Mechanocellular mechanisms of palatal shelf elevation

Morgan, Jack

Awarding institution:
King's College London

Mechanocellular mechanisms of palatal shelf elevation

Jack Darius Morgan

2023

A thesis submitted to King's College London for the degree of Doctor of Philosophy

Supervisors

Prof. Jeremy B.A. Green (primary)

Prof. Martyn T. Cobourne (secondary)

Declaration

I, Jack Darius Morgan, confirm that the work presented in this thesis, unless otherwise stated, is my own original work. The copyright of this thesis rests with the author and no quotation from it or information derived from it may be published without proper acknowledgement.

Acknowledgements

It is difficult to express my gratitude to the many wonderful people that have supported me throughout this Ph.D., and to those whom I have met as a result of it. The experiences shared have been truly inspiring; I am lucky to consider you all friends.

Firstly, thanks to my supervisor, Prof. Jeremy Green for the opportunity to carry-out this Ph.D. in your lab. Your training has shaped my scientific thinking and your enthusiasm and passion for science has been motivating. I will always be appreciative of our late Friday afternoon meetings discussing just about everything! Thanks also to my secondary supervisor, Prof. Martyn Cobourne, for your support throughout the Ph.D, which I extend to Dr. Cynthia Andoniadou, Prof. Agi Grigoriadis and Prof. Karen Liu.

I would also like to thank the wonderful group of KCL embryologists that inspired me to pursue developmental biology during my undergraduate degree: Pip, Ants, Esther, Clemens and Malcolm. Your exceptional teaching kindled my interests and I've never looked back.

A special note of thanks goes to the technical staff that provided invaluable support throughout this project: Chantal Hubens, for being an all-around technical wizard (en omdat je mij Nederlands leert), Wai-Lin, the Queen of histology, and Richard 'disengage the stage' Thorogate, master of the AFM.

Thanks to all the Green lab members past and present for your support. Mint, I will always cherish our afternoons looking at Echidnas and drinking tea. Claire, I will always be grateful to you for rescuing me from LAX! A particular note of thanks to my big brothers in the Green lab, Dom and Yushi. Be it in the lab (or in the pub), thank you for your guidance and friendship. Cathy, I felt lucky that you chose to do your MSc with us and feel even luckier now to call you a friend. Dan, thank you for helping with my final histology preparations and best of luck with the rest of the Ph.D.

Mo, thank you for being a wonderful friend and flatmate. Your support and reassurance have helped me beyond the written word during this Ph.D. I wouldn't have hurtled through our shared experiences with anybody else.

Jordan, thank you for everything. I am a better person for your steadfast friendship and support. I'm fortunate to have met you on our first day at King's and look forward to many more shared experiences in the future. Cheers for putting up with me, and cheers for that Yeats quote that I sign everything off with (I'll resist here!).

I am indebted to the Andoniadou lab family, members past and present. To Alice, Emily, Yasmine (French mum) and Cynthia. Your collective sheer kindness and unwavering support has been irreplaceable. Some of my favourite memories of the past few years have been forged with each of you, and I look forward to many more.

Thea, to cast your own words back at you: thank you for being my constant rock of support, too. You made coming to the lab fun, even when it wasn't. The past few years wouldn't have been half as bright without you, and I can't wait to visit you in San Diego.

Huge thanks to my friends and colleagues in the CCRB for welcoming me so kindly back in what now feels like a lifetime ago, and for continuing to inspire me along the way. Thank you to Wills Barrell, Neal Anthwal and James O'Sullivan for your wisdom (and shared love of Pokémon, music, and literature respectively) and for being there in all manner of crises. Ana and Leti, "ay-ay-ay!" Thank you both for your friendship and support throughout my Ph.D. I'd be remiss not to thank the extended Miller crew, with special shout outs to Michael and Dylan.

Voor mijn schatje, Nienke Annemijn Meeuwissen. Dank u voor uw blijvende liefde en steun. Je betekent de wereld voor mij. I couldn't have done this without you.

Thank you to my family for the love and support. Your encouragement has helped keep me going, and your comfort in rallying around me in the final moments helped me push through. I cannot thank each of you enough for helping me get to where I am today.

I dedicate this thesis to the memory of my grandfather, John Gwillim Morgan. 1930 – 2023.

Abstract

The mammalian palate is the physical and functional barrier between the oral and nasal cavities. It is also a common locus for human birth defects, with incidence of cleft lip/palate at 1:700 live births worldwide. Dysmorphias may arise at any stage of palatogenesis, from the initial ventral outgrowth of the paired palatal shelves (PSs), via their elevation above the tongue to their eventual fusion horizontally at the midline. Elevation is poorly understood, with no universally agreed-upon mechanism of action. It is thought to be driven by a force internal to the PSs in a heterogeneous manner, with the anterior 'flipping-up', and the posterior actively remodelling around the tongue. The cellular mechanisms of growth generating the internal shelf force are not well-understood, and little research has been carried out into both the biomechanics of this process and the material properties of the PSs and how they might facilitate elevation.

Initially, I set out to investigate the cellular mechanisms of growth underlying force generation in the PSs using an established hyperoxic *ex vivo* rolling culture system at E12.5 and E13.5. Surprisingly, it appeared that elevation was not occurring during culture, but rather via elastic recoil immediately on the removal of the tongue and mandible. However, 50% of cultured explants still displayed fused PSs, which posed the question as to how PS approximation can occur in the absence of growth *ex vivo*.

To interrogate this, I carried-out a 2D morphometric analysis of explanted maxillae-containing PSs, ‘maxillary explants’, during culture, which revealed that growth was poor and inconsistent across different metrics, and that the explants sometimes shrank. Increasing the gas change frequency marginally improved growth, though it remained inconsistent. On further morphometric analyses, I identified that PS fusion in *ex vivo* rolling culture is caused by a non-physiological deformation of the tissue, which narrows the space in the midline, causing the PSs to approximate.

PS elevation is a mammalian novelty, and non-mammalian PSs grow horizontally by default. This appeared to be the case in the anterior mouse PSs at E12.5, prior to contact and presumably downward deflection by the tongue. This led to the hypothesis that PS

elevation evolved as a consequence of the mammalian suckling requirement and large tongue, which I tested by producing a time course of palate development in a previously undescribed non-suckling mammal, the short-beaked echidna. The echidna shelves deflected just as in other mammals, disproving my hypothesis.

Finally, the *ex vivo* culture data suggested that elevation was an elastic, and potentially viscoelastic, event. Therefore, I carried out a series of experiments investigating the generation and mediation of the internal shelf force and the material properties of the PSs. Nuclear morphometrics studies revealed a complex picture of nuclear deformation and internuclear spacing across the PSs, but there were technical limitations in the segmentation model used and it was difficult to separate heterogeneity from noise. Further investigation into the presence of elastic fibres and collagens was carried out via histological staining and second harmonic imaging, which suggested that there are no mature elastic fibres or bundles of collagen present in the PSs at this time. Atomic force microscopy was used to measure the stiffness of the PSs. This suggested that the PSs comprise a relatively soft mesenchymal core, which was softer anteriorly and stiffer posteriorly, with a stiffer outer epithelial layer. This might suggest a more significant role for the epithelium during elevation than previously thought.

This work highlights new directions for the study of the biomechanics underlying PS elevation. It also provides the first early description of the material properties of the PSs at E13.5 and demonstrates that *ex vivo* rolling culture is an inappropriate system for the study of both PS elevation and growth. The limitations and future directions of the project are discussed, including directions for modelling PS elevation *in silico*.

Table of Contents

List of figures

List of tables

Abbreviations

AFM	Atomic force microscopy
AJ	Adherens junction
AP	Anteroposterior
Bm	Brillouin microscopy
BMP	Bone morphogenetic protein
BrdU	Bromodeoxyuridine
cKO	Condition knockout
CL/P	Cleft lip and/or palate
CNCC	Cranial neural crest cell
COL	Collagen
CPO	Isolated cleft palate
CPU	Central processing unit
Cre	Cyclic recombinase
DAPI	4’,6-diamidino-2-phenylindole
DiI	3,5-diiodopyridine-2,6-diamine
DMSO	Dimethylsulphoxide
DNA	Deoxyribonucleic acid
E	Young’s modulus
E	Embryonic day stage
ECM	Extracellular matrix
EdU	5-ethynyl 2´-deoxyuridine
EMT	Epithelial to mesenchymal transition
EtOH	Ethanol
FEM	Finite element model
FGF	Fibroblast growth factor
FN	Fibronectin
GAG	Glycosaminoglycan
GPU	Graphics processing unit

GRN	Gene regulatory network
H&E	Haematoxylin & Eosin
HA	Hyaluronic acid
Has	Hyaluronan synthase
IMS	Industrial methylated spirits
IoU	Intersection over union score
k	Spring constant
KO	Knockout
KO-DMEM	Knockout Dulbecco's modified Eagle's Medium
KSR	Knockout replacement serum
MA	Micropipette aspiration
Mdb	Mandible
MEE	Midline epithelial edge
MEPM	Mouse embryonic palatal mesenchyme
MES	Midline epithelial seam
microCT/μCT	Micro computed tomography
ML	Mediolateral
MMP13	Matrix Metallopeptidase 13
MPMT	Maxillae palate mandible tongue
Mya	Million years ago
NC	Neural crest
NCC	Neural crest cells
NS	Nasal septa
OSR2	Odd-skipped related 2
P-value	Probability value
PBS	Phosphate buffered saline
PCP	Planar cell polarity
PCR	Polymerase chain reaction
PFA	Paraformaldehyde

PPC	Parallel plate compression
PROMASS	Proliferation, reorientation, polarised matrix, addition, subtraction (apoptosis), shape/size
PS	Palatal shelf
PSA	Palatal shelf angle
PSI	Palatal shelf index
RNA	Ribonucleic acid
ROI	Region of interest
RPT	Rapid phase transition
RT	Room temperature
SD	Standard deviation
SHH	Sonic hedgehog
StarDIst	Object detection with star-convex shapes
SUN1	Sad1 And UNC84 Domain Containing 1
T/m	Tongue/mandible
TJ	Tight junction
TMJ	Temporomandibular joint
TUNEL	Terminal deoxynucleotidyl transferase dUTP nick end labelling
WNT1	Wingless-related integration site
WT	Wild type

1. Introduction

1.1 Cleft lip and/or palate

The mammalian palate is the physical and functional separation between the oral and nasal cavities. Anatomically, the palate consists of the primary palate and the secondary palate (the roof of the mouth), the latter further sub-divided into the bony 'hard palate' anteriorly and the muscular 'soft palate' posteriorly (Bush and Jiang, 2012). The two arise via different mechanisms of development and the secondary palate is the focus of this body of work.

Functionally, the two regions of the secondary palate serve both different and shared roles. The hard palate aids the processing of food and interoperates with the tongue in the production of specific so-called palatal and alveopalatal sounds (Helwany and Rathee, 2022). For example, in English the letter 't' is vocalised by pressing and releasing the blade of the tongue from the hard palate. The soft palate is valvular, closing-off the nasal airway for swallowing, and so is essential for proper feeding (Li, Lan, and Jiang, 2017). Palatal and glottal muscular contractions also direct airflow, which is partially responsible for sound variation during speech (Matsuo and Palmer, 2008). Therefore, normal development of the palate is essential for both structural form and in achieving functional feeding and communication.

The palate is also a common locus for craniofacial dysmorphology. One in seven hundred children are born with a cleft lip and/or palate (CL/P) (Dixon et al., 2011). CL/P is the most common craniofacial congenital anomaly and treatment is typically surgically invasive. There are various types of cleft, with both genetic and environmental causes, whose aetiologies are understood to varying extents.

1.1.1 Epidemiology

The number of live births with CL/P is typically stated as 1:700 globally (Dixon et al., 2011). However, this figure varies between studies, and is often quoted between 1 in 500 and 1 in 2500 live births (Christensen and Mitchell, 1996; Beaty et al., 2010; Klotz et al., 2010;

Mossey et al., 2009; Hammond and Dixon, 2022). This variation is linked to geographical location and ethnicity, with Asian and Indigenous American population CL/P incidence closer to 1:500, and European-derived populations closer to 1:1000. The incidence is lowest in African-derived populations, at 1:2500 (Dixon et al., 2011). This pattern is also observed in epidemiological studies of cases of cleft palate only/cleft palate without cleft lip (CPO) (Mossey and Modell, 2012). CPO is the least common form of clefting and occurs in between 1-25:10,000 live births (Burg et al., 2016).

CL/P and CPO may present as part of a syndrome, such as DiGeorge Syndrome (McDonald-McGinn et al., 2015), although 70% of CL/P cases and 50% of CPO cases are thought to be non-syndromic and occur in isolation (Stanier and Moore, 2004; Jugessur et al., 2009). CL/P is reportedly twice as common as CL overall (Jensen et al., 1988) and left sided unilateral clefts are twice as common as those affecting the right side (Gundlach and Maus, 2006).

Cleft lip alone (CL) is more prevalent in males, at a roughly 2:1 male:female ratio. This ratio is reversed in CPO, at a 2:1 female:male ratio (Shkoukani et al., 2013). Though mysterious, these sex differences may arise due to differences in developmental timing during male and female embryogenesis (Kosowski et al., 2012; Vanderas, 1987).

The relatively high frequency of CL/P renders palate development highly clinically relevant. Palate morphogenesis is a complex process and is developmentally sensitive to both genetic and environmental factors. This is evident from the epidemiology, though further studies could help identify and isolate particular risk factors.

1.1.2 Types of cleft

Clefting is thought occur at any site of union between the facial primordia and at any stage of palatogenesis; the anatomical location and extent of the cleft dictate their clinical description.

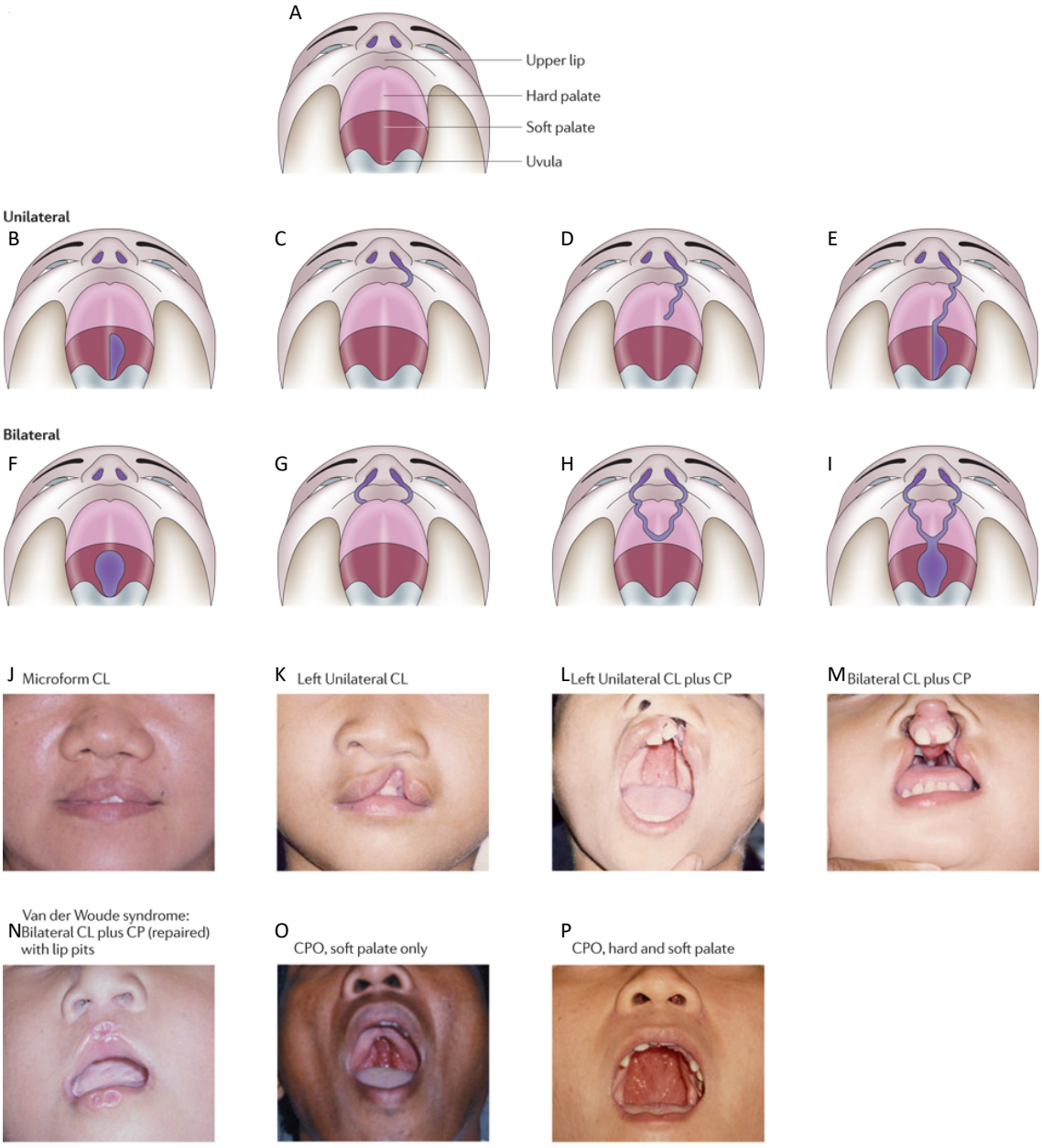

Figure 1.1 Diagrams and patient photographs demonstrating different types of CL/P

A) illustrative drawing of the palate and associated structures in the oral view. B) Unilateral soft palate cleft. C-E) Different degrees of unilateral CL/P. F) Bilateral soft palate cleft. G-I) Different degrees of bilateral CL/P. J-P) Patient photographs of different types of CL/P. CL, cleft lip; CP, cleft palate; CPO, cleft palate only (adapted from Dixon et al., 2011; Muenke, 2002).

1.1.2.1 Primary clefting

Primary palatal clefts occur when intermaxillary segment-derived or communicating structures fail to meet and/or fuse. This may occur if the paired maxillary prominences fail to meet and fuse (forming the philtrum), or if the maxillary and nasal prominences

fail to meet and fuse. Clefts here results in a 'cleft lip' (CL). In rarer cases, these clefts may continue superiorly along the craniofacial apparatus at sites of facial primordia fusion, namely between the lateral nasal prominences and the maxillary prominences. In severe cases, these so-called 'Tessier's clefts' may proceed up to the level of the eyes (Tessier, 1976).

1.1.2.2 Secondary palate clefting

Clefts of the secondary palate may affect the hard and/or soft palate (*see Figure 1.1*).

Secondary clefts are thought to arise due to the failure of the so-called paired palatal shelves (PSs) to undergo normal development. As with primary clefts, they may be syndromic or non-syndromic.

1.1.2.3 Prognoses and treatment

CL/P causes physical difficulties in feeding and speaking and may lead to mental health issues and social discrimination (Wehby and Cassell, 2010; Martín-Del-Campo et al., 2019; Zhou et al., 2023; Beaty et al., 2016). Treatment is typically surgical and consists of firstly repairing any CL via the translocation and stitching of upper lip tissue after 10 weeks. CPO repair is referred to as a palatoplasty, ideally performed between 9-15 months of age (Shkoukani et al., 2013). There are various types of palatoplasty depending on the type and severity of the CL/P, though all attempt to close the oronasal communication and repair any affected musculature in the soft palate to the point of functionality (Wang and Milczuk, 2014). This involves extensive tissue reconstruction, though success is variable, with patients often encountering further surgery-associated difficulties in communication and feeding (Sullivan et al., 2009; Annigeri et al., 2012).

1.1.3 Aetiologies

1.1.3.1 Syndromic vs non-syndromic

At least 275 known syndromes include CL/P as a primary feature and account for around 30% of all cases (Leslie and Marazita, 2013; Stanier and Moore, 2004). Of these syndromic clefts, Van der Woude syndrome is the most common, accounting for 2% of all CL/P cases

(Burdick, 1986). These are increasingly the focus of research and selected CL/P phenotype syndromes for which at least one relevant causative genetic locus mutation is known are listed in *Table 1.1*.

Table 1.1 Selected CL/P syndromes and implicated genes (adapted from Leslie & Marazita, 2014)

Syndrome/sequence	Cleft Type Observed	Gene	References
Ankyloblepharon-ectodermal dysplasia-clefting	CL/P	*TP63*	(McGrath et al., 2001)
Apert	CP	*FGFR2*	(Wilkie et al., 1995)
Bamforth-Lazarus	CP	*FOXE1*	(Bamforth et al., 1989)
Bartsocas-Papas	CL/P	*RIPK4*	(Kalay et al., 2012; Mitchell et al., 2012)
Branchio-oculo-facial	CL/P	*TFAP2A*	(Milunsky et al., 2008)
Campomelic dysplasia	CP	*SOX9*	(Foster et al., 1994; Wagner et al., 1994)
CHARGE	CP	*CHD7*	(Vissers et al., 2004)
CL/P ectodermal dysplasia	CL/P	*PVRL1*	(Suzuki et al., 2000)
Cornelia de Lange	CP	*NIPBL*	(Krantz et al., 2004; Tonkin et al., 2004)
Crouzon	CP	*FGFR2*	(Reardon et al., 1994)
DiGeorge	CP	*TBX1*	(Packham and Brook, 2003)
Ectrodactyly-ectodermal dysplasia-clefting	CL/P	*TP63*	(Celli et al., 1999)
Familial gastric cancer and CL/P	CL/P	*CDH1*	(Frebourg et al., 2006)
Gorlin	CL/P	*PTCH1*	(Hahn et al., 1996; Johnson et al., 1996)
Holoprosencephaly	CL/P	*GLI2*	(Roessler et al., 2003)
Holoprosencephaly	CL/P	*SHH*	(Roessler et al., 1996)
Holoprosencephaly	CL/P	*SIX3*	(Wallis et al., 1999)
Holoprosencephaly	CL/P	*TGIF*	(Gripp et al., 2000)

Syndrome/sequence	Cleft Type Observed	Gene	References
Isolated cleft palate	CP	*SATB2*	(FitzPatrick et al., 2003)
Kabuki	CL/P	*MLL2 KDM6A*	(Lederer et al., 2012; Ng et al., 2010)
Kallmann	CL/P	*FGFR1*	(Dodé et al., 2003)
Lethal and Escobar multiple pterygium	CP	*CHRNG*	(Morgan et al., 2006)
Loeys-Dietz	CP	*TGFBR1, TGFBR2*	(Loeys et al., 2005)
Miller	CP	*DHODH*	(Ng et al., 2010)
Oculofaciocardiodental	CP	*BCOR*	(Ng et al., 2004)
Opitz G/BBB	CL/P	*MID1*	(Quaderi et al., 1997)
Oro-facial-digital	CL/P	*GLI3*	(Johnston et al., 2010)
Oro-facial-digital type 1	CL/P	*OFD1*	(Ferrante et al., 2001)
Otopalatodigital types 1 and 2	CP	*FLNA*	(Robertson et al., 2003)
Pierre Robin	CP	*SOX9*	(Benko et al., 2009)
Popliteal pterygium	CL/P	*IRF6*	(Kondo et al., 2002)
Saethre-Chotzen	CP	*TWIST1*	(Ghouzzi et al., 1997; Howard et al., 1997)
Stickler type 1	CP	*COL2A1*	(Snead and Yates, 1999)
Stickler type 2	CP	*COL11A1, COL11A2*	(Snead and Yates, 1999)
Tetra-amelia with CL/P	CL/P	*WNT3*	(Niemann et al., 2004)
Tooth agenesis with or without cleft	CL/P	*MSX1*	(Van Den Boogaard et al., 2000)
Treacher Collins	CP	*TCOF1*	(Dixon et al., 1996)
Van der Woude	CL/P	*IRF6*	(Kondo et al., 2002)
X-linked cleft palate and ankyloglossia	CP	*TBX22*	(Braybrook et al., 2001)
Siderius X-linked intellectual disability	CL/P	*PHF8*	(Laumonnier et al., 2005)

Non-syndromic CL/P is genetically complex condition thought to be caused by interactions between genetic and environmental factors, though these are not fully understood. In the previous century, relative increases in clefting frequency in the family of those affected was identified (Fogh-Anderson, 1942), leading to segregation analyses (Marazita et al., 1984) and twin studies (Mitchell, 2002). However, familial risk of clefting is historically well-documented (Darwin, 1868; Rew, 1757; Sproule, 1863) and it is now known that the recurrence risk is around thirty-two times higher for individuals with a first degree relative with CL (Sivertsen et al., 2008). Genetic association has been further investigated using modern approaches. These include genome-wide association studies (GWAS) (Ludwig et al., 2012), investigations into genomic rearrangement (Alkuraya et al., 2006), copy number variations (Osoegawa et al., 2008) and standard candidate gene studies (Zucchero et al., 2004; Rahimov et al., 2008). Interestingly, the CL/P concordance rate is 40-60% in monozygotic twins, and 3-5% in dizygotic twins (Little and Bryan, 1986). This demonstrates that, despite clearly a strong component, the aetiology of CL/P cannot be purely genetic.

1.1.3.2 Environmental factors

Environmental factors may have a deleterious or protective effect on non-syndromic CL/P risk (Suazo, 2022). Risk factors include: maternal smoking (Wyszynski et al., 1997); medications such as beta-blockers (Puhó et al., 2007; Yakoob et al., 2013), benzodiazepine (Enato et al., 2011) and anti-convulsants (Veroniki et al., 2017) when taken during the first trimester; stress (Molina-Solana et al., 2013); and maternal alcohol consumption (DeRoo et al., 2016). The underlying molecular and cellular aetiologies are understood to varying extents. For example, nicotine in tobacco smoke causes apoptosis in embryonic cells under oxidative stress, which is linked to nucleic acid damage (Machado et al., 2019). Moreover, craniofacial neural crest cells in the first pharyngeal arch – major contributors to the craniofacial apparatus – demonstrate reduced DNA methylation in response to cigarette smoke. Methylation state changes have also been observed in the umbilical cord blood of smokers, wherein affected methylation sites are adjacent to genes involved in craniofacial dysmorphologies (Joubert et al., 2016). By contrast, it is debated as to whether maternal alcohol consumption increases the risk of CL/P at all (Garland et al., 2020). It should be noted, however, that extreme cases of foetal

alcohol syndrome may lead to holoprosencephaly, which often includes a CL/P (Roessler et al., 2003, 1996; Gripp et al., 2000; Wallis et al., 1999).

Maternal vitamin intake has also been linked to CL/P incidence, with folic acid supplementation found to have a protective effect against some types of cleft (Badovinac et al., 2007; Jahanbin et al., 2018). As with folic acid protection against some cases of spina bifida (Greene and Copp, 2014), the mechanism of protection in CL/P is largely unknown. However, a recent study identified that a reduction in the activity of an enzyme involved in intracellular folate retention is linked to an increased incidence of CL/P (Inostroza et al., 2021). Hence, further studies into the metabolism surrounding palatogenesis may help in our understanding of normal and dysmorphic palatal development.

1.1.4 CL/P summary

Overall, great progress has been and continues to be made in exploring the genetics underlying CL/P. However, this is in stark contrast with our understanding of the morphogenesis of the palate in normal development. In particular, very little is known about the cellular behaviours driving this process, nor the material properties or biomechanics of the tissue during palatogenesis. Understanding these components is key to bridging the gap between genotype and phenotype and it is hoped that, by understanding normal palate development, we can begin to interrogate the aetiologies underlying pathological palate development.

1.2 Palatogenesis

In keeping with the primary focus and model organisms of this work, all references to development and embryonic day staging are made in relation to the house mouse, *mus musculus*, which has the been the primary model used in historic CL/P research, unless stated otherwise.

1.2.1 Early craniofacial development overview

The external craniofacial apparatus arises as five cranial neural crest (CNCC)-derived primordia at E9.5 in the mouse and week four in humans; facial development is complete by E12.5 and week six respectively (Hinrichsen, 1985; Jiang et al., 2006).

The CNC cells migrate from the pharyngeal arches during embryonic development (Johnston, 1966; Knight and Schilling, 2013). The pharyngeal arches are a series of lateral bulges on the surface of the embryonic head, each containing a migratory population of neural crest cells (NCCs), which ultimately become much of the facial skeleton. The pharyngeal arches also contain a population of mesodermally-derived mesenchyme, which become the facial musculature (Mcgonnell et al., 1998). There are five pharyngeal arches in all amniotes (Graham et al., 2019), and CNCCs migrating from the first pharyngeal arch are designated the CNC and populate the maxilla and mandible (Francis-West et al., 1998). Regional proliferation of these structures results in the outgrowth of the facial primordia (Szabo-Rogers et al., 2010).

At E9.5, the primordia consist of the frontonasal process (FNP) rostrally, paired maxillary processes laterally and paired mandibular processes caudally (*Figure 1.2A*). By E10.5 depressions in the FNP form the nasal pits, which separate the FNP into the lateral and medial nasal processes (*Figure 1.2B&C*). Subsequently, the medial nasal processes fuse, forming the intermaxillary segment (*Figure 1.2D*) (Twigg and Wilkie, 2015). This region gives rise to the philtrum of the upper lip, the incisors, and the primary palate (Gritli-Linde, 2007). By E12.5, the lower lip and jaw are formed by fusion of the mandibular processes at the midline, whilst the commissures of the mouth are formed by the lateral fusion of the mandibular and maxillary processes (Hammond and Dixon, 2022). However, it is worth noting that the process may instead be considered a merging event, wherein mesenchyme populate the space from beneath, rather than strictly a fusion event, which would necessitate contact between distinct epithelial surfaces. In this thesis, the meeting of the palatal shelves is described as a fusion event, but whether or not the shelves have strictly undergone fusion as *in vivo* in the later described *ex vivo* culture studies was not investigated, so it may be considered that they 'abut' as a minimum.

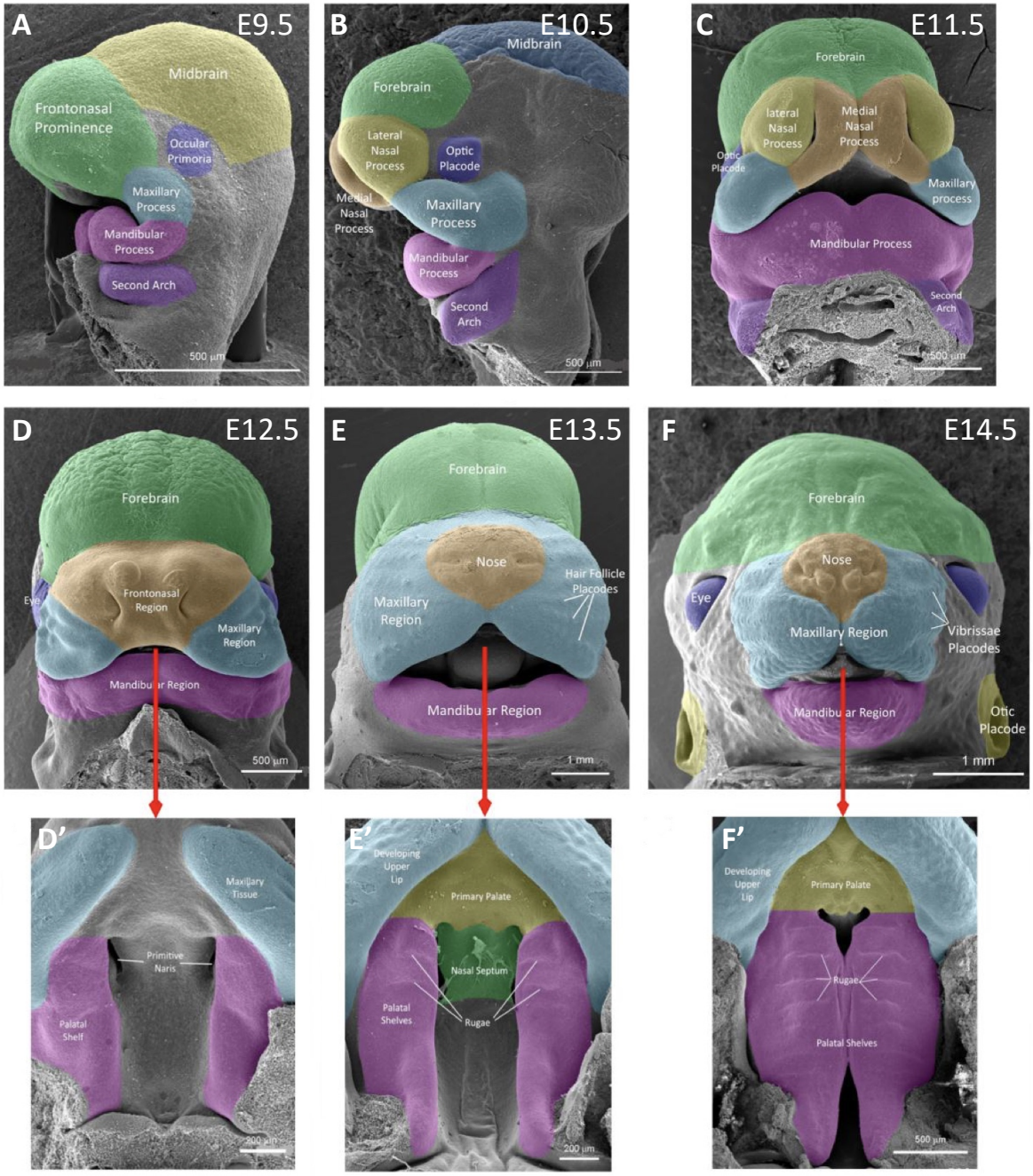

Figure 1.2 Scanning election micrographs (SEMs) of mouse head development

SEMs show a timecourse of facial development from the initial facial primordia (A) their further subdivision in the sagittal aspect (B), the development of the medial and lateral nasal processes from the FNP (C) and lateral state facial morphogenesis to final form (D – f) and the development of the secondary palate (D' – F') at corresponding stages. Scale bars are stated in each panel. SEMS are taken from facebase.org (Schuler et al., 2022) and the figure adapted from Brock, 2013.

Towards the end of this process, palatogenesis begins.

1.2.2 Primary palate formation overview

The primary palate consists of the upper-incisor region of the upper jaw anterior to the incisive foramen and the philtrum of the upper lip (Li, Lan, and Jiang, 2017). It is formed by the posteriorly extending intermaxillary segment in the oral aspect, which itself is formed by the fusion of the medial nasal processes (*Figure 1.2E'&F'*). Around E15.5, the primary palate fuses superiorly with the nasal septa to form the anterior roof of the oral cavity, and with the elevated palatal shelves of the posterior palate posteriorly – forming the continuous palate (Gritli-Linde, 2007).

CL may arise due to a failure of the complex fusion events during philtrum and primary palate development. At the contact point of the maxillary processes, the epithelium degenerates, and mesenchymal confluency is achieved, marking fusion. However, failures in these processes may result in an incomplete formation of the upper lip/philtrum region, the lambdoid junction, presenting as a CL (Deshpande and Goudy, 2019).

1.2.3 Secondary palate development

The secondary palate arises as paired outgrowths, the so-called palatal shelves (PSs), from the maxillary processes around E11.5 in the mouse, and at week six in human embryos. The PSs comprise a thin layer of epithelium surrounding a relatively large mesenchymal core. The development of the secondary palate has been summarised in a series of excellent reviews (Bush and Jiang, 2012; Li, Lan, and Jiang, 2017; Hammond and Dixon, 2022) and is conceptualised as a series of defined stages: ventral outgrowth, elevation, horizontal growth, and fusion, which are the transitions between the five stages illustrated in *Figure 1.3*, and is complete by around E15.5 in the mouse and week 12 in humans. Thereafter, in humans the posterior third of the palate undergoes myogenesis posteriorly, and ossification anteriorly, reflecting the final form and function of the palate along the AP axis (Depew et al., 2002). The fully developed palate separates the oral and nasal cavities, aiding and enabling intricately co-ordinated mastication, swallowing, and breathing (Matsuo and Palmer, 2009). Below, each of these stages are described in detail.

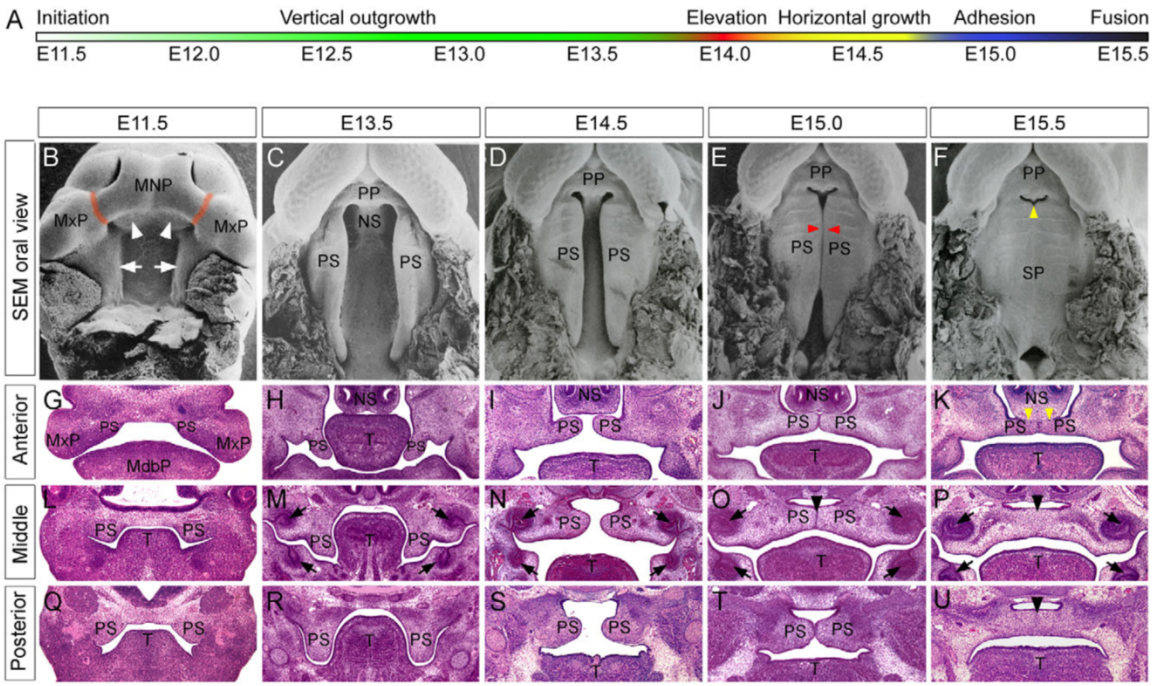

Figure 1.3 Murine palatogenesis

A) Timecourse of palate development in the mouse. B-F) Scanning electron micrographs of complete palate development in the oral view. G-U) Coronal (frontal) H&E-stained histological sections of the oral apparatus in the anterior (G-K), middle (L-P) and posterior (Q-U) regions at the indicated corresponding embryonic day stage. Orange lines, fusion sites (B); white arrowheads, early palatal outgrowths (B); red arrowheads, site of PS fusion (E); yellow arrowheads, space filled by fusion (F, K); black arrowheads, molar tooth germs and sites of epithelial seam degeneration (M-P); Mdbp, mandibular process; MNP, medial nasal process; MxP, maxillary process; NS, nasal septum; PP. primary palate; PS, palatal shelf; SP, secondary palate; T, tongue (Bush & Jiang, 2012).

1.2.3.1 Specification and outgrowth

During PS outgrowth, the paired PSs arise from the oral aspect of the maxillary prominences and are visible around E11.5 (*Figure 1.3B, G, L, Q*). They appear to grow ventrally, or 'downwards', either side of the tongue up until they elevate, and may be deflected in this orientation due to their anatomical relation and contact with the tongue (*Figure 1.3C, H, M, R*); this potential deflection will be revisited throughout this thesis.

The PSs also display subtly different morphologies along the AP axis, with the anterior PSs appearing more finger-like, and the posterior PSs appearing more rounded (Yu & Ornitz, 2011).

The role and mechanism of molecular signalling in initiating PS outgrowth is currently unknown, although SHH is thought to play a role given its regionalised expression patterns prior to and throughout palatogenesis (Bush and Jiang, 2012; Hammond and Dixon, 2022). *Shh* is expressed throughout the oral epithelium prior to elevation and becomes progressively restricted to the rugae. These are a series of periodic ridges on the oral surface of the mammalian hard palate and play a role in the sensing and processing of food (Pantalacci et al., 2009); they form as epithelial thickenings via a Turing reaction-diffusion patterning mechanism (Economou et al., 2012; Turing, 1952) followed by cell intercalation (Economou et al., 2013).

There is considerable molecular heterogeneity across the tissue throughout palatogenesis, confirmed by gene expression studies in both the anteroposterior (AP, running from the incisors towards the back of the throat) axis, and when comparing the presumptive oral and nasal aspects of the PSs (Hilliard et al., 2005; Hammond et al., 2019; Lan et al., 2015; Bush and Jiang, 2012; Han et al., 2009). For example, the transcription factor genes *Msx1* and *Shox2* are expressed in the anterior PSs only, whereas *Meox2* and *Tbx22* are expressed in the posterior PSs (Q. Li & Ding, 2007; Yu et al., 2005; Zhang et al., 2002, as reviewed by Bush & Jiang, 2012).

It is well-established that epithelial-mesenchymal interactions drive PS outgrowth and the literature on this aspect of palatogenesis is extensive. This is primarily via a positive feedback loop between epithelial SHH and mesenchymal FGF10, with various members of the signalling cascade and corresponding receptors investigated in mutant mouse studies (Bush and Jiang, 2012). Epithelial SHH signals to the underlying mesenchyme to promote proliferation and co-ordinate the subsequent PS outgrowth. This was confirmed by the tissue specific deletion of *Shh* in PS epithelium using *Krt-14*-Cre (Rice et al., 2004) and its receptor *Smo* in PS mesenchyme using *Osr2*-Cre (Lan and Jiang, 2009), which resulted in reduced outgrowth and clefting.

Multiple fibroblast growth factor family members converge on the regulation of *Shh* (Hammond and Dixon, 2022). *Fgf10* is expressed in the PS mesenchyme and its receptor, *Fgfr2b*, is expressed in the overlying epithelium between the periodic rugae (Welsh and

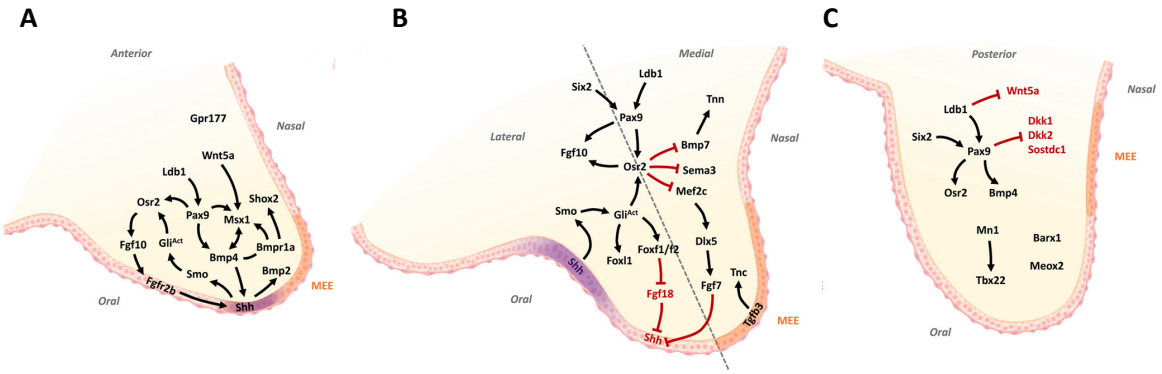

Figure 1.4 Molecular regulation of growth and patterning in the secondary palate

Schematic illustrating the extensive crosstalk and epithelial-mesenchymal interactions in the anterior (A), middle (B) and posterior (C) PSs. MEE, medial edge epithelia. Adapted from Hammond & Dixon, 2022; Li et al, 2017).

O'Brien, 2009; Rice et al., 2004). The reciprocal nature of epithelial-mesenchymal interactions via SHH and FGF10 has been shown by *Fgf10*$^{-/-}$ and *Fgfr2b*$^{-/-}$ embryos demonstrating overall reductions in proliferation, PS outgrowth and *Shh* expression; embryos also had a cleft palate (Welsh and O'Brien, 2009; Lan and Jiang, 2009; Rice et al., 2004). In the oronasal axis, *Fgf7* is expressed complementarily in the presumptive nasal mesenchyme before PS elevation (Veistinen et al., 2009). It is antagonised by *Dlx5*, which results in the restriction of *Shh* to the oral epithelium (Han et al., 2009). Therefore, FGF family members play an essential role in the outgrowth and oronasal patterning of the PSs.

The transcription factor Odd skipped-related 2 (OSR2) may play a particularly important role in PS outgrowth. *Osr2* is expressed the full AP length of the PSs and *Osr2*$^{-/-}$ mice display a cleft palate (Lan et al., 2004). Furthermore, *Osr2* functions downstream of SHH-SMO signalling (Lan and Jiang, 2009) and upstream of *Fgf10* (Zhou et al., 2013). *Osr2* has also been shown to act in a complex gene regulatory network (GRN) with, alongside SHH and FGF10, Pax9 and BMP4, hence appears to be a key intrinsic regulator of PS mesenchymal proliferation (Zhou et al., 2013).

In the anterior palate, ephrin-B1 signalling regulates PS mesenchymal cell proliferation by acting as a mitogen. In *ephrin-B1* heterozygous mutant mice, X-inactivation results in

ephrin-B1 expression mosaicism. This relieves endocytosis and degradation, causing a post-transcriptional up-regulation of EphB receptor expression. The authors further demonstrated that this ephrin-B1 driven control of anterior PS mesenchymal proliferation is mediated by regulation of the extracellular signal-regulated kinase/mitogen-activated protein kinase (RAS/MAPK) signalling pathway, and that the altered proliferation rates in mutants resulted in truncated anterior PSs (Bush & Soriano, 2010).

BMP family member crosstalk with SHH has also been observed during PS outgrowth, as has important cross-regulatory roles involving WNT signalling and various other molecular pathways (Hammond & Dixon, 2022). Further exploration and explanation of the genetic regulation of PS outgrowth is not essential to this thesis and is summarised in *Figure 1.4*.

1.2.3.2 Elevation

Following outgrowth, the PSs undergo an 'elevation' event, whereby they assume a horizontal position above the tongue from their previous vertical orientation either side of the tongue. In females, the PSs elevate later than in males, by a week in humans and by a few hours in mice (Burdi and Silvey, 1969; Goering et al., 2022). This could cause the higher incidence in CPO due to the relatively larger gap between the elevated shelves because of ongoing head growth. PS elevation is the focus of work in this thesis and is reviewed in-depth in section *1.3*.

1.2.3.3 Fusion

Following elevation, the PSs meet in the midline, adhere and fuse, resulting in a confluent mesenchyme (Bush and Jiang, 2012). It is contested as to whether growth following elevation contributes to bringing the PSs together, or whether they are immediately in contact on elevation (Goering et al., 2022).

As with PS outgrowth, there is a vast literature on PS fusion, particularly in the context of fusion-failure and clefting. Following elevation, the PSs abut immediately posterior to the second rugae, approximately between the anterior and middle region in the AP axis of

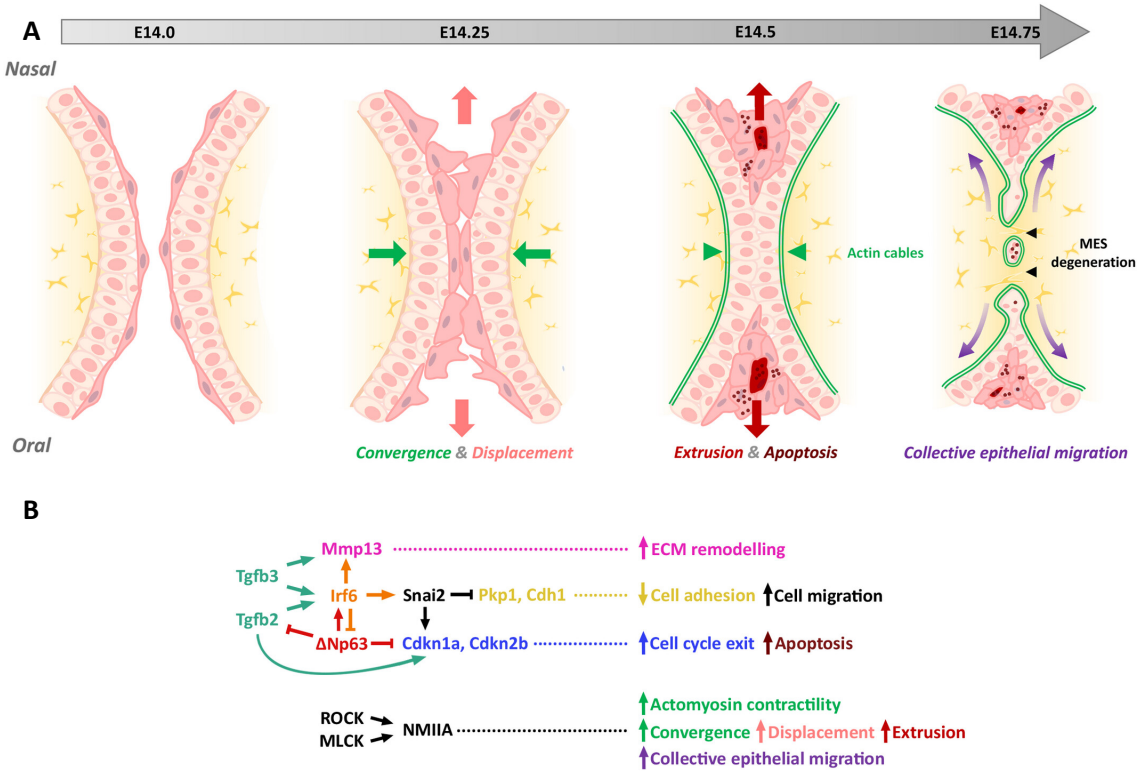

Figure 1.5 Mechanisms of PS fusion

Schematic representing A) the morphological changes during and B) the molecular control of PS fusion. MES degeneration begins when the PSs converge and TGFβ signalling promotes ECM remodelling acting on the transcription factors *Irf6 and Tp63.* These transcription factors act in a regulatory feedback loop to direct MEE cell fate. Ultimately, this results in the activation of non-muscle myosin, driving actomyosin contractility. The epithelia then migrate away, and mesenchymal confluence is achieved (adapted from Kim et al, 2015; Hammond & Dixon, 2022).

the PSs. Fusion than proceeds in a 'zippering' motion both anteriorly and posteriorly (*Figure 1.3E, J, O, T, F, K P U*). This occurs between E14.5 and E15.5 in the mouse and is typically complete by week 10 in human development (Danescu et al., 2015). However, fusion may be achieved earlier in static *ex vivo* culture if the PSs are brought into medial contact from E13.5 onwards (Kim et al., 2017; Morgan & Green, 2022).

Fusion competence must be tightly temporally regulated to prevent aberrant adhesion of the PSs to other oral surfaces, such has the tongue, as is seen in *Irf6* mutant mice (Richardson et al., 2009). Interestingly, mutations in *IRF6* are a prominent cause of CL/P in humans, causing Van Der Woude syndrome (Ghassibé et al., 2005; Kondo et al., 2002).

IRF6 is involved in the formation of periderm, a layer of flattened cells in the epithelial surface (Fitchett and Hay, 1989), which prevents inappropriate fusion. This stratified ectodermal layer is formed in part by a redistribution of membrane tension, promoting delamination following the onset of the expression of the vertebrate desmosomal cadherin desmoglein-1 (Nekrasova et al., 2018). Periderm cells are highly apicobasally polarised, and their adhesion complexes are fenced-off from the apical surface by tight junctions. Hence, the cells cannot adhere to adjacent ectodermal surfaces (Hammond and Dixon, 2022; Hammond et al., 2019). For PS fusion to occur, cells at the midline epithelial edge (MEE) are therefore required to become fusion-competent. When abutting, the adjacent medial PS MEE form the midline epithelial seam (MES) and the periderm barrier is not necessarily displaced prior to fusion, but rather mediates PS contact, before migrating out along with the basal MEE.

The mechanism by which the MES both adheres and degenerates has been contentious and extensively studied, with modulation of adhesion complex expression, cellular migration and apoptosis all implicated (Lough et al., 2017a; Bush and Jiang, 2012). It is now generally understood that extensive extracellular matrix (ECM) remodelling and cellular migration drive the morphological changes observed during PS fusion (Kim et al., 2015; Teng et al., 2022), and the process is summarised in *Figure 1.5*.

1.2.3.4 Summary of secondary palate formation stages

Development of the secondary palate is a multifaceted, complex and sensitive process. Normal development of the palate at the described stages is essential for its later ossification and innervation, creating the functional mature structure. The processes of palatal shelf outgrowth and fusion are well-understood both morphologically and molecularly. However, the cellular behaviours during these processes remain at least partially unresolved.

This is particularly the case during PS elevation; whilst the morphological changes are well-described, the mechanism by which the process occurs is unresolved both molecularly and at the level of cellular behaviours. The literature is relatively small, often in conflict and explored in detail below.

1.3 Palatal shelf elevation

PS elevation is the process by which the PSs elevate from their initial, ventrally-pointing orientation either side the tongue to their final horizontal position above the tongue (*Figure 1.3C, H, M, R, D, I, N, S*). The process is thought to happen rapidly in a heterogeneous manner along the AP axis, and the relevant literature is reviewed in detail below.

1.3.1 Early studies

The typically cited literature in modern palate elevation research date from around the mid-twentieth century. However, there is a fascinating earlier, predominantly German literature on the topic published between the mid-nineteenth to the early-twentieth century that appears to be largely overlooked.

From the earliest reference I can find based on early 20th century references, the first morphological description of palate elevation was based on observations from whole and frontally sectioned mammalian tissue, including human, staged by crown-rump length. In which, the tongue is described as moving away from both the lower aspect of the nasal septum and behind the base of the skull, losing contact with the PSs. The author states that the increased space in the oral cavity following tongue movement and loss of tongue-PS contact drives the PSs into their final, horizontal position (Dursy, 1869). Dursy also noted that, on elevation, the PSs are not yet able to meet in the midline, though no mechanism was proposed.

This account of the process was given credence by Wilhelm His in his landmark 'Anatomie Menschlicher Embryonen' (Anatomy of Human Embryos) and became the prevalent mechanism of elevation (His, 1885). In later work, His took sagittal sections of human embryos and described how the lateral aspect of the tongue became separated from the PSs during elevation, and that this supported the theory (His, 1901). His also offered a mechanism for elevation, on the assumption that 'muscle contractions' in the lower jaw at the end of the second month of gestation pulls the tongue under the PSs one at a time.

Here, His describes the newly inferiorly positioned tongue as moving the PSs from their vertical to a horizonal position, perhaps by pushing-up on them. This observation was made on the basis of a sample displaying unilateral elevation, which he considered an intermediate stage. Similar observations would surface later in the field (Chamberlain, 1966; Lazzaro, 1940; Poswillo & Roy, 1965; Walker, 1971a; Walker & Fraser, 1956; Wragg, Diewert, et al., 1972; Yu & Ornitz, 2011). Unilateral elevation was, however, controversial even at the time, with some considering it to be pathological (Fick, 1902; Polzl, 1905).

Furthermore, at this time mechanical interference preventing elevation was first proposed as a mode of clefting. In one study, two cases of CL/P were observed alongside micrognathia, and so it was proposed that the tongue had remained in the way of the PSs (Tandler, 1899), a mechanism later described as Pierre-Robin sequence (see below). His also reportedly suggested that clefts could be caused by the foetal body (chest) pushing-up on the mandible *in utero* and wedging the tongue high in the oronasal cavity (Pearn, 1967 citing His, 1885).

Another study using human tissue proposed a combination of external factors in driving elevation: an elongation of the mandible, increase in skull/oral cavity height and change in the angulation of the maxilla. This, combined with the space created by the lowering of the tongue, was said to cause elevation; the author postulates that it could happen passively without active muscle contraction (Polzl, 1905). Here, Polzl refers to elevation as an "Umlagerung" or a 'rearrangement' event and briefly outlines that, if one experimentally gives "a push of the thumb on the jaw" palate 'disruption' can be caused in whole samples.

Concurrently, there appears to have been a great interest in the evolution and comparative embryology of palate development, with the process described in humans (Dursy, 1869; His, 1885, 1901; Polzl, 1905; Schorr, 1908), pigs (Dursy, 1869), rabbits (Voit, 1909), wolves (Fick, 1902) and rats (Glas, 1904). There also appears to have been some comparison with amphibians (Fuchs, 1907), reptiles (Fuchs, 1908) and the echidna (Seydel, quoted by Polzl, 1905). In the latter, Polzl quotes the examination of an echidna sample brought back from an 'expedition to Australia and the Malay Archipelago' in

which an ‘O, Seydel’ (presumably a colleague) states there is ‘no evidence that, in the echidna, palatal processes first grow downwards, then horizontally, as in other higher order mammals’ (this will be especially relevant to Chapter 5 of this thesis).

Palatogenesis as a sequential process featuring an elevation/rearrangement event became known as the ‘classical model’ of palate development and was bolstered by several international-reaching reviews (Pearn, 1967, citing Inouye, 1912 and Ballantyne, 1905). This is perhaps best exemplified in the extremely detailed review of palate anatomy during development by Karl Peter, which is still occasionally referenced in the modern literature (Peter, 1924). In this work, Peter refers to paired, vertical ‘plates’ of tissue growing downward either side of the tongue, which ‘rotate inward’ to meet one another prior to apposition and fusion. This is likely the first description of PS elevation as a whole-tissue rotation event.

The early literature on palate development is often overlooked, perhaps due to a lack of readily available translations. It gives an insightful and detailed description of the morphogenesis of the palate. There also appears to be a particularly extensive comparative embryology and evolutionary literature on palate development from this period, but some papers have been particularly difficult to track down from the available references. This early literature is the first to describe palatogenesis as a series of progressive events and provides the first theories as to how elevation may occur, and how lack thereof may lead to CL/P. Many of these theories appear to centre around the PSs playing a largely passive role in elevation, with growth of surrounding structures and changes in PS-tongue apposition and oronasal geometry guiding the shelves into a horizontal position. A reported rapid elongation of the mandible at this stage was frequently highlighted in these studies (Polzl, 1905; Sicher, 1915). Elevation as a rearrangement (Polzl, 1905) or rotation (Peter, 1924) event would later be described independently by Walker & Fraser (1956) and Coleman (1965) respectively and experiments similar to Polzl’s manual manipulation of the mandible/tongue to manipulate the unelevated shelves would later become classical studies in the field (Walker and Fraser, 1956; Ferguson, 1978).

1.3.2 Intrinsic ability of shelves to elevate versus external factors

External factors (i.e., anything other than the PSs *per se*) are now thought to occupy a regulatory role in PS elevation, as it has been demonstrated that elevation can occur in partial isolation in a growth-independent manner. In a significant study, Wistar rat palatal shelves were shown to elevate via intrinsic forces prior to the onset of foetal reflexes following manual manipulation (Ferguson, 1978). Specifically, a blunt probe was inserted into the mouths of embryos with unelevated PSs and the tongue gently depressed. This resulted in the removal of the tongue as a physical barrier between the PSs, and the consequent rapid elevation of the PSs. This reportedly occurred faster in embryos that were closest to *in vivo* elevation, whilst at earlier stages the shelves were more likely to resume their vertical position either side of the tongue on removal of the instrument. The process occurred in seconds, too fast to be growth-dependent.

To further verify the intrinsic nature of the elevation process, in the same study the potential contributions of a pressure change in the nasal cavity or in the angulation of the cranial base were accounted for by dissecting out the developing skull, brain and nasal septum prior to probe insertion. The same results were seen as when these structures were present, consolidating the intrinsic nature of shelf elevation.

This study essentially mirrored earlier work in which the tongue was depressed using glass instruments in mice still attached to anaesthetised dams via the umbilicus in exteriorisation assays (Walker & Fraser, 1956). Here, the authors largely make the same observations as Ferguson and suggested that an 'internal shelf force' drives elevation. A particular strength of the Walker & Fraser study was their classification of developmental stage via shelf morphology, a histomorphological technique repeated under different parameters in the later literature owing to the extensive variability in PS morphology between embryos at the same embryonic day stage (Yu & Ornitz, 2011).

Despite these findings, extensive research was performed on the role of external factors driving PS elevation. These were documented previously (Ferguson, 1978, 1981a) and are updated and summarised in *Table 1.2*.

Table 1.2 Theories of PS elevation driven by factors external to the PSs (adapted from Ferguson, 1978, 1981).

Theory	References
Rapid growth of the mandible in relation to the maxilla, causing tongue descent.	(Asling et al., 1960; Burdi & Silvey, 1969; Coleman, 1965; Diewert, 1974; Polzl, 1905; Poswillo, 1968; H. Sicher, 1915; Sicher, 1966; Zeiler et al., 1964)
Downward growth of the nasal septa and primary palate, causing tongue descent.	(Zeiler et al., 1964; Abramovich, 1972; Fraser, 1967, 1969, 1971)
Descent of the tongue owing to tongue-intrinsic neuromuscular activity.	(Wragg, Smith, et al., 1972; Wragg, Diewert, et al., 1972)
The tongue pushing upwards on the shelves following descent.	(Arey, 1974; B. E. Walker, 1971; His, 1901)
Foetal mouth opening reflexes causing pressure and space differences, leading to tongue descent	(Humphrey, 1971, 1969, 1968; Friedl et al., 2019)
Angular changes in the anterior cranial base relative to the posterior, producing an elevating force.	(Larsson, 1974; Taylor and Harris, 1973; Verrusio, 1970; Harris, 1961, 1967; Polzl, 1905)
Lifting of the embryonic head from the chest causing tongue descent, driven by: i. Neck muscle contraction ii. Cervical vertebrae growth iii. Rapid increase in head height iv. Jaw muscle contraction	i. (Walker and Patterson, 1974; B. E. Walker, 1971; Walker, 1969) ii. (Ross et al., 1965) iii. (Joodeph and Wragg, 1971; Polzl, 1905) iv. (His, 1901)

Despite the PSs possessing an inherent ability to elevate on simple removal of the tongue, it is thought that this intrinsic ability acts in concert with external factors to ensure the proper regulation and timing of PS elevation. For example, it has been proposed that the constraint of the tongue drives the PSs into their final form and directs the proper timing of elevation (Yu & Yonemitsu, 2019).

Nevertheless, disruptions to these external, regulatory processes have been implicated in cleft palate phenotypes. This has perhaps been most extensively investigated in foetal mouth opening reflexes and tongue movements, often in the context of maternal nutrition and retinoid signalling. Retinoic acid dehydrogenase 10 (RDH10) is an enzyme required for the oxidation of vitamin A in retinoic acid (RA) synthesis (Sandell et al., 2012).

Disruption to retinoid signalling causes pharyngeal patterning defects, impairing the development of cranial nerve twelve (CN XII), which innervates the tongue and initiates motor activity around the time of elevation (Walker, 1969; Wragg et al., 1972). Perturbations in RA have been long known to cause CL/P (Hale, 1935; Sandell et al., 2007; Warkany, 1943; Wilson et al., 1953; Warkany, 1945), as have broader disruptions to tongue development and craniofacial innervation (Barrow and Capecchi, 1999; Oh et al., 2010a). Hence, undisturbed neuromuscular development and adequate levels of RA signalling are required for normal palate development. In a recent study utilising the *Rdh10*$^{delta/flox}$ mouse, deficient retinoid signalling resulted in reduced/absent foetal mouth opening movements and a cleft secondary palate in mutant embryos (Friedl et al., 2019). The cleft appears to be a secondary defect owing to the inability of the tongue to move out of the way. This further supports the idea that external factors play a supporting role in PS elevation but cannot be the sole mechanism by which elevation occurs. In Ferguson's probing experiment, it was noted that depression of the mandible alone was not sufficient to displace the tongue from between the shelves, and this only occurred if the mandible was depressed to the point of tearing (Ferguson, 1978).

Overall, there is a substantial body of evidence that external factors, such as mouth opening movements/foetal reflex onset and craniofacial neuromuscular activity, play a key role in the facilitation and regulation of PS elevation. There is also a substantial body of work investigating the intrinsic ability of the PSs to elevate, and these are explored below.

1.3.3 Intrinsic factors

The previously described series of experiments by Walker and Fraser (1956) and Ferguson (1977) provide compelling evidence for the PSs possessing an inherent ability to elevate independently from surrounding structures. Walker and Fraser (1956) proposed that elevation is driven by an 'internal shelf force' and that this force may reside in a network of elastic fibres in the shelves suggesting by a positive Gomori (acid fuchsin) stain (see section *1.4.5.5*). However, subsequent research failed to replicate Walker and Fraser's elastic fibre findings; this proposed mechanism of internal shelf force storage was

therefore disputed (Frommer and Monroe, 1969). Nonetheless, following Walker and Fraser or otherwise, a focus of palate elevation research has been on assessing the evidence for and the mechanism of the generation, storage, and action of the internal shelf force.

1.3.3.1 *Ex vivo* culture

Compelling evidence for the PSs intrinsic ability to elevate is given by research utilising *ex vivo* culture systems, which have been used extensively in previous research to investigate palate development.

PS elevation is difficult to visualise *in vivo* owing to the rapidity of the event and it's enclosure by surrounding tissues *in utero*. To try to apply live-imaging and microscopy to the dynamics of the process, e*x vivo* culture systems have been used extensively to overcome these physical barriers to investigate all stages of palatogenesis.

Historically, there have been a variety of culture systems used, often with subtle variation between research groups. However, they can broadly be categorised into three main set-ups:

1. Static air-liquid interface culture systems, also known as Trowell culture (Trowell, 1959)
2. Incubated 'dynamic' culture in bottles on roller apparatus (rolling culture)
3. Brinkley's 'improved' organ culture system (perfusion reactor)

All these systems were reviewed by Brinkley, and her lab (Lewis et al., 1980; Brinkley et al., 1975). Static culture systems involve placing excised PSs on filter paper or a metal grid, with tissue at the air-liquid interface (Myers et al., 1967; Pourtois, 1966; Lahti et al., 1972). Variations on this technique include the static anchoring of PS tissue in medium-covered nutrient agar discs or solidified plasma (Goss et al., 1970a; Chaudhry & Siar, 1967; Goss et al., 1970b; Moriarty et al., 1963; Reeve et al., 1966). A related technique, purportedly an improvement, simply placed palatal tissue in the centre of a petri dish and covered it in medium (Thompson and Schweisthal, 1969). However, it is well-documented

that culture of this nature results in unequal access to oxygen and nutrients across the tissue (Fainstat, 1972) and the adhesion of the PSs to the culture surface makes the study of any bulk-tissue PS movement events impossible. Nonetheless, this culture technique remains the standard for investigating PS fusion between explanted shelves placed directly in contact (Kim et al., 2017; Morgan & Green, 2022) but is of little use for the study of other aspects of palatogenesis, with growth arrested in the anteroposterior axis and severely slowed in the mediolateral axis (Economou et al., 2012).

Rolling culture systems are the most popular method used in the *ex vivo* study of palatogenesis. This technique was first used in response to the finding that circulation and oxygen-tension/gassing are vital to the development of whole embryo and large explant preparations *ex vivo* (Cockroft, 1973; New, 1967; New & Daniel, 1969; Robkin et al., 1972). For observing palate development, this technique involves the preparation of maxillary explants i.e., intact PSs attached to surrounding maxilla in the absence of tongue/mandible (t/m). The explants are submerged in supplemented media in bottles and gassed manually. To maintain a high oxygen tension the bottles are immediately sealed shut following gassing. They are then placed on roller apparatus and incubated for up to several days (see Chapter 2: Materials and Methods). It was thought that with this method the shelves grow normally, elevate and fuse at a time variably reported as analogous or at a reduced rate to the *in vivo* event (Abbott, 2000, 2019; Bulleit & Zimmerman, 1985; Chou et al., 2004; Lan et al., 2016; Oh et al., 2010; Shiota et al., 1990; Snyder-Warwick et al., 2010; Takahara et al., 2004; Wee et al., 1976). Hence, many of the studies influencing and shaping our understanding of palatogenesis are based in the use of this system, or variations on it. However, limitations in this system have been identified more recently owing to the removal of the mandible and tongue, and further variations have been suggested as an improvement, such as the inclusion of mandible and tongue during culture (Yonemitsu et al., 2020; Yu & Yonemitsu, 2019). Work in this thesis will go further, showing that in fact this culture system gives a palatal closure that is almost entirely artefactual in nature and a very poor model of *in vivo* development.

The most elaborate of the three, Brinkley's 'improved' culture system used specialised custom equipment in which tissue is suspended from metal hooks in an enclosed system

undergoing constant gas supply, with medium actively circulated via a pump (Brinkley et al., 1975; Lewis et al., 1980). It is claimed this enables close control of the partial pressure of the gas; closely mirrors conditions during gestation *in vivo;* and disrupts the 'boundary layer of wastes' that surround the tissue, which would limit adequate nutrient and oxygen perfusion otherwise. It was further claimed that this system is superior to the standard system of rolling culture, however this is not evident from the associated data, and examples the use of this system are limited. Interestingly, somewhat similar whole embryo culture (WEC) systems would find recent success in the recapitulation of whole embryo development *ex vivo* up to E12.5, although not beyond (Aguilera-Castrejon et al., 2021).

Notably, maxillary explant preparation is broadly the same in the latter two techniques, although Brinkley states in the 1980 paper that the mandible was in fact left attached with a 'mandibular vent' cut into it and the tongue removed. This is unclear, and the associated photomicrographs were taken with the mandible subsequently removed altogether. Nonetheless, palatal gap closure and the final state of palatal shelf fusion were taken as a metric of normal palatogenesis across the entire literature. It was thus assumed that with these methods, the shelves undergo normal successful outgrowth and elevation during culture, and this remained the standard measure to date (Morgan and Green, 2022). As will be shown in Chapter 3 below, this turns out to be wrong.

Our understanding of palate elevation has been greatly influenced by studies using the latter two culture systems. These are summarised in *Table 1.3*, and selected studies are highlighted throughout the rest of this chapter.

1.3.3.2 The rugae

It was previously theorised that the rugae may facilitate/assist PS elevation. The 'plaiting' of the rugae on the epithelial surface was thought to shrink the surface of the buccal slope of the PSs, consequently bulging the nasal slope of the PSs inward. It was proposed that, in concert with the tongue "sliding forward and downward", this motion would cause both PS elevation and tongue displacement (Pourtois, 1972). It was later theorised that the rugae themselves were providing the force driving elevation altogether, possibly

by rugae-dependent regional increases in PS stiffness (Brinkley, 1980; Luke, 1984; Orban, 1972).

Table 1.3 The use of *ex vivo* rolling culture and perfusion chamber culture in PS elevation research.

Research focus	References
Describing morphological changes to the PSs during elevation	(Abbott, 2000, 2019; Brinkley et al., 1975; Lewis et al., 1980; Shiota et al., 1990; Yu & Yonemitsu, 2019),
Fata mapping the PSs across elevation	(Chou et al., 2004)
Muscle activity during elevation	(Wee et al., 1976),
CL/P teratogen testing	(Kosazuma et al., 2004; Schreiner et al., 1986; Wee & Zimmerman, 1983),
Cell-type distribution	(Brinkley, 1984; Brinkley & Bookstein, 1986; Wee et al., 1981)
Mutant palatogenesis	(Oh et al., 2010a; Snyder-Warwick et al., 2010; Parada et al., 2015; Ito et al., 2003a; Almaidhan et al., 2014; Iseki et al., 2007; Tang et al., 2015, 2016)
ECM activity during elevation	(Morris-Wiman and Brinkley, 1993; Yonemitsu et al., 2020; Lan et al., 2019; Brinkley and Vickerman, 1982)
The effects of PS wounding/separation on elevation	(Brinkley and Vickerman, 1979; Bulleit and Zimmerman, 1985)
The influence of the cranial base and other surrounding structures on PS elevation.	(Brinkley et al., 1978; Brinkley & Vickerman, 1978)
Neurobiology and early craniofacial innervation during foetal mouth opening reflex onset.	(Friedl et al., 2019)
PS fusion mechanisms	(Takahara et al., 2004)
Growth factor distribution	(Brunet et al., 1993)
The role of YAP/TAZ	(Goodwin et al., 2020)
Cell shape, orientation and density changes	(Babiarz et al., 1979; Brinkley and Bookstein, 1986)
The effects of irradiation on palatogenesis	(Hiranuma et al., 2000)
The role of different neurotransmitters on palatogenesis.	(Wee et al., 1979; Wee & Zimmerman, 1983; Wee et al., 1981)
Metabolic regulation of palatogenesis	(Wee & Zimmerman, 1980)

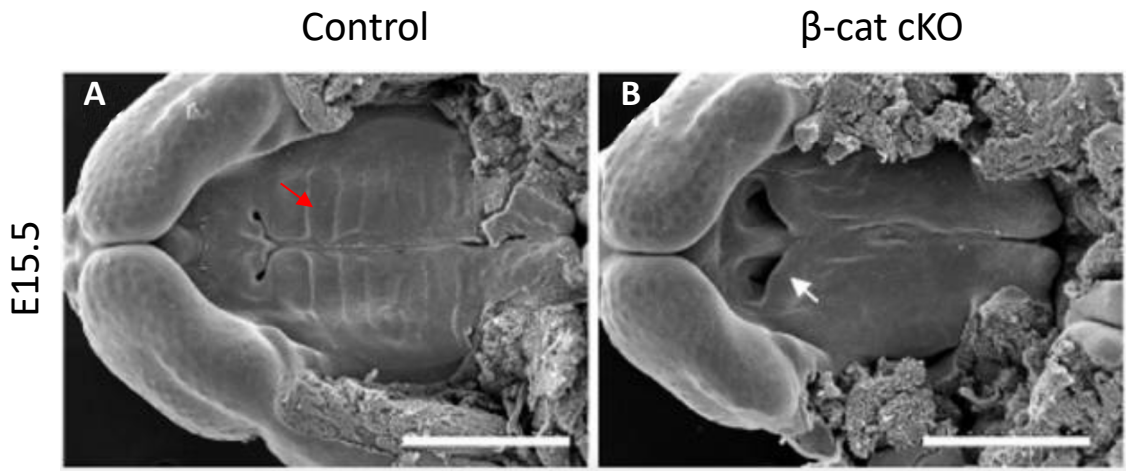

Figure 1.6 Palate elevation in the absence of the rugae

Scanning electron micrographs in the oral view of the elevated mouse palate at E15.5 in A) control and B) β-cat cKO mutant mice. In control mice, the rugae develop in the normal generative fashion (A), in the mutant, the rugae do not develop and the PSs still elevate fully (B). Red arrow, rugae 1; white arrow, failure of primary secondary palate fusion. Scale bars = 1 mm.

Subsequent research demonstrating the sequential development of the rugae throughout palate development further teased a role for them in PS elevation (Pantalacci et al., 2008; Welsh and O'Brien, 2009). However, an investigation into the role of Wnt-β-catenin signalling in orofacial development using the β-catenin conditional knockout (cKO) mouse model, resulted in the generation of rugae-less mice (Lin et al., 2011). In these mice, the PSs achieved elevation in a mostly morphologically and temporally normal manner, albeit not fusing with the primary palate (*Figure 1.6*). Therefore, it is unlikely that the rugae play a significant role in PS elevation.

1.3.4 The heterogeneity theory of PS elevation

Whilst there is no universally agreed-upon mechanism of elevation, it is generally stated in the literature that elevation progresses in a heterogeneous manner along the AP axis of the PSs. It is thought that the anterior elevates via a whole tissue rotation or 'flip-up' event (*Figure 1.7A&B*), while the posterior undergoes a tissue remodelling event (*Figure 1.7C&D*) (Coleman, 1965).

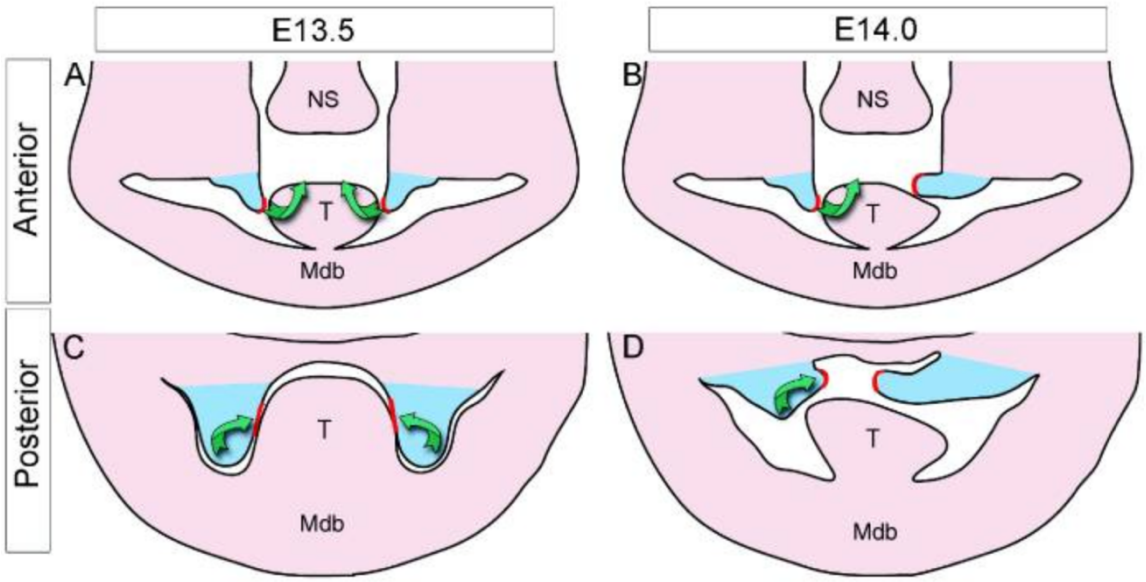

Figure 1.7 The heterogeneity theory of PS elevation

Schematic showing distinct mechanisms for PS elevation in the anterior (A&B) and the posterior (C&D) during the PS elevation window between E13.5 (A&C) and at E14.0 (B&D). Anteriorly, the PSs are thought to undergo a whole-tissue rotation event, essentially swinging upwards 90°, whereas posteriorly the PSs undergo a remodelling event, regressing in the ventral aspect and bulging medially via horizontal outgrowth. Green arrows, direction of elevation; Red lines, prospective site of midline epithelium; NS, nasal septum; T, tongue; Mdb, mandible (Bush & Jiang, 2012).

Prior to the heterogeneity theory, Walker and Fraser (1956) proposed a mechanism which encapsulates some aspects of both theories. Following their previously described exteriorisation assays, they found that the PSs elevate via a rapid remodelling event whereby the PSs concurrently regress their ventral portion and bulge medially at the lingual surface. This was said to be driven by their proposed 'internal shelf force' postero-anteriorly, enabled by reported highly deformable nature of the PSs. Although they discounted the rapid rotation event posted by Peter (1924) and Lazarro (1940) as the mechanism of elevation, they investigated the elastic nature of the process which would later be described as driving the anterior 'flip-up' event (Ferguson, 1978).

Further research has interrogated each aspect of this theory, with the internal shelf force (cause unknown) largely concerned with driving an elastic anterior rotation event, and

the posterior undergoing a remodelling event at the tissue level, which may include cellular mechanisms of growth. ECM activities are implicated in both methods of elevation and are reviewed separately in section *1.4.5*.

1.3.4.1 Evidence for anterior 'flip-up' elevation

Whole tissue rotation was proposed as a possible mechanism for elevation in early histomorphological studies (see *1.3.1*) (Peter, 1924; Lazzaro, 1940). However, it was only in later studies in the rat palate that this mode of elevation was referred to as rostral rotation, and a process distinct from any form of remodelling process (Coleman, 1965). This was later dubbed 'flip-up' elevation in the previously described rat tongue depression study, presumably because the rapidity and reversibility of the movement ruled out a tissue remodelling process (Ferguson, 1978).

Further evidence for the rapid rotation/flip-up elevation of the anterior palate has been documented on removal of the tongue during the preparation of maxillary explants in *ex vivo* culture work (Yu & Yonemitsu, 2019). Plus, an analysis of mesenchymal nucleus-Golgi orientation during elevation in the mouse found that anterior mesenchyme reorientates around 90° in the direction of elevation immediately prior to elevation, supporting anterior flip-up (Brock et al., 2016).

1.3.4.2 Evidence for posterior remodelling

Tissue remodelling was suggested as the mechanism of elevation in some of the earliest studies, as reviewed in *1.3.1*. It was proposed that growth was responsible for this remodelling (Pons-Tortella, 1937), but the identification of the event occurring on a timescale of seconds (Walker and Fraser, 1956) is strong evidence against this. Thereafter, Walker and Fraser proposed that instead an internal shelf force drove this remodelling around the tongue, and Coleman (1965) was the first to suggest this process occurred in the posterior palate only, thus posing the heterogeneity theory of elevation. It was also later suggested that a morphological transition zone in the midpalate shared elements of both flip-up and remodelling, but the supporting evidence is purely pictorial (*Figure 1.8*). (Yu & Ornitz, 2011). It is important to note that much of the evidence for

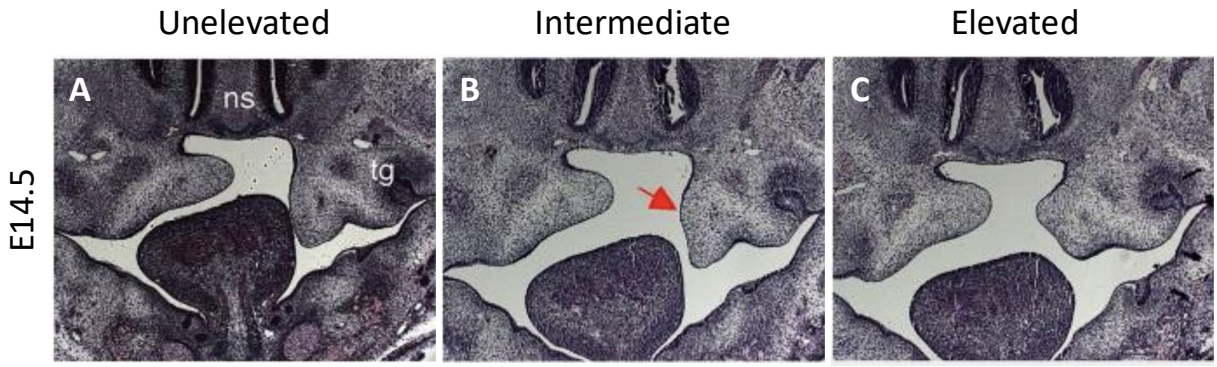

Figure 1.8 Histomorphological evidence for posterior remodelling

H&E-stained frontal sections of the WT mouse oral cavity at E14.5 showing unilateral elevation in three independent samples. A) the unelevated shelf is in a vertical orientation. B) the unelevated shelf shows sign of medial bulging. C) the mostly elevation shelf appears to be undergoing medial bulging a regression of the distal tip. Red arrow, medial bulge; ns, nasal septum; tg, tooth germ (adapted from Yu & Ornitz, 2011).

remodelling, i.e., ventral regression and medial bulging, is simply deduced from observations made in fixed frontal sections of embryos (Yu & Ornitz, 2011).

Furthermore, in the aforementioned study involving the nucleus-Golgi orientation assay, mesenchyme in the posterior palate were found to reorientate 180°, concomitant with a mechanism for the proposed ventral regression of cells at the distal tip of the unelevated PSs (Brock et al., 2016).

Plus, gene expression analysis of the MEE marker Matrix Metallopeptidase 13 (MMP13) in a mutant mouse strain exhibiting delayed PS elevation suggested that the medial aspect of the unelevated PSs corresponds to the distal tip of the elevated PS epithelium (Jin et al., 2010) (*Figure 1.7*, red lines). MMP13 is a known marker of the presumptive MEE in the PSs (Blavier et al., 2001) and its expression was tracked during elevation as a marker of remodelling events. Zinc-finger homeobox 1a (*Zfhx-1a*$^{-/-}$) mutant mice exhibit a delay in elevation up to forty-eight hours, with no apparent deficit in PS cell proliferation (Jin et al., 2008). At E14.5, the PSs of *Zfhx-1a*$^{-/-}$ embryos remain unelevated, but MMP13 expression is localised to the medial edge of the posterior unelevated shelves, suggesting that elevated PS MEE corresponds to the medial aspect of the PSs rather than the distal tips of unelevated PSs. However, gene expression may not necessarily be tied directly to

the same cells over time and may not truly represent elevation in the WT mouse; this caveat is further complicated by the mutant. *A fortiori*, this gene expression offers little in the way of elucidating the broader mesenchymal cell movements, which make up the majority of the PS bulk; epithelial markers are a poor marker of broad PS remodelling.

Similarly, in a fate mapping study utilising carbon labelling and *ex vivo* culture, it was asserted that the PSs elevate and come-together via a remodelling event in the anterior and posterior, with the midpalate exclusively elevating via a rotation event (Chou et al., 2004). This contradicts the typical posterior-only remodelling heterogeneity theory (Coleman, 1965).

An MRI-based study investigating PS elevation dynamics was recently posted to bioRxiv in preprint form (Goering et al., 2022). In this study, embryos were isolated at micro-stages across the elevation window and shelf movements recorded following fixation and MRI scanning. It was noted that the posterior PSs bulge medially around and above the tongue, and this proceeds in a posterior-to-anterior direction. Following this, the PSs adhere anterior-first; adhesion then proceeds posteriorly (*Figure 1.9A-D*).

Goering et al then performed proliferation (Ki-67), actomyosin contraction (pMLC2) and nuclear orientation analyses on the reorientating PS regions identified in their MRI scans, though it is unclear whether tissue was taken from across the entire AP axis, or consistently in one region. Interestingly, prior to elevation there was an increase in proliferation in the lingual region, and a change in nuclear orientation towards the tongue and increased phosphomyosin activity in the buccal region. This proliferation and orientation pattern persists during the 'bulging' phase, although phosphomyosin activity was now increased superiorly. This persists in elevated shelves, and the nuclei are then orientated horizontally over the surface of the tongue (*Figure 1.9E*)

These results suggest actomyosin contraction progresses in a wavelike fashion from buccal PS, with the wave of contraction continuing superiorly 'up' the shelf and 'over' the tongue. This drives elevation by remodelling over the tongue along the length of the PSs,

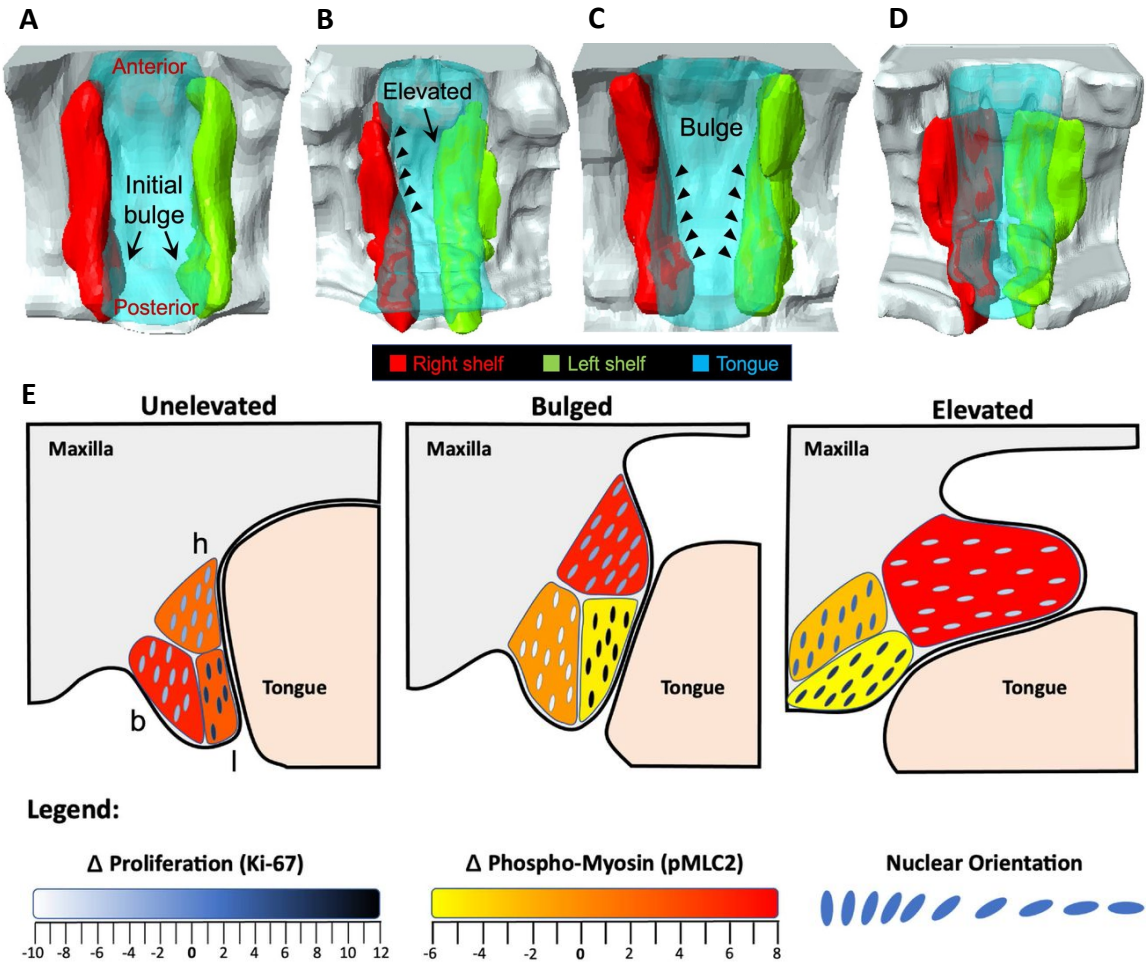

Figure 1.9 MRI scans and cellular behaviour schematic of elevation dynamics

Surface meshes rendered from MRI scans of fixed palate tissue, capturing bilaterally unelevated (A), laterally bulged (B), unilaterally elevated (C), and bilaterally elevated (D) PSs. E) schematic representing proliferation, contractile actomyosin and nuclear orientation dynamics in PS tissue during elevation (adapted from Goering et al, 2022).

originating posteriorly and proceeding anteriorly. The increased lingual proliferation suggests a method by which growth is known to be occurring but is evidently passive in elevation and not involved in the remodelling event *per se*. The moving wave of actomyosin contraction could either confer an orthogonal force, pushing the shelves over the tongue, or may exert a tensile force, 'pulling' the PSs over the tongue. The nuclear orientation data support both theories but offer no way to delineate between the two. Broadly, the nuclei appear to simply align in the direction of elevation, which has been noted in previous research (Chiquet et al., 2016). These data suggest that elevation is entirely driven by posterior-first remodelling events. It is unfortunate that the MRI,

typically used to image live tissue, was used on fixed material and not *in vivo*, which would give great insight into the live dynamics of the process.

1.3.5 The molecular-genetic control of PS elevation

With the advent of the molecular era, much of the focus of palate elevation research has been on generating mutants which appear to show a defect in elevation. Whilst several mouse lines have been generated with a cleft palate, it is often unclear as to whether the cleft is intrinsic to the palate, or if any identifiable failure in elevation is secondary to another defect. Therefore, it is arguable that work so far has been unsatisfying in fully understanding the cellular mechanisms of morphogenesis underlying PS elevation specifically.

For example, Gad1 and Viaat1 are important components of the GABA signalling cascade, with GABA having previously been shown to regulate cell migration, proliferation, differentiation, and survival (Varju et al., 2001). *Gad1* and *Viaat1* knockout mice appear to have PSs which fail to elevate (Oh et al., 2010a). Nonetheless, in the same study, the shelves were able to elevate during *ex vivo* explant culture, thus any elevation defect is evidently secondary to surrounding structures, such as in patients with micro or retrognathia (Pierre-Robin sequence). A similar 'rescue' of elevation has been reported subsequently during the culture of *GAD67*$^{-/-}$ embryo maxillary explants (Iseki et al., 2007).

To take another example, in both *Osr2*$^{-/-}$ and *Pax9*$^{-/-}$ embryos the PSs fail to elevate. It is evident from the histology in both studies that they adopt an abnormal morphology, and both mutants are linked to impaired palatal mesenchymal proliferation (Lan et al., 2004; Zhou et al., 2013). Moreover, in both instances, the histology at E15.5 (*Figure 1.10G-J*) clearly show elevated shelves; they are just smaller and have not met in the midline. Hence, it is unclear if elevation has completely failed, but could be considered defective in that it is delayed. Delays in elevation could be linked to the PSs not yet reaching the correct size, or the internal shelf force not yet having the threshold for overcoming the

external barriers, or delays in development of surrounding structures that prevent elevation.

Similarly, *Wnt1-Cre;Ldb1*$^{fl/-}$ mutants also have cleft phenotype, which has been described as a failure of elevation (Almaidhan et al., 2014). LIM domain binding protein 1 (LDB1) is a transcriptional co-factor and *Ldb1*$^{-/-}$ embryos also show reduced *Osr2* and *Pax9* expression in the palatal mesenchyme. Again, the failure of elevation is evidenced by histology, with frontal sections showing unelevated shelves with abnormal morphology beyond the normal elevation window. What is particularly interesting about this study, is that the authors also assayed for elevation in the absence of the tongue and mandible. This helps to identify whether the defect in elevation is secondary and should be a standard for all elevation defect studies. The authors report that removing the tongue and mandible does not restore elevation. However, in the anterior region of the representative histological section, the PSs have clearly elevated. Unfortunately, in their images representing the middle and posterior regions of the PSs, the sections are oblique, and it is not clear if they have captured the PSs at all (*Figure 1.10A-F*).

Disruption to cellular proliferation in a regional-specific manner has also been linked to a failure of elevation. *Fgfr2*$^{C342Y/C342Y}$ mutant mice display increased PS mesenchymal proliferation in the lateral half of the shelf, resulting in a cleft reportedly due to delayed elevation (Snyder-Warwick et al., 2010). Again, this is confusing as the representative image of the frontally sectioned oral cavity in these mutants clearly shows elevated shelves, at least in the posterior (*Figure 1.10L*). Bush and Jiang (2012) note that this regional perturbation is similar to that of the previously described *Osr2*$^{-/-}$ mutants (Lan et al., 2004). They go on to link this to the ERK/MAPK signal transduction pathway, noting that it is typically activated downstream of FGFR signalling, with the negative regulator of the ERK/MAPK pathway Sprouty 2 (*Spry2*) mutants also demonstrating a failure of PS elevation and an increase in proliferation in the anterior PSs (Matsumura et al., 2011). Interestingly, the *Spry2* KO PSs appear to show a delay in elevation and an aberrant morphology. However, in the supplied image at E16.5, the PS appears to have at least partially undergone elevation, with the shelf appear to somewhat flow around the tongue (*Figure 1.10K*), reminiscent of the classical description of posterior remodelling (Coleman,

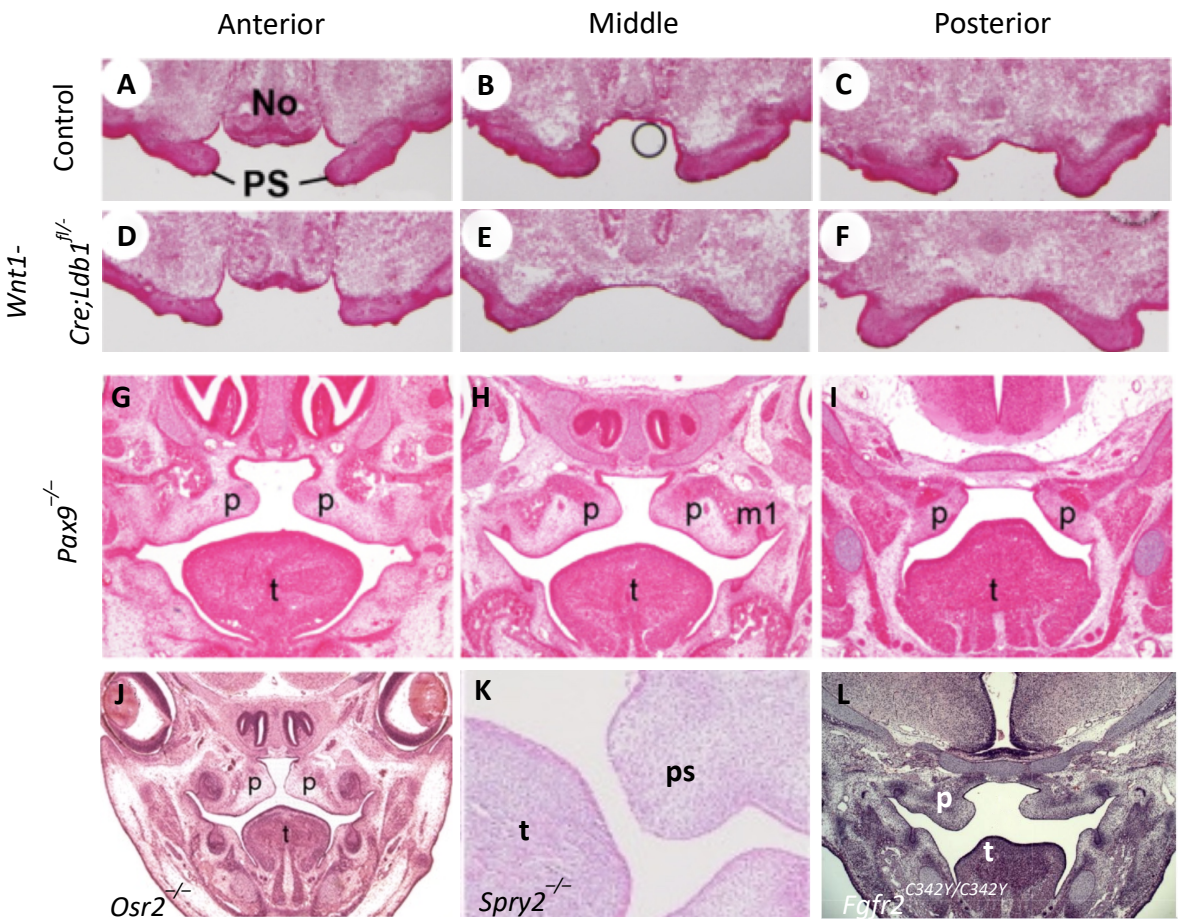

Figure 1.10 Excerpts from papers reporting PSs with elevation defects

Frontally sectioned H&E-stained mouse embryos for different mutations (stated in each panel). A-F) maxillary explants following *ex vivo* culture in control (A-C) and mutant (D-F) embryos. PSs are elevated in D, just smaller. In panel E, the embryos is tilted significantly forward and downwards, and the reverse appears to be true of F. G-I) PSs are elevated, albeit smaller, in all anatomical regions. J) Middle regions of mutant embryos showing complete elevation and failure to meet in the midline. K) Appears to roughly equate to the middle or posterior region. PS appears to be undergoing remodelling elevation around the tongue but is reduced in size. L) Apparent elevation. No, Nasal organ; PS/p/ps, palatal shelf; t, tongue; m1, molar (adapted from Almaidhan et al, 2014; Lan et al, 2004; Zhou et al, 2013; Matsumara et al, 2011; Synder-Warwick et al, 2010).

1965; Yu & Ornitz, 2011). In this instance, it does appear that ERK/MAPK plays an important role in PS growth, and that this may secondarily affect the completion of elevation.

There several other instances of mutant embryos displaying delays in elevation, many in embryos deficient in Wnt-planar cell polarity (PCP) components. *Wnt5a*$^{-/-}$ embryos

exhibit a failure of elevation in the posterior only, with elevated but small shelves anteriorly which do not meet in the midline (He et al., 2008). Ror2 is a receptor for Wnt5a and, in the same study, *Ror2*$^{-/-}$ embryos are described as failing to elevate. It is unclear if this is merely a delay, and images are only presented in the anterior oral cavity. The authors also identified that Wnt5a and Ror2 are required for the migration of the PS mesenchyme anteriorly during shelf growth, and so the posterior-specific elevation failure in *Wnt5a*$^{-/-}$ embryos could be due to a migration defect. Ror2 also interacts with frizzled (Fzd) proteins, forming coreceptor complexes, and *Fzd1*$^{-/-}$ and *Fzd2*$^{-/-}$ mutant mouse embryos exhibit clefts and reportedly fail to elevate (Yu et al., 2010). This appears to be primarily a fusion defect, and in representative frontal sections of embryos whose PSs have "failed to elevate", there appears to always be at least unilateral elevation. Mice deficient in the PCP pathway component Prickle1 have also been reported to fail to elevate (Yang et al., 2014). However, the representative images in the paper show that the PSs have in fact elevated but are small and fail to meet in the midline – again suggesting a growth defect rather than an elevation defect as such. Plus, it has been suggested that neueral crest-specfitic inactivation of the transmembrane Wnt-trafficking protein, Gpr177, results in elevation failure. Again, frontal sections from *Gpr177*$^{Wnt1\text{-}Cre}$ embryos appears to show elevation, or are at least horizontally orientated, and the defect appears to be quite convincingly growth related (Liu et al., 2015).

There are further examples specific to the regulation of the ECM and expression of ECM proteins. These are reviewed separately in section *1.4.5*.

Evidently, some of the literature suggesting elevation defects in particular signalling pathways instead appear to demonstrate clefting as a failing of shelf growth, causing the PSs to fail to meet in the midline. Thus, a major challenge to the goal of identifying pathways that are crucial for palate elevation is the rigorous and detailed phenotyping of mouse loss of function mutations. In these cases, the shelves often also have an aberrant morphology, and reside beside the tongue but are nonetheless horizontally orientated, suggesting either that elevation has in fact happened or that they were horizontal to begin with, and in the limited examples of 'rescue' experiments, where the tongue and mandible are removed, elevation can indeed happen. This bolsters the idea that a failure

of elevation may not exclusively be due to a defect in a shelf-intrinsic process driving elevation but may instead be more intimately linked to an extrinsic abnormality. Difficulties remain in the detailed phenotypic description of mutant shelves, which are often short/stubby, and so it is difficult to determine any extent of elevation.

1.3.6 The evolution of elevation

The secondary palate is a structure unique to amniotes, with differences in development and final form between and within the constituent clades Sauropsida and Synapsida (Abramyan and Richman, 2015). This is with the exception of Lepidosauria (e.g. snakes) and Testudines (e.g. turtles) which, like amphibians and other basal tetrapods, have no 'true' secondary palate (Jankowski, 2013). Broadly, Sauropsida possess PSs that grow horizontally, whilst extant Synapsida shelves face ventrally and elevate to their final horizontal position, which suggests elevation may be a mammalian novelty. Understanding the evolutionary basis of different modes of palate development may shed light on the developmental mechanisms underpinning palatogenesis and may inform the underlying mechanisms of mammalian PS elevation (note: this section and the cited literature are expanded upon in Chapter 5).

Members of clade Sauropsida with secondary palates include Aves (e.g., birds such as the chick *Gallus gallus*) and Crocodylia (e.g., crocodiles, alligators and gharials). In birds, the PSs growth horizontally above the tongue and meet in the midline. There is no ventral growth or elevation event and, although the PSs may abut in the midline, the MEE are keratinised, and fusion never occurs (Koch and Smiley, 1981). This results in birds possessing a naturally cleft palate. The Crocodilians are a particularly interesting case study, and much research has been carried out on the palate of the common American alligator, *Alligator mississippiensis* (Ferguson, 1981b). Crocodylians appear to develop a mammal-like secondary palate: while growing horizontally only, the PSs meet in the midline and fuse (Ferguson, 1981b).

The clade Synapsida consists of the Monotremata (echidna and platypus), Marsupalia (kangaroos and opossums) and the Placentalia (e.g., mice and humans). At least

morphologically, the PSs largely appear to develop similarly across Mammalia, with comparative studies carried out across several mammalian species (Ferguson, 1988).
In the Marsupial *Monodelphis domestica* (the opossum) PS elevate (Smith, 2006a), the PSs grow ventrally and elevate above the tongue, suggesting a conservation of this mode of palate development across the Theria.

The evolutionary relationship between the mammalian and non-mammalian palate is unresolved, and there are limited studies investigating this. At least molecularly, the mechanism of fusion is not conserved, and this cannot be induced *ex vivo*. In chimeric combination assays, the PSs of chicks, mice and crocodiles were placed in contact and culture *ex vivo* in a typical PS fusion assay. However, no heterologous fusion occurred between any of the groups tested (Ferguson et al., 1984).

The fossil record has also proven to be unhelpful in uncovering the ancestral state of elevation. The earliest known Synapsida ancestor, the reptile-like mammal *Promoschorhynchus*, has no ossified palate, and instead has bony palatine ridges (Maier et al., 1996). The authors hypothesise that the palate therefore consisted entirely of soft tissue bridging the gap between each palatine bone and suggest that the differing angulation of the bone (medial anteriorly, inferomedial posteriorly) informs the angle of projection of the tissue. Regardless, this does not give any insight into the origins of elevation.

From this comparative embryological perspective, a pattern emerges in that elevation appears to be a mammalian novelty, and specific behaviours could be linked to evolutionary pressures which may have caused this. The Sauropsida (non-mammals) are some of the earliest amniotes, and our early ancestors in the Synapsida branch are thought to share some of these traits (Maier et al., 1996). In the former, the PSs grow horizontally from the outset, suggesting that evolutionarily there could be a programme of default horizontal growth. This does not appear to be true of the mammals, and a major difference in the oral cavity of the mammals vs. non-mammals is the large muscular tongue, associated with differences in mechanisms of feeding (Jingtao Li et al., 2016). The differences in feeding between the mammals and non-mammals may provide the

evolutionary pressure that caused the PSs to be deflected ventrally, perhaps as a trade-off for space in the oral cavity.

Monotremes are the only non-suckling mammals (Griffiths, 1978; Werneburg and Sánchez-Villagra, 2011) and therefore provide an excellent opportunity to investigate the default programme of PS growth, and if the origins of elevation are linked to feeding mechanisms, i.e., suckling. There have been some assertions made in the literature that relate to the monotremes, typically with regard to the Echidna. As described in *1.3.1*, Polzl (1905) quotes an unreferenced study in which the assertion is made that there is no evidence for the PSs of the echidna growing ventrally and elevating. Plus, Ferguson (1981b) would later state that crocodiles are "the only animals which possess a true mammal-like secondary palate and develop in an egg." Given the lack of evidence of monotreme palate development in either of these statements, it remains unresolved as to how the monotreme palate develops embryologically, and this would give great insight into the evolutionary origins of palate elevation, and therefore its developmental basis.

1.4 The internal shelf force

It has been suggested that the internal shelf force may drive either both or one of the mechanisms of elevation in both the anterior and the posterior PSs (Ferguson, 1978; Walker and Fraser, 1956). There have been several attempts to characterise and identify the internal shelf force, which much of the modern literature shifting focus to the ECM. However, it is first important to consider the theoretical basis of how such a force might operate during elevation.

1.4.1 The mechanical basis of elevation

When theorising how the PSs might elevate, it is helpful to consider the event in the simplest sense. On the basis that elevation is driven by a force intrinsic to the tissue, in the case of a 'flip-up' elevation event the shelves can either be pushed or pulled to the horizontal position, or a combination of the two.

If pulling forces were responsible for PS elevation, the forces would be localised to regions immediately superior to the shelves, and perhaps running along the lingual surface of the unelevated shelf. The pulling (tensile) force could act in a drawbridge-like fashion in elevating the PSs. Plausibly, this type of force and action could be mediated by fibrous or cable-like elements of the cytoskeleton and/or the ECM.

Contrastingly, a pushing force may act inferiorly and be localised to the buccal side of the unelevated PSs, to 'push' them in the direction of elevation. This would act as a compressive force and can be conceptualised as the action of a hydraulic jack or piston, directing pressure to produce an upwardly-directed force. This type of force could be generated by any process that locally expands tissue, such as increasing turgor pressure in cells, fluid-induced swelling of ECM or increasing the number of nuclei by cell division (Green, 2022).

It has also been proposed that differential traction between the overlying epithelium and the underlying mesenchyme acts to constrain and direct the building force (Brinkley, 1984; Bulleit and Zimmerman, 1985) in much the same way that the rubber surface constrains an inflating balloon (Ferguson, 1988). This could help direct the force in the required direction for the shelves to elevate above the tongue.

1.4.2 The gross AP location of the internal shelf force

There is a small subsection of the literature investigating the location of origin of the internal shelf force and the subsequent direction of elevation (Brinkley & Vickerman, 1979; Bulleit & Zimmerman, 1985). In both studies, maxillary explants were generated, and lesions were made to the PSs in a transverse direction to various extents along the AP axis, separating the shelves into different regions e.g., splitting the shelves in anterior and posterior halves. The explants were then cultured *ex vivo* and the shelves elevated to differing extents by region. The anterior third (mostly presumptive hard) PS was able to elevate fully following separation, whilst the posterior (mostly soft) palate was only able to elevate fully if attached to the anterior palate. When two lesions were made, the midpalate was also able to elevate fully separated from the anterior palate, with the

posterior still not elevating (Brinkley and Vickerman, 1979). In these double-incision experiments, the midpalate elevated fully at the greatest frequency, and so it was inferred that the midpalate/posterior hard palate was the most stable PS region. Hence, it could be that the elevating force originates (or is strongest) in the midpalate, and that the posterior palate is dependent on the anterior/midpalate for elevation. However, the interpretation of these repots could be altered by limitations in *ex vivo* rolling culture, and these are explored in Chapter 4.

In the Bulleit and Zimmerman study, the PS epithelium was a particular focus, and was disrupted via either physical scraping of the surface, or by treatment of excised tissue with Ethylenediaminetetraacetic acid (EDTA), a chelating agent which removes epithelial cell layers (Bulleit and Zimmerman, 1985). In these epithelial wounding assays, the scraping wounds were said to penetrate 'deep into the mesenchyme.' Despite this, the greatest disruption to elevation was seen in the EDTA-treatment group only. While being limited by its observation in *ex vivo* culture alone, these data suggest an integral role for the epithelium in PS elevation, and by extrapolation, that the elevating force may at least in part be localised to the epithelium.

1.4.3 The AP progression of PS elevation

The results of the PS separation assay suggest that elevation might begin in the midpalate, with the posterior shelves exhibiting a dependency of the antero-midpalate to elevate (Brinkley and Vickerman, 1979). This supports a previously posed theory on the progression of PS elevation made on observed in rat embryos, which stated that elevation begins in the posterior hard palate (roughly the midpalate), before extending in a wavelike fashion in both anterior and posterior directions (Coleman, 1965). It should be noted that this result has previously been interpreted as evidence of 'anterior-first' elevation elsewhere in the literature (Ferguson, 1978). Whilst the relevant figure in the Coleman (1965) paper shows a sketch of the PSs elevating mostly in the anterior region, it is clearly described in text that the closure progresses both anteriorly and posteriorly from a mid-palate starting point.

Fittingly, this is a particularly contentious part of the literature, with reported evidence for anterior-first elevation (Andersen and Matthiessen, 1967; Burdi and Faist, 1967; Wragg, Diewert, et al., 1972; Ferguson, 1978; Pons-Tortella, 1937) and posterior-first elevation (Walker and Fraser, 1956; Zeiler et al., 1964; Larsson, 1962, 1974, 1960; Pourtois, 1972; Babiarz et al., 1975; Goering et al., 2022). The evidence cited mostly appears to be different interpretations of time courses of elevation from frontally sectioned mouse and rat histological studies.

Ferguson (1978) put forward a mechanism for anterior-first elevation, suggesting that the palate fuses with the nasal septum anteriorly, which he suggests the PSs use as a 'fulcrum' (meaning anchor point) to pull themselves up over the tongue in a wave extending posteriorly. More recently, Goering et al (2022) reported posterior-first elevation in a manner identical to that of Walker & Fraser's (1956) earlier observations, in that the PSs elevate posterior-first by forming medial bulges which spread over the tongue. Interestingly, Goering et al also found that although elevation proceeds posterior-first, fusion occurs anterior-first, zippering posteriorly. In some instances previously, there does not appear to have been a distinction between elevation and fusion, with the two events simply referred to as 'closure' (Coleman, 1965). It is much easier to observe fusion than elevation (Morgan & Green, 2022), and the lack of distinction between the two in earlier research might go some way to explain how the discrepancies in descriptions of the sequence of events arose.

1.4.4 Unilateral elevation as an obligate intermediate step

Unilateral elevation is referred to in the literature as the state where only one PS is elevated (Yu and Ornitz, 2011). As previously outlined in section *1.3.1*, unilateral elevation was observed in early research (His, 1901) but was rejected by some as being pathological, and not a part of normal palatogenesis (Fick, 1902; Polzl, 1905).

In one peculiar case, a human embryo was presented with the anterior shelves elevated and the posterior shelves unelevated (Pons-Tortella, 1937). However, as was pointed out at the time (Lazzaro, 1940) and since (Walker and Fraser, 1956) this particular sample

appears to be quite damaged in Pons-Tortella's original photomicrographs. Walker & Fraser point out that, although damaged, this sample appears to recapitulate what is observed upon manually manipulating the tongue and the shelves spontaneously elevating, which further suggests the sample may have adopted it's morphology in part via physical damage.

Nonetheless, unilateral elevation has been documented extensively in the literature in normal (Lazzaro, 1940; Walker and Fraser, 1956; Poswillo and Roy, 1965; Chamberlain, 1966; Bruce E. Walker, 1971; Wragg, Diewert, et al., 1972; Yu and Ornitz, 2011; Trasler and Fraser, 1963) and mutant (Liu et al., 2008; Hill et al., 2015; Hall et al., 2020; Butali et al., 2019; Goodwin et al., 2020) mice. It has been proposed that it is an obligate intermediate step in normal PS elevation. Goering et al (2022) recently investigated this in a detailed micro-staged time course using MRI, finding that the posterior 'bulges' observed move anteriorly in a bilateral fashion and, when one 'bulge' progressed more anteriorly than another, unilateral elevation may occur. They suggest that, if unilateral elevation is obligate at all, it occurs late and transiently in the elevation process. Conceivably, a mechanism of elevation by unilateral elevation may require the least energy input, in that the tongue is likely easier to displace if force is only applied to overcome it from one side. Further, the increased space afforded by a unilaterally elevated shelf in the oral cavity could make tongue displacement much easier in the case of the unelevated shelf.

1.4.5 The role of the extracellular matrix

Several ECM components have been implicated in producing and transducing the internal shelf force, and the role of the ECM in palatogenesis more broadly was reviewed twice recently (Wang et al., 2020; Paiva et al., 2019). Research documenting the role individual ECM components may play in PS elevation are summarised below.

1.4.5.1 Glycosaminoglycans (GAGs)

GAGs (or mucopolysaccharides) are negatively charged polysaccharides found in the ECM that bind water and influence the osmotic activity of tissues (Garantziotis and Savani,

2019). Hyaluronic acid (HA) is one such GAG found in regions of embryonic palate mesenchyme and can bind up to ten-times its molecular weight in water (Ferguson, 1988). It may also influence the viscosity of tissues (Mitra et al., 1983) with concentrations of just 0.1% (w/v) reportedly responsible for up to 80% of the total tissue viscosity of biological fluids (Balazs and Gibbs, 1970). It is also thought to have a regulatory role in morphogenesis, with early research establishing HA as directing mesenchymal differentiation (Toole et al., 1972), and GAGs are known to also regulate ECM dynamics via their conjugation to proteoglycans, which themselves interact with ECM remodelling enzymes and growth factors (Iozzo and Schaefer, 2015).

HA as the generator of the internal shelf force is substantially the most commonly hypothesised driver of elevation across the literature and warrants detailed review. Whilst there is substantial evidence supporting this theory, a recent mutant study casts serious doubt on its plausibility (Lan et al., 2019).

Chronologically, Lazzaro (1940) suggested that 'tissue turgor' could underlie rotational elevation, and Walker & Fraser (1956) were the first to explicitly suggest that HA could be the driver. They also report metachromasia (differences in tissue-dye complex colour versus the colour of the original dye) during aldehyde-fuchsin staining (Gomori, 1950) in embryos previously incubated with hyaluronidase and postulated that and that the loss of HA could be responsible for this. Hyaluronidase breaks GAGs into monosaccharides by cleaving glycosidic bonds, and so the metachromasia could indeed be a result of the loss of stainable acid mucopolysaccharides in the tissue. This is perhaps the earliest published evidence of the presence of HA in the elevating PSs.

The presence of GAGs in the PSs was confirmed by ^{35}S labelling and electrophoresis (Larsson, 1960) and 60% of these were later shown to be HA specifically (Pratt et al., 1973). However, ^{35}S labelling cannot detect HA, and this led to controversy in the field (Ferguson, 1978). ^{35}S incorporation into the palate mesenchyme has been tracked and measured following inhibition via glucocorticoid treatment. In these studies, no clefts occurred, and the authors conclude that GAG accumulation plays no role in PS elevation (Nanda, 1970; Andrew and Zimmerman, 1971). This was criticised heavily, given that HA,

the predominant GAG present in the palate at this time, cannot be tracked via this assay (Larsson, 1974; Ferguson, 1978).

The administration of the acid mucopolysaccharide (e.g., HA) synthesis inhibitor 6-diazo-5-oxonorleucine (DON) results in foetuses with a cleft palate phenotype (Pratt et al., 1973). Whilst the authors demonstrated a reduction in HA levels, they do not confirm that any resultant clefts are due to a failure of elevation specifically. Similarly, administration of the HA degradation enhancer chlorcyclizine (CHLR) (the common antihistamine) to pregnant mice also reportedly results in in offspring with a cleft palate, as does the exposure to its metabolite, norchlorcyclizine (NORCHLR) (Brinkley and Vickerman, 1982). Both CHLR and NOCHLR were previously found to reduce HA levels in the rat PSs without any appreciable change to DNA or protein synthesis, seemingly confirming the teratogenic (i.e. cleft-inducing) action of CHLR/NOCHLR as being via HA (Wilk et al., 1978). Strikingly, whilst CHLR and NORCHLR exposure both *in vivo* and in *ex vivo* culture was reported to cause clefting, it appears that the shelves were able to elevate during *ex vivo* culture specifically when cultured at stages immediately prior to elevation (given as E14.25) (Brinkley and Vickerman, 1982). However, the authors also culture at an earlier stage (given as E13.5) and describe a failure of posterior elevation only. This is the result described in the abstract and at a comparably greater length in the paper; it is easy to miss the 'rescue in culture' result. In the same study, the author's report a particular reduction in size of the posterior two thirds of the PSs following CHLR and NORCHLR treatment, with tighter mesenchymal nuclei packing. Their *in vivo* data also demonstrate a significant shortening of the mandible. Hence, on balance it appears much more likely that these clefts are a secondary defect owing to either reduced space in the oral cavity or a failure of the shelves to meet in the midline owing to an HA-degradation associated reduction in size. This does not suggest a role for HA in elevation.

As technology progressed, further research described HA distribution across the PSs to a more granular scale (Brinkley and Morris-Wiman, 1987a) and how this is altered following CHLR treatment (Brinkley and Morris-Wiman, 1987b). Several mutant mouse lines were also generated which show both a reduced expression of HA and clefting reportedly due to a reported failure of elevation (Li et al., 2021; Li, Lan, Krumlauf, et al., 2017; Lan et al.,

2016; Snyder-Warwick et al., 2010; Yonemitsu et al., 2020). Again, in each of these studies there is no clear evidence that the cleft phenotype is linked to an intrinsic failure of elevation.

Recently, strong evidence has been presented for HA contributing significantly to PS expansion during the elevation window, but not to elevation specifically, in studies using mice with HA synthesis deficits (Lan et al., 2019). There are three mammalian HA synthase genes, *Has1*, *Has2* and *Has3* (Tien and Spicer, 2005; DeAngelis, 1999). *Has2* shows the widest and highest expression during murine embryonic craniofacial development and so was selected for a targeted deletion study. Mutant mouse lines were generated which could inactivate *Has2* in a targeted fashion in: both the PSs and mandible, *Has2$^{f/f}$;Wnt1-Cre*; the PSs only, *Has2$^{f/f}$;Osr2-Cre*; and the mandible only, *Has2$^{f/f}$;Hand2-Cre* (*Figure 1.11*). Overall, it was found that when *Has2* is inactivated in the PSs only, the PSs are still able to elevate (*Figure 1.11B*). Clefting occurred as a failure of the PSs to meet in the midline. This was found to be due to a reduction in size of the PSs (*Figure 1.11E&F*). In both the mandible only and mandible-plus-PS group targeted *Has2* inactivation, the PSs failed to elevate due to the inability of the tongue to move out of the way of the shelves and was likely caused by a reduction in size of the mandible. These results are further supported by *ex vivo* rolling culture data from the same study, in which the PSs came together and fused on removal of the mandible and tongue in mutant explants.

Hence, HA contributes to PS size, presumably via osmotic swelling following secretion, but does not directly drive PS elevation, nor does it generate the internal shelf force. Rather, it regulates mandible expansion and secondarily impacts PS elevation, alongside contributing to the expansion of the PS ECM, therefore playing an important role in PS fusion. Although not necessarily reported this way in the older paper, the findings of Lan et al (2019) correlate with those of earlier studies (Brinkley and Vickerman, 1982). Conceivably, HA may play a role in assisting PS elevation by altering the material properties of the tissue. Increased viscoelasticity may aid the shelves during contact and movement over the tongue and may cause the seemingly slower elevation in the posterior, but this has not been investigated.

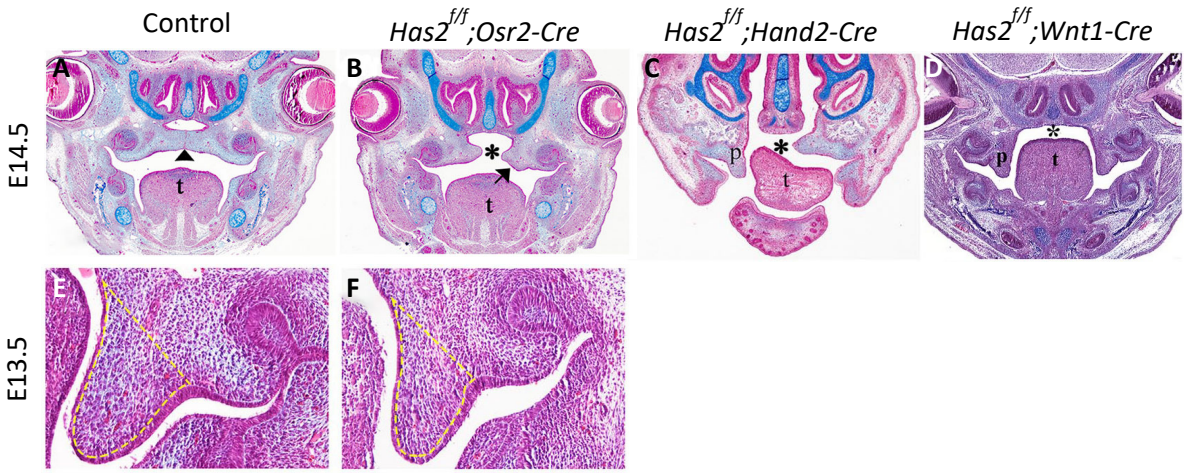

Figure 1.11 Region-specific deletion of *Has2* effects on PS elevation

PS elevation in control (A) and mutant (B-D) mouse embryos, with region-specific *Has2* inactivation in the PSs (B), mandible (C) and both PSs and mandible (D). In non-PS specific mutants (C&D) elevation is incomplete due to mandible and tongue defects. The shelves elevate as normal in PSs-only *Has2* inactivation (B). Clefting occurs PSs-only *Has2* inactivation due to small PSs which cannot meet in the midline, and the reduction in size is illustrated below (E&F) (adapted from Lan et al, 2019).

1.4.5.2 Collagen

Collagens are a major ECM component and categorised into fibrillar (types I, II, III, V, XI, XXIV and XXVII) and non-fibrillar types. Fibrillar collagens provide the three-dimensional framework for tissues, with some collagens forming cross-collagen cross-links (e.g., collagen XII) to modulate matrix and therefore tissue stiffness (Wang et al., 2020; Du et al., 2021). Another sub-group, the fibril-associated collagens, such as collagen IX, associate with fibrillar forms of collagen and bind them together, to create thick collagen fibres.

Collagens have long been proposed to play a role in PS elevation, with early suggestions made that the contraction of newly synthesised collagen may provide the physical action for elevation in the rat palate (Hassell and Orkin, 1976). Collagen-related theories were initially largely rejected on account of difficulty in identifying collagen in the embryonic PSs via traditional histochemical staining techniques (Ferguson, 1977), but again as technology advanced antibody staining techniques enabled a rich description of different collagen types across the PSs during the time of elevation (Chiquet et al., 2016; Ferguson,

1988; Paiva et al., 2019; Wang et al., 2020). Collagen I is expressed in the PS mesenchyme prior to elevation, particularly on the presumptive oral side in the middle and posterior PSs. Post-elevation, its expression is difficult to dissever from bone-forming mesenchymal condensations (Kurisu et al., 1992; Oka et al., 2012; Silver et al., 1981; Ohsaki et al., 1995). Furthermore, collagen II has been identified sparingly in the PS mesenchyme post elevation (Xu et al., 2018), collagen III in both the PS mesenchyme and basement membrane of the epithelium prior to elevation (Fantauzzo and Soriano, 2016; Ohsaki et al., 1995) and collagen IV in the epithelial basement membrane throughout, as would be expected (Wang et al., 2020; Ferguson, 1988).

Collagen gene mutations have been identified in syndromic clefts in humans, typically in Stickler syndrome (see *Table 1.1*) and collagen dysfunction has been linked to reported elevation defects in several mouse mutants. For example, lysyl oxidases (Loxl) play a role in cross-linking fibrillar collagens, and *Loxl3*$^{-/-}$ mice show delayed elevation *in vivo* and reduced collagen density (Zhang et al., 2015). Moreover, in a recent study the conditional deletion of *Yap/Taz* in the PS mesenchyme resulted in reduced *Loxl4* expression and a significant reduction in collagen, alongside a delay in PS elevation and clefting (Goodwin et al., 2020). As *Yap/Taz* are a part of the Hippo pathway, this suggests that mechanosensation may play a role during ECM remodelling during PS elevation (Hammond and Dixon, 2022).

Overall, given the ability of collagen fibrils to form stout bundles and fibres, they could be a strong candidate for transducing a tensile force 'pulling' the PSs during elevation. Further studies could be performed using modern, high resolution imaging techniques to identify the presence of collagen structures in aligned arrangements that may be capable to transduce a tensile elevating force.

1.4.5.3 Fibronectin

Along with collagen, fibronectin is another major structural (glyco)protein found in the ECM. Fibronectin is required for branching morphogenesis during development (Sakai et al., 2003) and, on adhesion, is upstream of the Hippo signalling cascade (Kim and Gumbiner, 2015).

Fibronectin is strongly expressed in the PS mesenchyme and MEE prior to elevation and is more localised to the MES post-elevation (Ohsaki et al., 1995; Dixon et al., 1993; Wang et al., 2020). Furthermore, various mutant mouse models with impaired fibronectin expression and/or deposition also have a cleft palate (Liang et al., 2014; Wang and Astrof, 2016; Tang et al., 2016). In one notable study, fibronectin may be linked directly to PS elevation. Rac1 is a RhoGTPase with roles in lamellipodium organisation and cell motility (Etienne-Manneville and Hall, 2002) and is required for proper fibronectin assembly (Dzamba et al., 2009). In *ex vivo* rolling culture, varying levels of Rac1 and cell density modulates the deposition of fibronectin in the midpalate (Tang et al., 2015). Downregulation of Rac1 by retinoic acid exposure resulted in a cleft palate phenotype, reportedly by delaying PS mesenchymal cell migration and the disarrangement of fibronectin (Tang et al., 2016). However, whilst the PSs did not elevate *in vivo,* it could just be a delay, but samples were not taken beyond E14.5. Plus, in their *ex vivo* rolling culture with retinoic acid, the PSs still elevated – another example of an apparent 'rescue' of an elevation failure phenotype.

1.4.5.4 Tenascin

Tenascins are another large group of ECM glycoproteins which roles in cellular migration, shape change and growth (Chiquet-Ehrismann, 2004). There are several types of tenascin which are differentially expressed in different tissues, with tenascin-C and tenascin-W expressed abundantly in developing tissues (Halper and Kjaer, 2014; Wang et al., 2020).

Tenascins are a known component of the PS mesenchymal ECM (Morris-Wiman and Brinkley, 1992; d'Amaro et al., 2012) and have distinct spatiotemporal expression patterns (d'Amaro et al., 2012). In the mid-posterior PSs prior to elevation, tenascin W is expressed in the future nasal aspect of the PS mesenchyme, before localising to the distal tip post-elevation (*Figure 1.12*). Tenascin C is expressed along the full length of the future nasal aspect of the PSs and in the distal tip, before settling in the distal tip and distal oral aspect of the elevated shelf (Chiquet et al., 2016).

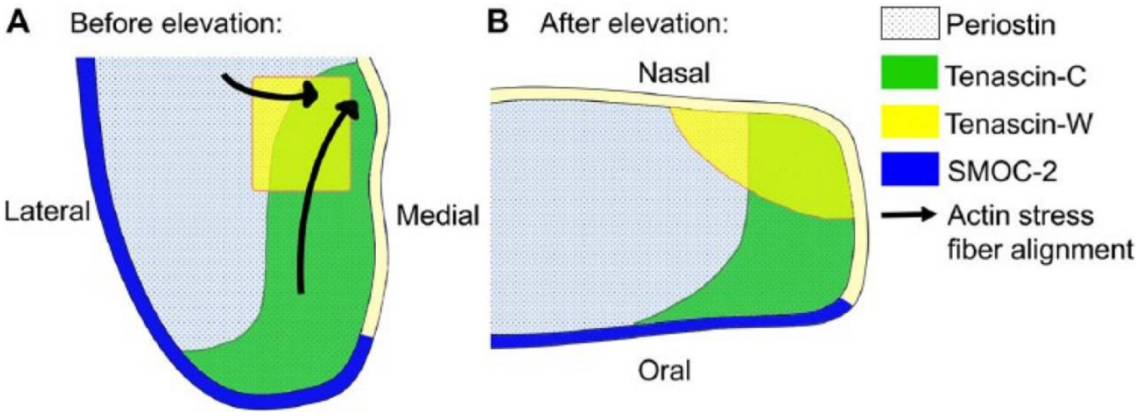

Figure 1.12 Tenascin and related ECM component expression during PS elevation

Schematic showing the expression of tenascin-C and tenascin-W before (A) and after (W) PS elevation. Note: the unelevated lateral and medial sides become the oral and nasal surfaces on elevation respectively (Li et al, 2017).

No mechanistic involvement of tenascins in shelf elevation have yet been demonstrated, but they could contribute to the mechanical properties of the tissue by their association with fibronectin as an ECM matrix interaction modulator and the actomyosin network (Wang et al., 2020). The same expression analysis identified that, in the mid-posterior PSs, tenascin aligned with actin bundles and the long axis of deformed nuclei, reportedly facing towards the bulging medial wall (Chiquet et al., 2016; Du et al., 2021).

1.4.5.5 Elastic fibres

'Elastic fibre' is the name given to bundles of fibrillin-rich microfibrils with or without an amorphous core of elastin (Feneck et al., 2018). Fibrillins are large extracellular glycoproteins which interact with integrins or activate transforming growth factor beta (Tgf-β) (Neptune et al., 2003). There are three isoforms (FBN1, FBN2, and FBN3). Together, fibrillins form microfibrils, which constitute a core structure of both elastic and non-elastic ECM (Wang et al., 2020). Elastin itself is an ECM protein responsible for giving elastic fibres their elastic properties, and its insufficiency is a known cause of congenital defects and structural mechanical failure, such as insufficient elastic recoil in the myocardium (Cocciolone et al., 2018). The elastic properties of elastic fibres depend on the ratio of microfibrils to elastin within the bundle, with higher elastin conferring more deformability. Elastic fibres are consequently categorised into three groups in order of

increasing maturity and elasticity: oxytalan fibres, elaunin (intermediate) fibres, and true elastic fibres (Feneck et al., 2018).

Walker and Fraser (1956) proposed that the internal shelf force responsible for driving the remodelling of the PSs was generated by a network of elastic fibres in the PSs. In support of this, they presented a standard Gomori stain of fixed tissue prior to elevation. It is particularly difficult to determine whether the staining really does show any sort of organised network, and subsequent research repeating the stain, and many traditional histochemical stains for elastic fibres, failed to replicate the result (Frommer and Monroe, 1969). The role of elastic fibres does not appear to have been researched further as a serious candidate for the internal shelf force until the later development of gene-specific *in situ* hybridisation probes. In the sole study on the matter, a weak *fibrillin-1* mRNA expression pattern was observed all throughout the PS mesenchyme prior to PS elevation. *Fibrillin-2* mRNA, however, was expressed highly on the presumptive nasal surface prior to elevation and expanded to the oral side of the PS mesenchyme following elevation (d'Amaro et al., 2012). Nonetheless, this does not suggest the presence of physiologically relevant elastic fibres, unless they appear transiently closer to the point of elevation. This contrasts Walker and Fraser's observation of elastic fibres, which they report supports the observation that, on manual manipulation, the PSs spring between two states (elevated and unelevated), indicating elasticity.

The picture is blurred further by the study described above (in the context of collagen cross-linking) using the *Loxl3*$^{-/-}$ mutant mouse (Zhang et al., 2015). Along with cross-linking collagens, Loxl3 also forms cross-links in mature elastin. Although collagen levels were significantly reduced in *Loxl3*$^{-/-}$ embryos with clefts, elastin levels were not significantly different to controls and cross-linked elastin (assayed by ELISA for the crosslink-associated amino acid desmosine) appeared to be present at detectable levels regardless.

In contrast, the spatially shifting expression of *fibrillin-2* mRNA may be more likely to be involved in PS fusion. Following elevation, expression was particularly expanded around *Tgf-β3*-positive cells. This is unsurprising, given Tgf-β plays a crucial role in PS fusion, and

so the increase in *fibrillin-2* expression at this stage is more likely related to Tgf-β activation during PS fusion (Zhang et al., 2015).

1.4.5.6 Summary of ECM roles in the palate

There are an abundance of studies asserting that the ECM plays a key role in PS elevation. The ECM components listed above are non-exhaustive but have so far been the primary focus of recent PS elevation research. The process is complicated by the extensive molecular crosstalk between ECM components. For example, HA synthesis can be upregulated by Tgf-β (McKeown-Longo and Higgins, 2021), which itself is activated by fibrillin (Neptune et al., 2003), whose assembly requires fibronectin (Sabatier et al., 2009), which accelerates collagen assembly (Paten et al., 2019), while collagen fibril formation catalyses co-localised fibronectin fibril formation (Paten et al., 2019). Combined with the ECM response to mechanosensation (Goodwin et al., 2020) and the yet unexplored intrinsic PS tissue-stiffness considerations, there is much scope for further research in this area.

1.4.6 Cellular mechanisms of growth

Growth as the direct driver of elevation has long been rejected in the field owing to rapidity of the event (Walker and Fraser, 1956; Ferguson, 1988). The molecular signalling underlying mechanisms of growth are relatively well-understood in PS outgrowth (section *1.2.3.1*), but the role that cellular mechanisms play in the growth and the associated generation of forces up to elevation have been largely neglected.

Different cellular mechanisms of growth are active at stages immediately prior to and during PS elevation, such as the relatively increased rate of proliferation in the presumptive nasal aspect of the PSs (Goering et al., 2022). Again, given the timescale of PS elevation, it is unlikely that this localised upregulation of proliferation causes elevation acutely, and in any case relatively more growth on the prospective nasal part of the shelf would be expected to depress rather than elevate a shelf, but it may somehow generate or contribute to the internal shelf force. Differential proliferation rates in developing tissue have previously been shown to generate mechanical stress in the wing disc of the

common fruit fly, *Drosophila melanogaster*, which is conferred on neighbouring cells. This results in the stretching of the cells around the edges of the disc, ultimately leading to reorientations in cell divisions and, when aligned, resulting in directed tissue growth (Mao et al., 2013).

Thus, cellular behaviours producing growth can result in the gradual build-up of elastic potential energy. In the pre-elevation palatal shelves, differential tissue growth could be translated into the internal shelf force, which work in this thesis will suggest is chronically stored elastic potential energy and maintained via cytoskeletal and/or ECM components.

There are, broadly, six ways that cells can behave to produce directional growth. These are given by the mnemonic PROMASS (Economou et al., 2013; Green, 2022) and they are listed with examples in Table 1.4. All directional tissue growth is captured by the product of one or more of these.

Beyond localised proliferation (Goering et al., 2022), ECM expansion via HA accumulation (Lan et al., 2019) and cellular reorientation (Brock et al., 2016) as described previously, there are few examples of where these processes have been investigated in the context of PS elevation specifically. However, a recent study identified cell shape change in mouse embryonic palatal mesenchyme (MEPM) cells following mutations in SPECC1L, the cytoskeletal scaffolding protein, and a potential role of the alignment of cell division in force generation. *Specc1l* is downstream of *Irf6*, mutations in which give a syndromic cleft in Van Der Woude syndrome, and is thought to organise cellular actin and myosin (Goering et al., 2022). Hence, it has been theorised that it may play a role in the alignment of actomyosin-based forces. Mutations in *SPECC1L* cause orofacial clefting in humans and delay PS elevation by one embryonic day in mice (Hall et al., 2020). In mice, it is thought that the delay in elevation is due to increased F-actin deposition at the cell edge, causing transient fusion events between the posterior tongue and palatal shelves (Goering et al., 2022). Furthermore, primary PS mesenchymal cell lines from *Specc1l* deficient mice have speed and directionality defects (Goering et al., 2021). The PS mesenchyme is known to contain contractile actomyosin (Lessard et al., 1974), and more recently patterns of active

Table 1.4 Known examples of cellular mechanisms of growth under the PROMASS framework

Cellular behaviour	Examples	References
Proliferation (anisotropic)	Chick limb outgrowth	(Niswander et al., 1994; Boehm et al., 2010a).
Rearrangement	Axial convergent extension	(Keller, 2006).
Orientated division	Directional growth in the cerebral cortex and wing bud; kidney tubule elongation	(Adams et al., 2002; Fischer et al., 2006; Mao et al., 2013).
EC**M** expansion/behaviours	ECM expansion in chick bone growth and palatal shelf expansion by HA accumulation	(Jingjing Li et al., 2016; Lan et al., 2019).
Addition/**S**ubtraction (apoptosis)	Interdigital webbing death	(Suzanne and Steller, 2013).
Shape/**S**ize changes	Later notochord elongation; metabolic growth and osmotic swelling	(Adams et al., 1990; Heisenberg and Bellaïche, 2013)

phosphorylated myosin (*Figure 1.9E*) and the actin cytoskeleton has been shown to become more disorganised following elevation (Chiquet et al., 2016). The fundamental requirement of the cytoskeleton in force generation during morphogenesis is increasingly being highlighted (Kindberg et al., 2020). These studies have begun to illuminate the role of collective cytoskeletal behaviour, and the consequent impacts on cellular shape and division orientation during PS elevation.

There have also been some attempts to document cell shape and nuclear shape change in the PS mesenchyme during elevation in association with contractile regions of the PSs. One such study utilised myosin ATPase histochemistry between muscle and non-muscle

contractile systems in the PSs themselves, the latter defined as 'filamentous rich mesenchymal cells' (Babiarz et al., 1975). The authors describe skeletal muscle cells on the oral side of the posterior palate, and non-muscular contractile systems in the midpalate on the lingual side towards the posterior limit and along the oral epithelium towards anterior limit. They describe 'elongated cells' present in the contractile regions. The same group would later report that PS mesenchymal cells were inherently contractile, and that this may be regulated by neurotransmitters such as serotonin (Zimmerman et al., 1983; reviewed by Ferugson, 1988). Plus, the non-muscle contractile system described by Babiarz et al (1975) was reportedly supported by the identification of filamentous posterior mesenchyme cells in a description of the PS mesenchyme ultrastructure, with the author suggesting that both the myofibrils in the skeletal muscle cells and the filamentous network in the mesenchymal cells may play a role in shelf reorientation (Innes, 1978).

Further measurements of PS mesenchymal cell shapes and a documentation of their changing orientation were made in these regions qualitatively (Babiarz et al., 1979). In summary, the PS mesenchyme appear to go from an elongated pre-elevation shape to rounded post elevation in the anterior and middle PSs at the presumptive oral aspect in immediately sub-epithelial cells (*Figure 1.13*). In the posterior oral aspect, the cells remain rounded throughout the AP axis. In the presumptive nasal side (referred to by the authors as 'tongue side opposite') the cells start rounded, adopt a medial/inferomedial orientation mid-elevation, and resume a rounded shape post-elevation. In the medial hinge region (referred to by the authors as the 'tongue side bend') the PSs recapitulate the pattern seen in the presumptive nasal region but to a more dramatic extent and are orientated more horizontally mid-elevation. The authors conclude that these data show a correlation between the shape and orientation of PS mesenchymal cells and shows a temporal cellular contraction, associated with shelf movement, beginning at the oral epithelium, and spreading towards the tongue-side as elevation proceeds. Interestingly, they noted that the changes were only observed in the peripheral mesenchyme immediately underlying the epithelium. Unfortunately, while the pre- and post-elevation data in this study came from samples fixed *in vivo*, the mid-stages of elevation were only captured while using the *ex vivo* rolling culture system. Given the flaws in this system,

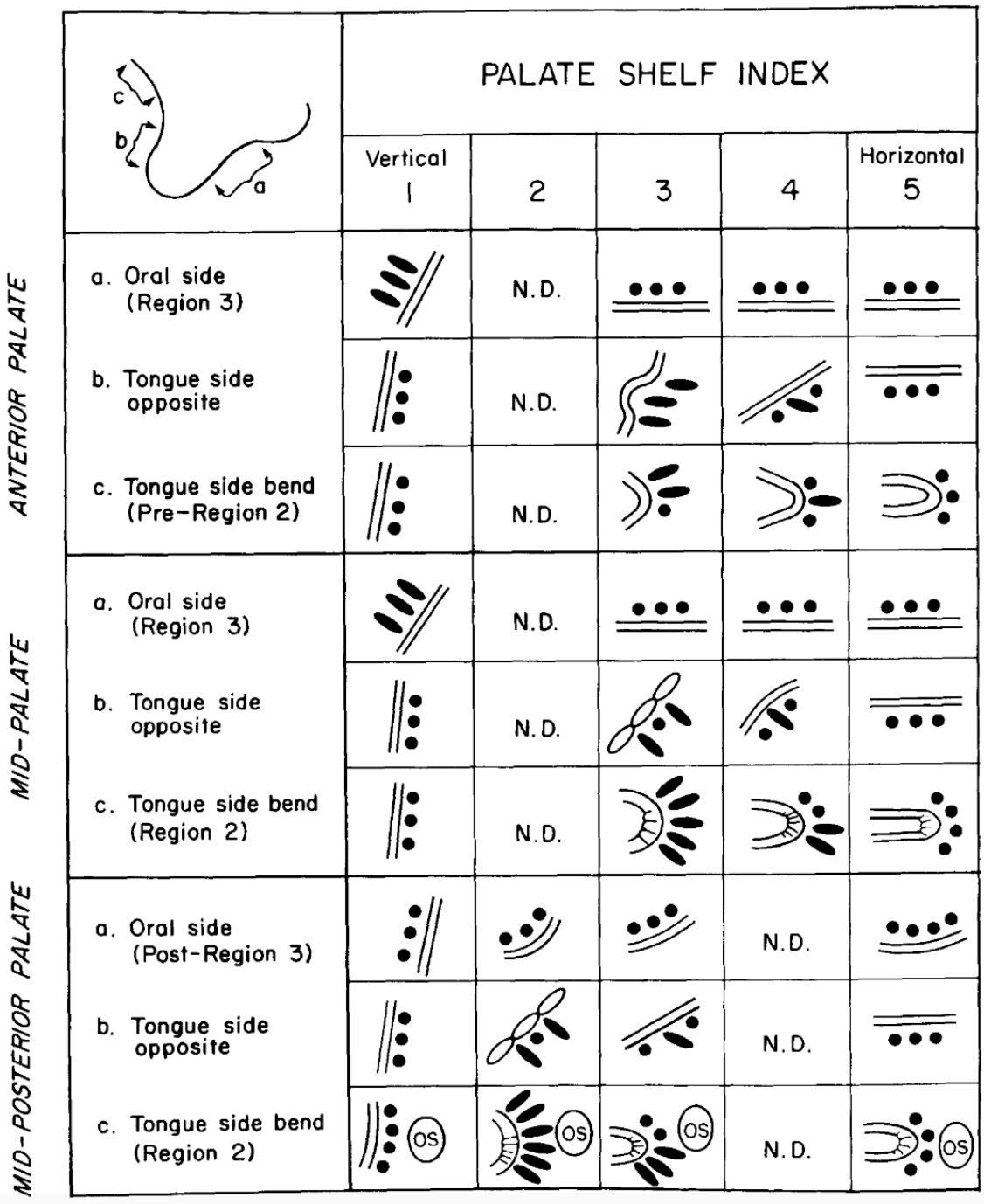

Figure 1.13 Diagram of PS cell shape changes during *in vivo* and *ex vivo* elevation

Sketches representing cell shape changes during PS elevation pre, during and post-elevation. Mesenchymal cells are presented by black shaded ellipses, and the epithelium is represented by the parallel lines. The key to each drawn region (a, b, c) is sketched in the top-left of the figure. The palate shelf index refers to extent of elevation, with 1: vertical and 5: horizontal. N.D., not determined; OS, ossification centre (Babiarz et al., 1979).

referred to above and analysed in detail in Chapter 4, care should be taken were drawing conclusions from these data.

A study utilising early computational analysis techniques investigated cellular spacing and proliferation during elevation (Brinkley & Bookstein, 1986). The author's noted region-specific patterns of changes in cell spacing from their 'smoothed spatial averaging' analysis (the work used image analysis and computation that was advanced for its time, using local blurring and interpolation algorithms to do the smoothing).

Nonetheless, the authors state that cell density increases over time in peripheral areas, and that density decreases in central maxillary areas. It is also suggested that other discrete and regional changes in density are observed in "areas associated with shelf reorientation" but that "commonalities among groups of contour maps are to be discerned by the researcher." Statistical testing was not performed during the analyses, and there are several other important factors to consider when interpreting these data. For example, the pre-elevation stage was captured after the tongue was removed, at which point elevation may have progressed to a significant extent already. Plus, the 're-modelling' of the contour lines is explored in detail but, given said contour lines were generated at smoothed points between the centre points of adjacent boxes, it is unclear how consistent these could really be between different samples collected at different time points. The density maps also look drastically different between the *in vivo* and *ex vivo* samples.

The analysis is innovative in the context of the literature at the time, and in the extensive discussion the authors raise several interesting points as to how cell-density could change under displacement by ECM expansion, and how the early osteogenic fronts in the shelves could influence cell spacing in the mid and posterior palate and influence the direction of PS remodelling.

Finally, the adhesive properties of PS mesenchymal cells were investigated in mouse embryos mutant in the *amputated* locus (Flint, 1980). In the *amputated* mutant mouse, embryos were characterised by multiple defects including short limbs, rib fusion, fore-facial hypoplasia, taillessness and cleft palate (Flint and Ede, 1978). The mutation is described as a single, autosomal recessive mutation; as a caveat, I have been unable to

link this to any modern genetic mutant description, and all references to the *amputated* mutant disappear from the literature by the 1980 (unfortunately, the only reference made to the mutant itself in this paper is to the author's PhD thesis, which I have also been unable to access). Regardless, the PSs in *amputated* mutant mice were found to be shortened, and it is stated that this was due to the mutant PS mesenchyme 'clumping together' with an increase in cell-density in the PSs, and larger areas of surface contact between cells than in controls. The authors state that this prevents adequate outgrowth for elevation to occur. Although limited in scope, the investigation of cell adhesion using modern imaging and immunohistochemical approaches could be an interesting avenue for future exploration.

1.4.7 Mechanisms of palate elevation summary

Overall, the trajectory of the PS elevation field is increasingly toward exploring the cellular mechanisms of growth and associated behaviours underlying force generation and remodelling events. Although some early attempts have been made to characterise these behaviours, there is still no clear mechanism for the generation, location or timing of the internal shelf force. The ECM appears to be a particularly promising avenue of exploration, with the focus shifting from HA accumulation and turgor pressure to the interplay between several ECM components and how they might work to together to drive large-scale tissue remodelling events such as PS elevation.

There is also a recent and growing interest in mechanically mediated biological phenomena (Norman et al., 2021), yet the role that tissue stiffness plays in PS elevation, facilitative or otherwise, is unexplored. The heterogeneous PSs could display heterogeneous material properties across the AP or dorsoventral axes; this would be particularly interesting to explore in the context of the higher concentration of GAGs in the posterior palate, conferring viscoelastic properties to the tissue.

Finally, the use of modern tools and image analysis techniques offers an excellent opportunity to map dynamic cellular behaviours responsible for directional tissue growth (J. Li et al., 2020; Panousopoulou and Green, 2016). This would give a clearer insight into

the location and nature of the internal shelf force, especially given the evidently often contradictory state of the literature. It would also help to clarify unclear aspects of the literature, such as whether appropriately aligned and orientated elastic and/or collagen fibres are present at the time of elevation. At the outset of this thesis project, combining these avenues with modern computational analyses and traditional *ex vivo* culture techniques offered an exciting opportunity to investigate PS elevation at both the whole tissue and cellular scale.

1.5 Project aims

Despite great advancements in our understanding of the genetics underlying orofacial clefting and the molecular genetics driving palatal outgrowth and fusion, comparatively little is understood about PS elevation mechanisms. As summarised at the end of each section in this introduction, there are many fundamental gaps in our knowledge of PS elevation, alongside scope for further investigation into the complex question of the generation, storage and mediation of the internal shelf force. Much of the research already done relies on the use of an *ex vivo* rolling culture system that does not appear to have been characterised morphometrically, and on mouse mutants which reportedly have an elevation defect but in fact do not. On the latter, there is a distinct lack of evidence that the failures are intrinsic to PS elevation itself and are demonstrably secondary to other defects (see *1.3.5*). Hence, these studies have done little to advance our understanding of the shelf-intrinsic mechanisms of PS elevation. Understanding cellular behaviours associated with growth mechanisms will be key to understanding the cause of heterogenous elevation mechanisms, as will characterising the material properties of the PSs and grasping the evolutionary basis of elevation.

Therefore, the project commenced with a broad scope which evolved throughout, led by the data, with specific aims as follows:

1. Characterise the nature of the internal shelf force via use of the *ex vivo* rolling culture system. The palatal severing/wounding studies by Brinkley and Vickerman

(1979) and Bulleit and Zimmerman (1985) were to be reproduced and built upon to identify mechanical dependencies of elevation along the AP and ML axes.

2. Identify and give the first description of palate development in a Monotreme. This was to be done via the Echidna, *Tachyglossus aculeatus*, to inform the evolutionary origins of PS elevation and an evolutionary default horizontal growth programme.
3. Map the internal shelf force in frontal *in vivo* sections of PS tissue prior to and after elevation. To do so at the scale required, an AI (deep learning) model of automatic nuclear segmentation was to be built and trained on embryonic PS mesenchyme, and nuclear deformation used as a measure of force as per Li et al, 2016 (outlined in chapter 6).
4. Characterise the cellular mechanisms of growth under the PROMASS framework that may be responsible for generating the internal shelf force, with a particular focus on ECM activities.
5. Characterise the material properties of the mouse PSs via atomic force microscopy (AFM) and use the results Young's Modulus data to populate a finite element model (FEM) of elevation.
6. Using second harmonic generation imaging, clarify whether mature, fibrillar collagen or elastic fibres are present in the PSs at the time of elevation.

Owing to surprising results, the first aim ultimately became an investigation into the elastic properties of the PSs via recoil studies, and a complete morphometric characterisation of the nature of growth and elevation in the *ex vivo* rolling culture system. This change of course is explained in the relevant chapters per the data that led the investigation. Aims 1 and 2 were thus expanded, Aims 3, 5 and 6 were reduced in depth while Aim 4 was abandoned but will be discussed under Future Work in the final Chapter of this thesis. What the work done will show is (1) internal shelf force is present well before actual elevation; (2) the rolling culture method is not a model for elevation or palatal growth since elevation occurs immediately upon explantation before culture and palatal shelf approximation occurs largely by progressive non-physiological deformation of the explant; (3) Echidna shelf elevation follows the typical mammalian course of downward tongue-side growth of the shelves followed by elevation and so does

not reveal the hoped-for link to a presumed ancestral direct horizontal growth; (4) AFM is a feasible approach to mapping stiffness in the palatal tissue and suggests the PSs are a composite structure, consisting of a stiff outer epithelial layer with relatively soft core mesenchyme, with a heterogeneity in stiffness between the stiffer posterior and softer anterior mesenchyme; (5) nuclear deformation and elastic relaxation show a complex and hard-to-interpret pattern before and after elevation; (6) no collagen fibrils or elastic fibres are detectable in the palatal shelves using multiple techniques.

2. Materials and methods

2.1 Animals

2.1.1 Mouse breeding

All procedures were carried out in accordance with the Animals (Scientific Procedures) Act 1986, under Home Office license with KCL ethical review approval. Mice were maintained on a 12:12 hour light:dark cycle and daily animal husbandry was undertaken by the Biological Services Unit (BSU) in New Hunt's House at King's College London, Guy's Campus.

2.1.2 Mouse lines

The majority of experiments presented in this thesis were performed on control strain (CD1) mice. However, preliminary studies were performed in a Sun1;Wnt1-cre reporter cross, and these mice are described below.

Sun1

Sun1, or B6;129-*Gt(ROSA)26Sor*$^{tm5(CAG\text{-}Sun1/sfGFP)Nat}$ mice were bred from a homozygous Sun1 reporter mouse gifted by the Streit lab (KCL) (JAX: 021039). Sun1-tagged mice use the INTACT (isolation of nuclei tagged in specific cell types) method for the immunopurification of nuclei. The cre-dependent removal of a floxed STOP cassette drives expression of the SUN1 inner nuclear membrane protein in a specific cell type. In a preliminary study, Sun1 expression was driven in craniofacial neural crest-derived cells using a constitutively active Wnt1-cre driver.

Wnt1-cre

Wnt1$^{cre/+}$ mice were bred from a heterozygous mouse gifted by the Tucker lab (KCL). This is a non-inducible/constitutively active cre controlled by mouse Wnt1, at the MMTV integration site 1, promoter and enhancer (JAX: 022501). These were crossed with Sun1 mice to generate Sun1;Wnt1-cre reporter embryos for the fluorescent outlining of the inner nuclear membrane.

2.1.3 Genotyping

In adult mice, ear clips were taken using a 1mm biopsy punch at P10. In embryos, tail clips were removed post-harvesting using watchmaker's forceps. A commercially available DNA lysis kit (PCR BIO rapid extract kit, cat. no: PB15.11-08) was used and DNA extraction performed according to the manufacturer's instructions in a heated block. Briefly, tissue was incubated in extraction buffer at 75°C for 5 minutes, with vortexing twice at intervals during incubation, followed by incubation at 95°C for 10 minutes. PCR grade deionised H_2O is then added to the mixture, which is centrifuged at high speed. The resultant supernatant contains the extracted DNA, which can be stored at -20°C indefinitely.

Primer information is included in *Table 2.1*.

Table 2.1 Primer information for PCR genotyping

Gene	Primer name	Sequence	Band size (bp)
Cre	CreA CreB	CCT GGA AAA TGC TTC TGT CCG CAG GGT GTT ATA AGC AAT CCC	WT: - Cre: 500
SUN1 (INTACT)	INTACT A + C INTACT B + D	ACA CTT GCC TCT ACC GGT TC AAG GGA GCT GCA GTG GAG TA	Mutant: 225 WT: 241

PCR genotyping was performed by genotyping technicians at the KCL Centre for Craniofacial & Regenerative Biology.

2.1.4 Echidnas

The short-beaked echidna (*Tachyglossus aculeatus*) is a protected monotreme found in Australia, New Zealand, and Tasmania. Access to this tissue was enabled by collaboration with The Tucker (KCL) and Renfree (University of Melbourne) labs. Tissue was collected and processed in the Renfree lab by Dr. Jane Fenelon, and access to microCT scans was shared with approval by Dr. Neal Anthwal (Tucker lab).

Tissue was harvested and processed as described previously (Fenelon et al., 2023a). Briefly: embryonic echidna samples were collected from a research breeding colony at Currumbin Wildlife Sanctuary (CWS), Queensland, Australia. Samples were dated based on the date of egg laying (oviposition), with samples varying in age from day 4 to day 9 after oviposition; hatching occurs on day 10. All samples were fixed in 4% paraformaldehyde (PFA) overnight, washed twice in PBS and stored in 70% EtOH at 4°C.

This study from which microCT scans of this tissue was received was approved by the University of Queensland Animal Ethics Committee (SAFS/334/17) in accordance with the National Health and Medical Research Council of Australia Guidelines. Wild short-beaked echidnas were obtained and maintained under the Queensland Government EPA scientific purposes permit (WISP153546614).

2.2 Explant culture and dissections

2.2.1 Landmarking

The PSs were landmarked along the anteroposterior (AP) axis using landmarks described previously (Yu and Ornitz, 2011) and anterior, middle and posterior regions were selected which correspond with anatomical places V, III and II in their study. PS regions were selected in the anterior, middle, and posterior regions of the oral cavity. These were demarcated by the epithelial invagination in the buccal side of the PS and the nasal septum superiorly (anterior), the molar tooth germ and the nasal epithelium (middle) and the molar tooth germ and the cranial base (posterior).

2.2.2 Explantation

All dissections were performed under a light microscope with additional fibre-optic lighting. Maxillary explants (explanted tissue containing the PSs and some surrounding maxilla only) were prepared and used in culture and recoil studies (Morgan and Green, 2022).

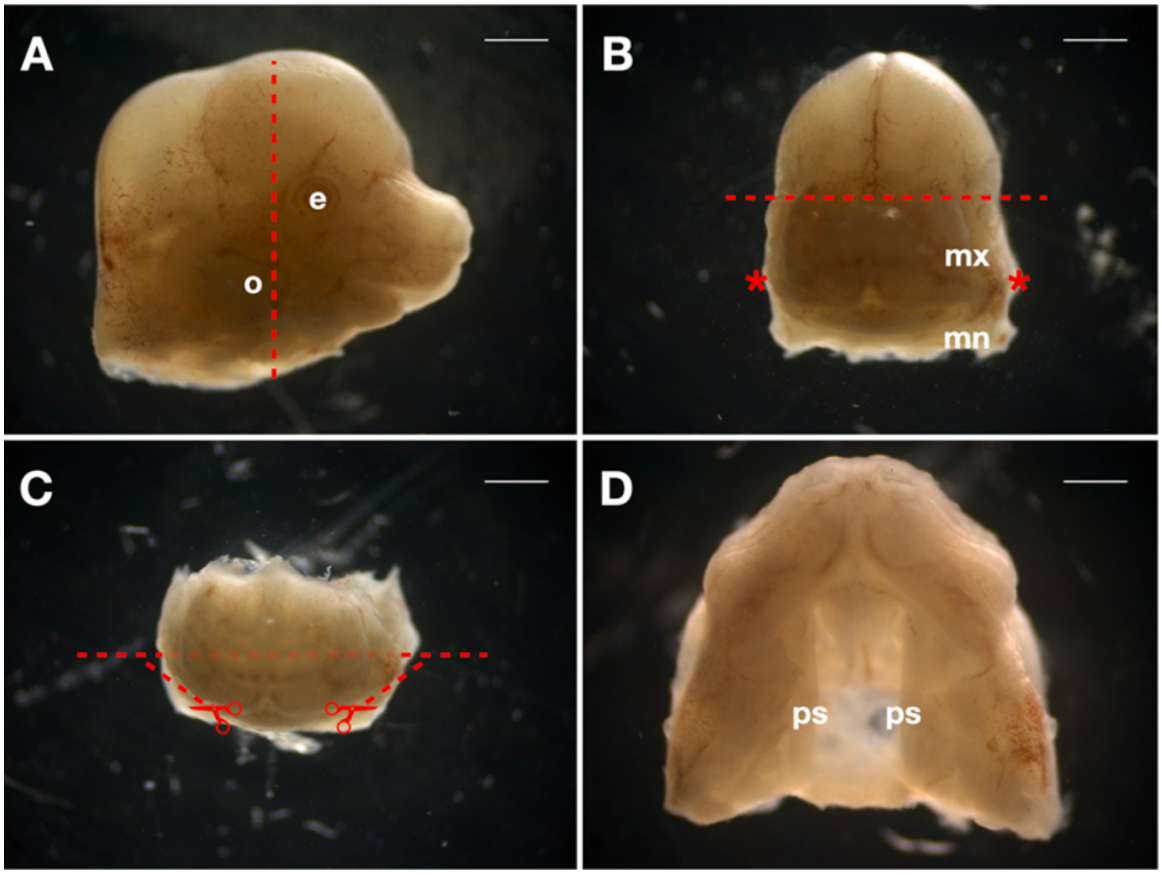

Figure 2.1 Maxillary explant dissection in an E13.5 mouse embryo

A) Decapitated E13.5 murine head facing sideways. An incision is made between the otic vesicle and the eye, splitting the tissue in half. B) The explant is reorientated onto its now flat posterior aspect, appearing to face upwards. Here, the number 10 surgical scalpel is used to remove all tissues above the maxillae/whisker pad. Red asterisk marks presumptive temporomandibular joints (TMJs). C) The mandible is then removed by inserting one microscissor blade into the oral cavity and cutting towards downwards the dish in the presumptive temporomandibular joint region (*). Any remaining connecting posterior tissue is cut away horizontally (red dashed lines). The tongue may also need to be cut away individually here in some samples. (d) Tipping the explant backwards reveals an oral view of the dissected maxillary explant. O., otic vesicle; e, eye; mx, maxilla; mn, mandible; ps, palatal shelf. Red dashed lines and scissors indicate paths of dissection. Scale bars = 250 µm (A, B&C) and 500 µm (D).

Freshly harvested embryos were removed from the uterine-sac using fine-tipped (watchmaker's) forceps, placed in a petri dish filled with PBS and decapitated using a number 10 sterile surgical scalpel. With the head facing sideways, an incision was made between the otic vesicle and the eye, resulting in a flat surface. Heads were rotated to lay on the flat surface to face upwards. A horizontal cut was made here with the scalpel to remove all tissue above the snout at the level of the eyes. Then, microdissection

scissors and/or scalpels were used to dissect-away the mandible and tongue (t/m) at the level of the future temporomandibular joint (TMJ). Only surrounding/lateral maxillae remain, exposing the palatal shelves, referred to as a maxillary explant (Figure 2.1).

Explants were then used in either culture or recoil studies. In recoil studies, explants were simply left in PBS for different lengths of time and fixed in 4% PFA when required.

2.2.3 *Ex vivo* rolling culture

2.2.3.1 Supplemented media composition

Supplemented culture media preparation was based on that used in previous reports investigating whole embryo culture (Kalaskar and Lauderdale, 2014a). Supplemented culture media consisted of KnockOut^{TM} Dulbecco's Modified Eagles Medium (KO-DMEM) (CTS, A12861-01) with: 10% Knockout serum replacement (KSR) (CTS, 10828010); 2% Bovine albumin fraction V (CTS, 10828010); 1% N-2 supplement (Thermofisher Scientific, 17502048) and 1% penicillin–streptomycin (Gibco, 15140122). The media mixture was made-up fresh on the morning of culture experiments.

2.2.3.2 Incubation conditions and hyperoxic culture maintenance

Under a laminar flow hood, 4 mL of supplemented media was added to glass scintillation vials and maxillary explants were transferred directly into the vials using a cut-to-size plastic Pasteur pipettes. The media was the then gassed with 95% oxygen, 5% carbon dioxide ('Carbogen') gas using a sterile Pastette® attached to the gas delivery tube. The Pastette tip was submerged in the explant-containing medium taking care not to compress the explants, and the gas was released until bubbles filled the vials. The vials were then closed-off in an airtight fashion with screw-top lids and the vials were placed on a rube roller (STARLAB) inside a humidified incubation chamber (37°C, 5% CO_2).

Cultures were maintained up to 72-hours and re-gassed either every 12-hours or every 4-hours depending on the experiment. The media was replaced every 24-hours. Following culture, explants were rinsed in PBS and fixed in 4% PFA at 4°C overnight.

2.2.4 DiI labelling

The fluorescent lipophilic dye, DiI (Invitrogen), was applied to maxillary explants prior to *ex vivo* rolling culture. Capillary needles were prepared using a Sutter puller and attached to rubber tubing, which was also connected to a pipette tip for use as a mouth pipette. Under a dissecting microscope, the capillary needle was placed directly into DiI (in DMSO) solution, which entered the needle via capillary action. Maxillary explants were orientated with the PSs towards the viewer, and DiI was applied directly to the PSs. The DiI would typically crystalise on the surface of the PSs on contact but would sometimes require pressure delivered by blowing down the mouth pipette. Explants were then placed back in culture, prior to photomicroscopy and fixation.

2.3 Tissue processing

2.3.1 Tissue collection

Embryos were staged via embryonic day (E) staging, with the day of vaginal plug discovery as day E0.5. Correspondence of E with developmental stage was confirmed by embryonic weighing (Peterka et al., 2002).

On reaching the required embryonic day stage, dams were sacrificed in accordance with the Animals (Scientific Procedures) Act 1986 via cervical dislocation, or by rising concentration of $CO_{2(g)}$. In both cases, death was confirmed by severing the femoral artery with a surgical scalpel.

At stages up to E13.5, the uterine sac was removed from the mother and placed immediately in either ice cold PBS if used in histology/immunohistochemistry, or in media if used in explanation, culture, or AFM studies. Under a dissection microscope, embryos were removed individually from the uterine sac, then the yolk sac and separated from the associated placenta using fine-tipped watchmakers' forceps. They were then weighed on a balance for stage confirmation. At E14.5, embryos were immediately dissected out of the uterine sac on dam sacrifice and decapitated.

2.3.2 Fixation

All tissue was fixed overnight at 4°C in 4% PFA solution. The next morning, embryos were rinsed twice in PBS under nutation, followed by a 1-hour wash in PBS at RT (room temperature) under nutation.

2.3.3 Embedding

2.3.3.1 Paraffin

Post-washing, tissue was incubated at RT during nutation through a dehydration series in EtOH (ethanol) at 70%, 80%, 90% and 100% for 1-hour each. Tissue was then placed in individual cassettes, which were loaded into a Leica ASP300 tissue processor. Equilibration in paraffin was performed via the automatic 'paraffin' programme, and the steps are outlined in *Table 2.2*. Fresh solution is loaded between each step.

Table 2.2 Leica ASP300 paraffin processing programme

Chemical	Temperature	Notes	Duration
EtOH (100%)	RT		1.5 h
EtOH (100%)	RT		1.5 h
EtOH (100%)	RT		1.5 h
Xylene	RT		1.5 h
Xylene	RT		1.5 h
Xylene	RT	Under increased pressure	1.5 h
Paraffin wax	60°C	Under increased pressure	1.5 h
Paraffin wax	60°C	Under increased pressure	1.5 h
Paraffin wax	60°C	Under increased pressure	1.5 h

After processing, the tissue was retrieved from the cassettes and placed in metal mounting trays. Trays were filled with liquid paraffin and the sample orientated in the desired position (for whole heads and maxillary explants, face down or face up) and plastic microtome mounting cassettes were placed on top of the tray. Trays were then

placed on a cooling plate until the wax solidified. Then, the paraffin wax-embedded samples were prised out of the metal tray attached to the cassette and stored at RT until microtome sectioning.

2.3.3.2 Gelatin

Gelatin embedding was used in the generation of vibratome-sectioned thick tissue samples for imaging at an extended Z-depth (up to 30µm) during confocal microscopy.

Gelatin was made-up to a 20% solution from SIGMA **G9382** Type B Gelatin from bovine skin. The gelatin solution was made in 1L batches by gradually dissolving 200g gelatin powder in 1 L PBS at 45-55°C during magnetic stirring. This was typically left overnight before aliquoting and storing at -20°C. The gelatin was heated to 55°C before use.

Following fixation and washing, samples were placed in a bijou filled with 20% gelatin and incubated at 55°C in a water bath. Samples were deemed to have equilibrated with the 20% gelatin when they sunk to the bottom of the bijou. Variably, this could take an hour, but the tissue was often left overnight. The variability could have been due to air-bubbles trapped in tissue cavities. Fresh 20% gelatin was poured into an embedding mould and the samples were placed in the centre of the mound and orientated (face-up for heads and maxillary explants). For fast solidification of the gelatin, which helps prevent disruption to the orientation, the embedding mounds were placed on ice until solidification. Then, the sample-containing 20% gelatin blocks were trimmed to a cuboid with a razor blade and placed in a bijou. The bijou was then filled with 4% ice cold PFA, which was kept at 4°C in a fridge for 3-4 days; any longer and the 20% gelatin block may go brittle. On the day of vibratome sectioning, the sample-containing 20% gelatin blocks were rinsed twice in PBS, and then washed in PBS twice for 1-hour. The block was then ready for sectioning.

2.3.4 Sectioning

2.3.4.1 Microtome

Paraffin blocks attached to cassettes were trimmed to an appropriate size using a razor blade and the cassette was mounted on a Leica RM2245 microtome and sectioned at 8 µm thickness. Correct alignment of sectioned tissue was ensured by sectioning from the posterior of whole heads until alignment of appropriate landmarks, in whole heads the four molars. Serial sections were floated in a deionised water bath at 42°C to help the sections 'stretch-out'. This prevented wrinkles when the serial sections were placed on slides. The serial sections were then mounted on Superfrost Plus slides which were left on a heating block overnight to dry before cover slipping.

2.3.4.2 Vibratome

After washing as described, gelatin blocks were superglued to a base plate and secured to the base of the well in a Leica VT1000 vibratome. The base plate was rotated to ensure the vibratome blade was flush with the straight edge of the gelatin block. The well was then filled with PBS until it comfortably covered the top of the block. Section thickness was set to 30 µm and sectioned were taken from the top of the gelatin block. The sections floated freely and were removed from the well while floating using a paintbrush, which was used to transfer the sections to a 24-well plate. Each well was filled with 1ml of PBS. Once filled, each full 24-well plate was store in a fridge at 4°C until required.

2.4 Histology

All staining was performed using an automatic slide stainer (Thermo Fisher Scientific Gemini AS).

2.4.1 Haematoxylin & Eosin (H&E)

Slides were loaded manually into the receptacle and deparaffinated via neo-clear (Merck) in 3 x 5-minute washes. Sections then underwent a rehydration series (100%, 90%, 70%, 50% and deionised water) using industrial methylated spirits (IMS) for 1-minute each. The

rehydrated tissue was then soaked in Ehrlich Haematoxylin solution (Solmedia) for 10-minutes before being washed with running water for 5 minutes. The slides were then rinsed with deionised water for 10 seconds and washed for 5 minutes in an acid-alcohol (5% HCL). The slides were then again washed with running water for 5-minutes and rinsed with deionised water for 10 seconds. The slides were then submerged in aqueous eosin Y in 2 mM acetic acid solution (Sigma-Aldrich) for counter-staining for 5 minutes. This was followed by 2 rinses (2-seconds each) before the sections underwent a dehydration series in IMS (70%, 90%, 100%) for a minute each, before soaking in 100% IMS for a further 5 minutes. The slides were final submerged in Neoclear for 3 x 5minutes and mounted using Neomount (Merck).

2.4.2 Trichrome with picrosirius red

Sections underwent the same deparaffination and rehydration series as described previously. Following rehydration, slides were soaked in 1% Alcian Blue 8GX (BDH) in 3% acetic acid (pH 2.5). This was washed with running water for 5-mintes and rinsed with deionised water for 10 seconds. Sections were then submerged in Ehrlich Haematoxylin solution (Solmedia) for 10-minutes before being washed with running water for 10 minutes and rinsed with deionised water. Slides were then soaked in 2.5 % phosphomolybdic acid (Acros Organic) as a differentiation step for 10 minutes, before being rinsed with deionised water. Slides were then submerged in Sirius red solution (Sigma direct red 80), with 0.5g in 500ml saturated aqueous solution of Picric acid. Slides were then rinsed twice in acetic acid to fix the sirius red, before undergoing the same Neoclear wash and mounting steps in 2.3.1.

2.4.3 Gomori (aldehyde-fuchsin) stain

Slides underwent the same deparaffination and rehydration series. Following rehydration, slides were soaked in acid fuchsin (Sigma-Aldrich) for 15 minutes. From here, the slides were immediately dehydrated, washed in Neoclear and mounted as in the previous staining protocols.

2.5 Fluorescent staining

DAPI staining was used to stain nuclei in free floating gelatin sections. Gelatin sections were first washed in individual wells with 1 x PBS for 5 minutes. This was removed with a pipette and replaced with 400µL of 0.1% triton in PBS (PBST) for 5 minutes at RT with nutation. Following this, the PBST was removed and 1:1000 DAPI (Sigma-Aldrich, D9542) was added to 400µL PBST, which was then added to each well. During this step, the 24-well plates were covered in tin foil and nutated for 20 minutes. After this, the gelatin sections were removed from the 24-well plates using a paint brush and placed on Superfrost Plus slides and either covered with a curing mountant (ProLong™ Glass Antifade Mountant) for confocal imaging, or with Dako fluorescent mounting medium (Agilent technologies). The slides were left to dry in the dark for one hour, before being stored at 4°C until required for imaging.

2.6 Imaging

2.6.1 Confocal

DAPI-stained sections were imaged using a Zeiss LSM 980 Airyscan 2 confocal microscope using a Plan-Apochromat CS 20x/0.8 (dry) objective for the identification of nuclei in the palatal shelves (PSs). For imaging, tile scans were set up (1024 x 1024) to capture the entire maxillary region (including the PSs). The Z-depth was set to 20 µm at a 0.5 µm Z-step and scans were started at least 2 µm below the tissues surface to avoid surface sectioning artefacts. Bidirectional scanning and 4 frame averages was used and tiles were automatically stitched together following imaging within Zeiss 'ZEN microscopy software' (Zeiss).

2.6.2 Second harmonic imaging

Second harmonic imaging was carried out on a Zeiss 7MP multiphoton microscope using a 20x water-dipping objective. DAPI-stained tissue mounted in aqueous Dako fluorescent mounting medium (Agilent technologies) and both DAPI and collagen fibres were imaged. The second harmonic signal was generated using an excitation wavelength of 930 nm.

2.6.3 Photomicroscopy

Brightfield photomicrographs were taken on an Olympus BX34F Brightfield microscope using a 10X objective. During the Photomicroscopy of frontally sectioned PSs, the samples were aligned by ensuring that the nasal septa (in anterior sections) or cranial base (in posterior sections) were flush to the horizontal. Small rotational corrections were performed during image analysis in Fiji (Schindelin et al., 2012).

2.7 Image analysis

All image analysis was performed in Fiji or R.

2.7.1 Palatal shelf angle

A new way to measure palatal shelf angle (PSA) was developed in this project and is described in detail with supporting schematics in Chapter 4. Briefly, sections of frontally sectioned PSs were opening in Fiji and straight lines were drawn using the line tool on both the oral and nasal surfaces of the PSs. The average angle of these two lines relative to the horizontal was calculated and designated the PSA, representing the extent of elevation.

2.7.2 2D-morphometrics

As with PSA, a customised approach to measuring the PSs was also used during this project in order to assess the extent of growth during culture, and this is described with supporting figures in Chapter 4.

2.7.3 Nuclear deformation

Nuclei were automatically segmented in Fiji using a StarDist model. Ellipses were fitted to the nuclear segmentation outline and the 'Measure' function was used in FIJI to extract the ellipse aspect ratio and X Y co-ordinates of the ellipse centroid. Then, in R, heatmaps were generated by plotting the X Y co-ordinates of the centroids of each nucleus. These

were represented as circles, which were colour-coded based on aspect ratio using the ggplot2 function.

2.7.4 Inter-nuclear spacing analyses

Nuclear spacing analyses were performed in R using code previously developed in the Green lab (Economou et al., 2013; Brock et al., 2016). Fitted ellipses from nuclear segmentation outlines were saved as ROIs and the X Y co-ordinates of the centroids saved as a .csv file. In R, the X Y co-ordinates were extracted from the .csv files and both custom macros written in the Green lab and in-built function in R were used to perform the analysis. The inbuilt 'Deldir' package was used to identify and draw line segments to the nearest neighbours of each nuclear centroid. The average distance between each centroid and its neighbours calculated, and each measured distance was assigned a colour-code from a user-defined scale. A double corona was then connected around each centroid (i.e., each centroid, it's nearest neighbours and their nearest neighbours) using a Voronoi tessellation, which tiled images into polygons, and the polygons were coloured as per the user-defined scale described previously, thus generateing heat maps of internuclear spacing.

2.7.5 microCT 3D rendering

To render microCT images (shared by collaborators in the Renfree and Tucker labs), stacks of .tif files were opened in Dragonfly, a commercially available scientific image analysis software. The software license was held by Mint Htun (Green lab) who assisted in generating the images. In Dragonfly, the desired range of image slices was selected manually, and the slices projected as a 3D image, which can be manipulated in the user interface. A plane of resection was moved to expose regions of interest in the 3D-rendered scans, and images were captured within the software.

2.8 StarDist deep learning auto-segmentation model

StarDist is a deep-learning tool that enables the training of user-generated models to automatically segment star-convex shapes (see Chapter 6 for custom model training detail).

A standard 'Google Colaboratory' notebook was used to train a model for PS mesenchyme automatic segmentation. Google Colaboratory (Colab) is a collaborative platform utilising a serverless Jupyter notebook, enabling the writing and execution of python code via browser. It is commonly used to prototype machine learning models on powerful GPUs and TPUs (Bisong, 2019). The Colab notebook is titled "StarDist (2D)" and is a part of the "Zero-Cost Deep-Learning to Enhance Microscopy" project (von Chamier et al., 2021) and is accessible at:

https://colab.research.google.com/github/HenriquesLab/ZeroCostDL4Mic/blob/master/Colab_notebooks/StarDist_2D_ZeroCostDL4Mic.ipynb

A detailed background to machine learning and StarDist model training is included in Appendix 9.3.

2.9 X-ray microcomputed tomography (microCT)

2.9.1 Sample and solution preparation

Dissections were performed on freshly-harvested CD1 mouse embryos at E13.5. Using watchmaker's forceps and a surgical scalpel, the minimum dissection was made without disrupting the integrity of the mandible, tongue, PSs and enclosing maxillae. This was achieved by following the maxillary explant dissection up to panel C in Figure 2.1., without subsequently removing the mandible or tongue. The dissected tissue was fixed in 4% PFA at 4°C overnight and washed in PBS as described previously, being a rinse with deionised water.

Phosphotungstic acid (PTA) was used as a soft-tissue stain for high-contrast microCT imaging in at 1% solution. 1% PTA (w/v) was prepared from white crystalline 99.7% purity PTA hydrate (Thermo Scientific, 040116.36) by dissolving 0.5 g of $PTA_{(s)}$ in 50 mL of deionised water. The PTA hydrate took 10 – 15 minutes to dissolve at RT with nutation.

2.9.2 Staining

15mL conical tubes were filled with 10mL of stock 1% $PTA_{(aq)}$ and dissected samples were placed directly in the solution using cut-to-size plastic pipettes. One sample was incubated per tube, which were sealed shut with a screw-top cap and parafilm. Samples were then incubated on a simple benchtop rocker (STARLAB) for 5 days. The solution was not changed during this period.

2.9.3 Scanning preparation

The PTA was found to leech quickly from the tissue upon removal from solution, so scanning was carried-out on the final incubation day. PTA-stained samples then needed to be secured in tubes for scanning. Sterile gauze was cut to 5cm strips and individual samples were placed carefully on one strip each with watchmaker's forceps. The frontal aspect of the tissue was aligned orthogonally with the edge of the gauze to help achieve a flush plane when scanning. 6mm scanning tubes were cleaned with EtOH, left to dry and the bottom-third filled with PBS. Samples were then 'rolled' in the gauze and placed directly in 6mm scanning tubes. Excess gauze preventing tube-entry was cut away with scissors, and PBS was pipetted into the top of the tube before the lid was secured.

2.9.4 Scanning parameters

MicroCT scanning was performed in a SCANCO microCT machine with settings set to 2048 x 2048 resolution, 4 µm voxel size, 90 kV energy, and 88 µA intensity with binning. Scan fidelity was checked in the proprietary SCANCO evaluation software and converted into a stack of .tif files for reconstruction, which was tested in both a landmark-free morphometric pipeline co-developed in the Green lab (Toussaint et al., 2021) or in DRAGONFLY as described previously (2.7.5).

2.10 Atomic force microscopy

Atomic force microscopy (AFM) was performed at the London Centre for Nanotechnology (UCL) with the technical assistance of Dr. Richard Thorogate, centre AFM technician. All AFM work and analysis were performed as per a recent bio-AFM protocol publication (Norman et al., 2021).

AFM was performed using JPK CellHesion 200 AFM with an inverted Olympus IX73, equipped with a motorized precision stage, placed on an active anti-vibration table (TMC), and controlled with JPK Scanning Probe Microscopy (SPM) software 5.0 (JPK Instruments) and force-distance curves were analysed using 'JPK/SPM data processing.'

2.10.1 Tissue preparation

AFM was performed on the presumptive nasal surface of isolated PSs. Maxillary explants were generated as previously described, and isolated PSs were dissected out of the explants using watchmaker's forceps and microdissection scissors (Vannas) and the dissection and mounting process is described and demonstrated alongside a figure in Chapter 6 (6.2.5.1). The night before AFM experiments, 4 µL of tissue-substrate adhesive (Corning® Cell-Tak™) was pipetted onto a petri dish under a laminar flow hood, left to dry at RT for 15-minutes, covered and stored at 4°C overnight. Following dissection, the Cell-Tak-containing petri-dish was filled with phenol red-free Leibovitz's L-15 medium (Gibco) (L-15) and the isolated PS floated over the top of the dried Cell-Tak and the medium was slowly aspirated via pipette, which lowered the PS into contact with the Cell-Tak. Following contact, fresh L-15 was pipetted directly onto the PS one single droplet at a time to avoid disturbing the tissue.

2.10.2 AFM parameters

Probing was performed with MLCT-O10 (Bruker) cantilevers C and D; cantilevers were only selected for use following calibration with spring constant (k) and frequency within the manufacturer's suggested acceptable range (k between 0.005 and 0.06 N/m,

frequency between 4 and 20 KHz). To increase surface area for probing, 37 µm polystyrene microspheres (Microparticles GmbH, PS-R-37.0) were glued to the end of each cantilever via probing directly onto the beads in a petri dish. The cantilever-bead complex was then cured under a UV lamp for 4 minutes.

Cantilevers were calibrated from a force – distance (F – D) curve generated from probing a glass slide with a beaded cantilever. This enabled the calculation of sensitivity (nm/V) from the extend curve, which used to calculate cantilever deflection lengths. The spring constant (K) of each cantilever was measured automatically by thermal noise fluctuation detection and cantilevers with K within the range previously stated were selected for use.

2.10.3 F – D curve generation and analysis

Force curves were generated from automatic force maps over different areas of the PSs. These were mapped in an 8 x 8 grid of points over a 100 x 100 µm area (i.e., at 12.5 µm intervals). Young's Modulus (*E*) was calculated using a Hertz model and the mean *E* was calculated from each grid of generated force-curves and used in statistical analyses. Force curve analysis was performed using JPK/SPM data processing software under the 'Hertz-fit' pre-selected analysis. The beaded cantilever tip radius was entered manually, and a Poisson ration of 0.5 was used. Curves were rejected if they demonstrated breakage events (a sudden downwards trajectory usually in the extend curve), did not achieve a constant baseline, or were noisy.

2.11 Statistics

All statistical analyses were performed in GraphPad Prism for Mac (version 10.0.3) under KCL user license, GraphPad Software, Boston, Massachusetts USA, www.graphpad.com. Statistical tests used are stated in figure legends and numerical P-values are displayed on graphs. A P-value of < 0.05 was selected to indicate statistical significance.

3. Morphometric analyses of PS elevation in *ex vivo* culture and recoil studies

3.1 Introduction

PS elevation is a complex, 3D event happening in a short timeframe. Therefore, being able to physically visualise the event could provide greater insight, informing timescales and morphogenetic movements along different aspects of the A – P axis.

PS elevation was difficult to visualise *in vivo* owing to the rapidity of the event and its enclosure by surrounding tissues *in utero*. To try to apply live-imaging and microscopy to the dynamics of the process, e*x vivo* culture systems have been used extensively to overcome these physical barriers to investigate all stages of palatogenesis. These were reviewed in the main introduction (1.3.3.1).

I originally sought to use the rolling culture technique to investigate the cellular mechanisms underlying the differences in the process of elevation in different parts of the palate: anterior flip-up and posterior remodelling. However, it became apparent that reported growth and palatogenesis in these systems were problematic in both publication and in my hands. This changed the course of my investigation and prompted a thorough morphometric characterisation of growth and palatogenesis during *ex vivo* culture.

This chapter documents the early observation that PS elevation does not occur in culture as previously described, but instead immediately on removal of the tongue and mandible (t/m) during explantation. I found that apparent palatogenesis in culture was a combination of misinterpretation and artefact, and these findings are documented in my growth morphometric studies in the next results chapter. Nonetheless, this provided valuable insight into the *in vivo* event, and in directing the rest of this project.

3.2 Results

3.2.1 Palatal shelf elevation does not occur in *ex vivo* rolling culture.

3.2.1.1 Maxillary explants display PS closure during rolling culture, but elevation is hard to identify

Maxillary explants were prepared as described (see Chapter 2 Materials & Methods) and cultured over 72-hours, with supplemented media replaced every 24-hours and the gas changed every 12-hours. Photomicrographs were taken every 12 hours from the perspective of the exposed oral surface of the maxillary explants (henceforth referred to as the 'oral view'), represented here in a time course (*Figure 3.1A*). In the first 24-hours of culture, the shelves appear to meet in the midpalate, and over the subsequent 48-hrs they 'zipper' bidirectionally, consistent with studies in the rat (Coleman, 1965), but contrary to both posterior-first (Walker and Fraser, 1956) and anterior-first reports (Ferguson, 1978). It was particularly difficult to observe the shelves' elevation angles from this perspective, so I followed palatogenic progress by observing so-called 'palatal gap closure', which has been used previously as a proxy for combined growth and elevation during culture (Brinkley et al., 1975; Lewis et al., 1980). Photomicrographs of fixed samples at E13.5 (immediately prior to elevation) (*Figure 3.1B*) and E14.5 (immediately post-elevation) (*Figure 3.1C*) demonstrated this more clearly than fresh, explanted material. Theoretically, the shelves were presumed to be unelevated at the beginning of culture, but this was not discernible in the top-down oral view. At fusion the surface contrast is so poor that structures cannot be distinguished. It was also difficult to highlight surface structures such as the fusion line and the palatal rugae with side-illumination alone. This can be improved with the addition of Indian ink, but this was not practical during culture (*Figure 3.1D*).

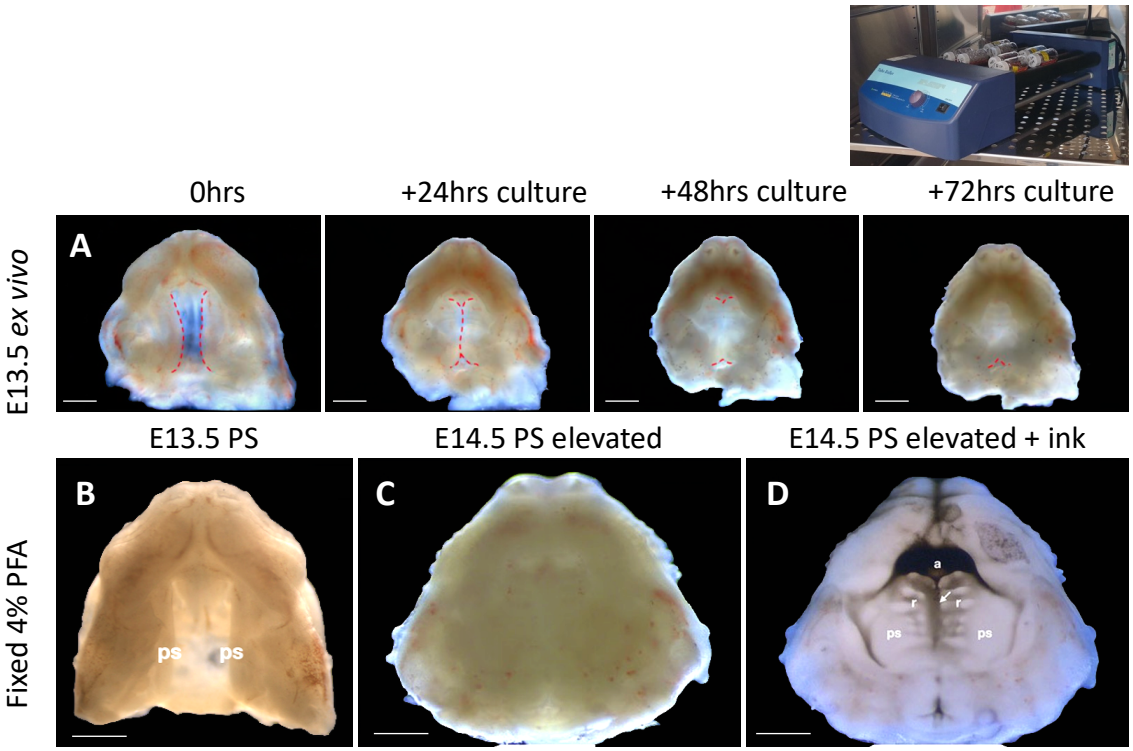

Figure 3.1 Time course of palatogenesis in cultured maxillary explants and W.T. visualisation in the oral aspect

A) Maxillary explants photographed every 12 hours of culture. B) Fixed E13.5 maxillary explant with unelevated PSs. C) Fixed E14.5 maxillary explants showing elevated and fused PSs. D) The sample as in C after layering with Indian ink, improving surface-contrast. Ps, palatal shelf; r, rugae; a, anterior palate (obscured by pooling ink). Red dotted lines show PS edges. Scale bars in A = 1mm; B-D = 500µm.

3.2.1.2 Fate mapping using DiI suggests PS elevation does not occur during rolling culture

In the oral view of a cultured head with the mandible removed at E13.5, the medial tips of the PSs have been assumed to be pointing towards the viewer (i.e., in effect ventrally) in their unelevated state, before rotating 90° medially away from the viewer upon elevation to the horizontal. However, in the oral view, this was difficult – in fact, virtually impossible, to determine. This lack of clarity is perhaps why 'palatal gap closure' has been used as a measure of elevation previously (Brinkley et al., 1975) but it is a dubious metric, seemingly based on false suggestions, as my results below suggest.

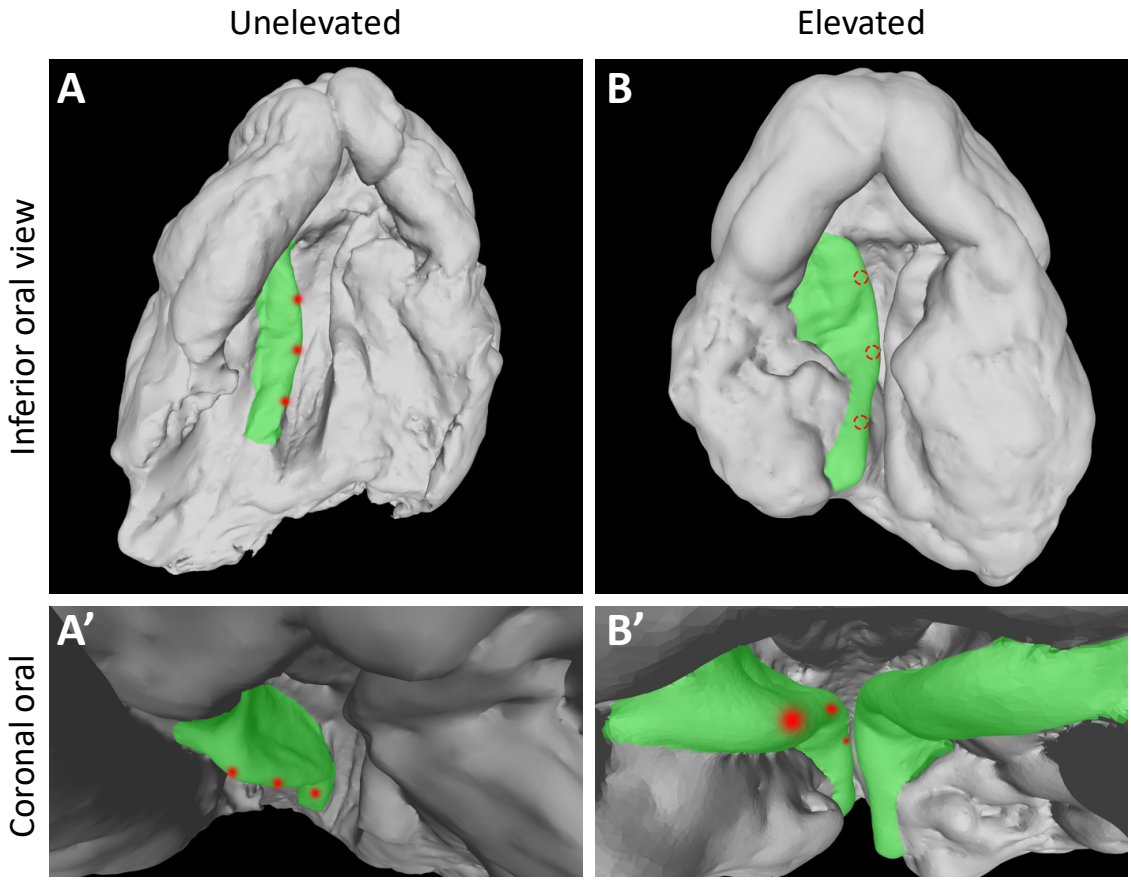

Figure 3.2 Conceptualisation of PS geometry and movements during elevation in microCT scanned maxillary explants.

A) E13.5 maxillary explant demonstrating the appearance of unelevated PSs in the oral view, with a corresponding view from the frontal orientation within the oral cavity (A') showing DiI placement. B) E14.5 maxillary explants demonstrating the appearance of elevated PSs in the oral view with obscured DiI, and a corresponding view from the frontal orientation within the oral cavity (B') demonstrating DiI movement in a flip up elevation event. Explant meshes were generated from microCT scanned maxillary explants at E13.5 and E14.5; red dots = DiI; green pseudo colour = palatal shelves.

Perhaps recognising the inadequacy of tracking the palatal gap closure, one study labelled the palatal shelves in maxillary explant rolling cultures using carbon particles (Chou et al., 2004). This study suggested that the midpalate, rather than the anterior palate, flips-up and elongates towards the midline, whilst the anterior and posterior thirds form via a remodelling event at the medial edge, contradicting the traditional anterior flip-up/ posterior remodelling theory (Chou et al., 2004). The limitations of carbon labelling are historically well-documented (Lipton and Jacobson, 1974) and there have since been no data supporting these findings. Hence, there was scope to fate map the PSs to track PS movements during culture using more modern techniques, such as the use of fluorescent

vital dye 1,1'-Dioctadecyl-3,3,3',3'-Tetramethylindocarbocyanine Perchlorate (DiI). Vital dyes can incorporate with living cells without inducing degenerative changes and are a staple tool of fate mapping experiments (Sulston et al., 1983; Vogt, 1929) (Selleck and Stern, 1991) and had previously been used to fate map the palatal epithelial seam in static culture (Carette and Ferguson, 1992).

DiI labelling the palatal shelves prior to culture was expected to enable distinction between flip-up or remodelling events: based on the assumption that in freshly explanted maxillae the shelf edges point ventrally (towards the viewer in the ventral view). I expected that labels placed on the medial side of these edges would swing out of sight as flip-up elevation (shelf rotation) proceeded, while they would remain clearly visible if and when elevation progressed through mesenchymal remodelling. Hence, in this experiment I planned to use the disappearance of DiI deposits post-culture as a metric for flip-up elevation having occurred.

I applied DiI label at a number of positions along the AP axis of palatal shelf edges in maxillary explants (*Figure 3.3A*) and cultured these for 48-hours using fluorescent microscopy to image them pre- and post-culture (*Figure 3.3B*). Unexpectedly, of all explants cultured (n=8 from 4 independent litters), DiI deposits did not disappear 'around the corner' in any (*Figure 3.3C*). Whilst the shelves appeared to come closer together, the DiI marks remained in roughly the same positions relative to the visible medial surface as where they had been deposited, regardless of A-P position. In some instances, rather than swinging medially out of sight, marks appeared to have moved away from the midline (i.e. there was an increase in visible tissue between the DiI and the medial PS edge post-culture). DiI marks also appeared to have slightly elongated, resembling finger-like projections from their original round shape, and some closely placed marks appeared to have merged, suggesting tissue/cellular rearrangement, or tissue shrinkage (*Figure 3.3A, B*, anterior-most deposits). The explants also appeared to have 'balled-up' on themselves.

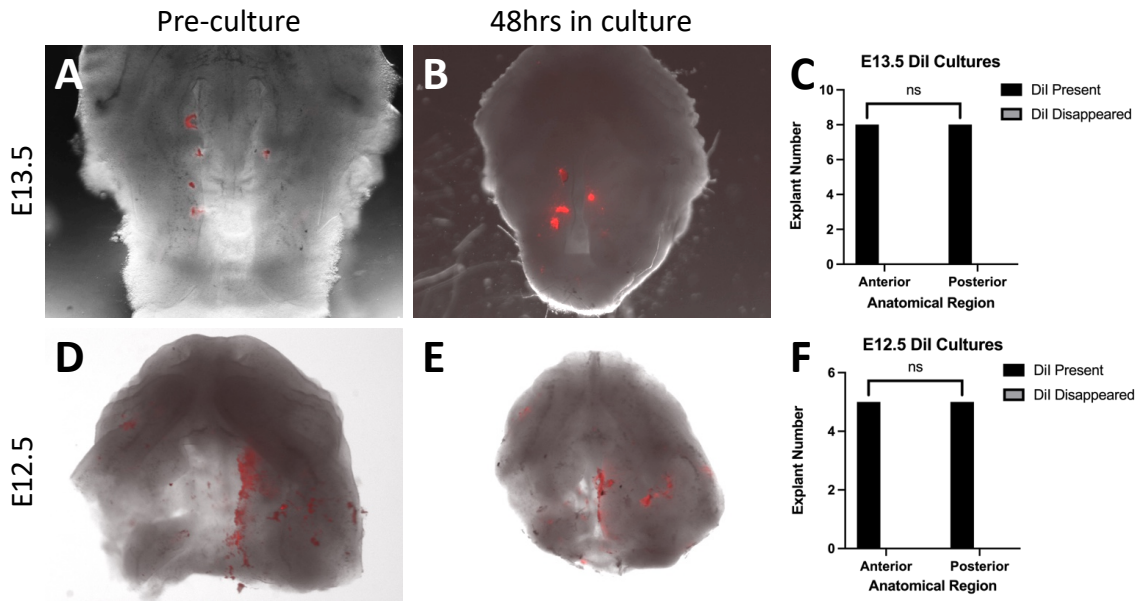

Figure 3.3 DiI labelling of cultured maxillary explants

A) E13.5 maxillary explant in the oral view with DiI labelling along the AP axis of the PS tip. B) The same explant after 48hrs in rolling culture. D) E12.5 maxillary explant with DiI labelled shelf, and adjacent shelf removed. E). The same explant after 48hrs in rolling culture. C&D) Graphs to show the proportion of explants with DiI that 'disappeared around the corner' (flip-up elevation proxy). No statistically significant difference between DiI placed in anterior or posterior PS regions confirmed by Fisher's Exact Test. Sample size = 8 (E13.5) and 6 (E12.5) Brightfield and fluorescent images were combined in Adobe Photoshop.

Given that there were no signs of flip-up elevation, I considered the possibility that the cultures might have been (repeatedly) carried out too late in development, essentially missing the elevation window. Therefore, I repeated this study at E12.5, in the hope of capturing the elevation event sometime over the subsequent 48-hours in culture. This was substantially more difficult technically owing to the much smaller size of maxillary explants at E12.5. Plus, owing to their smaller size, the PSs were particularly inaccessible. Therefore, I labelled single PSs on each explant by dissecting out the adjacent shelf, enabling access to the tip of the labelled shelves from the side (*Figure 3.3D*). Given the shelves were about as wide as the tip of the capillary needle, I was unable to reproducibly label the PS surface with neat spots as at E13.5. Instead, I layered DiI on the surface of the PS along the full AP axis. This proved to be messy, but in principle the same metrics can be applied. Of all explants cultured (n=6 from 3 independent litters), the disappearance of DiI was not observed in any of the explants (*Figure 3.3F*). Descriptions

of shape change were not possible owing to layering of the DiI, although the fluorescent signal does appear to have diluted over culture (*Figure 3.3E*).

The same general reduction in size (previously referred to as 'balling up') was observed, where the explants essentially appear to have somewhat deformed inwards on themselves. The usual issues with the visualisation of the PSs in the oral view also persisted.

The images and quantifications above show that the PS tissue tagged with DiI did not undergo any major reorientation event in culture, strongly suggesting that there was no "flip up" elevation event occurring *ex* vivo in this culture system, potentially undermining it as a model for palate elevation, despite the fact that the results above were consistent with those of all similar assays in the literature (Chou et al., 2004).

3.2.2 Palate fusion is abnormal in *ex vivo* rolling culture

To better understand the processes of palate elevation, both in explant culture and *in vivo*, I set out to identify when palate elevation occurs in each, and where and when does shelf growth occur in relation to elevation. These questions are addressed in the remainder of this chapter.

Given the limitations of measurement in the oral view, I opted to carry-out all further analyses on cultured maxillary explants in coronal (frontal) sections of fixed specimens. I chose to consider the palate in three regions, anterior, middle and posterior based on established landmarking criteria (Yu and Ornitz, 2011).

For the following experiments and analyses, 20x E13.5 and 20x E12.5 explants were prepared across 6 independent litters each, confirmed by weighing. All explants where cultured for 72-hours (ample opportunity for elevation to occur), and investigations were carried out at different gas change frequencies – 12-hours and 4-hours per stage (n=10 each) – to explore parameters that may affect growth in culture.

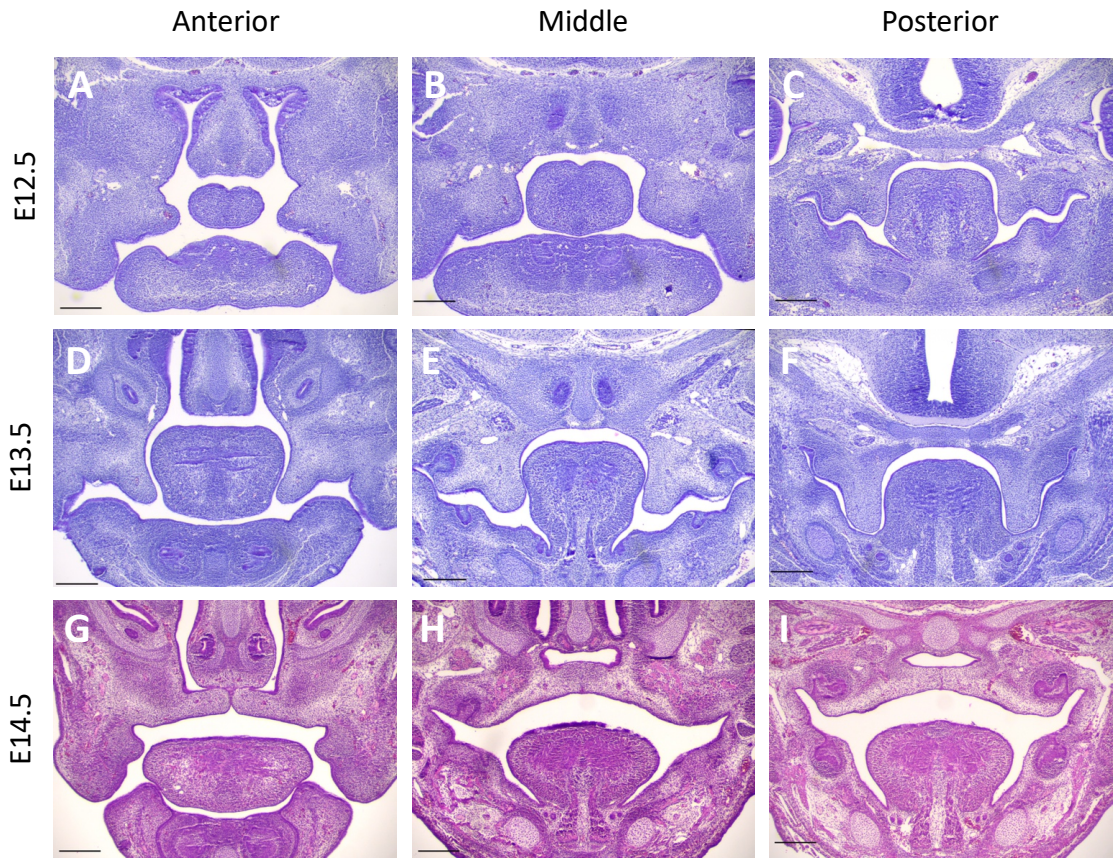

Figure 3.4 Time course of PS elevation in H&E stained frontally sectioned *in vivo* tissue

Representative morphologies of PSs undergoing elevation at E12.5, E13.5 and E14.5. Columns display anatomical regions according to Yu & Ornitz, 2011, and rows show embryonic day stage. Note the default horizontal orientation of the PSs in the anterior (A) prior to being deflected at E13.5 (D). Scale bars = 300µm

3.2.2.1 The PSs were deflected ventrally at E12.5 and elevate between E13.5 and E14.5 *in vivo*

For comparison of PS elevation during culture with normal elevation, I first generated histological images of a time course of *in vivo* PS elevation. It was particularly useful to highlight the PSs at E12.5, which are less often described in the literature than the stages immediately prior to and after elevation. The PSs were small yet horizontally orientated in the anterior region at E12.5 (*Figure 3.4A*). They are typically described as growing ventrally or downwards, yet this may demonstrate that the shelves grow medially before they reach the tongue, though this is not entirely clear from static images. In the middle at E12.5 (*Figure 3.4B*), the shelves barely project at all, with the tissue surface extending almost vertically down from the top of the nasal cavity and then obliquely down and laterally as it reaches the dorsal surface of the mandible. The PSs appear more elongated

in the posterior, closely resembling their shape at E13.5 (*Figure 3.4C*).

3.2.2.2 50% of maxillary explants demonstrate PS fusion when cultured from E13.5, but not E12.5

In maxillary explants, frontal sections give a clearer view of PS fusion and the extent of elevation than possible in the oral view. Across both stages the PSs appear to be elevated to a horizontal orientation (*Figure 3.5 A-I*). However, none of the explants cultured from E12.5 fused in any of the three anatomical regions surveyed (*Figure 3.5A-C, J*). This was despite shelves appearing to have been in contact, suggested by their complementary shapes at the tip (*Figure 3.5B*). It has been reported that the apparent space between them is an artefact of fixation (Greene and Kochhar, 1973; Diewert and Tait, 1979).

Cultured from E13.5, 50% of explants demonstrated PS fusion in all three anatomical regions *(Figure 3.5G-I, K*). The remaining 50% of explants – those with non-fused PSs – did not show complementary shapes in the PS tips, suggesting that they had not come into contact during culture, despite appearing elevated/horizontally orientated.

3.2.2.3 Increasing gas change frequency does not alter the fusion rate of maxillary explants

A high oxygen concentration – supplied during gestation by blood circulation – is critical in normal embryonic tissue development, and the requirement for this in palate development is well documented (Shiota et al., 1990). Further, palate development proceeds at a reduced rate, or is arrested altogether, during culture in normoxic conditions (Economou et al., 2012). Hyperoxic conditions are therefore used in explant rolling culture to overcome this limitation. However, constant oxygen perfusion requires expensive specialist equipment (Aguilera-Castrejon et al., 2021; Lewis et al., 1980) and most rolling head explant cultures have instead relied on batch replacement of oxygen-rich gas in sealed vials. It has not been established whether the frequency of replacement of the gas is limiting for the development of the explants. Therefore, to investigate the effects of oxygen availability (by gas change frequency) on palate development in rolling culture, I cultured sibling-littermate explants simultaneously at different gas change

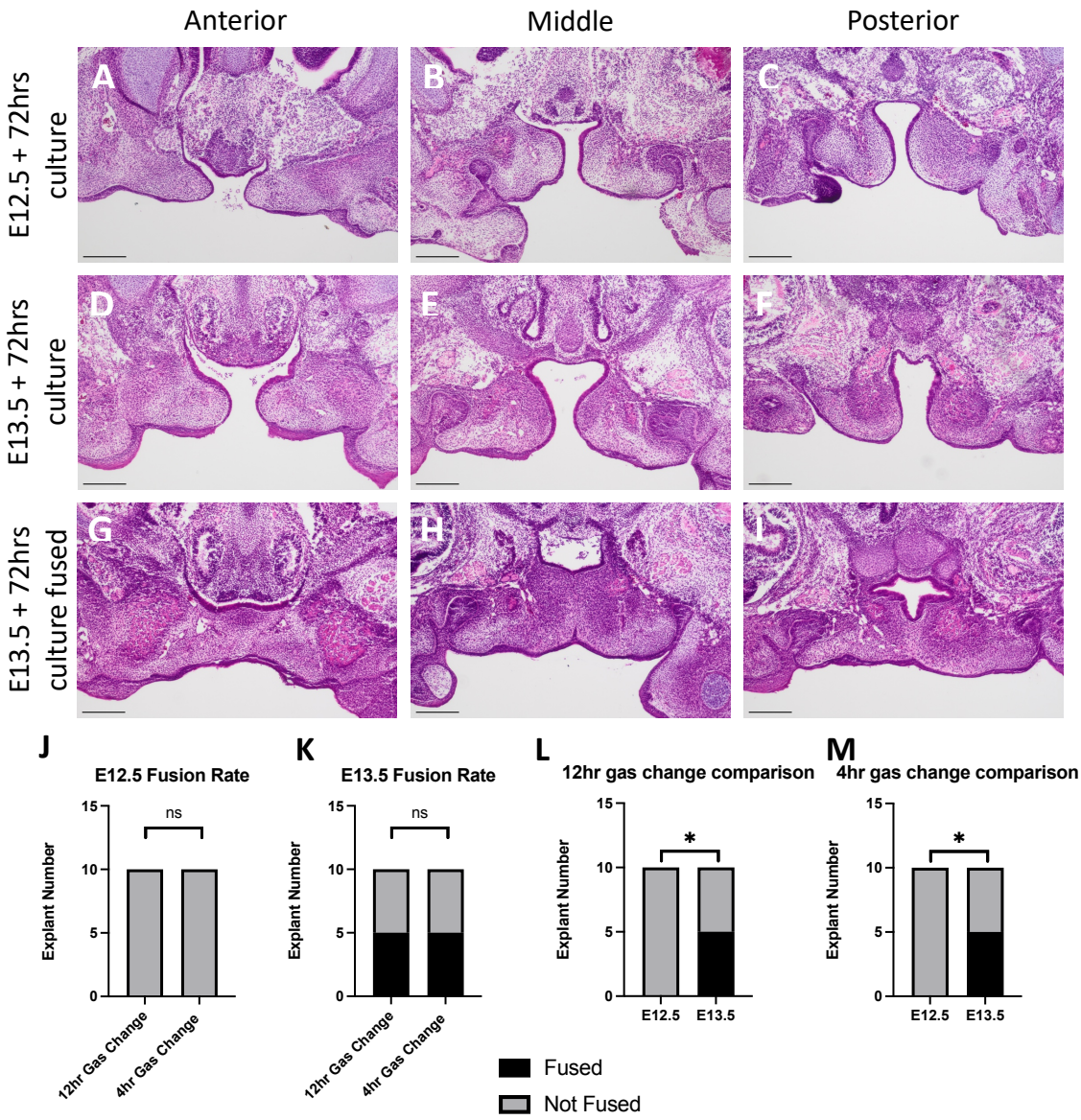

Figure 3.5 H&E Frontal sections of maxillary explants after 72-hours in culture at E12.5 and E13.5 with fusion rates

Columns represent anatomical regions. A-C) Explants cultured at E12.5. D-F) Explants cultured at E13.5 but which did not fuse. G-I Explants cultured at E13.5 which fused. J) E12.5 fusion rate. K) E13.5 fusion rate. L) 12-hour gas change group comparison between stages. M) L) 4-hour gas change group comparison between stages. Statistical significance determined by Fisher's Exact Test. Scale bars = 200 µm.

frequencies: manually replacing the gas at 12-hours for half of all explants, and every 4-hours for the other half, over 72-hours, excluding an overnight break (11pm – 7am).

Gas change frequency had no effect on the ratio of E13.5 explants displaying fusion during rolling culture (*Figure 3.5K-M*) and did not result in fusion in E12.5 cultured explants

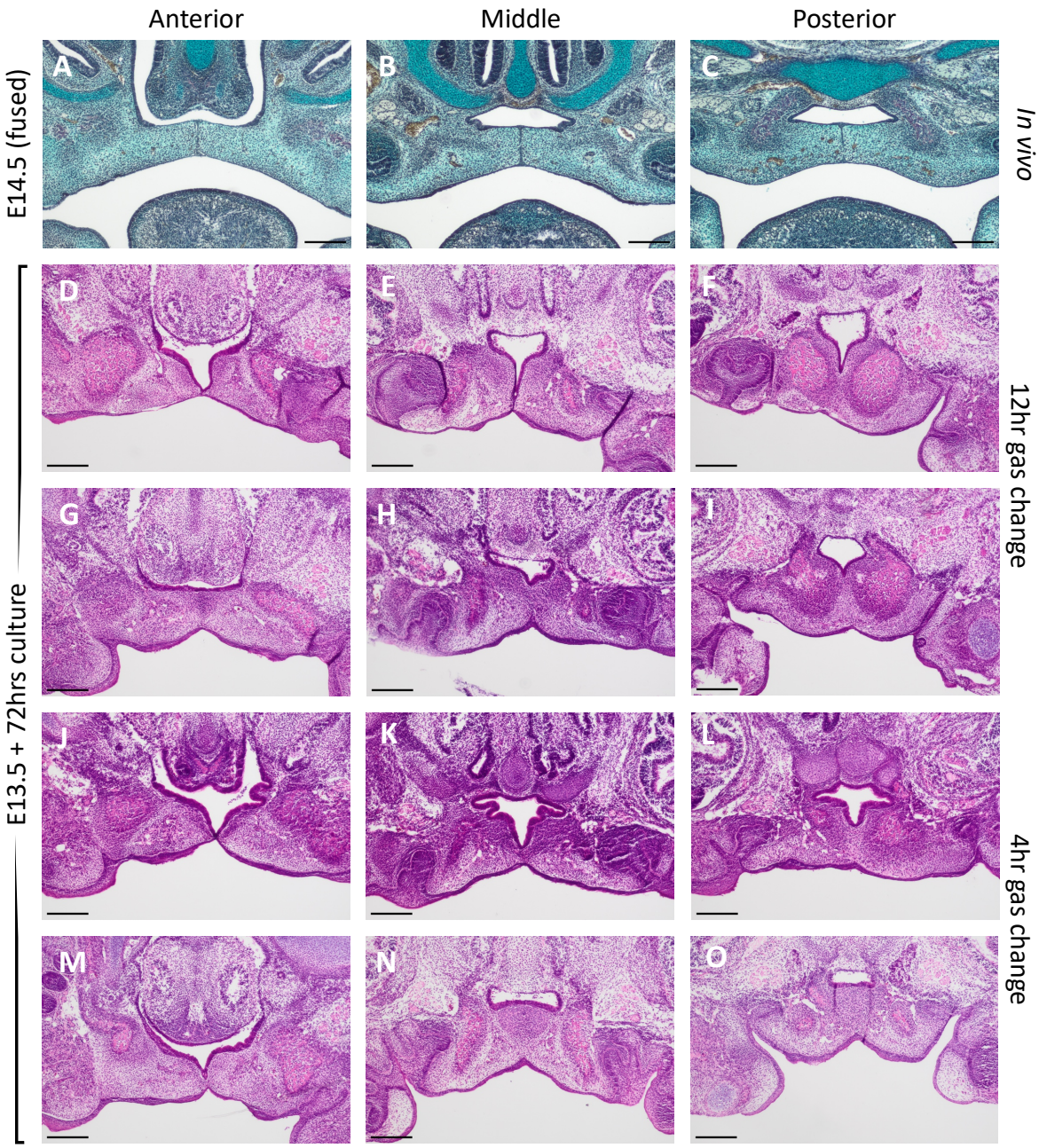

Figure 3.6 Frontal sections the morphological differences in fused PS morphology between E14.5 *in vivo* tissue and fused explants cultured at E13.5.

Columns represent anatomical regions. A-C) E14.5 *in vivo* fused tissue (trichrome stained for contrast to culture groups). D-I) Representative sections of fusion in explants cultured with a 12hr gas change. J-O) Representative sections of fusion in explants cultured with a 4hr gas change. Scale bars = 200 µm.

(*Figure 3.5L&M*).

3.2.2.4 PS fusion appears abnormal in cultured maxillary explants

The fusion achieved by 50% of all explants at E13.5 appeared morphologically abnormal

compared to *in vivo* fusion occurring at E14.5. *In vivo*, the palatal shelves appeared elongated, narrow, and adopted an arch-shaped oral surface, in concordance with the surface shape of the underlying tongue (*Figure 3.6A-C*). In cultured explants, fusion and mesenchymal confluence was also achieved but the fusion was often incomplete (*Figure 3.6 D-F, J-M*). Furthermore, in the posterior region the shelves appeared more rounded in shape than *in vivo*, not adopting the mediolaterally elongated, flattened shape observed in *in vivo* elevated and fused PSs (E14.5) (*Figure 3.6F, I, L, O*). The PSs were more elongated in shape, like E14.5, in the anterior, but the *in vivo* arched shape was only observed in the anterior region of 2 explants (*Figure 3.5G & 3.6F*). The arch was more convincingly recapitulated in the middle and posterior of one embryo in the 4-hour gas change group (*Figure 3.6 N&O*). The presence of the arch shape in the absence of the tongue, albeit in relatively few explants, could suggest that the tongue is less important in acquiring this final morphology.

3.2.3 Insights into palatogenesis *in vivo* and *ex vivo* from an alternative method of palatal shelf angle measurement

Given the difficulty in assessing elevation form the oral view, it was necessary to quantify PS elevation to get a better understanding of this process and how it is modelled in explant culture. This was to help determine whether or not elevation in culture faithfully or sufficiently recapitulates *in vivo* to any useful extent.

Palatal shelf angle (PSA) has been used previously as a metric to measure the extent of PS elevation *in vivo* embryos and cultured explants (Wee et al., 1976; Yonemitsu et al., 2020). The metric most used in the literature, the 'Palatal Shelf Index' (PSI) involves taking micrographs of palate frontal sections and drawing a line along the (prospective) nasal surface of the PS from a landmark, namely the meeting point between that surface and the lateral wall (or dorsal wall posteriorly) of the nasal cavity (*Figure 3.7*). The angle of that surface is scored relative to that of a horizontal line drawn across the nasal cavity to the same landmark on the contralateral side. A value of 1 is given when the PS surface is vertical (90° to the horizontal), 3 when 45° and 5 when horizontal. A value of 1 is given when the PS surface is vertical (90° to the horizontal), 3 when 45° and 5 when horizontal.

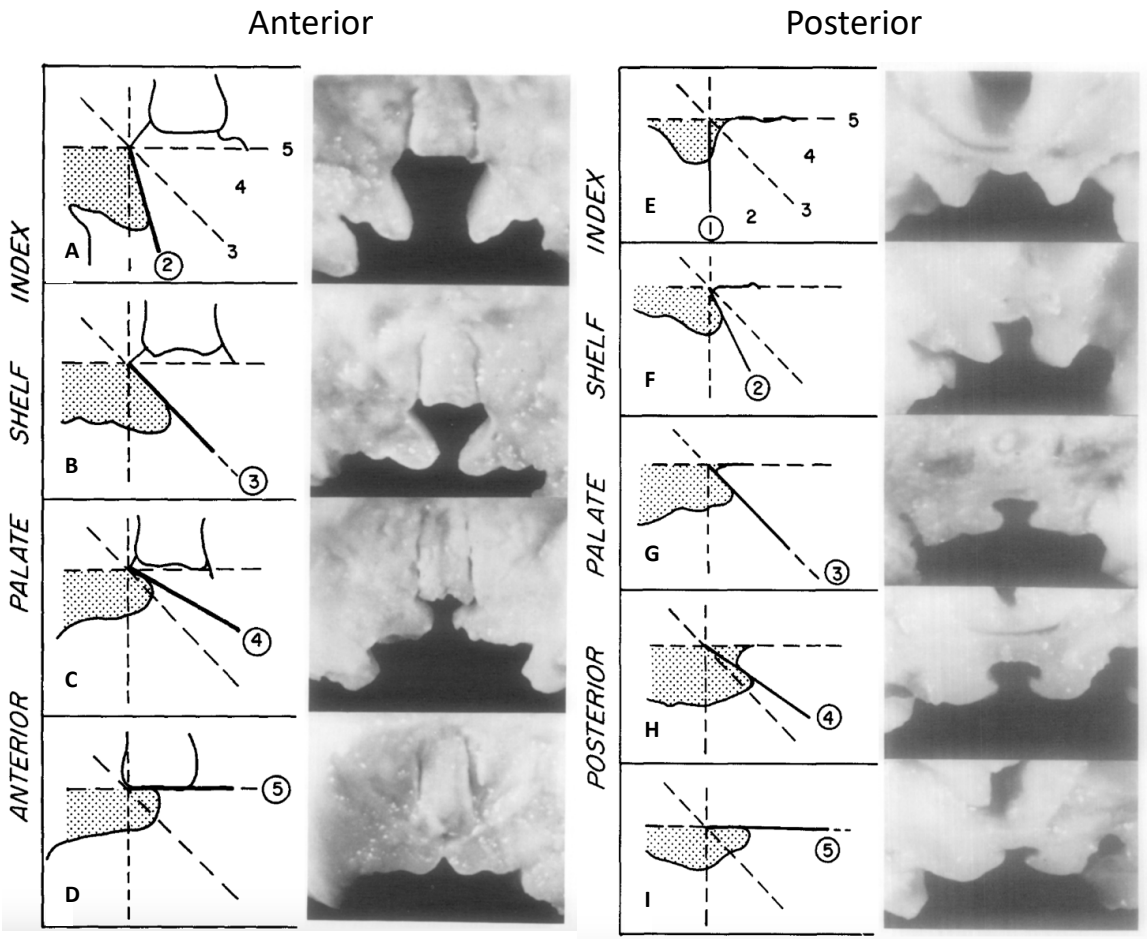

Figure 3.7 Schematic detailing how to measure the 'palatal shelf index' (PSI)

Representative schematics and their PSI value, with a corresponding example in anterior (A-D) and posterior (E-I) frontal sections. Adapted from Wee et al, 1976.

Angles between 90° and 45° and between 45° and 0° (horizontal) were designated 2 and 4 respectively. (*Figure 3.7*).

PSI may be a limited measurement in that only measuring the nasal surface of the PS fails to capture a complete picture of the elevation process because the oral surface and the PS morphology itself are totally ignored. This is particularly a problem when scoring premature elevation when the nasal surface is less clearly defined, and the shape of the shelves is stubbier. Therefore, an alternative method of measuring PSA might consider both the oral and nasal surfaces, and would use a continuous range of values, not being restricted by indexing.

To overcome these limitations, I devised a simple, repeatable method that considers both nasal and oral aspects of the shelf. A straight line was drawn along the surface of both the oral and nasal aspects of the PS tips. Then, a horizontal line was drawn at the origin of these lines, the resultant angles giving oral$^{\theta}$ and nasal$^{\theta}$. The average of these numbers gives the PSA (*Figure 3.8B*). This method was tested and validated on a small sample size of *in vivo* E13.5 PSs (n=5), and PSs from explants cultured *ex vivo* for 72hrs (n=5).

In vivo, this method of measuring PSA displayed the same trend in anterior, middle and posterior anatomical regions. As suspected, the nasal$^{\theta}$ consistently gave a higher elevation value (i.e., closure to 90°/less elevated) than the oral$^{\theta}$. In each anatomical region, the angle measured was statistically significantly different between nasal, oral and PSA measurements (*Figure 3.8C*), P values and tests reported in figure legend). The resultant PSA represents the average angle of the two, taking the entire surface of the PS into account. This trend was also repeated in cultured explants (*Figure 3.8D*). Here, negative PSA values reflected the oral surface angle above the horizontal, providing a quantification that could include the previously mentioned arch shape to the PS following elevation. Hence, this method might give a more meaningful indication of PS elevation as it captures the entire shelf and not just the nasal surface; it might therefore be more useful in this context as it used at earlier stages, where the nasal surface is less clear. Furthermore, it does not potentially lose information from indexing or 'binning' measurements.

As a working example, my previous histological elevation time course demonstrated that the PSs were horizontally orientated at E12.5 in the anterior (*Figure 3.4A*), before apparently meeting the tongue medially and being deflected ventrally (*Figure 3.4B*). This would be quantified as a PSA value being close to zero at E12.5 before increasing at E13.5 (downward deflection) and then decreasing again at E14.5 (elevation) (*Figure 3.9A*). This method of measurement was used to determine PSA in all reported *in vivo* and *ex vivo* measurements below.

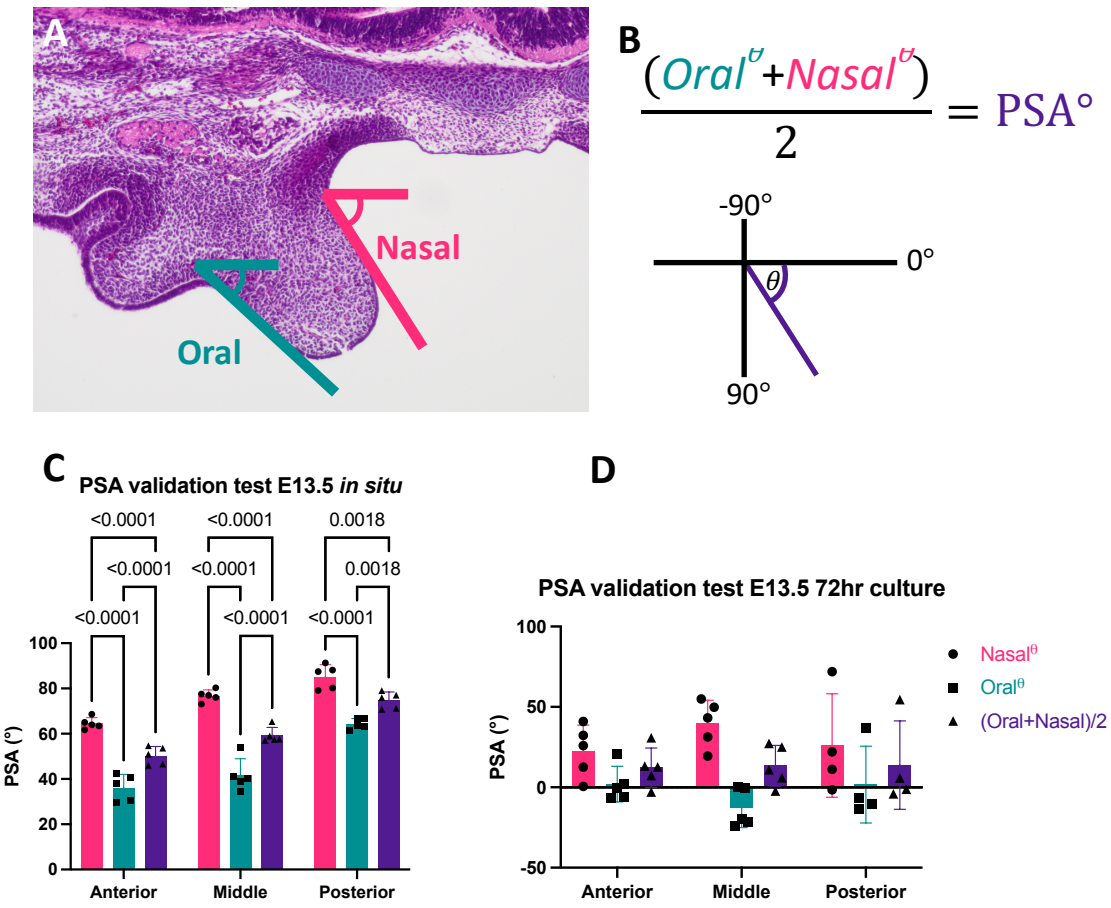

Figure 3.8 An alternative method of measuring PSA *in vivo and ex vivo.*

A) Guidelines for acquiring necessary angles. B) PSA calculation formula, and reference quadrant. C) PSA validation *in vivo*. D) PSA validation *ex vivo*. P values shown on graph and determined via 2-way ANOVA with Tukey's Multiple Comparisons Test; n=5 samples from 3 independent litters. Error bars = mean with SD.

3.2.3.1 Explants cultured at E13.5 reach a PSA similar *in vivo* elevated PSs, but explants cultured at E12.5 do not

Initially, I compared PSA *in vivo* at E12.5, E13.5 and E14.5 the anterior, middle and posterior regions to track how PSA changes across elevation. In each, the anterior, middle, and posterior PSA dropped to below 0° *in vivo* at E14.5 (*Figure 3.9A*). In the middle region, PSA statistically significantly increased between E12.5 and E13.5, suggesting that the PSs become more deflected closer to elevation. However, it is worth noting that the posterior PSs appear to grow to the greatest extent first, and so may be close to maximum deflection by E12.5 (*Figure 3.4*). PSA was consistently highest in the posterior regions.

Unsurprisingly, a comparison of *in vivo* unelevated shelves at E13.5 and PSs cultured from E13.5 for 72hrs reveals that there is a statistically significant reduction in PSA in each anatomical region during culture (*Figure 3.9D*). This demonstrates that PSA is detecting elevation in maxillary explants post-culture.

However, comparing the PSA of *in vivo* elevated PSs at E14.5 with the PSA of cultured E12.5 explants reveals that the PSs did not elevate to the extent of *in vivo* PSs over a similar timeframe (*Figure 3.9E*). This was despite 72-hours in culture, given that previous reports in the literature claiming palatogenesis proceeds normally in rolling culture during analogous timeframes (Abbott, 2019). This begins to suggest that maxillary explant culture at E12.5 is unsuitable for studying palate elevation.

3.2.3.2 Higher gas change frequency results in a PSA closer to *in vivo* elevated shelves in cultured explants

Comparing the PSAs of *in vivo* elevated PSs at E14.5 with the PSA of cultured E13.5 explants revealed that the PSs elevated to the full extent of *in vivo* elevated embryos at the higher gas change frequency (4-hours) (*Figure 3.9F*). In the 12-hour gas change group, this was only true in the middle region, with anterior and middle PSAs showing a statistically significant difference compared to *in vivo* elevated PSAs, perhaps suggesting that a higher gas change frequency is beneficial for investigating palatogenesis in rolling culture.

To further investigate how closely *ex vivo* fusion resembles that of the *in vivo* event at E14.5, I compared the PSAs of fused explants in E13.5+72h culture groups, and those *in vivo* at E14.5 (*Figure 3.9B*). It appeared that E13.5 explants fused after 72 hours in culture with a 4-hour gas change frequency show a final PSA alike *in vivo* elevated shelves in all three anatomical regions tested.

There was no statistically significant difference between the PSAs of the E13.5+72h 4-hour gas change group and E14.5 in vivo in any anatomical region, although the PSA of the cultured explants trended slightly higher throughout. This was also the case for the

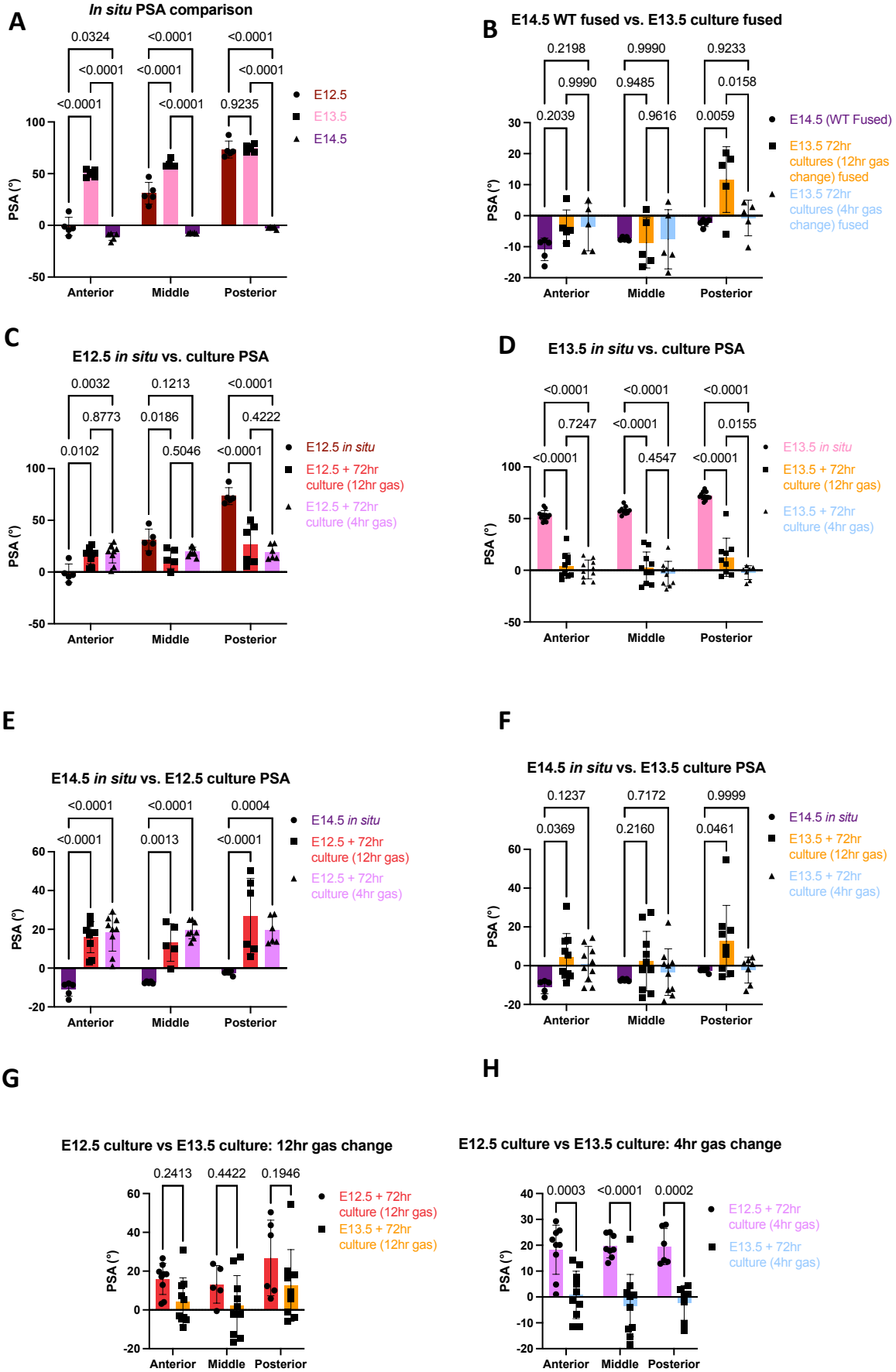
A
In situ PSA comparison
0.0324
<0.0001
<0.0001
<0.0001
<0.0001
<0.0001
<0.0001
<0.0001
0.9235
E12.5
E13.5
E14.5
PSA (°)
Anterior
Middle
Posterior
B
E14.5 WT fused vs. E13.5 culture fused
0.2198
0.9990
0.9233
0.9990
0.9485
0.0158
0.2039
0.9616
0.0059
E14.5 (WT Fused)
E13.5 72hr cultures (12hr gas change) fused
E13.5 72hr cultures (4hr gas change) fused
C
E12.5 in situ vs. culture PSA
0.0032
0.1213
<0.0001
0.8773
0.0186
0.4222
0.0102
0.5046
<0.0001
E12.5 in situ
E12.5 + 72hr culture (12hr gas)
E12.5 + 72hr culture (4hr gas)
D
E13.5 in situ vs. culture PSA
<0.0001
<0.0001
<0.0001
0.7247
<0.0001
0.0155
<0.0001
0.4547
<0.0001
E13.5 in situ
E13.5 + 72hr culture (12hr gas)
E13.5 + 72hr culture (4hr gas)
E
E14.5 in situ vs. E12.5 culture PSA
<0.0001
<0.0001
0.0004
<0.0001
0.0013
<0.0001
E14.5 in situ
E12.5 + 72hr culture (12hr gas)
E12.5 + 72hr culture (4hr gas)
F
E14.5 in situ vs. E13.5 culture PSA
0.1237
0.7172
0.9999
0.0369
0.2160
0.0461
E14.5 in situ
E13.5 + 72hr culture (12hr gas)
E13.5 + 72hr culture (4hr gas)
G
E12.5 culture vs E13.5 culture: 12hr gas change
0.2413
0.4422
0.1946
E12.5 + 72hr culture (12hr gas)
E13.5 + 72hr culture (12hr gas)
H
E12.5 culture vs E13.5 culture: 4hr gas change
0.0003
<0.0001
0.0002
E12.5 + 72hr culture (4hr gas)
E13.5 + 72hr culture (4hr gas)

Figure 3.9 PSA measurement comparison across *in vivo* and *ex vivo* PSs.

PSA measurements in PSs across 3 anatomical regions in E12.5 and E13.5 cultures at different gas change frequencies, and *in vivo* at E12.5, E13.5 and E14.5. Comparisons titled on each graph. Statistical significance (P values) are displayed on each graph and were calculated by 2-way ANOVA with Tukey's Multiple Comparisons Test (A, B, C&D), Dunnett's Multiple Comparisons Test (E&F) and Šidák's correction (G&H). See tables 3.1 and 3.2 for sample size and SD detail. Error bars = mean with SD.

12-hour gas change group in the anterior and middle regions, but in the posterior, there was a statistically significant difference compared to both the 4-hour gas change culture and the E14.5 in vivo conditions. This was particularly striking, in that only 1 sample (of 5) had a PSA below 0°. This further supports the previous observation that the posterior region of explants cultured with a 12-hour gas change fuses in a way that differs from normal *in vivo* fusion (*Figure 3.6F&I*).

The finding that elevation and fusion was more like the *in vivo* event in explants cultured with a 4-hour gas change frequency than a 12-hour gas change frequency at E13.5 suggests that increasing gas change frequency results in palatogenesis more closely resembling the *in vivo* event in culture. However, this was not the case in explants cultured from E12.5, with no statistically significant difference between both groups in any anatomical region (*Figure 3.9C*).

3.2.3.3 Summary: more frequent gas exchange may improve palate elevation in culture

Overall, in the 12-hour gas change group, there was – surprisingly - no statistically significant difference in PSA between explants culture from E12.5 versus those cultured from E13.5 (*Figure 3.9G*)**.** In contrast, when cultured with a 4-hour gas change frequency there was a highly statistically significant difference between the PSA of explants cultured from E12.5 and E13.5 in all 3 anatomical regions (*Figure 3.9H*). This strongly suggests a link between oxygen availability/tension and the ability to proceed with palate elevation resembling the *in vivo* event.

3.2.4 The majority of PS elevation occurs via elastic release immediately upon removal of the tongue, not during culture.

3.2.4.1 Hypothesis: Palate elevation in explants is elastic and early

The PSA measurements on cultured explants showed that the shelves underwent elevation, despite the fate mapping results described above that failed to show the expected movements (*Figure 3.3*). The elevation of the PSs was measured as PSA at the end point of the culture, rather than observed directly, which suggested the possibility that the shelves where actually largely undergoing elevation during the dissection, before lineage labels were applied, rather than during the culture process. This suggestion has been made or at least implied in early research in the field. In a seminal paper a potential underlying elasticity, reportedly residing in elastic fibres, was suggested to help facilitate rapid shelf elevation independently of the tongue (Walker and Fraser, 1956). It was proposed that an 'internal shelf force' was stored in these fibres and, on reaching a threshold, drove the rapid remodelling of the shelves, regressing ventrally and bulging medially in a posterior to anterior fashion. This was reported to cause elevation in a rapid, growth-independent manner. This could theoretically be facilitated early by removal of the tongue, as in the preparation of a maxillary explant, and was supported by a finding from the same study in which elevation was reversible and rescuable by manually depressing and releasing the tongue respectively prior to the elevation window. These observations were made in *ex vivo* whole embryos still attached to an anaesthetised dam via the umbilicus, i.e., in exteriorisation assays.

Since PS elevation at the time of explantation called into question the entire culture system and its associated published literature (about 35 papers) and would suggest that elevation itself was due not to a gradual build-up of force or cellular remodelling but purely due to release of elastic deformation by the tongue, it was clear that a well-defined and expanded series of experiments investigating the timing of elevation and the process of shelf approximation were required.

Therefore, to investigate the rapidity and potential elastic nature of PS elevation, maxillary explants were prepared as described previously at both E12.5 (*Figure 3.10*) and

E13.5 (*Figure 3.11*). For each stage, explants were fixed in ice-cold 4% PFA immediately upon removal of the tongue and mandible ('< 1 min fix') or left in PBS for 20 minutes before being fixed, ('20mins fix'). The inclusion of these two timepoints was to enable detection of effects of a purely elastic, and therefore immediate, release of stored potential energy (<1mins fix) as well as the viscoelastic (i.e., dampened) effects that would produce more gradual morphological changes, albeit occurring on a timeframe still too rapid for active cell migration or tissue growth to be a driving factor (20 mins fix). This also allows finer investigation of the previous finding that PS elevation occurs to a lesser extent at earlier stages in *ex vivo* culture (*Figure 3.8*), supported by the supposed reversibility of elevation *in vivo* at earlier stages (Ferguson, 1978; Walker and Fraser, 1956). Looking at both developmental stages was to enable interrogation of the reported gradual build-upon of the 'internal shelf force'. Theoretically, the later the stage prior to elevation, the greater the force; consequently, the greater extent to which elevation occurs.

3.2.4.2 Observations from E12.5 and E13.5 elastic recoil experiments

On removal of the tongue at E12.5 (*Figure 3.10A, D, G*), there was no statistically significant difference between *in vivo* PSA and either <1min fix (n=11 samples from 4 independent litters) or 20mins fix groups (n=10 samples from 4 independent litters) in the anterior (*Figure 3.12A*). This reflects the histology and is unsurprising given the PSs were horizontally orientated at E12.5 and have not yet undergone deflection.

However, the middle region PSA appears to decrease immediately upon removal of the tongue but increases after 20 minutes in PBS. There was a statistically significant decrease in PSA on removal of t/m in the middle region of E12.5 explants (<1mins fix), suggesting an immediate elastic elevation event. There was then a statistically significant increase in PSA (i.e., reversal of elevation) after 20 minutes in PBS (20mins fix group) (*Figure 3.10B, E, H & 3.12A*). Whilst initially confusing, this could be explained by the PS morphology. As described, the PSs were particularly 'blocky' in the E12.5 midpalate *in vivo* and it was difficult to distinguish a defined PS tip (*Figure 3.4B & 3.10B*). This is less prominent immediately after t/m removal, but the morphology is re-adopted by the end of 20

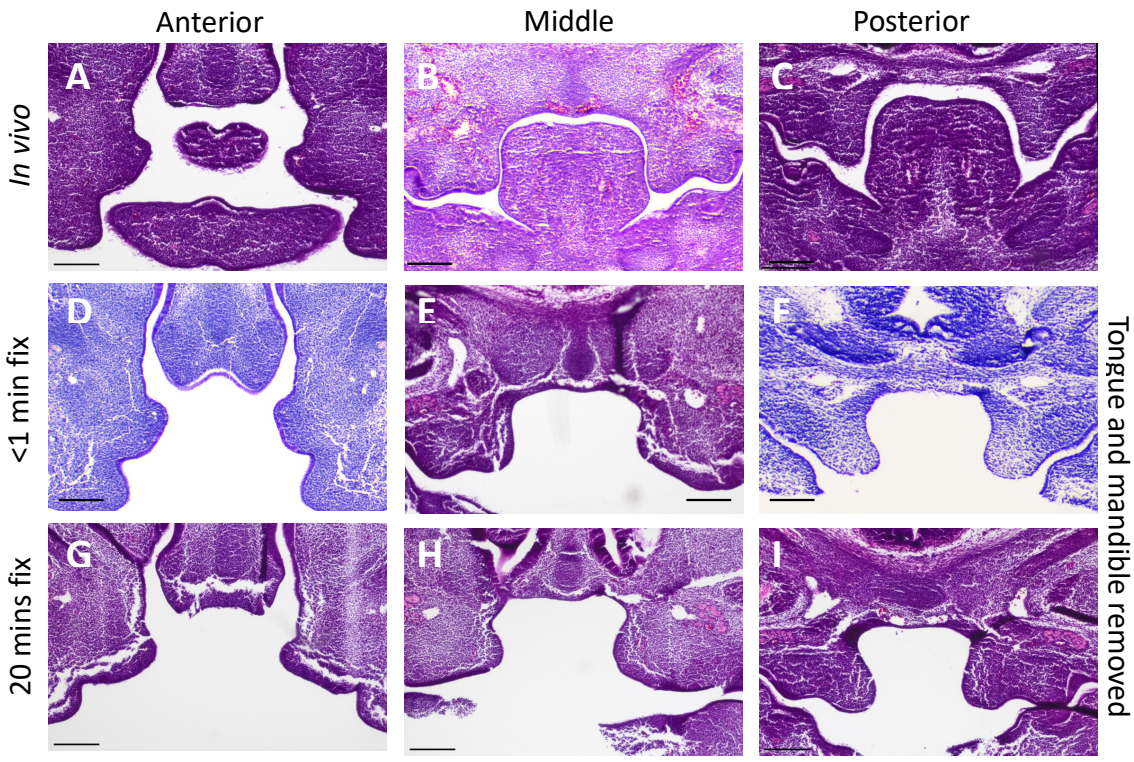

Figure 3.10 H&E frontal sections demonstrating PS morphology during recoil experiments at E12.5.

Columns represent anatomical regions. A-C) *In vivo* representative comparison, with intact t/m. D-E) PSs fixed less than a minute after t/m removal. G-I) PSs fixed after 20mins in PBS following t/m removal. *In vivo* and recoil explants were sibling controls, and samples were selected across at least 3 independent litters. See tables 3.1 and 3.2 for sample size and SD detail. Scale bars: 200 µm.

minutes spent in PBS (*Figure 3.10B*, anatomical right-side shelf). This shape gives a particularly steep nasal surface, thus a particularly high nasal$^{\theta}$, hence the PSA increases.

In the posterior region, PSA decreases significantly on t/m removal, suggesting immediate elastic elevation. There was a statistically significant decrease in PSA on t/m removal in the posterior region of E12.5 explants between *in vivo* and <1min fix and *in vivo* and 20mins fix group (*Figure 3.10C, F&I*). There was no statistically significant difference in PSA between <1min fix and 20mins fix group, however, demonstrating that the majority of PS elevation in this period ocurred via elastic recoil immediately upon t/m removal (*Figure 3.12A*).

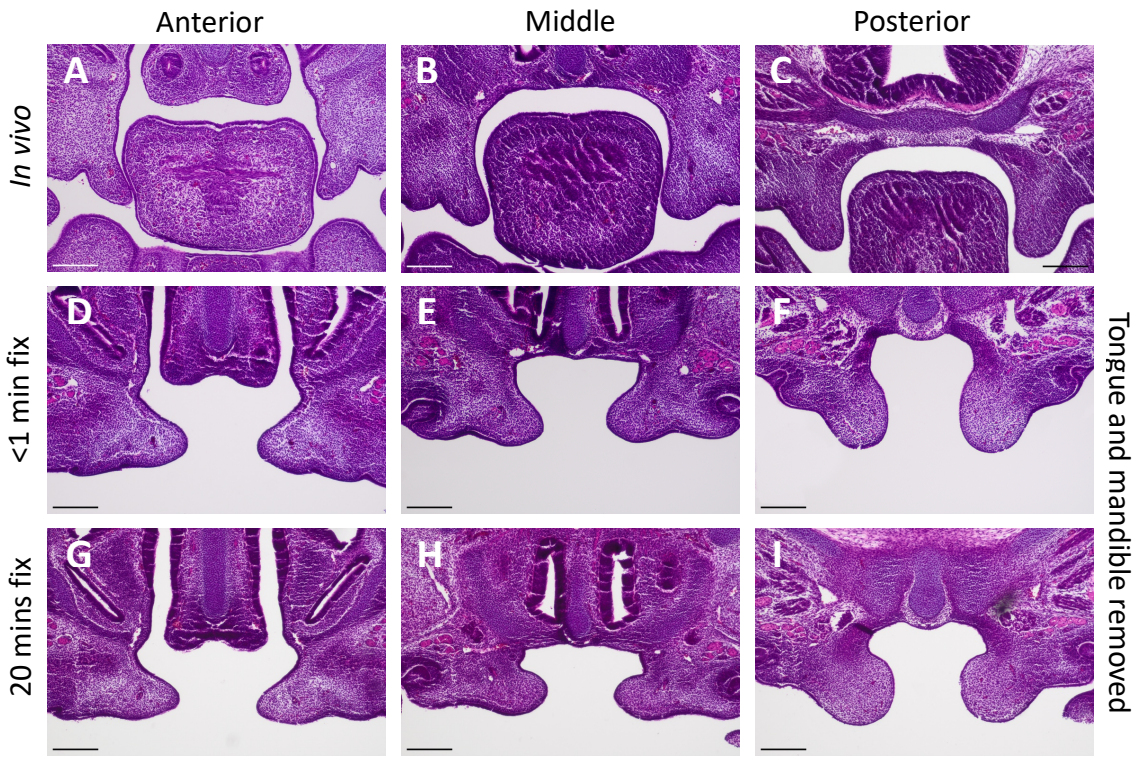

Figure 3.11 H&E frontal sections demonstrating PS morphology during recoil experiments at E13.5.

Columns represent anatomical regions. A-C) *In vivo* representative comparison, with intact t/m. D-E) PSs fixed less than a minute after t/m removal. G-I) PSs fixed after 20mins in PBS following t/m removal. *In vivo* and recoil explants were sibling controls, and samples were selected across at least 3 independent litters. See tables 3.1 and 3.2 for sample size and SD detail. Scale bars: 200µm.

At E13.5, the majority of PS elevation occurs immediately upon t/m removal in all three anatomical regions, with PSA decreasing more gradually between t/m removal and the later timepoints. There was a statistically significant difference between all conditions: *in vivo* to both <1mins and 20mins fix, and between <1mins and 20mins fix (*Figure 3.12B*). The difference in PSA was greater between the *in vivo* and <1mins groups (*Figure 3.11A&D*) than between the <1min and 20mins fix groups (*Figure 3.11D&G*) in all regions, most apparently in the anterior region (which also had the least (albeit still statistically significant) difference between <1min fix and 20mins fix) and least apparent in the posterior. In other words, in the anterior the majority of elevation observed occurred immediately upon t/m removal with little further elevation after 20 minutes, while t/m removal accounted for around 50% of elevation in the middle and posterior. By 20 minutes, and so within the elasticity and not growth timeframe, the middle PSs were two thirds elevated, and just over half elevated in the posterior.

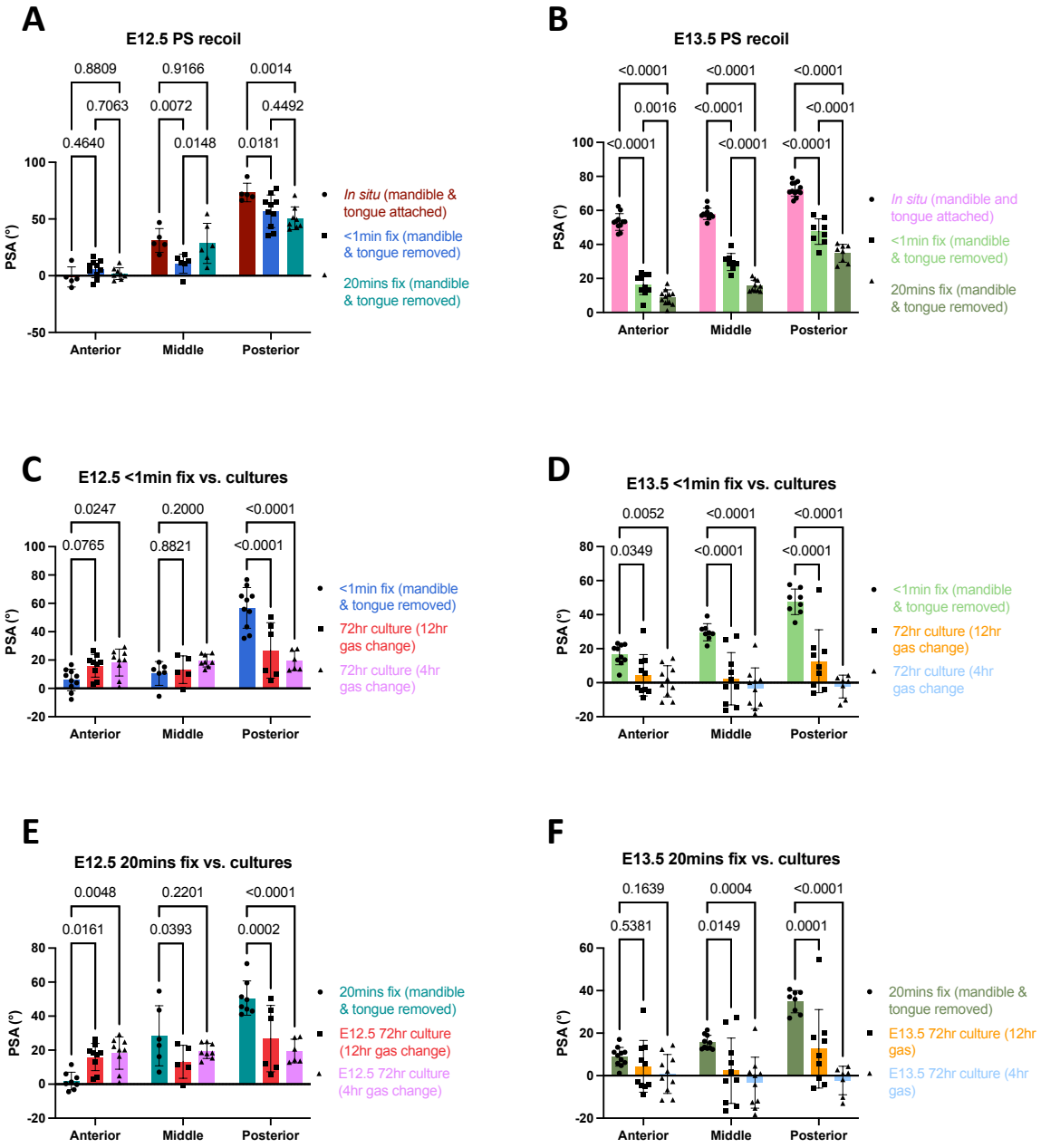

Figure 3.12 PSA measurement comparison across recoil study and *ex vivo* cultured PSs.

PSA measurements in PSs across 3 anatomical regions at E12.5 and E13.5 *in vivo,* in recoil studies, and in *ex vivo* culture at different gas change frequencies. Comparisons titled on each graph. Statistical significance (P values) are displayed on each graph and were calculated by 2-way ANOVA with Tukey's Multiple Comparisons Test (A&B) and Dunnett's Multiple Comparisons Test (C, D, E&F). See tables 3.1 and 3.2 for sample size and SD detail. Error bars = mean with SD.

In summary, it is clear that elevation happens immediately upon explantation. It is conceivable that this might not be any different to the elevation observed after culture.

Therefore, to determine if elevation occurs in culture at all, it was worth comparing the measuring PSAs from these recoil studies with those from cultured explants.

3.2.4.3 E12.5 recoil versus culture PSA comparison

After 72-hours in culture, explants in the <1min fix group showed less-elevated PSs. Comparing the <1min fix group with both E12.5 gas change frequencies (*Figure 3.12C*), there was a statistically significant increase (loss of elevation) in the 4-hour gas change group, and a non-significant increase in the 12-hour gas change group. This is clearly abnormal and represents a clear failure of the culture system to recapitulate palate development.

However, there was a surprising statistically significant increase in PSA between 20mins and culture (*Figure 3.12E*). In this instance, the difference was statistically significant between both groups, and greater than that of the <1min group, suggesting that the PSA increases from *in vivo* to <1min upon t/m removal, decreases between <1min and 20mins in PBS, before increasing again in culture. Again, this is likely due to the assay being designed to investigate elevation, and elevation is not happening in this region at this time in culture.

Furthermore, at E12.5 the posterior PSs elevate statistically significantly between the removal of the t/m and during culture. This represents a 42% decrease in PSA, and so a 42% increase in the extent of elevation in the posterior E12.5 PSs. Contrastingly, there was no significantly significant decrease in PSA in the midpalate between these groups. Moreover, the E12.5 middle and posterior region PSs in the 20-minute fix group showed further statistically significant differences in PSA when compared to culture. There was a statistically significant decrease in PSA (increase in elevation) in the middle-region PSs of the 20mins fix group and the 12-hour gas change group (*Figure 3.12E*). This represents an increase in PSA between the <1min group and 20min fix group, followed by a decrease following culture – the exact opposite trend of that observed in the anterior palate at E12.5. The comparably further-developed posterior PSs at E12.5 again show a statistically significant decrease in PSA, here between 20mins fix and 72hrs culture at both gas change

frequencies. There was no statistically significant difference in PSA between <1min and 20mins fix groups in the posterior PSs, and the same significant difference was observed between both of these stages with the culture groups.

3.2.4.4 Summary of elevation findings from PSA measurements in recoil and culture studies at E12.5.

For easier visualisation of the general trends in PSA change and elevation across these experiments, I re-plotted the mean PSA from each experimental group in a pseudo-chronological order from explantation to the end of the culture period along the x-axis (*Figure 3.13*).

The anterior and middle palate at E12.5 were the only regions that did not follow a general PSA decrease (elevating) trend. This was the case in the anterior as the PSs are horizontally orientated during the early outgrowth. In the middle palate, the PSs appear barely outgrown, and adopt a shape that was not easily measurable by either method of measuring PSA. In the posterior region at E12.5, 42% of all elevation occurs within 20 minutes of t/m removal. Therefore, the posterior palate appears to achieve a third the elevation recorded after 72 hours culture in the first 20 minutes.

The results may suggest that the majority of elevation at E12.5 occurred in culture. However, there are two major caveats to this. Firstly, the E12.5 anterior and posterior PSA is not particularly insightful owing to the relatively early development stage the PSs appear at. Secondly, there could be further elevation after the 20-minute mark assayed for here, and then little to no elevation during culture, and possibly even negative elevation. Nonetheless, these data strongly suggest that E12.5 is simply too early to study the nature of elevation, or to even capture it.

Notably, the horizontally orientated E12.5 PS was of particular interest. This could suggest that the mammalian palate too possesses the default horizontal growth programme by which in all non-mammalian species undergo palatogenesis (Ferguson, 1988). This finding serves as the basis for my third results chapter.

3.2.4.5 E13.5 recoil versus culture PSA comparison

At E13.5, these recoil experiments suggest that PS elevation is entirely due to elastic recoil in the anterior PSs. There was no statistically significant difference between the E13.5 anterior PSAs in the 20mins fix group with both culture groups (*Figure 3.12F*). Interestingly, this demonstrates that complete elevation occurs in the anterior PSs within the elastic recoil window. Therefore, the stored elastic potential energy is sufficient to cause the complete 'flip-up' elevation of the anterior palate immediately before the elevation window at E13.5.

Furthermore, the PSs elevate significantly between <1mins and both culture groups at E13.5 in all regions and was most significant posteriorly. Comparing the <1min fix group with both E13.5 gas change frequencies (*Figure 3.12D*) reveals a similar trend to that observed in the E13.5 recoil study (*Figure 3.12B*). Whilst there was a significant difference between the PSA of all tested groups, the difference was largest posteriorly, intermediate in the middle and least (but still statistically significant) in the anterior.

The PSs also elevated significantly between 20mins fix and both culture groups at E13.5 in all regions, and this was most significant posteriorly. Like the <1min fix group, but to a lesser extent, there was a statistically significant decrease in PSA between 20mins and 72hrs culture in both gas change groups (*Figure 3.12F*). This is consistent with the working model that elastic recoil alone is less sufficient to drive complete elevation more posteriorly along the AP axis, but still accounts for the majority of all PS elevation.

These results suggest that to differing degrees across the anatomical regions, elastic elevation may account for the majority of PS elevation, though not all of it. However, this is limited by the lack of a recorded time point after 20 minutes and prior to culture. It is feasible that by, for example, 1 hour, that elevation may have progressed in the posterior to the same extent as the anterior by 20 minutes.

3.2.4.6 Summary of elevation findings from PSA measurements in recoil and culture studies at E13.5.

If all PSA changes in both the <1min fix and 20mins fix group were considered to be due to elastic recoil only, the extent that elevation was due to elastic recoil/the release of stored elastic potential energy can be investigated, which Walker & Fraser (1956) termed the 'internal shelf force'.

This was done by calculating the difference between the mean *in vivo* PSA and mean 20mins fix PSA, which is presented as a percentage of the overall elevation. Overall elevation is given as the difference between the mean *in vivo* PSA and the mean +72hrs culture (4hr gas change), the latter previously demonstrated to give an elevation angle not statistically significantly different from that of *in vivo* E14.5 elevated shelves in all anatomical regions tested. This enables a simple yet effective interrogation of the established view of anterior 'flip-up' (i.e., elastic recoil) and posterior remodelling (i.e., elevation by cell movement, proliferation, shape change, or other cellular behaviours).

Up to 20-minutes post tongue/mandible (t/m) removal, elastic recoil accounts for at least 86% of elevation anteriorly, 69% in the midpalate, and 50% of elevation posteriorly. This demonstrates that the majority of PS elevation could be due to elastic recoil along the entire palate. However, what is perhaps more useful to consider is the differences between these regions. This suggests that the anterior palate stores a greater elastic potential energy prior to the removal of the tongue and mandible, hence it can elevate to a greater extent. This elastic potential may decrease posteriorly along the PSs, but still contributes to over half of all elevation in these regions. However, there could also be a greater viscoelasticity dampening the elasticity measured up to 20 minutes. Therefore, because of the lack of a further time point, it is not possible to fully separate elastic and other cellular behaviours which may be driving elevation in my results. Thus, the remaining elevation at this point could be due remaining elastic release, slowed by dampening, or a variety of other processes, including de novo elastic contraction due to cell migration or cell shape change, or non-elastic growth/tissue remodelling.

This quantification of elevation across the AP axis of the PSs gives an insight into the nature of elevation regionally and is directly comparable to previous (despite typically being qualitative) reports on PS elevation. This was performed on a larger sample number at E13.5, immediately prior to the elevation event occurring.

Finally, the revelation that the majority of PS elevation occurs immediately upon removal of the t/m, and not during culture has implications for the use of rolling culture to investigate PS elevation going forwards. Ultimately, it suggests that rolling culture is not an appropriate system for the study of palatal shelf elevation.

Table 3.1 Mean, SD and sample number (n) of PSA across each tested group in all anatomical regions at E13.5

E13.5	*In vivo*			<1min fix			20mins fix			+72hrs culture (12hr gas change)			+72hrs culture (4hr gas change)		
	Mean	SD	N	Mean	SD	N	Mean	SD	N	Mean	SD	N	Mean	SD	N
Anterior	53.233	4.906	11	16.58	6.014	10	8.909	4.408	11	4.37	12.167	10	0.809	9.162	10
Middle	57.999	3.336	11	29.683	5.025	8	15.612	3.381	10	2.314	15.378	10	-3.278	12.002	10
Posterior	72.372	4.043	12	47.559	7.497	8	34.791	5.219	8	12.617	18.475	9	-2.258	6.697	7

Table 3.2 Mean, SD and sample number (n) of PSA across each group tested in all anatomical regions at E12.5

E12.5	*In vivo*			<1min fix			20mins fix			+72hrs culture (12hr gas change)			+72hrs culture (4hr gas change)		
	Mean	SD	N	Mean	SD	N	Mean	SD	N	Mean	SD	N	Mean	SD	N
Anterior	-1.071	8.904	5	5.919	7.606	10	1.865	5.175	8	15.965	7.979	9	18.269	9.499	9
Middle	31.058	10.462	5	10.544	8.369	6	28.476	17.661	6	13.184	9.716	5	19.598	4.469	8
Posterior	73.388	8.148	5	56.828	14.366	10	50.646	10.078	8	26.794	19.519	6	19.485	6.97	6

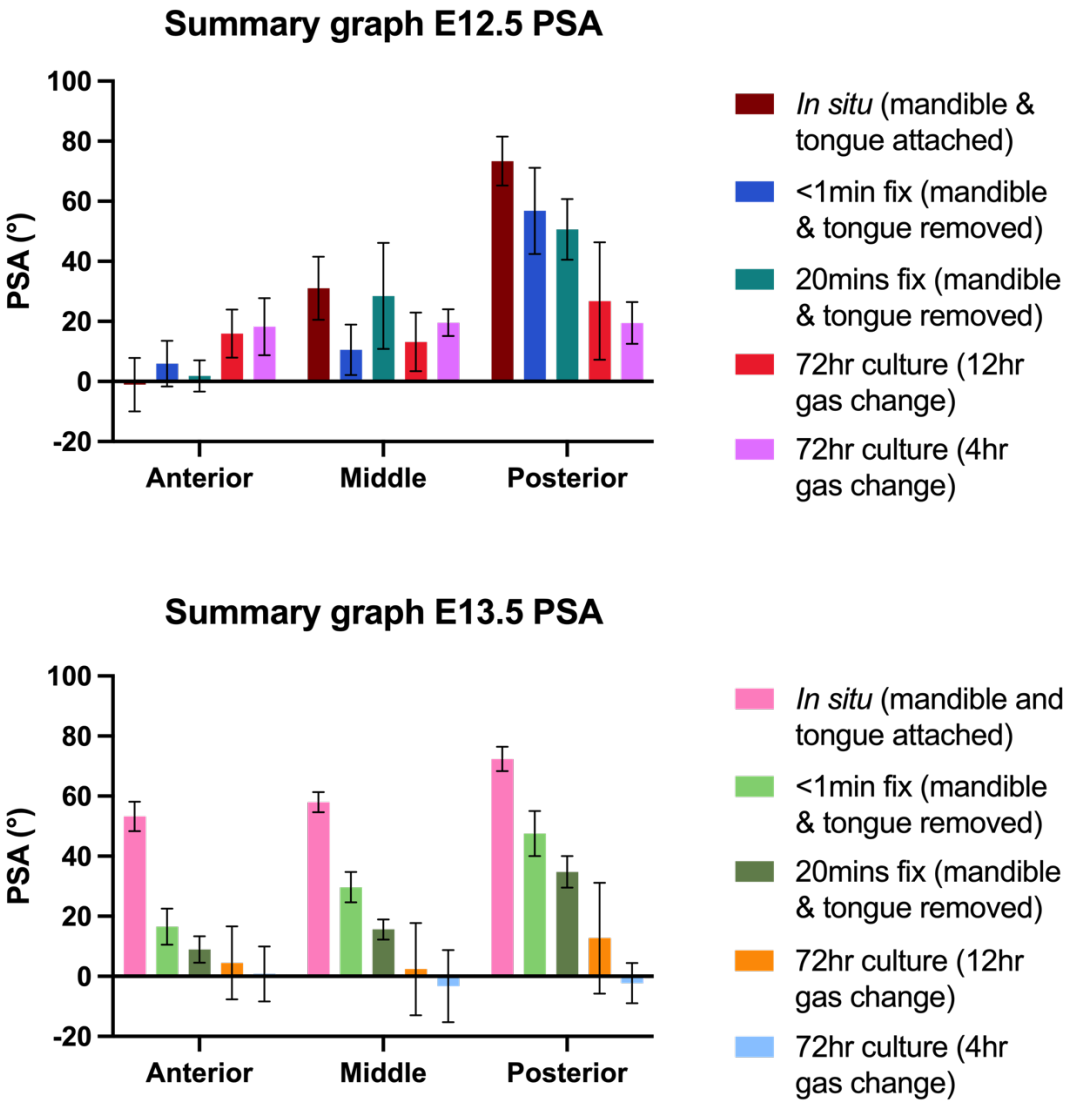

Figure 3.13 PSA Summary graphs

Summary graphs of PSA at E12.5 (A) and E13.5 (B). Error bars = mean with SD.

3.3 Discussion

In this results chapter, recoil experiments and subsequent PSA analysis revealed that elastic recoil immediately on removal of the tongue and mandible (t/m) is sufficient to drive 100% of elevation in the anterior, and 50% of elevation in the posterior at E13.5 i.e., immediately prior to elevation. This finding has informed the subsequent direction of the project. Although I quantified it, it is not surprising that elastic recoil is sufficient to drive

complete elevation, at least anteriorly, given classical descriptions of the rapidity of shelf movement on tongue depression (Polzl, 1905; Ferguson, 1978; Walker and Fraser, 1956).

Furthermore, the identification that posterior PS elevation can be driven to at least 50% completion by elastic recoil alone highlight that it is likely not a remodelling event alone as classically described, defined as ventral regression of the tip and medial bulging of the medial hinge (Yu and Ornitz, 2011). This was not highlighted in the recent preprint from Goering et al., (2022), which suggests elevation progresses entirely by a remodelling event driven by actomyosin contraction and proliferation. Therefore, there may be two different mechanism driving the remaining 50% of elevation, the first via some cellular rearrangement and proliferation, and the second via viscoelasticity which was not captured in my experiments due to a lack of later timepoint.

The former is ultimately the traditional theory and is reported throughout the literature (Goering et al., 2022; Brock et al., 2016; Brinkley and Bookstein, 1986). However, in the absence of compelling lineage labelling and/or genetic perturbation specifically restricted to the PS mesenchyme, this evidence remains entirely circumstantial. The latter suggests that the shape and changing position of the tongue permits a viscoelastic remodelling of the posterior PSs. This could explain the conformational shape changes between the tongue and the posterior PSs that are referred as the two remodelling about one another (Yu and Ornitz, 2011; Yonemitsu et al., 2020). Furthermore, viscoelastic posterior PSs may dampen the elastic response to tongue removal, which could suggest that I failed to capture the total release of viscoelasticity at 20 mins fixation post-t/m removal. Hence, any residual elastic elevation could be captured at a later time point. Plus, although it has now been demonstrated that glycosaminoglycans such as hyaluronic acid (HA) are necessary for *in vivo* PS elevation (but not intrinsically to the PSs) and rather PS expansion to ensure midline fusion (Lan et al., 2019), their heterogenous distribution along the A – P axis of the PSs may affect the speed at which the elasticity is converted into the internal shelf force. The anterior PSs contain more HA than the posterior PSs (Ferguson, 1988; Brinkley and Morris-Wiman, 1987a) and, although not the main driver of elevation, may exert an increased turgor pressure in the anterior, increasing the speed of elastic recoil on t/m removal.

In vivo, the tongue is free to move anteriorly, but anchored to the mandible (in adulthood by the genioglossus muscle) posteriorly (Parada and Chai, 2015). The early, at this stage, non-muscular attachment to the tongue may delay posterior elevation *in vivo*, with the geometry of the shelf-tongue apposition forcing a higher angle and the tongue not getting out of the way until after anterior elevation. The direction of elevation onset remains unresolved, but this suggestion is the opposite to that posed most recently (Goering et al., 2022). Again, the authors do not consider elasticity, nor the material properties of the PSs and, from my explantation and recoil assays, it is at least clear that elastic elevation occurs anterior first. The situation is more complicated *in vivo* owing to the changing geometry and PS communication with the tongue, which is more fixed in place posteriorly. Unfortunately, resolution to this question will require the so-far elusive *in vivo* live imaging of E13.5 embryos *in utero*. How elasticity may be stored in the PSs, however, is explored in chapter 6.

The other key finding from this results chapter is the lack of elevation during *ex vivo* rolling culture. This could seriously call into question the findings of the relatively large number of papers having used this technique. This is compounded by my finding that the PS growth is heavily stunted at best during *ex vivo* rolling culture, which is detailed in chapter 4. The results described in this chapter and those of results chapter 4 are related, and as such the implication of the unsuitability of *ex vivo* rolling culture are explored in detail in the discussion of the next chapter.

4. Morphometric analyses of PS growth during *ex vivo* rolling culture

4.1 Introduction

In the previous results chapter, I demonstrated that PS elevation does not occur during *ex vivo* rolling culture, and that the majority of elevation instead appears immediately on removal of the t/m via elastic recoil. However, in my E13.5 maxillary explant cultures, 50% of maxillary explants displayed fused palatal shelves. Palatal gap closure has previously been used as a metric of PS elevation (Brinkley et al., 1975; Lewis et al., 1980), but my results suggest that elevation is not occurring during culture.

Given that the PSs are said to grow in this system (Abbott, 2019; Shiota et al., 1990; Snyder-Warwick et al., 2010), I hypothesised that PS growth in this system might be responsible for bringing the shelves together, and this had instead been mistaken for elevation. To my surprise, it appeared there may have been only two attempts to study PS growth *ex vivo* previously. These were from the same group using Brinkley's 'advanced' incubation system as opposed to traditional rolling culture. Cross sectional area was measured by tracing around the basal lamina of the PS mesenchyme and connecting the medial and lateral aspects with a horizontal line. In the first of these investigations, they noted no statistically significant expansion of shelf area, but noted some non-significant expansion in the midpalate, concluding that shelf expansion is not a required part of PS elevation (Brinkley and Vickerman, 1982). My results suggest that the shelves might have elevated immediately on explantation. Therefore, it could be that the authors may not have captured elevation. However, the same group would then report that, *in vivo*, measuring cross-sectional area shows that the shelves increase in size in both anterior and posterior palate by up to 70% (Brinkley and Bookstein, 1986), which was not recapitulated by the culture system. Interestingly, this time in their cross-sectional area analyses in cultured explants they noted a statistically significant increase in shelf area reportedly concomitant with elevation in the anterior only. This was after 6 hours in culture at a stage approximately 30 hours before *in vivo* elevation, which I

assume to be sometime between E12.5 and E13.5. It appears the authors used explanted tissue with the tongue removed as their 0 hours (unelevated) stage, so again the reported expansion was unlikely to have occurred during elevation.

This raised the consideration that, if growth were not occurring (though the data were not previously available to suggest this), and elevation does not occur in culture, then how might the PSs approximate? Therefore, I carried out a morphometric analysis of PS growth (or, as my results will show, 'shape change' given the apparent lack of the former) on both *in vivo* tissue, and on the PSs of maxillary explants cultured at E12.5 and E13.5 for 72 hours, to produce the first detailed characterisation of growth in this system. The results below will demonstrate that growth is dramatically less in this system, with shrinkage occurring in some regions, and that the PSs are brought together by the progressive non-physiological deformation of the maxillary explants following recoil and during culture.

4.2 Results

4.2.1 Morphometric analyses reveal that PS growth is modest and inconsistent in the rolling culture of E12.5 explants

A masters project student in the Green lab, Dr. Catherine Liu, carried out a preliminary study under my day-to-day supervision and generated a preliminary dataset on palatal growth using landmarks and standard oral view images (*Figure 4.1*). Reliable topographical, or surface paired landmarks were identified from the oral view and lines were drawn between them (*Figure 4.1A&B*). These were measured in the same samples before and after 72-hours in rolling culture with 12-hour gas changes. In the samples fixed before culture, a steady increase in the distance between the paired landmarks was observed at each embryonic day stage between E12.5 and E15.5 (*Figure 4.1C*). To our surprise, not only did growth appear to be entirely arrested in cultured explants, but there was a shrinkage across all landmarks (n=17 maxillary explants) (*Figure 4.1D*). A reduction in mediolateral growth to a negligible rate had been reported previously in static PS culture (Economou et al., 2012). We speculated that this could be due to some

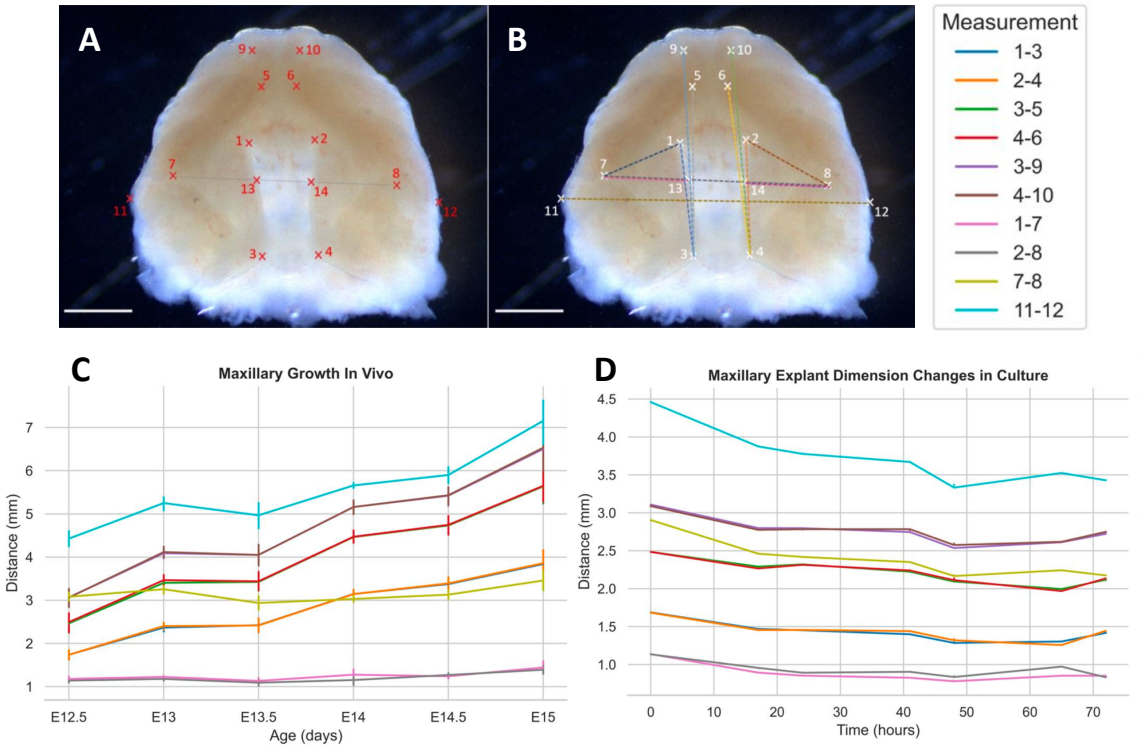

Figure 4.1 Growth measurements in cultured maxillary explants from surface landmarks

A) Paired surface landmarks on E13.5 maxillary explant. B) Measurement lines. C) Growth *in vivo* D) Growth *ex vivo*. Scale bars: 1mm. Adapted from C.Liu, MSc Thesis, 2022.

sort of 'balling-up' or 'crumpling' process during culture, therefore obscuring any true growth, but uncertainty

about this highlighted the inadequacies, mentioned previously, of assessing the 3D elevation event from the 2D oral view.

Therefore, following this observation, to better understand palatal shelf growth or lack thereof, I conducted morphometric measurements on frontally sectioned tissue on both fresh fixed embryos and cultured maxillary explants that had been used for the elevation analysis described in the previous chapter.

4.2.1.1 Defining metrics for palatal shelf growth

In order to measure growth, a reproducible technique enabling measurements at E12.5, E13.5 (pre-elevation) and E14.5 (post elevation) was required. Previous studies measuring the length of *in vivo* PSs have relied on drawing an intersect in the PS tip region to an arbitrary point on the superior medial surface of the PS and drawing a tangent from

the centre of this line to the tip of the PS (Yonemitsu et al., 2020). Whilst it is adequate to use the PS tip to measure elevation angles, when considering palatal growth, I wished to get a more complete picture of growth of the entire structure. Therefore, to encompass both tip and hinge regions, I used a simple method to measure the PS length, width, area, and perimeter in frontal sections. It was important to include all 4 to give a better overall and thorough measure of PS dimensions, so as not to bias the measurements towards any potential error introduced in one of the metrics. Also important was the selection of reliable, unambiguous landmarks. I chose the lateral side of the molar tooth bud neck which anchors the other measurements in both mediolateral and anterior-posterior dimensions in middle and posterior regions, and the epithelial invagination in anterior regions.

These were defined as follows:

1. **PS length.** A circle centred on the proximal point of the AP landmark (epithelial invagination for anterior, and molar tooth bud for middle and posterior) was expanded until the arc touches the last part of PS tissue medially. This was designated the tip. Then, the radius of this circle is taken, giving the PS length (*Figure 4.2A*).

2. **PS width.** A straight line was drawn from the proximal point of the AP landmark (i.e., the centre of the previously constructed circle) to the end of the superior landmark: anteriorly, this is the superior aspect of the PS in line with the nasal septum, and in the middle and posterior regions this is the corner of the roof of the nasal cavity (*Figure 4.2B*).

3. **PS area.** Using the 'PS width' line, the remaining outline of the PS was manually drawn around and area is calculated (*Figure 4.2C*).

4. **PS perimeter.** This is determined by calculating the perimeter of the outline of the shape used to determine PS area (*Figure 4.2D*).

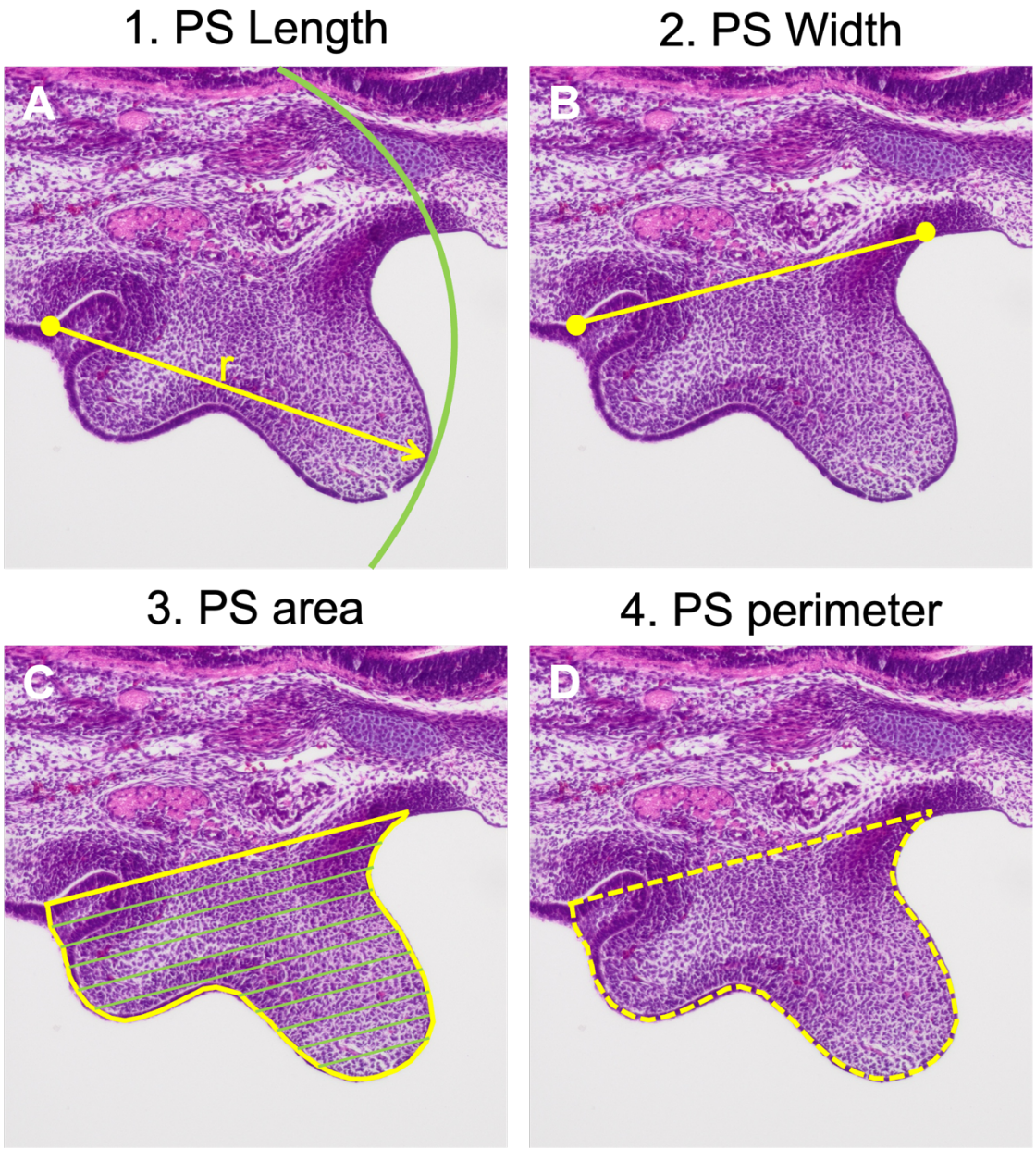

Figure 4.2 Schematic demonstrating how morphometric measurements were made on PSs

A) PS Length by circle radius. B) PS Width by landmark boundary. C) PS area by boundary line and tracing. D) Perimeter by outline.

4.2.1.2 Normal Palatal Shelf growth

A steady increase in growth across embryonic day stages was observed from measurements made on *in vivo* PSs (*Figure 4.3A, B, C & D*).

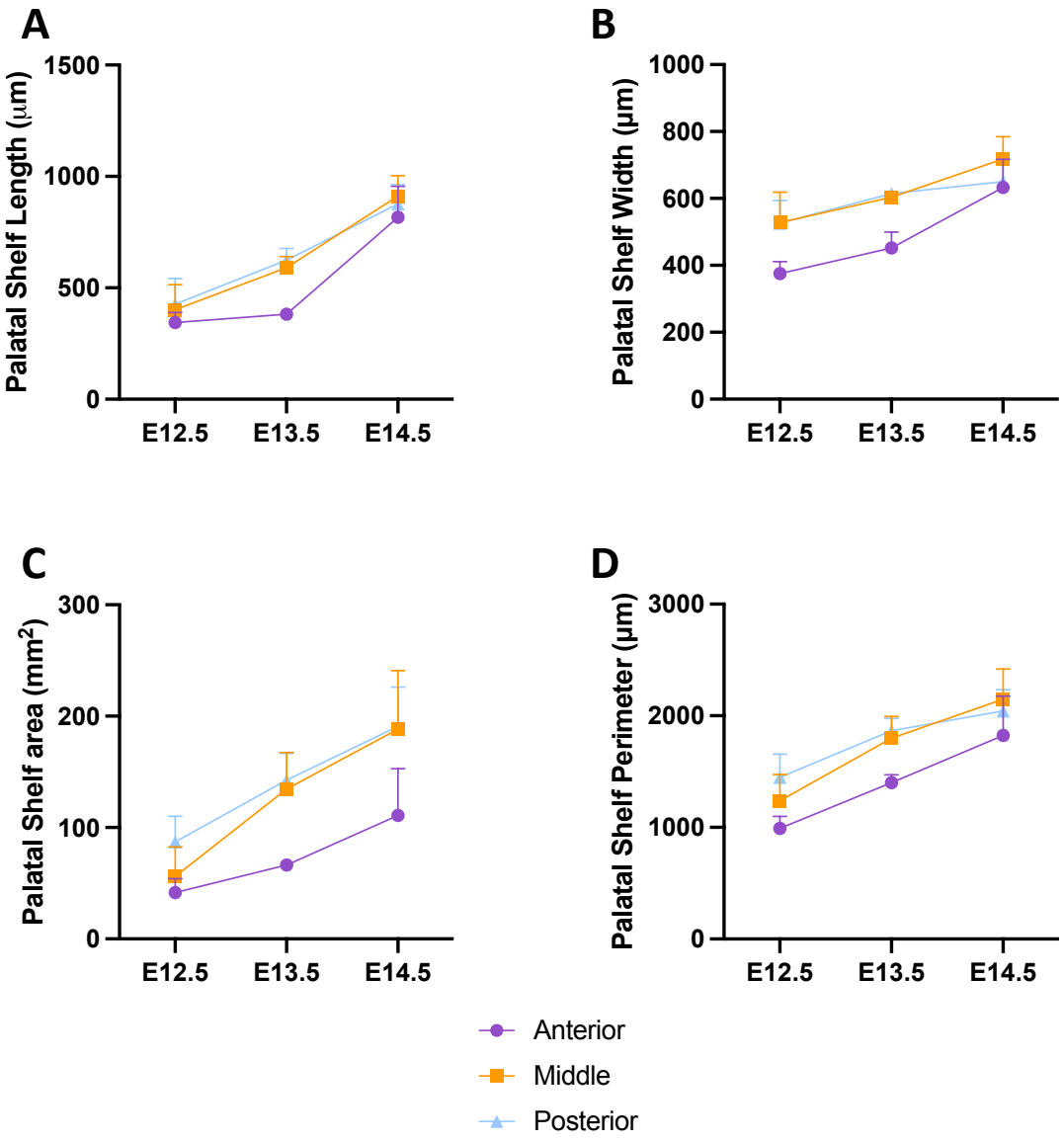

Figure 4.3 PSs growth as demonstrated by morphometric measurements in frontally sectioned fixed tissue.

In vivo, these measurements show that there is a steady increase in PS length (A), width (B), area (C) and perimeter (D). Sample size: n=5 at each stage from 3 independent litters. Error bars = mean with SD.

Notably, there appeared to be slight lag in shelf lengthening in the anterior between E12.5 and E13.5 (*Figure 4.3A*). Plus, overall length and area roughly double from E12.5 to E14.5, corresponding to a roughly 40% increase per day. PS width and perimeter increase more slowly as might be expected. Of course, it is unsurprising that growth was observed across these stages, and these measurements merely serve as a validation of the method.

4.2.1.3 At E12.5 there was statistically significant but modest growth in the anterior by all metrics, and in PS area in the middle region

In order to determine if E12.5 maxillary explant cultures exhibited PS growth during culture, I measured and compared the morphometrics described previously (*Figure 4.2*) between E12.5 *in vivo* PSs, and E12.5 PSs cultured for 72-hours in both gas change groups.

Between E12.5 *in vivo* and culture groups, there was a statistically significant increase in PS length in the 4hr gas change group in the anterior (*Figure 4.4A*). While mean increases in PS length were recorded between *in vivo* PS and cultured PSs in both gas change groups in all anatomical regions (*Figure 4.4A-A''*) these were not to statistical significance.

There was also a statistically significant increase in PS width in the 4hr gas change group in the anterior (*Figure 4.4B*). However, excluding this observation, there was a non-statistically significant decrease in PS width between E12.5 *in vivo* and both culture groups in all anatomical regions (*Figure 4.4B-B''*).

Plus, there was a statistically significant increase in PS area in the 4hr gas change group in the anterior (*Figure 4.4B*), and in both gas change groups in the middle (*Figure. 4.C'*) PSs. Similar to the PS width decreases, there was also a non-statistically significant decrease in PS are between E12.5 *in vivo* and both culture groups in the posterior region only (*Figure 4.4C*).

There was a statistically significant increase in PS perimeter in the 4hr gas change group in the anterior (*Figure 4.4D*). Here, there was no statistically significant difference between *in vivo* PSs and PSs in either culture group in the middle region, and a non-statistically significant decrease in the posterior PSs.

To assess whether the gas-change frequency, and therefore oxygen availability, impacted PS growth in culture, I also compared all four morphometric measures between the 4-hour and 12-hour gas change 72-hour cultures groups.

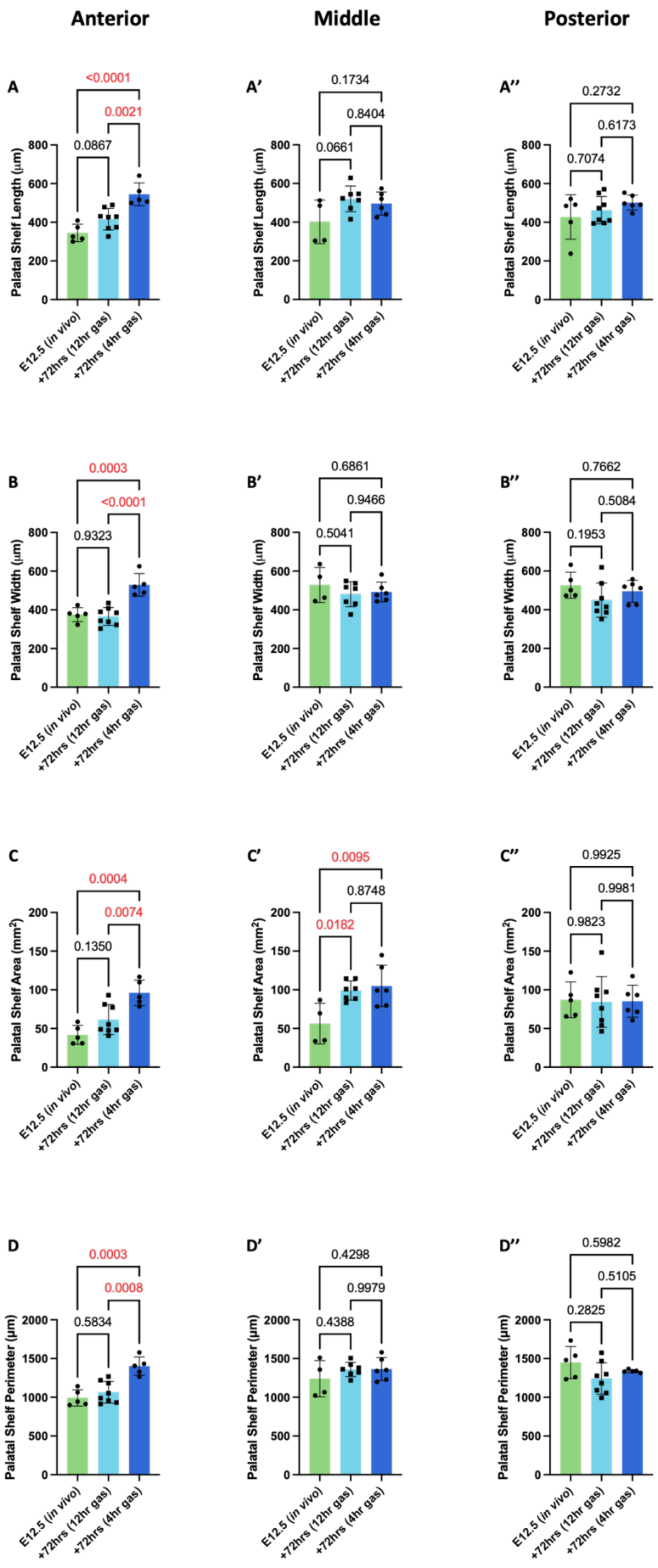
Anterior
Middle
Posterior
A
A'
A''
Palatal Shelf Length (µm)
<0.0001
0.0021
0.0867
0.1734
0.8404
0.0661
0.2732
0.6173
0.7074
B
B'
B''
Palatal Shelf Width (µm)
0.0003
<0.0001
0.9323
0.6861
0.9466
0.5041
0.7662
0.5084
0.1953
C
C'
C''
Palatal Shelf Area (mm²)
0.0004
0.0074
0.1350
0.0095
0.8748
0.0182
0.9925
0.9981
0.9823
D
D'
D''
Palatal Shelf Perimeter (µm)
0.0003
0.0008
0.5834
0.4298
0.9979
0.4388
0.5982
0.5105
0.2825
E12.5 (in vivo)
+72hrs (12hr gas)
+72hrs (4hr gas)

Figure 4.4 Comparisons of PS morphometrics between E12.5 *in vivo* and *ex vivo* cultured PSs, and between both gas change frequency groups

Measurements made to determine PS length (A-A''), width (B-B''), area (C-C'') and perimeter (D-D''). Statistical significance (P values) is shown on graphs and coloured in red where statistically significant ($P < 0.05$). Statistical significance was determined by one way ANOVA with Tukey's multiple comparisons test (A – D') and Brown-Forsythe & Welch's ANOVA tests with Dunnett's T3 multiple comparisons test (D'').

The anterior PSs were larger to statistical significance after 72-hours in culture in all four morphometric assays in the 4hr gas change group vs. the 12hr gas change group (Fig 4.4A, D, G&J). However, statistically significant differences were not observed in any other measurements in middle or posterior regions. Further, measurements in the 4-hour gas change PSs were larger in all measurements excluding PS length in the midpalate region, although none of these differences were to statistical significance.

Hence, an increased gas change frequency may only increase rate of growth in the PSs in the anterior region at E12.5.

4.2.1.4 PS growth is dramatically less in E12.5 *ex vivo* rolling culture than *in vivo* growth at comparable embryonic day stages.

While there was minor PS growth in culture in some regions and some culture conditions over 72 hours, this was quite apparently much less than growth of the same tissues *in vivo*. This is most clearly shown by plotting the values on a common time scale (*Figure. 4.5*).

On first glance, PS growth after 72-hours in culture seems to correspond to about 24-hours growth *in vivo* via PS length and area (*Figure 4.5A-A'', C-C'*). If this were consistently true then the *ex vivo* rolling culture of maxillary explants could be considered a faithful but slow system. However, there are substantial discrepancies, and even shrinkages across several regions (*Figure 4.5B-B'', C''&D''*). This makes the culture problematic as a model, both for PS elevation as demonstrated previously, and for PS growth at E12.5.

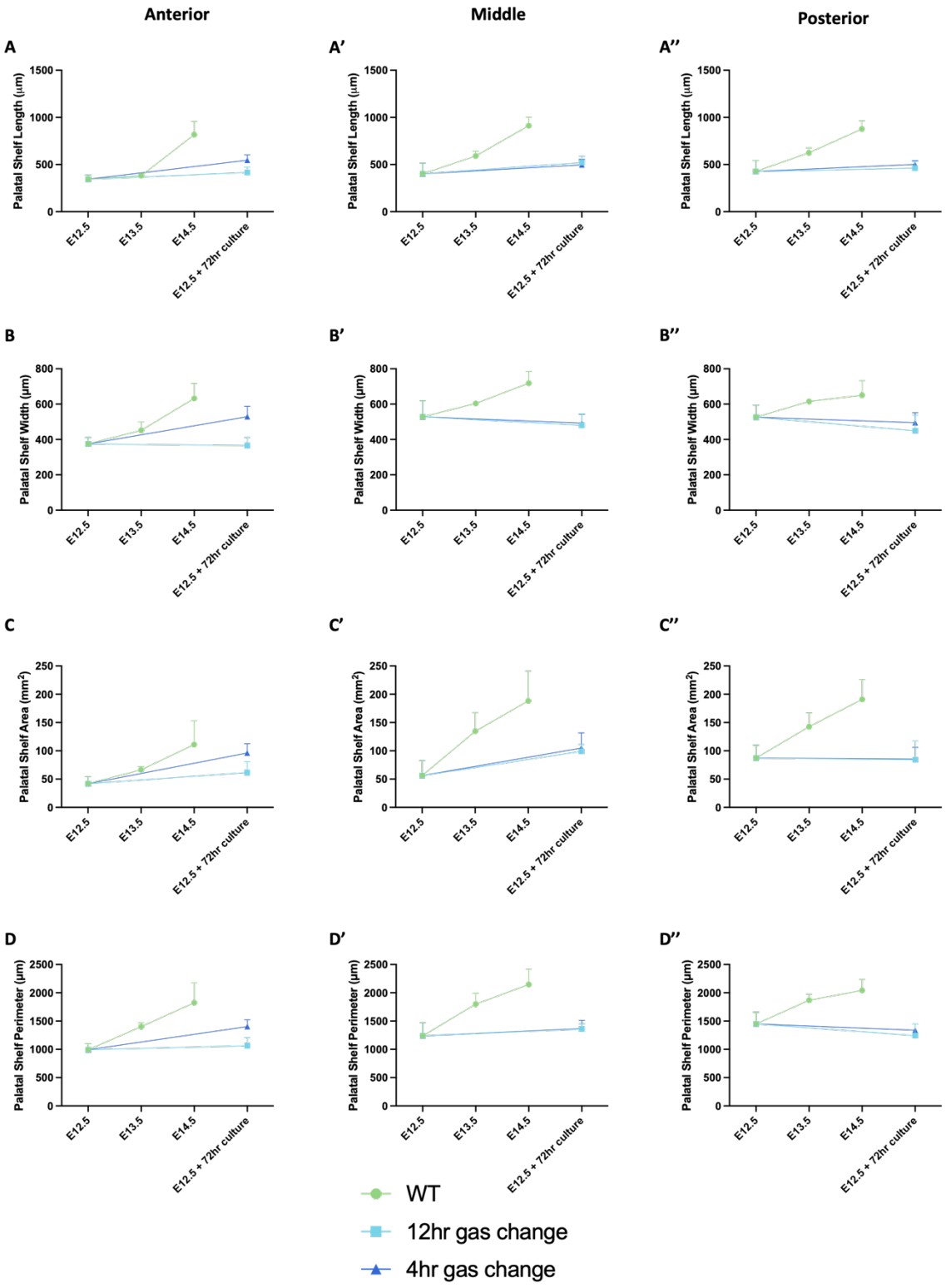

Figure 4.5 Morphometrics as a measurement of PS growth comparison between E12.5 *in vivo* and *ex vivo* culture groups over comparable embryonic day stages/days in culture.

Measurements made to determine PS length (A-A''), width (B-B''), area (C-C'') and perimeter (D-D''). Error bars = mean with SD.

Furthermore, these data suggest that, at least in the anterior PSs, increasing gas change frequency does appear to improve growth. Nonetheless, this growth appears to be very slight, with the PSs seemingly shrinking in some regions as much as they may be growing in others. It is also important to note that, from my data, it is not possible to determine whether the PSs are growing up to the 72-hour mark, or if growth reaches a maximum limit at some point earlier than this.

4.2.2 Morphometric analyses reveal that PS growth is modest and inconsistent in the rolling culture of E13.5 explants

4.2.2.1 At E13.5 there was more statistically significant PS shrinkage during culture than growth

The above analyses at E12.5 revealed serious shortcomings of the rolling culture system for PS growth analysis. Later-stage embryos could have been more robust for investigating morphogenesis than younger ones, thus there was some hope that E13.5 maxillary explants might do better in culture. Therefore, the same morphometric analyses performed at E12.5 were applied to E13.5 tissue and described in the same manner below.

There was a statistically significant increase in PS length in only the anterior region of explants cultured at E13.5, and this was apparent in both gas change groups (*Figure 4.6A*). There was no statistically significant increase in the other regions, and even a slight (statistically insignificant) decrease in PS length in the 12-hour gas change group in the posterior region. This is consistent with either explant shrinkage, or the previously suggested 'balling-up'.

There was a statistically significant shrinkage in PS width after 72-hours in culture in the 4-hour gas change group in the middle region (*Figure 4.6B'*), and in the 12-hour gas change group in posterior regions (*Figure 4.6B''*). There was also shrinkage in the anterior region across both gas change groups, but neither were statistically significant (*Figure 4.6B*).

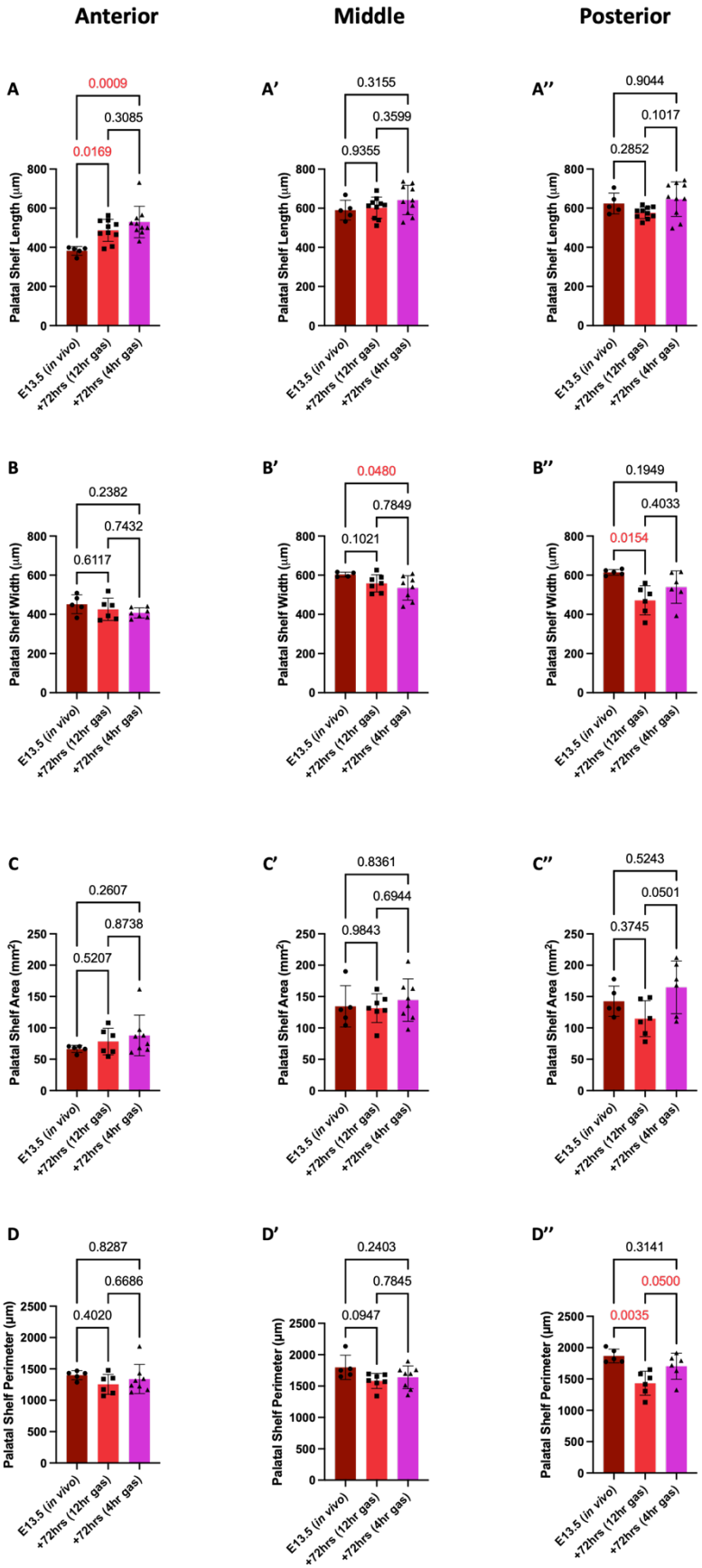
Anterior
Middle
Posterior
A
A'
A''
0.0009
0.3085
0.0169
0.3155
0.3599
0.9355
0.9044
0.1017
0.2852
Palatal Shelf Length (μm)
B
B'
B''
0.2382
0.7432
0.6117
0.0480
0.7849
0.1021
0.1949
0.4033
0.0154
Palatal Shelf Width (μm)
C
C'
C''
0.2607
0.8738
0.5207
0.8361
0.6944
0.9843
0.5243
0.0501
0.3745
Palatal Shelf Area (mm²)
D
D'
D''
0.8287
0.6686
0.4020
0.2403
0.7845
0.0947
0.3141
0.0500
0.0035
Palatal Shelf Perimeter (μm)
E13.5 (in vivo)
+72hrs (12hr gas)
+72hrs (4hr gas)

Figure 4.6 Comparisons of PS morphometrics between E13.5 *in vivo* and *ex vivo* cultured PSs, and between both gas change frequency groups

Measurements made to determine PS length (A-A''), width (B-B''), area (C-C'') and perimeter (D-D''). Statistical significance (P values) is shown on graphs and coloured in red where statistically significant ($P < 0.05$). Statistical significance was determined by one way ANOVA with Tukey's multiple comparisons test (A-A', B, C'-D'') and Brown-Forsythe & Welch's ANOVA tests with Dunnett's T3 multiple comparisons test (A'', B'-C).

Across all anatomical regions in both gas change groups, there is no statistically significant difference in PS area between *in vivo* PSs and either culture group (*Figure 4.6C-C''*). However, in both the middle and posterior regions during 72-hour culture at the lower gas change frequency, there was a statistically insignificant decrease in PS area (*Figure 4.6C-C'*). This was not the case at E12.5.

Plus, there is a statistically significant decrease in PS perimeter in the posterior region in the 12-hour gas change group. PS perimeter shrinkage was also observed in anterior and posterior regions between E13.5 *in vivo* PSs and both gas change groups, albeit not to statistical significance. Similar to the *ex vivo* rolling culture of E12.5 explants, the posterior region appears to fare particularly poorly at E13.5 too.

As before, I also compared all four morphometric measures between the 4-hour and 12-hour gas change 72-hour cultures groups to assess whether the gas-change frequency, and therefore oxygen availability, impacted PS growth in culture. There was a statistically significant increase in posterior perimeter in the 4-hour gas change group over the 12-hour gas change group (4.6D'') However, this was in the context of posterior PS shrinkage in both gas regimes. Otherwise, there were no significant differences or even consistent trends in growth metrics between the different gas change frequencies in the anterior or middle regions by any measure. PSs in the 4-hour gas change group were less shrunken in all regions and metrics, excluding the middle region PS width, which could suggest that the higher gas change frequency merely reduced or delayed overall shrinkage in most regions, rather than promoted growth.

4.2.2.2 PS growth is especially poor in E13.5 *ex vivo* rolling culture compared to *in vivo* growth

As in the E12.5 dataset, direct comparison of *in vivo* growth at E13.5 with growth in culture highlights the lack of growth in the latter (*Figure 4.7*). Overall, *ex vivo* maxillary explant cultures from E13.5 do an even poorer job at recapitulating *in vivo* growth than those cultured from E12.5 embryos; there is more shrinkage than growth, and once again the posterior region is most affected by shrinkage. Here, higher gas exchange frequency had minimal effects.

4.2.3 Greater PS length is not correlated with PS fusion in culture.

As shown in the previous chapter, most PS elevation occurs during dissection prior to culture; as shown above, PS growth during culture is minimal, zero or negative. Despite this, 50% of explants cultured at E13.5 fused. Since there was no correlation between PSA and fusion in culture, I asked if differences in growth were associated with fusion in culture. I compared PS length in the fused vs. not fused E13.5 cultured explants in each anatomical region under each gas change frequency regime (*Figure 4.8*).

In all anatomical regions, and across both gas change frequencies, there was no statistically significant difference is PS length, further suggesting that the PSs may approximate during *ex vivo* rolling culture by something other than growth.

4.2.4 PSs are brought together, and subsequently fuse, in rolling culture due to an abnormal narrowing of the oronasal cavity

Despite the abnormalities in maxillary explant cultures, the PSs still come together and fuse 50% of the time, raising the question: how? Given that the PSs do not fully elevate, do not grow, and instead shrink, I hypothesised that the PSs must be brought together in this system as a result of the 'balling-up' or 'crumpling' observed during culture. Such a general balling-up of the explant could bring the PSs towards one another by narrowing the whole maxilla during culture without PS growth, and this could be indicated by the shrinkages observed during culture, in particular at E13.5.

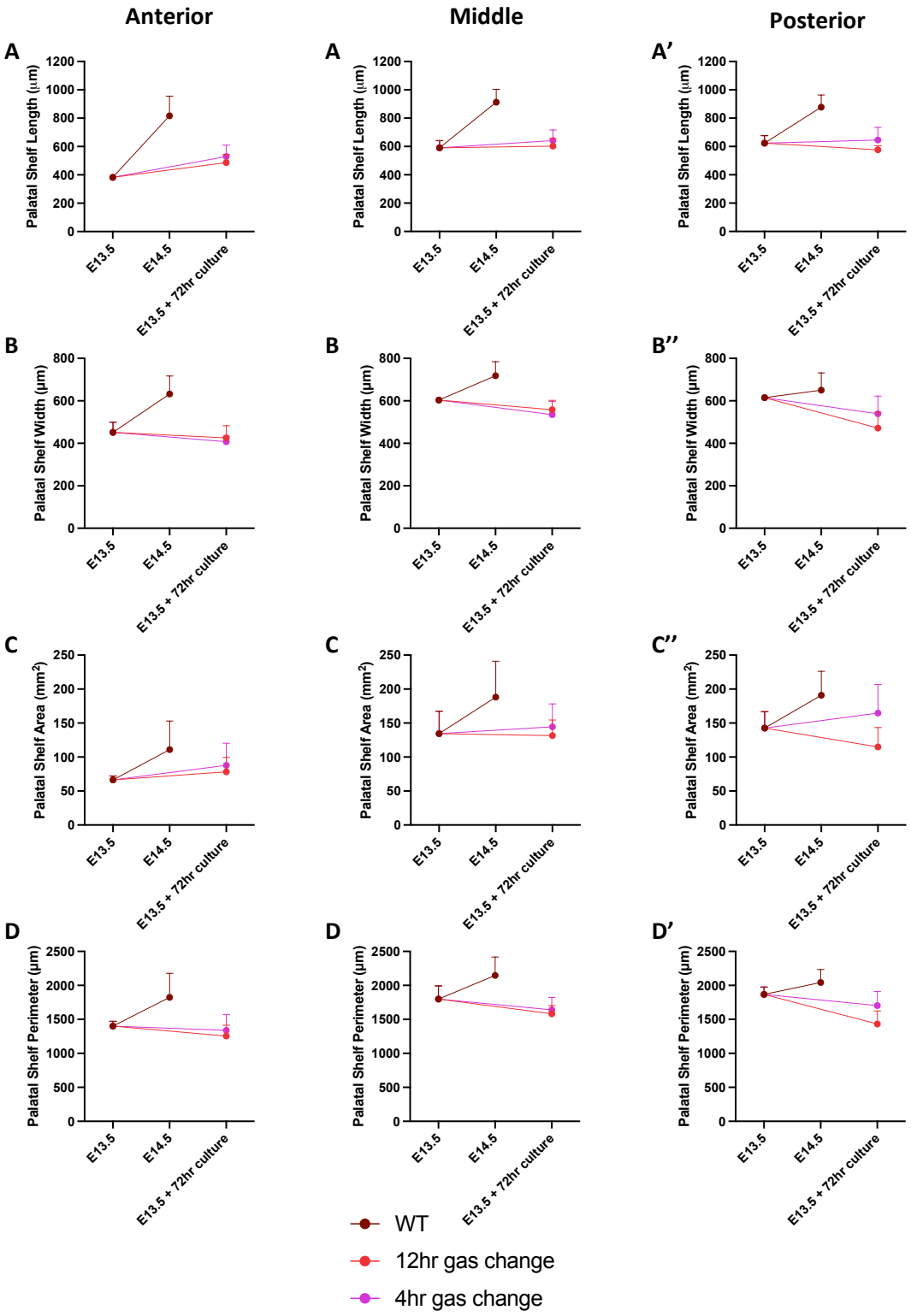

Figure 4.7 Morphometrics as a measurement of PS growth comparison between E13.5 *in vivo* and *ex vivo* culture groups over comparable embryonic day stages/days in culture.

Measurements made to determine PS length (A-A''), width (B-B''), area (C-C'') and perimeter (D-D''). Error bars = mean with SD.

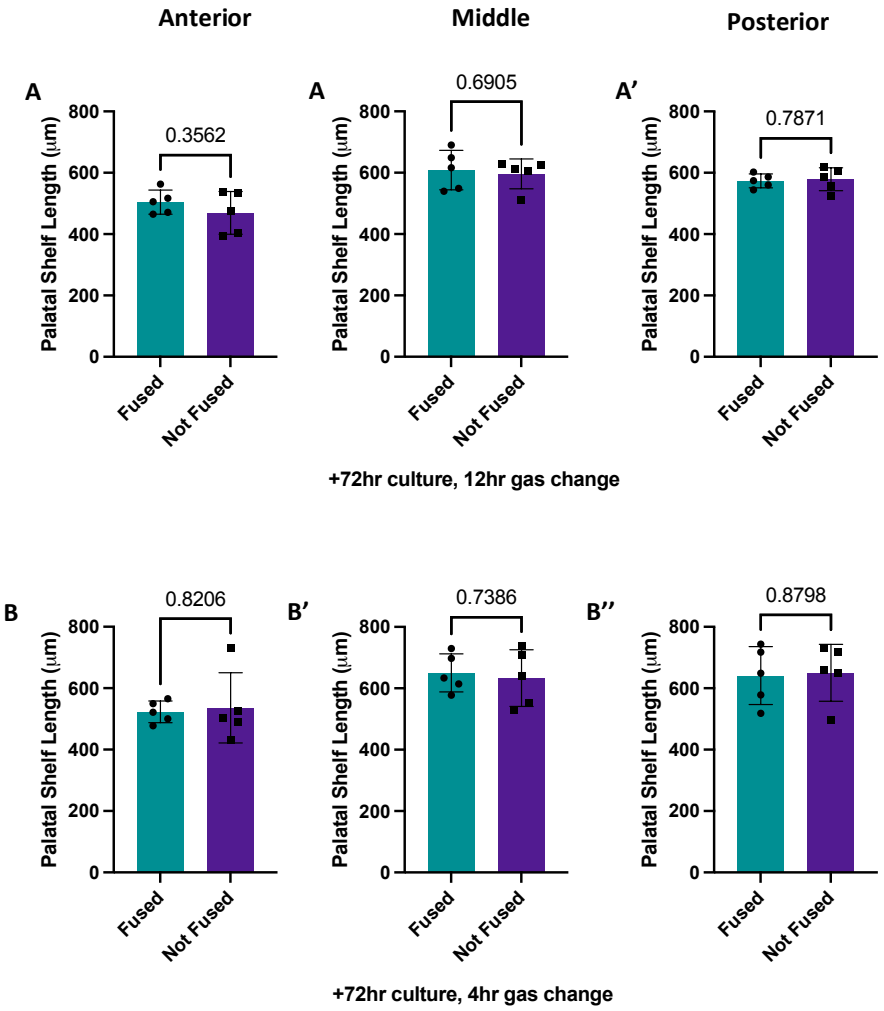

Figure 4.8 PS length comparison between fused and not-fused E13.5 culture explants at both gas change groups.

PS length measured both 12hr gas change group (A-A'') and 4hr gas change group (B-B''). Statistical significance (P values) was determined by two-tailed unpaired t-test (A, A'', B', B''); unpaired t-test with Welch's correction (B) and Mann-Whitney test (A'). Error bars = mean with SD.

To investigate this, I measured the width of the nasal cavity just dorsal to the PSs, the length of a horizontal line immediately below the superior landmark in each anatomical region (nasal septum/epithelium in anterior and middle, and the cranial base posteriorly). I henceforth refer to this space as the 'inter-hinge gap.' (*Figure 4.8A*).

In all three anatomical regions during normal development *in vivo*, there was no statistically significant change in nasal cavity width between E12.5 and E13.5, but between E13.5 and E14.5 is narrowed by about a third anteriorly and somewhat less in

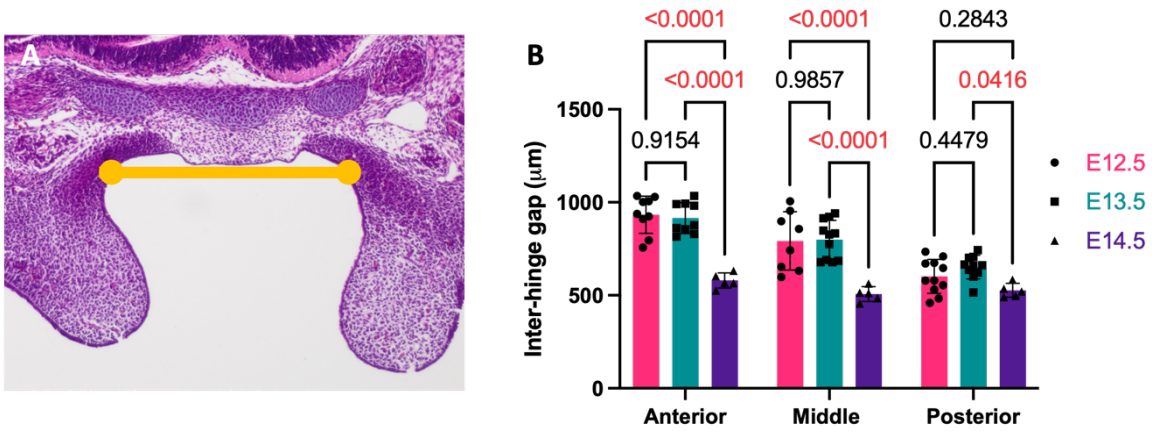

Figure 4.9 Inter-hinge gap measurements demonstration and *in vivo* measurements

A) horizontal line drawn immediately under the superior landmark (here, the cranial base) to the surface of the PSs either side. B) Graph comparing inter-hinge width differences at each embryonic day stage in anterior, middle and posterior regions. Statistical significance (P values) are displayed on the graphs and coloured in red where statistically significant ($P < 0.05$). Significance was determined by 2-way ANOVA with Tukey's Multiple Comparisons Test. Sample size: see tables 3.3, 3.4 and 3.5. Error bars = mean with SD.

the middle and posterior regions (*Figure 4.8B*). Therefore, a narrowing of the inter-hinge gap is a normal part of PS elevation/palatogenesis at this stage.

To investigate if the narrowing of the inter-hinge gap contributed to PS approximation during *ex vivo* culture, I measured the inter-hinge gap in all cultured explants described in this chapter at E12.5 and E13.5, and *in vivo* at E14.5 for comparison to that of *in vivo* tissue. I also measured the inter-hinge gap in the explants used in my recoil studies, to better establish when this narrowing is occurring.

This required extensive statistical comparison between the various conditions tested in results 1 and 2, and as a result the relevant graphs, P-values and associated descriptions have been placed in Appendix 2 (*9.2*). This is to help with ease of reading, in what would otherwise be a lengthy description of what was ultimately an artefact. Instead, I present the data in summary graphs below (*Figure 4.10*), which will overall reveal that PSs are brought together in a non-physiological progressive narrowing of the inter-hinge gap from the moment of t/m removal.

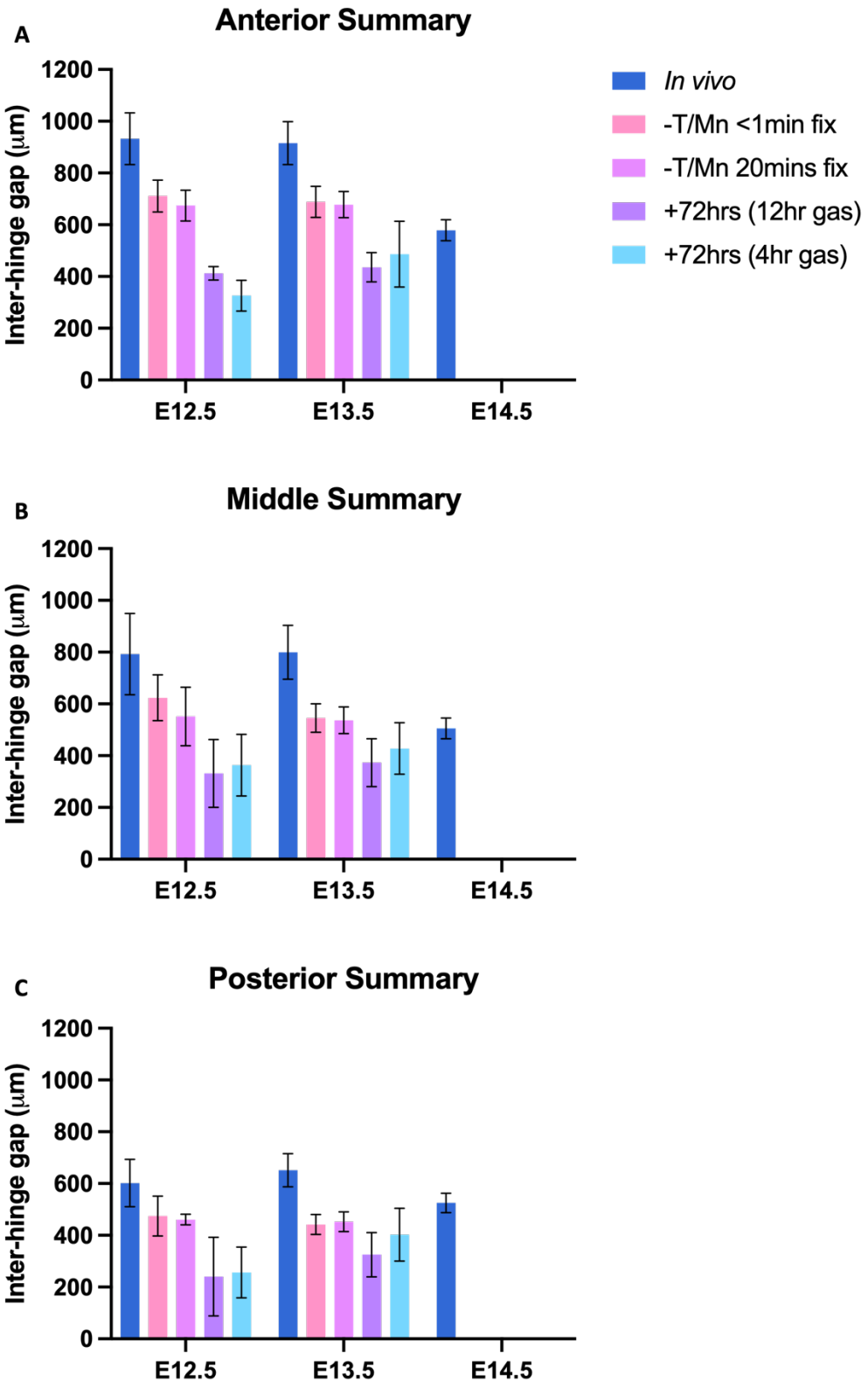

Figure 4.10 Inter-hinge gap summary graphs.

Graphs representing inter-hinge gap measurement across all experimental groups in the anterior (A), middle (B) and posterior (C). Error bars = mean with SD.

The inter-hinge gap is statistically insignificantly different *in vivo* at E12.5 and E13.5 and undergoes a statistically significant narrowing at E14.5, immediately following elevation. This gap is largest anteriorly and decreases antero-posteriorly. This pattern was observed across both recoil and gas change culture groups.

In the recoil groups, hence rapidly after the removal of the t/m, there was a statistically significant decrease in the inter-hinge gap, which immediately narrowed this gap to a corresponding (middle regions, *Figure 4.10B*) or smaller extent (posterior, *Figure 4.10B*) than *in vivo* at E14.5 following fusion. There was also a statistically significant decrease in inter-hinge gap by recoil anteriorly, but not to the extent of *in vivo* E14.5 PSs. Were growth proceeding at the normal rate, this decreased inter-hinge gap would be sufficient for PS contact to occur. However, growth did not occur in during culture, yet 50% of the time the PSs still fuse. This was due to a further statistically significant decrease in inter-hinge gap during culture, which then caused the PSs to approximate in all three anatomical regions along the A – P axis tested, resulting in fusion.

The inter-hinge gap narrowing following t/m removal in recoil studies implies that the mandible normally acts as a brace and helps spread the maxilla to its normal width. The further narrowing of the inter-hinge gap during culture provides an explanation as to how fusion occurs in the absence of additional elevation and growth. The correlation of fusion with nasal cavity width cements this explanation and offers an insight into how PS behaviour during culture may have been historically misinterpreted.

4.2.5 Constant gas supply may offer a marginal improvement on explant growth during culture

Given the poor growth and non-physiological mechanism of palate closure in the rolling culture system used in this study and most previous elevation studies, I considered potential avenues for improvement in the method. There were hints in the experiments described above that increased gas changes made some differences to the culture performance. I hypothesised that even with the more frequent gas change regime, a major limitation of my rolling culture system could be its inability to maintain a constant

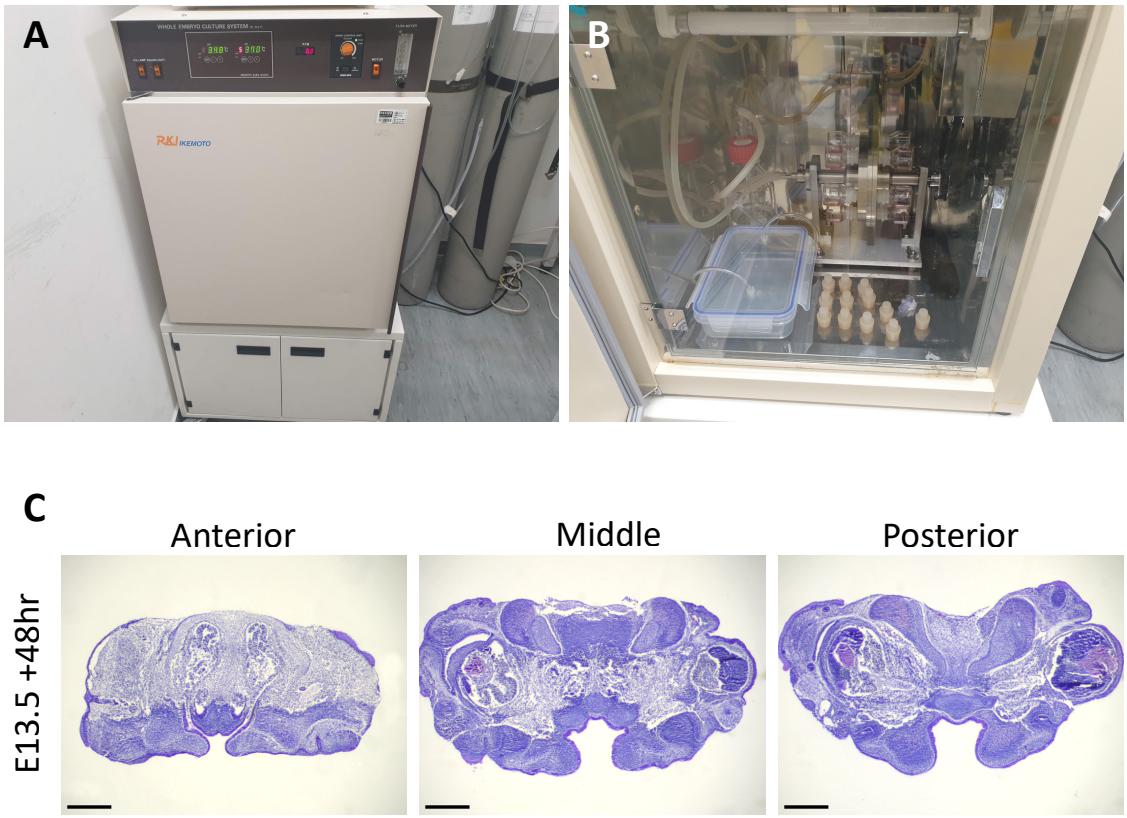

Figure 4.11 Ikemoto culture apparatus and explants.

A) Enclosed Ikemoto WEC system. B) Ikemoto apparatus interior, showing rotating drum, flasks, and airtight gas supply. C) Representative frontal section of H&E-stained tissue of E13.5 maxillary explants following 48hrs in Ikemoto culture. Scale bars = 400 µm.

high oxygen tension. To test this possibility, I carried out a pilot study using a whole embryo culture (WEC) so-called 'Ikemoto' system (*Figure 4.11A&B*). This system enabled the constant supply of gas in an enclosed system undergoing rotation.

The 'Ikemoto' system is a mass-produced variation on apparatus built in the 1970s to study embryonic development *ex vivo* (New and Cockroft, 1979). There is an extensive literature in which this system, and its similar predecessors, have been used to investigate, amongst others, whole embryo development, craniofacial development in the rat (specifically neural crest migration) and general neural development (D. A. T. New, 1967; Cockroft, 1976; Eto and Takakubo, 1985; Takahashi et al., 2008; Takahashi and Osumi, 2010). Notably, it is claimed that rodent embryos in this system undergo development at temporally matched stages to *in vivo* development up to E13.5.

I was unable to use the same gas composition (carbogen: 95% O_2, 5% CO_2) as used in the studies described above owing to limitations in the use of borrowed equipment. Instead, I used a lower [O_2] (65% O_2, 5% CO_2, 30% N_2). Despite the change, this is still a higher [O_2] than that used in other research claiming successful palate development in culture (Snyder-Warwick et al., 2010) and was therefore not considered a limiting factor. I was also only able to access the equipment for a 48-hour culture period so the following data should be considered preliminary.

4.2.5.1 PS fusion did not occur in Ikemoto culture, though growth may be marginally improved

To compare the development of maxillary explants cultured in traditional rolling culture vs. the Ikemoto system, I performed the morphometric analyses previously described in this chapter on E13.5 and E12.5 maxillary explants cultured in the Ikemoto system (n=3 per stage across 2 independent litters). None of the 3 explants cultured at E12.5 were viable, and entirely 'shrivelled up' during culture. This suggests a catastrophic failure such as contamination or media loss (though I did not identify either), and the explants were not analysed further.

The E13.5 explants were viable for analyses post-culture but appeared to be in poor condition (*Figure 4.11C*). Fusion did not occur in any of the explants, and the PSs did not appear to be adhered. They also adopted a seemingly 'flattened' appearance and, following H&E staining and sectioning, appeared to show consistent fading in superior regions of the explant in all anatomical regions. This was not observed in the PSs themselves.

Compared to both conventional rolling culture gas change culture groups, there was a statistically significant increase in PS length, area, and perimeter in the anterior and middle regions of explants cultured in the Ikemoto system (*Figure 4.12A, C&D*). There was also a significant increase in PS width in the anterior region only (*Figure 4.12B*). There was no statistically significant difference in the posterior region by any metric used.

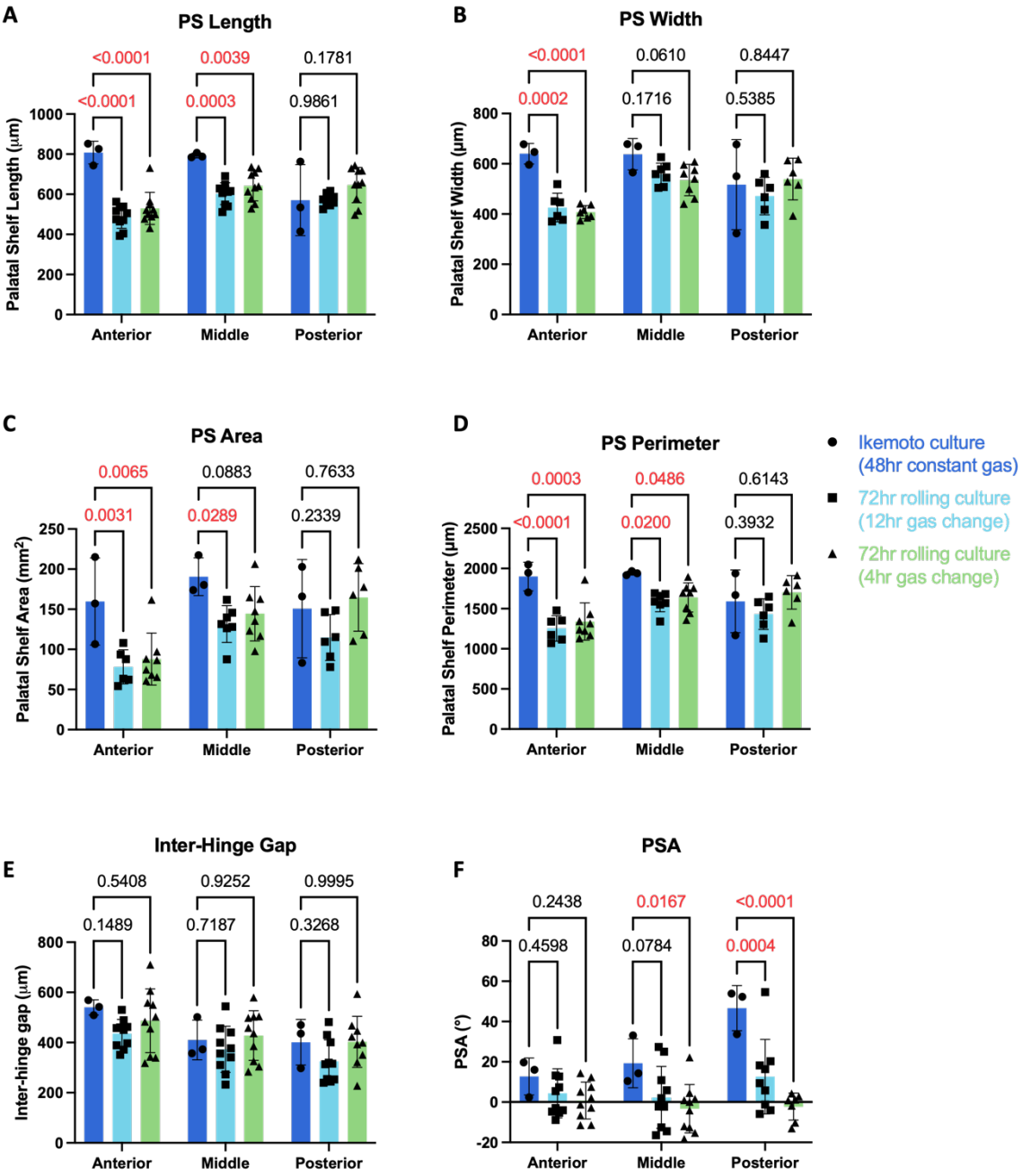

Figure 4.12 PS morphometrics of E13.5 maxillary explants following 48hrs in Ikemoto culture.

Measurements made to determine PS length (A), width (B), area (C), perimeter (D), inter-hinge gap (E) and PSA (F). Statistical significance (P values) is shown on graphs and determined two-way ANOVA with Dunnett's Multiple Comparisons test. Sample size (N) = 3 explants from 2 independent litters. Error bars = mean with SD.

Despite this, the increase was marginal and still significantly less than that of *in vivo* PSs (*Figure 4.7*).

There was also no statistically significant difference in the palatal shelf gap between Ikemoto explants and either gas change group in any anatomical region (*Figure 4.12E*).

4.2.5.2 There is less PS elevation in Ikemoto explants vs. rolling culture explants.

Middle and posterior region PSs had a statistically significantly higher PSA compared to explants cultured in traditional rolling culture at both gas changes (*Figure 4.12F*). PSA was also higher anteriorly, but not to statistical significance.

It is also important to consider that the narrowing of the inter-hinge gap could be contributing to a small amount of PS elevation, not just in these preliminary data, but also all throughout my PSA analysis. It is unlikely that this is impactful on the overall picture but is explored further in this chapter discussion.

This pilot study used a low number of explants, and morphometric measurements often had a high variance (e.g., PS width, *Figure 4.12C*). Visually, the explants had a particularly abnormal morphology and this likely impacted the measurements. Hence, care should be taken in drawing conclusions on the effects of a constant gas supply and a theoretically higher oxygen tension has on maxillary explant development at E13.5.

4.3 Discussion

The work in this chapter and the preceding one offers the first morphometric characterisation of the palatal shelves during *ex vivo* maxillary explant culture. On demonstrating that growth is severely reduced in this system, further investigation identified how the shelves may come together during culture in the absence of growth, which has previously been misidentified as a proxy for growth and elevation (Brinkley., 1975). Measuring the inter hinge gap demonstrated that fusion occurs during culture when this width narrows abnormally, much beyond the narrowing seen normally leading up to *in vivo* fusion at E14.5. The fusion event in culture has thus erroneously been used previously to suggest that all stages of palatogenesis: growth, elevation, and fusion, are recapitulated in explants. The conclusion must therefore be that batch-gassed rolling culture is an entirely inappropriate system in which to study palatogenesis. Preliminary

data using continuous gassing showed potential but in fact very marginal improvements on batch-gassed culture, showing that even this system is problematic but offering at least a little hope that a better *ex vivo* culture system might yet be developed, perhaps along the lines of the pressurised system recently shown to improve whole-embryo culture at earlier developmental stages (Aguilera-Castrejon et al., 2021), though potential limitations in application to the study of PS elevation are also discussed below.

4.3.1 The PSs do not elevate, and maxillary explants do not grow, in *ex vivo* rolling culture

Given PS elevation is occurring immediately on removal of the t/m, it was clear that PS elevation was therefore not occurring in culture, and in fact occurring during the preparation of the explant. However, the poor recapitulation of growth in the culture system was a surprising result. As described, not only was growth severely impaired, but in some instances the explants also appeared to be shrinking. This was in fact due to progressive non-physiological deformation of the explant, which I identified was due to the narrowing of the inter-hinge gap, thus driving PS approximation by non-physiological deformation during culture. This had previously been misidentified as the completion of elevation and growth. Thus, the *ex vivo* rolling culture of maxillary explants is an entirely inappropriate system in which to study PS elevation or growth, since neither appear to happen in this system. However, it should be noted that, as it has been for me, the system has still provided valuable insight into the nature of PS elevation.

Small differences were observed in explant behaviour in culture between 4-hour or 12-hour gas change frequencies. However, in cases of overall shrinkage compared to equivalent *in vivo* embryonic day development, the higher gas change frequency did not indicate any marked improvement in growth, but perhaps that the higher gas change frequency decreased the rate of shrinkage. This could perhaps be due to a presumably higher oxygen tension in the more frequent gas change group, but this is speculative, and any further investigation would be into what is essentially an artefactual system for my purposes, so this was not pursued.

As described in this chapter introduction, there have been two reports of PS area changes both *in vivo* and during culture *ex vivo* previously (Brinkley and Vickerman, 1982; Brinkley and Bookstein, 1986). Interestingly, my data agree both with their increase in PS area of up to 70% in *in vivo* PSs, and in the statistically significant anterior growth at reported in explants cultured at E13.5. Moreover, they also report statistically insignificant increases in the other anatomical regions, but this is not elaborated. Nonetheless, my PS growth in roller culture findings seem to approximate their incubation chamber findings.

4.3.2 Implications for previously published studies using *ex vivo* rolling culture

These results could influence the way previous reports are interpreted, given that there are at least thirty-five papers in published palate development literature reporting findings following the use of this system (Table 1.3). However, it is not possible to apply broad brush strokes to previous reports in response to these findings. The studies incorporate rolling culture to various extents, and some do not form the basis of the primary results of the paper; these are outlined below.

The artefactual nature of this system may not be too impactful for many of the papers, especially in those performing rescue-like experiments where mutant or drug-treated PSs elevate in culture despite not having done so *in vivo* (Iseki et al., 2007; Oh et al., 2010b; Brinkley and Vickerman, 1982; Tang et al., 2016; Snyder-Warwick et al., 2010; Ito et al., 2003b). In these papers, the use of the explant system is often to attempt a rescue of elevation by adjusting the culture environment, such as chemical treatments. As my findings show, this elevation would have occurred during explantation. Whilst this aspect of the papers would therefore be invalid, where elevation does occur it does interestingly confirm that any elevation defect must have been secondary to something else. There is no reason to believe that the invalidation of the culture system has any bearing on the *in vivo* results, which most of these papers focus on.

However, some papers could be undermined by this finding, and this typically relates to the older literature. Investigations solely focussing on bulk morphological changes (Lewis

et al., 1980; Brinkley et al., 1975; Shiota et al., 1990), fate-mapping (Chou et al., 2004), cellular morphometrics (Babiarz et al., 1979; Brinkley and Bookstein, 1986; Brinkley, 1984; ElizabethL. Wee et al., 1981), mechanical dependencies (Bulleit and Zimmerman, 1985; Brinkley and Vickerman, 1979; Brinkley et al., 1978; Brinkley and Vickerman, 1978) are most affected. Given these investigations apply analyses to what has been mistaken as progressive elevation throughout culture, elevation has therefore not been investigated in this research. Again, it is important to note, as in my experience, the use of the system provided insight, but in these cases the changes reported mostly concern the post-elevation PSs.

The arrestment or negligible progression of growth also suggests that investigations focussed on metabolic processes (Wee and Zimmerman, 1980), growth factor distribution (Brunet et al., 1993) and ECM activities, typically assaying HA accumulation and distribution (Morris-Wiman and Brinkley, 1993; Yonemitsu et al., 2020; Lan et al., 2019; Brinkley and Vickerman, 1982) could be unreliable as growth appears inconsistently across different metrics. Were this consistent, the system could still be used to investigate growth, albeit at a reduced rate.

This finding might not have much bearing on studies investigating PS fusion; although the shelves approximate in a growth-independent manner, fusion competency does not seem to be affected (Takahara et al., 2004). However, given that static culture is simpler and demonstrably more reliable method for investigating fusion (Kim et al., 2017; Morgan and Green, 2022), rolling culture may not be the most appropriate choice of assay for PS elevation.

It was noted in a recent paper that, in traditional explant rolling culture, elevation may not be occurring like the *in vivo* event (Yu and Yonemitsu, 2019). The author's then present their new culture method, which involves leaving the t/m intact, stating that it more accurately recapitulations *in vivo* elevation. While is true to the extent that the bottom half of the oral cavity is present, it remains to be confirmed morphometrically whether PS elevation occurs as per the *in vivo* event, if growth occurs at all, and if their explants experience the same progressive deformation maxilla-only explants experience

during culture as per these investigations. It could very well be less affected by artefacts given the mandible (and tongue) stays intact, thus the inter-hinge gap narrowing could occur to a lesser extent. Nonetheless, it appears that the limitations of this system may have been recognised previously, but this had not been investigated quantitatively.

Overall, my results suggest that previously used culture systems are not suitable for the *ex vivo* study of palate elevation. Until an adequate *in utero* live imaging system is developed, studies investigating palate elevation may benefit from returning to the exteriorisation assays developed by Walker & Fraser (1956). Modern techniques such as light sheet microscopy could then be combined with live-imaging techniques to investigate the overall tissue movements during *in vivo* palatogenesis. Advanced culture methods and variations on incubation conditions are explored in the limitations section of this discussion.

4.3.3 Limitations

The impact of inter-hinge gap narrowing on PS elevation

In this results chapter I identified that PS approximation is brought about by a progressive narrowing of the inter-hinge gap immediately below the nasal septum/cranial base. Comparing my timed recoil and culture data revealed that most of this narrowing happens in two stages, one immediately on removal of the t/m, and another decrease sometime during 72 hours in culture. The narrowing is conserved in all three anatomical regions along the A – P axis.

It is conceivable that this narrowing may contribute to some extent to PS elevation, in that the superior aspect of the explant is continuous and remains stationary, while the 'freely hanging' lateral maxillae, which include the PSs, must come together to close this gap. This narrowing may contribute to some PS elevation, although it may only be a small amount. Given the gap increases fairly consistently in all three regions, any change would be global, which helps simplify the matter. Moreover, it is clear from the photomicrographs that the inferior maxilla is still pointing downwards – were the whole tissue to be rotating to any significant extent, the maxillae would point medially, and

consequently the PSs, would point upwards into the nasal cavity, thus seriously influencing the extent of elevation. This does not appear to be happening in my culture or recoil studies.

Nonetheless, to avoid this issue altogether, the investigation could be repeated in explants retaining the mandible but in absence of the tongue. The experimental design here is non-trivial; in my experience it is difficult to remove the tongue at its posterior genioglossal insertion into the mandible, especially without disturbing the PSs directly, opening more room for error. Plus, at this stage it is difficult to distinguish posterior tongue from maxilla under a stereoscope during dissection, thus it is likely some tissue would be in the way, preventing elevation. Alternatively, one might consider devising a metric to calculate how much the free inferior maxillae move medially on narrowing and subtract this from the PS measurement. However, this too is non-trivial given the inferior maxillae hang freely and are continuous with the rest of the explant, making landmarking difficult. Ultimately, given the lateral maxillae movements are not as pronounced as the PS movements, any impact inter-hinge gap narrowing may have on elevation is likely to be minimal.

The potential for sub-optimal medium and other culture conditions

As described in the rolling culture mini review (1.3.3.1) there are several variations in media, supplementation and gas concentration across rolling culture techniques (Abbott, 2019, 2000; Morgan and Green, 2022). Evidently, the system cannot be optimised to study PS elevation, as the event is not happening in culture. However, if the system could be optimised to stimulate real tissue growth, even if just a delayed rate more consistent across the explants, it could prove useful for other stages of palatogenesis. This begs the question, could growth have been improved by exploring other media and gas compositions and supplementations? As described, I used a KO-DMEM based supplemented media in hyperoxic conditions (Kalaskar and Lauderdale, 2014b), but other studies use BGJb with varying supplementation in a more balanced oxygen:nitrogen:carbon dioxide gas composition, for example all of the work from the Brinkley lab, which makes up much of the early literature using this method as described previously. Taking my results and the published literature together, it does not appear

that currently reported rolling culture techniques are suitable to study growth during palatogenesis, but future variations on condition (e.g., media and gas composition) may yield more faithful recapitulation of the *in vivo* event than those used here.

Unfortunately, there appear to be significant technological limitations. Perhaps the most advanced culture system in use today is the 'enhanced *ex utero* rolling culture' system recently devised in the Hanna lab, which enables faithful recapitulation of embryogenesis in the mouse from the pre-gastrulation stage (E5.5) up to hind limb formation (E11) (Aguilera-Castrejon et al., 2021). This was confirmed by histological, molecular and single-cell RNA-sequencing validations, which appear to show the system models *in utero* development exactly. It required a consistent partial pressure of 6 – 7 psi and used a complex supplemented media closely resembling nutrient concentrations supplied by maternal blood, alongside an increasing concentration of oxygen gas per embryonic day. However, even in this system, the authors note that growth simply does not occur normally after E11, and the embryos resemble foetuses effected by *hydrops foetalis*, an oedematous condition marked by pericardial effusion and death. This is caused by insufficient oxygenation and nutrient supply, suggesting that from E11 there is currently no known replacement for the maternal blood supply. The majority of palatogenesis occurs after this stage, thus it is completely unsurprising that it cannot be faithfully recreated *ex vivo*.

Therefore, while the fallibility of traditional rolling culture is evident from the work in this thesis, the culture findings by the Hanna lab may call into question the efficiency of current culture methods reportedly more closely recapitulating palatogenesis, such the as the 'MPMT' explants in roller culture reported recently (Yu and Yonemitsu, 2019; Yonemitsu et al., 2020) due to it being used beyond E12.5.

Potential for poor tissue health and resulting tissue death

This is a specific instance of the previous potential limitation and an obvious risk in any explant culture system. However, in my cultured specimens, I did not observe any fragmented nuclei or increased eosin, hallmarks of cell death. Despite this, I did observe 'faded' tissue (i.e., paler H&E) in the superior region of the maxillary explants, particularly

in the nasal septa or nasal epithelium (e.g., *Figure 4.11C*). These are also observed in previous culture papers and are referred to as "degenerative changes… mostly affecting the nasal septa region" (Lewis et al., 1980). Despite this, the PS tissue itself appear perfectly viable. A viability stain could be performed to confirm this, and this does not appear to have been performed previously. Tissue degeneration in this superior anatomical region could contribute to the second significant narrowing of the inter-hinge gap during culture: this is supported by my finding that narrowing occurs mostly anteriorly, and less posteriorly, mirroring the pattern of "fading" and therefore potential degeneration observed in both my own experiments and in the literature.

Potential for mismeasurement due to poorly chosen or poorly applied landmarks

There are extensive documented limitations in landmarking tissue in general. Landmark based methods are well-established and provide valuable insight into development via both manual and automated methods. As described, the landmarking methods used in this work follows that of Yu & Ornitz, 2011, in which landmarks were provided both on the PSs themselves, and the surrounding tissue, both superiorly and inferiorly. This helped prevent the use of oblique sections, which could have resulted in the mis-comparison of different AP regions assumed to be the same, a real risk given the relative smallness of the tissue and its anatomical heterogeneity (it is surprisingly easy to accidentally compare tissue that includes both anterior and posterior PS tissue when sections are oblique). The consistent attainment of both superior and inferior landmarks helps prevent this specifically. However, a major limitation of landmarking cultured explants was that the inferior landmarks were always lost on removal of the tongue and mandible. This is also a limitation of the anterior inferior landmark (the PS epithelial invagination), the prominence of which is reduced significantly following elevation. Whilst every care was taken to align the PSs and superiorly landmarks in each anatomical region, this is limiting factor that may affect reproducibility. However, this may not be particularly concerning given the consistency of data obtained and high sample numbers. Theoretically, this could be ameliorated altogether by repeating the investigation in 3D using landmark-free morphometry as in a previous work from the Green lab (Toussaint et al., 2021; Redhead et al., 2023). Given the consistency of the data demonstrating the

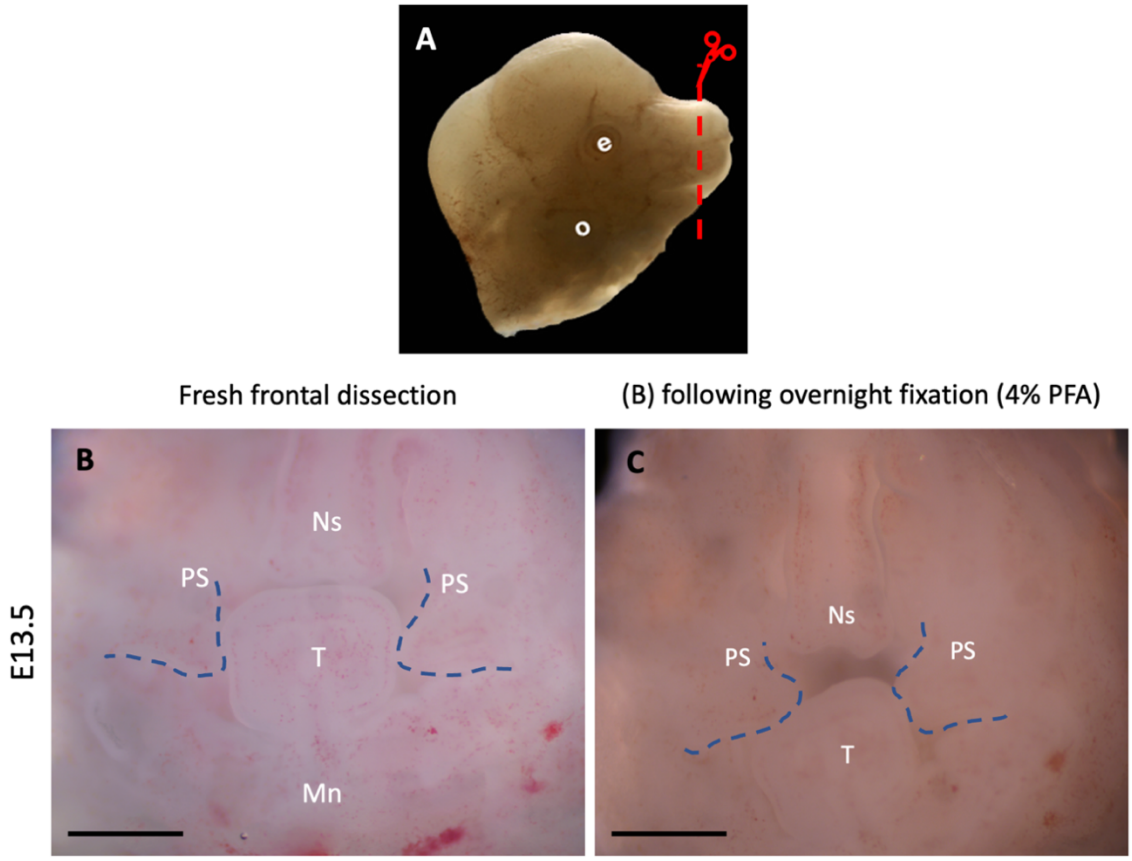

Figure 4.13 Artefactual elevation following overnight incubation in 4% PFA.

Representative photomicrographs of an E13.5 embryonic head dissected to give a 'faceplant' (A), and the oral cavity immediately following dissection (B) and after overnight incubation in 4% PFA at 4°C. The PSs appear to elevatate in a unilateral fashion, and a patent gap between the tongue and nasal septa is produced which is not observed *in vivo*. e, eye; o, otic vesicle; PS, palatal shelf; Ns, Nasal septa; Mn, mandible; T, tongue. Scale bars: 400µm.

inadequacy of this system in recapitulating growth and PS elevation, this would likely not be pursued.

Fixation artefacts influencing elevation

It is well-documented that fixation with PFA causes tissue shrinkage, and this is previously documented in the palate, resulting in geometric and spacing artefacts (Greene and Pratt, 1976; Greene and Kochhar, 1973). By my own observation, shelves which are completely unelevated at E13.5 may be artificially elevated following overnight incubation in PFA (*Figure 4.13*). This appears unlikely to affect tissue fixed following elastic recoil and culture described here, as elevation had already occurred. However, the shrinkage could have a variable impact on different anatomical regions of the PSs, and it could perhaps

exacerbate the extent of the narrowing of the inter-hinge gap. If the tissue were affected in a consistent manner by the fixative, one could assume that the effects are global and the effects on data interpretation would be minimal. However, I did not assay for this, and so cannot interpret the effects of tissue fixation from my data.

The definition and semantics of 'elevation'

These recoil, culture and morphometric experiments highlight the need for clarity and precision when using the term 'elevation.' Classically, elevation has often been thought of as the physical act of the shelves assuming their horizontal position above the tongue, following their initial vertical orientation, whilst also being used to refer to the entire process (Walker & Fraser, 1956; Bush & Jiang, 2012). However, if elevation is the result of the release of a gradual build-up of force (perhaps elastic potential energy) during loading against the tongue, then elevation could be considered to begin much earlier. In this sense the entire process of elevation, or at least the mechanism by which it occurs, may not be an entirely distinct process from PS outgrowth.

Therefore, for any future work in this area, and any further publication arising from these data, it will be imperative to make distinctions between i) the overall mechanism of elevation, which arises over a longer time period (e.g., potentially from the moment of first contact with the tongue) and ii) the rapid act of elevation itself. It may be of use to refer to the latter, rapid event as 'reorientation', or the 'reorientation event' which is the ultimate stage in the longer process of 'elevation' (i.e., the mechanistic former), regardless of the precise mechanism by which it occurs.

4.3.4 Summary

Overall, the work presented in this chapter demonstrate the first detailed morphometric characterisation of PS growth in the commonly used *ex vivo* rolling culture system, and the identification that growth is poor and inconsistent across the tissue. This builds on the findings in the previous chapter which showed that the majority of PS elevation occurs via elastic recoil immediately on removal of the t/m. Together, these results highlight that *ex vivo* rolling culture is an inappropriate system in which to study PS

elevation. Thus, live imaging of PS elevation *in vivo* remains elusive, but a combination of Walker's classical embryonic exteriorisation and vivisection assays (Walker and Quarles, 1976) combined with modern imaging techniques such as MRI could yield future progress.

Furthermore, I identified that a progressive, non-physiological narrowing of the inter-hinge gap is responsible for bringing the PSs into contact during culture, which in my studies resulted in fusion in E13.5 explants 50% of the time. The use of the closure of the palatal shelf gap as a marker of elevation seems to suggest that, because the PSs have come together during culture, elevation must have occurred. This post-hoc fallacy has permeated the literature to become the dominant narrative, and these results demonstrate this falsehood quantifiably.

The observed elasticity during recoil shifted the course of this project in questioning how the internal shelf force could be stored, and how the material properties of the PSs may contribute to and/or facilitate this event. Plus, the identification of horizontally orientated pre-deflected anterior shelves at E12.5 also suggest a default horizontal growth programme, as in all palate-bearing non-mammals.

Therefore, these findings provide novel insight into PS elevation and form the basis for future investigations into a) the evolutionary origins of palate elevation and ii) the nature and storage of the internal shelf force in relation to the material properties of the PSs, each of which are interrogated in the subsequent results chapters in this thesis.

5. The evolution of palatal shelf elevation and default horizontal growth

5.1 Introduction and theory

This chapter deviates from the previous morphometric investigations and uses a comparative embryology approach to investigate the evolutionary origins of PS elevation. PS elevation is a mammalian novelty, and the PSs grow horizontal by default in the Avia and Crocodylia (Ferguson, 1981b; Foreman et al., 1991), and it is unclear if this is the case in mammals, though there is evidence in mice for brief horizontal outgrowth before ventral deflection by the PSs (3.2.2).

It has been suggested previously that the large mammalian tongue may play a role in directing the PSs during outgrowth (Hayward and Avery, 1957; (Moxham, 2003). The role the tongue plays in directing ventral PS outgrowth was investigated in the hamster by measuring 3H-thymidine incorporation in the PSs and tongue as a marker of DNA synthesis, which the authors use as an index for growth in both structures (Young et al., 1991; reviewed by Moxham, 2003). 3H-thymidine incorporated in the anterior palatal primordia whilst the tongue and mandible incorporated 3H-thymidine posteriorly, thus it was suggested that the tongue may not determine the direction of the developing PSs. However, 3H-thymidine incorporation alone cannot take into account the changes in orofacial growth and angulation at this stage (Diewert and Tait, 1979). Plus, 3H-thmidine incorporation has since bene identified as a defective measure of DNA synthesis, inducing cell cycle arrest and apoptosis (Hu et al., 2002). Therefore, the role that the tongue may place in directing PS growth remains unclear.

On consideration of the structural and functional differences between mammalian and (amniotic) non-mammalian oral cavities, one difference is the mechanism of feeding. Mammals suckle, whilst non-mammals do not, adopting a variety of different mechanisms to feed between taxa. The biomechanics of suckling has been studied thoroughly, and it is understood that mammals require a large muscular tongue for

proper feeding: on forming a vacuum around the maternal teat with the mouth, the ventral displacement of a large tongue creates a relatively large vacuum, thus creating a pressure gradient ultimately drawing-in milk (Crompton et al., 2019). Having a large, muscular tongue is therefore a requirement for post-partum survival in mammals, but so is separating the oral and nasal cavities via the palate. Hence, it could be considered that there is a trade-off for space in the oral cavity between two (counting the paired PSs singularly) essential structures, the tongue, and the palatal shelves. Theoretically, to ensure both structures can grow adequately in a confined space, one structure could evolve to be more deformable than the other. I.e., the PSs can deform around the tongue, presumably by having a lower elastic modulus. The tongue sits high in the common oronasal cavity and is anchored to the mandible inferiorly and, in later mature form, the hyoid bone via the genioglossus muscle posteriorly (Parada and Chai, 2015). Therefore, the only direction the PSs can be deflected is ventrally. The internal shelf force could build during the continued growth of the shelves in this compressed manner, with the force released elastically the moment the tongue moves out of the way. On this basis, I hypothesised that PS elevation is a consequence of the mammalian suckling requirement.

I was presented with a serendipitous opportunity to interrogate this theory as a colleague had access to monotreme tissue. Monotremes are the only non-suckling mammals and, via collaborative work with the Tucker (KCL, UK) and Renfree (Melbourne, AUS) labs, I had access one of two extant monotreme species tissue, the echidna (*Tachyglossus aculeatus)*. Palate development in monotremes at this stage was previously unknown and, in this chapter, I present a time course of palate development in a monotreme. Whilst this did not support my theory of the PSs growing horizontally in all non-suckling animals, it led to the further theory that mammalian and non-mammalian palates are homoplasic structures, arising via convergent evolution. I also describe preliminary data via collaboration with the Goodwin lab (USCF) suggesting possible default horizontal PS growth in mutant mice with pronounced microglossia.

5.1.1 Default horizontal PS growth in non-mammals

Not all non-mammals have a palate similar that of mammals, although the secondary palate is thought to arise from the maxillary processes in all vertebrates (Foreman et al., 1991). However, this may not be strictly true. For example, only some species of Lepidosauria (e.g., snakes) and Testudines (e.g., turtles) possess such a structure, and if so, it is commonly a posterior extension of the primary palate, often remaining cleft (Fuchs, 1907; Ferguson, 1988). It is unclear whether Lepidosauria and Testudines can be considered comparable structures to the mammalian secondary palate and may have a different evolutionary structural origin (Cadena, 2015). Therefore, these different species are referred to as not having a 'true palate' in this chapter.

On the other hand, Aves and Crocodylia appear to have a comparable 'mammal-like' secondary palate between the oral and nasal cavities. This has been investigated comparatively to the mouse in both the chick, *Gallus gallus* (Foreman et al., 1991) and the American alligator, *Alligator mississippiensis* (Ferguson, 1981b). At least in the alligator, the palate shares functional features with the mammalian palate in that it assists in the processing of food, albeit in the absence of rugae (Ferguson, 1979). In the chicken, the PSs meet in the midline but never fuse. While chickens do not chew their food, instead swallowing it whole, the chicken palate still plays a role in feeding and contains a diverse array of tastebuds (Kawabata and Tabata, 2022; Rajapaksha et al., 2016) though these differ in form to those of humans (Liu et al., 2018).

In both chick and alligator, the PSs grow horizontally by default and never undergo an elevation event. In the chick, palatogenesis occurs approximately between embryonic days 7 and 8.5 – 9, before hatching on day 21 (Martinsen, 2005). The PSs arise from the maxillary processes at HH31 (*Figure 5.1A*), extend horizontally over the tongue at HH33 (*Figure 5.1B*), and meet in the midline at HH35 (*Figure 5.1C*) (Foreman et al., 1991; Hamburger and Hamilton, 1951); the MEE keratinises, and the PSs subsequently do not fuse (Shah et al., 1988; Koch and Smiley, 1981). In the alligator, the PSs arise from the maxillary processes on embryonic day 18 (*Figure 5.1D*), are in contact in the midline by

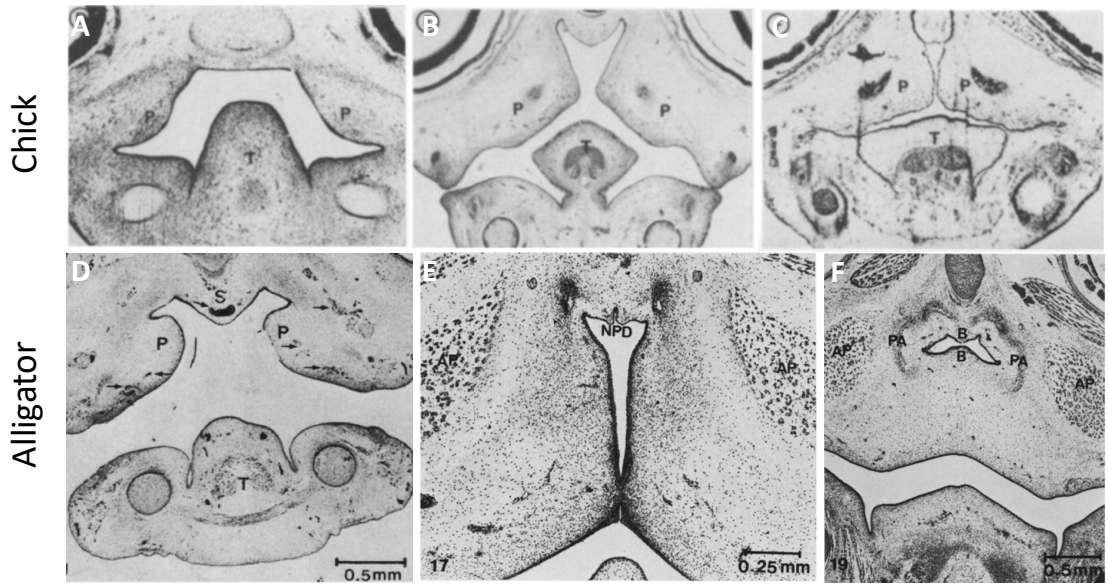

Figure 5.1 Default horizontal PS growth with no elevation event in Aves and Crocodylia

Photomicrographs of the frontally sectioned oral cavity of chick embryos (A-C) and alligator embryos (D-F). In both, the PSs arise as paired outgrowths from the maxillary prominences (A&D). The PSs then extend horizontally towards the midline immediately, showing no elevation event (B&E). Note the relatively small and inferiorly positioned tongue in both (B&D). The PSs meet in the midline and fuse in crocodiles (F), but not in the chick (C). P, palatal shelf; T, tongue; AP, anterior pterygoid muscle; PA, ossifying palatine bones; NPD, future nasopharyngeal duct; B, insipient bulges partitioning the nasopharyngeal dutch. Scale bars stated in the panels where available (adapted from Foreman et al., 1991; Ferguson, 1981).

day 24 (*Figure 5.1E*) and are fused with full mesenchymal confluency by day 28, with eggs hatching around day 65 (*Figure 5.1F*) (Ferguson, 1981b).

In Amniotes, the extant non-mammals are evolutionarily older than the mammals, and this could suggest that the programmed horizontal growth is the default mechanism of palatogenesis. However, this assumes that an early ancestor did not simply lose the process of elevation, and so it should be acknowledged that the inverse could also be true (though there is even less evidence of this, given no known non-mammals elevate their PSs). Therefore, this gives early evidence that the mammals may have acquired PS elevation at some point during their evolution from the early 'reptile-like' ancestral amniotes (Maier et al., 1996). Understanding the selection pressures that drove this potential evolutionary shift may provide insights into modern day mammalian PS elevation, namely in establishing if there is a default horizontal growth programme underlying the processes, which could suggest a passivity to the process of elevation.

5.1.2 Is PS elevation a consequence of the mammalian suckling requirement?

Palatogenesis has been studied extensively in a variety of mammals (1.3.1), and in this chapter elevation is considered in representative species from across the three extant subdivisions of class Mammalia. These are the Placentalia (Eutheria), Marsupalia (Metatheria) and Monotremata; each of which are briefly introduced below.

Placentalia were thought of as the only mammals to access foetal nourishment via a placenta, and include mice, rats, and humans. Although still used, Placentalia is an historic misnomer as marsupials also have a placenta (Renfree, 2010). Eutheria is commonly used to refer to what was once thought of as placental mammals instead. Other anatomical features are now used to distinguish the eutherians from marsupials, such as the absence of the epipubic bones (Novacek et al., 1997). Moreover, relative to the marsupials, they carry their young *in utero* until a late stage in development, thus feeding mechanically by suckling as described previously (*5.1*) at a later point.

Marsupials (e.g., the opossums, kangaroos, and the Tamar wallaby) are commonly distinguished from eutherians by the pouch in which they carry their young. They are born relatively early, possess highly developed upper limbs and climb from the birth canal into their mother's pouch (Tyndale-Briscoe and Renfree, 1987; Sharman, 1973). Here, they latch on to the maternal teat and feed by suckling relatively early in development (Kelly et al., 2019). Unlike eutherians, milk produced by marsupials varies as the pouch young age, essentially replacing the placenta, though an early placenta is indeed present during marsupial gestation (Renfree, 2010). Both marsupials and eutherians evolved from a common Therian ('wild beast') ancestor and, interestingly, branched-off when ancient transposable elements altered the uterine regulatory landscape and transcriptome to suppress the maternal immune system (Lynch et al., 2015). This enabled prolonged pregnancy and elaborated placental development, ultimately giving birth to relatively protected, mature young. The marsupials did not undergo this adaptation to the same extent as the eutherians, hence they maintain short pregnancies and much of their early

development still occurs *ex utero.* Furthermore, the fossil record indicates that there were a diverse range of mammals that shared eutherian and marsupial traits, but were more closely related to extant marsupials, hence the extant marsupials and the fossils are referred to together as Metatherian (Williamson et al., 2014). Evidently, common to each of these sub and infraclasses is their mechanism of feeding: suckling.

Monotremata are the most ancient of the extant mammals now represented by only five extant species: the platypus, *Ornithorhynchus anatinus,* and four species of echidna (Zhou et al., 2021). Described as "extraordinary" in their first scientific description by Shaw in the late 18th Century, an historic debate arose as to how the monotremes related to mammals, with some suggesting they do not fit within Linnaean groupings, instead representing a link between mammals and reptiles (Saint-Hilaire, 1803). We now understand the monotremes to have branched off from the Prototherians, our earliest reptile-like mammalian ancestors, and apparently retained some of their features. The monotremes are explored in further detail with respect to palate development in the next section, but it is important to note here that they are thought to be non-suckling (Crompton et al., 2019).

Hence, eutherians and marsupials display suckling behaviour and undergo PS elevation during palatogenesis, while non-mammalian amniotes with PSs display immediate horizontal growth to the midline, with no elevation event, and they do not exhibit suckling behaviours. The monotremes evolved from ancient, reptile-like mammals and do not suckle, though palatogenesis in the order is completely undescribed. These comparisons can be visualised in *Figure 5.2*. The seemingly anomalous combination of a non-suckling mammal presents an exciting opportunity to investigate how form may follow function in investigating the evolutionary origins of PS elevation.

5.1.3 The short-beaked echidna, *Tachyglossus aculeatus*

The short-beaked echidna, Tachyglossus aculeatus, is one of four extant species of echidna and was the first described monotreme (Shaw, 1792). They possess a bird-like beak and lay their young in eggs directly into a maternal pouch at the early somite stage

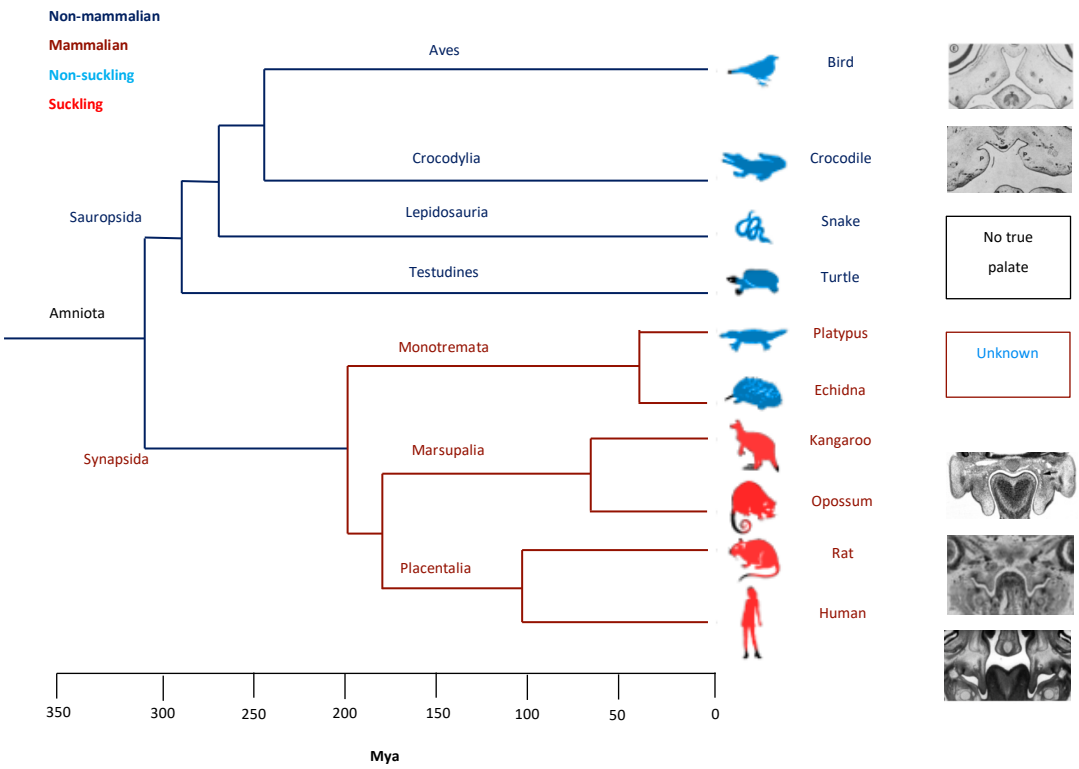

Figure 5.2 Amniotic phylogenetic tree of PS elevation and feeding mechanisms

Amniotic phylogenetic tree displaying mammals (burgundy lines) and non-mammals (dark blue lines) of the clade Amniota, their relative evolutionary origins, and coloured sketches displaying whether they suckle (light blue) or do not suckle (light red). Alongside each is a photomicrograph of the frontally sectioned PSs in representative species, showing immediately horizontally orientated PSs (hence no elevation event) in the chick (Foreman et al., 1991) and the alligator (Ferguson, 1981), i.e., no elevation event in non-mammalian amniotes which have a secondary palate. Vertically elevated PSS, immediately prior to elevation, are observed in representative photomicrographs of Placentalia (eutherians) in the human (Sperber, 2002) and the rat (Coleman, 1965). The same observation is made in the marsupials, represented here by the grey short-tailed opossum, *Monodelphis domestica* (Smith, 2006b). However, as demarcated by the light blue colouring, monotremes it is not known whether the monotremes elevate their PSs, and their development is undescribed. Given their novel position in this comparison and relatively ancient origin, they provide a novel opportunity to investigate the evolutionary origins of PS elevation. Note: the early synapsids are not considered mammalian. Mya, millions of years ago. The tree structure was traced (Krubitzer and Campi, 2009).

(Griffiths, 1968), wherein the egg hatches after just 10 – 10.5 days incubation (Dutton-Regester et al., 2021). The hatchlings break their way out of the egg using their sole 'egg tooth' (which falls out shortly after hatching) and caruncle, a thick, keratinised epithelium located above the nasal cartilage (*Figure 5.3A*) (Hill and de Beer, 1950; Fenelon et al., 2023b). From hatching, the young are bald and referred to as 'puggles' (*Figure 5.3B*), until

the point they develop mature spines and reach adult mass between four and five years (*Figure 5.3C*) (Griffiths, 1978).

Despite this oviparity, the young hatch after a relatively short timeframe and are still nursed on milk (Griffiths, 1965). At the anterolateral margins of the pouch lie two patches of mammary gland-associated skin, the mammary areolae, which secrete milk into a skin invagination along with an invading hair follicle (Rismiller and Grutzner, 2019). It is often reported that, owing to the complete lack of nipple, the echidna simply 'laps' the milk from the skin patches it is secreted into, somewhat reminiscent of human sweating (Crompton et al., 2019). However, this appears to be a contentious area in the literature, with early reports suggesting the echidna suckle from the hair or surrounding epithelial structures (Bresslau, 1920) and that, when in the pouch, puggles make sounds consistent with suckling, detected via sonogram (Griffiths, 1965). A more recent study suggested that the echidna areolae could be projected outwards, giving the appearance of a nipple and enabling suckling, whilst the platypus instead laps milk in the way contentiously associated with echidnas (Koyama et al., 2013). Support for licking may be found in anatomical studies of the echidna tongue, with muscular arrangements and vascular stiffening mechanisms enabling rapid licking, hence '*Tachyglossus*', meaning 'fast tongue' (up to a hundred actions a minute) (Doran and Baggett, 1970; Griffiths, 1978).

Moreover, palate development has not been studied in any monotreme. As outlined in 1.3.1, there is a single study which claims there is no evidence the PSs in echidnas first grow vertically before assuming a horizontal position, i.e., no evidence of an elevation event (Seydel, 1899). This is quoted in contemporaneous research from the time (Polzl, 1905) and is frequently cited in more recent literature (Fenelon et al., 2023b; Rismiller and Grutzner, 2019; Rismiller and Seymour, 1991), but I have been unable to track down a copy of what would appear to be the only published research documenting embryonic echidna palate growth.

The role of suckling has been studied in the context of palate development previously albeit at a later stage, with suckling onset coinciding with transient palatal chondrogenesis, investigated via finite element modelling (FEM) (Jingtao Li et al., 2016).

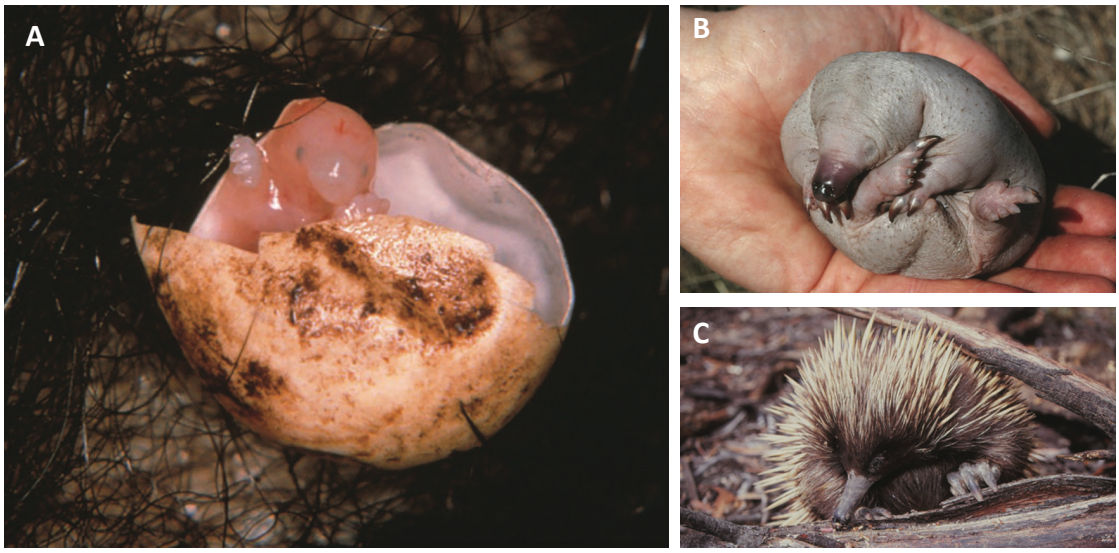

Figure 5.3 Photographs of the major life stages of the short-beaked echidna, *Tachyglossus aculeatus*

Photographs of the short-beaked echidna in various life stages. A) Echidna hatchling on the abdomen of the mother, note the well-developed forelimbs, similar to those of marsupials. B) a so-called 'puggle', the juvenile echidna stage before they develop spines and a filly elongated beak. C) the adult echidna, with a fully developed beak and mature spines (adapted from Rismiller and Grutzner, 2019).

The authors state that the reported growth plates are maintained via the mechanical strain from suckling, and that the growth plates, ergo the head, stop expanding laterally and the palate ossifies with the onset of weaning. In discussion, the authors suggest that that monotremes would be the perfect model for testing this.

Therefore, the availability of echidna tissue provided the opportunity to both describe palatogenesis in a monotreme (essentially completing the representative mammalian phylogenetic tree of palatogenesis), and to give an insight into the evolutionary origins of mammalian feeding and palate development. In the absence of suckling activities in the more reptile-like monotreme it is conceivable that, as in crocodiles and birds, the tongue may be relatively small, and the PSs grow horizontally by default. If this is the case in the echidna, it suggests that the PSs attempt to grow horizontally, and that elevation is therefore merely an elastic release of PS prior PS deflection by the tongue.

5.1.4 Echidna tissue and data acquisition

The short-beaked Echidna is a protected animal endemic to Australia and eastern New

Guinea, and it is uncommon to acquire them for scientific research purposes. This work was done in collaboration with groups that already have access to the animals/animal tissue. Histological sections and microCT scanned .tiff files of embryonic echidnas were provided by Dr. Neal Anthwal (Tucker lab, KCL) who had received them in collaboration with the Renfree lab (Melbourne). The echidnas were harvested and processed by Dr. Jane Fenelon (Renfree lab), acquired from the recently established breeding colony at the Currumbin Wildlife Sanctuary (CWS) (Queensland, Australia).

5.2 Results

5.2.1 On hatching, echidnas have horizontally orientated, unfused PSs, with a small inferiorly positioned tongue

Echidna tissue availability was very limited. Prior to the palate study, a hatchling stage echidna (P0) was processed for a separate investigation into the middle ear (Anthwal et al., 2020). From this, trichrome stained, frontally sectioned P0 echidna sections were generated, showing the PSs and tongue in what appears to be the anterior region as per the nasal septa (*Figure 5.4A*) and a slightly more posterior section, perhaps in the midpalate (*Figure 5.4B*). I have referred to them as the rostral and caudal sections respectively, as they are not equivalent to anterior and posterior regions defined in the mouse palate elsewhere in this thesis.

At P0, the PSs are elevated in both provided anatomical regions, and resemble those of any other mammal. They remain cleft in the anterior and abut in the more caudal section. This is interesting as echidnas blow mucosal bubbles out of their nostrils, which burst over their beak/face and keeps them cool, therefore playing a key role in thermoregulation (Cooper and Withers, 2023). A naturally cleft palate in the anterior region, immediately inferior to the nasal septa, could be the anatomical feature that enables this physiological function.

Also of note is the particularly small tongue in the anterior, especially relative to the available space towards the mandible (*Figure 5.4A*). The PSs might not contact the tongue

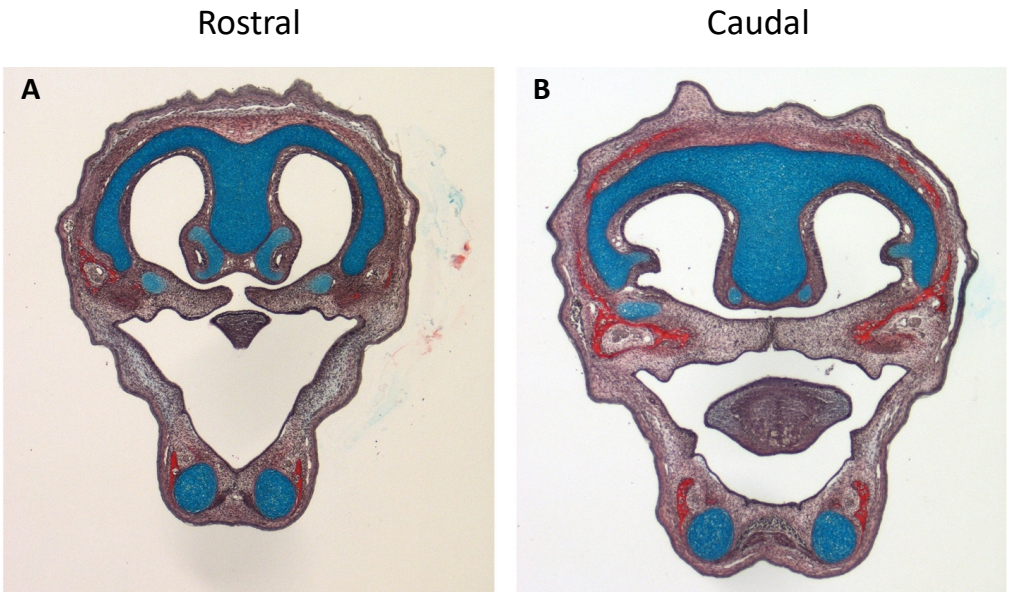

Figure 5.4 Frontal sections of the P0 short-beaked echidna

Photomicrographs of a trichrome stained frontally sectioned P0 short-beaked echidna in the anterior region, demarcated by the nasal septa (A), and somewhat more posteriorly, towards the midpalate (B). Notable features include the relatively large space in the oral cavity relative to the small tongue, particularly rostrally, and the cleft at birth. Tissue prepared by Neal Anthwal (Tucker lab, KCL).

here in the anterior. More caudally, probably closer to the midpalate given the cranial base is not in the plane of section, rather than the posterior, the tongue is much larger. However, it is also not connected to the mandible and there is much free space, unlike in eutherians and marsupials, bearing closer resemblance to the oral cavity in non-mammalian amniotes (*Figure 5.4B*).

These photomicrographs highlight the cleft at birth phenotype of the echidna, however any information on embryological palate development could only be inferred.

5.2.2 The embryonic echidna PSs elevate like all other mammals

To characterise how the echidna PSs develop embryologically, I reconstructed microCT scans of embryonic echidnas taken by Jane Fenelon (Renfree lab, Melbourne). Four echidnas were collected at different stages *in Ovo* after oviposition at day 1 (D1), D6, 7, 8 and 9, with hatching occurring on D10. Following 3D rendering I resected the 3D projections in the frontal plane at the level of the nasal septa, which was designated

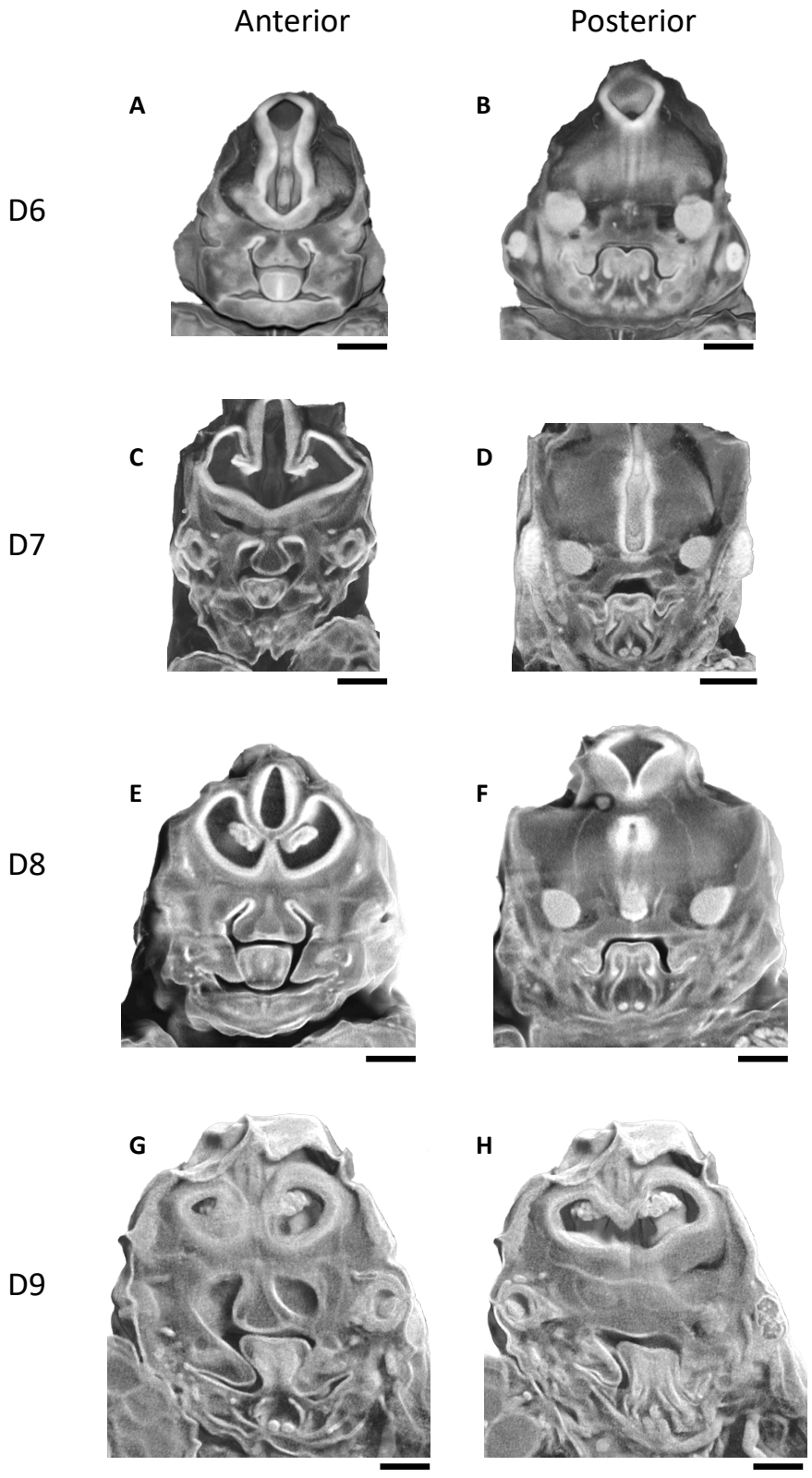

Figure 5.5 Frontal resections of embryonic echidna heads from microCT scans

Time course of PS development in the embryonic short-beaked echidna at D6, 7, 8&9 in the anterior (A, C, E&G) and the posterior (B, D, F&H). The time course is described in detail in the main text. Scale bars = 100 µm.

Figure 5.6 Sagittal resection of a reconstructed 3D microCT scan of a D9 short-beaked echidna

Sagittal resection of the D9 echidna microCT scan showing relationship between tongue and PS. Note the relative high position of the tongue and the large gap below to the mandible. The tongue is casting a shadow on the anterior PS, and the posterior PS is adjacent to the muscular insertion of the tongue to the mandible.

anterior, and to the level of the cranial base, which was designated posterior, and made a time-course (*Figure 5.5*).

At all stages, D6, 7, 8 and 9, the PSs are vertically orientated in the anterior (*Figure 5.5A, C, E&G*) and the posterior (*Figure 5.5B, D, F&H*). The pattern appears to be identical to that observed in all other mammals: the shelves are vertically orientated and have more defined tips in the anterior, and appear more rounded in the posterior, progressively getting larger with each 'D' stage. As with other mammals, the tongue is also not attached anteriorly, but attached to the mandible posteriorly. This does not appear to be the case at D9, with an anterior tongue attachment (*Figure 5.5G*). However, it is important to note that this embryo appears to have been compressed against the tube when scanning, and as a result some of the anatomical relations are a bit out of place due to whole tissue bending, which also made it particularly difficult to get a non-oblique plane for the representative image. It is also plausible that the sample could have been damaged during harvesting.

In the anterior at D6, the PSs somewhat resemble those of the mouse PSs at E12.5 (*Figure 5.7*G), in that they are smaller and appear to be somewhat horizontally orientated, suggesting subsequent deflection (*Figure 5.5A*). Between D8 and D9, both anterior and posterior PSs also appear to be reorientating to the horizontal, albeit still stuck underneath the tongue, suggesting anterior elastic elevation (*Figure 5.5E-H*). Furthermore, the previous figure demonstrates that, immediately post-hatching on D10 (then referred to as P0) the echidna PSs are elevated (*Figure 5.4*). This suggests that the echidna PSs must elevate sometime between D9 – D10, immediately before or perhaps during hatching.

The communication between the echidna tongue and PSs along the entire A – P axis immediately prior to elevation is best observed in the sagittal plane (*Figure 5.6*). The (anatomical) left PS can be clearly seen to run, from the viewers perspective, behind the tongue and curling underneath it in the anterior aspect, as confirmed in the corresponding frontal image (*Figure 5.5G*). The tongue can be seen casting a shadow on the presumptive nasal surface of the unelevated PS and the egg tooth is clearly visible.

As with other mammals, the tongue appears to sit high in the anterior oral cavity, pressing against the nasal septum, and is not attached to the mandible. There is a pronounced empty space below the tongue to the mandible, as observed in the P0 section (*Figure 5.4A*). Posteriorly, the tongue is anchored to the mandible and the PSs run parallel to both the muscular insertion itself and the tongue. The changing geometry and tissue communications explain how the PSs appear to partly elevate beneath the tongue in the anterior yet remain vertically orientated in the posterior (*Figure 5.4*). There is relatively large amount of space beneath the unanchored tongue in the anterior for 'flip-up' elastic elevation movements to occur, whereas in the posterior there is no such space nor give in the tongue.

Overall, these scans do not support my theory that the PSs only undergo elevation in non-suckling mammals (unless they do indeed suckle). Nonetheless, this work provides the first description of palatogenesis in a monotreme. As the tongue is still large/gets in the way of the PSs, it is not possible to assess the default horizontal growth theory. However, preliminary evidence for this has been identified in a mutant mouse model, and this is presented below.

5.2.3 Preliminary evidence for default horizontal PS growth in a microglossia mutant mouse

Despite elevation perhaps not being linked to suckling behaviour itself, the PSs physical communication with the tongue throughout suggests that, at least in mammals, the relatively larger tongue plays a role in directing the PSs ventrally. Theoretically, this could be tested easily in mammals with microglossia. However, mutant mice with microglossia appear to typically be associated with either micrognathia or retrognathia, thus the tongue obstructs the PSs regardless (Suzuki et al., 2018).

This question is being addressed in collaboration with the Goodwin lab (UCSF) via a mutant mouse enabling the conditional activation of diphtheria toxin A (DTA) in the tongue via a *Hand2-cre* driver. Briefly, DTA is a segment of diphtheria toxin, and its expression is known to inhibit cellular proliferation and intracellular protein synthesis

(Zhang et al., 2012). As described in relation to the *Has2$^{f/f}$;Hand2-Cre* mouse previously (1.4.5.1) *Hand2* is expressed in NCCs in the mandibular and posterior pharyngeal arches (Ruest et al., 2003; Xu et al., 2019; Lan et al., 2019). This could suggest that the same micrognathia issue could be encountered using this mutant, but these preliminary data do not suggest that this is the case (*Figure 5.7*). However, the mouse model used here is a new mutant line, with some key differences. In the former model, Hand2-cre is expressed in the heart, while the latter only uses the pharyngeal arch enhancer, with no cardiac expression (Charité et al., 2001). Therefore, the mutant mouse *DTA$^{/+}$;Hand2-cre* is being used to investigate the direction of growth of the PSs in the absence of contact with the tongue.

In the anterior at E13.5 the mutant tongue is considerably smaller than that of control mice, and the PSs are horizontally orientated (*Figure 5.7*A&D). The same is true of the midpalate *(Figure 5.7*B&E), with the PSs horizontally orientated above the much smaller tongue. The posterior mutant PSs appear to be angled slightly infero-medially ('diagonally downwards') but appear to be unilaterally elevated, with the anatomically right-hand shelf elevated above the tongue (*Figure 5.7*F). The adjacent PS appears to be in contact with the tongue, but in either case they certainly do not resemble those of the control tissue at E13.5 (*Figure 5.7*C&F).

To draw conclusions from this study, a full time-course will need to be completed from the point of WT shelf emergence (E11.5) through to WT elevation (E14.5) and compared. However, supporting evidence for default horizontal growth is also given from *in vivo* sections in the anterior at E12.5 (*Figure 5.7*G) and in the extreme posterior at E13.5 (*Figure 5.7*H). As described in Chapter 3 (3.2.2), in the anterior at E12.5 the PSs are horizontally orientated and are some distance from the tongue, suggesting they have not yet been deflected (*Figure 5.7*G). There is a similar situation in the extreme posterior end of the PSs at E13.5, with the PSs not quite horizontally orientated, but certainly not vertically and nor are they in contact with the tongue, again suggesting the tongue is at least playing some role in their deflection (*Figure 5.7*G).

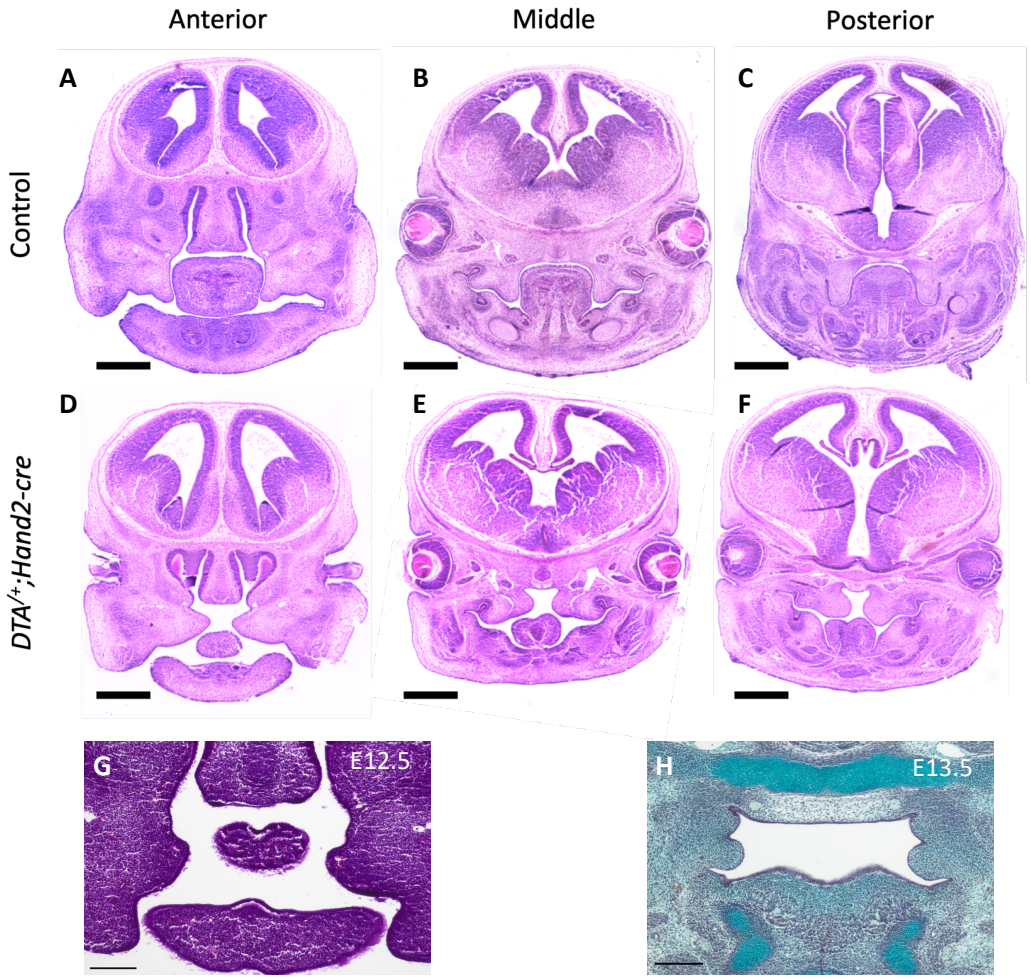

Figure 5.7 PS orientation at E13.5 in control and *DTA$^{/+}$;Hand2-cre* mice, with WT evidence for default horizontal growth

Photomicrographs of frontally sectioned H&E (A-G) and trichrome (H) stained heads and oral cavities in control (A-C, F&G) and *DTA$^{/+}$;Hand2-cre* (D-F) mutant mice in the anterior (A, D&D), middle (B&E) and posterior (C, F&H) anatomical regions (n = 2). In each mutant section, there is no evidence of primary vertical growth, and evidence for default horizontal growth is given from control tissue in the anterior at E13.5 (G) and the extreme posterior end at E13.5 (H). Scale bars = 500 µm (A-F); 200 µm (G&H).

Therefore, the anterior E12.5 and extreme posterior E13.5 data, in combination with the preliminary data from our collaboration with the Goodwin lab, suggest that the mammalian PSs might grow horizontally by default anteriorly, and horizontally with a slight inferior tilt posteriorly.

5.3 Discussion

5.3.1 Palatogenesis in the echidna and functional insights

This work provides the first description of palatogenesis in a monotreme and does not support Seydel's early suggestion that the PSs are not primarily ventrally orientated in the monotreme, nor Ferguson's suggestion that the alligator is the only animal with a 'mammal-like' palate that also hatches from an egg. (Ferguson, 1981b; Polzl, 1905). It appears that PS elevation is a conserved process across all mammalian orders.

Moreover, the data disprove my theory that the PSs elevate as a consequence of the mammalian suckling requirement. There are two main caveats to this: firstly, the little we know about post-partum feeding in the echidna is limiting. The ongoing disagreement as to whether they suckle or lick blurs the situation; these findings could suggest evidence for suckling, given the requirement of the early large muscular tongue and the conservation of the palatogenesis across all orders of mammal. If this is the case, the revelation of monotreme elevation might instead be unsurprising.

Secondly, whilst the echidnas and the platypus are the only extant monotremes, the fossil records indicate that there are millions of years of extinct monotremes with varying dentition and, in some cases, in total absence of a beak (Pascual et al., 2002). This suggests differential mechanisms of feeding in the more ancient monotremes. This was reported previously by Crompton et al (2019), reporting that monotremes once suckled, but lost this ability in the more recent, extant species to do so. This could be an alternative explanation as to why the shelves still elevate, if indeed they do not suckle. In other words, PS elevation in a non-suckling extant monotreme might represent early conservation of developmental traits (Richardson and Keuck, 2002; Oppenheimer, 1959). This would fulfil Baer's third law, which states that basic traits are conserved at the higher level of taxonomic groupings and appear in earlier stages of embryogenesis, where more specialised traits are more likely to be shared by lower taxa, with PS elevation between mammalian orders fulfilling the latter (von Baer, 1828). The typically given examples in support of Baer's third law are the notochord and pharyngeal arches, being chordate-shared features developing relatively early across the vertebrates (Uesaka et al., 2022;

Abzhanov, 2013). Similarly, this might be demonstrated genetically via the resistance of the Hox code expression across evolutionary variation (Duboule, 1994) and the relative conservation of the mid-embryogenesis vertebrate transcriptome (Hu et al., 2017). Further evidence for this is given by the relatively large embryonic echidna tongue, and the juvenile and adult long, thin tongue.

Furthermore, the description of the embryonic echidna oral cavity could highlight other regions of interest in the craniofacial apparatus that may be relevant to PS elevation. The relatively large space in the mandibular cavity (*Figure 5.6*) could explain why the PSs appear, relative to the mouse, somewhat horizontally elevated whilst still under the tongue (*Figure 5.5A, C, G&E*). It is unclear if this large space remains during postnatal development, or if it serves any particular function during feeding. Otherwise, of note is the open anterior palate on hatching, compared to the closed palate posteriorly (*Figure 5.4*). This may play a role in the echidna blowing mucosal bubbles over its snout to maintain both thermoregulation and electroreception, the latter utilised in hunting ants (Gregory et al., 1989; Cooper and Withers, 2023). The open anterior palate may enable extra pressure to be built in this partial continuum of the oronasal cavities, thus blowing a bigger bubble. It would be helpful to identify if the anterior palate remains patent in the adult echidna, though it does seem to be from photographs of the adult echidna skull in the oral view (Rismiller and Grutzner, 2019). However, it is unclear which parts of the echidna embryonic craniofacial apparatus relate to which anatomical location in the adult skill, particularly between maxillae, snout and beak. The adult echidna snout has been described previously (Higashiyama et al., 2021), but no reference is made to the palate, thus it remains difficult to determine the relationship between the embryonic and adult structures, and if the anterior palate even remains open, without further investigation.

Overall, these findings provide an interesting description of early palatogenesis in Monotremata but do little to directly inform us on the origins of PS elevation, nor the extant mechanism underlying the event. Arguably, it simply demonstrates that the event is a few million years older than may have been inferred previously. It would be informative to generate a similar time-course on embryonic platypus tissue. Whilst the echidna and platypus reportedly diverged around 112.5 million years ago based on

phenotypic description (hence 'living fossils'), a multigene and fossil analysis study reported that the echidna in fact branched off from the platypus 19 – 48 million years ago (Phillips et al., 2009). Therefore, the platypus could provide a better insight into the evolutionary state of palate development based on any extant mammal. However, the platypus is potentially less available for scientific research than the echidna, as it is comparatively more conversationally threatened. Future possible work could include completing the time-course of echidna craniofacial development across all 10 days *in Ovo*, but again this would depend on the availability of what is relatively rare issue.

5.3.2 The mammalian and amniotic non-mammalian palates could be homoplasic structures

The identification of elevation in the echidna demonstrates that PS elevation is a trait common to all three mammalian orders, who also ossify at least part of their palate. The only extant non-mammalian amniotes with a mammalian-like secondary palate are the Crocodylia, with the chick palate somewhat similar besides the permanent cleft.

It is helpful in building a picture of how these structures might have evolved in different clades to consider the basal amniotes, i.e., the root of the amniotic tree (*Figure 5.8*). The amniote ancestors evolved from amphibious Reptiliomorpha, tetrapods sharing a closer common ancestor with amniotes that extant amphibians, just over 300 million years ago (Benton and Donoghue, 2007). These early amniotes split into the clades outlined previously, Sauropsida and Synapsida and, whilst Synapsida would eventually give rise to the mammalian orders, the earliest synapsids were reptile-like and are not considered mammalian. There is fossil evidence of some of these early non-mammalian synapsids, such as *Promoschorhynchus*, which exhibits rudimentary palatal outgrowth that are cleft (Maier et al., 1996). This inter-palatal gap may indeed have been bridged by soft tissue, but beyond this the early synapsid palate very much resembles that of the more ancient extant sauropsids: Testudines (e.g., turtles) and Lepidosauria (e.g., snakes). I previously referred to these orders as not having 'true palates' and when compared to the Aves, Crocodylia and all mammalian orders they stand out as described. However, they do closely resemble the reptile palate, and therefore likely that of the amniotic ancestors,

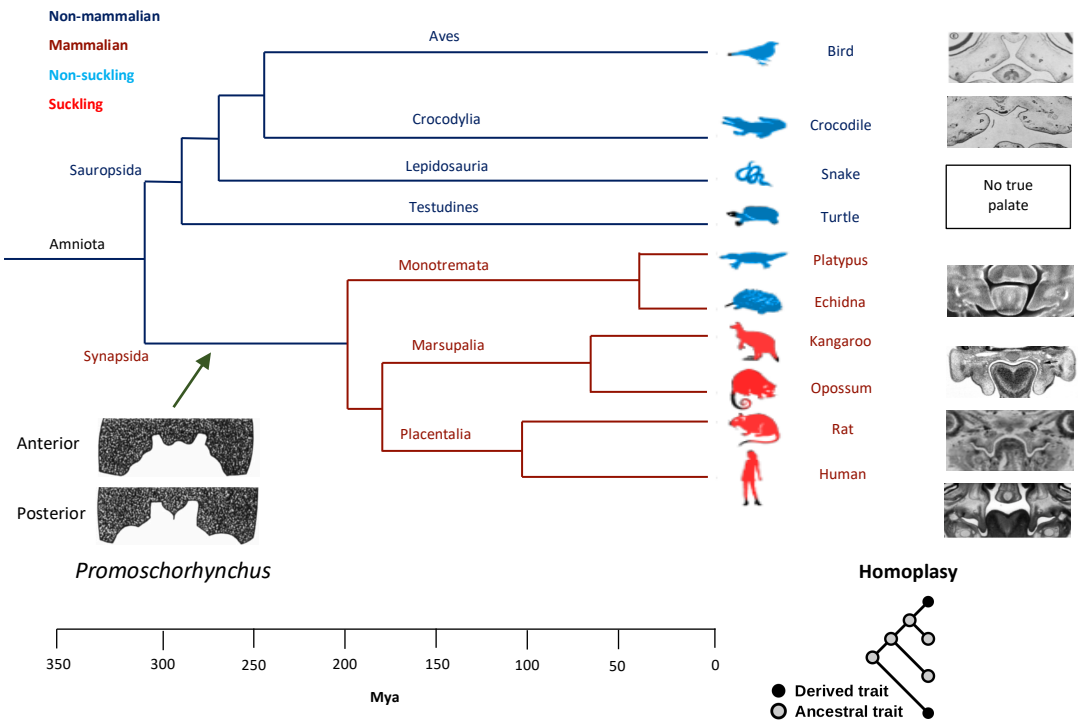

Figure 5.8 Updated amniotic phylogenetic tree of PS elevation and feeding mechanisms including the echidna palate demonstrating suggesting palatal homoplasy

Updated amniotic phylogenetic tree displaying mammals (burgundy lines) and non-mammals (dark blue lines) of the clade Amniota, their relative evolutionary origins, and coloured sketches displaying whether they suckle (light blue) or do not suckle (light red). Previously presented photomicrographs have been updated to include that of the short-beaked echidna from this work, and the ancient non-mammalian synapsid, *Promoschorhynchu*s (Maier et al., 1996). As before, representative photomicrographs are from the chick (Foreman et al., 1991), alligator (Ferguson, 1981), human (Sperber, 2002) rat (Coleman, 1965), and the grey short-tailed opossum (Smith, 2006b). Green arrow, approximate date of origin of the *Promoschorhynchus* fossil. Mya, millions of years ago. The tree structure was traced (Krubitzer and Campi, 2009). Homoplasy diagram adapted from Page & Holmes, 1998.

Reptiliomorpha, and perhaps the non-mammalian synapsid ancestors to the extant mammalian orders, such as *Promoschorhynchus* (*Figure 5.8*, green arrow).

The fused secondary palate appears to be a much more recent feature acquired independently in both the sauropsids (Crocodylia only) and the synapsids (mammalian orders only), with analogous roles in mastication. However, the mechanism by which the structure develops is acquired by different means between the groups, with elevation only occurring in the mammals. Hence, the synapsid and sauropsid palates may be homoplasic: structures which are independently acquired in immediately unrelated

lineages. There are two types of homoplasy that could be true of the palate: parallel evolution (the independent evolution of the same trait from the same ancestral condition) and convergent evolution (the independent evolution of the same trait from different ancestral conditions) (*Figure 5.8*) (Page and Holmes, 1998). On the fossil-record informed inference that the non-mammalian synapsid palate resembled that of the extant more ancient extant sauropsids, it appears that the secondary palate between Crocodylia/Aves and the mammals are homoplasic structures acquired by parallel evolution.

Furthermore, there is functional evidence for this from cross-species palatal shelf heterologous recombination experiments. In static, Trowell-type culture, the PSs of the chick, alligator and mice were placed in contact in each possible combination and incubated for 3.5 days. There was no fusion observed between any vertebrate heterologous combination, with full fusion observed in a mouse homologous PS pairing only (Ferguson et al., 1984). This demonstrates that the molecular crosstalk between the PSs driving fusion in mammals is not sufficient to induce fusion in the non-mammals.

Finally, the apparent default horizontal growth of the mouse PSs in the microglossia mutant mouse, the anterior E12.5 and extreme posterior end E13.5 PS orientation, resemble that of palatogenesis seen in the non-mammal amniotes. This suggests that, in the absence of the large tongue, mammalian PS development becomes more non-mammalian and perhaps more reptile-like, i.e., representative of what is likely the ancestral state of palatogenesis. However, a larger sample size across a wider range of stages is required to investigate this further, and these data are preliminary.

5.3.3 Summary

The work in this chapter describes palatogenesis in a monotreme, the echidna, and highlights regions of interest in the anterior palate and mandibular oral cavity. The latter may facilitate underlying echidna thermoregulation and feeding methods. It also gives evidence for the mammalian and non-mammalian palates being homoplasic structures, arising via parallel evolution. The preliminary data from the microglossia mutant mouse

supports the hypothesis that there is an evolutionarily conserved default horizontal growth programme, but that the mammalian acquirement of a large tongue may cause their ventral deflection.

6. Investigating the location, generation and mediation of the internal shelf force, and the material properties of the PSs

6.1 Introduction

This results chapter is broad in scope, encompassing a variety of experimental techniques. However, the overarching goal of the experiments collectively was to map and quantify the internal shelf force throughout the surrounding mesenchyme, identify and establish if it may be stored by fibrous structures in the ECM, and how the event may be facilitated by the material properties of the PSs.

Therefore, this chapter can be considered in five distinct but related sections. The first concerns the training of a deep learning/AI-powered model of automatic segmentation specific to the PS mesenchyme, and the second and third sections describe the application of the model to nuclear morphometrics. Specifically, the model was used to quantify nuclear aspect ratio as a measure of nuclear deformation for force mapping during elevation, and to extract centroid co-ordinates for nuclear spacing analyses. In the fourth section, I seek to resolve conflict in the literature by establishing whether an organised network of mature, aligned elastic or collagen fibres were present in the PSs during elevation. In the fifth section, I provide the first characterisation of the material stiffness of the PSs. The workflow for the first three sections is presented as a flow diagram below (*Figure 3.1*).

As will be described in this chapter, the PS mesenchyme is densely packed and overlapping. Therefore, traditional methods of segmentation by thresholding and watershedding do not work well for the segmentation of PS mesenchymal nuclei. This, combined with the often irregular or stellate shape of mesenchyme cells (Boehm et al., 2010b), and the sheer number of cells in the region provided non-trivial challenges in accurate segmentation. This renders manual outlining impractical. In recent years, deep

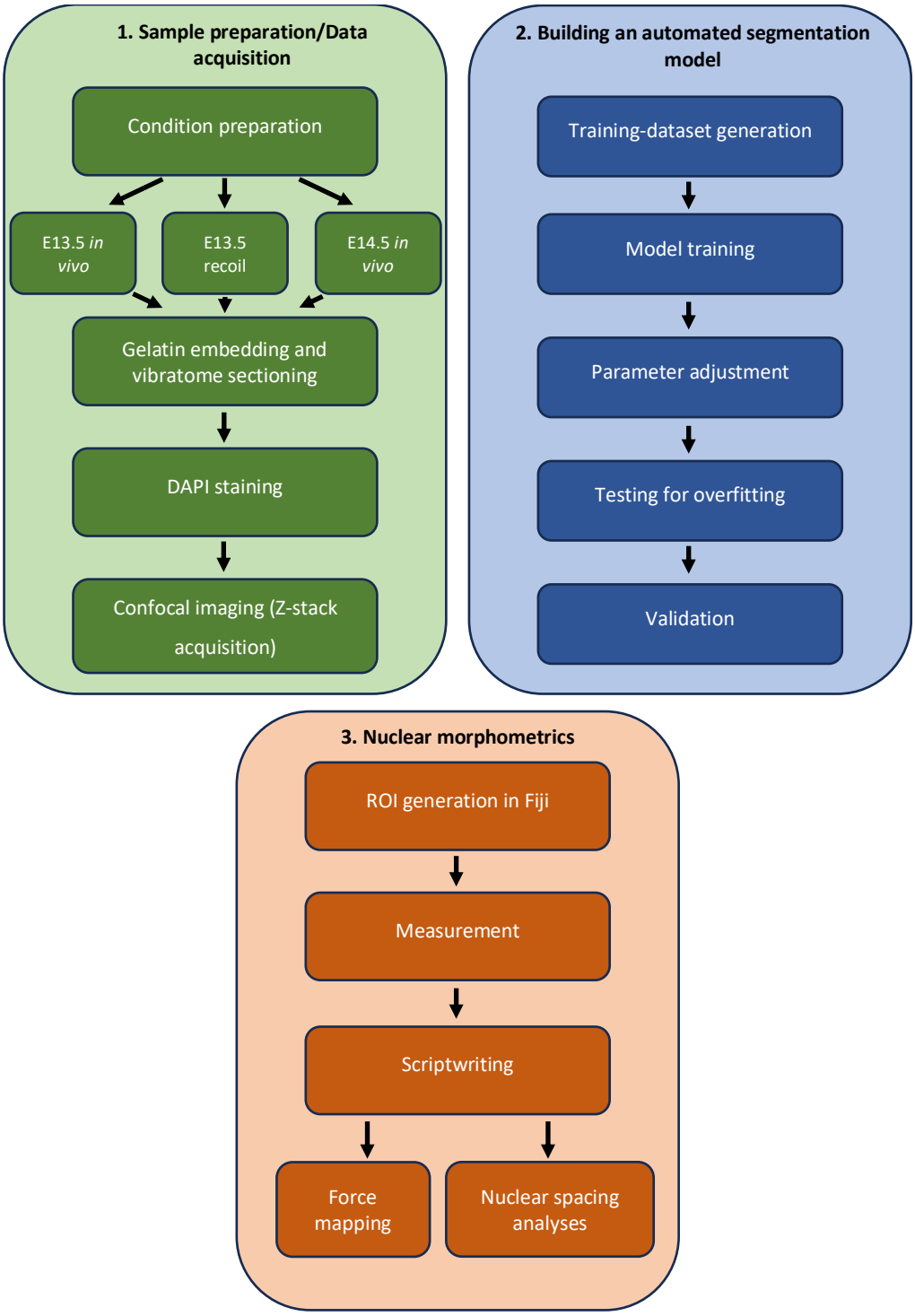

Figure 6.1 Workflow and relation between recoil experiments (sample preparation), StarDist model training and nuclear morphometric studies

Diagram overviewing how samples were prepared for the various analyses throughout this results chapter (1), a simplification of the steps taken to train a StarDist nuclear segmentation model (2) and how the model generated (2) was applied to the sample conditions (1) for nuclear morphometric studies including force mapping via nuclear aspect ratio and nuclear spacing analyses (3). Detailed explanations are given for each box in the relevant sections of this chapter.

learning pipelines have been constructed to address these challenges, and there are currently several options when training a model for automated nuclear segmentation. Recent inter-pipeline comparisons suggest that StarDist, a deep learning model of object detection with star-convex polygons, is the superior model of nuclear segmentation in terms of accurately segmentally overlapping nuclei (Kleinberg et al., 2022). Further details and the technical aspects are outlined below in the training results (*6.2.1*). Several properties can be extracted from accurately segmented nuclei, including their aspect ratio, shape, relative angle, and centroid co-ordinates. The accurate and large-scale acquisition of these data enables extensive nuclear morphometric studies, such as force mapping by nuclear deformation mapping and nuclear spacing analyses.

The presence of forces in tissues undergoing morphogenesis can be mapped using nuclear deformation (i.e., nuclear aspect ratio) as a proxy marker for force. since relaxed nuclei are generally spherical in shape and, when subject to force, adopt an ellipsoid shape that reverts to spherical when the force is removed (e.g. *Figure 6.2*). Mapping the collective aspect ratios of nuclei (i.e. the extent of deformation) gives a spatial representation of the presence of forces in tissues (Friedl et al., 2012; Krause et al., 2013) This application of deformation mapping has been used previously in investigating parabasal contraction in the invaginating tooth placode (Panousopoulou and Green, 2016). Whilst nuclear deformation studies provide evidence as to where forces may be active, they cannot distinguish between tensile forces in one direction versus compressive forces in an orthogonal direction. However, as previously described (*1.4.1*) I reasoned that the location of deformed nuclei in palatal shelf would suggest which type of force is active at any given locus, since only tensile forces acting superiorly and/or pushing forces inferiorly could result in elevation. Therefore, the nuclear deformation mapping described in this chapter promised to provide an insight into the previously undescribed tissue-scale location of forces during PS elevation.

Regional changes in cell density could also be indicative of differences in localised cellular behaviours. For example, it could represent an increase in matrix production between cells either pushing cells together or apart, and a sudden increase in density might represent a burst of proliferation. Increased cell density is also thought to direct

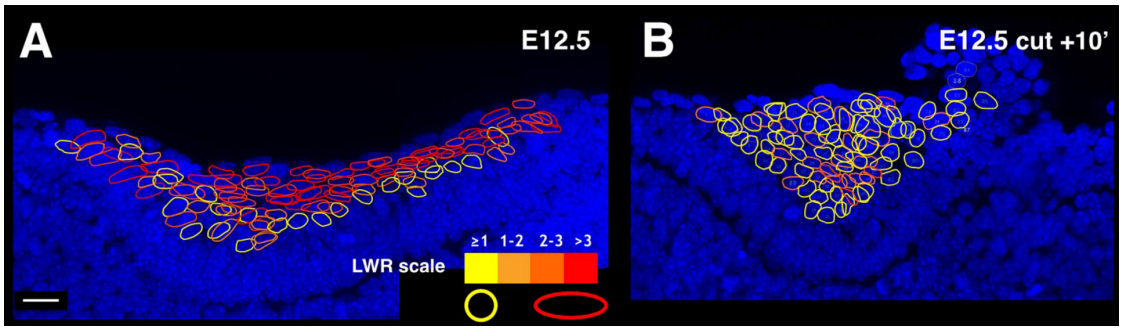

Figure 6.2 Nuclear deformation in the invaginating tooth placode

Nuclear shape signature maps tension in the cells during tissue morphogenesis. A) E12.5 tooth placode with nuclei outlined in yellow (low aspect ratio, relaxed) and red (high aspect ratio, under tension). B) Cut and recoil experiment causing the release of placodal tension, marked by previously deformed nuclei (red) adopting a spherical relaced shape (yellow). Scale bar = 30 µm (adapted from Green & Panousopoulou, 2016).

fibronectin deposition in the midpalate (Tang et al., 2015) as described previously (*1.4.5.3*), suggesting spacing changes may influence ECM behaviours. As with Brinkley and Bookstein's (1986) computational study into cell density during elevation (*1.4.6*) descriptions of cell density/spacing changes during elevation have been qualitative. In the Wistar rat, Ferguson (1977) describes the mesenchyme as densely packed during vertical PS growth, followed by an increase in spacing immediately prior to elevation, predominantly in the anterior PSs; the same observations were made earlier in the 'Swiss white' mouse (Sweney and Shapiro, 1970). Cellular spacing has also been linked to CL/P, with the embryos of pregnant 'Wistar Hannover' rats injected with the synthetic corticosteroid displaying a decrease in density and CL/P. However, from the photomicrographs provided in Sweney and Shapiro (1970), it appears that the PSs have in fact elevated, but not fused, which may suggest that change in cell spacing do not play a role in elevation itself. Similarly, in a study investigating the teratogenic effects of hydrocortisone on the hamster palate found that elevation occurred with no delay, cell spacing increased between vertical growth and immediately prior to elevation (Shah et al., 1989). More recently, heat maps of palatal spacing were generated in the Green lab using semi-automatically segmented nuclei by specialist image analysis software (Volocity). The results are reported as being complex/difficult to interpret, but broadly seem to agree with the published literature in that the PS mesenchyme are less densely packed immediately prior to elevation than during vertical growth (Brock et al., 2016).

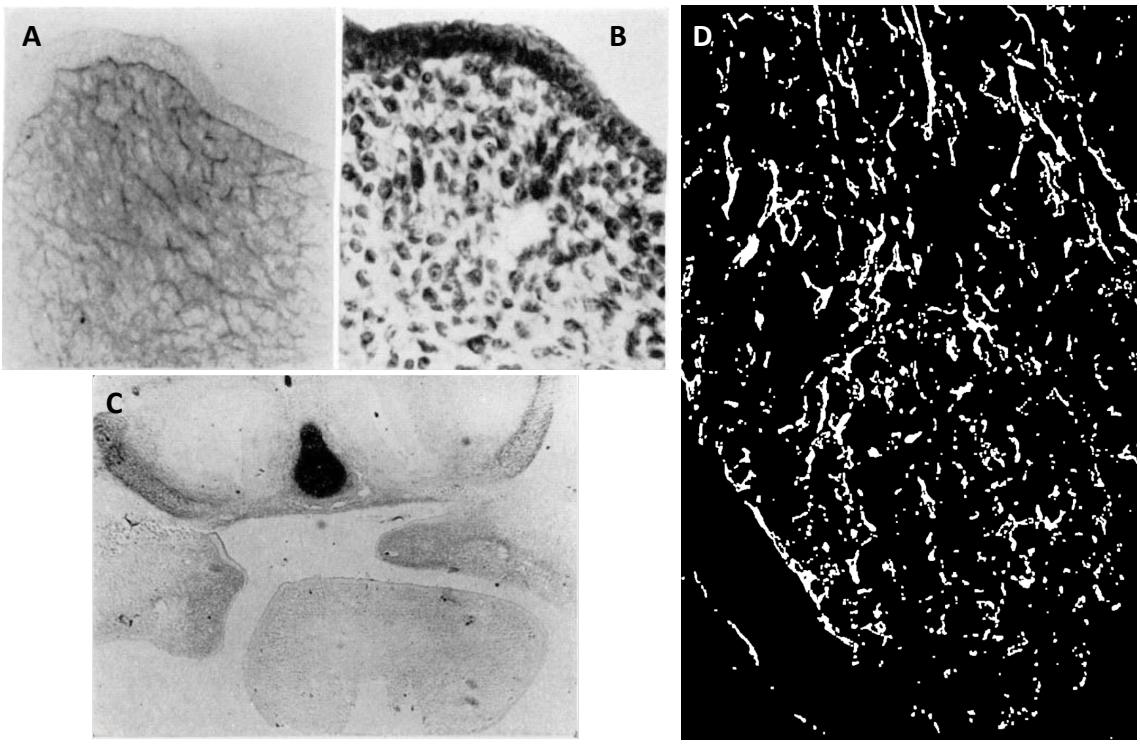

Figure 6.3 Reported evidence of elastic and collagenous fibres

Reported evidence for elastic fibres (A-C) and collagen bundles in the PSs during elevation. A) PS tissue following Gomori staining for elastic fibres with corresponding H&E stain (B). C) Gomori-stained PSs in a captured instance of unilateral elevation. The authors do not describe the orientation of the PSs in A&B nor the relative A – P position, and so this is difficult to interpret. D) Unelevated Wistar rat PS stained with an antibody against collagen I. The author states that, centrally, there are clear stout bundles of collagen fibres running from base to tip. Adapted from Walker & Fraser, 1956 (A – C) and Ferguson, 1988 (D).

However, segmentation methods have improved dramatically since that study and so it made sense to revisit the analysis with the more reliable machine-learning StarDist tool.

While shape and spacing of nuclei promised to locate forces within the palate mesenchyme, they could give only limited clues as to the mechanism of force generation. There was an unresolved conflict in the literature not only as to whether the internal shelf force is tensile and mediated by fibrous ECM components or not, but also whether such tensile components are present at all. Walker and Fraser (1956) proposed that a network of elastic fibres running throughout the core of the PSs drives elevation (*Figure 6.3A&C*), but subsequent research failed to identify the structures reported by Walker and Fraser (Frommer and Monroe, 1969). This does not appear to have been addressed since. It was later proposed that collagen fibres instead fulfil this role, with Ferguson (1988) staining

unelevated rat palate with a collagen I antibody, reporting that it shows stout organised bundles (*Figure 6.3D*). Again, this is unclear and despite great advancements in imaging techniques the role of even presence of the reported collagen bundles have not been confirmed. Therefore, it seemed fairly straightforward to repeat Walker & Fraser's experiment to settle the elastic fibre literature conflict, and to use modern imaging techniques that would enable interrogation of the nature of mature bundles of collagen in the PSs (*6.2.4.3*).

Finally, the material properties of the PSs appear to remain entirely uncharacterised during or in relation to elevation. In the last decade atomic force microscopy (AFM) has been used to characterise the material properties, typically the elastic modulus, in a variety of different biomaterials such as human brain (Long et al., 2018), mouse ovarian follicles (Hopkins et al., 2021) and various disease model cell lines (Gautier et al., 2015). This is referred to as 'bio-AFM' and its increasingly popularity has resulted in recent protocol publications making the technique more accessible for first-time users (Norman et al., 2021). A characterisation of the material properties of the PSs during elevation could be helpful to understanding the apparent heterogeneity in elevation and may explain the way they appear to interact differently with the tongue along the AP axis. Therefore, I performed AFM on the surface and the mesenchymal cores of isolated PSs and provide the first description of differential stiffness along the A – P axis, between the epithelial surface and mesenchymal core, and between sub-regions in the same A – P plane.

6.2 Results

6.2.1 Building a deep learning model of automated nuclear segmentation

Mesenchymal nuclear deformation mapping was used to map the presence of force in the PSs prior to and immediately after elevation in *in vivo* frontal sections, and in embryos following tongue removal and the elastic recoil elevation of the PSs. However, from the outset it was clear that there were several hurdles to overcome when designing these analyses.

Foremost, it was clearly not feasible to manually outline nuclei in the PSs and immediately surrounding maxillary region at E13.5 due to the sheer number of nuclei (≈8000 nuclei per PS). Hence, manually outlining both anterior and posterior PS mesenchyme in three study groups across 4 samples (totalling 24 images ≈192000 nuclei) was not an option. Therefore, I opted to train a user-generated deep-learning model of automatic nuclear segmentation, StarDist (see Materials and Methods for detailed background information of StarDist models and machine learning).

Alongside building a new model from scratch, StarDist suggests that the user-generated model includes weight from their own 'versatile nuclei' model. This is a community generated model with users consistently add their training datasets to. Theoretically, it can automatically outline any objects it is trained on, and so could eventually work on any nuclei The 'versatile mode' can be used in a simple and straightforward manner on images via a plugin in Fiji, and I carried out a pre-training Z-depth optimisation using this model.

6.2.1.1 2.5 µm is the optimum Z-projection for nuclear recognition in StarDist

Before generating training images for the model, there was an opportunity to maximise the future accuracy of the model. Z-projections are commonly used in confocal microscopy in the context of cellular or nuclear morphology analysis give a more complete idea of shape. Essentially, the greater the Z-depth of the image(s) captured, the more likely one is to capture the widest part of the nucleus. This echoes 'Wicksell's corpuscle problem' which is that planar sections lead to two opposing but not cancelling artefacts in corpuscle (e.g. nucleus) size estimation, namely grazing (which underestimates diameter) and inclusion bias (which favours larger diameters) (Wicksell, 1925). However, since I was interested in shape rather than size, only the problem of misleading grazing sections was of greater concern. I reasoned that using Z-projection images here had the potential to improve the number of objects successfully recognised, and a greater chance of capturing the centre or widest point of the generally spheroid nuclei, which would be a better indicator of gross deformation. I set out to test empirically what the optimal Z-projection depth should be.

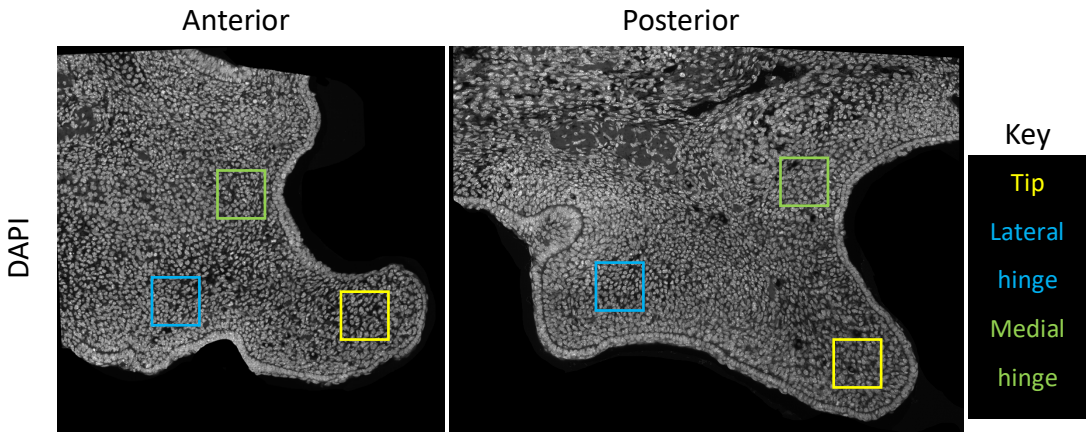

Figure 6.4 Regions selected for StarDist nuclear recognition testing on different Z-projections.

Representative confocal images of DAPI-stained anterior and posterior with regions selected for StarDist nuclear segmentation at difference Z-projections. Names of each region are given in the colour-coded key and are used throughout this chapter.

For this optimisation, I used the "versatile" (henceforth 'default') nuclear segmentation model within Stardist. I sampled 256 x 256 pixel areas of the tile scans generated for this analysis (see Materials and Methods) and compared different Z-projection depths 12.5 µm, 5 µm, 2.5 µm and 0.5 µm (single slice) consisting of 25, 10, 5 and one 0.5 µm optical sections respectively. In all cases, Z-stacks were started 2 µm deep into the tissue surface to avoid physical sectioning artifacts.

Sample regions were taken from three separate locations, designated the tip, medial hinge and lateral hinge (*Figure 6.4*) across *in vivo* E13.5 unelevated shelves, E13.5 elevated PSs via tongue and mandible (t/m) removal and *in vivo* E14.5 elevated PSs in both the anterior and the posterior (n = 5 samples from each condition).

In Fiji (Schindelin et al., 2012), I then manually counted the number of nuclei and ran the StarDist default model, recording the number of objects identified in each. I then calculated the percentage difference between the ground truth (taken as number of nuclei counted manually).

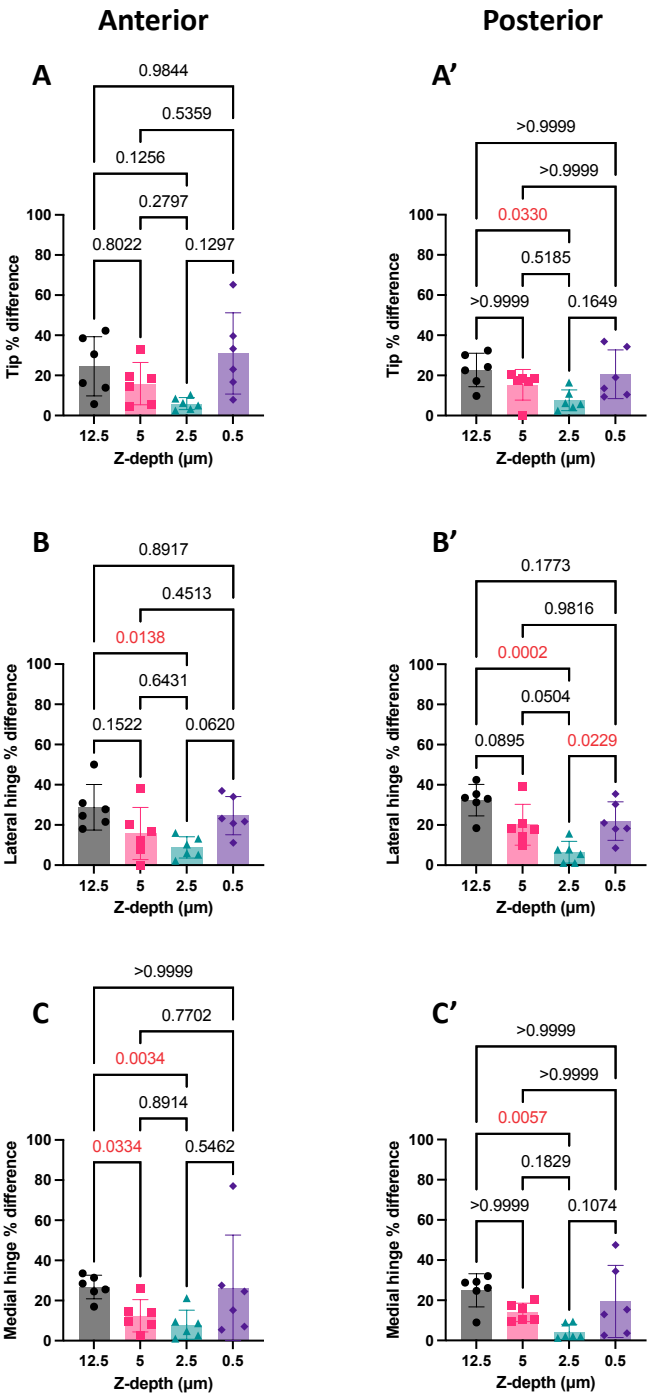

Figure 6.5 Percentage difference between manually counted vs. StarDist default model detected nuclei count

Graphs show % difference between manual and automated counts of nuclei at different Z-projection depths in the PS tip (A&A'), lateral hinge (B&B') and medial hinge (C&C') regions. This was tested in both the anterior (A, B, C) and posterior (A', B', C') PSs. Statistical significance (P values) is shown on graphs and determined by Brown-Forsythe & Welch's ANOVA tests (A&C) with Dunnett's T3 multiple comparisons, ordinary one-way ANOVA (B&B') with Tukey's multiple comparisons, and Kruskal-Wallis test (A'&C') with Dunn's multiple comparisons test. Error bars = mean with SD.

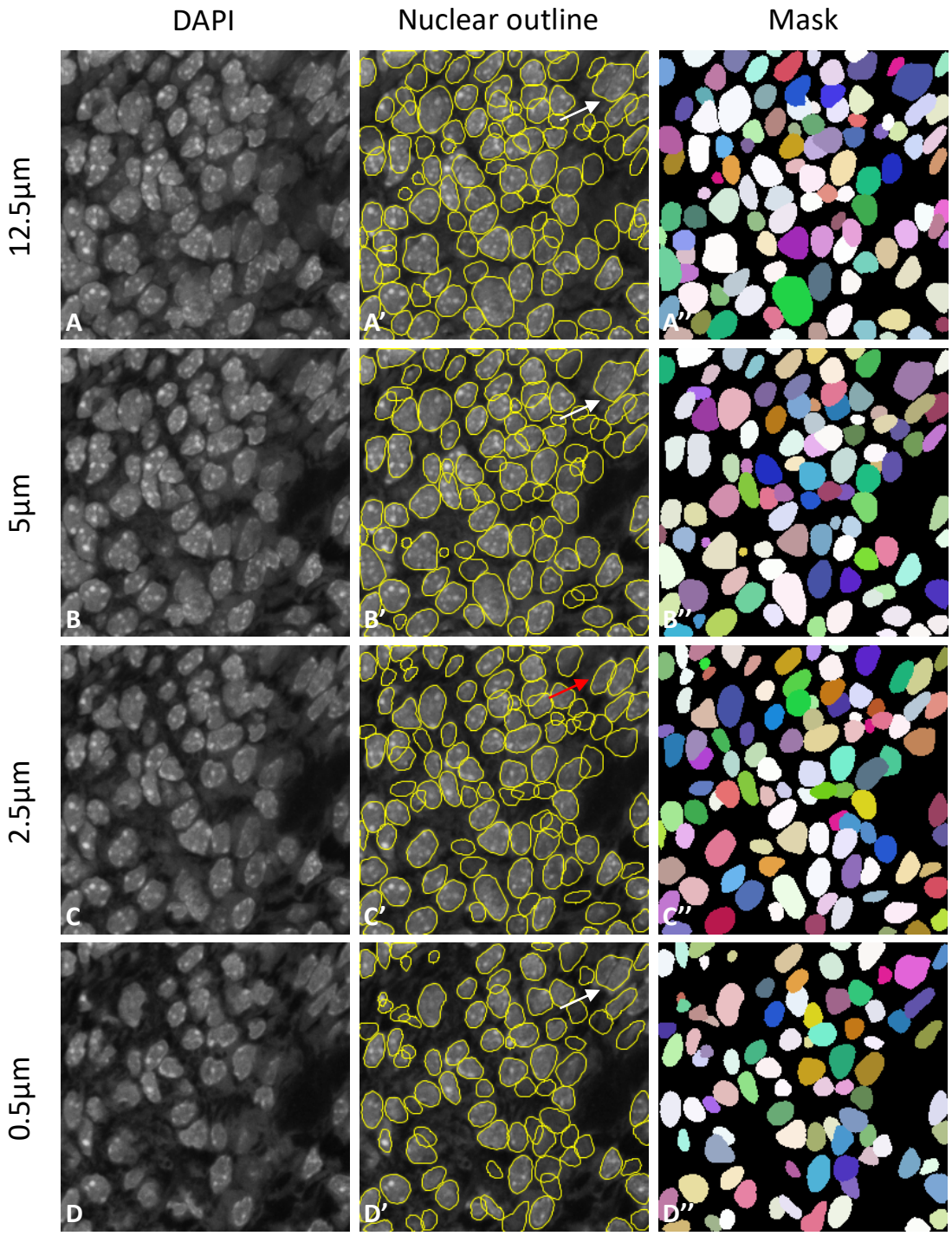

Figure 6.6 StarDist default model object detection at different Z-projections

Representative confocal images of DAPI-stained sample regions selected for StarDist nuclei recognition testing at 12.5 µm (A-A''), 5 µm (B-B''), 2.5 µm (C-C'') and in single 0.5 µm slices (D-D''). Yellow outlines are the ROIs automatically generated to outline nuclei by the StarDist default model, and masks are filled graphical representations of the segmented ROIs. White arrows represented erroneously segmented nuclei; red arrow represents corresponding accurately segmented nuclei example.

In all three regions in both anterior and posterior, a Z-projection of 2.5 µm (5 optical slices) resulted in the default StarDist model most accurately counting the number of nuclei (*Figure 6.5*). Comparing the original images side-by-side with the ROI overlay generated by StarDist *(Figure 6.6*) it was easily apparent that the greater the Z-depth, the more nuclei were included and the more there was overlap. Hence, it was unsurprising that the 12.5 µm Z-projection had the lowest nuclear recognition accuracy. On the other hand, in the single slices several small objects, such as grazing sections of nuclei, or individual nucleoli were identified as separate objects (*Figure 6.6D-D''*). Thus a Z-projection of 2.5 µm was a 'sweet spot' where enough of the nuclei were captured that they were detected accurately (and outlined), but not so much information was present in the image that overcrowding became an issue (*Figure 6.6C-C''*). This effect was captured in these representative sample images. In the right-hand corner of each image there are aligned, elongated nuclei, marked by arrows in *Figure 6.6A', B', C', D'*. In the 2.5 µm Z-projection, the default model accurately identified the nuclei and two separate, elongated objects (red arrow) despite not going a great job of accurately outlining them. In each other group, the model failed to recognise them as separate objects, and instead outlined one large, inaccurate shape over the top of them.

I observed that while the default model recognised a similar number of nuclei as counted manually, it was not particularly good at accurately outlining them. This was particularly problematic in elongated nuclei (whose accurate outlining was essential to this study), in regions of overlap and in small, grazing sections of nuclei, thus I did not trust they accurately reflected the nuclear shapes. This provided impetus to train the model from scratch. By training the model on images that included overlapping and elongated nuclei, and excluding the small, grazing sections of nuclei from the training set, a model could theoretically only detect the nuclei useful for the shape assessment. Thus, I determined that a model should be trained from scratch for this particular application, and that a Z-projection of 2.5 µm was a good starting point for generating a training dataset.

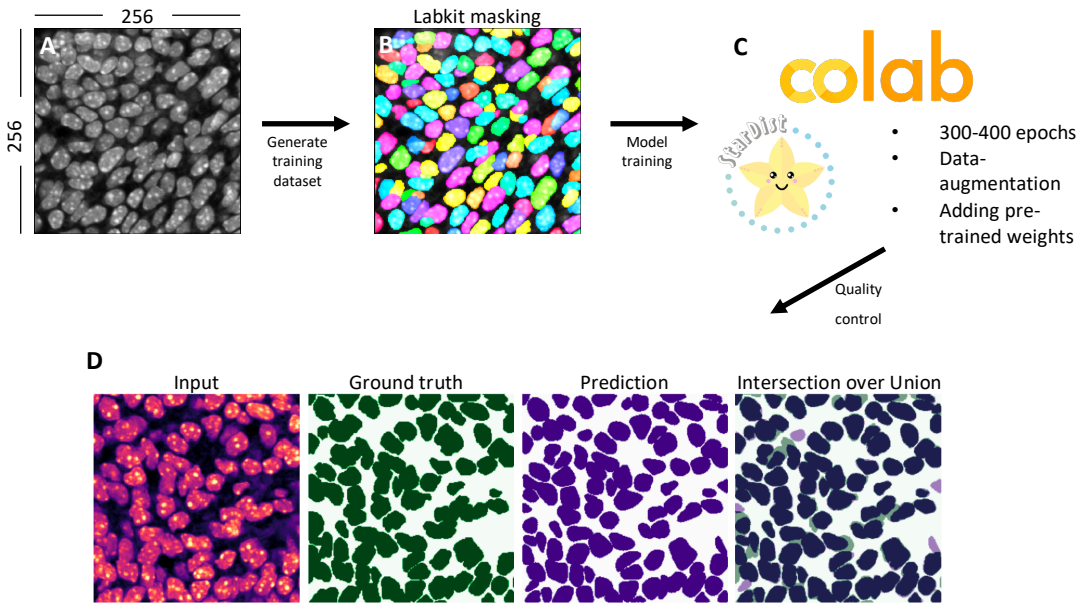

Figure 6.7 StarDist model generation pipeline

Workflow outlining the generation of the training dataset (A), generating the ground truth manually segmented dataset for comparison by the model (B), the use of Google Colab with key training parameter for model generation (C) and quality control via intersection over union analysis (D). Each step is outlined in detail in the associated text.

6.2.1.2 Paired training dataset generation

With the optimum Z-projection identified for use with the default nuclear segmentation model, I then generated the training set of images (i.e., the training dataset) from the large tile scans obtained as described in the materials and methods (*2.6.1*). In total, twenty-four 256 x 256 windows were placed over the tile scanned PS images broadly around the regions outlined in *Figure 6.4*. These 24 samples consisted of 8 each from E13.5 *in vivo* (unelevated), E13.5 t/m removed (elevation by elastic recoil) and E14.5 *in vivo* (elevated) divided equally between the anterior and posterior PS (n = 4 embryos from 3 independent litters per condition).

Next, 'ground truth' (manual) segmentations were generated from the training dataset. Following the recommended StarDist model training procedure, I manually masked nuclei within the FIJI plugin 'LABKIT' using its manual masking 'nuclei painting' feature (Arzt et al., 2022). Each sample image was loaded into LABKIT as a background layer, and nucleus was manually painted over with a paintbrush tool and assigned its own label. Each sample region contained between 100 – 250 nuclei, with each image taking around one – two

hours to manually segment. I found that better results were obtained if the training mask was as close to pixel perfect as possible.

Following the StarDist protocol (see *2.8* and *9.3* for details) I set out to test several parameters for the machine learning. I first varied the number of "epochs" (training passes through the dataset) to maximise learning without over-fitting, then applied data augmentation (flipping and rotating the training images between passes to further prevent over-fitting) and finally added information from pre-trained models ("transfer learning") which can further enhance the training. In materials and methods section *2.8*, and appendix 3 (*9.3*) I give a detailed background to machine learning, model building and performance assessment. This may be helpful in interpreting my training results in the rest of this section.

In my model training, loss and validation loss did not converge (flatten out with increasing epoch number) as completely or quickly when adding weights from the pretrained default model (*Figure 6.8A*), compared to when leaving them out (*Figure 6.8B*). Training loss decreased as a steady rate, suggesting its predictions were closely matching that of the ground state dataset, while validation loss decreased slightly, before levelling-off early (*Figure 6.8A*). The slight increase in validation loss also suggests it was not performing well on the test data. Unintuitively, however, when my model was trained without added weight from the pretrained model, both training and validation loss curves converged (levelled-off) quickly (*Figure 6.8B*). This suggests that the model is fully trained, and no overfitting had occurred. In theory, the pre-trained weight from a much more diverse set of nuclei could have improved convergence if the data themselves and the training parameters were similar enough, though it might also result in them taking longer to converge as it has a larger dataset to train on. These results therefore suggested that either my images and segmentation were significantly different from the default training set and/or that further fine-tuning of the hyperparameters would be required to achieve the full potential from the model.

At this stage the model is technically ready for use but further quality control training in the Colab notebook was possible. Before continuing with quality control training, I tested

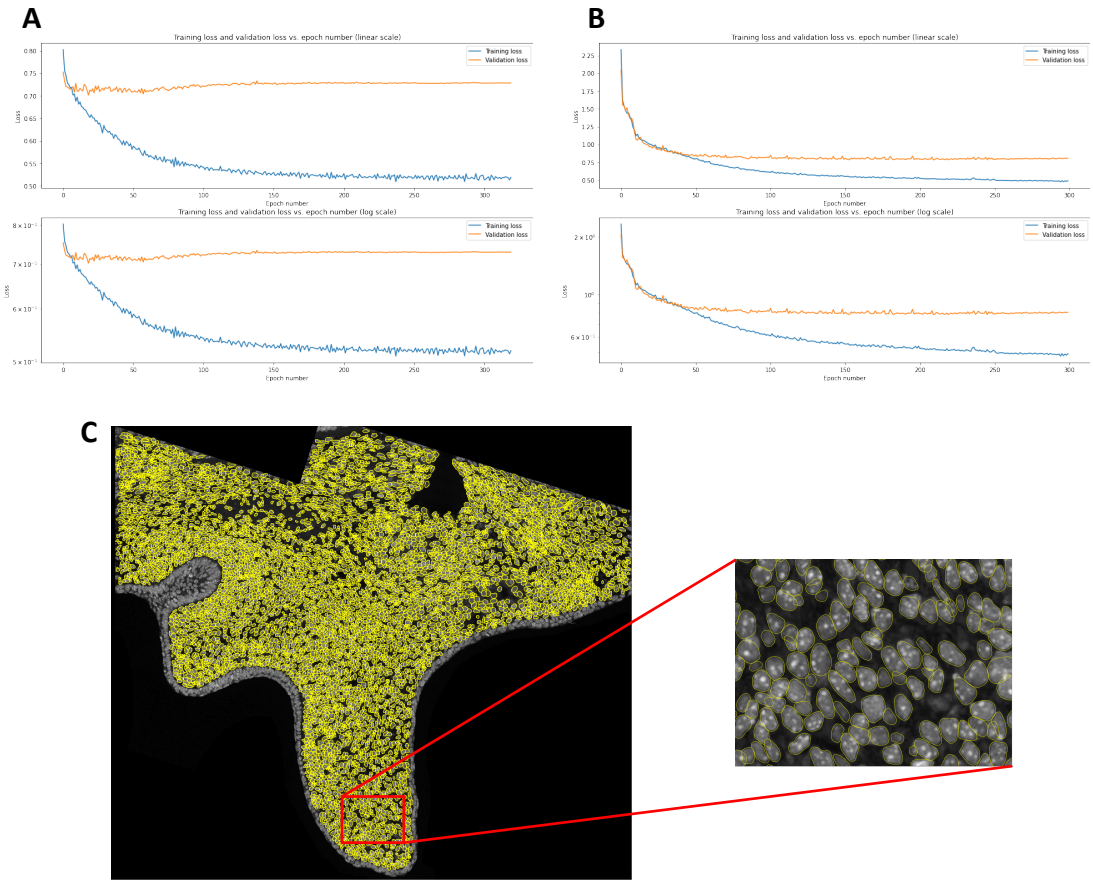

Figure 6.8 StarDist model loss function plots and test run on an unseen image

Graphs generated during model training by Colab showing training loss (blue) and validation loss (orange) in a model built using pre-trained weights (A) and without (B). C) Model testing: posterior unelevated PS at E13.5 after running StarDist. Yellow circles are ROIs generated in Fiji by my model.

the model with the added weights (*Figure 6.8A*) on a larger-scale tile scanned image of the unelevated posterior PS (approximately 8000 nuclei) first. Despite the apparent less complete convergence and higher values of the training and validation loss functions at the end of the training, the model appeared to faithfully outline nuclei on visual inspection (*Figure 6.8C*). It appeared to ignore grazing sections of nuclei, and mostly outlined individual and overlapping nuclei extremely well. It was not trained on epithelia, and so generally ignored these. There were instances where the model would erroneously outline over the top of several epithelia or confuse the boundaries between particularly challenging overlapping nuclei. However, this was easily corrected via a quick manual clean-up over the image, and the majority od the PS epithelium was manually

Table 6.1 Quality control testing results for PS mesenchyme nuclear automatic segmentation StarDist model on three unseen images

Test image	Intersection over union (IoU)	False positive	True positive	False negative	Precision	Recall	Accuracy	F1 score	N_True	N_Pred	Mean true score	Mean matched score	Panoptic quality
1	0.86	18	83	33	0.822	0.716	0.619	0.765	116	101	0.583	0.815	0.623
2	0.823	18	108	39	0.857	0.735	0.655	0.791	147	126	0.57	0.776	0.614
3	0.827	4	77	26	0.951	0.748	0.72	0.837	103	81	0.602	0.806	0.674
Average	**0.837**				**0.877**	**0.733**	**0.665**	**0.798**			**0.585**	**0.799**	**0.637**

Table key: False positive: N_Pred – true positive. **True positive**: an identified object with an IoU value of > 0.5. **False negative:** N_True – true positive. **Mean matched score**: mean IoUs of matched true positives. **Mean true score**: mean IoUs of matched true positives normalised by N_True. **Precision**: True positives / (True positives + False positives). **Recall:** True positives / (True positives + False negatives). **F1 score:** indicates the balance between the precision and recall of the model by 2 [(Precision x Recall) / (Precision + Recall)]. **Accuracy**: True positives / N_Pred. **Panoptic quality**: evaluates the ability of the model to segment both and between defined/discrete objects and background uncountable elements This is a complex measure explained in detail elsewhere (Kirillov et al., 2018), but is not required for interpreting my model.

deleted in Fiji during the initial image processing. Nonetheless, to better assess how the model was performing, I continued with the in-built quality control feature.

6.2.1.3 Quality control

Quality control testing was performed on the images that were removed from the training dataset during initialisation. The Colab automatically generated a table of the quality metrics.

The **intersection over union (IoU)** score is a criterion typically used to quantify the percentage overlap between the model prediction and mask/ground truth image across deep learning models. The closer to 1, the better the model is performing. This is represented visually in *Figure 6.7D*. In the Colab notebook, IoU is calculated both over the whole image (which is what the raw IoU score in the table represents) and over each individual object detected, from which all other metrics in the table are calculated. These are documented in *Table 6.1* and explained in the attached table key.

According to the Colab metrics, the model performed better in some areas than others. However, some of the metrics appeared misleading. For example, the accuracy is fairly low at an average of 0.665, despite high IoU, Precision and F1 scores. When the model is employed, errors that might be expected with a low accuracy score are rarely encountered and, moreover, any that are can be simply manually corrected within Fiji. However, these metrics represent the model nonetheless. The false positive and false negative rates are quite high, compared to a relatively low true positive rate. In fact, it suggests that the model is missing around 30% of the objects. While this is still an improvement on manually outlining this number of nuclei, it is an important criticism to recognise.

IoU is the most commonly used method to evaluate the quality of segmentation models (Sánchez-Peralta et al., 2020). However, IoU thresholds are considered based on the complexity of the images supplied, and there is not a regimented IoU threshold for what is considered a 'good' model common to all images (Schmidt et al., 2018). Hence, interpreting the IoU value should be done in the context of the specific data being evaluated. In the documentation for the default StarDist model, the authors use 0.5 as a threshold value for IoU in comparison to other models. Further, several papers recently used deep learning to identify polyps and colorectal cancers, with model IoU scores of 0.694 (Wichakam et al., 2018), 0.516 (Vázquez et al., 2017), 0.767 (Wickstrøm et al., 2018) and 0.889 (Nguyen and Lee, 2018). Hence, taking the proposed minimum threshold by the StarDist authors, comparison to published models and the physical performance of the model evaluated by the eye into account, this model was deemed satisfactory for the task of segmenting PS mesenchyme nuclei during elevation.

Furthermore, in this application of the model I was specifically trying to measure deformation. Therefore, unlike in the medical applications of deep learning tools, it should be sufficient to sample, i.e., even if the model only detects nuclei with unambiguous shapes, the relatively high IoU versus the counting metrics almost acts as a quality control.

6.2.2 Nuclear deformation analyses reveal a complex distribution of force throughout the PSs during elevation

The trained model was run directly on confocal images within Fiji via the StarDist plugin, and I found the model took approximately 30 seconds to completely segment and generate ROIs for the entire PS area of each tile-scanned composite image. This is several days, and maybe weeks, faster than attempting to segment the same number of nuclei in a single sample image manually.

I hypothesised that elongated nuclei would be predominant in either the medial (prospective nasal) or lateral (prospective oral) hinge regions (or both) prior to elevation and would adopt a more rounded shape post-elevation, acting as a proxy marker for the presence and subsequent relaxation of force. Hence, this could reveal the location of the internal shelf force and indicate whether it was tensile (medial hinge nuclear deformation) or compressive (lateral hinge deformation) or both.

I had initially planned to investigate nuclei deformation in frontal sections *in vivo* at E13.5 (unelevated) and E14.5 (elevated), and with t/m removed at E13.5 (immediately post-elevation by elastic recoil). However, on further inspection of PS mesenchymal nuclei at E14.5, it was decided that there were too many non-elevation specific activities in the tissue at this time to dissever nuclear deformation/elastic relaxation from elevation compared with other factors. For example, the development of the sphenoid bone at this point may exert compression on surrounding nuclei, and the invading vasculature does this strikingly (*Figure 6.8*). Plus, in some samples at E14.5 the process of fusion appears to have begun which could conceivably result in the transfer of force between the opposing PSs to the extent that the underlying mesenchymal nuclei deform, similar to cranial suture fusion (Katsianou et al., 2016; Malde et al., 2019). Therefore, nuclear deformation analyses were not performed on the E14.5 *in vivo* tissue, and instead just on the *in vivo* E13.5 unelevated and t/m removed E13.5 elevated tissue. These two conditions represent the “before” and “after” of a rapid release elastic elevation event, and therefore represent the purest measure of elastic effects.

6.2.2.1 Regionalising the palate in frontal sections

Although I hypothesised that any pronounced differences in nuclear deformation/aspect ratio would be in the medial or lateral hinge regions, it could conceivably be focussed anywhere else, or be present sparsely all throughout. The degree and variability as well as the size and location of any region of nuclear deformation were unknowns. Weak deformations would only be detected by averaging large numbers of cells, but large areas could also contain non-deformed nuclei which would dilute any deformation signal. Therefore, to improve the chance of capturing any effect, I took a progressive regionalisation approach to the images, i.e., I started with the whole image, then divided the structure into progressively smaller regions, measuring the average nuclear aspect ratio in each and comparing like-regions between unelevated and elevated PSs in both the anterior and the posterior.

Reproducible landmarks were set for consistent regionalisation of the PSs between samples for each region measured in both the anterior (*Figure 6.9A-C)* and posterior (*Figure 6.9D-F*). Prior to all regionalisation, the epithelium of the original raw tile scans was manually trimmed away using the freehand shape tool and delete function in Fiji. The same approach was taken to remove the molar tooth bud in posterior regions. This was to reduce the manual labour in deleting the ROIs erroneously placed over the epithelium by the model, as there is no option to delete several ROIs at once in Fiji. Anterior 'Whole' PS regions were segmented away from adjacent maxilla in the epithelium-less tile scans by drawing a line straight up from the epithelial invagination, and horizontally from the point that the PS blade (tip) curves medially in the superior-most aspect (*Figure 6.9A*, in green). In the posterior, a line was drawn upwards from the lateral aspect of the molar tooth bud, joining a line drawn horizontally from the point which the superior part of the PS tip begins to slope upwards (*Figure 6.9D*, in green).

'Upper and tip' regions were drawn by taking the 'whole' regions previously segmented and dividing them and the base of the finger-like projection (i.e., the tip). The remaining region was referred to as the 'upper' regions and this was the same in both the anterior and the posterior (*Figure 6.9B&E*, in blue and orange respectively).

Figure 6.9 Regionalisation of the anterior and posterior PSs for quantitative analyses of the mesenchymal nuclei

Representation of the regions analysed during nuclear deformation and spacing analyses in this chapter in the anterior (A-C) and posterior (D-F) PSs. Green shading represents the 'whole' PS tissue (A&D), orange and blue the 'upper' and 'tip' regions respectively (B&E) and purple and yellow the lateral and medial hinges (C&F). Representative images are in unelevated PSs at E13.5.

'Lateral hinge' regions (*Figure 6.9C&F*, purple) were drawn by drawing a curve between two points. Theoretically, this is where a pushing or compressive force could be acting. In the anterior, the first was placed at the halfway point between the epithelial and the inferior-most point of the 'upper' region invagination (hence the bottom left corner of the image). The second was placed halfway down the tip of the PS. In the posterior, the first was placed at the halfway point between the molar tooth bud and the inferior-most point of the 'upper' region halfway down (hence the bottom left corner of the image). The second was placed halfway down the tip of the PS. In both cases, the curve was

limited such that only a few layers of mesenchyme were included; this is where the greatest extent of overall cell shape change was noted in previous research (Babiarz et al., 1979).

'Medial hinge' regions (*Figure 6.9C&F*, yellow regions) where draw by selecting the first few layers of cells along the whole of the medial surface of the tip region up to the points of acute curvature increase superiorly described previously. This region is where tensile forces could be operating and, if mediated by some fibrous network, could run the full length of this aspect of the PSs. The same approach was applied to both the anterior and posterior PSs in these regions.

6.2.2.2 Heat maps of nuclear aspect ratio show sparse and inconsistent regions of deformation and relaxation throughout the anterior and posterior PSs

To aid visualisation and pattern recognition, heat maps were generated from the nuclear deformation data. This was plotted in R. Briefly: ROIs were generated on the appropriate regionalised confocal images of DAPI stained PS mesenchyme via my StarDist model within Fiji. A manual check of the ROIs was performed, and any detected erroneous segmentation corrected. All ROIs generated over nuclei at image boundaries were manually deleted to prevent edge artefacts. Ellipses were fitted to each ROI and, using

the measure function in Fiji, X & Y co-ordinates and the aspect ratio of the fitted ellipses were extracted. For visualisation, the ellipses were plotted and filled with a colour corresponding to the natural logarithm of each aspect ratio [Ln(AR)] (a log scale enhances colour contrast and improves the ability to distinguish between regions with subtle but potentially biologically meaningful differences in aspect ratio).

Maps were generated for 'whole' regions (as outlined in *6.2.2.1*) and are shown in full for each sample used in each region (n = 4 for each condition in both anterior and posterior) in *Figure 6.10* and *Figure 6.11* The colour scale was normalised to the maximum AR, giving a top value of Ln(AR) = 1.4 representing an AR of 4.05.

In the anterior, between all four samples, the nuclear distribution was difficult to interpret by eye. There appeared to be no conserved pattern of deformation within unelevated (*Figure 6.10A-D*) or unelevated PSs (*Figure 6.10E-F*) in anterior *Figure 6.10* or posterior (*Figure 6.11*) PSs.

Moreover, there were no immediately obvious regions where nuclei were particularly deformed prior to elevation, and relaxed following elevation. If anything, it appeared that nuclei might be more deformed in the medial hinge region post-elevation (*Figure 6.10E&F*).

Posteriorly, the heat maps were arguably even more uninformative, with highly deformed nuclei present sparsely all throughout the PS tip both prior to and following elevation (*Figure 6.11*). However, the aligned regions of deformation in the dorsal parts of each posterior heat map (magenta regions towards the top of all panels in *Figure 6.11*) are somewhat reassuring. These regions of high deformation represent the nuclei either side of the invading vasculature, known to compress the adjacent nuclei as described above (*6.2.2*). Unfortunately, while the accurate detection of these highly deformed vasculature-adjacent nuclei further validated the methodology, it bolstered the fact that nuclear deformation patterns in the PSs were either extremely subtle or not operating in the way I had hypothesised.

6.2.2.3 Elastic relaxation occurs in the anterior medial and lateral hinges on elevation

There are several ways in which nuclei could be buffered against prominent deformation partly or completely (see chapter discussion) but it remained possible that biologically relevant differences in nuclear aspect ratio between unelevated and elevated PSs not immediately visually apparent might be detectable quantitatively. I therefore conducted statistical analyses for each sub-region outlined in *Figure 6.9*. While no statistically significant difference in nuclear aspect ratio between unelevated and elevated shelves was identified in the broader whole, upper or tip PS regions (*Figure 6.12*), this was not

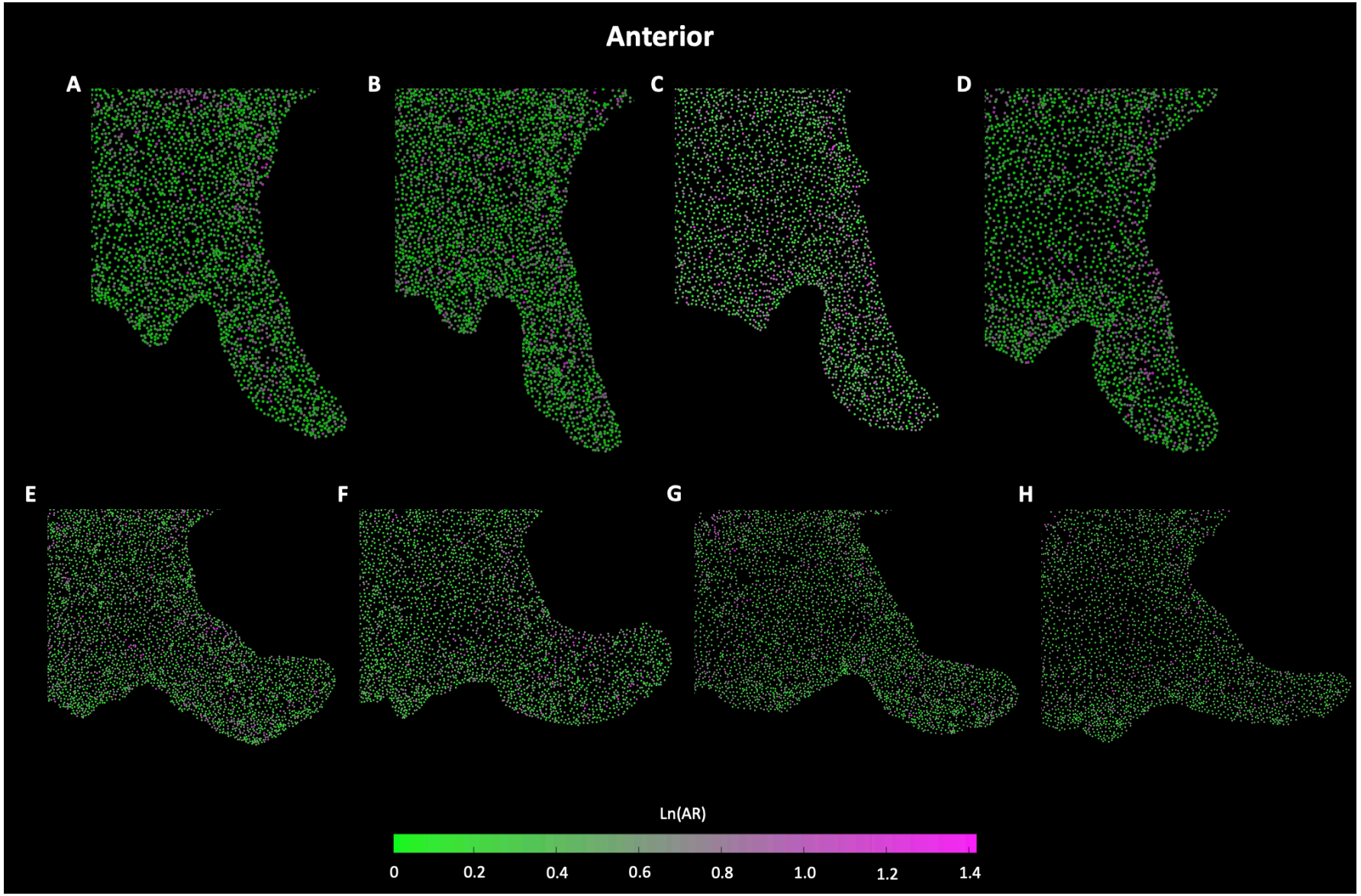

Figure 6.10 Heat maps of nuclear deformation in the anterior PSs

Heat maps of nuclear aspect ratio in the anterior unelevated (A-D) and elevated (E-F) PSs at E13.5 in 4 independent samples per condition. Each circle represents the exact XY co-ordinates of a nucleus segmented via StarDist in Fiji. Deformation is given as the natural log (LN) of each aspect ratio (AR), with 0/green representing rounded nuclei and purple/1.4 representing particularly deformed nuclei.

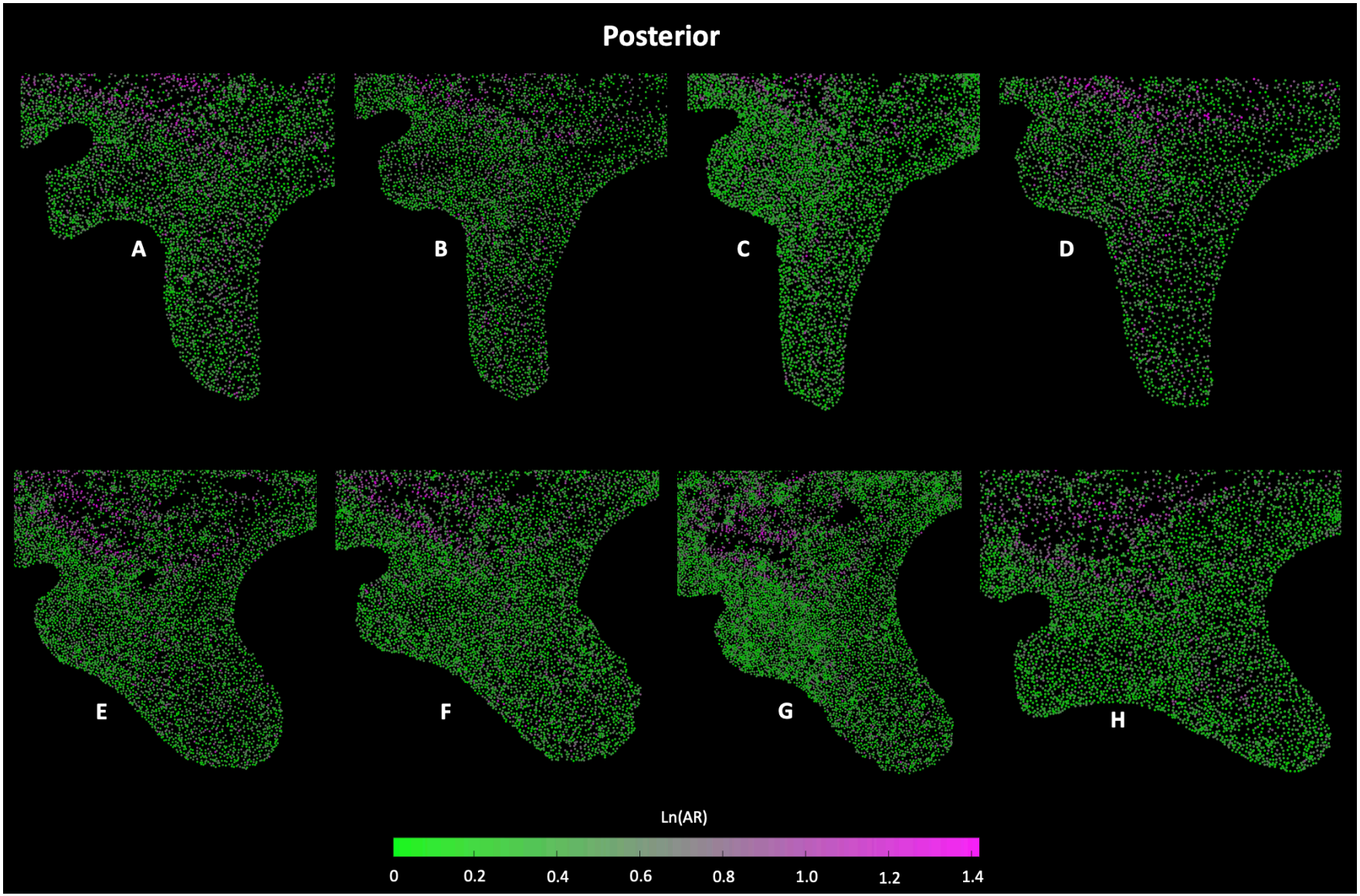

Figure 6.11 Heat maps of nuclear deformation in the posterior PSs

Heat maps of nuclear aspect ratio in the posterior unelevated (A-D) and elevated (E-F) PSs at E13.5 in 4 independent samples per condition. Each circle represents the exact XY co-ordinates of a nucleus segmented via StarDist in Fiji. Deformation is given as the natural log (LN) of each aspect ratio (AR), with 0/green representing rounded nuclei and purple/1.4 representing particularly deformed nuclei.

the case in smaller regions of interests. Specifically, in the anterior of both the medial and lateral hinges of the PSs, nuclei were more elongated prior to elevation, and more rounded post-elevation (*Figure 6.13A&B*). This suggests that, in both hinge regions, the nuclei were under stress and therefore deformed prior to elevation and underwent elastic relaxation following elevation. This could suggest that the internal shelf force is localised to both the lateral and medial shelves during elevation, and that this drives anterior elevation only, supporting the heterogeneity theory of elevation. However, although statistically significant, it is unclear whether a reduction in nuclear aspect ratio this small (≤ 0.1 difference; ~7% change) are biologically significant. Potential biological significance and biological and technical reasons for the smallness of the measured change are discussed in the chapter discussion below (*6.3.1*).

6.2.2.4 The force responsible for nuclear deformation does not appear to be stronger in either the anterior or the posterior PSs, nor in either of the hinges

To investigate any potential heterogeneity in elevating force along the AP axis of the shelves, I compared nuclear aspect ratio between the anterior and posterior aspects of the medial and lateral hinges in both unelevated and elevated tissue (*Figure 6.14A-B'*). There was no statistically significant difference detected in any comparison. Similarly, I wanted to assess whether the force might be acting more strongly in either the lateral or medial hinge in unelevated and elevated shelves, and considered the extent of nuclear deformation as a proxy for this (*Figure 6.14C-D'*). Again, there was no statistically significant difference in any condition tested.

Overall, these results are somewhat surprising and could suggest that the internal shelf force is either diffuse throughout the core mesenchymal tissue, that a small enough region simply was not located, or that nuclear deformation is not a suitable proxy marker for the presence of the internal shelf force. These considerations are also further explored in the chapter Discussion below.

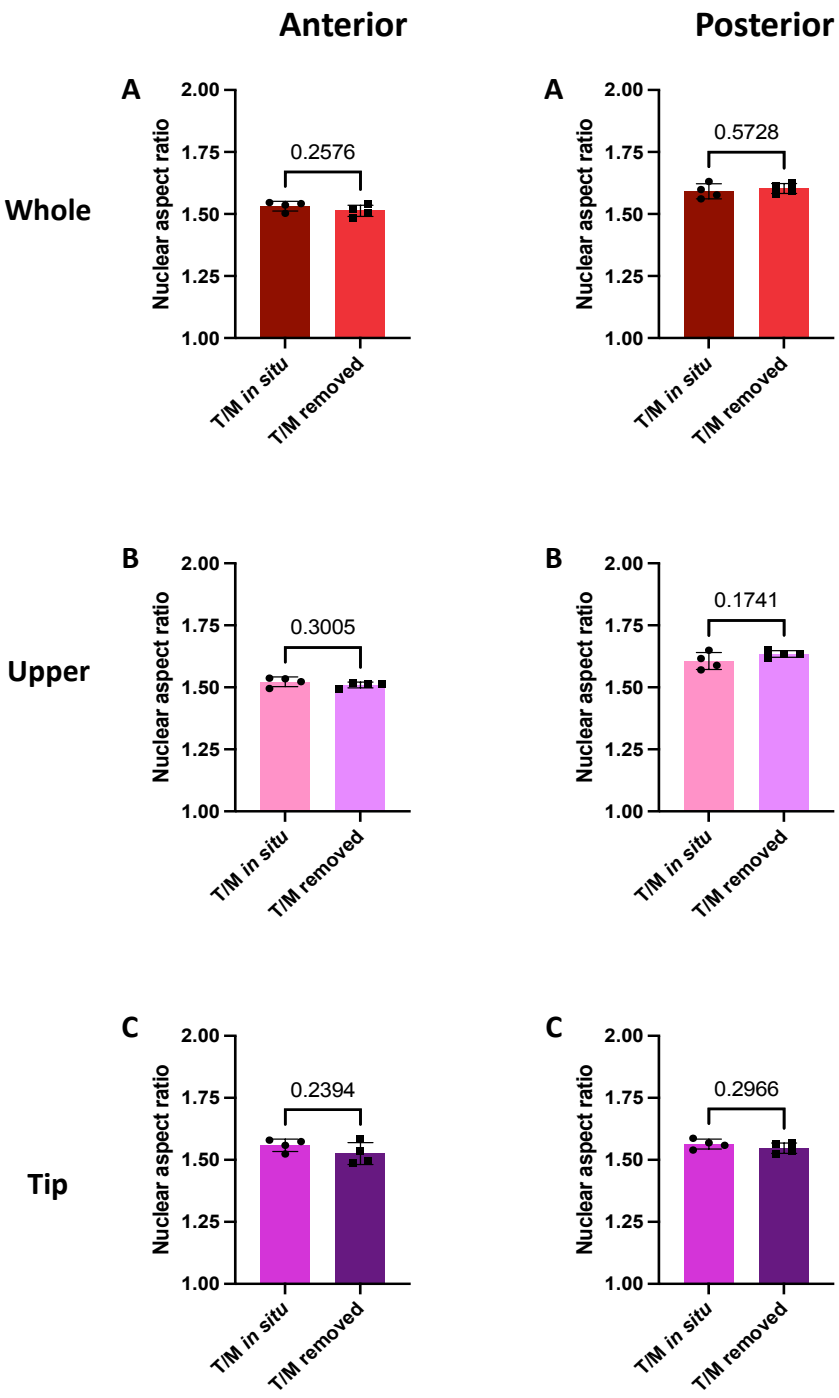

Figure 6.12 Comparison of nuclear aspect ratio in unelevated and elevated PSs in broad PS regions

Graphs comparing the average nuclear aspect ratio across whole PSs (A&A'), the upper region (B&B') and the tip region (C&C') in both anterior (A, B &C) and posterior (A', B'&C') PSs. TM in situ refers to unelevated PSs, and T/M removed refers to elastically elevated PSs following tongue and mandible removal. There was no statistically significant difference between unelevated and elevated PS nuclear aspect ratio at any point in these broader PS regions. Statistical significance (P values) is displayed on each graph and was determined by two-tailed unpaired t-tests. Error bars = mean with SD.

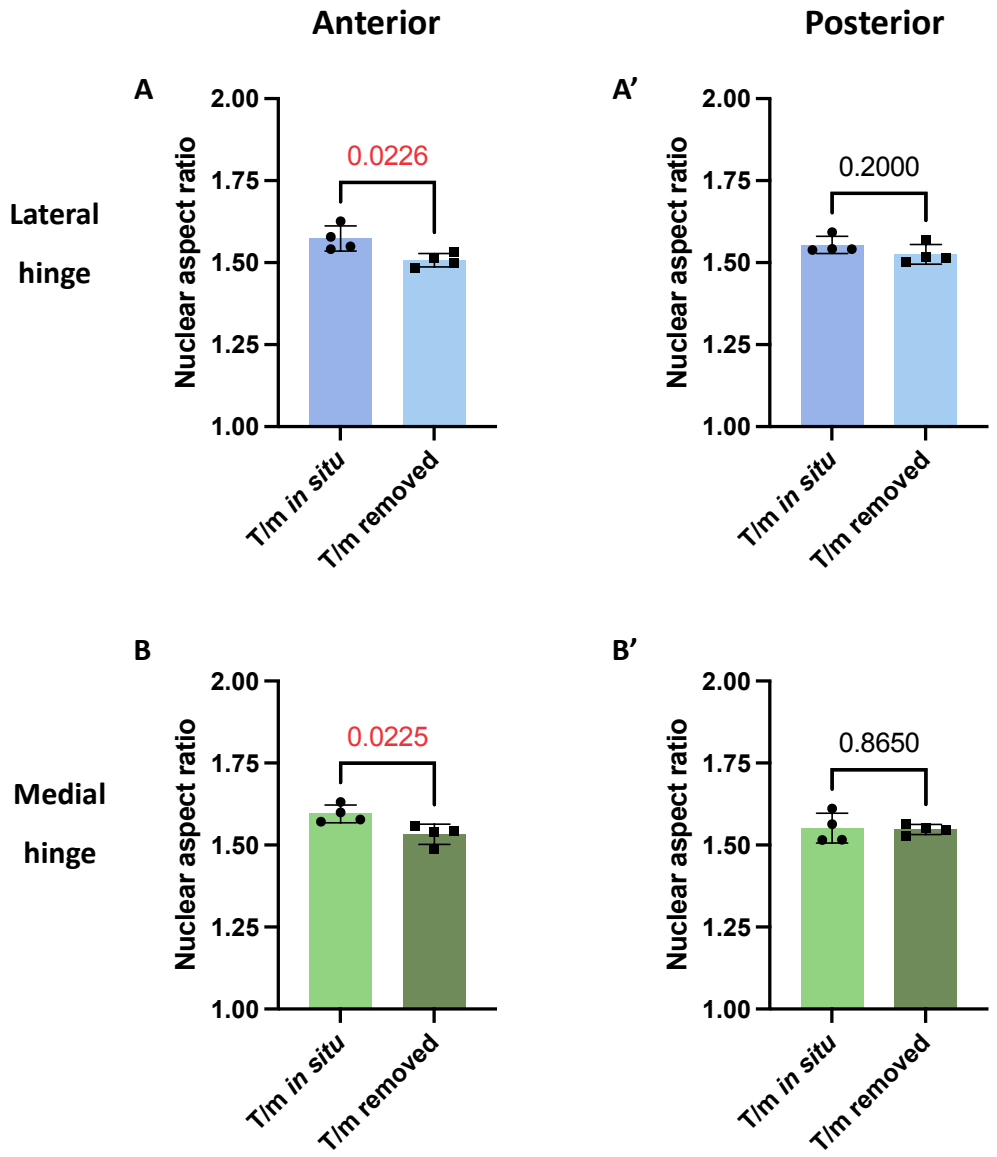

Figure 6.13 Comparison of nuclear aspect ratio in unelevated and elevated PSs in the medial and lateral hinge regions

Graphs comparing the average nuclear aspect ratio across the lateral hinge (A&A') and the medial hinge (B&B') in both anterior (A&B) and posterior (A'&B') PSs. T/M in situ refers to unelevated PSs, and T/M removed refers to elastically elevated PSs following tongue and mandible removal. There was a statistically significant difference between unelevated and elevated PS nuclear aspect ratio in the anterior lateral (A) and medial (B) hinges. Statistical significance (P values) is displayed on each graph and was determined by two-tailed unpaired t-tests (A, C&D) and Mann-Whitney test (B). Error bars = mean with SD.

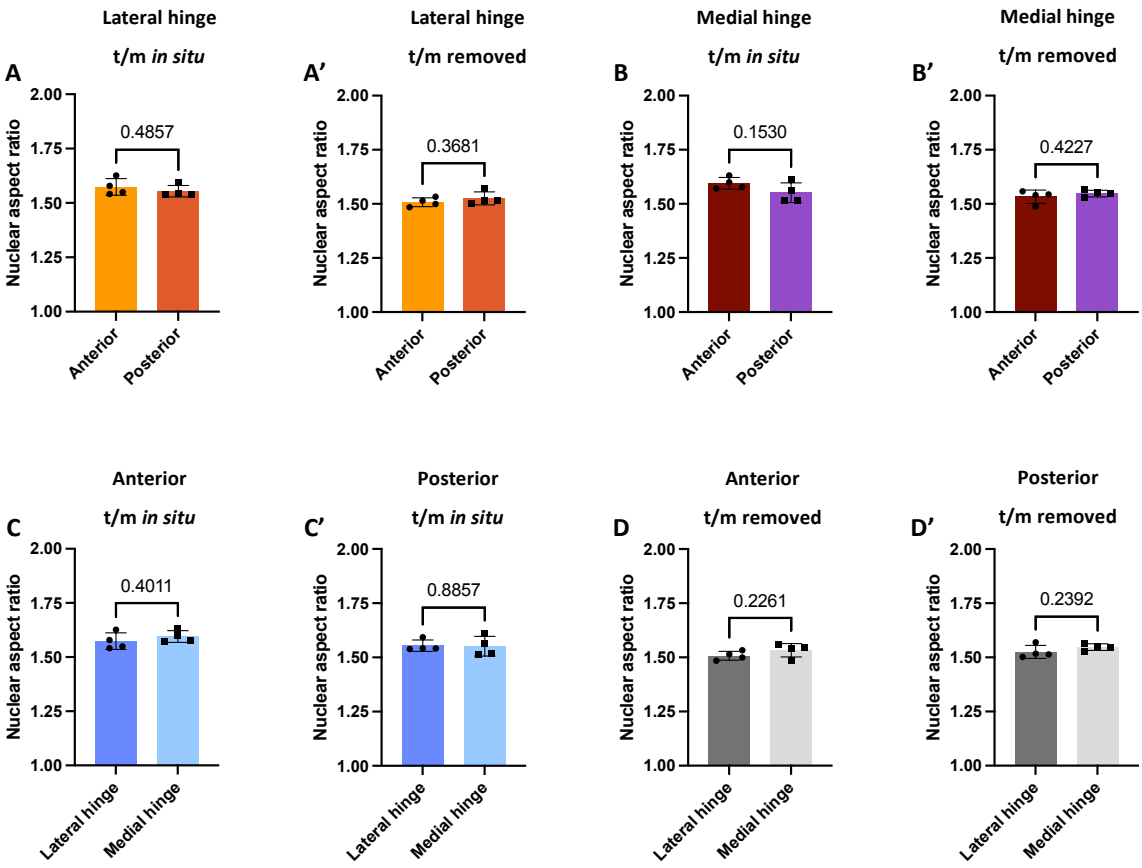

Figure 6.14 Comparison of nuclear aspect ratio in unelevated and elevated PSs in broad PS regions

Graphs comparing the average nuclear aspect ratio between the anterior and posterior regions of the lateral (A&A') and medial (B&B') hinge PS mesenchyme. Comparisons were also made between the hinges in the anterior and posterior in unelevated (C&C') and elevated (D&D') hinge PS mesenchyme. No statistical significance was identified in any of these cases. Statistical significance (P values) is displayed on each graph and was determined by two-tailed unpaired t-tests (A'-C, D&D') and Mann-Whitney test (A&C'). Error bars = mean with SD.

6.2.3 Nuclear spacing analyses reveal decreased PS mesenchymal inter-nuclear spacing following PS elevation

Use of the StarDist model in nuclear morphometrics and whole-tissue spatial analyses enabled the interrogation of several different aspects of morphogenesis during PS elevation. Investigating cellular distribution across the PSs prior to and immediately following elevation is one such use. Differences in cellular spacing (via nuclear spacing as a proxy marker) could represent changes in organisation and alignment, indicating which cellular behaviours and mechanisms of growth are active in generating the internal shelf

force. Furthermore, cell density itself could provide feedback to the individual cells to direct these behaviours, such as directing ECM secretions (Tang et al., 2015), or it could be a direct result of changes in cellular shape and size, which might also be contact-dependent.

Previous studies have typically included differences in cellular spacing/density as a qualitative measure, often as a by-observation (Brinkley and Bookstein, 1986; Furukawa et al., 2004; Shah et al., 1989; Sweney and Shapiro, 1970; Ferguson, 1977). The difficulty in heat map interpretation noted in previous studies could be due to difficulties in PS mesenchyme segmentation and centroid identification (Brock et al., 2016) and so the use of StarDist both utilises aspects of this previous research and builds upon it.

6.2.3.1 Spatial mapping using R

Code was previously written in the Green lab that generates internuclear spacing heatmaps (Economou et al., 2013). Briefly, centroid XY coordinates were extracted for each nucleus segmented by my StarDist model. In R, the 'nearest neighbours' to each centroid were identified using a Delaunay triangulation function and the average distance between each centroid and its neighbours calculated, with distances assigned a colour-code based on a user-defined scale. Then, a Voronoi tessellation was performed to tile the image into polygons containing the centroids and the polygons filled based on the colour-code assigned previously, representing the average internuclear spacing in this region. Averaging on this scale improves pattern recognition within the heat maps, and the combinatorial use of Delaunay triangulation and Voronoi tessellation in analysis is a tried-and tested method used in image and various other biological analyses (Qu et al., 2017).

6.2.3.2 Heat maps of nuclear density show sparse and inconsistent regions of nuclear spacing throughout the anterior and posterior PSs

Internuclear spacing heat maps were generated on the same samples described in the nuclear deformation study (*6.2.2.2*), i.e., unelevated and elevated (enabled by t/m removal) in both anterior (*Figure 6.15*) and posterior (*Figure 6.16*) PSs. As with the nuclear

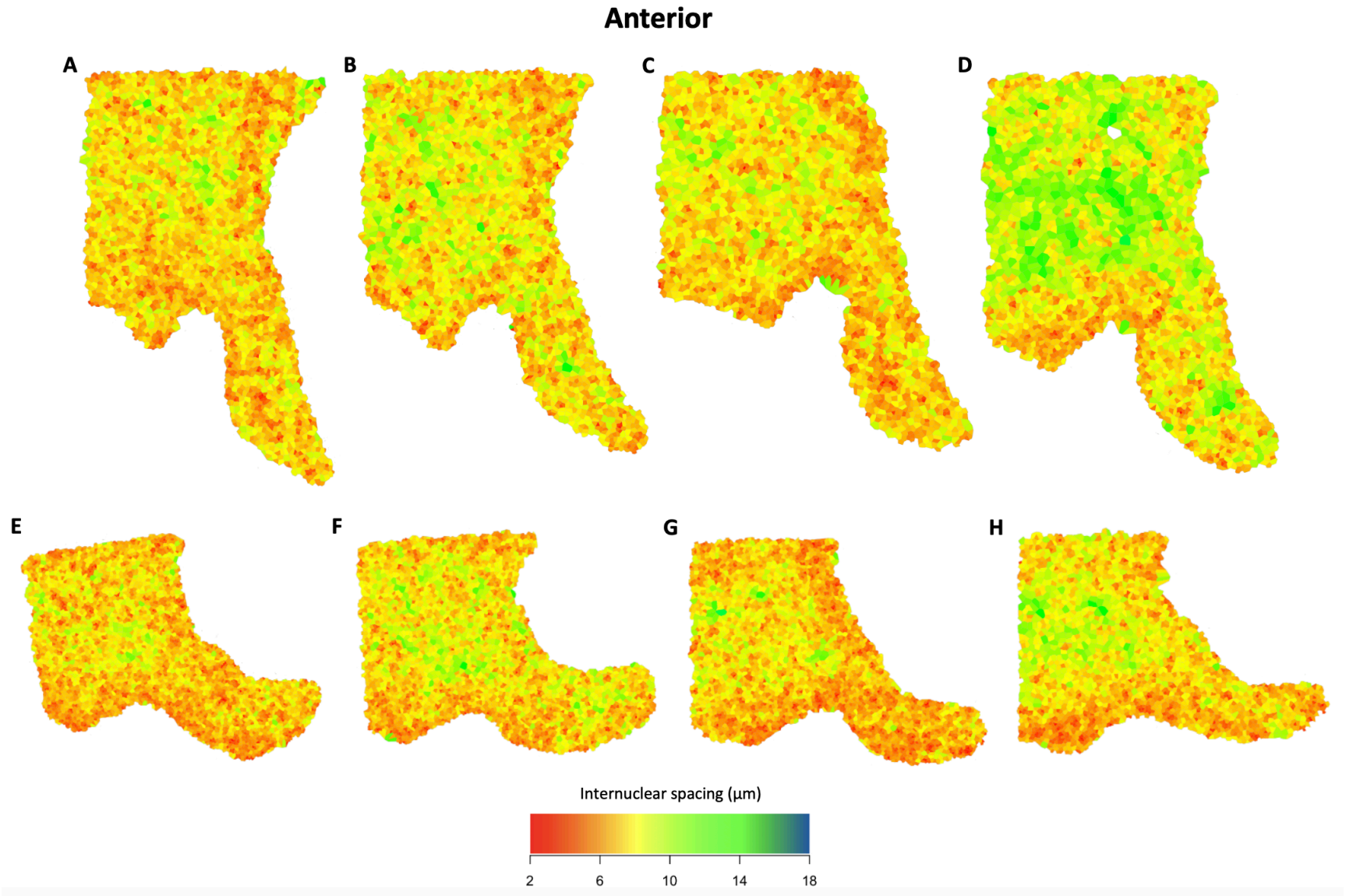

Figure 6.15 Heat maps showing average internuclear spacing in the anterior PSs prior to and following elevation

Heat maps of localised average internuclear spacing in the anterior unelevated (A-D) and elevated (E-F) PSs at E13.5 in 4 independent samples per condition. Each coloured tile represents the average distance between the centroid of a nucleus and its nearest neighbours, colour coded as per the scale bar included, ranging between 2 µm and 18 µm.

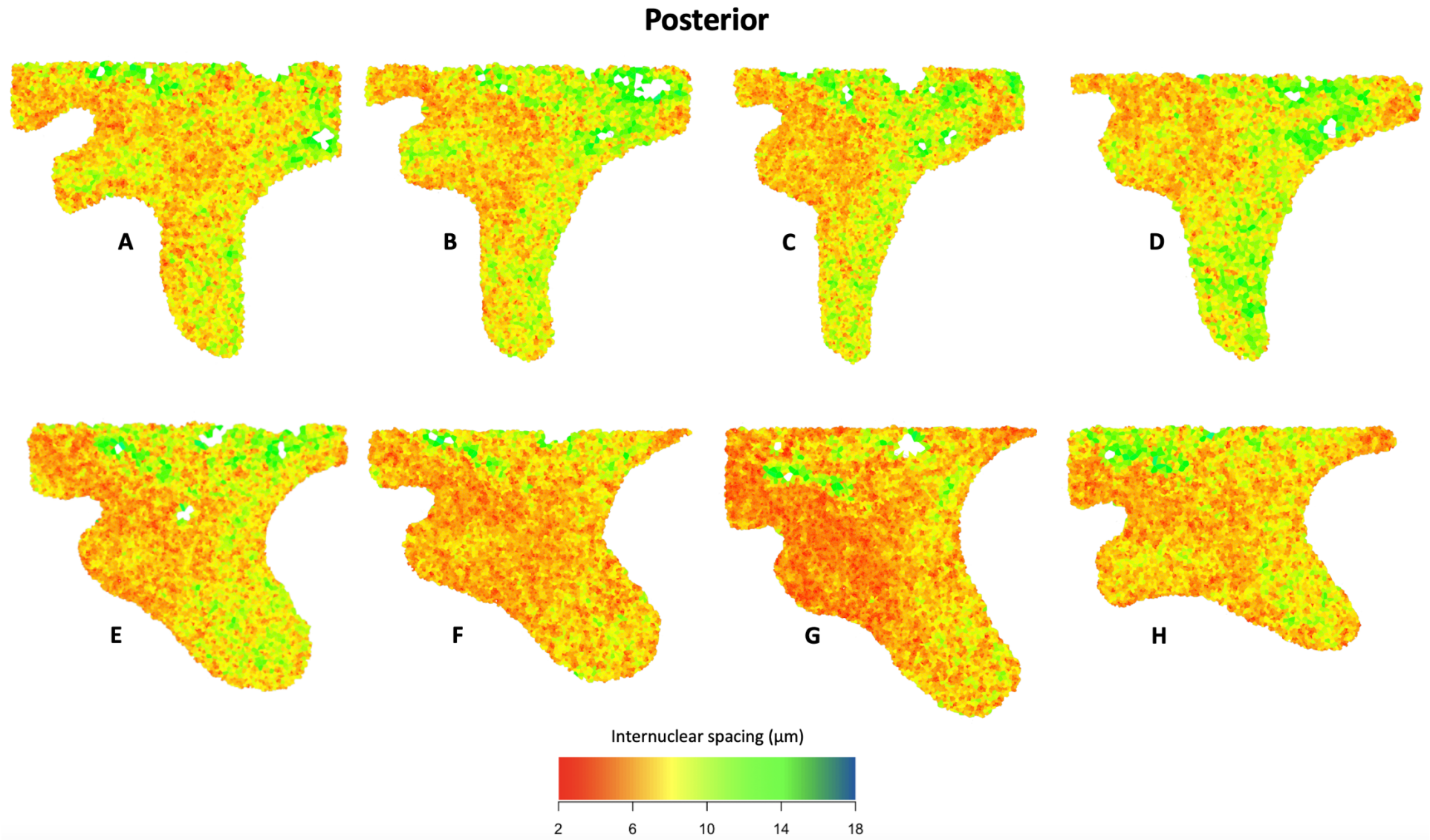

Figure 6.16 Heat maps showing average internuclear spacing in the posterior PSs prior to and following elevation

Heat maps of localised average internuclear spacing in the posterior unelevated (A-D) and elevated (E-F) PSs at E13.5 in 4 independent samples per condition. Each coloured tile represents the average distance between the centroid of a nucleus and its nearest neighbours, colour coded as per the scale bar included, ranging between 2 µm and 18 µm.

deformation maps, the internuclear spacing maps did not show dramatic consistent changes. Anteriorly, it appeared that the periphery of the PSs, particularly around the lateral hinge and tip, are densely populated both pre and post elevation but there were no easily discernible differences between the unelevated and elevated heat maps. In the posterior, there appeared perhaps to be somewhat consistent regions of higher nuclear density in the lateral hinge regions the unelevated PSs (*Figure 6.16A-D*). Furthermore, it appeared there was a consistent region of lower density in the medial hinge region and the medial side of the unelevated shelf that became denser after elevation. Therefore, although not immediately clear, there are some pointers towards regions of interest in density change between the unelevated and elevated PSs (*Figure 6.16E-H*).

Therefore, a quantitative assessment exploring potential differences in average nuclear spacing between the two regions were carried out in the regions outlined previously (*Figure 6.9*). As before, this was carried out over the whole image, and then in the medial and lateral hinges and PS tip specifically.

6.2.3.3 Nuclei are more densely packed in the medial hinge of the posterior palate following elevation

Internuclear spacing was only statistically significantly reduced (i.e., cell density was higher) in the medial hinge region of the posterior elevated PSs vs. unelevated PSs (*Figure 6.17D*). Anteriorly, whilst the average spacing was reduced in each region tested, this was not statistically significant in any tested region (*Figure 6.17*). The reduction in the medial hinge represented about a 10% reduction in space, i.e., a 10% increase in cell packing.

This could be comparable to the changes in contour length along the surface of the medial PSs, at least in the posterior, though if this is the case, there is not concomitant increase in cell spacing on the lateral side of the PSs. Differences in internuclear spacing across large areas could be indicative of different cellular behaviours, but which behaviours specifically, cannot be inferred directly from these analyses.

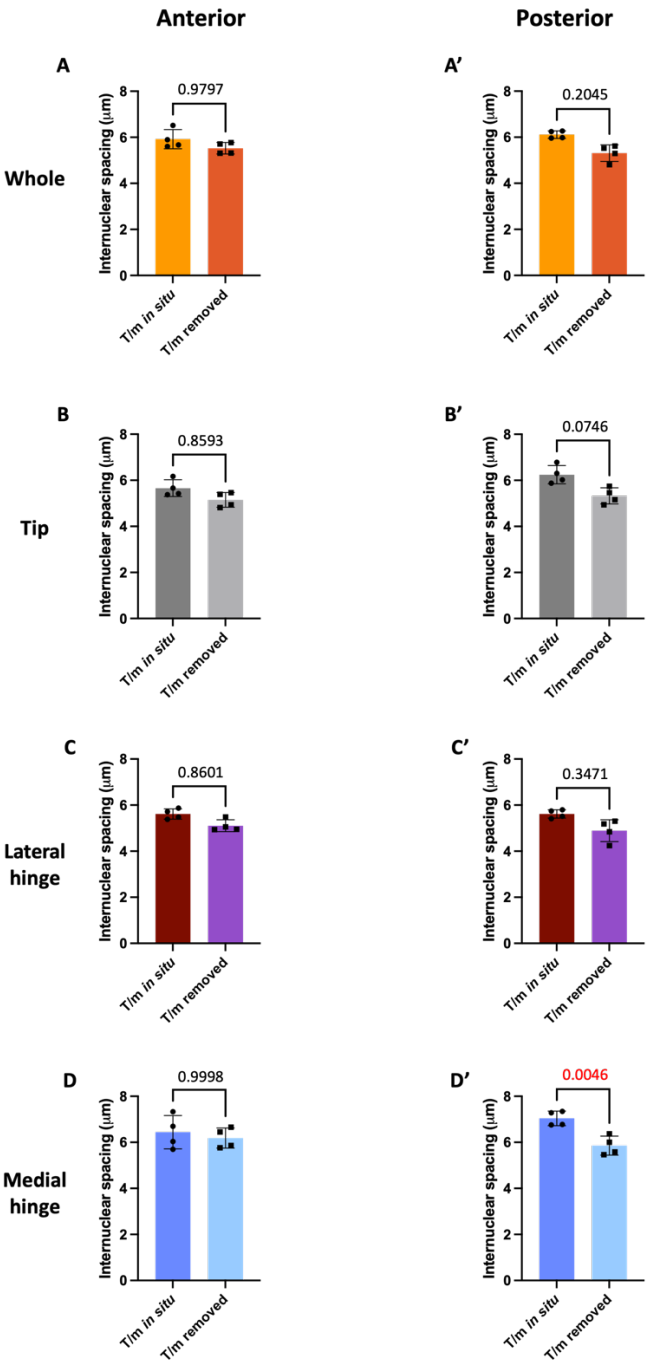

Figure 6.17 Comparison of localised average internuclear spacing between unelevated and elevated PSs in the anterior and posterior regions

Graphs comparing the average internuclear spacing across whole PSs (A&A'), the tip region (B&B') and the lateral hinge (C&C') and the medial hinge (D&D') pre and post elevation. T/M in situ refers to unelevated PSs, and T/M removed refers to elastically elevated PSs following tongue and mandible removal. Statistical significance (P values) is displayed on each graph and coloured in red where significant ($P < 0.05$). Statistical significance was determined by one-way ANOVA with Tukey's multiple comparisons tests. Error bars = mean with SD.

The posterior results are especially intriguing. As in the anterior, the mesenchymal cell density in all posterior regions tested increase following elevation, but none to a statistically significant degree (*Figure 6.18A', B', C'&D'*). I was surprised to find that average internuclear spacing decreased following elevation in both hinge regions (*Figure 6.18C'&D'*). It would be more intuitive if internuclear spacing had simultaneously increased in the lateral hinge and decreased in the medial hinge upon release of downward deflection by the tongue (just as would be the case with removing a load from a cantilever beam). However, the data suggest a more global release of tension and increase in compression, and this is explored further in the chapter discussion (*6.3.2*).

6.2.3.4 Internuclear spacing is not significantly different between the anterior and posterior regions either before or after elevation

To investigate how internuclear spacing may relate to the AP heterogeneity theory of elevation, I compared the average internuclear spacing between anterior and posterior each tested region in unelevated (*Figure 6.18A, B, C&D*) and elevated (*Figure 6.18A', B', C'&D'*) PSs. I found no statistically significant difference between anterior and posterior in any region or condition tested (*Figure 6.18).*

6.2.3.5 Summary of nuclear deformation and spacing analyses

Overall, the deformation data were disappointingly unrevealing besides statistically significant but sublte decrease in nuclear aspect ratio in both medial and lateral hinges (*Figure 6.13*). Notwithstanding, the data could be mined further to reveal more finely localised regions of change or changes in direction or coherence (see discussion). The internuclear spacing data were more promising but rather noisy, so again a significant data-mining project is needed in order to better define the signal and subsequent modelling will be required to help interpret the findings.

Prominently, these assays also highlight the utility of nuclear segmentation on this scale, now possible due to modern analysis techniques such as the application of StarDist nuclear segmentation models. The reduction in time and labour spent segmenting enable

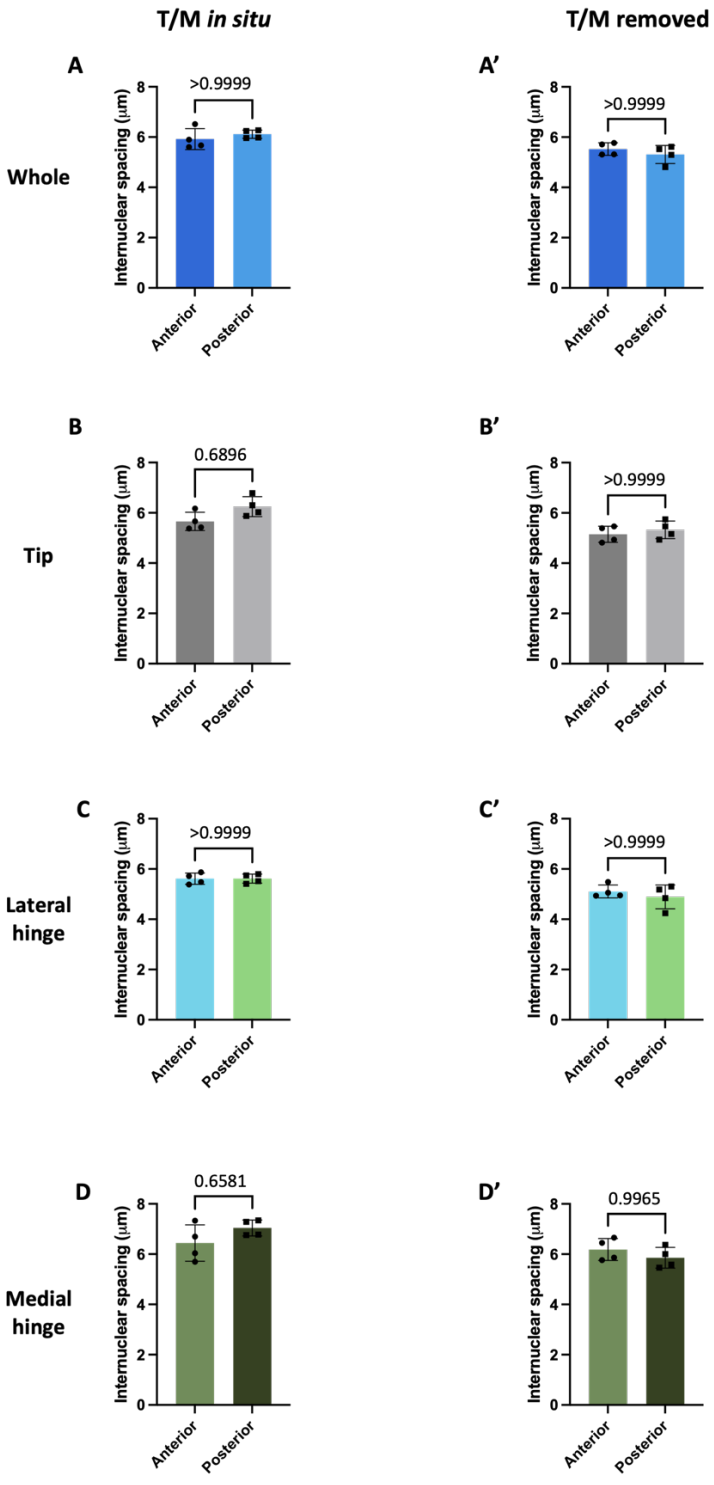

Figure 6.18 Comparison of localised average internuclear spacing between the anterior and posterior regions of unelevated and elevated PSs

Graphs comparing the average internuclear spacing across between the anterior and posterior of whole PSs (A&A'), the tip region (B&B') and the lateral hinge (C&C') and the medial hinge (D&D') in unelevated (T/M in situ) and elevated (T/M removed) conditions. Statistical significance (P values) is displayed on each graph and was determined by one-way ANOVA with Tukey's multiple comparisons tests. Error bars = mean with SD.

a more detailed investigation into more regions of the tissue than done before (Brock et al., 2016), with my early data demonstrating quantifiable differences in multiple nuclear morphometric assays during elevation. This could be useful in any future PS morphometrics investigations.

6.2.4 There are no mature, aligned elastic or collagen fibres driving PS elevation

As outlined previously there are conflicting reports in the literature as to whether aligned, fibrous structures in the developing PSs that could facilitate or generate the internal shelf force driving PS elevation (Walker and Fraser, 1956) (Frommer and Monroe, 1969). Recent studies have created high resolution SEM images clearly detailing organised elastic fibre networks (Lewis et al., 2021) and it remains plausible that they might mediate the elasticity observed during elevation (*1.4.5.5*).

Alongside elastic fibres, collagen bundles are the next obvious candidate for a structure mediating a tensile force during PS elevation. Yet, it also remains unclear whether mature bundles of collagen are even present during PS elevation; positive antibody stains certainly suggest that collagen is present, but it could be immature and disorganised (*1.4.5.2*). It has previously been posed that "stout bundles of collagen fibres" drive elevation (Ferguson, 1978) but there is little evidence that the structures are present in a mature form at this stage, with the supplied images lacking context and clarity (*Figure 6.3*).

Therefore, I wanted to resolve once and for all whether these structures were even present in the PSs at this time by performing two common histological stains for elastic fibres and collagen, and by utilising confocal microscopy with second harmonic generation (SHG) imaging (*6.2.4.3*) to generate a higher resolution and more sensitive pictures of any collagen bundles or networks of elastic fibres present. As the following results will show, neither of these structures were found.

6.2.4.1 The PSs stain lightly with aldehyde-fuchsin, with no visible network of elastic fibres

As shown previously, the elastic fibre theory of PS elevation arose from photomicrographs from Walker & Fraser (1956) reporting a network of elastic fibres in the PSs (*Figure 6.3*). The figure itself is unclear, and a subsequent study claiming to have performed the same histological staining technique reported a total lack of staining but did not show any pictorial evidence of this (Frommer and Monroe, 1969).

Therefore, as a first pass I wanted to repeat the protocol used in these investigations to determine whether or not a network of elastic fibres, which may be involved in elevation, truly run throughout the PSs at this time. The stain in question is a simple aldehyde-fuchsin, or 'Gomori' stain (Gomori, 1950). Briefly, Gomori staining binds to non-ionic proteins and peptides in unoxidized cells and tissues, and it is thought to react with an acid in elastic fibres specifically (Fuller and Lillie, 1957). This type of staining has low specificity, and it was noted shortly after its inception that it is difficult to distinguish between elastic fibres, connective tissue fibres and, in one study, pancreatic islet cells

The weakness of the stain also tends to undermine the possibility of elastic fibres, although the non-specificity of the stain makes this conclusion tentative.

6.2.4.2 Trichrome staining with picric acid suggests there are no aligned or mature bundles of collagen in the PSs during elevation

Aligned bundles of mature collagen fibres could drive the 'flip-up' elevation of PSs (1.4.5.2). Given their relative strength and structure, fibrillar collagens specifically are arguably the strongest candidate for facilitating any tensile forces driving elevation. Although the Gomori stain happens to stain for collagens as well as elastic fibres, the non-specificity impedes the ability to visualise any bundles of collagen, and Gomori stains are not typically used to assay for collagen.

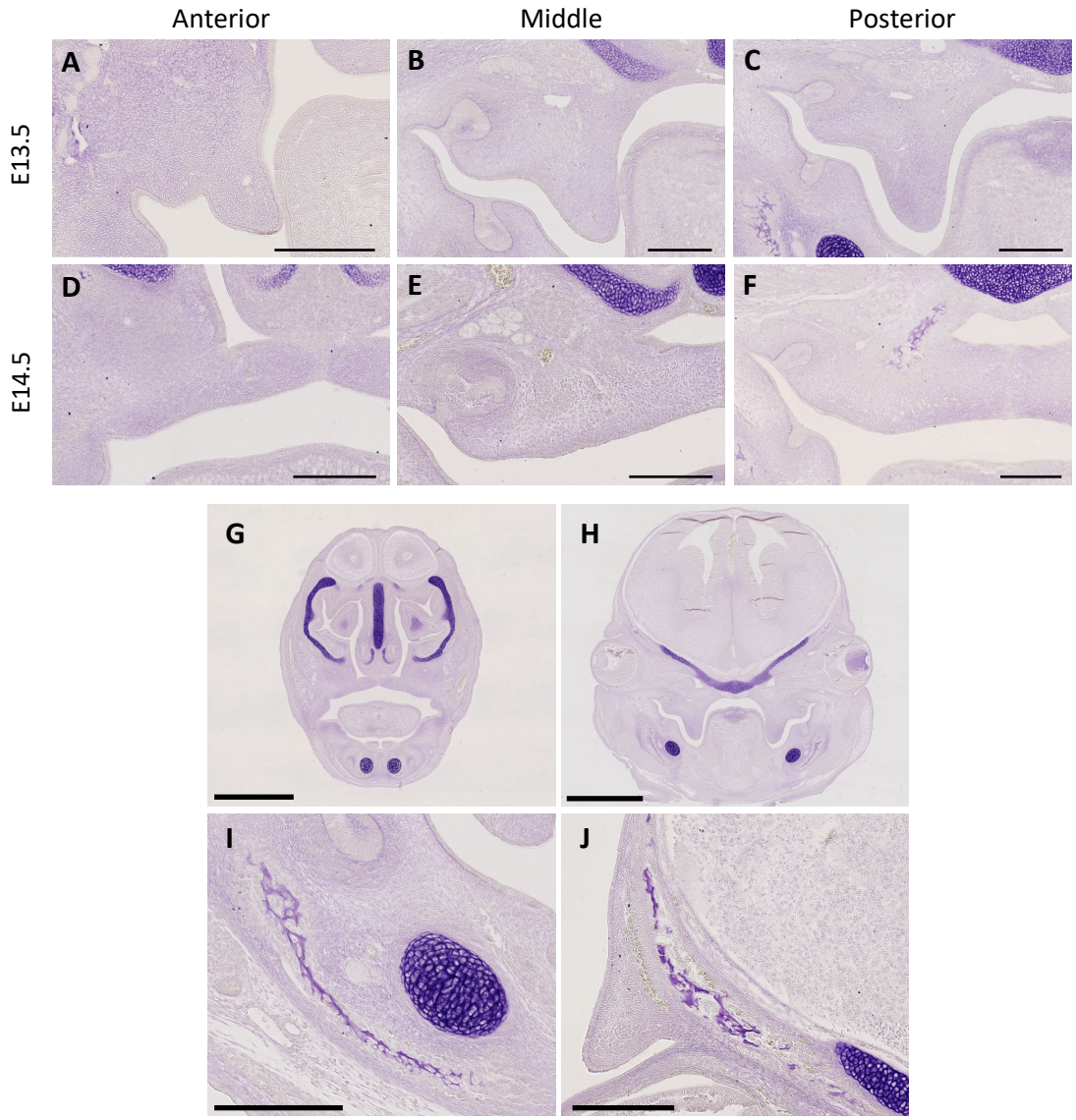

Figure 6.19 Gomori staining in the palatal shelves and wider craniofacial apparatus

Representative photomicrographs of frontally sectioned heads with Gomori staining in the PSs at E13.5 (A-C) and E14.5 (D-F), in whole heads at E14.5 (G) and E13.5 (H), and in the mandible (I) and frontal bone (J) at E13.5. Staining is especially weak throughout the PS mesenchyme at both stages and is only really pronounced in the PSs basement membrane of the epithelium. Examples of 'true' positive staining are given in the nasal septum (G), cranial base (H), mandibular bone and Meckel's cartilage (I) and the frontal bone (J). N = 4 embryos from 3 independent litters. Scale bars A-F, I&J = 250 µm; G&H = 1 mm.

Histochemically, the gold-standard in staining for collagen fibres hads been the use of the azodye picrosirius red (sometimes referred to as sirius red) combined with polarised light microscopy (Junqueira et al., 1979). Picrosirius red is prepared from picric acid (trinitrophenol) which itself has been used varyingly as a stain and an explosive for

centuries (Woulfe, 1771). The chemical reaction between picrosirius red and collagen fibres is frequently referred to as one of the best understood in histology (Rittié, 2017; Liu et al., 2021) and is often used as a part of a 'trichrome' stain, which I performed on sibling tissue to the samples prepared in Gomori staining (*6.2.4.1*).

In this trichrome staining variant, I used alcian blue to stain for chondrocytes (blue), Ehrlich haematoxylin for nuclei (dark blue) and picrosirius red to stain for collagen (red). This was photographed as standard under a stereoscope and then combined with polarised light microscopy (PLM). The latter depends on birefringence, which is the measure of the difference between the refractive indices of two light pathways moving at different speeds through an object. This occurs when light enters an anisotropic structure, such as fibrous collagen bundles when running longitudinally in transverse sections (Caamaño et al., 2010; Liu et al., 2021). Two polarising filters were placed in the light path: one over the slide, and one over the illuminator, rotated 90° to each other. Fundamentally, this causes the double-refraction of polarised light, which interferes with itself. I.e., birefringence effectively rotates the plane of incident light polarisation so that when viewed through crossed polarising filters, it gives transmitted light an intermediate polarisation angle which has a component that can pass through the nearer filter. The effect is wavelength-dependent, hence may appear to emit different colours. Thus, the birefringent material appears to "glow" (Segnani et al., 2015).

Picrosirius red is a birefringent material itself and binds directly to eosinophilic collagen fibres. On binding, the picrosirius red molecules align parallel to the longitudinal axis of collagen fibres, which enhances the birefringence already arising from aligned collagen fibres (Wolman, 1975; Liu et al., 2021). Interestingly, it is reported that under birefringent conditions, type 1 collagen fibres appear reddish yellow, whilst type 3 collagen appears green (Liu et al., 2021). However, recent studies argue that this is an historic misinterpretation, and the ability to use the colour of birefringence to differentiate between type 1 and type 3 collagen remains contentious (López De Padilla et al., 2021).

Hence, this is a straightforward yet powerful combination of histochemical and optical manipulation techniques which shed light on the theory of bundles of collagen fibres facilitating PS elevation via tensile forces (Ferguson, 1988).

In frontally sectioned tissue: prior to elevation at E13.5 (*Figure 6.20A-C'*) I found no picrosirius red staining in the PSs, nor did the PSs exhibit birefringence in any region. Post elevation at E14.5, there was extensive picrosirius red staining in the anterior (*Figure 6.20D&D'*) and posterior PSs (*Figure 6.20F&F'*). However, staining and birefringence was only visible in regions of ossification of the maxillary bone anteriorly (*Figure 6.20D&D'*) and the palatine bone more posteriorly (*Figure 6.20F&F'*). There was no detectable birefringence in the PSs in the middle region at this stage.

In the middle and posterior regions at both E13.5 (*Figure 6.20B-C'*) and E14.5 (*Figure 6.20E-F'*) the ossifying mandibular bone could be seen stained red in bright field and glowing bright green under birefringence optics. A clearer picture of this is given as a control image for both picrosirius red and birefringence (*Figure 6.20H&H'*). The frontal bone was also undergoing ossification at E14.5, providing another clear control, and highlighted the different colours exhibited by birefringent collagen fibres (*Figure 6.20G&G'*).

No collagen fibres were detected in the PSs in sagittally sectioned tissue either. Sections were taken in different sagittal planes at E13.5, capturing the shelf only (*Figure 6.21A-B'*) or both shelf and tongue (*Figure 6.21C-E'*). Again, some picrosirius red staining and birefringence was observed in the anterior (*Figure 6.21F&F'*) and posterior (*Figure 6.21H&H'*) at E14.5, but these once again simply marked the ossifying maxillary and palatine bones respectively.

Overall, the use of trichrome staining with picrosirius red and PLM did not reveal the presence of any "stout bundles" of collagen fibres. Although unlikely, presence of immature or subtle collagen fibres could potentially have been masked or obscured by the surrounding alcian blue and Ehrlich haemoxylin stains. This is the case with Meckel's

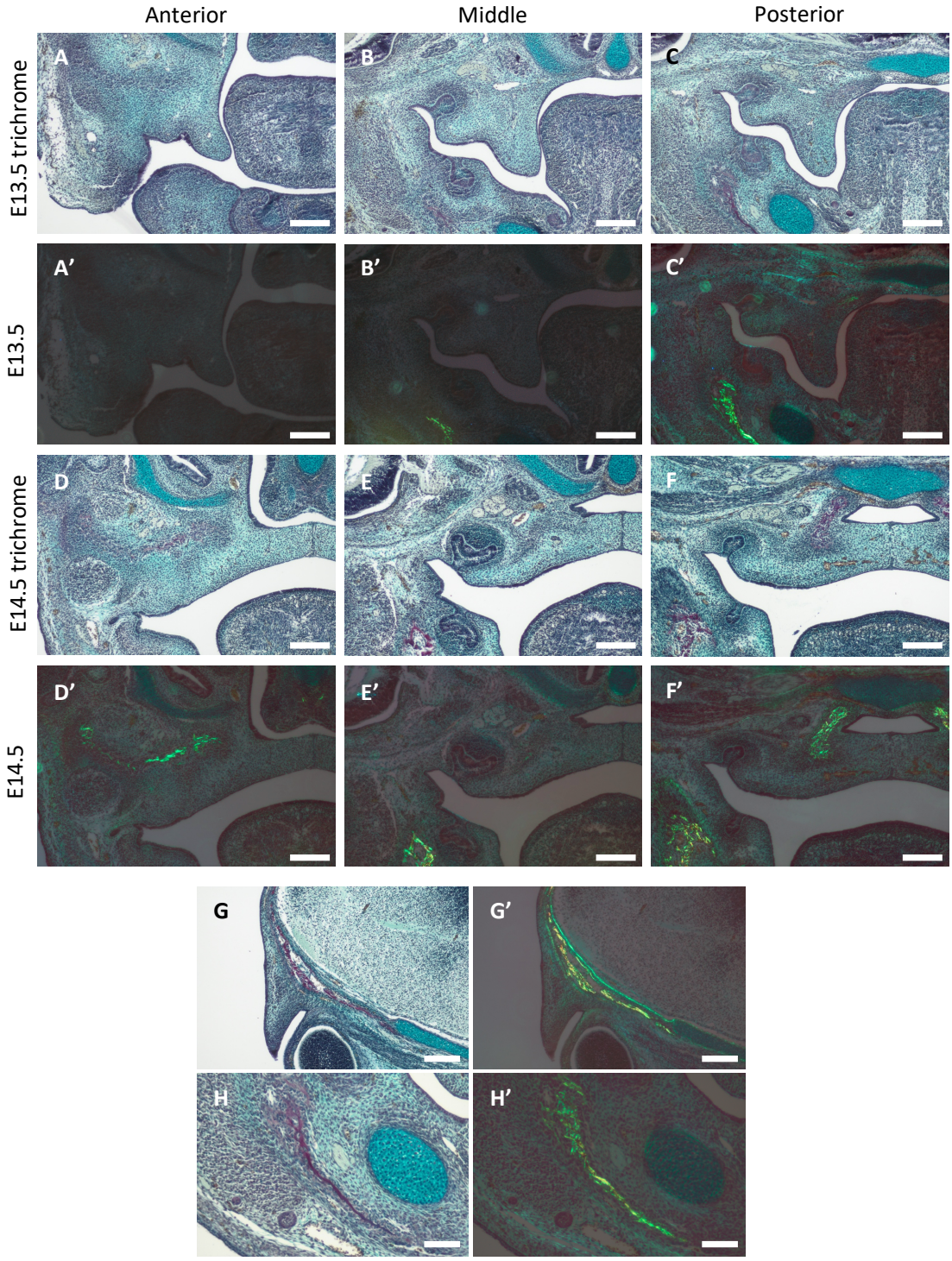

Figure 6.20 Trichrome (picrosirius red) staining with birefringence in frontally sectioned PSs

Photomicrographs of frontally sectioned heads with trichrome staining in the PSs at E13.5 (A-C) and E14.5 (D-F), the frontal bone at E14.5 (G) and the mandibular bone at E13.5 as controls. Corresponding birefringence images are marked (‘). There is no picrosirius red (red) staining in the PSs in any anatomical region at E13.5, and the positive stain and signal in the anterior (D) and posterior (F) at E14.5 are the ossifying maxillary and palatine bones respectively. mandibular bone and Meckel’s cartilage (I) and the frontal bone (J). N = 4 embryos from 3 independent litters. Scale bars = 200 µm.

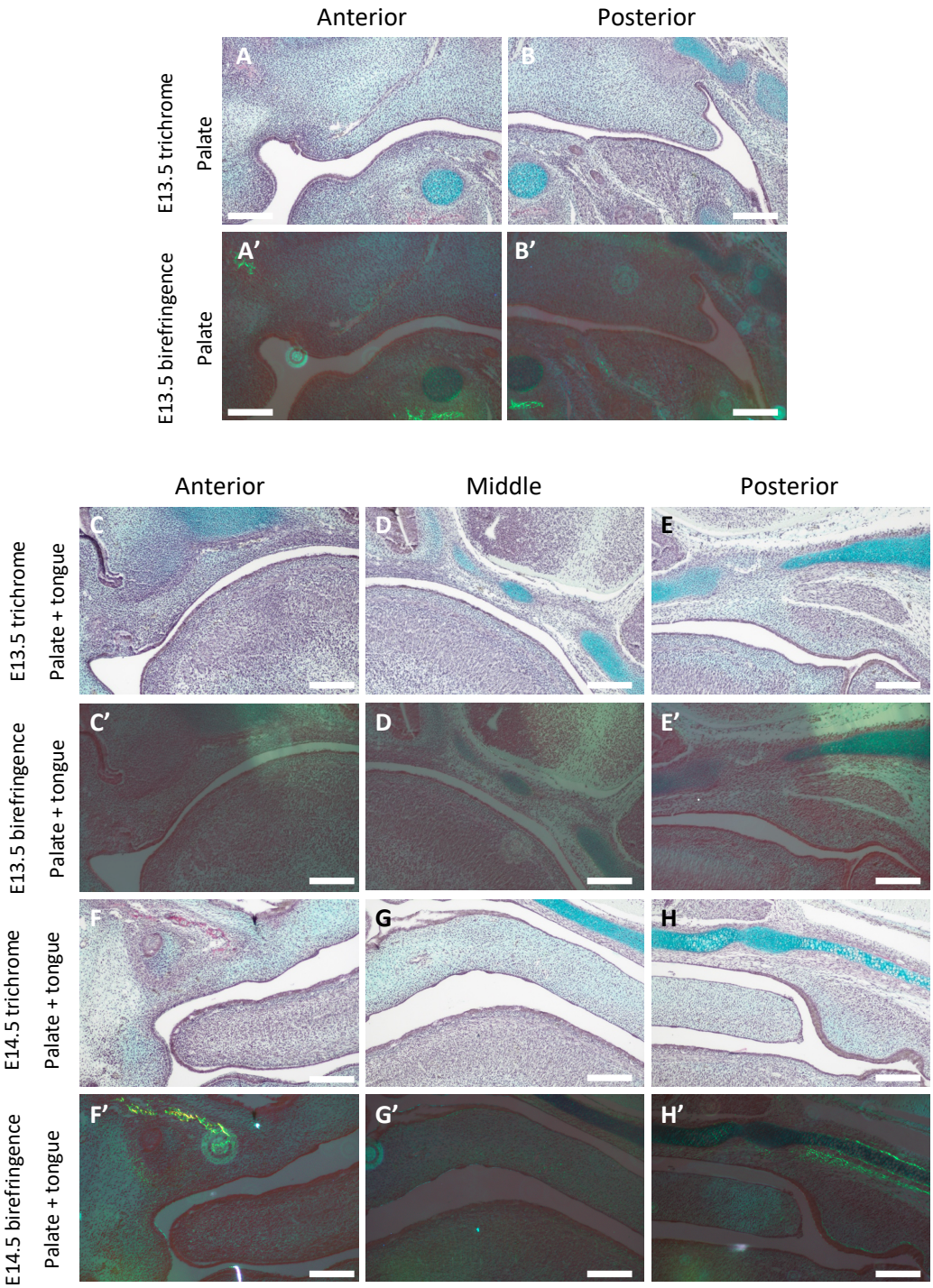

Figure 6.21 Trichrome (picrosirius red) staining with birefringence in sagittally sectioned PSs

Photomicrographs of sagittally sectioned heads with trichrome staining in the PSs in two different aspects at E13.5 and centrally at E14.5. All corresponding birefringence images are marked (‘). Sections capturing palate only (A&B) and palate with tongue (C-E) did not show any picrosirius red or collagen staining. At E14.5, picrosirius red and birefringence was observed in the anterior (F) and posterior (H) regions, again marking the ossifying maxillary and palatine bones respectively. N = 4 embryos from 3 independent litters. Scale bars = 200 µm.

cartilage, hence it tests positive in a Gomori stain (*Figure 6.19I*) but not in a trichrome stain or under birefringence (*Figure 6.20H*).

6.2.4.3 Second harmonic generation imaging does not reveal any collagen fibres in the PSs during elevation

Given the possibility of subtle or immature collagen fibres, to provide higher resolution evidence as to the potential presence of collagen fibres in the PSs during elevation I carried out a final assay for collagen detection. Second harmonic generation (SHG) is a type of nonlinear optical phenomenon with a wide variety of applications in research and medical diagnostics (Chen et al., 2012; Campagnola and Dong, 2011). Briefly, when two gamma-photons of equal frequency interact with an anisotropic (or nonlinear) material, they may be combined and produce a new photon with double the frequency and half of the wavelength of the original photon. Hence, the energy of the photon is doubled, and coherence is maintained. This results in the interacting nonlinear material appearing to "glow" bright white; the technique can be performed in combination with powerful microscopes, in this case a two-photon microscope, to produce high resolution images of the detailed structures of nonlinear materials. Collagen reportedly generates the largest second harmonic of all mammalian tissue structures (Cox and Kable, 2006) and has been investigated extensively with SHG imaging, but not in the PSs (Yildirim et al., 2016; Silva et al., 2013).

Therefore, to resolve any potential ambiguity in the picrosirius red staining and birefringence data, I performed SHG imaging using a two-photon microscope on PS tissue prior to (E13.5) and immediately after (E14.5) elevation. I had initially planned to re-use my trichrome-stained tissue. However, on imaging my first sample I noticed what appeared to be 'bubbling' in my region of interest, followed by tissue destruction on later slide inspection. The salts of picric acid are explosive, and the laser excitation may have been triggering this on a microscopic scale and destroying my tissue. Therefore, I produced frontally sectioned tissue as before, stained only with DAPI for help in tissue orientation during imaging, and cover-slipped under an aqueous mountant (n = 3 samples from 3 independent litters).

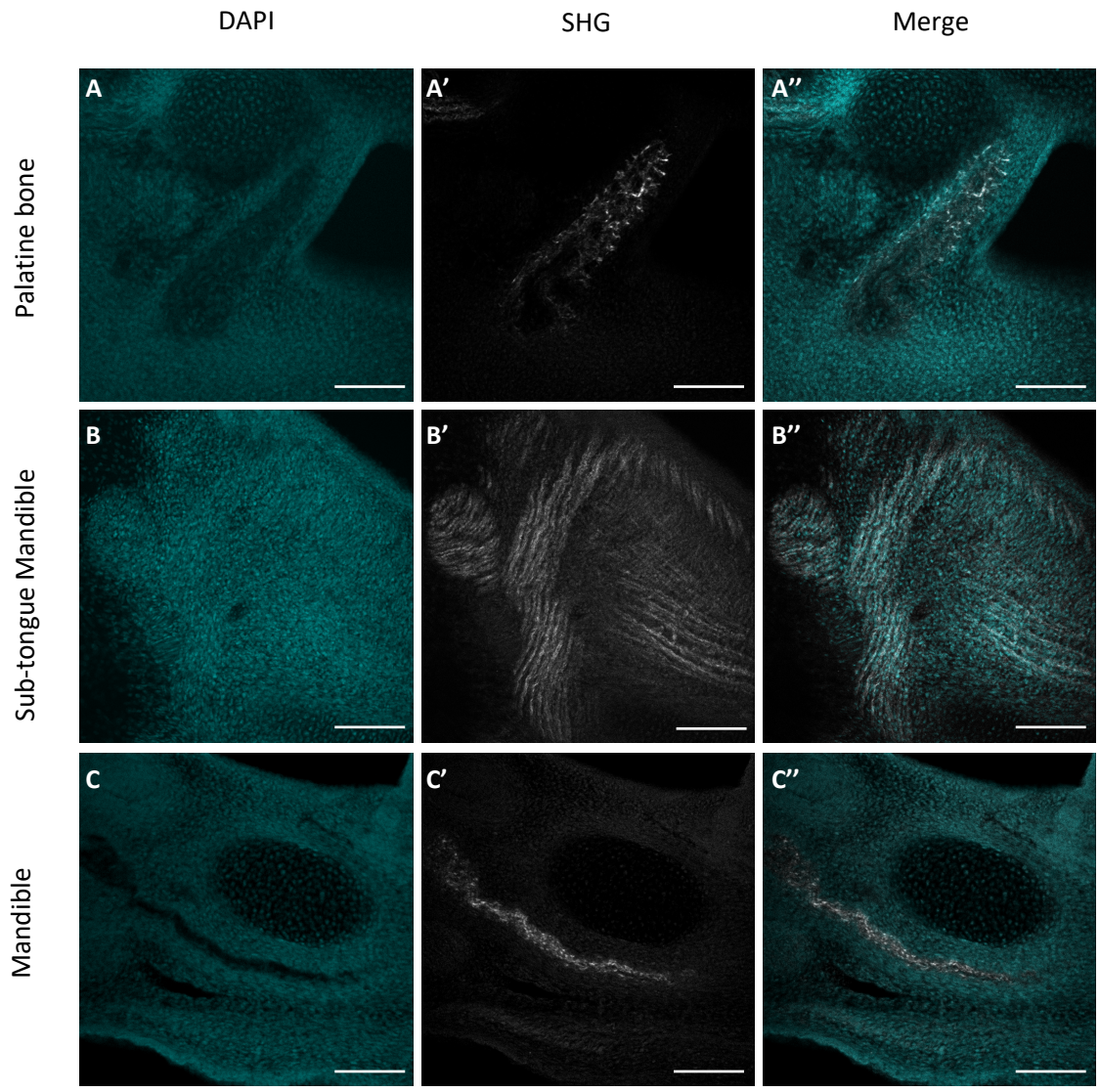

Figure 6.22 Second harmonic generation in frontally sectioned collagen-positive tissue regions

Images of collagen control regions capture on a two-photon microscope stained with DAPI (A-C), under SHG conditions (A'-C') and merged (A''-C''). Images were captured in the palatine bone at E14.5 (A), in the sub-tongue mandible at E13.5 (B) and in the mandibular bone at E13.5 (C). The bright white regions are nonlinear structures undergoing SHG. Scale bars = 100 µm.

I was initially unsure as to how SHG may look in embryonic tissue collagen, so I first imaged regions which previously stained strongly for picrosirius red, or which demonstrated strong SHG on scanning across the tissue. Satisfactorily, some of the resultant images were quite striking. At E14.5, the ossifying palatine bone (*Figure 6.22A-A''*) and E13.5 mandibular bone (*Figure 6.22C-C''*) produced patterns similar to that

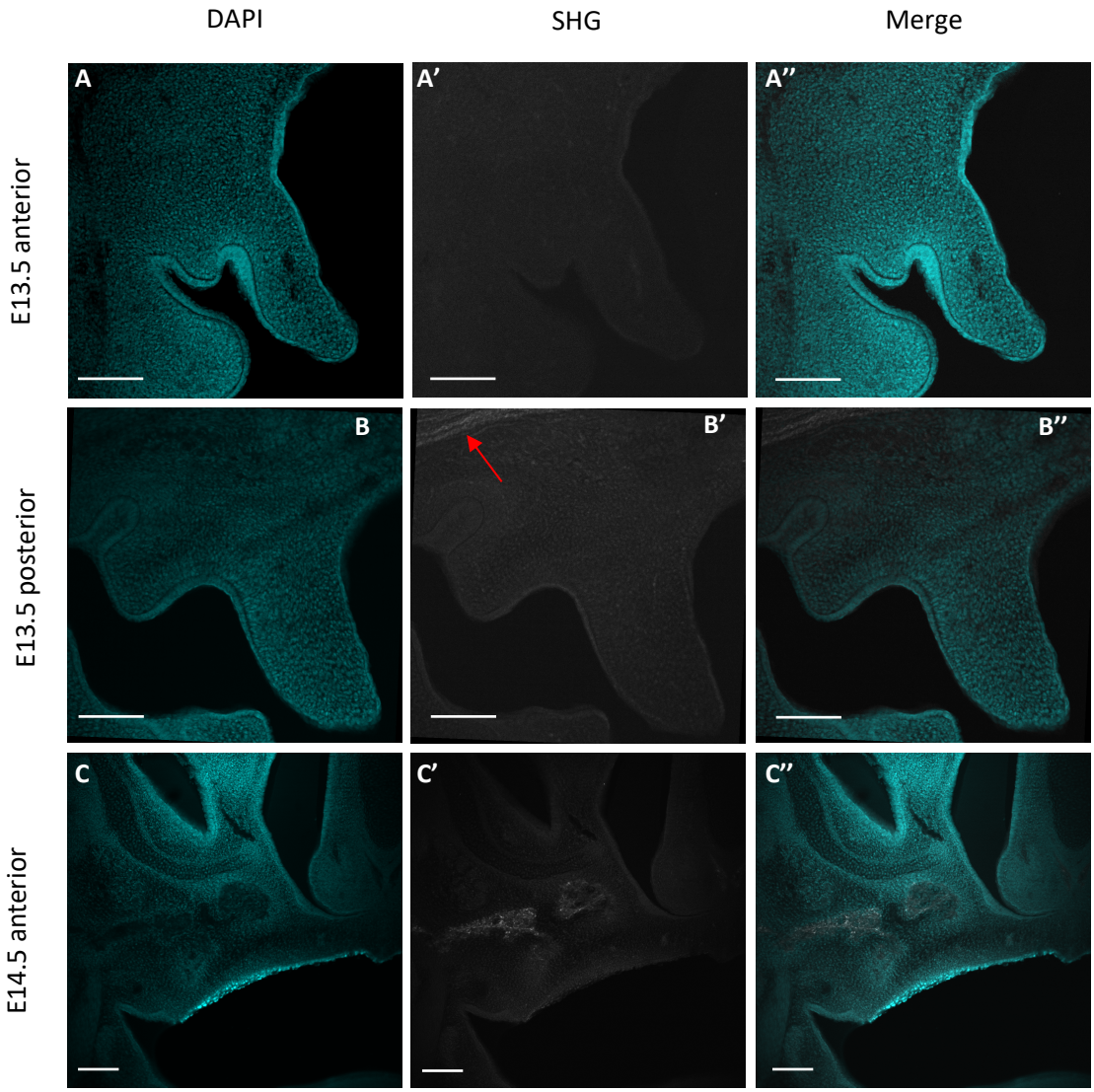

Figure 6.23 Second harmonic generation in frontally sectioned PSs

PSs captured on a two-photon microscope stained with DAPI (A-C), under SHG conditions (A'-C') and merged (A''-C''). Images were captured in the anterior (A) and posterior (B) PSs at E13.5 and in the anterior PSs at E14.5 (C). No SHG was detected in these regions. The red arrow points to faint SHG from the cranial base (B'). Scale bars A-B'' = 200 µm; C-C'' = 300 µm.

observed via both Gomori and trichrome staining. However, immediately inferior to the tongue, perhaps at the muscular insertion site into the mandible, the extensive alignment of collagen fibres was observed (*Figure 6.22B-B''*). This identification of these structures under SHG confirmed that this was a suitable technique to investigate collagen alignment in embryonic craniofacial tissue.

Due to limitations in equipment availability and time, I was able to image adequately E13.5 anterior and posterior and E14.5 anterior regions only (*Figure 6.23*). Whilst some positive SHG signal is present in the posterior region at E13.5 (*Figure 6.23B'* red line), this was just the collagen rich cranial base and no SHG fibrillar signal was detected in any part of the PSs.

6.2.4.4 Summary of staining and imaging for ECM fibres

Taken together, my Gomori, Trichrome (with picrosirius red and birefringence) and SHG imaging data demonstrate both that there is no network of elastic fibres running through the PSs prior to elevation, nor are there bundles of collagen fibres facilitating elevation via mediating a tensile force. This is in disagreement with Walker & Fraser's (1956) and Ferguson's (1988) theories on elastic fibre and collagen-mediated elevation respectively and validates Frommer & Monroe's (1969) claims in their inability to replicate Walker & Fraser's data. This is not to say that neither collagen nor elastic fibres are present in immature and non-aligned forms, as Ferguson had partially suggested in an earlier study (Ferguson, 1978). The collagen antibody staining investigations suggest that the protein is at least present (Ohsaki et al., 1995), but these data suggest that stout bundles of collagen fibres and networks of elastic fibres are not the primary ECM component drivers of PS elevation.

6.2.5 The PSs display regional variations in stiffness at E13.5

While material properties of the PSs have been investigated in relation to feeding (Jingtao Li et al., 2016), they not yet been investigated in relation to elevation. Differential material properties across the PSs, namely the tissue stiffness, could facilitate the heterogeneous manner of elevation. To inform this, I carried-out atomic force microscopy (AFM) and generated stiffness map of the PSs, both topographically on the tissue surface and in frontal slices to access the mesenchymal core. This may be the first description of the material properties of the PSs at this stage. The work would not only establish methods to enable the exploration of further material properties of the PSs via AFM, such as viscoelasticity testing, but it will also enable proper finite element modelling (FEM) in due course.

Briefly, the terminology used when describing material properties differs when speaking colloquially or in a scientific manner (Baumgart, 2000). This is particularly relevant to the term 'stiffness', used in materials science to describe the resistance of an elastic structure to deformation by applied force (Norman et al., 2021). I.e., stiffness could be considered as simply as load divided by deformation (Baumgart, 2000). Furthermore, when describing deformation, stress refers to the defined force per unit area applied to the material, whilst strain refers to a measure of the deformation of that material under stress. Finally, the elastic or 'Young's' modulus (*E*) describes the fundamental property of a material to resist deformation on the application of stress, i.e., *E* = tensile or compressive stress divided by axial strain (Muiznieks and Keeley, 2017; Davidson and Keller, 2007; Davidson, 2011). Thus, for a physicist "elasticity" is resistance to deformation (the opposite of the colloquial meaning) and high elasticity means a structure is stiffer. The simple stress/strain relationship is true for linear-elastic solids, though tissues with different properties exhibit different types of related behaviours. For example, some materials are described being 'viscoelastic.' This refers to an **an**elastic behaviour, where there is a temporal delay between the application of stress on the observable resultant strain, but an ultimately elastic return to form following deformation (Capurro and Barberis, 2014). However, developing and even some adult tissues may display the opposite behaviour. On short timescales tissues are often elastic, but on longer timescales the stress is relaxed by (viscous) fluid deformation, which is permanent. This could be true of developing tissues with high GAG content, such as the PSs at E13.5 (Lan et al., 2019).

This results section will demonstrate that the PSs show statistically significant differences in *E* between anterior and posterior, within sub-regions in the same plane when sectioned frontally, and on the exterior surface compared to the inner mesenchymal core. I also highlight the challenges and limitations of this technique, and how the data should be interpreted accordingly.

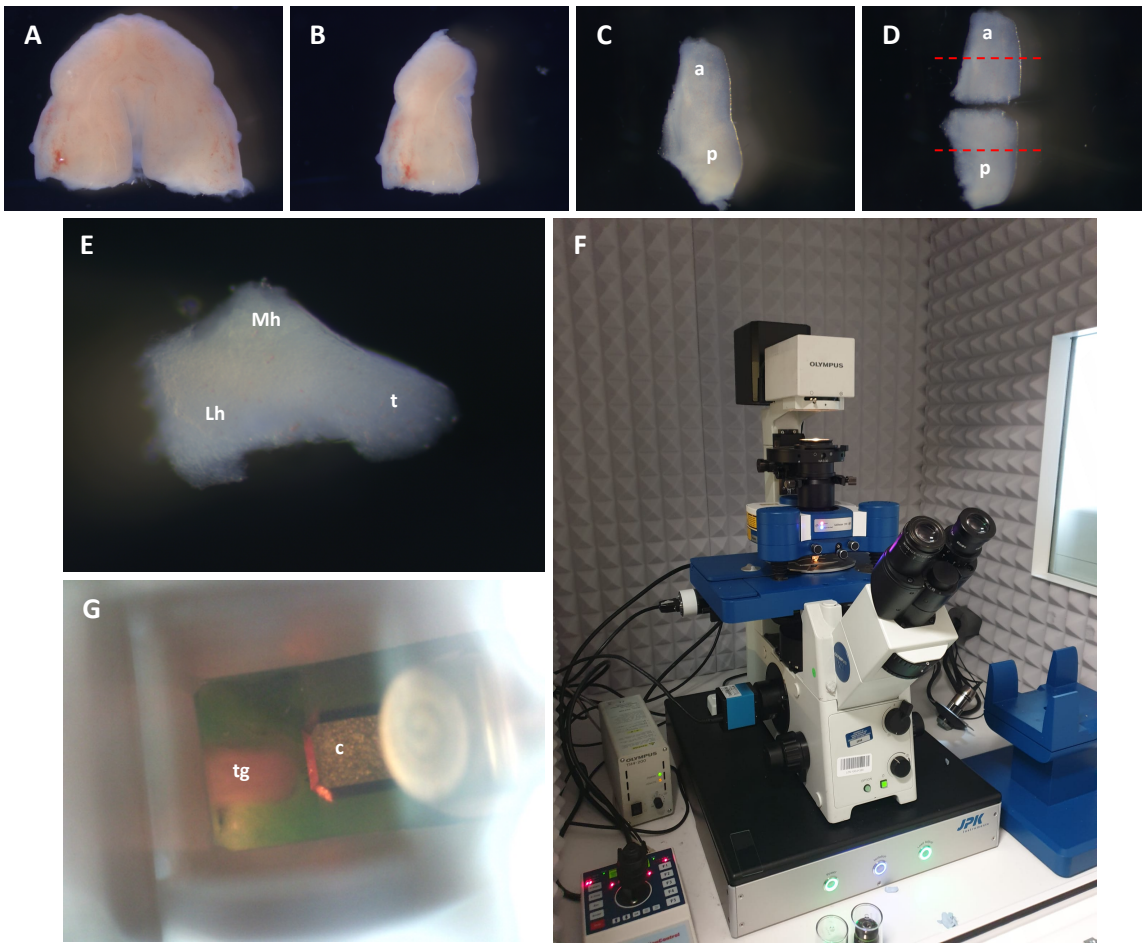

Figure 6.24 Tissue preparation for AFM and experimental set-up

Photomicrographs of PS dissection (A-E) in preparation for stiffness mapping by AFM (G&F). Maxillary explants (A) were prepared and bisected longitudinally (B), before further resection of maxillary tissue (C) to isolate whole PSs, on which surface measurements were made (C). For core mesenchymal measurements, whole isolated PSs where bisected latitudinally into anterior and posterior halves (D), which were then bisected in half again to generate opposing flat surfaces (red dotted lines). Each half was then flipped onto a flat surface to expose the mesenchymal core of the tissue (E) and each described region was probed. G) top-down view of tongue surface AFM measurements. F) JPK CellHesion 200 AFM on an inverted Olympus IX73 equipped with a motorized precision stage placed on a TMC active anti-vibration table in an isolation cabinet. a, anterior; p, posterior; Mh, medial hinge; Lh, lateral hinge; t, tip; tg, tongue' c, chip-containing-cantilever.

6.2.5.1 Experimental set-up and parameters

A detailed explanation of AFM and the selected parameters for this work are described in the materials and methods. AFM is an extremely high-resolution type of scanning probe microscopy which enables the measurement of the material properties of an object via contact with a mechanical probe. Essential parts of the process for interpreting the results are condensed and described here.

Freshly dissected maxillary explants were prepared as in other parts of this project (Chapter 3). Explants were then bisected longitudinally *(Figure 6.24A&B*) and remaining lateral maxillar tissue was trimmed-away with microdissection scissors, isolating the PS (*Figure 6.24C*). For samples undergoing topographical surface mapping, the dissection stopped here, and stiffness mapping was performed in the anterior (*Figure 6.24C,* 'a') or posterior (*Figure 6.24C,* 'p') halves of the tissue on the presumptive nasal surface (as the oral surface was easier to later secure down to the Petri dish, likely due to the curvature of the PSs at this stage). For samples undergoing mesenchymal (henceforth 'core') mapping, further preparation was required. The isolated PS was bisected to separate the anterior and posterior into halves (*Figure 6.24D*), and these halves were halved again in the same manner to expose the frontally sectioned anterior and posterior mesenchymal cores (*Figure 6.24D*, red dashed lines). The middle two pieces could then be carefully 'flipped' 90° end-on to rest on one cut surface and expose the newly cut surfaces uppermost, which provided a flat object to which the AFM could be applied. This procedure generated explants with recognisable PS anatomy, as pictured (*Figure 6.24E*). AFM measurements were taken in the three regions described in frontal sections for force and spacing mapping previously (*Figure 1.12*) and are labelled (*Figure 6.24E*). The explants were mounted on plastic petri dishes on a drop of Cell-Tak™, submerged in Leibovitz's L-15 medium without phenol red (L-15). This dissection was demanding and time consuming, taking around 30 minutes per sample from whole embryo to mounted PS region. However, it ensured no variability/potential artefacts in stiffness measurements from encapsulating immobilising mountants such as agarose used in other protocols (Hopkins et al., 2021).

Force mapping was performed in 8 x 8 grid of points over a 100 x 100 µm area (i.e. at 12.5 µm intervals), and the probes consisted of 37 µm polystyrene beads glued to cantilevers. This grid-size spacing prevented the same point being indented twice, avoiding hysteresis effects. Bead-mounted cantilevers were only accepted with a measured spring constant (k) within the manufacturer's suggested range for the cantilever use (see materials and methods *2.10*).

The data are less widely distributed in the tongue than in the PSs (The processing and analysis of the data was performed as per a recently published bio-AFM protocol (Norman et al., 2021). To outline, the mean *E* was calculated from each grid of generated force-curves via a Hertz model and used in statistical analyses. In some cases, several grids were taken in different regions of the same PS, and this is marked clearly in my graphs. Furthermore, in AFM analysis, the median of the data is typically represented graphically. Given the wide variance of force curve values this gives a better idea of the central tendency of the data than the mean and is helpful when assessing if differences in stiffness are biologically relevant. Therefore, all comparisons using the mean are displayed as bar graphs with individual datapoints and are accompanied by box and whisker plots.

6.2.5.2 There is no significant difference in the surface stiffness between the anterior or posterior regions of the PSs and the tongue

Differences in the surface stiffness of the PSs and the tongue, across the changing geometry of the oral cavity, could help facilitate shelf remodelling and elevation. To test these properties, I performed AFM as described on the surface of anterior and posterior PSs, and on the tongue. Tongue measurements were taken along much of the full length and not in anterior and posterior regions specifically. This is due to issues faced when mounting the tongue as the curvature in the posterior was often too large for the Z-piezo on the AFM to overcome, and the probes would crash. Given the tongue moves somewhat freely at this point in development, it was not deemed an issue, as both anterior and posterior aspects of the PSs come into contact with much of the A – P axis of the tongue.

Figure 6.25*Figure 6.25A*). Although the median *E* values were more uniform in the PSs than in the tongue, the variance in each individual sample was much greater in the PSs (*Figure* 6.25*A-C*). This suggests that there are small regions of increased stiffness in the PSs at this stage.

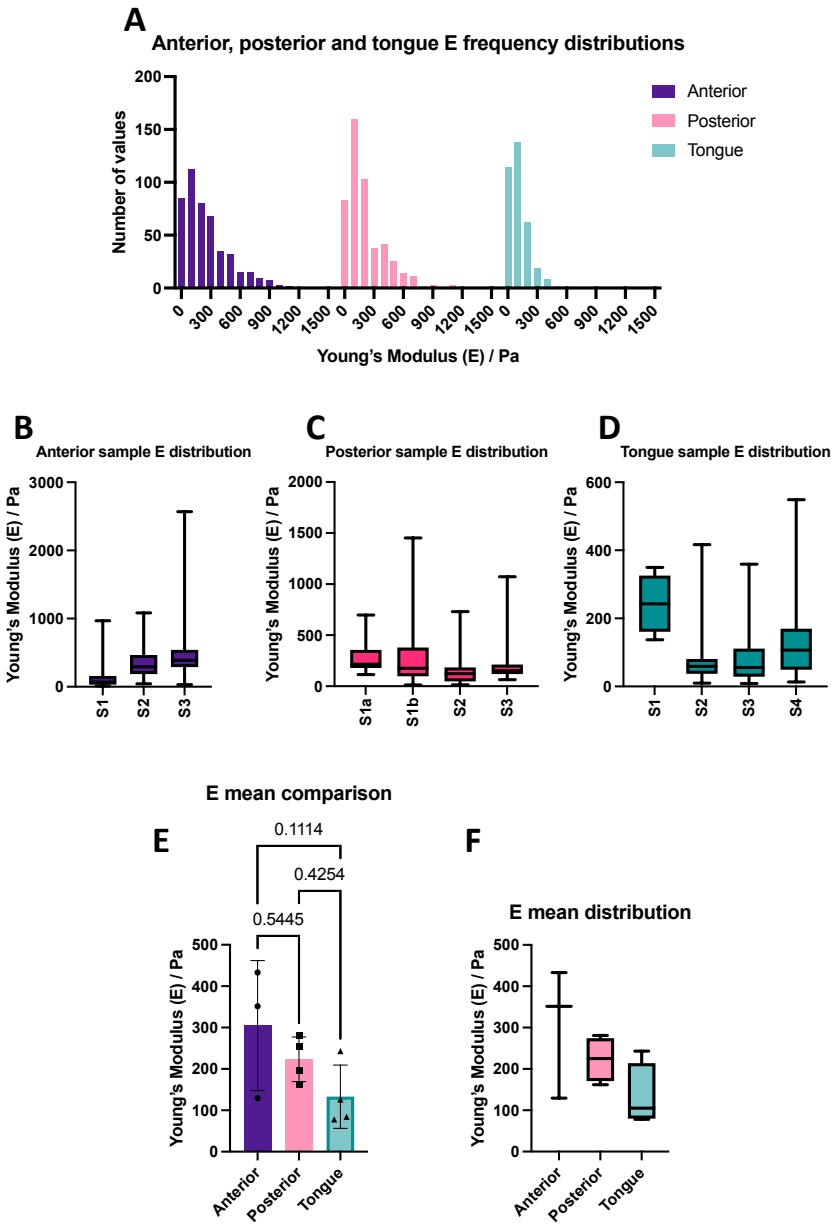

Figure 6.25 *E* measurements made on the surface of anterior, posterior and tongue tissue at E13.5 by AFM

Graphs showing A) overall sample distribution of *E* generated from force curves generated across all measured sample in all tested regions as per the key displayed in a frequency distribution. Individual sample *E* distributions displayed as box and whisker plots from AFM measurements made on the anterior (B), posterior (C) and tongue (C) surfaces. Each individual sample is denoted SX where X is the sample number, and subsequent lettering represents force maps taken in different regions of the same sample. D) Sample mean comparisons between tested regions (E) and the associated spread of the mean datapoints shown as a box and whisker plot (F). All box and whisker plots show the minimum and maximum values (whiskers), the 1st and 3rd quartiles (bounding box) and the median value (horizontal line). Statistical significance (P values) is displayed on each graph and was determined by ordinary one-way ANOVA with Tukey's multiple comparisons (E). Error bars = mean with SD.

While the median *E* was lower in the tongue than either PS region, the mean difference in *E* between all three regions was not statistically significant in any comparison (*Figure* 6.25*E-F*). This suggests that the surface stiffness of the PSs and tongue are somewhat uniform at this stage, which could be due to the lack of mature structures at this stage: in each instance, a single layer of epithelium is likely being probed.

Notably, there was a challenging degree of probe-tissue adhesion in these surface measurements, and the irregularly shaped tissue were particularly difficult to secure, often coming detached from the substrate. Therefore, a focus was put on the subsequent 'core' mesenchymal probing, where the majority of measurements were made.

6.2.5.3 In the anterior, the medial hinge is softer than the lateral hinge

Dissecting and mounting the tissue as described (*Figure 6.24*) enabled direct access to the mesenchymal core of the PS, which is the bulk of the tissue, and to map differences in stiffness in this plane. Such differences must influence how PSs elevate, since elevation is movement in this plane.

In the anterior, the tip region had a particularly wide *E* variance between samples, with some particularly stiff regions encountered when force mapping (*Figure 6.26A&B*). Widely varying *E* distributions were observed within samples in the both the lateral (*Figure 6.26C*) and medial (*Figure 6.26D*) hinge regions too, but the maximum values were an order of magnitude lower compared to the variance in tip region samples. The medial hinge was particularly soft and had the narrowest spread of data – the mean *E* was consistently below 50 Pa, and the central tendency of the data even lower (*Figure 6.26A, D, E&F*). The medial hinge was statistically significantly softer than the lateral hinge region (*Figure 6.26E*); this could represent the compression of the lateral hinge at this stage and will be explored in discussion. There was no significant difference between other regional comparisons in the anterior (*Figure 6.26E&F*).

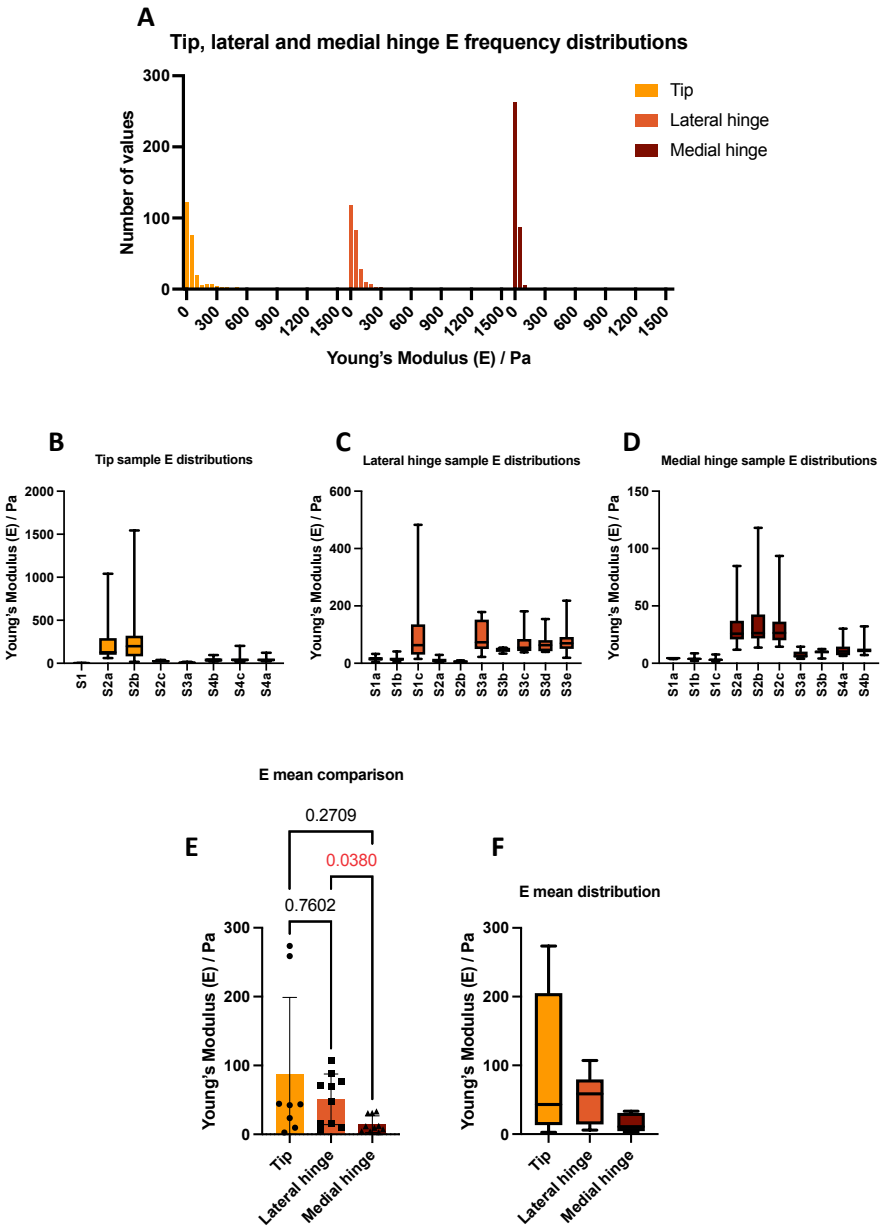

Figure 6.26 Regional comparison of *E* in the anterior PS mesenchymal core

Anterior region core stiffness mapping graphs showing A) overall sample distribution of *E* generated from force curves generated across all measured sample in all tested regions as per the key displayed in a frequency distribution. Individual sample *E* distributions displayed as box and whisker plots from AFM measurements made on the tip (B), lateral hinge (C) and medial hinge (C) core mesenchyme. Each individual sample is denoted SX where X is the sample number, and subsequent lettering represents force maps taken in different regions of the same sample. D) Sample mean comparisons between tested regions (E) and the associated spread of the mean datapoints shown as a box and whisker plot (F). All box and whisker plots show the minimum and maximum values (whiskers), the 1st and 3rd quartiles (bounding box) and the median value (horizontal line). Statistical significance (P values) is displayed on each graph and coloured in red where significant ($P < 0.05$), determined by Brown-Forsythe and Welch ANOVA tests with Dunnett's T3 multiple comparisons test (E). Error bars = mean with SD.

Posteriorly there was less overall variance across each region, with tissue exhibiting similar relative distributions to the anterior dataset, albeit on a reduced scale (*Figure 6.27A-D*). However, in the posterior there is no statistically significant difference in *E* between any of the regions investigated (*Figure 6.27E&F*).

6.2.5.4 The anterior medial hinge is softer than the posterior medial hinge, revealing heterogeneous material properties along the A – P axis of the PSs

The observed difference in behaviours between the anterior (flipping-up) and the posterior (remodelling) PSs could be due to, or at least facilitated by, differences in stiffness along the AP axis of the PSs. Anterior flip-up might suggest greater stiffness, and posterior remodelling greater fluidity, i.e. lower stiffness. However, each of these regions are likely to be composites of stiffer and softer regions and, moreover, the type of movement could just as easily be dominated by different geometries as different material properties. On the one hand, faster elastic recoil implies higher stiffness, on the other, it also implies greater resistance to deformation. Depending on the exact nature and localisation of the elevation-driving and elevation-resisting parts of the PS, there could be many different stiffness distributions. Therefore, to investigate any potential differences in regional stiffness between the anterior and posterior PSs, I compared the tip, medial and lateral hinges between the anterior and the posterior regions.

The mean *E* in the tip (*Figure 6.28A&B*) and lateral hinge (*Figure 6.28C&D*) trended higher in the posterior than the anterior, but not to statistical significance. This could suggest that the posterior is overall stiffer than the anterior but given the high variance, which is typical of AFM measurements in biological tissues (Norman et al., 2021), the low sample size should be increased.

However, the mean *E* was statistically significantly greater in the posterior medial hinge than the anterior medial hinge (*Figure 6.28E&F*). Interestingly, the spread of the individual datapoints (sample means) almost appear bimodal in this instance (*Figure 6.28E*), though it is not possible to uncover what is causing this from these data alone, and again n should be increased.

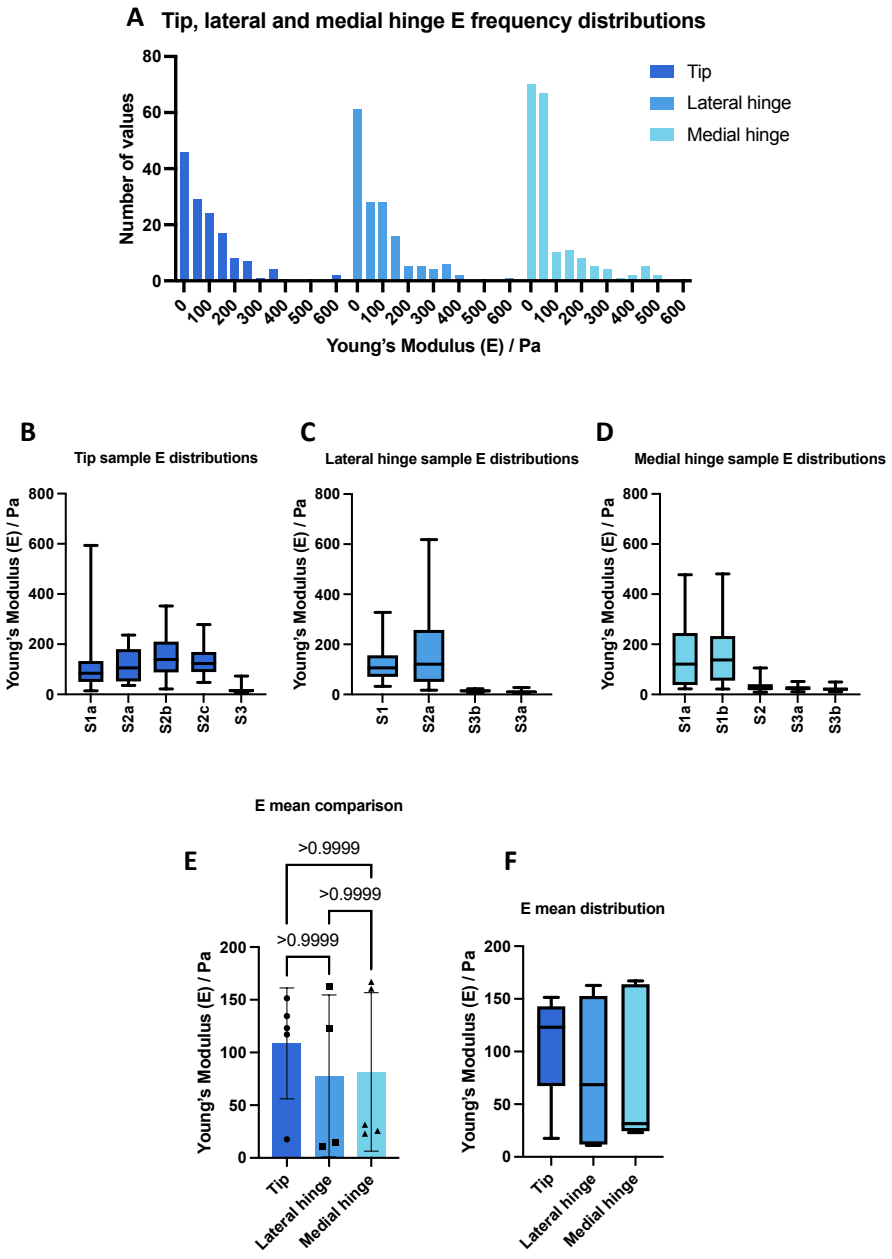

Figure 6.27 Regional comparison of *E* in the posterior PS mesenchymal core

Posterior region core stiffness mapping graphs showing A) overall sample distribution of *E* generated from force curves generated across all measured sample in all tested regions as per the key displayed in a frequency distribution. Individual sample *E* distributions displayed as box and whisker plots from AFM measurements made on the tip (B), lateral hinge (C) and medial hinge (C) core mesenchyme. Each individual sample is denoted SX where X is the sample number, and subsequent lettering represents force maps taken in different regions of the same sample. D) Sample mean comparisons between tested regions (E) and the associated spread of the mean datapoints shown as a box and whisker plot (F). All box and whisker plots show the minimum and maximum values (whiskers), the 1st and 3rd quartiles (bounding box) and the median value (horizontal line). Statistical significance (P values) is displayed on each graph and determined by Kruskal-Wallis test with Dunn's multiple comparisons test (E). Error bars = mean with SD.

Overall, the core mesenchyme of the posterior palate is stiffer than that of the anterior, to statistical significance in the medial hinge. This suggests that the material properties of the PSs are heterogeneous along the A – P axis and, given this metric assesses deformability, will very likely play an important role in how these regions and the overall shelves will change shape during elevation. The anterior springs up rapidly and so actively moves whereas the posterior in effect oozes more slowly. Therefore, the A – P stiffness difference is counter-intuitive in this light, but as my subsequent results will show, this can be unified and described by a stiff outer later and a softer internal mesenchyme.

6.2.5.5 The PSs consist of a stiff outer surface surrounding a significantly softer core

Differential stiffness between the surface and the mesenchymal core of the PSs may play an important role in shaping directional growth and morphogenesis during elevation. Notably, a stiffer surface might lend credence to the balloon analogy drawn by Ferguson (1988) (*1.4.1*). Although this was previously posed in light of the theorised differential traction between the overlying epithelium and the underlying mesenchyme constraining and directing the internal shelf force (Brinkley, 1984; Bulleit and Zimmerman, 1985), it could be that differences in stiffness do this instead. Hence, differential stiffness between the outer surface and inner core of the PSs may assist in directing the elevating force driving the PSs above the tongue.

To investigate the potential difference in *E* between the outer surface and inner core of the PSs, I compared the surface measurements with the corresponding core measurements. For the core, I averaged all three regions (tip, lateral hinge and medial hinges) to give a single number. As a result of this, the disparity in sample size (n) between surface and core is particularly high in favour in the core measurements (*Figure 6.29A&C*), and this should be taken into consideration when interpreting the data.

In both the anterior (*Figure 6.29A&B*) and the posterior (*Figure 6.29C&D*), the mesenchymal core is not only statistically significantly but in fact dramatically softer than the outer surface of the PSs. This effect is greatest in the anterior, though there is much

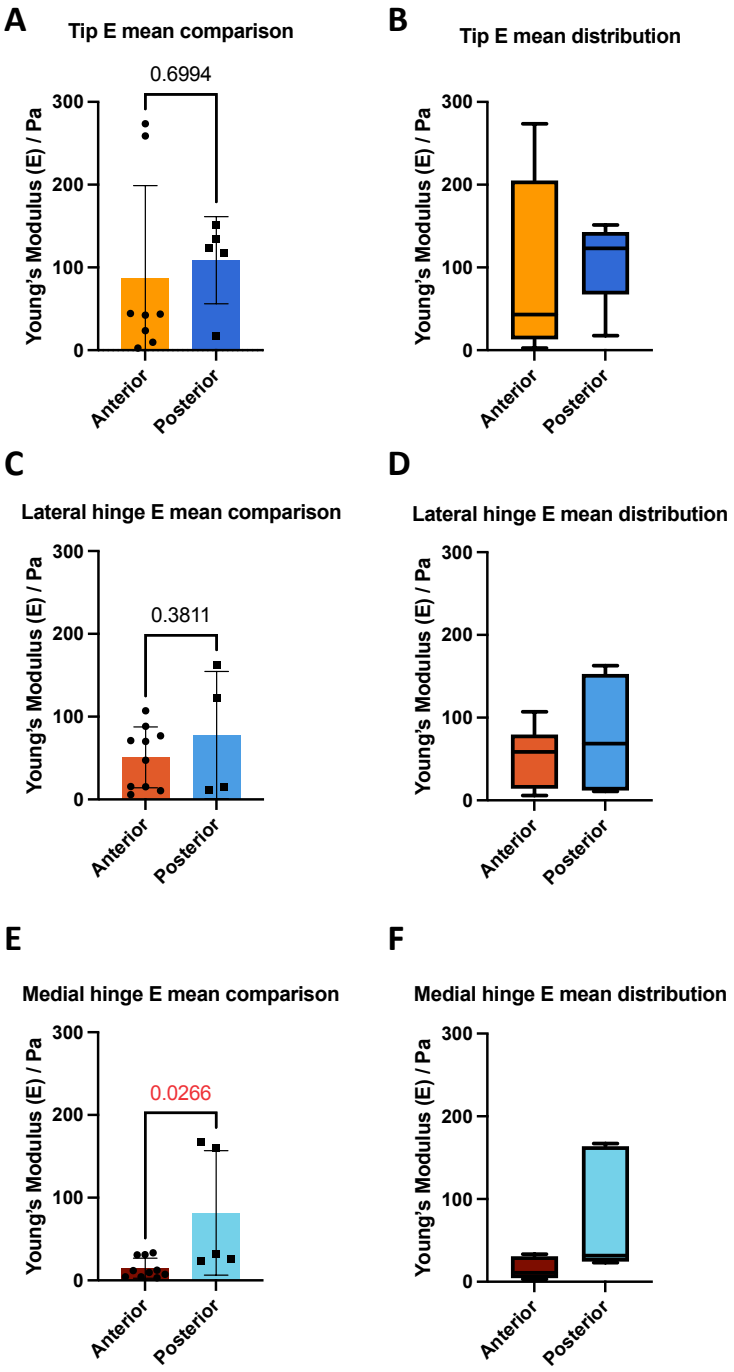

Figure 6.28 *E* comparisons between the anterior and posterior PSs

Graphs comparing the sample mean of *E* between the anterior and posterior PSs in the tip (A), lateral hinge (C) and medial hinge (E), with corresponding distributions of the mean values presented as box and whisker plots (B, D &F). Box and whisker plots show the minimum and maximum values (whiskers), the 1st and 3rd quartiles (bounding box) and the median value (horizontal line). Statistical significance (P values) is displayed on each graph and coloured in red where significant ($P < 0.05$), determined by two-tailed unpaired t-tests (A&C) and Mann-Whitney test (E). Individual datapoints are show on each graph. Error bars = mean with SD.

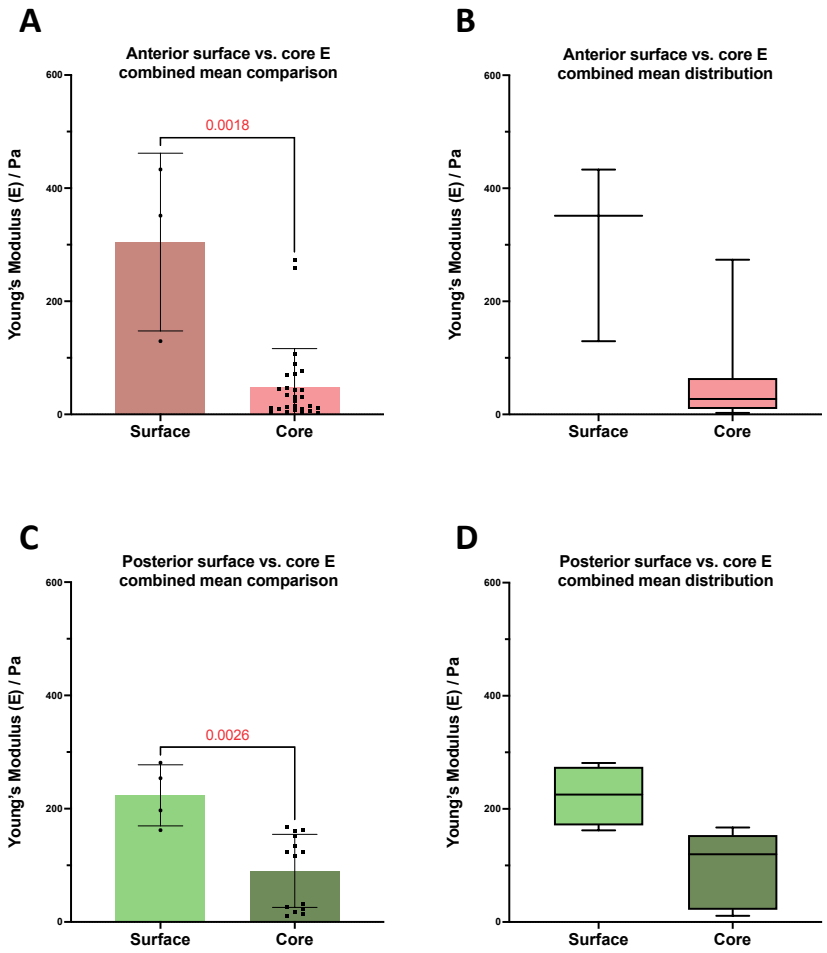

Figure 6.29 *E* comparisons between the outer surface and mesenchymal core of the PSs in both anterior and posterior regions

Graphs comparing the sample mean of *E* between the outer surface and mesenchymal core of the PSs in the anterior (A&B) and posterior (C&D) or the PSs. Core data was compiled from tip, lateral hinge and medial hinge data; hence the overall n is considerably higher (shown on bars in A&C). Corresponding distributions of the mean values are presented as box and whisker plots (B&D). Box and whisker plots show the minimum and maximum values (whiskers), the 1st and 3rd quartiles (bounding box) and the median value (horizontal line). Statistical significance (P values) is displayed on each graph and coloured in red where significant ($P < 0.05$), determined by Mann-Whitney tests. Error bars = mean with SD.

less overlap between the datasets in the posterior measurements (*Figure 6.29D*). This suggests that, alongside the regional core stiffness heterogeneity between anterior and posterior medial hinges, the outer surface of the PSs is stiffer than the core the full length of the PSs. The disparity in stiffness between the (soft) core mesenchyme and (stiff) surface epithelium strongly suggests that they may be the elusive driver of elastic movement during elevation, and this is explored in the discussion. The differences in

motion are thus dominated by the differences in resistance to motion, which would be consonant with a stiffer or more viscous posterior mesenchyme.

6.2.5.6 Summary of stiffness mapping studies

Overall, these data may provide a novel insight into the material properties of the PSs immediately prior to *in vivo* elevation. The data suggest the PSs comprise of a stiff outer later with a soft core, which also has distinct regions of softness along the A – P axis: notably the anterior medial hinge. There are several ways in which this might also point towards an essential role for the epithelium, and these are explored in discussion. Moreover, bio-AFM on PSs is technically difficult and there are some limitations to the method and caveats in the data as pointed-out throughout this results chapter, and these are further explored in discussion below.

6.3 Discussion

In this chapter I trained and applied modern deep-learning analyses and performed advanced microscopy (SHG and AFM) techniques to interrogate outstanding questions in the PS elevation field, in particular with respect to the nature of the internal shelf force. In doing so, I trained a StarDist specifically for the segmentation of nuclei in PS mesenchyme images (which, despite having limitations, may be an improvement on previous segmentation techniques), investigated nuclear morphometrics, demonstrated a lack of mature elastic or collagen fibres driving elevation of the type previously proposed, and provided the first description of the material properties (namely the stiffness) of the PSs. The AFM data are particularly interesting in suggesting elastic behaviours may be driven by a stiff epithelium, rather than the mesenchyme itself; this is introduced in this chapter discussion but, given it informs a shift in the future direction of this work, it is explored in detail in the general discussion (*7.2*). In this chapter discussion, I address these results in the context of the wider literature and highlight the technical limitations of each.

6.3.1 The elevating force might be dispersed throughout the entire PSs

Historically, it appears that investigations into the nature of the internal shelf force have considered it to act within relatively localised tensile structures, which would make sense were the event tensile and mediated by fibrous structures (Bulleit and Zimmerman, 1985; Ferguson, 1988). While my analyses demonstrate this is not mediated by collagen or elastic fibres, there may be further fibres which the techniques I used did not detect, such as fibronectin (*6.3.3*).

Recent studies describe the PS mesenchymal nuclei as aligning their long axes more or less vertically before elevation and horizontally afterwards (Chiquet et al., 2016; Goering et al., 2022). This could be interpreted to mean they are being pulled in a horizontal direction or compressed vertically upon elevation. While my nuclear deformation heatmaps suggests that the nuclei are deformed in the medial hinge in both the anterior (*Figure 6.10*) and posterior (*Figure 6.11*), I require nuclear orientation data to make the full comparison. This could be extracted from ROIs measuring the relative angle of fitted ellipses to segmented nuclei in the StarDist model in future. Alternatively, there are several ready-to-use plugins available to use in Fiji, such as 'OrientationJ', which automatically generate quiver plots for localised object orientation and calculates the associated coherence (Fonck et al., 2009; Püspöki et al., 2016).

This is similar to the previously described PS cellular shape investigation (Babiarz et al., 1979) in which the authors sketched their observations (*Figure 1.13*). Here, it was stated that the cells immediately underlying the epithelium were particularly elongated/deformed, and that the major shape changes between PSs pre and post elevation in *in vivo* tissue were situated within their 'oral side' region, which is approximate to my medial hinge. The statistically significant relaxation of the nuclei in my hinge regions supports this observation (*Figure 6.13*). They also explicitly state there were no observed shape changes in their 'oral side' (the lateral hinge in my study), which was not the case in this investigation. However, further analysis using progressively smaller (and perhaps more clearly defined) sub-regions of the PSs would be required to substantiate this in my study. Moreover, as with the other mapping data in this chapter,

I am limited by relatively low sample number (n = 4 embryos from 3 independent litters per condition). Furthermore, some differences between the Babiarz et al (1979) data and mine could be due to differences in experimental set up: I described shape changes in PSs which had elevated via elastic recoil immediately on removal of the t/m, whereas the previously outlined study was performed on cultured maxillary explants and E13.5 vs. E14.5 tissue. Although informative, neither study really captures the full extent of the *in vivo* event, given that the tongue may exert an upwards pressure on the underside of the PSs, which is not captured here.

While the mapping did not reveal any particularly promising regions of interest, the large-scale relaxation of nuclei is very likely to be a response to an elastic change. The smallness of the change, however, could mean the relaxation may not be a consequence of elevation. It may also, or alternatively, suggest that there is not much force transmitted to the nuclear envelope by the gross tissue movements, or that the force is rapidly dissipated more rapidly by rearrangement. Furthermore, and perhaps more likely given the pronounced difference between surface epithelial stiffness and soft mesenchymal core, the latter could act as a viscoelastic fluid and dissipate the tension rapidly.

Alternatively, it could be that nuclear deformation is not acting as a proxy marker for force in this tissue, unlike in the tooth placode in previous research (Panousopoulou and Green, 2016). The cells analysed in the developing tooth placode study are epithelial, compared to the mesenchyme here. The tooth also demonstrates a clear bidirectional contraction during development, whereas the PSs exhibit a relatively complex rotation/remodelling event. Plus, the tooth placode is clearly a tensile structure, and there is still little indication as to what is tensile or compressive in the elevating PSs. These are stark differences between systems. It is worth noting that my mapping accurately detected the known deformation caused by invading vasculature in the PS, most strikingly in the posterior PSs (*Figure 6.15A&D*), but this may not extend to the rest of the PSs.

Finally, there could very much be systematic changes in orientation that could shed further light on the complex and somewhat difficult to interpret patterns of nuclear deformation observed in these maps. Without this, it remains difficult to distinguish

between noise and heterogeneity in the tissue. Tentatively, nuclear deformation perhaps not being linked strongly to elevation may explain how the medial and lateral hinge nuclei can relax at the same time (*Figure 6.13*). Otherwise, a large pushing or pulling force might result in nuclei relaxing and deforming in a side specific manner during elevation, but that was not seen here. The lack of a clear driver, or any particularly striking region of interest altogether, further suggests that the mesenchymal core may be more passive than previously envisioned. While the cellular mechanisms of growth should still be explored in relation to the mesenchyme immediately underlying the epithelium, there is an increasing body of evidence from this work suggesting that epithelium is the locus of force generation, and the mesenchyme responds passively.

6.3.2 The observed changes in nuclear spacing during elevation are non-intuitive

I had hypothesised that, as the shelves elevated, nuclear spacing would increase in the lateral hinge, and decrease in the medial hinge. This is based on the idea that, pre-elevation, cells/nuclei are under compression in the lateral hinge and/or under tension on the medial side, storing elastic potential energy as a consequence of the deflection of default horizontal growth, energy that would be released on elastic elevation. However, this hypothesis was not supported by my observations. The finding that nuclear spacing decreased in both the lateral and the medial hinge post-elevation is not easily reconciled with the direction of PS movements.

In a previously described study (Brinkley and Bookstein, 1986) the authors do appear to have shown a decrease in spacing in a region approximate to my lateral hinge following elevation in their anterior heat maps (*1.4.6*). However, they do not show a decrease in spacing in the medial hinge, as observed in this work in the posterior only (*Figure 6.16*). However, the authors tracked cell density changes during elevation in maxillary explant culture. As demonstrated in this thesis, elevation does not occur in culture, instead happening immediately upon removal of the tongue. Therefore, their 'unelevated' datapoints may be more comparable to my 'elevated' data. Comparing these groups instead still does not reconcile the two studies. Notably, Brinkley and Bookstein (1986)

report a particularly densely packed PS tip, which was also not observed via heat mapping or quantified statistically in either anterior or posterior regions in my data (*Figure 6.17*).

Nuclear spacing did decrease in the medial hinge region following elevation (*Figure 6.17*). As outlined previously, this could represent an overall shortening of the medial contour of the shelf during elevation (*6.2.3.3*). It is unclear both if the medial side of the PSs do undergo any major shrinking during elevation, and why it might happen in the posterior only as per my results. It is also not possible to separate this from any PFA shrinkage artefacts in the data at present. This would require further morphometric study; it might be more suitable to do this in 3D via a landmark-free analysis, which would be better at capturing the full extent of the sloping surface of the PSs post-elevation than via the traditional landmarking methods as in this work (Toussaint et al., 2021; Redhead et al., 2023).

There is also no way to currently determine what might be increasing cell density in the posterior medial hinge post-elevation in my data. However, some inferences can be made on the timescale of the event. Given the rapidity of this elastic event, the increase in nuclear density observed is unlikely due to cell death or sudden displacement by the growth of surrounding structures. Again, the data are pointing towards the mesenchyme being more passive in the process, despite making up the physical bulk, than previously thought. Mesenchymal cells are often migratory populations and form few cell junctions, including punctate junctions between protrusions, though there is some evidence for transient junction formation in mesenchymal neural crest cells (Theveneau and Mayor, 2011). Therefore, the mesenchyme may instead be moving to a small extent passively in response to a non-mesenchymal driver of the elevating force. The lack of mature structures in the PSs at this stage, and the relatively stiffer outer epithelium further points towards the epithelium playing a more active role in elevation than previously thought.

6.3.3 Fibrous structures: applying modern techniques to answer old questions

Data in this chapter suggest that there are neither mature, aligned bundles of collagen fibres, nor a network of elastic fibres driving PS elevation of the nature reported previously (Walker and Fraser, 1956; Ferguson, 1988). Had they been detected, this might have rather straightforwardly explained elevation. There are also limitations to this analysis. Foremost, imaging with SHG is a poor way to identify fibres aligned in the optical Z-axis. I attempted to overcome this by generating both frontal and sagittal sections, but in the absence of substantial Z-depth this is a limitation. This could be addressed in future studies by the use of the recent 'Fast Green' technique for the orientation-independent identification of collagen fibres (Timin and Milinkovitch, 2023). Briefly, this impressive and reportedly simple technique involves the use of the common synthetic food dye (and histological stain) 'fast green' which has a high specificity for collagen, in anhydrous conditions. Combined with either clearing and light sheet, or just confocal, microscopy, the authors demonstrate highly detailed 3D architectures of collagen networks. Acting independently of SHG principles or birefringence (as in picrosirius red), there are no limitations dependent on the orientation of the fibres, though it can also be combined with sirius red staining and SHG to enhance signal. Thus, there are now readily available superior techniques in visualising collagen networks, and this could be applied to the PSs.

Repeating Walker & Fraser's (1956) Gomori stain, assaying for collagen via trichrome staining (with sirius red) and imaging under SHG conditions displayed very weak and diffuse staining/signal. The subtle staining seen in each instance, taken together with positive collagen antibody stains shown previously (*Figure 6.3D*) might suggest that these components are indeed present in the PS mesenchyme at this time, albeit in an immature form. This is consistent with my nuclear spacing and deformation maps, in suggesting a passivity to the mesenchyme: the internal shelf force, and what may be generating it, is either acting in a rather dispersed manner in the PS mesenchyme or is in the epithelium. It not localised to any distinct region, which might be the case if the force were tensile and mediated by elastic or collagen fibres. This could be further investigated in the case

of elastic fibres by immunostaining for elastin and comparing detected levels to those of functional elastic structures at a similar stage, such as the myocardium.

The lack of investigation into fibronectin is a limitation of this work. Fibronectin (Fn) is perhaps the only other ECM component sizeable enough to confer or mediate a force of the scale to drive a whole tissue elevation event as a principle driver. However, the lack of organised collagens may already suggest an answer, in that Fn binds to collagen I and mediates collagen fibril assembly in the ECM (Sevilla et al., 2013). It is not possible to observe Fn under SHG (Sevilla et al., 2013), and so it would not have been detected in my investigation. Previous investigations using antibody stains against FN again produced a somewhat diffuse patten across the PSs (Ohsaki et al., 1995; Kurisu et al., 1992; Morris-Wiman and Brinkley, 1992), suggesting again that fibrous ECM components might be too immature to be playing a force-mediation role during elevation.

Complex changes in the distribution of the previously described ECM components, alongside laminin, have been described previously during maxillary explant cultures in *ex vivo* rolling culture (Morris-Wiman and Brinkley, 1993). However, given the identification that elevation is in fact not happening in culture, these patterns cannot be translated to *in vivo* elevation. In the emerging epithelium-centric model of palate elevation, the epithelium could be instructing the layers of mesenchyme immediately underlying to co-ordination behaviours facilitating elevation. This may involve several ECM components working in tandem with the epithelium to drive elevation, and these are explored in the general discussion.

6.3.4 Stiffness mapping with AFM suggests an epithelial driver of PS elevation

The identification of heterogeneities in PS stiffness between both the epithelial surface and mesenchymal core, and between the medial hinge regions of the anterior and posterior PSs demarcated a narrative shift in this project. The lack of a smoking gun in the mesenchyme could be explained by its being soft and passive relative to the epithelium.

Epithelium (and conceivably sub-adjacent mesenchyme) could be the elusive driver of elevation. This notion is bolstered by the identification of epithelium being much stiffer than the PSs (*Figure 6.29*). Considering the PSs as composite structures, the stiffer epithelium may drive both anterior and posterior elevation, but the posterior PSs have a greater core stiffness, and is therefore more resistant to shape change. I.e., differences in motion are thus dominated by the differences in resistance to motion, which would be consonant with a stiffer or more viscous posterior mesenchyme.

Furthermore, this theory could still point to there being particular regions of interest within the mesenchyme during elevation, just perhaps more sub-epithelial. For example, if the shelf is stiff *per se*, then tension needs only be restricted to the proximal part of the medial hinge (a useful analogy being the fairly proximal insertion of the bicep in the forearm). Thus, there is an expansive array of consideration and discussion points arising from these data. As such, the further elaboration and discussion of this theory forms much of the general discussion. For the remainder of this chapter discussion, I discuss the technical limitations of AFM broadly, and specifically in my work.

The stiffness mapping presented in this thesis suggest that AFM is an adequate tool in measuring Young's modulus across the PSs. However, the use of AFM in soft embryonic tissue is relatively new and there are several limitations to this work, and in the technique more generally, that must be considered alongside the data. Owing to equipment and space constraints, the AFM setup was not optimal for force-mapping on live/explanted tissue. Between harvesting, transportation to a separate site (UCL), dissection and mounting, it could be up to an hour before the first sample underwent AFM; the tissue was kept on ice where possible. This timing could be variable depending on the success of the simultaneous calibration of the AFM apparatus. On the latter, I was fortunate to have the assistance of Dr. Richard Thorogate, the head AFM technician at the LCN, assisting in calibration and set up whilst I dissected. I was also unable to use a heat plate during measurements, which took place in an isolation cabinet. This was warmer than room temperature, and the explants were kept in media, but the conditions from explantation throughout probing could not be considered physiological.

Moreover, PSs were already elevated at the time of probing, occurring via elastic recoil during dissection. This might affect the ability to detect any pre-elevation regions of tension or compression that might relate to a difference in stiffness. Alternative methods of mounting were considered, such as mounting the tissue in low melting temperature agarose and vibratome sectioning, but it is unclear how the stiffness may be affected by fully embedding the target tissue in this medium. Similar studies have done so whilst the top half of the tissue remains exposed, in one case the mouse ovary, but the adult mouse ovary is considerably more robust than embryonic PSs and less likely to deform than the considerably softer PSs (Hopkins et al., 2021).

Several technical challenges were also encountered during AFM measurements. During surface PS and tongue measurements, both structures were substantially curved enough that they would on occasion come loose from the dish. Here, the cantilevers were prone to crashing into the tissue, breaking the beaded cantilevers used for measurements. Plus, although adding beads to the cantilever increases surface area and enables greater sampling of stiffness contributions from the tissues, it also interferes with the calibration of the cantilevers and lowers the cantilever spring constant (k), which could make measurements more variable, and may explain the high variance seen in my data and reported elsewhere (Hopkins et al., 2021; Norman et al., 2021). There are also assumptions made by the Hertz model, which is applied in the case of the spherical indentations typical of bio-AFM. Here, the Hertz model assume that there is a linear elastic relationship between the beaded-cantilever tip and the tissue, and that tip – tissue adhesion/other surface interactions can be neglected (Kontomaris, 2018).

Hence, there are a variety of limitations to consider when performing bio-AFM, but this is not atypical of the method (Norman et al., 2021). However, there are some limitations that are specific to this study as I have outlined here. Nonetheless, alternative techniques in force mapping face many of the same technical challenges and use the same assumptions in the Hertz mode, such as in nanoindentation (He and Swain, 2017). There are a variety of alternative methods that could be used in the future characterisation of the material properties of the PSs, and these are explored in more detail within the future

directions of the project in the general discussion. In this work, AFM has served as a useful preliminary tool in describing the stiffness of the PSs at E13.5.

7. General discussion

7.1 Overview of key findings

At the outset of this project, I had originally intended to characterise the cellular mechanisms of growth underlying palatal shelf elevation via the PROMASS framework (Green, 2022). However, the early discovery of the inherent elastic nature of the PSs during elevation via observing an almost complete rapid elevation upon tongue removal led to a reconsideration of how the internal shelf force is generated and how it drives PS elevation (Chapter 3). I then conducted a thorough morphometric characterisation of the nature of growth and elevation in the widely used *ex vivo* rolling culture system to understand whether it provided a model for palatal elevation or growth in other ways (Chapter 4). This revealed that growth is extremely poor and inconsistent in this system and, in combination with the recoil assays, confirm that the majority of PS elevation occurs immediately on removal of the tongue and is too rapid to be primarily driven by growth, the latter supporting the historic theory (Walker and Fraser, 1956). These findings might also influence the way we interpret many of the frequently cited papers in the wider literature, and these were discussed in the Chapter 4 Discussion.

Adjacently, whilst exploring the background literature on the comparative embryology of palate development, I was intrigued as to why PS elevation appeared to be a mammalian novelty. I hypothesised that the selection pressure that drove the acquisition of elevation is likely the differences in mechanisms of feeding between mammals and the more ancient extant Sauropsida. Specifically, I conjectured that the mammalian suckling requirement would have selected for a larger tongue that would obstruct the type of direct horizontal palate growth observed in reptiles and birds. I sought to test the theory via investigating palate elevation in the only non-suckling mammals, the monotremes (Chapter 5). My findings both disproved my hypothesis and led to several interesting insights into the evolution of PS elevation. I presented the first description of palatogenesis in Monotremata, via the short-beaked echidna, in collaboration with the Tucker (KCL) and Renfree (Melbourne) labs. This enabled me to complete the amniotic phylogenetic tree of elevation and suggested that that the mammalian and non-

mammalian palates are homoplasic structures, acquired via parallel evolution, and a preliminary investigation into the default horizontal nature of PS growth was undertaken in collaboration with the Goodwin lab (UCSF), whom kindly shared photomicrographs of the frontally sectioned oral cavity in a microglossia mutant. These preliminary data suggest that the mammalian PSs may indeed grow horizontally by default, just as in every non-mammal.

I then carried-out a series of experiments and analyses aimed at identifying how the force may be generated and stored, and how the previously undescribed material properties of the PSs may influence the elevation event (Chapter 6). I took advantage of the drastic improvement in methods of object segmentation in recent years and trained a machine-learning StarDist tool specific to the automatic segmentation of mesenchymal nuclei. It enabled quantitative analysis on at a resolution and scale previously not feasible. However, the software also segmented false positives and negatives, some requiring manual clean-up, during which some of these technical errors could have been missed due to user-error, which may have impacted results. Based on the segmentation, I performed nuclear morphometric analyses, namely deformation and centroid spacing, before and after elastic elevation. However, no clear patterns emerged, suggesting weak, dispersed forces and therefore passive mesenchymal behaviour.

I also attempted to address and resolve some contradictions in the literature on the presences of elastic/fibrous structures in the PSs, either mature collagen or elastic fibrils, that could potentially provide the PS elevating tension. I repeated the histological techniques used previously and carried out a higher-resolution investigation via 2-photon microscopy with SHG (Chapter 6). My data support the notion that there are no bundles of collagen fibres, nor a network of mature elastic fibres present in the PSs during elevation. However, while those findings could not rule out the possibility that fibres of fibronectin or non-fibrous elastic structures may also be present, if present they might also be consistent with mesenchymal passivity. I also highlighted the fact that the use of palatal gap closure cannot be used as a metric for PS elevation it the way it has been previously (Chapter 4). This metric arose from the early misconception that the PSs undergo gradual elevation in culture (Brinkley et al., 1975). As I demonstrated, elevation

instead occurs immediately upon explantation before culture (Chapter 3), and that any further PS approximation occurs instead by the progressive non-physiological deformation of the explant during culture (Chapter 4).

Finally, I measured the stiffness of the medial/prospective nasal epithelial surface and mesenchyme of the PSs (Chapter 6). These data inspired the reconsideration of the PSs as composite structures consisting of a stiffer, elastic epithelial surface layer, covering a much softer and potentially relatively passive mesenchymal core. Further AP heterogeneities in mesenchymal core stiffness would then additionally provide an explanation as to why the less stiff anterior PSs elevate quicker than the stiffer posterior. These data are exciting, but there is much future work to be done to expand on this potentially unifying theory of PS elevation. The epithelium could also be interacting with the immediately sub-epithelial layers of mesenchyme, which may still play an important role in elevation. Thus, these findings help narrow the focus of future cellular investigations. This hypothesis, and the future directions the project may take in addressing them, are discussed below.

7.2 The epithelium as the driver of PS elevation

7.2.1 Background and hypothesis

The material properties of the PSs during elevation are hitherto undescribed in the literature, and this assessment of surface and core stiffness in this chapter may therefore be their first characterisation. In part this is due to historic technological limitations in the ability to measure the properties of soft tissues. It might also be the case that previous elastic theories of elevation lacked the significance that these data might lend to this mode of elevation, which indicate a prominence for the material properties of the tissue.

Based on the conventional view of PS elevation and my initial results showing PS elevation to be primarily elastic, the most plausible elasticity-based elevation hypothesis was that the anterior PS 'flip-up' would be the relief of elastic deflection while posterior remodelling would be the relief of elastic compression. For this to be the case, I had

initially thought the posterior PSs might broadly have to be softer than the anterior PSs, what with the PSs appearing to be compressed over the posteriorly anchored tongue *in vivo* and its relative slowness in elevating upon tongue removal in my recoil studies. Instead, the opposite was true, with the anterior medial hinge significantly softer than that of the posterior (*Figure 6.28E&F*) and no further differences between anterior and posterior regions observed in other core regions or the surface.

I had also thought that, even as early as E13.5, the future muscular tongue would be much stiffer than the PSs, hence their deflection. However, I found the tongue to have a surface stiffness no different to that of the PSs (*Figure 6.12*). On reflection, this may not have much significance, given the tongue is in part anchored to the mandible, and is experiencing similar forces either side from the paired PSs. The finding that the tongue has a similar surface stiffness to the PSs may also be supported by previous observations in the literature that the PSs and tongue appear to undergo conformational changes about each other during posterior remodelling (Yu and Ornitz, 2011). Rather than an active event, this could instead be relatively soft materials impressing on one-another.

Furthermore, the medial hinge mesenchyme was found to have a statistically significant lower *E* than the lateral hinge and tip regions in both anterior and posterior. This suggests that the PS medial hinge mesenchyme is more deformable under applied stress, and may facilitate a medially directed elevation event, highlighting it as a prominent future region of interest.

In combination with the lack of any major indicator of a mesenchymal driver, both from my results and the literature, these findings have led to the early working hypothesis that the epithelium could be playing a much more significant role in elevation than previously thought. These results are consistent with the literature; they suggest that the anterior mesenchyme really does rotate but the posterior does not (Brock et al., 2016), but that both stiffness/viscosity differences and mostly geometry are the main factors for the difference, rather than a posterior remodelling event directed by growth.

At the start of the project, the epithelium was partly discounted in that it makes up such a small part of the bulk of the PSs. Below, I discuss evidence for epithelial involvement in PS elevation, and the different cellular behaviours, ECM dynamics and biomechanical phenomena that could be involved in facilitating and/or driving PS elevation.

7.2.2 What causes material heterogeneity in the PSs?

Whilst my data describe a heterogenous elastic modulus across the PSs, I encountered no direct cellular evidence as to what causes this. It is well-established that differential tissue stiffness affects the way tissues respond to force, i.e., tissue rheology, and there are several ways in which the rheological properties of the PSs could be acquired.

Starting broadly, the structural properties and relative organisation of the PS epithelial versus mesenchymal cells alone could cause difference in elastic modulus. Epithelia are tightly packed, anchored to a basal lamina and kept in direct, close in close communication by junctional complexes (J. Li et al., 2020). The PS mesenchymal cells, on the other hand, are by definition not anchored to a basal lamina, nor connected by permanent junctional complexes, which could result in them displaying relatively fluid properties i.e., they could rearrange more easily in response to mechanical stress (Theveneau and Mayor, 2011).

The mesenchyme overall could be viscous owing to the somewhat gelatinous nature of hydrated GAGs, such as HA, which are prominent in the tissue ECM (Brinkley and Morris-Wiman, 1987a). However, while these properties describe the constituent PS epithelium and mesenchyme, it is too simplistic a view to convincingly describe how the tissue may behave. For example, despite the lack of basal lamina or junctional connections, and so the potentially fluid-like behaviour of mesenchymal cells, they are in fact very tightly packed, as demonstrated in this thesis. Nuclei are relatively stiff (McCreery et al., 2021), and tightly packed mesenchymal cells, even with some local rearrangement, could convey a higher elastic modulus on the tissue scale.

Cell junctions are an important consideration. Epithelial cells are connected via junctional complexes, including those containing tight junctions (TJs) and adherens junctions (AJ)s. TJs effectively seal adjacent epithelia together by fusion of their cell membranes, and AJs confer the primary adhesive and mechanical properties to the epithelium (Adil et al., 2021). Both have been shown to play an essential role in epithelial adhesions following periderm removal and PS fusion (Lough et al., 2017b), but junctional dynamics in the PSs are unclear at the time of elevation. Molecularly, AJs contain a cadherin-catenin complex at their core, which directly engage microtubules and actin (Harris and Tepass, 2010), thus playing an essential role in epithelial remodelling (explored in the context of PS elevation in *7.3.3*). Actin remodels in response to applied stress (X. Li et al., 2020) thus it is conceivable that the PS epithelium responds directly to mechanical stress applied to the tongue during vertically deflected PS growth, possibly mediated by AJs (*7.4.4*)

The basal lamina itself could also play a role in the increased stiffness measured in the PS epithelium. The basal lamina is a thin ECM layer separating the epithelia, in the case of the PSs, form the underlying mesenchyme (Matlin et al., 2017). Alongside integrins, laminins are a major component of the basal lamina. Laminins are a family of glycoproteins and acts in conjunction with focal adhesion kinase (FAK) as a mechanotransducer to mediate cytoskeletal reorganisation in response to the stiffness of the local microenvironment (Zhou et al., 2022). Collagen IV is another major component of the basal lamina and, given its fibrous structure, could confer material stiffness to the epithelial layer via laminin. As would be expected, collagen IV is found in the basement membrane throughout the elevation window (Wang et al., 2020). Collagen III, which is also fibrillar has also been identified in the PS epithelium immediately prior to elevation (Fantauzzo and Soriano, 2016; Ohsaki et al., 1995). Mutant mice with mutations in collagen cross-linking enzymes have also been found to have a cleft palate (Goodwin et al., 2020). Interestingly, this could suggest that there is still a role for fibrous collagen during PS elevation in the epithelium, rather than the mesenchyme as investigated in this work, and various other examples of collagen mutations linked to CL/P were reviewed in the thesis introduction (*1.4.5.2*).

7.2.3 Epithelial remodelling

In an epithelium-centric model of PS elevation, the epithelium itself may be responding to deflection/deformation by the tongue whilst the shelves grow in a predefined medial and lateral rate. This could be in a biomechanical response to stress as outlined previously, which could cause whole tissue elevation. This is like the classical model of posterior remodelling (Coleman, 1965), except this method of elevation would be driven almost entirely by the epithelium (and perhaps the immediately sub-epithelial mesenchyme). If the mesenchyme is behaving in a fluid manner relative to the epithelium, the core mesenchyme could be largely passive in this process, with localised mesenchymal cellular behaviours, such as proliferation (Goering et al., 2022) not necessarily contributing to elevation itself. This paints a similar picture to that reported previously, of the PS epithelium exerting a differential traction serving to constrain and direct the elevating force (previously thought to be osmotic turgor via GAG accumulation) similar to the outer skin constraint on a balloon (Bulleit and Zimmerman, 1985; Ferguson, 1988; Brinkley, 1984).

Moreover, as reviewed in the thesis introduction, it is well-established that epithelial mesenchymal signalling interactions drive PS outgrowth, and there is an extensive literature on the topic (*1.2.3*). Briefly, PS outgrowth is driven by a positive feedback loop between SHH, which is restricted to the epithelium, and mesenchymal FGF10. The role of epithelial-mesenchymal signalling interactions is less understood during the elevation window, with most genetic studies reporting abnormal elevation in mutant mice and delayed elevation (Hammond and Dixon, 2022). Although processes primarily focussed on PS outgrowth are unlikely to underlie elastic PS elevation, there is evidence that genetic perturbation to the epithelial – mesenchymal signalling loop may influence elevation. A cKO of the Fgfr2 receptor was driven in the epithelium in a *K14-Cre;Fgfr2*$^{fl/fl}$ mouse, which are born with clefts (Hosokawa et al., 2009). It is unclear from this study if the PSs were able to elevate, or if the cleft was caused by fusion failure, but this does highlight epithelial – mesenchymal signalling interactions as a particular area for future investigation.

Epithelial bending events could also drive a larger-scale tissue remodelling/elevation event. As with the recently identified vertical telescoping cell movements during in the formation of epithelial placodes (J. Li et al., 2020), co-ordinated cellular shape changes wedging in distinct regions of the PS epithelium play a role in driving PS elevation. The scale of epithelial shape change could be much more subtle than those seen in driving buckling events during molar tooth bud development (Marin-Riera et al., 2018) or the folding events in drosophila wing disc formation (Tozluoğlu et al., 2019).

Ultimately, large scale epithelial and mesenchymal remodelling events are driven by cellular and ECM behaviours. A combination of these could drive PS elevation, and these are explored in *7.4*.

7.3 Limitations

As highlighted throughout the thesis, there are a range of limitation and caveats to the project, some which may be more impactful on the work that the others. These have been described technically in the discussion section of each results chapter and are further explored here.

7.3.1 Landmarking issues

Landmarks were selected to demarcate anterior, middle, and posterior regions in the PSs according to Yu & Ornitz, 2011 as described in the materials and methods (Chapter 2). The main strength of this metric is that landmarks are provided below, above and within the PSs and, so long as the 4-molars were aligned during sectioning, sections were obtained consistently in the correct plane. However, this cannot be said of cultured tissue, or any tissue previously explanted. Owing to the nature of the dissection, the majority of landmarks used to identify A – P regions along the PSs are lost. Internal ps (epithelial invagination and molar tooth bud) landmarks are maintained, but the inferior landmarks (tongue attachments and mandibular cartilages) are lost entirely. Furthermore, although it is still relatively easy to identify the nasal septa from culture maxillary explants, it was sometimes difficult to distinguish this from the middle region

superior landmark, the nasal epithelium, owing to the significant narrowing of the inter-hinge gap. Therefore, oblique and tilted sectioning was much more of a problem in the sectioning of cultured or recoiled tissue. Attempts were made to control for this by not including sections that were clearly oblique or had particularly unrecognisable landmarks, but it could still be the case that sections representing each region do not correspond perfectly between samples. In theory, this could be avoided in future by repeating the investigations using a landmark-free morphometrics approach (Redhead et al., 2023; Toussaint et al., 2021) and comparing total rendered geometric differences between samples in 3D, rather than selected regions based on landmarks.

7.3.2 Inter-hinge gap narrowing and PSA

The implications of the effects of the inter-hinge gap narrowing on palatal shelf angle (PSA) were discussed at length in the Chapter 4 discussion. Although likely subtle, the free movement of the lateral maxillae towards one another likely affects the extent to which the PSs elevate. As demonstrated by the inter-hinge gap narrowing, this non-physiological deformation occurs to the greatest extent during culture. Therefore, this issue may have less of an impact on samples used in elastic (immediately fixed following t/m removal) or viscoelastic (fixed after 20-minutes) recoil studies compared to PSA measurements in culture. The inter-hinge gap narrowing was fairly consistent across culture but given the inconsistent nature of growth/shrinkage across the entire tissue, as demonstrated in the morphometric studies, it would be difficult and likely not possible to determine how much these narrowing events influence elevation, thus PSA, in this work. This could potentially be ameliorated by repeating the studies leaving the mandible intact and only remove the tongue. However, having attempted this, it is difficult to remove the tongue without contacting or potentially damaging the PSs owing to the intimate communicate between the structures. This is particularly a problem in the posterior oral cavity, what with the potentially total lack of free space and sharp downward angulation of the cavity towards the oesophagus. One could attempt to remove the tongue in the extreme posterior aspect by making small incisions in the mandible inferiorly and pulling the tongue through the resultant gap. However, this could disrupt mandibular integrity, which would undermine the reason for the exercise. In a

pilot study, attempts were made to cast small, low melting temperature blocks of agarose, replace the tongue with them, and measure the relative indentations along the A – P axis of the block, potentially as a comparative metric for recoil. However, there was extremely experimentally demanding, and there was a particular issue with keeping the blocks inside the oral cavity, thus the pilot was abandoned. Overall, there is not a straightforward way to resolve this from the data I have. If the extent of influence of narrowing on elevation were known in each region, this could simply be subtracted from the measured PSA, but it is not possible to determine that value from the data presented here.

7.3.3 Recoil study timepoints

In my recoil studies, fixation immediately after removal of the t/m was designated as an assay for primarily elastic elevation, whilst fixation after 20-minutes in PBS following explantation was designated as an assay for elastic and viscoelastic elevation. It would be informative to have a third, further time point closer to or at the one-hour mark. It could very well be the case that the posterior PSs would have completed elevation had there been a longer timepoint, which up to and beyond an hour is still far too rapid for morphological changes to be due to significant proliferation or cell migration events. The posterior PSs were generally horizontally elevated in the posterior at the end of 72hours in culture, but from the data there is no way of determining whether that remaining elevation occurred any time up to that point, or within culture itself, which could have very different drivers. If it happened sooner, it would provide further support for the posterior PSs behaving in a viscoelastic manner.

7.3.4 Sub-optimal growth during culture

Comparisons between media compositions and types of culture were made in the discussion section of Chapter 4, which suggest that the conditions during my rolling cultures could have been sub-optimal. Whilst the slightly improved growth in the higher gas-change frequency groups in my culture studies was observed, the inconsistency across the PSs remains. Furthermore, the most-advanced culture systems in use today cannot recapitulate embryonic growth beyond E12.5 owing to a failure to recapitulate

the maternal bloody supply at later stages (Aguilera-Castrejon et al., 2021). On the whole, this inconsistency, with the fact that elevation primarily does not occur in culture, makes the system inappropriate for use in answering the questions posed in this thesis. However, if the growth rate could be made consistent by further alterations to the incubation or media conditions, it could at least be useful in PS growth investigations (albeit likely at a substantially reduced rate). The slight improvement in the higher gas change frequency group suggests that further improvements could be made, but future work to investigate this would require extensive parameter exploration with differing methods of gas delivery, gas concentrations/compositions and media type/supplementation.

7.3.5 Sample number limitations in echidna and pilot default horizontal growth studies

A particular issue with the comparative embryology description of the echidna palate (Chapter 5) is the low sample number, 1 from each of the 4 developmental stages presented. Thus, there are no biological replicates. Although the simple fix is to increase the sample number, the difficulty associated with acquiring echidna eggs highlighted previously makes this difficult. The only solution to this is hope that more samples are acquired from the echidna breeding programme our collaborators are a part of, but low-breeding rates make the acquisition of tissue for scientific results even less likely. The only alternative species to investigate palatogenesis in a monotreme is the platypus, but this is more endangered thus an even less possible course of action. The only solution to this appears to be waiting for more tissue, so this will just be a time consideration. Similarly, although the data from images shared by the Goodwin lab (UCSF) suggest that the PSs are growing horizontally by default in the mouse, this is only a pilot and sample number needs to be increased at more stages. Furthermore, the data were described qualitatively in this thesis, but future work with a higher samples size will require quantitative assessment of nature of the potentially default horizontal outgrowth, and PSA could be a useful metric for comparison between WT and mutant samples.

7.3.6 StarDist model issues

The use of a StarDist model helps tackle the time and labour requirements that have previously made large-scale quantification of object segmentation impractical. However, it has several caveats, and these mainly stem from the quality of the model. Although it appeared to faithfully segment nuclei to the eye, the quality control testing revealed a relatively high false negative and false positive object detection rates. While sample should be adequate in determining nuclear morphometric heterogeneities in these studies, it is unclear whether much of the somewhat chaotic patterns of deformation and spacing was due to true heterogeneity or just noise. Manual clean-ups were performed after each sample segmentation, but it is highly likely that many were missed due to user error on account of there being several thousands of nuclei per image. This was less likely to have been an issue in the smaller PS regions selected during deformation and spacing comparisons as there were less ROIs to deal with. Therefore, data obtained using the StarDist model could be particularly noisy, and further training should be carried out to try and improve the quality of the model. Filters could also be applied post-segmenting to see if these reduces the rate of false positive and false negative detection, based on object size.

7.3.7 Nuclear morphometrics ROI selection

Nuclear morphometric comparisons were exploratory, and potential regions of interest were selected qualitatively studying the larger heat maps of these quantities in the PSs pre and post elevation. However, this was not done systematically, and further sub-regions of interest could exist within the smallest regions I investigated, such as the lateral and medial hinge regions. This particularly became apparent in the final stages of the project, when the epithelium, and potentially immediate sub-epithelial regions of mesenchyme, were highlighted as a region of interest in AFM studies. This, combined with the persisting limitations of the StarDist model, suggest that further patterns other than those presented in this thesis could remain unidentified in my data, or could have been missed altogether owing to limited regions of investigation. This could be improved by dividing the PSs in a more systematic manner and running the investigations again.

However, before doing so, the method of nuclear segmentation needs to be improved as discussed previously.

7.3.8 Narrow selection of fibrous ECM components and analyses

The investigation into the presence of elastic and collagen fibres in the PSs supports the notion that they are not present in a mature form at the time of elevation and may therefore not be a primary driver of the event. These were selected for investigation as it appeared unresolved in the literature as to whether or not they were present, and this could have had a large impact on how the event is conceptualised. However, although the use of SHG to study collagen is higher resolution than previous histological stain, the elastic fibre investigation was simply a repeat of Walker and Fraser's (1956) Gomori staining. Moreover, fibronectin could be the only other ECM component playing a potential similar role to that previously thought of collagen in mediating tensile forces due to its sheer bulk. Therefore, the lack of its inclusion in these analyses leaves a gap in investigating the presence of large ECM components in the PSs prior to elevation that could also be crucial to future modelling approaches *in silico*. Antibody staining has been carried out previously as described in the introduction (Silver et al., 1981; Ohsaki et al., 1995). Methods for carrying out these investigations are suggested below in 'Future Directions' (*7.4*).

7.3.9 AFM issues

The application of Bio-AFM to embryonic tissues is a relatively recent use of scanning probe microscopy and I have not found an example of its use in the embryonic palate. This was a particularly exploratory part of the project and there are multiple technical limitations and caveats to the data obtained.

There are several limitations in the experimental set-up. The use of isolated PSs was necessary as it was not possible to access the PSs for probing with virtually any surrounding maxillary tissue left intact. However, this means that each PS measured was in post-recoil elevated state, and the internal shelf force would be released during

dissection. Therefore, the data collected here cannot be said to strictly represent the elasticity of the PSs immediately prior to PS elevation.

It was also continually difficult to mount the tissue in a way which prevented movement during probing, but which kept enough tissue intact that the dish was not contributing to the stiffness data obtained. I eventually settled on the use of Cell-Tak in sticking isolated PSs down to the dish to overcome this, but the PSs only stayed attached to the dish when mounted presumptive oral surface down. Therefore, surface measurements were obtained on the presumptive nasal aspect of the PSs only and a relatively low sample number (3 in the anterior and 4 in the posterior). The lack of probing on the oral surface of the PSs is a fairly substantial gap in the data as this comprises half of all PS epithelium and could behave in a different manner to the future nasal (medial) PS epithelium, which is under compression by the tongue. The pre-elevation PS may experience compression against the tongue on the medial aspect pre-elevation, and the oral aspect of the epithelium post-elevation. Plus, the technical limitations of the AFM were particularly apparent when generating surface measurements, as discussed in Chapter 6. The typical curve to the shelves was consistently larger than the Z-range of the AFM used, which resulted in several broken cantilevers and unusable force maps (hence the low n).

Plus, although data was obtained at a more successful frequency in the mesenchymal core surface measurements, the regions selected for measurement (medial and lateral hinges and tip region) were approximations. Therefore, these data represent samples of each region and may not overlap to a particularly rigorous extent, highlighting the requirement for a more systematic approach to measuring PS elasticity.

Finally, the conditions under which the samples were measured were far-removed from physiological. As outlined in Chapter 6, due to equipment/space limitation at the time, the tissue was not heated on a warming plate. Plus, being explanted in an exposed dish meant it was not possible to maintain the high oxygen tension required for tissue viability. Plus, with embryo harvesting, transport to the AFM and dissection collectively taking up and sometimes over an hour, the tissue could have been affected by the early stages of degeneration (though this was not apparent under the microscope).

Overall, the picture painted by the AFM data is interesting and differences in stiffness values obtained between core and surface measurements were substantially different in the relatively low sample number comparisons. However, the caveats to this investigation are numerous and further investigations into the material properties of the PSs are imperative to verify the early findings before inferring the biology beyond conjecture. Future directions for measuring the material properties of the PSs are explored below.

7.4 Future directions

The research presented in this thesis leaves many questions unanswered. This, in the light of the relatively sparse literature on PS elevation (compared to the other stages of palatogenesis) suggests several avenues for future exploration. These include *in silico* modelling approaches, the outstanding requirement for a complete description of cellular behaviours during PS elevation and further biomechanical interrogation of both the PS mesenchyme and epithelium.

7.4.1 Material and biomechanical investigations

Further characterisation of the material and biomechanical properties of the PSs will be essential in understanding the basis of the elastic PS elevation process. Here, I offer suggestions as to how several material and biomechanical properties could be investigated in the PSs to inform how they may play a role in driving or facilitating elevation.

7.4.1.1 Stiffness (elasticity) and viscoelasticity

Initially, it would be informative and interesting to further the characterisation of the elastic modulus (stiffness) of the PSs and would be essential for quantitative modelling of the process (*7.4.2*).

It is clear in the light of the very low-resolution AFM stiffness mapping I achieved that it could be completed at a much higher resolution than that presented in this thesis, which would be useful and informative because it could help identify potential further heterogeneities. Specifically, it would be interesting to measure the elastic modulus of the mesenchyme immediately underlying the epithelium, which could be altering their behaviours in response to the overlying epithelium, thus informing any future modelling approaches *in silico*. The AFM experiments presented here were limited by a small Z-range, which was problematic in PS surface measurements, and fairly restrictive mapping options in the software (Chapter 6 discussion). The use of a larger Z-piezo, and software with and the ability to physically define regions of interest for mapping could enable a user-defined stiffness map specific to the geometry of the tissue, unlike the regional sampling methods in my own mapping. These technical improvements in combination with the method of tissue-mounting via Cell-Tak described in this thesis would be adequate to create a detailed stiffness map of the PSs.

AFM can also be used to measure viscoelasticity (Efremov et al., 2019), which could explain the delay in elevation timing seen in the posterior in my recoil experiments. The investigation of viscoelasticity might be of particular interest due to the observed behaviours of the posterior PSs.

Alongside AFM, several techniques could be used to investigate the viscoelastic (and elastic) behaviours of the PSs, one such example being Brillouin microscopy (Bm). Bm uses the scattering of laser light from acoustic waves that are created by fluctuations in density within a tissue sample to measure viscoelasticity (Prevedel et al., 2019). In short, this creates a spectrum from which the longitudinal modulus (an approximation of elastic modulus) can be extracted. This technique has several advantages when applied to the PSs in that it is entirely non-invasive, simply using light, and could potentially be used to live-image the PSs. The density and refractive index of the tissue are required to generate accurate measurements, which could be difficult to measure in entire PSs. Nonetheless, Bm has been used to measure the longitudinal modulus in the ECM of live zebrafish (Bevilacqua et al., 2019) and could perhaps at least be applied to the epithelial surface and sub-epithelial layers of mesenchyme in the PSs.

Another alternative to AFM is nanoindentation. Nanoindentation works under the same principals as AFM; in biological studies it utilising scanning probe microscopy via spherical cantilever and typically fits measured quantities to a Hertz model to calculate Young's Modulus (Griepentrog et al., 2013). The essential difference is that the cantilever tips used in nanoindentation are larger than those used in AFM and so can measure deformability of areas of tissue up to several tens of microns in diameter (versus under 25 microns for standard AFM), so it is possible to sample larger tissue areas. Whilst somewhat larger areas can be achieved in AFM by using non-standard probe tips (e.g. gluing glass or polystyrene beads to cantilevers similar to the beads used in my studies), this affects the stability of the cantilever. AFM is therefore much better suited to the nanoscale for which it was originally invented, to the extent that the DNA double helix has been probed (Leung et al., 2012). Nanoindentation is a more recent technique but is becoming increasingly commercially available and so future work might benefit from the use of this technique over the AFM.

It could also be relatively straightforward to apply parallel plate compression (PPC) to measure overall sample elasticity. This could be useful in determining whether the tongue is stiffer than the PSs, hence PS vertical deflection, or if it is just the genioglossal anchoring of the tongue to the mandible that drives this (which could also be useful for FEM). Simply, PPC compresses samples at a constant strain between two rigid plates, and the force exerted back onto the plates is recorded until equilibrium is reached (Forgacs et al., 1998). This is then used to calculate the overall elasticity and viscosity of the tissue and has been used in characterising the material properties of explanted zebrafish tissue (Schötz et al., 2013). This could readily be applied to explanted/isolated PSs and the tongue, but the straightforwardness is to the detriment of resolution, which AFM provides. Moreover, this more destructive technique is unlikely to be well-suited for tissues as soft as the embryonic palate and tongue in the way that AFM and nanoindentation are, thus this may not be the best approach.

Micropipette aspiration (MA) could also be used to interrogate the elasticity (and surface tension and viscosity) of the PSs (von Dassow et al., 2010). During MA, a constant negative

pressure is applied to the sample via a micropipette, which induces deformation in the tissue at a rate-dependent manner based on the resistance of the tissue to deformation (Petridou and Heisenberg, 2019). The tissue deformation is recorded in relation to flow, from which elasticity viscosity and surface tension can be calculated. However, as with PPA, MPA is relatively low resolution, and heterogeneities in the tissue properties could be missed via this method.

Potentially of particular utility, ferrofluid oil droplets (FDs) can be used both *in vivo* and *ex vivo* to quantify mechanical properties during development over a variable spatial scale (Serwane et al., 2017). Here, FDs are inserted between cells, and initial spherical shape is maintained by applying a magnetic field. The spherically shaped oil droplet is deformed by the surrounding cells, and this can be imaged to measure the local viscosity and elasticity in a region-specific manner (Petridou and Heisenberg, 2019). The droplet may also be tagged with a fluorphore to improve visualisation of the extent of deformation. This is likely not possible *in vivo* in mice, but could conceivably be combined in exteriorisation assays or, ideally, improved future stationary culture methods that enable the observation of PS elevation. An advantage of this technique in particular is the ability to investigate cellular behaviours and material properties concurrently, and several droplets could be applied in different regions of the same PS sample. Thus, this could be a particularly desirable technique to investigate the material properties (combined with the cellular topology) of the PS epithelium, the sub-epithelial mesenchyme, and the mesenchyme more broadly.

7.4.1.2 Membrane tension

Membrane tension regulates mechanosensitive ion channels (Wang et al., 2014) and, although the relationship between membrane tension and bulk tissue tension is not entirely clear, it could be conjectured that this might a dynamic role in the PS epithelium during elevation. This could occur on a global scale, or in isolated regions of interest during PS contact with the tongue during PS outgrowth/ventral deflection. Changes in membrane tension can be measured and monitored via the application of the fluorescent lipid tension reporter, FlipR (Colom et al., 2018). The fluorescence lifetime of the probe

is linearly dependent on cellular membrane tension and is typically quantified via fluorescence lifetime imaging microscopy (FLIM). This could be applied to the PS explants to track changes in membrane tension in regions of interest, such as the medial hinge. Ideally, this would be used in combination the generation of a 'faceplant', a whole embryonic head with the nasal prominences and frontal maxillae excised, revealing the intact oral cavity and unelevated PSs at E13.5, to track membrane tension in the unelevated state for short periods, per tissue viability. However, it is further unclear whether membrane tension could even be a driver compared to the cytoskeleton or ECM. Therefore, FlipR dyes could instead potentially be a useful reporter for tissue tension if it could be correlated with bulk tension, which could be measured using one of the approaches outlined above.

7.4.1.3 Cortical actomyosin contractility

The contraction of the cortical actomyosin cytoskeleton is the major cell-based generator of forces in morphogenesis. Forces generated in this fashion are transmitted via adhesive complexes, and underlie cell shape change, division, migration and, in combination with biochemical signalling, co-ordinate tissue morphogenesis during development (Murrell et al., 2015). Therefore, understanding the dynamics of actomyosin contractility during PS elevation and their relation to the ECM will be a crucial step in further exploration of the forces driving palatogenesis.

Briefly, the cortical actomyosin cytoskeleton lies immediately beneath the plasma membrane in eukaryotic cells and consists of bundles of overlapping filamentous 'F'-actin microfilaments, ATP-dependent myosin motors and various actin binding proteins (ABPs) (Clark et al., 2014; Salbreux et al., 2012). In non-muscular systems, the complex network of F-actin microfilaments is bound by ABPs and myosin II motors physically 'pull' on the network. This generates cortical stresses and, combined with local changes in organisation and composition, results in tension gradients across cells (Chugh and Paluch, 2018). These gradients instruct cellular behaviour, for example, rearward cortical tension gradients provide the forces which propel migrating cells forwards (Bergert et al., 2015; Chugh and Paluch, 2018). Furthermore, F-actin fibres can transition between their

cortical arrangement and in alignment as ‘stress-fibres’, which occurs in response to different stimuli and as cells exit mitosis. Stress fibres are involved in mechanosensation, cell migration and cell adhesion (Santa-Cruz Mateos et al., 2020), thus actomyosin tension can be regulated by changes in substrate stiffness (Du et al., 2021).

Regarding the palate, a recent preprint was highlighted in this thesis (*1.3.4.2*) which tracks phosphorylated actin dynamics across the process of elevation in static sections (Goering et al., 2022). To recap, the authors used a phospho-myosin antibody (a marker of myosin phosphorylation, and actomyosin activity by proxy) and measured regional differences in staining between micro-stages of elevation to track actomyosin activity during elevation. They suggest that actomyosin contraction progresses in a wavelike fashion, originating in the buccal PSs and spreading superiorly as the PSs pass over the tongue (*Figure 1.9*, see *1.3.4.2* for detailed review). However, while descriptions of actomyosin dynamics are key to the progress, especially if they could be captured during live imaging, it remains unclear how actomyosin contractility/force generation interacts with the ECM to drive morphogenesis during PS elevation.

The cortical cytoskeleton is intimately linked with ECM components, which may store/transmit and be directed by the actomyosin-generated forces to drive morphogenesis. Structurally, F-actin filaments anchor into the cell membrane and form focal adhesions (FAs). These connect the cytoskeleton to the ECM via the transmembrane integrin receptors (Eyckmans et al., 2011). The integrin receptor itself adopts a high-affinity state in response to force, whereas a reduction in cytoskeletal tension via myosin II inhibition results FA disassembly (Eyckmans et al., 2011; Friedland et al., 2009; Kirfel et al., 2004). Hence, integrin-mediated communication between the ECM and the actin cytoskeleton could be responding to the loading of the PSs against the tongue during PS outgrowth, potentially playing a role in their eventual reorientation over the tongue.

Elastic fibres are one such ECM component which binds to integrins (Neptune et al., 2003) (see 1.4.5.5), thus tension could be generated and transferred by the contractile actomyosin network via integrins and to elastic fibres directly to influence morphogenesis during palate elevation. However, this may be unlikely given the apparent lack of mature

elastic fibres at this time from work presented in this thesis. The published literature investigating the roles of individual ECM components during PS elevation were reviewed in *1.4.5,* and how particular components of interest may be interrogated experimentally in future are proposed later in this discussion (*7.4.3.3*).

The actomyosin network may also play a role in the non-reversibility of PS elevation at later stages post-E13.5. It has been demonstrated in the *Drosophila* wing that myosin II forms polarised cables following mechanical stretch, increasing overall tissue stiffness. Interestingly, the relationship between stretch and polarisation was found to be linear, with more stretch causing more polarisation, thus the consequent stiffening of the epithelium prevents further deformation (Duda et al., 2019). The PS epithelium may act in a similar manner, with epithelial stretch potentially occurring on the opposing side of compression by the tongue during outgrowth i.e., on the lateral surface during outgrowth and on the nasal surface post-elevation. This could build until the PSs stiffen to an adequate extent to prevent reversion to the pre-elevated state, which is well-documented in the literature following tongue-probing experiments (Walker & Fraser, 1956; Ferguson, 1977). This would be challenging to test *in vivo*, but could be explored as in Duda et al., 2019 by isolating individual PSs and placing them on a stretch device.

Furthermore, junctions mediating cortical actomyosin and ECM communication, such as FAs, also act as distinct signalling centres. However, of particular interest here may be EPH/EPHRIN signalling. A recent study identified a role for EPH/EPHRIN signalling in modulating cell contact strength (Kindberg et al., 2021). Both using cellular aggregates and mouse genetics, the authors demonstrated that EPH/EPHRIN signalling increases cortical actomyosin contractility, resulting in an increased interfacial tension and decreasing cell contact. This was sufficient, independent of cell migration, to drive cell segregation. Ephrin family members may play a role in mediating cell contact strength to enable the appropriate extent of deformation of the PSs during elevation. Previous research has demonstrated that ephrin-B1 perturbation results in truncated anterior PSs via reduced proliferation (Bush and Soriano, 2010), and is regulated by the RAS/MAPK pathway (see *1.2.3.1*). The Ras protein is found in FAs (Eyckmans et al., 2011), thus a complex role for ephrin family members is being elucidated in the development of the

palate, and this may directly relate to actomyosin dynamics throughout outgrowth/elevation.

Overall, there is much scope for future investigation into the role of actomyosin generated forces, and how they interact with the ECM in morphogenesis during palate elevation. As suggested, this will require combinatorial *in vivo* and *in vitro* approaches, with mouse genetic perturbation studies being of particular value (*7.4.5*).

7.4.2 Finite element modelling

Greater confidence in the elastic nature of palate elevation would be achieved if stiffness measurements made by one or more of the above methods were combined with mechanical modelling of the process. Finite element modelling (FEM) would be the method of choice for this. FEM is a powerful modelling technique increasingly utilised in developmental biology (Malde et al., 2019; Jingtao Li et al., 2016; Tozluoğlu et al., 2019). FEM reduces a system down into finite-sized elements and applies equations describing the elastic and/or viscous behaviours of each element. These are constructed and solved per-element to determine the overall behaviour of the system (Brodland, 1994).

As with wider computational modelling, FEM enables significant user-freedom in testing hypotheses and, along with other types of models, can be applied in biology to investigate the biomechanics of morphogenetic process (Fletcher et al., 2014). FE models are often coded from scratch by groups seeking to answer specific questions (Tozluoğlu et al., 2019), but can also be purchased as commercial software, such as COMSOL (Jingtao Li et al., 2016), increasing accessibility to the method.

As such, there is great scope to apply FEM techniques to the process of PS elevation. Fundamental to the modelling, however, is a thorough understanding of the properties/behaviours of the individual elements comprising the model. Thus, the more information one can programme into the system, the more faithfully the model may recapitulate *in vivo* behaviour. In the case of PS elevation, this at minimum requires knowledge of the material properties throughout the entire PS volume. My AFM data are

the first steps towards this. Naturally, knowledge of spatial force distribution and cell-cell junction and signalling behaviour would assist in building a better model.

When modelling complex morphogenetic processes in biology, such as PS elevation, the 3D geometry of the model is a particularly important consideration (Paci and Mao, 2021). Therefore, in applying FEM to morphogenesis, it is essential to recreate complex 3D geometries observed *in vivo*. There is, of course, great value in simplifying 3D biological shapes in asking questions about morphogenesis, but in the case of PS elevation the intimate communication between the tongue and PSs over a changing geometry of the oral cavity creates a very specific situation.

To obtain the detailed geometry of the PSs and tongue, one could also take advantage of several imaging and microscopy tools to render much more accurate geometries of tissues undergoing morphogenesis. Firstly, extremely high-resolution tissue scans can be acquired via micro-computed tomography (microCT). This has recently been used in the Green lab to investigate craniofacial phenotypes in mouse model of Down syndrome (Redhead et al., 2023; Toussaint et al., 2021). Using contrast agents such as iodine or phosphotungstic acid (PTA), excellent contrast can be achieved in soft tissues, making the technique suitable for the study of embryos (Fenelon et al., 2023b). Subsequently, these scans could be rendered as 3D meshes, which can be full volumetric or surface (hollow) recreations of the subject. These meshes can then be imported into FEM software; hence an authentic, complex 3D geometry of a biological tissue, such as the PSs, could be relatively straightforwardly rendered for use in FEM investigations. It would be important to import meshes of both pre-and post-elevation PSs, which would enable the use of a target geometry in modelling. Towards the end of this project, I generated pilot meshes from microCT-stained tissue and successfully re-rendered the geometries in COMSOL. Unfortunately, due to time constraints the modelling was not performed, but included are representative images from my preliminary meshes which highlight the potential for future work (*Figure 7.1*).

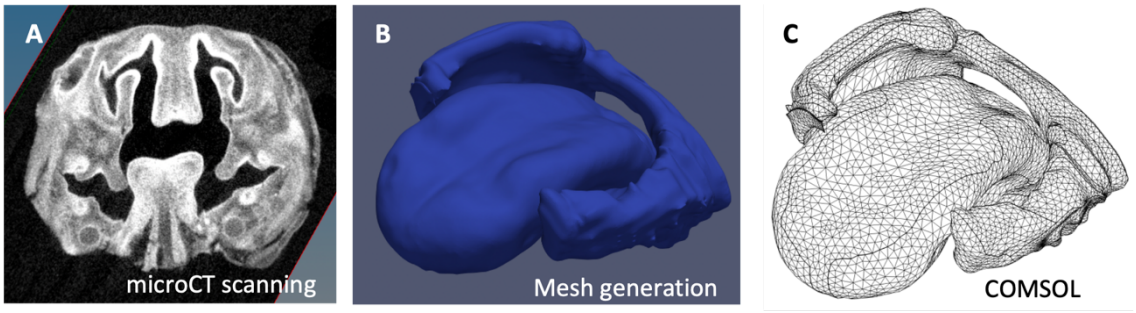

Figure 7.1 Pilot PS and tongue mesh and FEM geometry

Representative images of a single slice from microCT scanned E13.5 embryonic oral cavity (A) which was rendered in a landmark free-morphometric pipeline (Toussaint et al., 2021) and false coloured in blue (B). Meshes were then imported in COMSOL and re-rendered as a user-defined polygonal surface mesh (C).

With the complex geometries rendered, there is virtually no limit as to the information that can be programmed into each element. Therefore, on modelling PS elevation, further *in vivo* analyses will inform the modelling and, hopefully, the modelling will inform further work at the bench. These further analyses could include building a more detailed picture of the 3D material properties of the PSs and modelling cellular behaviours, ideally captured in their entirety under the PROMASS framework, alongside investigations into phase transitions and cell/tissue jamming. There are several ways in which both biomechanical and cellular behaviours could be explored to better-understand PS elevation, and these are explored below.

7.4.3 Cellular behaviours and ECM components

The collective behaviours of cells and polarised ECM secretions during PS morphogenesis will ultimately be responsible for generating the forces that drive PS elevation. As referred to all throughout this thesis, cellular behaviours underlying growth can be systematically quantified under the PROMASS framework (Green, 2022). The major strength of this particular framework is that it captures all the possible ways in which cells might be behaving during growth, thus bridging the gap between genotype and phenotype. These processes were summarised in a table in the thesis introduction (*Table 1.4*).

While investigations into one or more of these processes are often reported, there is an often-unexploited wealth of knowledge in investigating all of them. It is not possible to establish significance between processes in the absence of a complete picture. PS elevation is no different, with no complete description of the cellular behaviours underlying the normal *in vivo* event available in the literature. Therefore, to understand what drives PS elevation it will be crucial to investigate these processes. The new focus on the epithelium does not change this: it is likely that sub-epithelial layers of mesenchyme are in communication with the epithelium, and in turn these could direct localised cellular behaviours in the mesenchymal core. Below, I discuss ways in which PROMASS can be investigated in the PSs, alongside suggesting future investigations into components of interest in the ECM. Notably, the PROMASS framework can be applied to both simply testing whether individual processes are important and making a quantification of growth by summing them. Thus, in applying this framework, the importance of each individual component and their contribution to overall growth could be identified.

7.4.3.1 Proliferation

Although a lingual-side dominant proliferation gradient in the PS mesenchyme prior to elevation has been reportedly recently (Goering et al., 2022), future work is required to establish whether this gradient aligns with a differing growth rate compatible with PS growth leading up to the elevation window. Differential rates of proliferation across different aspects of the PS (whether mesenchymal or epithelial) could in principle play the key role in generating the internal shelf force. This is with the caveat that previous genetic perturbation affecting proliferation have reduced PS size but have not necessarily prevented elevation (Lan et al., 2004; Goodwin et al., 2020). Previous research has established advanced ways to model proliferation rates in relation to actual growth rates in the developing limb bud, and this could be applied here (Boehm et al., 2010a). Briefly, this involves generating a numerical description of shape change during morphogenesis and a quantitative cell cycle map in 3D, before combining both with a finite element model. This could be directly translated to the PSs. It is worth noting that classical metrics of proliferation such as indexing via DNA label incorporation (EdU/BrdU) are not sufficient

to give an accurate description of the event, in that they only capture cells in S-phase. Thus, double labelling techniques are used to overcome this (Shibui et al., 1989). Similarly, valuable information could be extracted from genetic lineage labelling in mapping localised directional growth and clonal spread, and both the mesenchyme and epithelium could be investigated here by crossing a tamoxifen-inducible pCAG-cre with mTmG or Confetti mice.

7.4.3.2 Orientation of division

Orientated cell division has been investigated previously in the PSs (Brock, 2012, PhD thesis), however these data showed that biases in cell division are weak or absent. However, this work investigated the orientation of division across several stage of palatogenesis, and instead a future study could focus on capturing elevation could be especially usefully in interrogating mechanical contact events between the epithelium and sub-epithelial mesenchyme immediately prior to elevation. There are several ways this could be readily investigated in histological sections of the PSs. This could be achieved by immunostaining with an antibody against gamma-tubulin, alongside a phalloidin or similar membrane stain, could create a clearer picture of division. Difficulties could be encountered in that it is likely a relatively low number of cells will be in anaphase/telophase, but this can be overcome with experimental repeats/a high sample number.

7.4.3.3 Directional ECM production and expansion and ECM components

Investigations into matrix production during morphogenesis concern the mesenchyme more than epithelia owing to the spatial restrictions of the latter. In the case of the PSs, this is the exception to the typical scarcity of PROMASS in the elevation literature, with extensive documentation of the role of GAGs as described throughout this thesis. Although GAGs are no longer thought to be driving elevation (Lan et al., 2019), the GAG content of the PS mesenchyme could play an important role in conferring mechanical properties to the tissue. The distribution of specific GAGs, namely HA, have been mapped in the PSs previously (Brinkley and Morris-Wiman, 1987a), and future, higher resolution mapping of PS elasticity should be compared to GAG distribution. However, it might be

pertinent to discuss ECM components of interest here. Fibronectin (Fn) remains a particular object of interest in PS elevation. It is present throughout both the mesenchyme and the epithelium during PS elevation and interacts extensively with several other ECM components (*1.4.5.3*). The study of Fn function, especially *in vivo*, are not as common as that of collagen, and Fn gene knockout mice are embryonic lethal owing to the failure of the development of mesodermal structures (George et al., 1993). Promisingly, a tamoxifen inducible conditional Fn gene knockout mouse has recently been generated (Yuan et al., 2020). Initially, it would be interesting simply to establish whether the PSs elevate if the model is induced globally at stages immediately prior to elevation, and again prior to PS outgrowth. Specific drivers could then be used to drive recombination in the PSs specifically by using cre-drivers such as Osr2, similar to the *Has2* cKo study described previously (Lan et al., 2019).

Although not strictly a component of the ECM, future work could also include cKOs of junctional components. In epithelia, adherens junctions couple the contractile cytoskeletal components of cells, thus generating tissue-scale tension (Charras and Yap, 2018) (which, as discussed previously, could be mapped in the PSs using 'FliptR'). These changes in tension are detected by mechanotransduction pathways, which subsequently regulate localised cellular behaviours in the PSs in response to stress or stiffness (Charras and Yap, 2018). While individual junctions can be identified and ablated via laser ablation studies, this resolution of ablation is not suitable in studying PS elevation (which requires much larger regions of ablation as discussed previously). Thus, genetic perturbations of constituent adherens junctional proteins could inform the role of cell:cell communication in driving PS elevation. Vinculin would be an appropriate target, as it anchors adherens junctions to the cytoskeleton. Vinculin mutations are associated with heart defects, and hemizygous KO mice have been generated to study this. (Zemljic-Harpf et al., 2009; Martínez-Sanz et al., 2008). These mice could be used to investigate PS elevation in disrupted junctional-cytoskeletal communication. As with each of these assays in mice, it would first be useful to identify whether the PSs elevate *in vivo*. Again, similar to the potential Fn cKO, this could be investigated in a localised fashion in the PSs using an Osr2 driver. However, it would also be informative to investigate junctional activities in the epithelium only, which could be achieved using a K14-cre driver.

7.4.3.4 Cell addition/subtraction

As discussed previously under the concept of cellular rearrangement, it is unlikely that cell subtraction (such as by apoptosis) is occurring during PS elevation. Nonetheless, this could be confirmed with a simple TUNEL stain. Localised cellular rearrangements could be driven by epithelial-mesenchymal signalling to the sub-epithelial mesenchyme. If this hypothetical event plays a role in organising the latter, the signals driving this would first have to be identified. Following that, genetic perturbations could be used to disrupt the behaviour to identify its effects. In the context of PS elevation, this may not be a priority for research in the immediate future.

7.4.3.5 Cell size and shape change

Changes in cell shape and size could be measured in histological sections via the use of automatic segmentation tools such as the StarDist model presented in this thesis. While this is difficult in the often stellate-shaped mesenchyme (Boehm et al., 2010a) this could be readily applied to the PS epithelium. Changes in epithelial cell shape/size could cause localised bending, likely short of buckling, in tensile regions of the PSs. If, for example, the epithelial medial hinge region was tensile, co-ordinated shape change could bend the epithelium concomitant with PS elevation. Furthermore, this work suggests that the elastic potential of the shelves is present much earlier on during palatogenesis before normal elevation stages (e.g., at E12.5), and so the shapes will have to be outlined from the point of PS outgrowth (E10.5 – E11.5).

7.4.4 A useful tool for the live imaging of nuclear morphometrics

The nuclear morphometric analyses carried-out in this thesis were informative and should be expanded in future investigations into PS elevation, firstly at a larger sample size. However, DAPI-staining combined with auto-segmentation might not be the optimal method for outlining nuclei (or, conceivably, epithelial cell shapes), and an alternative technique using a mouse reporter line is discussed below.

DAPI is a fluorescent dye which binds to adenosine – thymidine-rich regions of nuclear DNA (hence staining particularly strongly in the nucleoli) electrostatically (Tarnowski et al., 1991). It is extremely versatile and widely used but may not be the most suitable method for automated nuclear segmentation. DAPI intensity reportedly varies widely between cells, thus signal detection issues are encountered when thresholding, and some nuclear edges can appear blurred or obscured (Kesler et al., 2019). Moreover, DAPI is not typically used in the live staining of cells or tissues due to plasma autofluorescence in live cells and the dye's relative impermanence (Howell et al., 2017). This poses a particular problem in investigating palate elevation given that research to date, including data presented in this thesis, clearly points towards future live imaging of the PSs and the investigating of cellular behaviours, for which nuclear morphometrics is a powerful tool. Plus, DAPI staining requires a manual step, unlike the use nuclear reporters.

There are several nuclear fluorescent reporter lines which can be used to overcome these issues; as some of the work here required accurate nuclear outlining, I focussed on nuclear membrane markers. Of particular interest here was the SUN1 reporter mouse. The SUN1 protein is a conserved inner nuclear membrane protein which provides a direct connection between the nuclear lamina and the cytoskeleton (Lei et al., 2009; Haque et al., 2010), here fused to a superfolder GFP (sfGFP). I thought this might be a useful tool to outline nuclei in the PSs minus the steps required for the use of DAPI while also opening up the potential for live imaging. Therefore, I was grateful to receive a SUN1 mouse from the Streit lab (KCL) and I subsequently crossed it with a constitutively active Wnt1-cre mouse, generating a B6;129-Gt(ROSA)26Sor$^{tm5(CAG-Sun1/sfGFP)}$;Wnt1-cre reporter (henceforth referred to simply as the SUN1;Wnt1-cre mouse). This resulted in the constitutively active fluorescence of the mesenchymal nuclear membranes in the PSs and a representative test image from the fused E15.5 mouse palate is shown here (*Figure 7.2*). The images demonstrate how precisely the reporter outlined nuclei. With testing and optimisation, I had hoped to generate fluorescence-intensity consistently and accurately outlined nuclei which could be segmented readily in FIJI via simple thresholding and watershedding techniques. Unfortunately, I generated this cross between the first two COVID-19 lockdowns and was therefore not able to expand the colony at the required period. Furthermore, the KCL BSU encountered several consistent

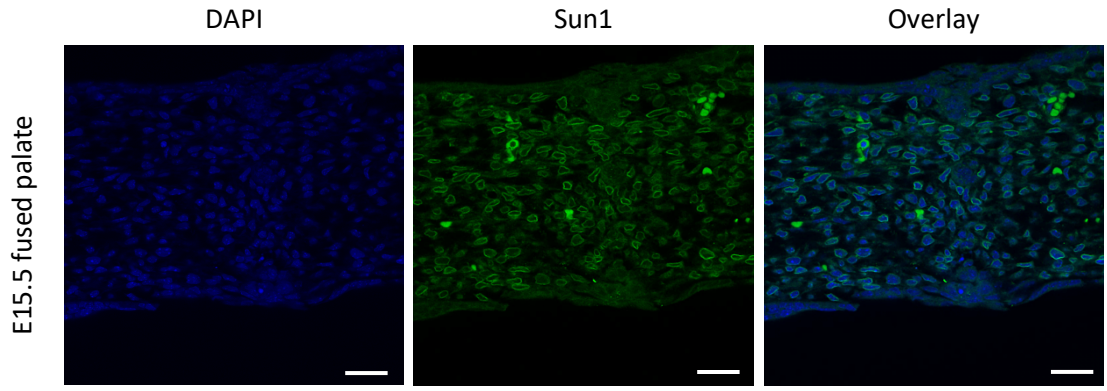

Figure 7.2 Preliminary images demonstrating fluorescent nuclear outlines in the Sun1;Wnt1-cre mouse

Confocal images of a frontally sectioned E15.5 fused palate in the midline from the Sun1;Wnt1-cre mouse. The tissue was also stained with DAPI, and the two are overlaid for comparison. Scale bars = 50 µm.

issues with day-night cycle lighting and staff shortages, which resulted in many groups having issues with mouse breeding. This too was my experience, with my mice not breeding reliably. Due to this, I encountered low mouse numbers and, faced with restricted time in the PhD, the production of this colony was abandoned in favour of using CD-1 mice and DAPI staining. Had I not encountered this limitation, I may not have needed to train the StarDist model.

More importantly, future studies using nuclear morphometrics to assay for cellular behaviours could likely benefit from this mouse line due to the potential for use in live imaging studies, perhaps being of particular interest in 3D.

7.4.5 Investigating elevation in mutant mice

Relatively simple experiments could be performed on genetic mutant mice with defects in elevation, which were reviewed in the thesis introduction (*1.3.5*). As described, mice with elevation defects often show either a delay in elevation, or a cleft phenotype at birth which is likely secondary to other defects, such as micrognathia; failure of elevation is often reported from frontal sections of *in vivo* tissue with the tongue in the way, thus the capacity of the PSs inherent ability to elevate independent of surrounding structures is not being tested. Therefore, to investigate whether the defect is inherent to the PSs or

any particular process or ECM component involved in the generation or mediation of the internal shelf force, the recoil experiments described in this thesis could simply be repeated in mutants.

Finally, it would be informative to combine the approaches outlined in this general discussion and apply them to mutant mice. By understanding the processes affected in the mutant, one could apply these techniques to determine how the material properties of the PSs are affected, thus building a picture of how deviations from the normal material properties of the tissue may contribute to palatogenesis. For example, the previously mentioned Osr2 mutant mouse has defects in mesenchymal proliferation (Lan et al., 2004). While proliferation is unlikely to drive elevation as outlined it could affect localised, for example, localised cell-packing in stages prior to elevation which may influence stiffness. This will be particularly interesting in the case of mutants that maintain fusion competence (*1.3.5*), further narrowing the mutant genes for selection. Thus, techniques such as AFM could be applied here to measure the elasticity of these tissues demonstrating deviations from normal development and compared to the future WT dataset. This could not only be informative to the *in vivo* event, but could simultaneously inform modelling approaches *in silico,* namely FEM.

7.5 Conclusions

At the beginning of this project, I aimed to describe and quantify the cellular mechanisms of growth directing palatal shelf elevation. The ensuing project was led by intriguing and often surprising data, leading to the application of a variety of techniques in a novel fashion to interrogate the material properties of the palatal shelves, and the biomechanics of the event.

The use of the *ex vivo* rolling culture system in the early phases of the project provided valuable insights into elevation, which included the identification that growth is poor and inconstant in the system, and that the system is neither suitable for the study of palatal growth nor elevation. Not only this, but during explant preparation it became clear that the PS were elevating elastically immediately upon the removal of the tongue and

mandible (Chapter 3). The design and application of suitable 2D morphometrics provided quantitative evidence both for elevation by elastic recoil, measured by palatal shelf angle, and for the poor growth observed in culture. Further quantification of maxillary explants post-culture revealed that PS approximation in culture is caused by a progressive non-physiological deformation of the whole explant. This gap closure had previously and extensively been misused in the literature as evidence of elevation having occurred in culture, and the implications for specific reports were discussed (Chapter 4). During morphometric analyses, it was identified that the PSs appear to be horizontally orientated in several regions along the A – P axis at E12.5, before presumably being deflected ventrally by E13.5. This suggested a default horizontal growth programme and served as the basis for the work presented in Chapter 5.

The identification of horizontally orientated shelves at E12.5 prior to their vertical orientation at E13.5 led to the hypothesis that mammals possess a default horizontal growth programme, just like all other palate-bearing Amniotes. Furthermore, I hypothesised that this was due to the requirement for a large tongue in mammals, a consequence of the suckling requirement, and the trade-off for space in the oral cavity. The serendipitous presentation of Monotreme tissue via collaboration with the Tucker (KCL) and Renfree (Melbourne) labs enabled me to test this theory in a non-suckling mammal, the short-beaked echidna. I generated a time course of palate elevation in the echidna, which disproved my theory. However, the completion of the amniotic phylogenetic tree of palate development provided further insights into the origins of the palate, and led to the further hypothesis that mammalian and non-mammalian palates are homoplasic and arose via parallel evolution (Chapter 5).

Having quantified elevation by elastic recoil, I then aimed to investigate how this force might be generated and mediated (Chapter 6). This resulted in the training of a StarDist automatic nuclear segmentation model, which enabled quantifiable analyses on a large scale but leaves room for improvement. Applying this model in nuclear morphometric studies investigating i) nuclear deformation as a proxy for stress and ii) internuclear spaces analyses painted a potentially noisy and heterogenous picture. The further demonstration that collagen and elastic fibres do not appear to be present in the PSs

immediately prior to elevation shed the mesenchyme in a more passive light than previously considered. This was bolstered by the novel characterisation of the elasticity (stiffness) across the palatal shelves. These data suggest that the PSs comprise a stiff outer epithelium with a relatively soft mesenchymal core, with further heterogeneities in the A – P axis in the medial hinge region. Here, the posterior medial hinge is stiffer than that of the anterior. This led to a reconsideration of the roles of the palatal epithelium versus the mesenchyme, and poses interesting questions regarding the role of a potential epithelial driver of elevation. The mesenchymal core could behave like a viscoelastic fluid that dissipates tension, while an active outer epithelium directs elevation in response to mechanical cues. The stiffer, and therefore less deformable, posterior PSs could explain why the posterior PSs appear to elevate more slowly in my recoil studies.

The wide scope for future directions in this project has been discussed at length and falls into 3 categories, better material/mechanical quantification, *in silico* modelling, and investigations into the cellular mechanisms of growth that generate the internal shelf force, including the use of future genetic models of perturbed elevation.

Overall, the work presented in this thesis begins to elucidate the mechanocellular underpinnings of PS elevation. It also raises as many questions as it answers, but this provides impetus to build on the work presented here in the hope of eventually understanding what drives PS elevation. Not only is this interesting from a scientific perspective, but could one day play a role in understanding the aetiologies underlying CL/P. Thus, it is hoped that this thesis informs future work into PS elevation, which may eventually translate into improved healthcare outcomes for people with CL/P.

8. Bibliography

Abbott, B. D. (2019) Embryonic midfacial palatal organ culture methods in developmental toxicology. *Methods in Molecular Biology*. [Online] 196593–105. [online]. Available from: https://link.springer.com/protocol/10.1007/978-1-4939-9182-2_7 (Accessed 11 May 2023).

Abbott, B. D. (2000) Palatal dysmorphogenesis. Palate organ culture. *Methods in molecular biology (Clifton, N.J.)*. [Online] 136195–201. [online]. Available from: https://link.springer.com/protocol/10.1385/1-59259-065-9:195 (Accessed 15 May 2023).

Abramovich, A. & Buenos Arres, D. (1972) Cleft Palate in the Fetuses of Lathyric Rats and Its Relation to Other Structures: Nasal Septum, Tongue and Mandible. *The Cleft Palate Journal*. 9 (1), 73–83. [online]. Available from: https://cleftpalatejournal.pitt.edu/ojs/cleftpalate/article/view/417 (Accessed 6 August 2023).

Abramyan, J. & Richman, J. M. (2015) Recent insights into the morphological diversity in the amniote primary and secondary palates. *Developmental dynamics : an official publication of the American Association of Anatomists*. [Online] 244 (12), 1457. [online]. Available from: /pmc/articles/PMC4715671/ (Accessed 4 September 2023).

Abzhanov, A. (2013) von Baer's law for the ages: lost and found principles of developmental evolution. *Trends in genetics : TIG*. [Online] 29 (12), 712–722. [online]. Available from: https://pubmed.ncbi.nlm.nih.gov/24120296/ (Accessed 22 September 2023).

Adams, D. S. et al. (1990) The mechanics of notochord elongation, straightening and stiffening in the embryo of Xenopus laevis. *Development*. [Online] 110 (1), 115–130.

Adams, J. et al. (2002) Cyclooxygenase-2 Induction in Cerebral Cortex: An Intracellular Response to Synaptic Excitation. *Journal of Neurochemistry*. [Online] 66 (1), 6–13.

Adil, M. S. et al. (2021) Cell-cell junctions: structure and regulation in physiology and pathology. *Tissue Barriers*. [Online] 9 (1), . [online]. Available from: /pmc/articles/PMC7849786/ (Accessed 28 September 2023).

Aguilera-Castrejon, A. et al. (2021) Ex utero mouse embryogenesis from pre-gastrulation to late organogenesis. *Nature*. [Online] 593 (7857), 119–124.

Alkuraya, F. S. et al. (2006) SUMO1 haploinsufficiency leads to cleft lip and palate. *Science (New York, N.Y.)*. [Online] 313 (5794), 1751. [online]. Available from: https://pubmed.ncbi.nlm.nih.gov/16990542/ (Accessed 23 July 2023).

Almaidhan, A. et al. (2014) Neural crest-specific deletion of Ldb1 leads to cleft secondary palate with impaired palatal shelf elevation. *BMC Developmental Biology*. [Online] 14 (1), 3. [online]. Available from: /pmc/articles/PMC3899388/ (Accessed 28 August 2023).

Andersen, H. & Matthiessen, M. (1967) Histochemistry of the early development of the human central face and nasal cavity with special reference to the movements and fusion of the palatine processes. *Acta Anatomica*. [Online] 68 (4), 473–508. [online]. Available from: https://dx.doi.org/10.1159/000143050 (Accessed 28 August 2023).

Andrew, F. D. & Zimmerman, E. F. (1971) Glucocorticoid induction of cleft palate in mice; no correlation with inhibition of mucopolysaccharide synthesis. *Teratology*. [Online] 4 (1), 31–37. [online]. Available from: https://pubmed.ncbi.nlm.nih.gov/5541174/ (Accessed 29 August 2023).

Annigeri, V. M. et al. (2012) Outcome analysis of palatoplasty in various types of cleft palate. *Journal of Indian Association of Pediatric Surgeons*. [Online] 17 (4), 157. [online]. Available from: /pmc/articles/PMC3518993/ (Accessed 22 July 2023).

Anthwal, N. et al. (2020) Transient role of the middle ear as a lower jaw support across mammals. *eLife*. [Online] 91–36.

Arey, L. B. (1974) *Developmental anatomy. A textbook and laboratory manual of embryology*. 7th edition. Philadelphia & London: W. B. Saunders & Co.

Arzt, M. et al. (2022) LABKIT: Labeling and Segmentation Toolkit for Big Image Data. *Frontiers in Computer Science*. [Online] 4777728.

Asling, C. W. et al. (1960) The development of cleft palate resulting from maternal pteroylglutamic (folic) acid deficiency during the latter half of gestation in rats. *Surg Gynecol Obstet.* [Online] 11119–28.

Babiarz, B. S. et al. (1979) Palate morphogenesis - III. Changes in Cell Shape and rientation During Shelf Elevation. *Teratology*. [Online] 20 (1), 249–278.

Babiarz, B. S. et al. (1975) Ultrastructural evidence of contractile systems in mouse palates prior to rotation. *Developmental Biology*. [Online] 47 (1), 32–44.

Badovinac, R. L. et al. (2007) Folic acid–containing supplement consumption during pregnancy and risk for oral clefts: A meta-analysis. *Birth Defects Research Part A: Clinical and Molecular Teratology*. [Online] 79 (1), 8–15. [online]. Available from: https://onlinelibrary.wiley.com/doi/full/10.1002/bdra.20315 (Accessed 23 July 2023).

von Baer, K. E. (1828) *Über Entwickelungsgeschichte der Thiere: Beobachtung und Reflexion - Karl Ernst von Baer*. Konigsberg: Gebrüder Borntraeger. [online]. Available from: https://books.google.nl/books?hl=en&lr=&id=yHXKEpRguGEC&oi=fnd&pg=PA3&ots=OYjvGl3sMT&sig=5olJemiY7YjH1cWQ2DdMOfeCYlo&redir_esc=y#v=onepage&q&f=false (Accessed 22 September 2023).

Balazs, E. A. & Gibbs, D. A. (1970) *Chemistry and Molecular Biology of the Intercellular Matrix*. Vol. 3. London: Academic Press.

Ballantyne, J. W. (1905) *Manual of antenatal pathology and hygiene: the embryo*. 1st edition. Edinburgh: W Green & Sons. [online]. Available from: https://wellcomecollection.org/works/sebb25b7 (Accessed 6 August 2023).

Bamforth, J. S. et al. (1989) Congenital hypothyroidism, spiky hair, and cleft palate. *Journal of Medical Genetics*. [Online] 26 (1), 49. [online]. Available from: /pmc/articles/PMC1015536/?report=abstract (Accessed 23 July 2023).

Bangle, R. (1954) Gomori's paraldehydefuchsin stain. I. Physico-chemical and staining properties of the dye. *The journal of histochemistry and cytochemistry : official journal of the Histochemistry Society*. [Online] 2 (4), 291–299. [online]. Available from: https://journals.sagepub.com/doi/10.1177/2.4.291 (Accessed 12 September 2023).

Barrow, J. R. & Capecchi, M. R. (1999) Compensatory defects associated with mutations in Hoxa1 restore normal palatogenesis to Hoxa2 mutants. *Development (Cambridge, England)*. [Online] 126 (22), 5011–5026. [online]. Available from: https://pubmed.ncbi.nlm.nih.gov/10529419/ (Accessed 7 August 2023).

Baumgart, F. (2000) Stiffness — an unknown world of mechanical science? *Injury*. [Online] 31 (SUPPL.2), 14–84.

Beaty, T. H. et al. (2010) A genome-wide association study of cleft lip with and without cleft palate identifies risk variants near MAFB and ABCA4. *Nature genetics*. [Online]

42 (6), 525. [online]. Available from: /pmc/articles/PMC2941216/ (Accessed 20 July 2023).

Beaty, T. H. et al. (2016) Genetic factors influencing risk to orofacial clefts: today's challenges and tomorrow's opportunities. *F1000Research*. [Online] 5. [online]. Available from: /pmc/articles/PMC5133690/ (Accessed 23 July 2023).

Benko, S. et al. (2009) Highly conserved non-coding elements on either side of SOX9 associated with Pierre Robin sequence. *Nature genetics*. [Online] 41 (3), 359–364. [online]. Available from: https://pubmed.ncbi.nlm.nih.gov/19234473/ (Accessed 23 July 2023).

Benton, M. J. & Donoghue, P. C. J. (2007) Paleontological Evidence to Date the Tree of Life. *Molecular Biology and Evolution*. [Online] 24 (1), 26–53. [online]. Available from: https://dx.doi.org/10.1093/molbev/msl150 (Accessed 22 September 2023).

Bergert, M., Erzberger A., Desai R. A., Aspalter I. M., Oates A. C., Charras G., Salbreux G., Paluch E. K. Force transmission during adhesion-independent migration. Nat Cell Biol. 2015 Apr;17(4):524-9. doi: 10.1038/ncb3134. Epub 2015 Mar 16. PMID: 25774834; PMCID: PMC6485532.

Bevilacqua, C. et al. (2019) Imaging mechanical properties of sub-micron ECM in live zebrafish using Brillouin microscopy. *Biomedical optics express*. [Online] 10 (3), 1420. [online]. Available from: https://pubmed.ncbi.nlm.nih.gov/30891356/ (Accessed 28 September 2023).

Bisong, E. (2019) Google Colaboratory. *Building Machine Learning and Deep Learning Models on Google Cloud Platform*. [Online] 59–64. [online]. Available from: https://link.springer.com/chapter/10.1007/978-1-4842-4470-8_7 (Accessed 7 September 2023).

Blavier, L. et al. (2001) TGF-β3-induced palatogenesis requires matrix metalloproteinases. *Molecular Biology of the Cell*. [Online] 12 (5), 1457–1466. [online]. Available from: https://www.molbiolcell.org/doi/10.1091/mbc.12.5.1457 (Accessed 27 August 2023).

Bodner, J. W. et al. (1970) Fusion capability of rat embryonic extra-oral tissue in vitro. *Archives of Oral Biology*. [Online] 15 (9), 861-IN12.

Boehm, B. et al. (2010a) The role of spatially controlled cell proliferation in limb bud morphogenesis. *PLoS Biology*. [Online] 8 (7), .

Boehm, B. et al. (2010b) The Role of Spatially Controlled Cell Proliferation in Limb Bud Morphogenesis. *PLoS Biology*. [Online] 8 (7), 1000420. [online]. Available from: /pmc/articles/PMC2903592/ (Accessed 15 September 2023).

Van Den Boogaard, M. J. H. et al. (2000) MSX1 mutation is associated with orofacial clefting and tooth agenesis in humans. *Nature genetics*. [Online] 24 (4), 342–343. [online]. Available from: https://pubmed.ncbi.nlm.nih.gov/10742093/ (Accessed 23 July 2023).

Braybrook, C. et al. (2001) The T-box transcription factor gene TBX22 is mutated in X-linked cleft palate and ankyloglossia. *Nature genetics*. [Online] 29 (2), 179–183. [online]. Available from: https://pubmed.ncbi.nlm.nih.gov/11559848/ (Accessed 23 July 2023).

Bresslau, E. (1920) *The mammary apparatus of the Mammalia*. London: Methuen & Co.

Brinkley, L. et al. (1975) A new in vitro system for studying secondary palate development. *Journal of Embryology and Experimental Morphology*. 34 (2), 485–495.

Brinkley, L. et al. (1978) Effects of craniofacial structures on mouse palatal closure in vitro. *Journal of dental research*. [Online] 57 (2), 402–411. [online]. Available from: https://pubmed.ncbi.nlm.nih.gov/277540/ (Accessed 5 June 2023).

Brinkley, L. L. (1984) Changes in cell distribution during mouse secondary palate closure in vivo and in vitro. I. Epithelial cells. *Developmental Biology*. [Online] 102 (1), 216–227.

Brinkley, L. L. (1980) 'In vitro studies of palatal shelf elevation', in R. M. Pratt & R. L. Christiansen (eds.) *Current Research Trends in Prenatal Craniofacial Development*. 1st edition Amsterdam: Elsevier. pp. 203–220.

Brinkley, L. L. & Bookstein, F. L. (1986) Cell distribution during mouse secondary palate closure. II. Mesenchymal cells. *Journal of Embryology and Experimental Morphology*. VOL. 96111–130.

Brinkley, L. L. & Morris-Wiman, J. (1987a) Computer-assisted analysis of hyaluronate distribution during morphogenesis of the mouse secondary palate. *Development*. 100 (4), 629–635.

Brinkley, L. L. & Morris-Wiman, J. (1987b) Effects of chlorcyclizine-induced glycosaminoglycan alterations on patterns of hyaluronate distribution during morphogenesis of the mouse secondary palate. *Development*. 100 (4), 637–640.

Brinkley, L. L. & Vickerman, M. M. (1979) Elevation of lesioned palatal shelves in vitro. *Journal of Embryology and Experimental Morphology*. Vol. 54229–240.

Brinkley, L. L. & Vickerman, M. M. (1982) The effects of chlorcyclizine-induced alterations of glycosaminoglycans on mouse palatal shelf elevation in vivo and in vitro. *Journal of Embryology and Experimental Morphology*. Vol. 69193–213.

Brinkley, L. L. & Vickerman, M. M. (1978) The mechanical role of the cranial base in palatal shelf movement: an experimental re-examination. *Development*. [Online] 48 (1), 93–100. [online]. Available from: https://journals.biologists.com/dev/article/48/1/93/50400/The-mechanical-role-of-the-cranial-base-in-palatal (Accessed 21 May 2023).

Brock, L. J. et al. (2016) Mapping cellular processes in the mesenchyme during palatal development in the absence of Tbx1 reveals complex proliferation changes and perturbed cell packing and polarity. *Journal of Anatomy*. [Online] 228 (3), 464–473.

Brodland, G. W. (1994) Finite Element Methods for Developmental Biology. *International Review of Cytology*. [Online] 150 (C), 95–118.

Brunet, C. L. et al. (1993) The distribution of epidermal growth factor binding sites in the developing mouse palate. *The International Journal of Developmental Biology*. [Online] 37 (3), 451–458. [online]. Available from: https://ijdb.ehu.eus/article/8292539 (Accessed 5 June 2023).

Bulleit, R. F. & Zimmerman, E. F. (1985) The influence of the epithelium on palate shelf reorientation. *Journal of Embryology and Experimental Morphology*. VOL. 88265–279.

Burdi, A. R. & Faist, K. (1967) Morphogenesis of the palate in normal human embryos with special emphasis on the mechanisms involved. *American Journal of Anatomy*. [Online] 120 (1), 149–159. [online]. Available from: https://onlinelibrary.wiley.com/doi/full/10.1002/aja.1001200112 (Accessed 28 August 2023).

Burdi, A. R. & Silvey, R. G. (1969) The relation of sex-associated facial profile reversal and stages of human palatal closure. *Teratology*. [Online] 2 (4), 297–303. [online]. Available from: https://pubmed.ncbi.nlm.nih.gov/5362423/ (Accessed 6 August 2023).

Burdick, A. B. (1986) Genetic epidemiology and control of genetic expression in van der Woude syndrome. *Journal of Craniofacial Genetics and Developmental biology. Supplement*. 2 (SUPPL. 2), 99–105. [online]. Available from: https://europepmc.org/article/med/3491128 (Accessed 23 July 2023).

Burg, M. L. et al. (2016) Epidemiology, Etiology, and Treatment of Isolated Cleft Palate. *Frontiers in physiology*. [Online] 7 (MAR), . [online]. Available from: https://pubmed.ncbi.nlm.nih.gov/26973535/ (Accessed 20 July 2023).

Bush J. O. & Soriano P. Ephrin-B1 forward signaling regulates craniofacial morphogenesis by controlling cell proliferation across Eph-ephrin boundaries. Genes Dev. 2010 Sep 15;24(18):2068-80. doi: 10.1101/gad.1963210. PMID: 20844017; PMCID: PMC2939368.

Bush, J. O. & Jiang, R. (2012) Palatogenesis: Morphogenetic and molecular mechanisms of secondary palate. *Development*. [Online] 139 (4), 828.

Butali, A. et al. (2019) Genomic analyses in African populations identify novel risk loci for cleft palate. *Human Molecular Genetics*. [Online] 28 (6), 1038–1051. [online]. Available from: https://dx.doi.org/10.1093/hmg/ddy402 (Accessed 29 August 2023).

Caamaño, J. N. et al. (2010) Polarized Light Microscopy in Mammalian Oocytes. *Reproduction in Domestic Animals*. [Online] 45 (SUPPL. 2), 49–56. [online]. Available from: https://onlinelibrary.wiley.com/doi/full/10.1111/j.1439-0531.2010.01621.x (Accessed 12 September 2023).

Cadena, E. (2015) The first South American sandownid turtle fromthe Lower Cretaceous of Colombia. *PeerJ*. [Online] 2015 (12), e1431. [online]. Available from: https://peerj.com/articles/1431 (Accessed 19 September 2023).

Campagnola, P. J. & Dong, C. Y. (2011) Second harmonic generation microscopy: principles and applications to disease diagnosis. *Laser & Photonics Reviews*. [Online] 5 (1), 13–26. [online]. Available from: https://onlinelibrary.wiley.com/doi/full/10.1002/lpor.200910024 (Accessed 12 September 2023).

Capurro, M. & Barberis, F. (2014) Evaluating the mechanical properties of biomaterials. *Biomaterials for Bone Regeneration: Novel Techniques and Applications*. [Online] 270–323.

Carette, M. J. M. & Ferguson, M. W. J. (1992) The fate of medial edge epithelial cells during palatal fusion in vitro: An analysis by DiI labelling and confocal microscopy. *Development*. 114 (2), 379–388.

Celli, J. et al. (1999) Heterozygous germline mutations in the p53 homolog p63 are the cause of EEC syndrome. *Cell*. [Online] 99 (2), 143–153. [online]. Available from: https://pubmed.ncbi.nlm.nih.gov/10535733/ (Accessed 23 July 2023).

Chamberlain, J. G. (1966) Development of cleft palate induced by 6-aminonicotinamide late in rat gestation. *The Anatomical Record*. [Online] 156 (1), 31–39. [online]. Available from: https://onlinelibrary.wiley.com/doi/full/10.1002/ar.1091560106 (Accessed 5 August 2023).

von Chamier, L. et al. (2021) Democratising deep learning for microscopy with ZeroCostDL4Mic. *Nature Communications 2021 12:1*. [Online] 12 (1), 1–18. [online]. Available from: https://www.nature.com/articles/s41467-021-22518-0 (Accessed 7 September 2023).

Charité J., McFadden D. G., Merlo G., Levi G., Clouthier D. E., Yanagisawa M., Richardson J. A., Olson E. N. Role of Dlx6 in regulation of an endothelin-1-dependent, dHAND branchial arch enhancer. Genes Dev. 2001 Nov 15;15(22):3039-49. doi: 10.1101/gad.931701. PMID: 11711438; PMCID: PMC312822

Charras, G. & Yap, A. S. (2018) Tensile Forces and Mechanotransduction at Cell–Cell Junctions. *Current Biology*. [Online] 28 (8), R445–R457.

Chaudhry, A. P. & Siar, S. (1967) In Vitro Study of Fusion of Palatal Shelves in A/Jax Mouse Embryos. *Journal of Dental Research*. [Online] 46 (1), 257–260. [online]. Available from: https://journals.sagepub.com/doi/10.1177/00220345670460012101 (Accessed 21 May 2023).

Chen, X. et al. (2012) Second harmonic generation microscopy for quantitative analysis of collagen fibrillar structure. *Nature Protocols 2012 7:4*. [Online] 7 (4), 654–669. [online]. Available from: https://www.nature.com/articles/nprot.2012.009 (Accessed 12 September 2023).

Chiquet, M. et al. (2016) Mesenchymal remodeling during palatal shelf elevation revealed by extracellular matrix and F-actin expression patterns. *Frontiers in Physiology*. [Online] 7 (SEP), .

Chiquet-Ehrismann, R. (2004) Tenascins. *The International Journal of Biochemistry & Cell Biology*. [Online] 36 (6), 986–990.

Chou, M. J. et al. (2004) Palatal shelf movement during palatogenesis: A fate map of the fetal mouse palate cultured in vitro. *Anatomy and Embryology*. [Online] 208 (1), 19–25.

Chugh P., Paluch E. K. The actin cortex at a glance. J Cell Sci. 2018 Jul 19;131(14):jcs186254. doi: 10.1242/jcs.186254. PMID: 30026344; PMCID: PMC6080608.

Christensen, K. & Mitchell, L. E. (1996) Familial recurrence-pattern analysis of nonsyndromic isolated cleft palate--a Danish Registry study. *American Journal of Human Genetics*. 58 (1), 182. [online]. Available from: /pmc/articles/PMC1914943/?report=abstract (Accessed 20 July 2023).

Clark A. G., Wartlick O., Salbreux G., Paluch E. K. Stresses at the cell surface during animal cell morphogenesis. Curr Biol. 2014 May 19;24(10):R484-94. doi: 10.1016/j.cub.2014.03.059. PMID: 24845681.

Clarke Fraser, F. (1967) Cleft lip and cleft palate. *Science (New York, N.Y.)*. [Online] 158 (3808), 1603–1606. [online]. Available from: https://pubmed.ncbi.nlm.nih.gov/17816632/ (Accessed 6 August 2023).

Cocciolone, A. J. et al. (2018) Elastin, arterial mechanics, and cardiovascular disease. *American Journal of Physiology - Heart and Circulatory Physiology*. [Online] 315 (2), H189–H205. [online]. Available from: https://journals.physiology.org/doi/10.1152/ajpheart.00087.2018 (Accessed 30 August 2023).

Cockroft, D. L. (1976) Comparison of in vitro and in vivo development of rat foetuses. *Developmental Biology*. [Online] 48 (1), 163–172.

Cockroft, D. L. (1973) Development in culture of rat foetuses explanted at 12·5 and 13·5 days of gestation. *Development*. [Online] 29 (2), 473–483. [online]. Available from: https://journals.biologists.com/dev/article/29/2/473/49702/Development-in-culture-of-rat-foetuses-explanted (Accessed 21 May 2023).

Coleman, R. D. (1965) Development of the Rat Palate. *The Anatomical Record*. 151 (1), 107–117.

Colom, A. et al. (2018) A Fluorescent Membrane Tension Probe. *Nature chemistry*. [Online] 10 (11), 1118. [online]. Available from: /pmc/articles/PMC6197433/ (Accessed 28 September 2023).

Cooper, C. E. & Withers, P. C. (2023) Postural, pilo-erective and evaporative thermal windows of the short-beaked echidna (Tachyglossus aculeatus). *Biology Letters*. [Online] 19 (1), .

Cox, G. & Kable, E. (2006) Second-harmonic imaging of collagen. *Methods in molecular biology (Clifton, N.J.)*. [Online] 31915–35. [online]. Available from: https://pubmed.ncbi.nlm.nih.gov/16719349/ (Accessed 13 September 2023).

Crompton, A. W. et al. (2019) Origin of Suckling in Therian Mammals Matthias Starck (ed.). *Journal of Morphology*. [Online] 280 (S1), S128–S128. [online]. Available from: https://onlinelibrary.wiley.com/doi/full/10.1002/jmor.21003 (Accessed 17 September 2023).

d'Amaro, R. et al. (2012) Putative functions of extracellular matrix glycoproteins in secondary palate morphogenesis. *Frontiers in Physiology*. [Online] 3 SEP31636.

Danescu, A. et al. (2015) Analysis of human soft palate morphogenesis supports regional regulation of palatal fusion. *Journal of Anatomy*. [Online] 227 (4), 474–486. [online]. Available from: https://onlinelibrary.wiley.com/doi/full/10.1111/joa.12365 (Accessed 4 August 2023).

Darwin C (1868) *The Variation of Animals and Plants Under Domestication*. 1st edition. Vol. 2. London: John Murray, Albermale Street. [online]. Available from: https://books.google.co.uk/books?hl=en&lr=&id=B8o6AAAAcAAJ&oi=fnd&pg=PA1&ots=NAJevJhkYp&sig=9qmLt70kWpOcFdZiUmApHMgv1yA&redir_esc=y#v=onepage&q&f=false (Accessed 23 July 2023).

von Dassow, M. et al. (2010) Surprisingly Simple Mechanical Behavior of a Complex Embryonic Tissue. *PLoS ONE*. [Online] 5 (12), . [online]. Available from: /pmc/articles/PMC3011006/ (Accessed 28 September 2023).

Davidson, L. A. (2011) Embryo Mechanics: Balancing Force Production with Elastic Resistance During Morphogenesis. *Current Topics in Developmental Biology*. [Online] 95215–241.

Davidson, L. & Keller, R. (2007) Measuring Mechanical Properties of Embryos and Embryonic Tissues. *Methods in Cell Biology*. [Online] 83425–439.

DeAngelis, P. L. (1999) Hyaluronan synthases: fascinating glycosyltransferases from vertebrates, bacterial pathogens, and algal viruses. *Cellular and molecular life sciences : CMLS*. [Online] 56 (7–8), 670–682. [online]. Available from: https://pubmed.ncbi.nlm.nih.gov/11212314/ (Accessed 30 August 2023).

Depew, M. J. et al. (2002) 'Craniofacial Development', in *Mouse Development*. [Online]. Academic Press. pp. 421–498. [online]. Available from: https://linkinghub.elsevier.com/retrieve/pii/B9780125979511500238 (Accessed 30 July 2023).

DeRoo, L. A. et al. (2016) Maternal alcohol binge-drinking in the first trimester and the risk of orofacial clefts in offspring: a large population-based pooling study. *European Journal of Epidemiology*. [Online] 31 (10), 1021–1034. [online]. Available from: https://link.springer.com/article/10.1007/s10654-016-0171-5 (Accessed 23 July 2023).

Deshpande, A. S. & Goudy, S. L. (2019) Cellular and molecular mechanisms of cleft palate development. *Laryngoscope Investigative Otolaryngology*. [Online] 4 (1), 160. [online]. Available from: /pmc/articles/PMC6383315/ (Accessed 30 July 2023).

Diewert, V. M. (1974) A cephalometric study of orofacial structures during secondary palate closure in the rat. *Archives of Oral Biology*. [Online] 19 (4), 303–315.

Diewert, V. M. & Tait, B. (1979) Palatal process movement in the rat as demonstrated in frozen sections. *Journal of Anatomy*. 128 (3), 609–618. [online]. Available from: /pmc/articles/PMC1232912/?report=abstract (Accessed 13 May 2023).

Dixon, J. et al. (1996) Positional cloning of a gene involved in the pathogenesis of Treacher Collins syndrome. The Treacher Collins Syndrome Collaborative Group. *Nature genetics*. [Online] 12 (2), 130–136. [online]. Available from: https://pubmed.ncbi.nlm.nih.gov/8563749/ (Accessed 23 July 2023).

Dixon, M. J. et al. (2011) Cleft lip and palate: Understanding genetic and environmental influences. *Nature Reviews Genetics*. [Online] 12 (3), 167–178. [online]. Available from: http://dx.doi.org/10.1038/nrg2933.

Dixon, M. J. et al. (1993) Epidermal growth factor and transforming growth factor alpha regulate extracellular matrix production by embryonic mouse palatal mesenchymal cells cultured on a variety of substrata. *Roux's Archives of Developmental Biology*.

[Online] 203 (3), 140–150. [online]. Available from: https://link.springer.com/article/10.1007/BF00365053 (Accessed 30 August 2023).

Dodé, C. et al. (2003) Loss-of-function mutations in FGFR1 cause autosomal dominant Kallmann syndrome. *Nature genetics*. [Online] 33 (4), 463–465. [online]. Available from: https://pubmed.ncbi.nlm.nih.gov/12627230/ (Accessed 23 July 2023).

Doran, G. A. & Baggett, H. (1970) The vascular stiffening mechanism in the tongue of the echidna (Tachyglossus aculeatus). *The Anatomical Record*. [Online] 167 (2), 197–204.

Du, W. et al. (2021) FACEts of mechanical regulation in the morphogenesis of craniofacial structures. *International Journal of Oral Science 2021 13:1*. [Online] 13 (1), 1–16. [online]. Available from: https://www.nature.com/articles/s41368-020-00110-4 (Accessed 30 August 2023).

Duboule, D. (1994) Temporal colinearity and the phylotypic progression: a basis for the stability of a vertebrate Bauplan and the evolution of morphologies through heterochrony. *Development*. [Online] 1994 (Supplement), 135–142. [online]. Available from: https://dx.doi.org/10.1242/dev.1994.Supplement.135 (Accessed 22 September 2023).

Duda M., Kirkland N. J., Khalilgharibi N., Tozluoglu M., Yuen A. C., Carpi N., Bove A., Piel M., Charras G., Baum B., Mao Y. Polarization of Myosin II Refines Tissue Material Properties to Buffer Mechanical Stress. Dev Cell. 2019 Jan 28;48(2):245-260.e7. doi: 10.1016/j.devcel.2018.12.020. PMID: 30695698; PMCID: PMC6353629

Dursy, E. (1869) *Zur Entwicklungsgeschichte des Kopfes des Menschen und der höheren Wirbeltiere*. 1st edition. Tubingen: H Laupp. [online]. Available from: https://books.google.co.uk/books?hl=en&lr=&id=T9g-AAAAcAAJ&oi=fnd&pg=PA5&ots=ArUfS72NPv&sig=a5Eg2eXRqkIb5R0tN41Z6wV86l0&redir_esc=y#v=onepage&q&f=false (Accessed 5 August 2023).

Dutton-Regester, K. et al. (2021) Plasma progesterone secretion during gestation of the captive short-beaked echidna. *Reproduction*. [Online] 162 (4), 267–275. [online]. Available from: https://rep.bioscientifica.com/view/journals/rep/162/4/REP-21-0110.xml (Accessed 20 September 2023).

Dzamba, B. J. et al. (2009) Cadherin Adhesion, Tissue Tension and Non-Canonical Wnt Signaling Regulate Fibronectin Matrix Organization. *Developmental cell*. [Online] 16

(3), 421. [online]. Available from: /pmc/articles/PMC2682918/ (Accessed 30 August 2023).

Economou, A. D. et al. (2012) Periodic stripe formation by a Turing mechanism operating at growth zones in the mammalian palate. *Nature Genetics*. [Online] 44 (3), 348–351.

Economou, A. D. et al. (2013) Whole population cell analysis of a landmark-rich mammalian epithelium reveals multiple elongation mechanisms. *Development (Cambridge)*. [Online] 140 (23), 4740–4750.

Efremov, Y. M. et al. (2019) Measuring viscoelasticity of soft biological samples using atomic force microscopy. *Soft Matter*. [Online] 16 (1), 64–81. [online]. Available from: https://pubs.rsc.org/en/content/articlehtml/2020/sm/c9sm01020c (Accessed 24 September 2023).

Enato, E. et al. (2011) Motherisk Rounds: The Fetal Safety of Benzodiazepines: An Updated Meta-analysis. *Journal of Obstetrics and Gynaecology Canada*. [Online] 33 (1), 46–48.

Etienne-Manneville, S. & Hall, A. (2002) Rho GTPases in cell biology. *Nature*. [Online] 420 (6916), 629–635. [online]. Available from: https://pubmed.ncbi.nlm.nih.gov/12478284/ (Accessed 30 August 2023).

Eto, K. & Takakubo, F. (1985) Improved development of rat embryos in culture during the period of craniofacial morphogenesis. *Journal of Craniofacial Genetics and Developmental Biology*. 5 (4), 351–355. [online]. Available from: https://europepmc.org/article/med/4077955 (Accessed 20 May 2023).

Eyckmans J., Boudou T., Yu X., Chen C. S. A hitchhiker's guide to mechanobiology. Dev Cell. 2011 Jul 19;21(1):35-47. doi: 10.1016/j.devcel.2011.06.015. PMID: 21763607; PMCID: PMC3155761

Fainstat, T. (1972) Submerged organ culture: An improved method. *In Vitro 1972 7:5*. [Online] 7 (5), 300–303. [online]. Available from: https://link.springer.com/article/10.1007/BF02661718 (Accessed 21 May 2023).

Fantauzzo, K. A. & Soriano, P. (2016) PDGFRβ regulates craniofacial development through homodimers and functional heterodimers with PDGFRα. *Genes & development*. [Online] 30 (21), 2443–2458. [online]. Available from: https://pubmed.ncbi.nlm.nih.gov/27856617/ (Accessed 30 August 2023).

Feneck, E. M. et al. (2018) A comparative study of the elastic fibre system within the mouse and human cornea. *Experimental Eye Research*. [Online] 17735. [online]. Available from: /pmc/articles/PMC6280038/ (Accessed 30 August 2023).

Fenelon, J. C. et al. (2023a) Getting out of a mammalian egg: the egg tooth and caruncle of the echidna. *Developmental Biology*. [Online] 4958–18.

Fenelon, J. C. et al. (2023b) Getting out of a mammalian egg: the egg tooth and caruncle of the echidna. *Developmental biology*. [Online] 4958–18. [online]. Available from: https://pubmed.ncbi.nlm.nih.gov/36565838/ (Accessed 16 September 2023).

Ferguson, M. W. J. (1981a) Developmental mechanisms in normal and abnormal palate formation with particular reference to the aetiology, pathogenesis and prevention of cleft palate. *British journal of orthodontics*. [Online] 8 (3), 115–137. [online]. Available from: https://pubmed.ncbi.nlm.nih.gov/6455154/ (Accessed 5 August 2023).

Ferguson, M. W. J. et al. (1984) Differentiation of cultured palatal shelves from alligator, chick, and mouse embryos. *The Anatomical Record*. [Online] 209 (2), 231–249.

Ferguson, M. W. J. (1978) Palatal shelf elevation in the Wistar rat fetus. *Journal of Anatomy*. 125 (3), 555–577.

Ferguson, M. W. J. (1988) Palate development. *Development*. 103 (Supplement 9), 41–60.

Ferguson, M. W. J. (1979) The American Alligator (Alligator mississipinensis): A new model for investigating developmental mechanisms in normal and abnormal palate formation. *Medical Hypotheses*. [Online] 5 (10), 1079–1090.

Ferguson, M. W. J. (1977) The mechanism of palatal shelf elevation and the pathogenesis of cleft palate. *Virchows Archiv A Pathological Anatomy and Histology*. [Online] 375 (2), 97–113. [online]. Available from: https://link.springer.com/article/10.1007/BF00428098 (Accessed 28 August 2023).

Ferguson, M. W. J. (1981b) The structure and development of the palate in Alligator mississippiensis. *Archives of Oral Biology*. [Online] 26 (5), 427–443.

Ferrante, M. I. et al. (2001) Identification of the Gene for Oral-Facial-Digital Type I Syndrome. *American Journal of Human Genetics*. [Online] 68 (3), 569. [online]. Available from: /pmc/articles/PMC1274470/ (Accessed 23 July 2023).

Fick, R. (1902) Bemerkungen zur Wolfsrachenbildung. *Arch. f. klin. Chir.* 68299–299.

Fischer, E. et al. (2006) Defective planar cell polarity in polycystic kidney disease. *Nature Genetics*. [Online] 38 (1), 21–23.

Fitchett, J. E. & Hay, E. D. (1989) Medial edge epithelium transforms to mesenchyme after embryonic palatal shelves fuse. *Developmental biology*. [Online] 131 (2), 455–474. [online]. Available from: https://pubmed.ncbi.nlm.nih.gov/2463946/ (Accessed 4 August 2023).

FitzPatrick, D. R. et al. (2003) Identification of SATB2 as the cleft palate gene on 2q32-q33. *Human molecular genetics*. [Online] 12 (19), 2491–2501. [online]. Available from: https://pubmed.ncbi.nlm.nih.gov/12915443/ (Accessed 23 July 2023).

Fletcher, A. G. et al. (2014) Vertex models of epithelial morphogenesis. *Biophysical journal*. [Online] 106 (11), 2291–2304. [online]. Available from: https://pubmed.ncbi.nlm.nih.gov/24896108/ (Accessed 28 September 2023).

Flint, O. & Ede, D. A. (1978) Facial development in the mouse; a comparison between normal and mutant (amputated) mouse embryos. *Journal of embryology and experimental morphology*.

Flint, O. P. (1980) Cell behaviour and cleft palate in the mutant mouse, amputated. *Journal of Embryology and Experimental Morphology*. Vol. 58131–142.

Fogh-Anderson, P. (1942) Inheritance harelip and cleft palate. *Opara exdome biologiae hareditariae universities hafniensis*. [Online] 41-. [online]. Available from: https://cir.nii.ac.jp/crid/1572543024780215040 (Accessed 23 July 2023).

Fonck, E. et al. (2009) Effect of aging on elastin functionality in human cerebral arteries. *Stroke*. [Online] 40 (7), 2552–2556.

Foreman, D. M. et al. (1991) Comparative biochemistry of mouse and chick secondary-palate development in vivo and in vitro with particular emphasis on extracellular matrix molecules and the effects of growth factors on their synthesis. *Archives of Oral Biology*. [Online] 36 (6), 457–471.

Forgacs, G. et al. (1998) Viscoelastic properties of living embryonic tissues: a quantitative study. *Biophysical journal*. [Online] 74 (5), 2227–2234. [online]. Available from: https://pubmed.ncbi.nlm.nih.gov/9591650/ (Accessed 28 September 2023).

Foster, J. W. et al. (1994) Campomelic dysplasia and autosomal sex reversal caused by mutations in an SRY-related gene. *Nature*. [Online] 372 (6506), 525–530. [online].

Available from: https://pubmed.ncbi.nlm.nih.gov/7990924/ (Accessed 23 July 2023).

Francis-West, P. et al. (1998) Signalling interactions during facial development. *Mechanisms of Development*. [Online] 75 (1–2), 3–28.

Fraser, F. C. (1971) 'Etiology of cleft lip and palate', in W C Grabb et al. (eds.) *Cleft lip and palate, surgical, dental and speech aspects*. 1st edition Boston: Little Brown Co. pp. 54–65. [online]. Available from: https://adams.marmot.org/Record/.b1717448x (Accessed 6 August 2023).

Fraser, F. C. (1969) 'Gene-environment interactions in the production of cleft palate, In Melted•· for teratological studies in experimental animals and man', in H Nishimura & J R Miller (eds.) *Methods for teratological studies in experimental animals and man*. 1st edition Tokyo: Igaku Shoin. pp. 34–38. [online]. Available from: https://www.google.com/search?client=safari&rls=en&sxsrf=AB5stBh3jYcWHMqKP0bCtCovR3auKQgqrg:1691361941004&q=Fraser,+F.+C.+(1969)+Gene-environment+interactions+in+the+production+of+cleft+palate,+In+Melted%E2%80%A2%C2%B7+for+teratological+studies+in+experimental+animals+and+man,+H.+Nishimura+and+J.+R.+Miller+(Eds.),+pp.+34-38,+Tokyo:+igaku+Shoin.&spell=1&sa=X&ved=2ahUKEwivi7idjsmAAxWogf0HHShoA5YQBSgAegQICRAB&biw=2240&bih=1086&dpr=2 (Accessed 6 August 2023).

Frebourg, T. et al. (2006) Cleft lip/palate and CDH1/E-cadherin mutations in families with hereditary diffuse gastric cancer. *Journal of Medical Genetics*. [Online] 43 (2), 138. [online]. Available from: /pmc/articles/PMC2564630/ (Accessed 23 July 2023).

Friedl, P. et al. (2012) Nuclear mechanics during cell migration. *Current Opinion in Cell Biology*. [Online] 23 (1), 55–64.

Friedl, R. M. et al. (2019) RDH10 function is necessary for spontaneous fetal mouth movement that facilitates palate shelf elevation. *DMM Disease Models and Mechanisms*. [Online] 12 (7), .

Frommer, J. & Monroe, C. W. (1969) Further Evidence for the Absence of Elastic Fibers during Movement of the Palatal Shelves in Mice. *Journal of Dental Research*. [Online] 48 (1), 155.

Fuchs, H. (1908) Untersuchungen uber Ontogenie und Phylogenie der Gaumenbilding bei den Wirbeltieren Zweite Mitteilung. Uber das Munddach der Rhynchocephalen,

Saurier, Schlangen, Krokodile und Sauger und den zusammenhong zwrischen Mund und Nasenhohle bei diesen Tieren. *Z. Morph. und Anth.* 11153–248. [online]. Available from: https://cob.silverchair-cdn.com/cob/content_public/journal/dev/103/supplement/10.1242_dev.103.supplement.41/5/develop_103_s_41.pdf?Expires=1694294748&Signature=ChAGQ8yit8ou-VgGYqJe5JP6SW9-JOnsYhhx4P34Ecoyvl-CysEtRTkVudiJsYNG1I8KqtbcOVG~oykNXvG3y7LJv~dToIc7LmL8xrNdpZpWmpDb6Wcj6XaKT7jM6UUqLSPwZ0-hWsES2aRr~gO4VL1hY1TT9Ooe1sqzkXBOUkh~9zldh5PQbG16ZHiP4gomQVcx5sSBZrJzKkTeGSFD402PC6C~lCPoSJ2t7Mzo3HpUjUUnWqUz3gPQhiO91KVulYYT34j4K9Y7hQ8x00kdpHtQWm6ijKsxRsQh5tbggE8FOFhbPfljMLN9HB2dWokJFzVzh7ovQQpV5DGUyvnWJw__&Key-Pair-Id=APKAIE5G5CRDK6RD3PGA (Accessed 6 August 2023).

Fuchs, H. (1907) Untersuchungen uber Ontogenie und Phylogenie der Gaumenbildungen bei den Wirbeltieren Erste Mitteilung Uber den Gaumen der Schildkroten und seine Entwicklungsgeschichte. *Z. Morph. und Anth.* 10409–463. [online]. Available from: https://www.zobodat.at/pdf/Archiv-Naturgeschichte_74-2_1_0001-0146.pdf (Accessed 6 August 2023).

Fuller, H. M. & Lillie, R. D. (1957) The staining of collagen with elastic tissue stains. *Journal of Histochemistry & Cytochemistry*. [Online] 5 (1), 11–14. [online]. Available from: https://journals.sagepub.com/doi/abs/10.1177/5.1.11 (Accessed 12 September 2023).

Furukawa, S. et al. (2004) Histopathological findings of cleft palate in rat embryos induced by triamcinolone acetonide. *The Journal of veterinary medical science*. [Online] 66 (4), 397–402. [online]. Available from: https://pubmed.ncbi.nlm.nih.gov/15133269/ (Accessed 11 September 2023).

Garantziotis, S. & Savani, R. C. (2019) Hyaluronan biology: A complex balancing act of structure, function, location and context. *Matrix Biology*. [Online] 78–791–10.

Garland, M. A. et al. (2020) Environmental mechanisms of orofacial clefts. *Birth Defects Research*. [Online] 112 (19), 1660–1698. [online]. Available from: https://onlinelibrary.wiley.com/doi/full/10.1002/bdr2.1830 (Accessed 23 July 2023).

Gautier, H. O. B. et al. (2015) Atomic force microscopy-based force measurements on animal cells and tissues. *Methods in Cell Biology*. [Online] 125211–235.

George, E. L. et al. (1993) Defects in mesoderm, neural tube and vascular development in mouse embryos lacking fibronectin. *Development (Cambridge, England)*. [Online] 119 (4), 1079–1091. [online]. Available from: https://pubmed.ncbi.nlm.nih.gov/8306876/ (Accessed 29 September 2023).

Ghassibé, M. et al. (2005) Interferon regulatory factor-6: a gene predisposing to isolated cleft lip with or without cleft palate in the Belgian population. *European Journal of Human Genetics 2005 13:11*. [Online] 13 (11), 1239–1242. [online]. Available from: https://www.nature.com/articles/5201486 (Accessed 4 August 2023).

Ghouzzi, V. El et al. (1997) Mutations of the TWIST gene in the Saethre-Chotzen syndrome. *Nature genetics*. [Online] 15 (1), 42–46. [online]. Available from: https://pubmed.ncbi.nlm.nih.gov/8988167/ (Accessed 23 July 2023).

Glas, E. (1904) Über die Entwickelung und Morphologie der inneren Nase der Ratte. *Beiträge und Referate zur Anatomie und Entwickelungsgeschichte*. [Online] 25 (2), 273–341. [online]. Available from: https://link.springer.com/article/10.1007/BF02300760 (Accessed 6 August 2023).

Goering, J. P. et al. (2022) Novel insights into the fundamentals of palatal shelf elevation dynamics in normal mouse embryos. *bioRxiv*. [Online] 2022.06.02.494562. [online]. Available from: https://www.biorxiv.org/content/10.1101/2022.06.02.494562v1 (Accessed 15 May 2023).

Goering, J. P. et al. (2021) SPECC1L-deficient primary mouse embryonic palatal mesenchyme cells show speed and directionality defects. *Scientific Reports*. [Online] 11 (1), 1–13. [online]. Available from: https://doi.org/10.1038/s41598-021-81123-9.

Gomori, G. (1950) Aldehyde-fuchsin: a new stain for elastic tissue. *American journal of clinical pathology*. [Online] 20 (7), 665–666. [online]. Available from: https://pubmed.ncbi.nlm.nih.gov/15432365/ (Accessed 29 August 2023).

Goodwin, A. F. et al. (2020) YAP/TAZ Regulate Elevation and Bone Formation of the Mouse Secondary Palate. *Journal of Dental Research*. [Online] 99 (12), 1387–1396.

Goss, A. N. et al. (1970) In Vitro Fusion of Cleft Palate Shelves. *The Cleft Palate Journal*. 7 (3), 737–747. [online]. Available from:

https://cleftpalatejournal.pitt.edu/ojs/cleftpalate/article/view/350 (Accessed 21 May 2023).

Graham, A. et al. (2019) A reappraisal and revision of the numbering of the pharyngeal arches. *Journal of Anatomy*. [Online] 235 (6), 1019–1023. [online]. Available from: https://onlinelibrary.wiley.com/doi/full/10.1111/joa.13067 (Accessed 30 July 2023).

Green, J. B. A. (2022) Resolving morphogenesis into quantifiable cell behaviours. *Development (Cambridge)*. [Online] 149 (21), . [online]. Available from: https://dx.doi.org/10.1242/dev.199794 (Accessed 28 August 2023).

Greene, N. D. E. & Copp, A. J. (2014) Neural Tube Defects. *Annual review of neuroscience*. [Online] 37221. [online]. Available from: /pmc/articles/PMC4486472/ (Accessed 23 July 2023).

Greene, R. M. & Kochhar, D. M. (1973) Palatal closure in the mouse as demonstrated in frozen sections. *American Journal of Anatomy*. [Online] 137 (4), 477–482.

Greene, R. M. & Pratt, R. M. (1976) Developmental aspects of secondary palate formation. *Journal of Embryology and Experimental Morphology*. 36 (2), 225–245.

Gregory, J. E. et al. (1989) Responses of electroreceptors in the snout of the echidna. *The Journal of Physiology*. [Online] 414 (1), 521. [online]. Available from: /pmc/articles/PMC1189155/?report=abstract (Accessed 22 September 2023).

Griepentrog, M. et al. (2013) Comparison of nanoindentation and AFM methods for the determination of mechanical properties of polymers. *Polymer Testing*. [Online] 32 (3), 455–460.

Griffiths, M. (1968) 'Embryology', in *Echidnas*. 1st edition Oxford: Pergamon Press. pp. 156–172. [online]. Available from: https://books.google.nl/books?hl=en&lr=&id=WArLBAAAQBAJ&oi=fnd&pg=PP1&ots=hh97OLc7WQ&sig=i0bBty_v28MAbO68ohC9ApVV9vM&redir_esc=y#v=onepage&q=incubation&f=false (Accessed 20 September 2023).

Griffiths, M. (1965) Rate of growth and intake of milk in a suckling echidna. *Comparative Biochemistry and Physiology*. [Online] 16 (4), 383–392.

Griffiths, M. (1978) 'Reproduction and embryology', in *The Biology of the Monotremes*. New York, San Francisco, London: Academic Press. pp. 209–254.

Gripp, K. W. et al. (2000) Mutations in TGIF cause holoprosencephaly and link NODAL signalling to human neural axis determination. *Nature genetics*. [Online] 25 (2), 205–208. [online]. Available from: https://pubmed.ncbi.nlm.nih.gov/10835638/ (Accessed 23 July 2023).

Gritli-Linde, A. (2007) Molecular control of secondary palate development. *Developmental Biology*. [Online] 301 (2), 309–326.

Gundlach, K. K. H. & Maus, C. (2006) Epidemiological studies on the frequency of clefts in Europe and world-wide. *Journal of cranio-maxillo-facial surgery : official publication of the European Association for Cranio-Maxillo-Facial Surgery*. [Online] 34 Suppl 2 (SUPPL. 2), 1–2. [online]. Available from: https://pubmed.ncbi.nlm.nih.gov/17071381/ (Accessed 23 July 2023).

Hahn, H. et al. (1996) Mutations of the human homolog of Drosophila patched in the nevoid basal cell carcinoma syndrome. *Cell*. [Online] 85 (6), 841–851. [online]. Available from: https://pubmed.ncbi.nlm.nih.gov/8681379/ (Accessed 23 July 2023).

Hale, F. (1935) The Relation of Vitamin a to Anophthalmos in Pigs. *American Journal of Ophthalmology*. [Online] 18 (12), 1087–1093.

Hall, E. G. et al. (2020) SPECC1L regulates palate development downstream of IRF6. *Human Molecular Genetics*. [Online] 29 (5), 845–858. [online]. Available from: https://dx.doi.org/10.1093/hmg/ddaa002 (Accessed 29 August 2023).

Halper, J. & Kjaer, M. (2014) Basic components of connective tissues and extracellular matrix: elastin, fibrillin, fibulins, fibrinogen, fibronectin, laminin, tenascins and thrombospondins. *Advances in experimental medicine and biology*. [Online] 80231–47. [online]. Available from: https://pubmed.ncbi.nlm.nih.gov/24443019/ (Accessed 30 August 2023).

Hamburger, V. & Hamilton, H. L. (1951) A series of normal stages in the development of the chick embryo. *Journal of Morphology*. [Online] 88 (1), 49–92. [online]. Available from: https://onlinelibrary.wiley.com/doi/full/10.1002/jmor.1050880104 (Accessed 19 September 2023).

Hammond, N. L. et al. (2019) Periderm: Life-cycle and function during orofacial and epidermal development. *Seminars in Cell & Developmental Biology*. [Online] 9175–83.

Hammond, N. L. & Dixon, M. J. (2022) Revisiting the embryogenesis of lip and palate development. *Oral Diseases*. [Online] 28 (5), 1306–1326. [online]. Available from: https://onlinelibrary.wiley.com/doi/full/10.1111/odi.14174 (Accessed 20 July 2023).

Han, J. et al. (2009) Indirect modulation of Shh signaling by Dlx5 affects the oral-nasal patterning of palate and rescues cleft palate in Msx1-null mice. *Development (Cambridge, England)*. [Online] 136 (24), 4225–4233. [online]. Available from: https://pubmed.ncbi.nlm.nih.gov/19934017/ (Accessed 2 August 2023).

Haque, F. et al. (2010) Mammalian SUN protein interaction networks at the inner nuclear membrane and their role in laminopathy disease processes. *The Journal of biological chemistry*. [Online] 285 (5), 3487–3498. [online]. Available from: https://pubmed.ncbi.nlm.nih.gov/19933576/ (Accessed 24 September 2023).

Harris, J. W. S. (1967) Experimental studies on closure and cleft formation in the secondary palate. *Scientific Basis of Medicine Annual Reviews*. 354–370.

Harris, J. W. S. (1961) Growth changes in the cranial base and lower jaw during the closure of the secondary palate in two strains of rat. *Journal of Anatomy*. 95286.

Harris, T. J. C. & Tepass, U. (2010) Adherens junctions: from molecules to morphogenesis. *Nature Reviews Molecular Cell Biology 2010 11:7*. [Online] 11 (7), 502–514. [online]. Available from: https://www.nature.com/articles/nrm2927 (Accessed 28 September 2023).

Hassell, J. R. & Orkin, R. W. (1976) Synthesis and distribution of collagen in the rat palate during shelf elevation. *Developmental biology*. [Online] 49 (1), 80–88. [online]. Available from: https://pubmed.ncbi.nlm.nih.gov/1254099/ (Accessed 30 August 2023).

He, F. et al. (2008) Wnt5a regulates directional cell migration and cell proliferation via Ror2-mediated noncanonical pathway in mammalian palate development. *Development*. [Online] 135 (23), 3871–3879.

He, L. H. & Swain, M. V. (2017) Microindentation. *Comprehensive Biomaterials II*. [Online] 144–168.

Heisenberg, C. P. & Bellaïche, Y. (2013) Forces in tissue morphogenesis and patterning. *Cell*. [Online] 153 (5), 948.

Helwany, M. & Rathee, M. (2022) Anatomy, Head and Neck, Palate. *StatPearls*. [online]. Available from: https://www.ncbi.nlm.nih.gov/books/NBK557817/ (Accessed 25 July 2023).

Higashiyama, H. et al. (2021) Mammalian face as an evolutionary novelty. *Proceedings of the National Academy of Sciences of the United States of America*. [Online] 118 (44), e2111876118. [online]. Available from: https://www.pnas.org/doi/abs/10.1073/pnas.2111876118 (Accessed 22 September 2023).

Hill, C. et al. (2015) Cranial neural crest deletion of VEGFa causes cleft palate with aberrant vascular and bone development. *Cell and Tissue Research*. [Online] 361 (3), 711–722. [online]. Available from: https://link.springer.com/article/10.1007/s00441-015-2150-7 (Accessed 29 August 2023).

Hill, J. P. & de Beer, G. R. (1950) Development of the Monotremata VII. The Development and Structure of the Egg-Tooth and the Caruncle in the Monotremes and on the Occurrence of Vestiges of the Egg-tooth and Caruncle in Marsupials. *The Transactions of the Zoological Society of London*. [Online] 26 (6), 503–544. [online]. Available from: https://onlinelibrary.wiley.com/doi/full/10.1111/j.1096-3642.1950.tb00226.x (Accessed 20 September 2023).

Hilliard, S. A. et al. (2005) Regional regulation of palatal growth and patterning along the anterior–posterior axis in mice. *Journal of Anatomy*. [Online] 207 (5), 655–667. [online]. Available from: https://onlinelibrary.wiley.com/doi/full/10.1111/j.1469-7580.2005.00474.x (Accessed 2 August 2023).

Hinrichsen, K. (1985) The early development of morphology and patterns of the face in the human embryo. *Advances in anatomy, embryology, and cell biology*. [Online] 98. [online]. Available from: https://pubmed.ncbi.nlm.nih.gov/4083112/ (Accessed 30 July 2023).

Hiranuma, H. et al. (2000) Effect of X Irradiation on Secondary Palate Development in Mice. *https://doi.org/10.1667/0033-7587(2000)154[0034:EOXIOS]2.0.CO;2*. [Online] 154 (1), 34–38. [online]. Available from: https://bioone.org/journals/radiation-research/volume-154/issue-1/0033-7587_2000_154_0034_EOXIOS_2.0.CO_2/Effect-of-X-Irradiation-on-Secondary-

Palate-Development-in-Mice/10.1667/0033-7587(2000)154[0034:EOXIOS]2.0.CO;2.full (Accessed 5 June 2023).

His, W. (1885) *Anatomie menschlicher Embryonen III: Zur Geschichte der Organe*. 1st edition. Leipzig: F C W Vogel. [online]. Available from: https://books.google.co.uk/books?hl=en&lr=&id=nPxJAQAAMAAJ&oi=fnd&pg=PA1&ots=TEpGh1h1ks&sig=BWBuE3tw9oAp3muTrA1QGxqgfHg&redir_esc=y#v=onepage&q=gaumen&f=false (Accessed 5 August 2023).

His, W. (1901) *Beobachtungen zur geschichte der nasen und gaumenbildung beim menschlichen embryo*. 1st edition. Leipzig: B G Teubner. [online]. Available from: https://books.google.co.uk/books/about/Beobachtungen_zur_geschichte_der_nasen_u.html?id=j8YZzwEACAAJ&redir_esc=y (Accessed 5 August 2023).

Hopkins, T. I. R. et al. (2021) Micromechanical mapping of the intact ovary interior reveals contrasting mechanical roles for follicles and stroma. *Biomaterials*. [Online] 277. [online]. Available from: https://pubmed.ncbi.nlm.nih.gov/34537501/ (Accessed 14 September 2023).

Hosokawa, R. et al. (2009) Epithelial-specific requirement of FGFR2 signaling during tooth and palate development. *Journal of Experimental Zoology Part B: Molecular and Developmental Evolution*. [Online] 312B (4), 343–350. [online]. Available from: https://onlinelibrary.wiley.com/doi/full/10.1002/jez.b.21274 (Accessed 30 September 2023).

Howard, T. D. et al. (1997) Mutations in TWIST, a basic helix-loop-helix transcription factor, in Saethre-Chotzen syndrome. *Nature genetics*. [Online] 15 (1), 36–41. [online]. Available from: https://pubmed.ncbi.nlm.nih.gov/8988166/ (Accessed 23 July 2023).

Howell, M. et al. (2017) Live Cell Fluorescence Microscopy to Observe Essential Processes During Microbial Cell Growth. *Journal of visualized experiments : JoVE*. [Online] 2017 (129), . [online]. Available from: https://pubmed.ncbi.nlm.nih.gov/29286454/ (Accessed 24 September 2023).

Hu, H. et al. (2017) Constrained vertebrate evolution by pleiotropic genes. *Nature ecology & evolution*. [Online] 1 (11), 1722–1730. [online]. Available from: https://pubmed.ncbi.nlm.nih.gov/28963548/ (Accessed 22 September 2023).

Hu, V. W. et al. (2002) 3H-thymidine is a defective tool with which to measure rates of DNA synthesis. *FASEB journal : official publication of the Federation of American Societies for Experimental Biology*. [Online] 16 (11), 1456–1457. [online]. Available from: https://pubmed.ncbi.nlm.nih.gov/12205046/ (Accessed 22 September 2023).

Humphrey, T. (1971) Development of oral and facial motor mechanisms in human fetuses and their relation to craniofacial growth. *Journal of dental research*. [Online] 50 (6), 1428–1441. [online]. Available from: https://pubmed.ncbi.nlm.nih.gov/5289050/ (Accessed 7 August 2023).

Humphrey, T. (1968) The dynamic mechanism of palatal shelf elevation in human foetuses, . *Anatomical Record*. 160369.

Humphrey, T. (1969) The relation between human fetal mouth opening reflexes and closure of the palate. *American Journal of Anatomy*. [Online] 125 (3), 317–344.

Innes, P. B. (1978) The ultrastructure of the mesenchymal element of the palatal shelves of the fetal mouse. *Journal of Embryology and Experimental Morphology*. Vol. 43 (1961), 185–194.

Inostroza, V. et al. (2021) Maternal genotypes of folate/one-carbon metabolism gene variants and nonsyndromic cleft lip with or without cleft palate risk in Chile. *European journal of oral sciences*. [Online] 129 (5), . [online]. Available from: https://pubmed.ncbi.nlm.nih.gov/34289180/ (Accessed 23 July 2023).

Inouye, M. (1912) Die Entwickelung des Sekundären Gaumens Einiger Säugetiere . *Beiträge und Referate zur Anatomie und Entwickelungsgeschichte*. [Online] 46 (1), 3–184. [online]. Available from: https://link.springer.com/article/10.1007/BF02214425 (Accessed 6 August 2023).

Iozzo, R. V. & Schaefer, L. (2015) Proteoglycan form and function: A comprehensive nomenclature of proteoglycans. *Matrix Biology*. [Online] 4211–55.

Iseki, S. et al. (2007) Experimental induction of palate shelf elevation in glutamate decarboxylase 67-deficient mice with cleft palate due to vertically oriented palatal shelf. *Birth defects research. Part A, Clinical and molecular teratology*. [Online] 79 (10), 688–695. [online]. Available from: https://pubmed.ncbi.nlm.nih.gov/17849453/ (Accessed 28 August 2023).

Ito, Y. et al. (2003a) Conditional inactivation of Tgfbr2 in cranial neural crest causes cleft palate and calvaria defects. *Development (Cambridge, England)*. [Online] 130 (21),

5269–5280. [online]. Available from: https://pubmed.ncbi.nlm.nih.gov/12975342/ (Accessed 5 June 2023).

Ito, Y. et al. (2003b) Conditional inactivation of Tgfbr2 in cranial neural crest causes cleft palate and calvaria defects. *Development*. [Online] 130 (21), 5269–5280. [online]. Available from: https://journals.biologists.com/dev/article/130/21/5269/52163/Conditional-inactivation-of-Tgfbr2-in-cranial (Accessed 5 June 2023).

Jahanbin, A. et al. (2018) Maternal folic acid supplementation and the risk of oral clefts in offspring. *Journal of Craniofacial Surgery*. [Online] 29 (6), e534–e541. [online]. Available from: https://journals.lww.com/jcraniofacialsurgery/Fulltext/2018/09000/Maternal_Folic_Acid_Supplementation_and_the_Risk.79.aspx (Accessed 23 July 2023).

Jankowski, R. (2013) 'The complex formation of the secondary palate and nose in evolution', in *The Evo-Devo Origin of the Nose, Anterior Skull Base and Midface*. Springer-Verlag. pp. 41–61.

Jiang, R. et al. (2006) Development of the Upper Lip: Morphogenetic and Molecular Mechanisms. *Developmental dynamics : an official publication of the American Association of Anatomists*. [Online] 235 (5), 1152. [online]. Available from: /pmc/articles/PMC2562450/ (Accessed 30 July 2023).

Jin, J. Z. et al. (2008) Analysis of Zfhx1a mutant mice reveals palatal shelf contact-independent medial edge epithelial differentiation during palate fusion. *Cell and Tissue Research*. [Online] 333 (1), 29–38.

Jin, J. Z. et al. (2010) Mesenchymal cell remodeling during mouse secondary palate reorientation. *Developmental Dynamics*. [Online] 239 (7), 2110–2117.

Johnson, R. L. et al. (1996) Human homolog of patched, a candidate gene for the basal cell nevus syndrome. *Science (New York, N.Y.)*. [Online] 272 (5268), 1668–1671. [online]. Available from: https://pubmed.ncbi.nlm.nih.gov/8658145/ (Accessed 23 July 2023).

Johnston, J. J. et al. (2010) Molecular analysis expands the spectrum of phenotypes associated with GLI3 mutations. *Human mutation*. [Online] 31 (10), 1142. [online]. Available from: /pmc/articles/PMC2947617/ (Accessed 23 July 2023).

Johnston, M. C. (1966) A radioautographic study of the migration and fate of cranial neural crest cells in the chick embryo. *The Anatomical record*. [Online] 156 (2), 143–155. [online]. Available from: https://pubmed.ncbi.nlm.nih.gov/5969670/ (Accessed 30 July 2023).

Joodeph, D. R. & Wragg, L. E. (1971) Facial growth during the secondary palate closure in the rat. *American journal of orthodontics*. [Online] 60 (1), 88–89. [online]. Available from: https://pubmed.ncbi.nlm.nih.gov/5281456/ (Accessed 7 August 2023).

Joubert, B. R. et al. (2016) DNA Methylation in Newborns and Maternal Smoking in Pregnancy: Genome-wide Consortium Meta-analysis. *American Journal of Human Genetics*. [Online] 98 (4), 680–696. [online]. Available from: http://www.cell.com/article/S0002929716000707/fulltext (Accessed 23 July 2023).

Jugessur, A. et al. (2009) The genetics of isolated orofacial clefts: from genotypes to subphenotypes. *Oral diseases*. [Online] 15 (7), 437–453. [online]. Available from: https://pubmed.ncbi.nlm.nih.gov/19583827/ (Accessed 23 July 2023).

Junqueira, L. C. U. et al. (1979) Picrosirius staining plus polarization microscopy, a specific method for collagen detection in tissue sections. *The Histochemical Journal*. [Online] 11 (4), 447–455. [online]. Available from: https://link.springer.com/article/10.1007/BF01002772 (Accessed 12 September 2023).

Kalaskar, V. K. & Lauderdale, J. D. (2014a) Mouse embryonic development in a serum-free whole embryo culture system. *Journal of Visualized Experiments*. [Online] (85), 1–8.

Kalaskar, V. K. & Lauderdale, J. D. (2014b) Mouse Embryonic Development in a Serum-free Whole Embryo Culture System. *Journal of Visualized Experiments : JoVE*. [Online] (85), 50803. [online]. Available from: /pmc/articles/PMC4122383/ (Accessed 24 September 2023).

Kalay, E. et al. (2012) Mutations in RIPK4 Cause the Autosomal-Recessive Form of Popliteal Pterygium Syndrome. *American Journal of Human Genetics*. [Online] 90 (1), 76. [online]. Available from: /pmc/articles/PMC3257895/ (Accessed 23 July 2023).

Katsianou, M. A. et al. (2016) Signaling mechanisms implicated in cranial sutures pathophysiology: Craniosynostosis. *BBA Clinical*. [Online] 6165. [online]. Available from: /pmc/articles/PMC5144105/ (Accessed 8 September 2023).

Kawabata, F. & Tabata, S. (2022) Bitter Taste Perception in Chickens. *The Journal of Poultry Science*. [Online] 59 (1), 8. [online]. Available from: /pmc/articles/PMC8791780/ (Accessed 19 September 2023).

Keller, R. (2006) Mechanisms of elongation in embryogenesis. *Development*. [Online] 133 (12), 2291–2302.

Kelly, E. M. et al. (2019) The Development of Integration in Marsupial and Placental Limbs. *Integrative Organismal Biology*. [Online] 1 (1), 1–11. [online]. Available from: /pmc/articles/PMC7671123/ (Accessed 19 September 2023).

Kesler, B. et al. (2019) Automated cell boundary and 3D nuclear segmentation of cells in suspension. *Scientific reports*. [Online] 9 (1), . [online]. Available from: https://pubmed.ncbi.nlm.nih.gov/31308458/ (Accessed 24 September 2023).

Kim, N. G. & Gumbiner, B. M. (2015) Adhesion to fibronectin regulates Hippo signaling via the FAK-Src-PI3K pathway. *The Journal of cell biology*. [Online] 210 (3), 503–515. [online]. Available from: https://pubmed.ncbi.nlm.nih.gov/26216901/ (Accessed 30 August 2023).

Kim, S. et al. (2015) Convergence and Extrusion Are Required for Normal Fusion of the Mammalian Secondary Palate. *PLOS Biology*. [Online] 13 (4), e1002122. [online]. Available from: https://journals.plos.org/plosbiology/article?id=10.1371/journal.pbio.1002122 (Accessed 4 August 2023).

Kim, S. et al. (2017) Live Imaging of Mouse Secondary Palate Fusion. *Journal of visualized experiments : JoVE*. [Online] (125), 1–8.

Kindberg, A. et al. (2020) Forced to communicate: Integration of mechanical and biochemical signaling in morphogenesis. *Current Opinion in Cell Biology*. [Online] 6659–68.

Kindberg A. A., Srivastava V., Muncie J. M., Weaver V. M., Gartner Z. J., Bush J. O. EPH/EPHRIN regulates cellular organization by actomyosin contractility effects on cell contacts. J Cell Biol. 2021 Jun 7;220(6):e202005216. doi: 10.1083/jcb.202005216. PMID: 33798261; PMCID: PMC8025214.

Kirillov, A. et al. (2018) Panoptic Segmentation. *Proceedings of the IEEE Computer Society Conference on Computer Vision and Pattern Recognition*. [Online] 2019-June9396–

9405. [online]. Available from: https://arxiv.org/abs/1801.00868v3 (Accessed 8 September 2023).

Kleinberg, G. et al. (2022) Usability of deep learning pipelines for 3D nuclei identification with Stardist and Cellpose. *Cells & Development*. [Online] 172203806.

Klotz, C. M. et al. (2010) Revisiting the Recurrence Risk of Nonsyndromic Cleft Lip with or without Cleft Palate. *American journal of medical genetics. Part A*. [Online] 152A (11), 2697. [online]. Available from: /pmc/articles/PMC2965308/ (Accessed 20 July 2023).

Knight, R. D. & Schilling, T. F. (2013) *Cranial Neural Crest and Development of the Head Skeleton*. Landes Bioscience. [online]. Available from: https://www.ncbi.nlm.nih.gov/books/NBK6075/ (Accessed 30 July 2023).

Koch, W. E. & Smiley, G. R. (1981) In-vivo and in-vitro studies of the development of the avian secondary palate. *Archives of Oral Biology*. [Online] 26 (3), 181–187.

Kondo, S. et al. (2002) Mutations in IRF6 cause Van der Woude and popliteal pterygium syndromes. *Nature genetics*. [Online] 32 (2), 285. [online]. Available from: /pmc/articles/PMC3169431/ (Accessed 23 July 2023).

Kontomaris, S.-V. (2018) The Hertz Model in AFM Nanoindentation Experiments: Applications in Biological Samples and Biomaterials. *Micro and Nanosystems*. [Online] 10 (1), 11–22.

Kosazuma, T. et al. (2004) Organ culture of the fetal mouse palate for screening the developmental toxicity of chemicals: A validation study. *Congenital Anomalies*. [Online] 44 (2), 60–71. [online]. Available from: https://onlinelibrary.wiley.com/doi/full/10.1111/j.1741-4520.2004.00010.x (Accessed 21 May 2023).

Kosowski, T. et al. (2012) Cleft Palate. *Seminars in Plastic Surgery*. [Online] 26 (4), 164. [online]. Available from: /pmc/articles/PMC3706041/ (Accessed 22 July 2023).

Koyama, S. et al. (2013) The nipple: A simple intersection of mammary gland and integument, but focal point of organ function. *Journal of Mammary Gland Biology and Neoplasia*. [Online] 18 (2), 121–131. [online]. Available from: https://link.springer.com/article/10.1007/s10911-013-9289-1 (Accessed 20 September 2023).

Krantz, I. D. et al. (2004) Cornelia de Lange syndrome is caused by mutations in NIPBL, the human homolog of Drosophila melanogaster Nipped-B. *Nature genetics*. [Online] 36 (6), 631. [online]. Available from: /pmc/articles/PMC4902017/ (Accessed 23 July 2023).

Krause, M. et al. (2013) Probing the compressibility of tumor cell nuclei by combined atomic force-confocal microscopy. *Physical biology*. [Online] 10 (6), . [online]. Available from: https://pubmed.ncbi.nlm.nih.gov/24304807/ (Accessed 8 September 2023).

Krubitzer, L. & Campi, K. (2009) 'Neocortical Organization in Monotremes', in *Encyclopedia of Neuroscience*. [Online]. Academic Press. pp. 51–59.

Kurisu, K. et al. (1992) Heterogeneous distribution of the precursor of type I and type III collagen and fibronectin in the rough endoplasmic reticulum of palatal mesenchymal cells of the mouse embryo cultured in ascorbate-depleted medium. *Cell and tissue research*. [Online] 267 (3), 429–435. [online]. Available from: https://pubmed.ncbi.nlm.nih.gov/1571957/ (Accessed 30 August 2023).

Lahti, A. et al. (1972) The effect of hydrocortisone on the closure of the palatal shelves in two inbred strains of mice in vivo and in vitro. *Teratology*. [Online] 6 (1), 37–41. [online]. Available from: https://onlinelibrary.wiley.com/doi/full/10.1002/tera.1420060106 (Accessed 21 May 2023).

Lan, Y. et al. (2015) Cellular and Molecular Mechanisms of Palatogenesis. *Current topics in developmental biology*. [Online] 11559–84. [online]. Available from: https://pubmed.ncbi.nlm.nih.gov/26589921/ (Accessed 2 August 2023).

Lan, Y. et al. (2016) Golgb1 regulates protein glycosylation and is crucial for mammalian palate development. *Development (Cambridge)*. [Online] 143 (13), 2344–2355. [online]. Available from: https://journals.biologists.com/dev/article/143/13/2344/47434/Golgb1-regulates-protein-glycosylation-and-is (Accessed 21 May 2023).

Lan, Y. et al. (2004) Odd-skipped related 2 (Osr2) encodes a key intrinsic regulator of secondary palate growth and morphogenesis. *Development (Cambridge, England)*. [Online] 131 (13), 3207–3216. [online]. Available from: https://pubmed.ncbi.nlm.nih.gov/15175245/ (Accessed 2 August 2023).

Lan, Y. et al. (2019) Requirement of Hyaluronan Synthase-2 in Craniofacial and Palate Development. *Journal of Dental Research*. [Online] 98 (12), 1367–1375.

Lan, Y. & Jiang, R. (2009) Sonic hedgehog signaling regulates reciprocal epithelial-mesenchymal interactions controlling palatal outgrowth. *Development*. [Online] 136 (8), 1387–1396. [online]. Available from: https://dx.doi.org/10.1242/dev.028167 (Accessed 2 August 2023).

Larsson, K. S. (1974) 'Mechanisms of cleft palate formation', in D. T. Janerich et al. (eds.) *Congenital defects, new directions in research*. 1st edition pp. 255–275. [online]. Available from: https://journals.sagepub.com/doi/epdf/10.1179/bjo.8.3.115 (Accessed 7 August 2023).

Larsson, K. S. (1960) Studies on the closure of the secondary palate: II. Occurrence of sulpho-mucopolysaccharides in the palatine processes of the normal mouse embryo. *Experimental Cell Research*. [Online] 21 (3), 498–503.

Larsson, K. S. (1962) Studies on the closure of the secondary palate: V. Attempts to study the teratogenic action of cortisone in mice. *Acta Odontologica Scandinavica*. [Online] 20 (1), 1–13.

Laumonnier, F. et al. (2005) Mutations in PHF8 are associated with X linked mental retardation and cleft lip/cleft palate. *Journal of Medical Genetics*. [Online] 42 (10), 780. [online]. Available from: /pmc/articles/PMC1735927/?report=abstract (Accessed 23 July 2023).

Lazzaro, C. (1940) Sul meccanismo di chiusura del palato secondario. *Monit. zool. ital.* 51249–265. [online]. Available from: https://scholar.google.com/scholar_lookup?journal=Monit.+Zool.+Ital.&title=Sul+meccanismo+di+chiusura+del+palato+secondario&author=C.+Lazzaro&volume=51&publication_year=1940&pages=249-273&#d=gs_cit&t=1691269054213&u=%2Fscholar%3Fq%3Dinfo%3AbSX4gr0bp84J%3Ascholar.google.com%2F%26output%3Dcite%26scirp%3D0%26hl%3Den (Accessed 5 August 2023).

Lederer, D. et al. (2012) Deletion of KDM6A, a Histone Demethylase Interacting with MLL2, in Three Patients with Kabuki Syndrome. *American Journal of Human Genetics*. [Online] 90 (1), 119. [online]. Available from: /pmc/articles/PMC3257878/ (Accessed 23 July 2023).

Lei, K. et al. (2009) SUN1 and SUN2 play critical but partially redundant roles in anchoring nuclei in skeletal muscle cells in mice. *Proceedings of the National Academy of Sciences of the United States of America*. [Online] 106 (25), 10207. [online]. Available from: /pmc/articles/PMC2700906/ (Accessed 24 September 2023).

Leslie, E. J. & Marazita, M. L. (2013) Genetics of Cleft Lip and Cleft Palate. *American journal of medical genetics. Part C, Seminars in medical genetics*. [Online] 163 (4), 246. [online]. Available from: /pmc/articles/PMC3925974/ (Accessed 23 July 2023).

Lessard, J. L. et al. (1974) Presence of contractile proteins in mouse fetal palate prior to shelf elevation. *Teratology*. [Online] 9 (1), 113–125.

Leth Jensen, B. et al. (1988) Cleft lip and palate in Denmark, 1976-1981: epidemiology, variability, and early somatic development. *The Cleft Palate Journal*. 25 (3), 258–269. [online]. Available from: https://europepmc.org/article/med/3262457 (Accessed 23 July 2023).

Leung, C. et al. (2012) Atomic force microscopy with nanoscale cantilevers resolves different structural conformations of the DNA double helix. *Nano Letters*. [Online] 12 (7), 3846–3850. [online]. Available from: https://pubs.acs.org/doi/abs/10.1021/nl301857p (Accessed 28 September 2023).

Lewis, C. A. et al. (1980) An improved culture system for secondary palatal elevation. *In Vitro*. 16 (6), 453–460.

Lewis, P. N. et al. (2021) Contrast-enhanced tissue processing of fibrillin-rich elastic fibres for 3D visualization by volume scanning electron microscopy. *Methods and Protocols*. [Online] 4 (3), .

Li, C., Lan, Y., Krumlauf, R., et al. (2017) Modulating Wnt Signaling Rescues Palate Morphogenesis in Pax9 Mutant Mice. *https://doi.org/10.1177/0022034517719865*. [Online] 96 (11), 1273–1281. [online]. Available from: https://journals.sagepub.com/doi/10.1177/0022034517719865 (Accessed 29 August 2023).

Li, C., Lan, Y. & Jiang, R. (2017) Molecular and Cellular Mechanisms of Palate Development. *Journal of Dental Research*. [Online] 96 (11), 1184. [online]. Available from: /pmc/articles/PMC5613875/ (Accessed 2 June 2023).

Li, J. et al. (2020) Epithelial invagination by a vertical telescoping cell movement in mammalian salivary glands and teeth. *Nature Communications*. [Online] 11 (1), 1–9. [online]. Available from: http://dx.doi.org/10.1038/s41467-020-16247-z.

Li, Jingjing et al. (2016) Epithelial stratification and placode invagination are separable functions in early morphogenesis of the molar tooth. *Development*. [Online] 143 (4), 670–681.

Li, Jingtao et al. (2016) Linking suckling biomechanics to the development of the palate. *Scientific Reports*. [Online] 6 (August 2015), 1–9. [online]. Available from: http://dx.doi.org/10.1038/srep20419.

Li, Q. & Ding, J. (2007) Gene expression analysis reveals that formation of the mouse anterior secondary palate involves recruitment of cells from the posterior side. *The International journal of developmental biology*. [Online] 51 (2), 167–172. [online]. Available from: https://pubmed.ncbi.nlm.nih.gov/17294368/ (Accessed 2 August 2023).

Li, R. et al. (2021) The Fibroblast Growth Factor 9 (Fgf9) Participates in Palatogenesis by Promoting Palatal Growth and Elevation. *Frontiers in Physiology*. [Online] 12653040.

Li, X. et al. (2020) Tensile force-induced cytoskeletal remodeling: Mechanics before chemistry. *PLOS Computational Biology*. [Online] 16 (6), e1007693. [online]. Available from: https://journals.plos.org/ploscompbiol/article?id=10.1371/journal.pcbi.1007693 (Accessed 28 September 2023).

Liang, D. et al. (2014) Mesodermal expression of integrin α5β1 regulates neural crest development and cardiovascular morphogenesis. *Developmental biology*. [Online] 395 (2), 232–244. [online]. Available from: https://pubmed.ncbi.nlm.nih.gov/25242040/ (Accessed 30 August 2023).

Lin, C. et al. (2011) The inductive role of Wnt-β-Catenin signaling in the formation of oral apparatus. *Developmental Biology*. [Online] 356 (1), 40–50. [online]. Available from: http://dx.doi.org/10.1016/j.ydbio.2011.05.002.

Lipton, B. H. & Jacobson, A. G. (1974) Experimental analysis of the mechanisms of somite morphogenesis. *Developmental Biology*. [Online] 38 (1), 91–103.

Little, J. & Bryan, E. (1986) Congenital anomalies in twins. *Seminars in perinatology*. 10 (1), 50–64. [online]. Available from: https://pubmed.ncbi.nlm.nih.gov/3532342/ (Accessed 23 July 2023).

Liu, H.-X. et al. (2018) An Update on the Sense of Taste in Chickens: A Better Developed System than Previously Appreciated. *Journal of nutrition & food sciences*. [Online] 8 (2), . [online]. Available from: /pmc/articles/PMC5951165/ (Accessed 19 September 2023).

Liu, J. et al. (2021) Picrosirius-Polarization Method for Collagen Fiber Detection in Tendons: A Mini-Review. *Orthopaedic Surgery*. [Online] 13 (3), 701–707. [online]. Available from: https://onlinelibrary.wiley.com/doi/full/10.1111/os.12627 (Accessed 12 September 2023).

Liu, W. et al. (2008) The Mn1 transcription factor acts upstream of Tbx22 and preferentially regulates posterior palate growth in mice. *Development*. [Online] 135 (23), 3959–3968. [online]. Available from: https://dx.doi.org/10.1242/dev.025304 (Accessed 29 August 2023).

Liu, Y. et al. (2015) Gpr177-mediated Wnt signaling is required for secondary palate development. *Journal of Dental Research*. [Online] 94 (7), 961–967. [online]. Available from: https://journals.sagepub.com/doi/10.1177/0022034515583532 (Accessed 28 August 2023).

Loeys, B. L. et al. (2005) A syndrome of altered cardiovascular, craniofacial, neurocognitive and skeletal development caused by mutations in TGFBR1 or TGFBR2. *Nature genetics*. [Online] 37 (3), 275–281. [online]. Available from: https://pubmed.ncbi.nlm.nih.gov/15731757/ (Accessed 23 July 2023).

Long, K. R. et al. (2018) Extracellular Matrix Components HAPLN1, Lumican, and Collagen I Cause Hyaluronic Acid-Dependent Folding of the Developing Human Neocortex Correspondence. *Neuron*. [Online] 99702-719.e6. [online]. Available from: https://doi.org/10.1016/j.neuron.2018.07.013 (Accessed 15 September 2023).

López De Padilla, C. M. et al. (2021) Picrosirius Red Staining: Revisiting Its Application to the Qualitative and Quantitative Assessment of Collagen Type I and Type III in Tendon. *Journal of Histochemistry and Cytochemistry*. [Online] 69 (10), 633–643. [online]. Available from:

https://journals.sagepub.com/doi/10.1369/00221554211046777 (Accessed 12 September 2023).

Lough, K. J. et al. (2017a) Closing the Gap: Mouse Models to Study Adhesion in Secondary Palatogenesis. *Journal of Dental Research*. [Online] 96 (11), 1210–1220. [online]. Available from: https://journals.sagepub.com/doi/10.1177/0022034517726284 (Accessed 4 August 2023).

Lough, K. J. et al. (2017b) Closing the Gap: Mouse Models to Study Adhesion in Secondary Palatogenesis. *https://doi.org/10.1177/0022034517726284*. [Online] 96 (11), 1210–1220. [online]. Available from: https://journals.sagepub.com/doi/10.1177/0022034517726284 (Accessed 28 September 2023).

Ludwig, K. U. et al. (2012) Genome-wide meta-analyses of nonsyndromic cleft lip with or without cleft palate identify six new risk loci. *Nature genetics*. [Online] 44 (9), 968. [online]. Available from: /pmc/articles/PMC3598617/ (Accessed 23 July 2023).

Luke, D. A. (1984) Epithelial proliferation and development of rugae in relation to palatal shelf elevation in the mouse. *Journal of Anatomy*. 138 (Pt 2), 251. [online]. Available from: /pmc/articles/PMC1164065/?report=abstract (Accessed 26 August 2023).

Lynch, V. J. et al. (2015) Ancient transposable elements transformed the uterine regulatory landscape and transcriptome during the evolution of mammalian pregnancy. *Cell reports*. [Online] 10 (4), 551–561. [online]. Available from: https://pubmed.ncbi.nlm.nih.gov/25640180/ (Accessed 19 September 2023).

Machado, R. A. et al. (2019) Interactions between superoxide dismutase and paraoxonase polymorphic variants in nonsyndromic cleft lip with or without cleft palate in the Brazilian population. *Environmental and Molecular Mutagenesis*. [Online] 60 (2), 185–196. [online]. Available from: https://onlinelibrary.wiley.com/doi/full/10.1002/em.22239 (Accessed 23 July 2023).

Maier, W. et al. (1996) New therapsid specimens and the origin of the secondary hard and soft palate of mammals. *Journal of Zoological Systematics and Evolutionary Research*. [Online] 34 (1), 9–19.

Malde, O. et al. (2019) An Overview of Modelling Craniosynostosis Using the Finite Element Method. *Molecular Syndromology*. [Online] 10 (1–2), 74. [online]. Available from: /pmc/articles/PMC6422121/ (Accessed 8 September 2023).

Mao, Y. et al. (2013) Differential proliferation rates generate patterns of mechanical tension that orient tissue growth. *The EMBO Journal*. [Online] 32 (21), 2790–2803. [online]. Available from: https://onlinelibrary.wiley.com/doi/full/10.1038/emboj.2013.197 (Accessed 30 August 2023).

Marazita, M. L. et al. (1984) Genetic analysis of cleft lip with or without cleft palate in Danish kindreds. *American journal of medical genetics*. [Online] 19 (1), 9–18. [online]. Available from: https://pubmed.ncbi.nlm.nih.gov/6496575/ (Accessed 23 July 2023).

Marin-Riera, M. et al. (2018) Differential tissue growth and cell adhesion alone drive early tooth morphogenesis: An ex vivo and in silico study. *PLoS computational biology*. [Online] 14 (2), . [online]. Available from: https://pubmed.ncbi.nlm.nih.gov/29481561/ (Accessed 28 September 2023).

Martín-Del-Campo, M. et al. (2019) Biomaterials for Cleft Lip and Palate Regeneration. *International Journal of Molecular Sciences*. [Online] 20 (9), . [online]. Available from: /pmc/articles/PMC6540257/ (Accessed 22 July 2023).

Martínez-Sanz, E. et al. (2008) Alteration of medial-edge epithelium cell adhesion in two Tgf-β3 null mouse strains. *Differentiation; Research in Biological Diversity*. [Online] 76 (4), 417. [online]. Available from: /pmc/articles/PMC2346164/ (Accessed 29 September 2023).

Martinsen, B. J. (2005) Reference guide to the stages of chick heart embryology. *Developmental Dynamics*. [Online] 233 (4), 1217–1237. [online]. Available from: https://onlinelibrary.wiley.com/doi/full/10.1002/dvdy.20468 (Accessed 19 September 2023).

Matlin, K. S. et al. (2017) Laminins in Epithelial Cell Polarization: Old Questions in Search of New Answers. *Cold Spring Harbor Perspectives in Biology*. [Online] 9 (10), . [online]. Available from: /pmc/articles/PMC5629996/ (Accessed 28 September 2023).

Matsumura, K. et al. (2011) Sprouty2 controls proliferation of palate mesenchymal cells via fibroblast growth factor signaling. *Biochemical and Biophysical Research Communications*. [Online] 404 (4), 1076–1082.

Matsuo, K. & Palmer, J. B. (2008) Anatomy and Physiology of Feeding and Swallowing: Normal and Abnormal. *Physical Medicine and Rehabilitation Clinics of North America*. [Online] 19 (4), 691–707.

Matsuo, K. & Palmer, J. B. (2009) Coordination of mastication, swallowing and breathing. *Japanese Dental Science Review*. [Online] 45 (1), 31–40.

McCreery, K. P. et al. (2021) Nuclear stiffness decreases with disruption of the extracellular matrix in living tissues. *Small (Weinheim an der Bergstrasse, Germany)*. [Online] 17 (6), e2006699. [online]. Available from: /pmc/articles/PMC7891867/ (Accessed 28 September 2023).

McDonald-McGinn, D. M. et al. (2015) 22q11.2 deletion syndrome. *Nature reviews. Disease primers*. [Online] 115071. [online]. Available from: /pmc/articles/PMC4900471/ (Accessed 20 July 2023).

Mcgonnell, I. M. et al. (1998) Fate Map of the Developing Chick Face: Analysis of Expansion of Facial Primordia and Establishment of the Primary Palate. *Dev. Dyn*. [Online] 212102–118. [online]. Available from: https://onlinelibrary.wiley.com/terms-and-conditions (Accessed 30 July 2023).

McGrath, J. A. et al. (2001) Hay-Wells syndrome is caused by heterozygous missense mutations in the SAM domain of p63. *Human molecular genetics*. [Online] 10 (3), 221–229. [online]. Available from: https://pubmed.ncbi.nlm.nih.gov/11159940/ (Accessed 23 July 2023).

McKeown-Longo, P. J. & Higgins, P. J. (2021) Hyaluronan, Transforming Growth Factor β, and Extra Domain A-Fibronectin: A Fibrotic Triad. *Advances in Wound Care*. [Online] 10 (3), 137–152. [online]. Available from: https://www.liebertpub.com/doi/10.1089/wound.2020.1192 (Accessed 30 August 2023).

Milunsky, J. M. et al. (2008) TFAP2A Mutations Result in Branchio-Oculo-Facial Syndrome. *American Journal of Human Genetics*. [Online] 82 (5), 1171. [online]. Available from: /pmc/articles/PMC2427243/ (Accessed 23 July 2023).

Mitchell, K. et al. (2012) Exome Sequence Identifies RIPK4 as the Bartsocas- Papas Syndrome Locus. *American Journal of Human Genetics*. [Online] 90 (1), 69. [online]. Available from: /pmc/articles/PMC3257958/ (Accessed 23 July 2023).

Mitchell LE (2002) *Twin Studies in Oral Cleft Research - Cleft Lip & Palate: From Origin to Treatment*. 1st edition. Wyszyski DF (ed.). Oxford University Press. [online]. Available from: https://doctorlib.info/surgery/treatment/18.html (Accessed 23 July 2023).

Mitra, A. K. et al. (1983) Hyaluronic acid: Molecular conformation and interactions in the tetragonal form of the potassium salt containing extended chains. *Journal of Molecular Biology*. [Online] 169 (4), 813–827.

Molina-Solana, R. et al. (2013) Current concepts on the effect of environmental factors on cleft lip and palate. *International Journal of Oral and Maxillofacial Surgery*. [Online] 42 (2), 177–184. [online]. Available from: http://www.ijoms.com/article/S0901502712004213/fulltext (Accessed 23 July 2023).

Morgan, J. D. & Green, J. B. A. (2022) Methods of Palate Culture in Later Palatogenesis: Elevation, Horizontal Outgrowth, and Fusion. *Methods in molecular biology (Clifton, N.J.)*. [Online] 240363–80. [online]. Available from: https://pubmed.ncbi.nlm.nih.gov/34913117/ (Accessed 12 May 2023).

Morgan, N. V. et al. (2006) Mutations in the Embryonal Subunit of the Acetylcholine Receptor (CHRNG) Cause Lethal and Escobar Variants of Multiple Pterygium Syndrome. *American Journal of Human Genetics*. [Online] 79 (2), 390. [online]. Available from: /pmc/articles/PMC1559492/ (Accessed 23 July 2023).

Moriarty, T. M. et al. (1963) The Development in vitro and in vivo of Fusion of the Palatal Processes of Rat Embryos. *Development*. [Online] 11 (3), 605–619. [online]. Available from: https://journals.biologists.com/dev/article/11/3/605/36582/The-Development-in-vitro-and-in-vivo-of-Fusion-of (Accessed 21 May 2023).

Morris-Wiman, J. & Brinkley, L. (1992) An extracellular matrix infrastructure provides support for murine secondary palatal shelf remodelling. *The Anatomical Record*. [Online] 234 (4), 575–586.

Morris-Wiman, J. & Brinkley, L. (1993) Rapid changes in the extracellular matrix accompany in vitro palatal shelf remodelling. *Anatomy and Embryology*. [Online] 188 (1), 75–85.

Mossey, P. A. et al. (2009) Cleft lip and palate. *Lancet (London, England)*. [Online] 374 (9703), 1773–1785. [online]. Available from: https://pubmed.ncbi.nlm.nih.gov/19747722/ (Accessed 20 July 2023).

Mossey, P. A. & Modell, B. (2012) Epidemiology of oral clefts 2012: an international perspective. *Frontiers of oral biology*. [Online] 161–18. [online]. Available from: https://pubmed.ncbi.nlm.nih.gov/22759666/ (Accessed 20 July 2023).

Moxham, B. J. (2003) The development of the palate - a brief review. *European journal of anatomy*. 7 (1), 53–74. [online]. Available from: https://eurjanat.com/data/pdf/eja.03S10053.pdf (Accessed 18 September 2023).

Muenke, M. (2002) The pit, the cleft and the web. *Nature genetics*. [Online] 32 (2), 219–220. [online]. Available from: https://pubmed.ncbi.nlm.nih.gov/12355077/ (Accessed 22 July 2023).

Muiznieks, L. D. & Keeley, F. W. (2017) Biomechanical Design of Elastic Protein Biomaterials: A Balance of Protein Structure and Conformational Disorder. *ACS Biomaterials Science and Engineering*. [Online] 3 (5), 661–679. [online]. Available from: https://pubs.acs.org/doi/abs/10.1021/acsbiomaterials.6b00469 (Accessed 13 September 2023).

Murrell M., Oakes P. W., Lenz M., Gardel M. L. Forcing cells into shape: the mechanics of actomyosin contractility. Nat Rev Mol Cell Biol. 2015 Aug;16(8):486-98. doi: 10.1038/nrm4012. Epub 2015 Jul 1. PMID: 26130009; PMCID: PMC7443980.

Myers, G. S. et al. (1967) Cultivation of embryonic rat palate in defined and semi-defined media. *Archives of Oral Biology*. [Online] 12 (4), 565-IN31.

Nanda, R. (1970) The role of sulfated mucopolysaccharides in cleft palate production. *Teratology*. [Online] 3 (3), 237–244. [online]. Available from: https://onlinelibrary.wiley.com/doi/full/10.1002/tera.1420030305 (Accessed 29 August 2023).

Nekrasova, O. et al. (2018) Desmosomal cadherin association with Tctex-1 and cortactin-Arp2/3 drives perijunctional actin polymerization to promote keratinocyte delamination. *Nature Communications 2018 9:1*. [Online] 9 (1), 1–18. [online]. Available from: https://www.nature.com/articles/s41467-018-03414-6 (Accessed 4 August 2023).

Neptune, E. R. et al. (2003) Dysregulation of TGF-beta activation contributes to pathogenesis in Marfan syndrome. *Nature genetics*. [Online] 33 (3), 407–411. [online]. Available from: https://pubmed.ncbi.nlm.nih.gov/12598898/ (Accessed 30 August 2023).

New, D. A. (1967) Development of explanted rat embryos in circulating medium. *Development*. [Online] 17 (3), 513–525. [online]. Available from: https://journals.biologists.com/dev/article/17/3/513/49133/Development-of-explanted-rat-embryos-in (Accessed 21 May 2023).

New, D. A. T. (1967) Development of explanted rat embryos in circulating medium. *Embryol. exp. Morph*. 17513–538.

New, D. A. T. & Cockroft, D. L. (1979) A rotating bottle culture method with continuous replacement of the gas phase. *Experientia*. [Online] 35 (1), 138–140. [online]. Available from: https://link.springer.com/article/10.1007/BF01917926 (Accessed 20 May 2023).

New, D. A. T. & Daniel, J. C. (1969) Cultivation of Rat Embryos explanted at 7.5 to 8.5 Days of Gestation. *Nature 1969 223:5205*. [Online] 223 (5205), 515–516. [online]. Available from: https://www.nature.com/articles/223515a0 (Accessed 21 May 2023).

Ng, D. et al. (2004) Oculofaciocardiodental and Lenz microphthalmia syndromes result from distinct classes of mutations in BCOR. *Nature genetics*. [Online] 36 (4), 411–416. [online]. Available from: https://pubmed.ncbi.nlm.nih.gov/15004558/ (Accessed 23 July 2023).

Ng, S. B. et al. (2010) Exome sequencing identifies MLL2 mutations as a cause of Kabuki syndrome. *Nature genetics*. [Online] 42 (9), 790. [online]. Available from: /pmc/articles/PMC2930028/ (Accessed 23 July 2023).

Nguyen, Q. & Lee, S. W. (2018) Colorectal Segmentation Using Multiple Encoder-Decoder Network in Colonoscopy Images. *Proceedings - 2018 1st IEEE International Conference on Artificial Intelligence and Knowledge Engineering, AIKE 2018*. [Online] 208–211.

Niemann, S. et al. (2004) Homozygous WNT3 Mutation Causes Tetra-Amelia in a Large Consanguineous Family. *American Journal of Human Genetics*. [Online] 74 (3), 558. [online]. Available from: /pmc/articles/PMC1182269/ (Accessed 23 July 2023).

Niswander, L. et al. (1994) Function of FGF-4 in limb development. *Molecular Reproduction and Development*. [Online] 39 (1), 83–89.

Norman, M. D. A. et al. (2021) Measuring the elastic modulus of soft culture surfaces and three-dimensional hydrogels using atomic force microscopy. *Nature protocols*. [Online] 16 (5), 2418–2449. [online]. Available from: https://pubmed.ncbi.nlm.nih.gov/33854255/ (Accessed 3 September 2023).

Novacek, M. J. et al. (1997) Epipubic bones in eutherian mammals from the late Cretaceous of Mongolia. *Nature*. [Online] 389 (6650), 483–486. [online]. Available from: https://pubmed.ncbi.nlm.nih.gov/9333234/ (Accessed 19 September 2023).

Oh, W. J. et al. (2010a) Cleft Palate Is Caused by CNS Dysfunction in Gad1 and Viaat Knockout Mice. *PLOS ONE*. [Online] 5 (3), e9758. [online]. Available from: https://journals.plos.org/plosone/article?id=10.1371/journal.pone.0009758 (Accessed 21 May 2023).

Oh, W. J. et al. (2010b) Cleft Palate Is Caused by CNS Dysfunction in Gad1 and Viaat Knockout Mice. *PLoS ONE*. [Online] 5 (3), 1–10.

Ohsaki, Y. et al. (1995) Localization of Types I and III Collagen and Fibronectin in the Developing Mouse Palatal Shelves. *Acta Anatomica*. [Online] 153 (3), 161–167. [online]. Available from: https://dx.doi.org/10.1159/000147696 (Accessed 30 August 2023).

Oka, K. et al. (2012) Roles of collagen and periostin expression by cranial neural crest cells during soft palate development. *The journal of histochemistry and cytochemistry : official journal of the Histochemistry Society*. [Online] 60 (1), 57–68. [online]. Available from: https://pubmed.ncbi.nlm.nih.gov/22205681/ (Accessed 30 August 2023).

Oppenheimer, J. M. (1959) Embryology and Evolution: Nineteenth Century Hopes and Twentieth Century Realities. *The Quarterly Review of Biology*. [Online] 34 (4), 271–277. [online]. Available from: https://www.journals.uchicago.edu/doi/10.1086/402827 (Accessed 22 September 2023).

Orban, B. (1972) 'Orban's oral histology and embryology', in *Annual session of thr American Dental Association*. pp. 1004–1016.

Osoegawa, K. et al. (2008) Identification of novel candidate genes associated with cleft lip and palate using array comparative genomic hybridization. *Journal of medical genetics*. [Online] 45 (2), 81. [online]. Available from: /pmc/articles/PMC3732463/ (Accessed 23 July 2023).

Paci, G. & Mao, Y. (2021) Forced into shape: Mechanical forces in Drosophila development and homeostasis. *Seminars in Cell & Developmental Biology*. [Online] 120160–170.

Packham, E. A. & Brook, J. D. (2003) T-box genes in human disorders. *Human molecular genetics*. [Online] 12 Spec No 1 (REV. ISS. 1), . [online]. Available from: https://pubmed.ncbi.nlm.nih.gov/12668595/ (Accessed 23 July 2023).

Page, R. D. M. & Holmes, E. C. (1998) *Molecular Evolution: A Phylogenetic Approach*. Oxford: Blackwell Publishing Ltd. [online]. Available from: www.blackwell-science.com (Accessed 22 September 2023).

Paiva, K. B. S. et al. (2019) Extracellular Matrix Composition and Remodeling: Current Perspectives on Secondary Palate Formation, Cleft Lip/Palate, and Palatal Reconstruction. *Frontiers in Cell and Developmental Biology*. [Online] 7457025.

Panousopoulou, E. & Green, J. B. A. (2016) Invagination of Ectodermal Placodes Is Driven by Cell Intercalation-Mediated Contraction of the Suprabasal Tissue Canopy. *PLoS Biology*. [Online] 14 (3), 1–15.

Pantalacci, S. et al. (2009) Heterochronic shifts explain variations in a sequentially developing repeated pattern: Palatal ridges of muroid rodents. *Evolution and Development*. [Online] 11 (4), 422–433.

Pantalacci, S. et al. (2008) Patterning of palatal rugae through sequential addition reveals an anterior/posterior boundary in palatal development. *BMC Developmental Biology*. [Online] 81–17.

Parada, C. et al. (2015) Disruption of the ERK/MAPK pathway in neural crest cells as a potential cause of pierre Robin sequence. *Development (Cambridge)*. [Online] 142 (21), 3734–3745. [online]. Available from: /pmc/articles/PMC4647211/ (Accessed 5 June 2023).

Parada, C. & Chai, Y. (2015) Mandible and Tongue Development. *Current topics in developmental biology*. [Online] 11531. [online]. Available from: /pmc/articles/PMC4869709/ (Accessed 1 June 2023).

Pascual, R. et al. (2002) New data on the Paleocene monotreme Monotrematum sudamericanum, and the convergent evolution of triangulate molars. *Acta Palaeontologica Polonica*. 47 (3), 487–492. [online]. Available from: http://www.paleo.pan.pl/acta/acta47/app47 (Accessed 22 September 2023).

Paten, J. A. et al. (2019) Molecular Interactions between Collagen and Fibronectin: A Reciprocal Relationship that Regulates De Novo Fibrillogenesis. *Chem*. [Online] 5 (8), 2126–2145. [online]. Available from: http://www.cell.com/article/S2451929419302219/fulltext (Accessed 30 August 2023).

Pearn, J. H. (1967) *An experimental study of the embryopathogenic effects of indospicine with particular reference to the production of cleft palate*. Queensland: University of Queensland.

Peter, K. (1924) Die entwicklung des Säugetiergaumens. *Ergebn. Anat. EntwGesch*. 25448–564. [online]. Available from: https://scholar.google.com/scholar_lookup?title=Die%20Entwicklung%20des%20Saugetiergaumens&author=K.%20Peter&publication_year=1924&journal=Ergebn.%20Anat.%20EntwGesch&volume=25&pages=448-564 (Accessed 5 August 2023).

Peterka, M. et al. (2002) Body weight in mouse embryos specifies staging of tooth development. *Connective tissue research*. [Online] 43 (2–3), 186–190. [online]. Available from: https://pubmed.ncbi.nlm.nih.gov/12489157/ (Accessed 29 September 2023).

Petridou, N. I. & Heisenberg, C.-P. (2019) Tissue rheology in embryonic organization. *The EMBO Journal*. [Online] 38 (20), e102497. [online]. Available from: https://onlinelibrary.wiley.com/doi/full/10.15252/embj.2019102497 (Accessed 28 September 2023).

Phillips, M. J. et al. (2009) Molecules, morphology, and ecology indicate a recent, amphibious ancestry for echidnas. *Proceedings of the National Academy of Sciences of the United States of America*. [Online] 106 (40), 17089–17094. [online]. Available from: https://www.pnas.org/doi/abs/10.1073/pnas.0904649106 (Accessed 22 September 2023).

Polzl, A. (1905) Zur Entwicklungsgechichte des menchlichen Gaumens. *Anatomische Hefte*. Bd. 27245–281. [online]. Available from: http://www.biodiversitylibrary.org/item/28445.

Pons-Tortella, E. (1937) Über die Bildungsweise des sekundären Gaumens. *Anat. Anz*. 8413–17. [online]. Available from: https://scholar.google.com/scholar_lookup?title=%C3%9Cber%20die%20Bildungsweise%20des%20sekundaren%20Gaumens&author=E.%20Pons-Tortella&publication_year=1937&journal=Anat.%20Anz&volume=84&pages=13-17#d=gs_cit&t=1691271708793&u=%2Fscholar%3Fq%3Dinfo%3AopRSmNs-HVoJ%3Ascholar.google.com%2F%26output%3Dcite%26scirp%3D0%26hl%3Den (Accessed 5 August 2023).

Poswillo, D. E. (1968) Cleft Palate in the Rat. *Laboratory Animals*. [Online] 2 (2), 181–190.

Poswillo, D. & Roy, L. J. (1965) The pathogenesis of cleft palate. An animal study. *The British journal of surgery*. [Online] 52 (11), 902–913. [online]. Available from: https://pubmed.ncbi.nlm.nih.gov/5842981/ (Accessed 5 August 2023).

Pourtois, M. (1972) 'Morphogenesis of the Primary and Secondary Palate', in *Developmental Aspects of Oral Biology*. [Online]. Academic Press, Inc. pp. 81–108. [online]. Available from: http://dx.doi.org/10.1016/B978-0-12-648350-5.50010-3.

Pourtois, M. (1966) Onset of the acquired potentiality for fusion in the palatal shelves of rats. *Development*. [Online] 16 (1), 171–182. [online]. Available from: https://journals.biologists.com/dev/article/16/1/171/49100/Onset-of-the-acquired-potentiality-for-fusion-in (Accessed 21 May 2023).

Pratt, R. M. et al. (1973) Acid mucopolysaccharide synthesis in the secondary palate of the developing rat at the time of rotation and fusion. *Developmental Biology*. [Online] 32 (1), 230–237.

Prevedel, R. et al. (2019) *Brillouin microscopy - a revolutionary tool for mechanobiology?* [online]. Available from: https://arxiv.org/abs/1901.02006v1 (Accessed 28 September 2023).

Puhó, E. H. et al. (2007) Drug Treatment during Pregnancy and Isolated Orofacial Clefts in Hungary. *https://doi.org/10.1597/05-208.1*. [Online] 44 (2), 194–202. [online]. Available from: https://journals.sagepub.com/doi/10.1597/05-208.1 (Accessed 23 July 2023).

Püspöki, Z. et al. (2016) Transforms and operators for directional bioimage analysis: A survey. *Advances in Anatomy Embryology and Cell Biology*. [Online] 21969–93.

Qu, R. et al. (2017) Using Delaunay triangulation and Voronoi tessellation to predict the toxicities of binary mixtures containing hormetic compound. *Scientific Reports 2017 7:1*. [Online] 7 (1), 1–10. [online]. Available from: https://www.nature.com/articles/srep43473 (Accessed 11 September 2023).

Quaderi, N. A. et al. (1997) Opitz G/BBB syndrome, a defect of midline development, is due to mutations in a new RING finger gene on Xp22. *Nature genetics*. [Online] 17 (3), 285–291. [online]. Available from: https://pubmed.ncbi.nlm.nih.gov/9354791/ (Accessed 23 July 2023).

Rahimov, F. et al. (2008) Disruption of an AP-2α binding site in an IRF6 enhancer is strongly associated with cleft lip. *Nature genetics*. [Online] 40 (11), 1341. [online]. Available from: /pmc/articles/PMC2691688/ (Accessed 23 July 2023).

Rajapaksha, P. et al. (2016) Labeling and analysis of chicken taste buds using molecular markers in oral epithelial sheets. *Scientific Reports*. [Online] 6. [online]. Available from: /pmc/articles/PMC5112566/ (Accessed 19 September 2023).

Reardon, W. et al. (1994) Mutations in the fibroblast growth factor receptor 2 gene cause Crouzon syndrome. *Nature genetics*. [Online] 8 (1), 98–103. [online]. Available from: https://pubmed.ncbi.nlm.nih.gov/7987400/ (Accessed 23 July 2023).

Redhead, Y. et al. (2023) Craniofacial dysmorphology in Down syndrome is caused by increased dosage of Dyrk1a and at least three other genes. *Development (Cambridge, England)*. [Online] 150 (8), . [online]. Available from: https://pubmed.ncbi.nlm.nih.gov/37102702/ (Accessed 31 May 2023).

Reeve, W. L. et al. (1966) In vitro closure of the rat palate. *Journal of dental research*. [Online] 45 (5), 1375–1380. [online]. Available from: https://pubmed.ncbi.nlm.nih.gov/5225493/ (Accessed 21 May 2023).

Renfree, M. B. (2010) Review: Marsupials: Placental Mammals with a Difference. *Placenta*. [Online] 31 (SUPPL.), S21–S26.

Rew, C. (1757) Sistens plura exempla palati deficientis. *Nova acta physico-medica academiae caesarae Leopoldion-Carolinae*. 1 (1), 445–447. [online]. Available from: https://scholar.google.com/scholar_lookup?journal=Leopoldion-Carolinae&title=Sistens+plura+exempla+palati+deficientis.+Nova+Acta+Physico-

Medica+Academiae+caesarae&author=CJ+Trew&volume=1&publication_year=1757&pages=445-447& (Accessed 23 July 2023).

Rice, R. et al. (2004) Disruption of Fgf10/Fgfr2b-coordinated epithelial-mesenchymal interactions causes cleft palate. *The Journal of Clinical Investigation*. [Online] 113 (12), 1692–1700. [online]. Available from: http://www.jci.org (Accessed 2 August 2023).

Richardson, M. K. & Keuck, G. (2002) Haeckel's ABC of evolution and development. *Biological reviews of the Cambridge Philosophical Society*. [Online] 77 (4), 495–528. [online]. Available from: https://pubmed.ncbi.nlm.nih.gov/12475051/ (Accessed 22 September 2023).

Richardson, R. J. et al. (2009) Integration of IRF6 and Jagged2 signalling is essential for controlling palatal adhesion and fusion competence. *Human Molecular Genetics*. [Online] 18 (14), 2632. [online]. Available from: /pmc/articles/PMC2701335/ (Accessed 4 August 2023).

Rismiller, P. D. & Grutzner, F. (2019) Tachyglossus aculeatus (Monotremata: Tachyglossidae). *Mammalian Species*. [Online] 51 (980), 75–91. [online]. Available from: https://dx.doi.org/10.1093/mspecies/sez012 (Accessed 16 September 2023).

Rismiller, P. & Seymour, R. (1991) The Echidna. *Scientific American*. 264 (2), 96–103. [online]. Available from: https://www.jstor.org/stable/pdf/24936795.pdf?refreqid=excelsior%3A2f04412d52d0a1378c6dbec12c41b945&ab_segments=&origin=&initiator=&acceptTC=1 (Accessed 17 September 2023).

Rittié, L. (2017) Method for Picrosirius Red-Polarization Detection of Collagen Fibers in Tissue Sections. *Methods in molecular biology (Clifton, N.J.)*. [Online] 1627395–407. [online]. Available from: https://pubmed.ncbi.nlm.nih.gov/28836216/ (Accessed 12 September 2023).

Robertson, S. P. et al. (2003) Localized mutations in the gene encoding the cytoskeletal protein filamin A cause diverse malformations in humans. *Nature genetics*. [Online] 33 (4), 487–491. [online]. Available from: https://pubmed.ncbi.nlm.nih.gov/12612583/ (Accessed 23 July 2023).

Robkin, M. A. et al. (1972) A new in vitro culture technique for rat embryos. *Teratology*. [Online] 5 (3), 367–376. [online]. Available from:

https://onlinelibrary.wiley.com/doi/full/10.1002/tera.1420050312 (Accessed 21 May 2023).

Roessler, E. et al. (2003) Loss-of-function mutations in the human GLI2 gene are associated with pituitary anomalies and holoprosencephaly-like features. *Proceedings of the National Academy of Sciences of the United States of America*. [Online] 100 (23), 13424. [online]. Available from: /pmc/articles/PMC263830/ (Accessed 23 July 2023).

Roessler, E. et al. (1996) Mutations in the human Sonic Hedgehog gene cause holoprosencephaly. *Nature genetics*. [Online] 14 (3), 357–360. [online]. Available from: https://pubmed.ncbi.nlm.nih.gov/8896572/ (Accessed 23 July 2023).

Ross, R. B. et al. (1965) The Cervical Vertebrae as a Factor in the Etiology of Cleft Palate. *The Cleft Palate Journal*. 2 (3), 273–281. [online]. Available from: https://cleftpalatejournal.pitt.edu/ojs/cleftpalate/article/view/81 (Accessed 7 August 2023).

Ruest, L. B. et al. (2003) dHAND-Cre transgenic mice reveal specific potential functions of dHAND during craniofacial development. *Developmental biology*. [Online] 257 (2), 263. [online]. Available from: /pmc/articles/PMC2830752/ (Accessed 21 September 2023).

Sabatier, L. et al. (2009) Fibrillin Assembly Requires Fibronectin. *Molecular Biology of the Cell*. [Online] 20 (3), 846. [online]. Available from: /pmc/articles/PMC2633374/ (Accessed 30 August 2023).

Saint-Hilaire, É. G. (1803) Extrait des observations anatomiques de M Home, sur l'echidne. *Bulletin de la Société philomathique de Paris*. 3125–127.

Sakai, T. et al. (2003) Fibronectin requirement in branching morphogenesis. *Nature*. [Online] 423 (6942), 876–881. [online]. Available from: https://pubmed.ncbi.nlm.nih.gov/12815434/ (Accessed 30 August 2023).

Sánchez-Peralta, L. F. et al. (2020) Deep learning to find colorectal polyps in colonoscopy: A systematic literature review. *Artificial Intelligence in Medicine*. [Online] 108101923.

Salbreux G., Charras G., Paluch E. Actin cortex mechanics and cellular morphogenesis. Trends Cell Biol. 2012 Oct;22(10):536-45. doi: 10.1016/j.tcb.2012.07.001. Epub 2012 Aug 4. PMID: 22871642.

Sandell, L. L. et al. (2007) RDH10 is essential for synthesis of embryonic retinoic acid and is required for limb, craniofacial, and organ development. *Genes & development*. [Online] 21 (9), 1113–1124. [online]. Available from: https://pubmed.ncbi.nlm.nih.gov/17473173/ (Accessed 7 August 2023).

Sandell, L. L. et al. (2012) RDH10 oxidation of vitamin A is a critical control step in synthesis of retinoic acid during mouse embryogenesis. *PLoS ONE*. [Online] 7 (2), .

Santa-Cruz Mateos C., Valencia-Expósito A., Palacios I. M., Martín-Bermudo M. D. Integrins regulate epithelial cell shape by controlling the architecture and mechanical properties of basal actomyosin networks. PLoS Genet. 2020 Jun 1;16(6):e1008717. doi: 10.1371/journal.pgen.1008717. PMID: 32479493; PMCID: PMC7263567.

Schindelin, J. et al. (2012) Fiji: an open-source platform for biological-image analysis. *Nature Methods 2012 9:7*. [Online] 9 (7), 676–682. [online]. Available from: https://www.nature.com/articles/nmeth.2019 (Accessed 16 September 2023).

Schmidt, U. et al. (2018) Cell Detection with Star-convex Polygons. *Lecture Notes in Computer Science (including subseries Lecture Notes in Artificial Intelligence and Lecture Notes in Bioinformatics)*. [Online] 11071 LNCS265–273. [online]. Available from: https://arxiv.org/abs/1806.03535v2 (Accessed 7 September 2023).

Schorr, G. (1908) Zur Entwickelungsgeschichte des Sekundären gaumens bei Einigen Säugetieren und beim Menschen. *Beiträge und Referate zur Anatomie und Entwickelungsgeschichte*. [Online] 36 (1), 69–106. [online]. Available from: https://link.springer.com/article/10.1007/BF02214280 (Accessed 6 August 2023).

Schötz, E. M. et al. (2013) Glassy dynamics in three-dimensional embryonic tissues. *Journal of the Royal Society, Interface*. [Online] 10 (89), . [online]. Available from: https://pubmed.ncbi.nlm.nih.gov/24068179/ (Accessed 28 September 2023).

Schreiner, C. M. et al. (1986) Caffeine effects on cyclic AMP levels in the mouse embryonic limb and palate in vitro. *Teratology*. [Online] 34 (1), 21–27.

Schuler, R. E. et al. (2022) FaceBase: A Community-Driven Hub for Data-Intensive Research. *Journal of Dental Research*. [Online] 101 (11), 1289–1298.

Segnani, C. et al. (2015) Histochemical Detection of Collagen Fibers by Sirius Red/Fast Green Is More Sensitive than van Gieson or Sirius Red Alone in Normal and Inflamed

Rat Colon. *PLoS ONE*. [Online] 10 (12), . [online]. Available from: /pmc/articles/PMC4682672/ (Accessed 12 September 2023).

Selleck, M. A. J. & Stern, C. D. (1991) Fate mapping and cell lineage analysis of Hensen's node in the chick embryo. *Development (Cambridge, England)*. [Online] 112 (2), 615–626. [online]. Available from: https://pubmed.ncbi.nlm.nih.gov/1794328/ (Accessed 12 May 2023).

Serwane, F. et al. (2017) In vivo quantification of spatially-varying mechanical properties in developing tissues. *Nature methods*. [Online] 14 (2), 181. [online]. Available from: /pmc/articles/PMC5524219/ (Accessed 30 September 2023).

Sevilla, C. A. et al. (2013) Regional fibronectin and collagen fibril co-assembly directs cell proliferation and microtissue morphology. *PloS one*. [Online] 8 (10), . [online]. Available from: https://pubmed.ncbi.nlm.nih.gov/24116223/ (Accessed 16 September 2023).

Seydel, O. (1899) Der Eizahn von Echidna. Seine Entwicklung und sein Bau. . *Denkschriften der Medicinish-Naturwissenschaftlichen Gesellschaft zu Jena*. 6519–532.

Shah, R. M. et al. (1988) Embryogenesis of the Secondary Palate in Pigeons. *Poultry Sciences*. 67865–870.

Shah, R. M. et al. (1989) Growth of the secondary palate in the hamster following hydrocortisone treatment: shelf area, cell number, and DNA synthesis. *Teratology*. [Online] 40 (2), 173–180. [online]. Available from: https://pubmed.ncbi.nlm.nih.gov/2772852/ (Accessed 11 September 2023).

Sharman, G. B. (1973) Adaptations of Marsupial Pouch Young for Extra-uterine Existence. *The Mammalian Fetus in vitro*. [Online] 67–90. [online]. Available from: https://link.springer.com/chapter/10.1007/978-1-4899-7212-5_3 (Accessed 19 September 2023).

Shaw, G. (1792) The Spiny Ant Eater. *The Naturalist's Miscelany*. 3 (36), 108–112.

Shibui, S. et al. (1989) Double labeling with iodo- and bromodeoxyuridine for cell kinetics studies. *The journal of histochemistry and cytochemistry : official journal of the Histochemistry Society*. [Online] 37 (7), 1007–1011. [online]. Available from: https://pubmed.ncbi.nlm.nih.gov/2659659/ (Accessed 28 September 2023).

Shiota, K. et al. (1990) Development of the fetal mouse palate in suspension organ culture. *Acta Anatomica*. [Online] 137 (1), 59–64.

Shkoukani, M. A. et al. (2013) Cleft Lip – A Comprehensive Review. *Frontiers in Pediatrics*. [Online] 1 (DEC), . [online]. Available from: /pmc/articles/PMC3873527/ (Accessed 22 July 2023).

Sicher, H. (1915) Die Entwickelung des sekundaeren Gaumens beim Menchen. . *Anal. Anz.* 47513–562. [online]. Available from: https://www.academia.edu/18878110/Spatial_relations_in_the_oral_cavity_and_the_mechanism_of_secondary_palate_closure_in_the_rat (Accessed 6 August 2023).

Sicher, M. (1966) *Orban's oral histology and embryology*. 6th edition. St. Louis: . [online]. Available from: https://www.google.com/search?client=safari&rls=en&q=Sicher%2C+M.+(1966)+Orban%27s+oral+histology+and+embryology%2C+6th+edn%2C+Ch.+I%2C+St+Louis%3A+C.+V.+Mosby+Co.&ie=UTF-8&oe=UTF-8 (Accessed 6 August 2023).

Silva, D. F. T. et al. (2013) Birefringence and second harmonic generation on tendon collagen following red linearly polarized laser irradiation. *Annals of Biomedical Engineering*. [Online] 41 (4), 752–762. [online]. Available from: https://link.springer.com/article/10.1007/s10439-012-0720-3 (Accessed 13 September 2023).

Silver, M. H. et al. (1981) Distribution of fibronectin and collagen during mouse limb and palate development. *Differentiation; research in biological diversity*. [Online] 18 (3), 141–149. [online]. Available from: https://pubmed.ncbi.nlm.nih.gov/7035260/ (Accessed 4 August 2023).

Sivertsen, Å. et al. (2008) Familial risk of oral clefts by morphological type and severity: population based cohort study of first degree relatives. *BMJ : British Medical Journal*. [Online] 336 (7641), 432. [online]. Available from: /pmc/articles/PMC2249683/ (Accessed 23 July 2023).

Smith, K. K. (2006a) Craniofacial development in marsupial mammals: Developmental origins of evolutionary change. *Developmental Dynamics*. [Online] 235 (5), 1181–1193. [online]. Available from: https://onlinelibrary.wiley.com/doi/full/10.1002/dvdy.20676 (Accessed 4 September 2023).

Smith, K. K. (2006b) Craniofacial development in marsupial mammals: Developmental origins of evolutionary change. *Developmental Dynamics*. [Online] 235 (5), 1181–1193. [online]. Available from: https://onlinelibrary.wiley.com/doi/full/10.1002/dvdy.20676 (Accessed 18 September 2023).

Snead, M. P. & Yates, J. R. W. (1999) Clinical and molecular genetics of Stickler syndrome. *Journal of Medical Genetics*. [Online] 36 (5), 353. [online]. Available from: /pmc/articles/PMC1734362/?report=abstract (Accessed 23 July 2023).

Snyder-Warwick, A. K. et al. (2010) Analysis of a gain-of-function FGFR2 Crouzon mutation provides evidence of loss of function activity in the etiology of cleft palate. *Proceedings of the National Academy of Sciences of the United States of America*. [Online] 107 (6), 2515–2520. [online]. Available from: https://www.pnas.org/doi/abs/10.1073/pnas.0913985107 (Accessed 15 May 2023).

Sperber, G. H. (2002) 'Palatogenesis: Closure of the Secondary Palate ', in Diego F. Wyszynski (ed.) *Cleft Lip & Palate: From Origin to Treatment*. 1st edition Oxford, UK: Oxford University Press. p. [online]. Available from: https://doctorlib.info/surgery/treatment/3.html (Accessed 20 September 2023).

Sproule, J. (1863) Hereditary Nature of Hare-Lip. *British Medical Journal*. 1 (120), 412. [online]. Available from: https://www.ncbi.nlm.nih.gov/pmc/articles/PMC2324860/ (Accessed 23 July 2023).

Stanier, P. & Moore, G. E. (2004) Genetics of cleft lip and palate: syndromic genes contribute to the incidence of non-syndromic clefts. *Human molecular genetics*. [Online] 13 Spec No 1 (REV. ISS. 1), . [online]. Available from: https://pubmed.ncbi.nlm.nih.gov/14722155/ (Accessed 20 July 2023).

Suazo, J. (2022) Environmental factors in non-syndromic orofacial clefts: A review based on meta-analyses results. *Oral Diseases*. [Online] 28 (1), 3–8.

Sullivan, S. R. et al. (2009) Palatoplasty outcomes in nonsyndromic patients with cleft palate: a 29-year assessment of one surgeon's experience. *The Journal of craniofacial surgery*. [Online] 20 Suppl 1 (SUPPL. 1), 612–616. [online]. Available from: https://pubmed.ncbi.nlm.nih.gov/19169156/ (Accessed 22 July 2023).

Suzanne, M. & Steller, H. (2013) Shaping organisms with apoptosis. *Cell Death and Differentiation*. [Online] 20 (5), 669–675.

Suzuki, A. et al. (2018) Gene datasets associated with mouse cleft palate. *Data in Brief*. [Online] 18655–673.

Suzuki, K. et al. (2000) Mutations of PVRL1, encoding a cell-cell adhesion molecule/herpesvirus receptor, in cleft lip/palate-ectodermal dysplasia. *Nature genetics*. [Online] 25 (4), 427–430. [online]. Available from: https://pubmed.ncbi.nlm.nih.gov/10932188/ (Accessed 23 July 2023).

Sweney, L. R. & Shapiro, B. L. (1970) Histogenesis of Swiss white mouse secondary palate from nine and one-half days to fifteen and one-half days in utero. I. Epithelial-mesenchymal relationships--light and electron microscopy. *Journal of morphology*. [Online] 130 (4), 435–449. [online]. Available from: https://pubmed.ncbi.nlm.nih.gov/4245153/ (Accessed 10 September 2023).

Szabo-Rogers, H. L. et al. (2010) New directions in craniofacial morphogenesis. *Developmental Biology*. [Online] 341 (1), 84–94.

Takahara, S. et al. (2004) Programmed cell death is not a necessary prerequisite for fusion of the fetal mouse palate. *The International Journal of Developmental Biology*. [Online] 48 (1), 39–46. [online]. Available from: https://ijdb.ehu.eus/article/15005573 (Accessed 21 May 2023).

Takahashi, M. et al. (2008) Transferring genes into cultured mammalian embryos by electroporation. *Development, Growth & Differentiation*. [Online] 50 (6), 485–497. [online]. Available from: https://onlinelibrary.wiley.com/doi/full/10.1111/j.1440-169X.2008.01046.x (Accessed 20 May 2023).

Takahashi, M. & Osumi, N. (2010) The Method of Rodent Whole Embryo Culture using the Rotator-type Bottle Culture System. *Journal of Visualized Experiments : JoVE*. [Online] 42 (42), . [online]. Available from: /pmc/articles/PMC3156024/ (Accessed 20 May 2023).

Tandler, J. (1899) Zur Entwicklungsgeschichte des Uranoschisma. *Wiener klin. Wochenschr*. 12153–156. [online]. Available from: https://espace.library.uq.edu.au/data/UQ_360971/THE1387_V1.pdf?Expires=1691367525&Key-Pair-Id=APKAJKNBJ4MJBJNC6NLQ&Signature=OE0mRmWLstVGJyw8033E3bWuagXfW4J

NmwmQRXgpMOyCNknbXmSIiS-eYZ~PvshTwfN42NnHePdIxvYP2YfuVdgjmskrznevxrvMTsGe97NrOrVElzefHTVA5B9EiXszxPFhY5BGJ2Tg7aneZNZaoVgLhQXlr8wBWthc6Tjq~eRmuPsPcZXG9WR9MqQmFZC3ImPTXqCzXxJ2yr0xhVJDvWIslV41a6agg2lL3Fzo1-T~8OjeuN9zXL4pYGUbNd~g96W7eDwcVWoiTs8FG7MBAaIxElqnzX-iMFhEuu1XbF-kfZDYJlDfH6ya1m4DfvjR2hHBKnaFZwI4EcDBYWd4aw__ (Accessed 6 August 2023).

Tang, Q. et al. (2016) Novel insights into a retinoic-acid-induced cleft palate based on Rac1 regulation of the fibronectin arrangement. *Cell and Tissue Research*. [Online] 363 (3), 713–722. [online]. Available from: https://link.springer.com/article/10.1007/s00441-015-2271-z (Accessed 30 August 2023).

Tang, Q. et al. (2015) Role of region-distinctive expression of Rac1 in regulating fibronectin arrangement during palatal shelf elevation. *Cell and Tissue Research*. [Online] 361 (3), 857–868. [online]. Available from: https://link.springer.com/article/10.1007/s00441-015-2169-9 (Accessed 30 August 2023).

Tarnowski, B. I. et al. (1991) DAPI as a Useful Stain for Nuclear Quantitation. *Biotechnic & Histochemistry*. [Online] 66 (6), 296–302. [online]. Available from: https://www.tandfonline.com/doi/abs/10.3109/10520299109109990 (Accessed 24 September 2023).

Taylor, R. G. & Harris, J. W. S. (1973) Growth and spatial relationships of the cranial base and lower jaw during closure of the secondary palate in the hamster. *Journal of Anatomy*. 115149–150.

Teng, T. et al. (2022) A unique form of collective epithelial migration is crucial for tissue fusion in the secondary palate and can overcome loss of epithelial apoptosis. *Development (Cambridge)*. [Online] 149 (10), . [online]. Available from: /pmc/articles/PMC9188751/ (Accessed 4 August 2023).

Tessier, P. (1976) Anatomical classification facial, cranio-facial and latero-facial clefts. *Journal of maxillofacial surgery*. [Online] 4 (2), 69–92. [online]. Available from: https://pubmed.ncbi.nlm.nih.gov/820824/ (Accessed 20 July 2023).

Theveneau, E. & Mayor, R. (2011) Can mesenchymal cells undergo collective cell migration?: The case of the neural crest. *Cell Adhesion & Migration*. [Online] 5 (6),

490. [online]. Available from: /pmc/articles/PMC3277782/ (Accessed 25 September 2023).

Thompson, J. F. & Schweisthal, M. R. (1969) Study of Closure of the Embryonic Rat Palate In Vitro with the Effects of Certain Chemicals. *http://dx.doi.org/10.1177/00220345690480041201*. [Online] 48 (4), 568–572. [online]. Available from: https://journals.sagepub.com/doi/10.1177/00220345690480041201 (Accessed 21 May 2023).

Tien, J. Y. L. & Spicer, A. P. (2005) Three vertebrate hyaluronan synthases are expressed during mouse development in distinct spatial and temporal patterns. *Developmental dynamics : an official publication of the American Association of Anatomists*. [Online] 233 (1), 130–141. [online]. Available from: https://pubmed.ncbi.nlm.nih.gov/15765504/ (Accessed 30 August 2023).

Timin, G. & Milinkovitch, M. C. (2023) High-resolution confocal and light-sheet imaging of collagen 3D network architecture in very large samples. *iScience*. [Online] 26 (4), 106452.

Tonkin, E. T. et al. (2004) NIPBL, encoding a homolog of fungal Scc2-type sister chromatid cohesion proteins and fly Nipped-B, is mutated in Cornelia de Lange syndrome. *Nature genetics*. [Online] 36 (6), 636–641. [online]. Available from: https://pubmed.ncbi.nlm.nih.gov/15146185/ (Accessed 23 July 2023).

Toole, B. P. et al. (1972) *Hyaluronate in Morphogenesis: Inhibition of Chondrogenesis In Vitro (chick somites/chick limb buds/cartilage nodule formation)*. 69 (6), 1384–1386. [online]. Available from: https://www.pnas.org (Accessed 29 August 2023).

Toussaint, N. et al. (2021) A landmark-free morphometrics pipeline for high-resolution phenotyping: application to a mouse model of Down syndrome. *Development (Cambridge, England)*. [Online] 148 (18), . [online]. Available from: https://pubmed.ncbi.nlm.nih.gov/33712441/ (Accessed 31 May 2023).

Tozluoğlu, M. et al. (2019) Planar Differential Growth Rates Initiate Precise Fold Positions in Complex Epithelia. *Developmental Cell*. [Online] 51 (3), 299-312.e4. [online]. Available from: http://www.cell.com/article/S1534580719307385/fulltext (Accessed 27 September 2023).

Trasler, D. G. & Fraser, F. C. (1963) Role of the tongue in producing cleft palate in mice with spontaneous cleft lip. *Developmental Biology*. [Online] 6 (1), 45–60.

Trowell, O. (1959) The Culture of Mature Organs in a Synthetic Medium. *Cell Research*. 147118–147.

Turing, A. M. (1952) The chemical basis of morphogenesis. *Bulletin of Mathematical Biology*. [Online] 52 (1–2), 153–197.

Twigg, S. R. F. & Wilkie, A. O. M. (2015) New insights into craniofacial malformations. *Human Molecular Genetics*. [Online] 24 (R1), R50–R59.

Tyndale-Briscoe, H. & Renfree, M. (1987) 'Marsupials and the evolution of mammalian reproduction', in *Reproductive Physiology of Marsupials*. Cambridge: Cambridge University Press. pp. 396–424. [online]. Available from: https://books.google.nl/books?hl=en&lr=&id=HpjovN0vXW4C&oi=fnd&pg=PR13&dq=Tyndale-Biscoe+CH,+Renfree+M.+1987.+Reproductive+physiology+of+marsupials.+Cambridge:+Cambridge+University+Press.+&ots=9rQ6J6PAPE&sig=i6dOBcEZycCLd_7zLV5qVmKGGxU&redir_esc=y#v=onepage&q=Tyndale-Biscoe%20CH%2C%20Renfree%20M.%201987.%20Reproductive%20physiology%20of%20marsupials.%20Cambridge%3A%20Cambridge%20University%20Press.&f=false (Accessed 19 September 2023).

Uesaka, M. et al. (2022) The developmental hourglass model and recapitulation: An attempt to integrate the two models. *Journal of Experimental Zoology. Part B, Molecular and Developmental Evolution*. [Online] 338 (1–2), 76. [online]. Available from: /pmc/articles/PMC9292893/ (Accessed 22 September 2023).

Vanderas, A. (1987) Incidence of cleft lip, cleft palate, and cleft lip and palate among races: a review. *Cleft Palate Journal*. 24 (3), 216–225. [online]. Available from: https://scholar.archive.org/work/fqmthhivjvgsnbphlkxbtvj2i4/access/wayback/https://cleftpalatejournal.pitt.edu/ojs/cleftpalate/article/download/1155/1155 (Accessed 22 July 2023).

Varju, P. et al. (2001) GABA signalling during development: new data and old questions. *Cell and tissue research*. [Online] 305 (2), 239–246. [online]. Available from: https://pubmed.ncbi.nlm.nih.gov/11545261/ (Accessed 28 August 2023).

Vázquez, D. et al. (2017) A Benchmark for Endoluminal Scene Segmentation of Colonoscopy Images. *Journal of Healthcare Engineering*. [Online] 2017.

Veistinen, L. et al. (2009) Convergent signalling through Fgfr2 regulates divergent craniofacial morphogenesis. *Journal of experimental zoology. Part B, Molecular and developmental evolution*. [Online] 312B (4), 351–360. [online]. Available from: https://pubmed.ncbi.nlm.nih.gov/19205045/ (Accessed 2 August 2023).

Veroniki, A. A. et al. (2017) Comparative safety of anti-epileptic drugs during pregnancy: A systematic review and network meta-analysis of congenital malformations and prenatal outcomes. *BMC Medicine*. [Online] 15 (1), 1–20. [online]. Available from: https://bmcmedicine.biomedcentral.com/articles/10.1186/s12916-017-0845-1 (Accessed 23 July 2023).

Verrusio, A. C. (1970) A mechanism for closure of the secondary palate. *Teratology*. [Online] 3 (1), 17–20. [online]. Available from: https://pubmed.ncbi.nlm.nih.gov/5418331/ (Accessed 7 August 2023).

Vissers, L. E. L. M. et al. (2004) Mutations in a new member of the chromodomain gene family cause CHARGE syndrome. *Nature genetics*. [Online] 36 (9), 955–957. [online]. Available from: https://pubmed.ncbi.nlm.nih.gov/15300250/ (Accessed 23 July 2023).

Voit, M. (1909) Das Primordialcranium des Kaningchens - Unter Berücksichtigung der Deckknochen. *Beiträge und Referate zur Anatomie und Entwickelungsgeschichte*. [Online] 38 (3), 425–616. [online]. Available from: https://link.springer.com/article/10.1007/BF02214638 (Accessed 5 August 2023).

Wagner, T. et al. (1994) Autosomal sex reversal and campomelic dysplasia are caused by mutations in and around the SRY-related gene SOX9. *Cell*. [Online] 79 (6), 1111–1120. [online]. Available from: https://pubmed.ncbi.nlm.nih.gov/8001137/ (Accessed 23 July 2023).

Walker, B. E. (1969) Correlation of embryonic movement with palate closure in mice. *Teratology*. [Online] 2 (3), 191–197.

Walker, Bruce E. (1971) Induction of cleft palate in rats with antiinflammatory drugs. *Teratology*. [Online] 4 (1), 39–42.

Walker, B. E. (1971) Palate morphogenesis in the rabbit. *Archives of Oral Biology*. [Online] 16 (3), 275-IN7.

Walker, B. E. & Fraser, F. C. (1956) Closure of the Secondary Palate in Three Strains of Mice. *Journal of Experimental Embryology*. 4 (2), 176–189.

Walker, B. E. & Patterson, A. (1974) Induction of cleft palate in mice by tranquilizers and barbiturates. *Teratology*. [Online] 10 (2), 159–163. [online]. Available from: https://onlinelibrary.wiley.com/doi/full/10.1002/tera.1420100212 (Accessed 7 August 2023).

Walker, B. E. & Quarles, J. (1976) Palate development in mouse foetuses after tongue removal. *Archives of Oral Biology*. [Online] 21 (7), 405–412.

Wallis, D. E. et al. (1999) Mutations in the homeodomain of the human SIX3 gene cause holoprosencephaly. *Nature genetics*. [Online] 22 (2), 196–198. [online]. Available from: https://pubmed.ncbi.nlm.nih.gov/10369266/ (Accessed 23 July 2023).

Wang, T. D. & Milczuk, H. A. (2014) Cleft Lip and Palate. *Cummings Pediatric Otolaryngology*. [Online] 105–122.

Wang, X. et al. (2020) Extracellular Matrix Remodeling During Palate Development. *Organogenesis*. [Online] 16 (2), 43. [online]. Available from: /pmc/articles/PMC7531623/ (Accessed 29 August 2023).

Wang, X. & Astrof, S. (2016) Neural crest cell-autonomous roles of fibronectin in cardiovascular development. *Development (Cambridge)*. [Online] 143 (1), 88–100. [online]. Available from: https://pubmed.ncbi.nlm.nih.gov/26552887/ (Accessed 30 August 2023).

Wang, Y. et al. (2014) Single molecule FRET reveals pore size and opening mechanism of a mechano-sensitive ion channel. *eLife*. [Online] 2014 (3), . [online]. Available from: https://pubmed.ncbi.nlm.nih.gov/24550255/ (Accessed 28 September 2023).

Warkany, J. (1943) Congenital malformations induced in rats by maternal nutritional deficiency: IV. Cleft palate. *American Journal of Diseases of Children*. [Online] 65 (6), 894.

Warkany, J. (1945) The Importance of Prenatal Diet. *The Milbank Memorial Fund Quarterly*. [Online] 23 (1), 77.

Wee, B. E. L. et al. (1979) Palate Morphogenesis IV. Effects of serotonin and its antagonisys on rotation in embryo culture. *Journal of Embryology and Experimental Morphology*. 53 (1), 75–90.

Wee, E. L. et al. (1981) Palate morphogenesis VI. Identification of stellate cells in culture. *Cell and Tissue Research*. 217 (1), 143–154.

Wee, E. L. et al. (1976) Palate shelf movement in mouse embryo culture: Evidence for skeletal and smooth muscle contractility. *Developmental Biology*. [Online] 48 (1), 91–103. [online]. Available from: http://www.sciencedirect.com/science/article/pii/0012160676900488.

Wee, E. L. & Zimmerman, E. F. (1983) Involvement of GABA in palate morphogenesis and its relation to diazepam teratogenesis in two mouse strains. *Teratology*. [Online] 28 (1), 15–22.

Wee, E. L. & Zimmerman, E. F. (1980) Palate morphogenesis: II. Contraction of cytoplasmic processes in ATP-induced palate rotation in glycerinated mouse heads. *Teratology*. [Online] 21 (1), 15–27.

Wee, ElizabethL. et al. (1981) Palate morphogenesis V. Effects of cholinergic agonists and antagonists on rotation in embryo culture. *Cell and Tissue Research*. [Online] 217 (1), 177–193.

Wehby, G. L. & Cassell, C. H. (2010) The impact of orofacial clefts on quality of life and healthcare use and costs. *Oral diseases*. [Online] 16 (1), 3–10. [online]. Available from: https://pubmed.ncbi.nlm.nih.gov/19656316/ (Accessed 22 July 2023).

Welsh, I. C. & O'Brien, T. P. (2009) Signaling integration in the rugae growth zone directs sequential SHH signaling center formation during the rostral outgrowth of the palate. *Developmental Biology*. [Online] 336 (1), 53–67. [online]. Available from: https://pubmed.ncbi.nlm.nih.gov/19782673/ (Accessed 2 August 2023).

Werneburg, I. & Sánchez-Villagra, M. R. (2011) The early development of the echidna, Tachyglossus aculeatus (Mammalia: Monotremata), and patterns of mammalian development. *Acta Zoologica*. [Online] 92 (1), 75–88.

Wichakam, I. et al. (2018) Real-Time Polyps Segmentation for Colonoscopy Video Frames Using Compressed Fully Convolutional Network. *Lecture Notes in Computer Science (including subseries Lecture Notes in Artificial Intelligence and Lecture Notes in Bioinformatics)*. [Online] 10704 LNCS393–404. [online]. Available from: https://link.springer.com/chapter/10.1007/978-3-319-73603-7_32 (Accessed 8 September 2023).

Wicksell, S. D. (1925) The Corpuscle Problem: A Mathematical Study of a Biometric Problem. *Biometrika*. [Online] 17 (1/2), 84.

Wickstrøm, K. et al. (2018) Uncertainty modeling and interpretability in convolutional neural networks for polyp segmentation. *IEEE International Workshop on Machine Learning for Signal Processing, MLSP*. [Online] 2018-September.

Wilk, A. et al. (1978) Degradation of Palatal Glycosaminoglycans. *Experimental Teratology*. 18 (2), 199–209.

Wilkie, A. O. M. et al. (1995) Apert syndrome results from localized mutations of FGFR2 and is allelic with Crouzon syndrome. *Nature genetics*. [Online] 9 (2), 165–172. [online]. Available from: https://pubmed.ncbi.nlm.nih.gov/7719344/ (Accessed 23 July 2023).

Williamson, T. E. et al. (2014) The origin and early evolution of metatherian mammals: the Cretaceous record. *ZooKeys*. [Online] (465), 1–76. [online]. Available from: https://pubmed.ncbi.nlm.nih.gov/25589872/ (Accessed 19 September 2023).

Wilson, J. G. et al. (1953) An analysis of the syndrome of malformations induced by maternal vitamin A deficiency. Effects of restoration of vitamin A at various times during gestation. *The American journal of anatomy*. [Online] 92 (2), 189–217. [online]. Available from: https://pubmed.ncbi.nlm.nih.gov/13030424/ (Accessed 7 August 2023).

Wolman, M. (1975) Polarized light microscopy as a tool of diagnostic pathology. A review. *Journal of Histochemistry and Cytochemistry*. [Online] 23 (1), 21–50.

Woulfe, P. (1771) Experiments to show the Nature of Aurum Mosaicum. *Philosophical transactions of the Royal Society of London*. 61114–130. [online]. Available from: https://www.biodiversitylibrary.org/item/206643 (Accessed 12 September 2023).

Wragg, L. E., Smith, J. A., et al. (1972) Myoneural maturation and function of the foetal rat tongue at the time of secondary palate closure. *Archives of oral biology*. [Online] 17 (4), 673–682. [online]. Available from: https://pubmed.ncbi.nlm.nih.gov/4505459/ (Accessed 6 August 2023).

Wragg, L. E., Diewert, V. M., et al. (1972) Spatial relations in the oral cavity and the mechanism of secondary palate closure in the rat. *Archives of Oral Biology*. [Online] 17 (4), 683–690.

Wyszynski, Dr. D. F. et al. (1997) Maternal Cigarette Smoking and Oral Clefts: A Meta-analysis. *https://doi.org/10.1597/1545-1569_1997_034_0206_mcsaoc_2.3.co_2*. [Online] 34 (3), 206–210. [online]. Available from: https://journals.sagepub.com/doi/10.1597/1545-1569_1997_034_0206_mcsaoc_2.3.co_2 (Accessed 23 July 2023).

Xu, J. et al. (2018) FGF8 Signaling Alters the Osteogenic Cell Fate in the Hard Palate. *Journal of dental research*. [Online] 97 (5), 589–596. [online]. Available from: https://pubmed.ncbi.nlm.nih.gov/29342370/ (Accessed 30 August 2023).

Xu, J. et al. (2019) Hedgehog signaling patterns the oralaboral axis of the mandibular arch. *eLife*. [Online] 8.

Yakoob, M. Y. et al. (2013) The risk of congenital malformations associated with exposure to β-blockers early in pregnancy: A meta-analysis. *Hypertension*. [Online] 62 (2), 375–381. [online]. Available from: https://www.ahajournals.org/doi/abs/10.1161/HYPERTENSIONAHA.111.00833 (Accessed 23 July 2023).

Yang, T. et al. (2014) Analysis of PRICKLE1 in human cleft palate and mouse development demonstrates rare and common variants involved in human malformations. *Molecular Genetics & Genomic Medicine*. [Online] 2 (2), 138. [online]. Available from: /pmc/articles/PMC3960056/ (Accessed 28 August 2023).

Yildirim, M. et al. (2016) Quantitative differentiation of normal and scarred tissues using second-harmonic generation microscopy. *Scanning*. [Online] 38 (6), 684–693.

Yonemitsu, M. A. et al. (2020) Hyaluronic acid is required for palatal shelf movement and its interaction with the tongue during palatal shelf elevation. *Developmental Biology*. [Online] 457 (1), 57–68. [online]. Available from: https://doi.org/10.1016/j.ydbio.2019.09.004.

Yu, H. et al. (2010) Frizzled 1 and frizzled 2 genes function in palate, ventricular septum and neural tube closure: General implications for tissue fusion processes. *Development*. [Online] 137 (21), 3707–3717. [online]. Available from: /pmc/articles/PMC2964100/ (Accessed 28 August 2023).

Yu, K. & Ornitz, D. M. (2011) Histomorphological study of palatal shelf elevation during murine secondary palate formation. *Developmental Dynamics*. [Online] 240 (7), 1737–1744.

Yu, K. & Yonemitsu, M. A. (2019) In Vitro Analysis of Palatal Shelf Elevation During Secondary Palate Formation. *Anatomical Record*. [Online] 302 (9), 1594–1604.

Yu, L. et al. (2005) Shox2-deficient mice exhibit a rare type of incomplete clefting of the secondary palate. *Development (Cambridge, England)*. [Online] 132 (19), 4397–4406. [online]. Available from: https://pubmed.ncbi.nlm.nih.gov/16141225/ (Accessed 2 August 2023).

Yuan, X. et al. (2020) Construction of fibronectin conditional gene knock-out mice and the effect of fibronectin gene knockout on hematopoietic, biochemical and immune parameters in mice. *PeerJ*. [Online] 8. [online]. Available from: /pmc/articles/PMC7605225/ (Accessed 29 September 2023).

Zeiler, K. B. et al. (1964) A study of the morphology and the time of closure of the palate in the albino rat. *Archives of Oral Biology*. [Online] 9 (5), 545–554.

Zemljic-Harpf, A. et al. (2009) Vinculin and Talin: Focus on the Myocardium. *Journal of investigative medicine : the official publication of the American Federation for Clinical Research*. [Online] 57 (8), 849. [online]. Available from: /pmc/articles/PMC2810504/ (Accessed 29 September 2023).

Zhang, J. et al. (2012) Functional verification of the diphtheria toxin A gene in a recombinant system. *Journal of Animal Science and Biotechnology*. [Online] 3 (1), 29. [online]. Available from: /pmc/articles/PMC3523071/ (Accessed 17 September 2023).

Zhang, J. et al. (2015) Loss of lysyl oxidase-like 3 causes cleft palate and spinal deformity in mice. *Human molecular genetics*. [Online] 24 (21), 6174–6185. [online]. Available from: https://pubmed.ncbi.nlm.nih.gov/26307084/ (Accessed 30 August 2023).

Zhang, Z. et al. (2002) Rescue of cleft palate in Msx1-deficient mice by transgenic Bmp4 reveals a network of BMP and Shh signaling in the regulation of mammalian palatogenesis. *Development (Cambridge, England)*. [Online] 129 (17), 4135–4146. [online]. Available from: https://pubmed.ncbi.nlm.nih.gov/12163415/ (Accessed 2 August 2023).

Zhou, C. et al. (2022) Microenvironmental stiffness mediates cytoskeleton re-organization in chondrocytes through laminin-FAK mechanotransduction. *International Journal of Oral Science 2022 14:1*. [Online] 14 (1), 1–10. [online].

Available from: https://www.nature.com/articles/s41368-022-00165-5 (Accessed 28 September 2023).

Zhou, J. et al. (2013) Pax9 regulates a molecular network involving Bmp4, Fgf10, Shh signaling and the Osr2 transcription factor to control palate morphogenesis. *Development (Cambridge, England)*. [Online] 140 (23), 4709–4718. [online]. Available from: https://pubmed.ncbi.nlm.nih.gov/24173808/ (Accessed 2 August 2023).

Zhou, X. et al. (2023) Incidence of cleft lip and palate, and epidemiology of perinatal deaths related to cleft lip and palate in Hunan Province, China, 2016-2020. *Scientific reports*. [Online] 13 (1), . [online]. Available from: https://pubmed.ncbi.nlm.nih.gov/37365256/ (Accessed 22 July 2023).

Zhou, Y. et al. (2021) Platypus and echidna genomes reveal mammalian biology and evolution. *Nature 2020 592:7856*. [Online] 592 (7856), 756–762. [online]. Available from: https://www.nature.com/articles/s41586-020-03039-0 (Accessed 16 September 2023).

Zimmerman, E. F. et al. (1983) Serotonin regulation of palatal cell motility and metabolism. *J. Craniofac. Genet, devl Biol.* 3371–385.

Zucchero, T. M. et al. (2004) Interferon regulatory factor 6 (IRF6) gene variants and the risk of isolated cleft lip or palate. *The New England journal of medicine*. [Online] 351 (8), 769–780. [online]. Available from: https://pubmed.ncbi.nlm.nih.gov/15317890/ (Accessed 23 July 2023).

9. Appendices

9.1 Mechanical dependencies during elevation in culture

Below is a representative photomicrograph from a preliminary investigation aimed at identifying if any anatomical regions depended on another during elevation in culture. This was essentially a repeat of previously studies (Brinkley & Vickerman, 1979; Bulleit & Zimmerman, 1985). However, during these preliminary studies, it was identified that PS elevation is not occurring during cultures, and the experiments were abandoned.

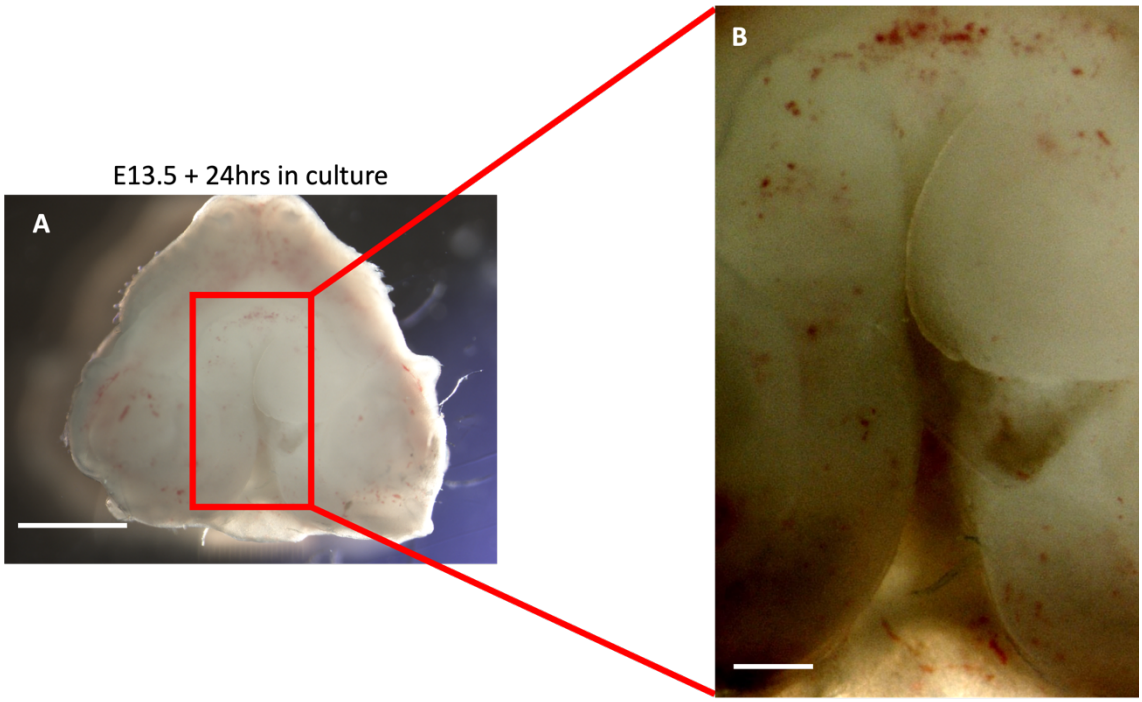

Figure 9.1 PS severing during culture

Representative photomicrograph of maxillary explants after 24 hours in culture following PS severing via microdissection scissors. Scale bars: A: 1000um, B: 250um

9.2 Inter-hinge gap statistics

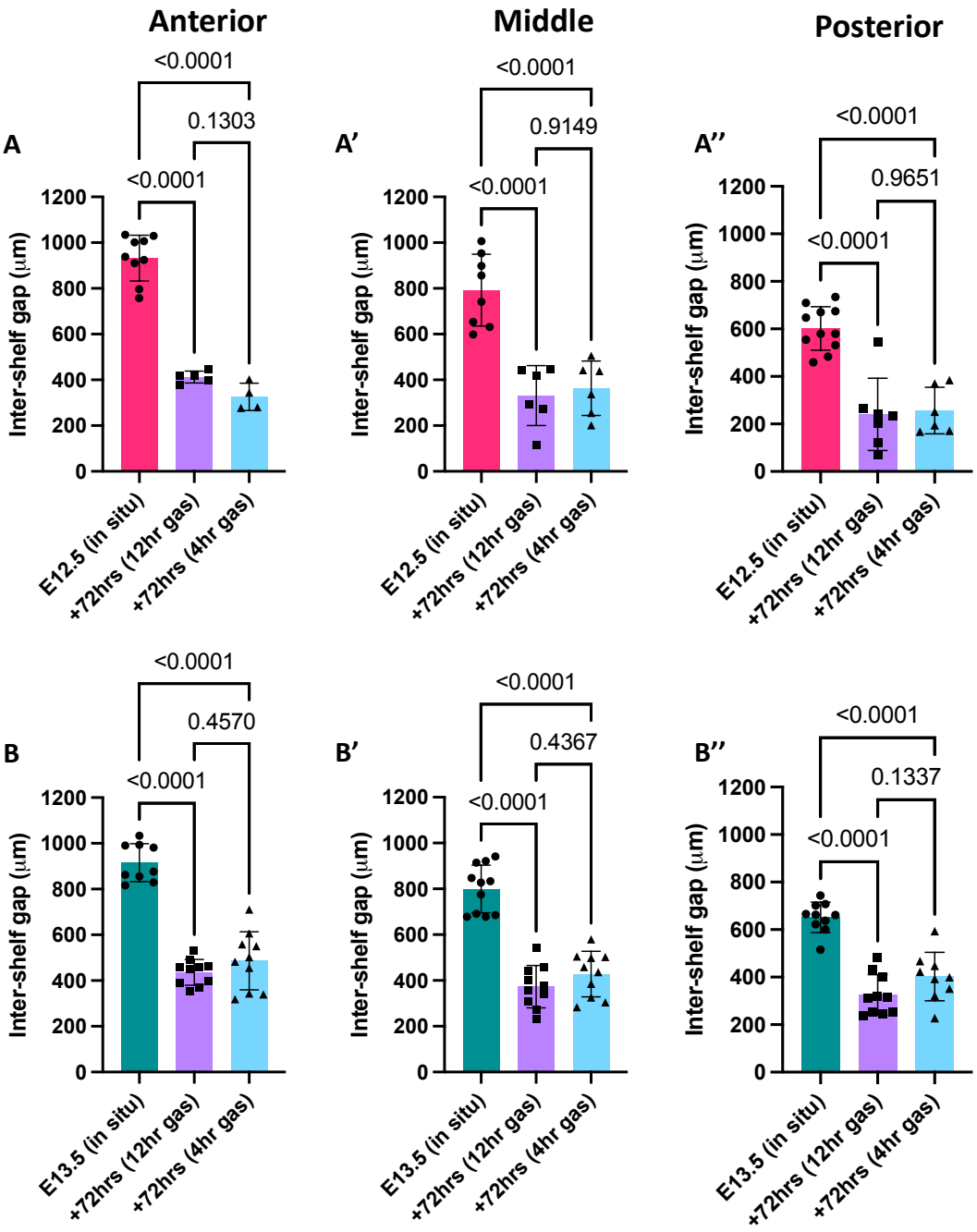

Figure 9.2 Inter-hinge gap comparison between E12.5 and E13.5 *in situ* and *ex vivo* PSs.

Graph comparing inter-hinge width difference between E12.5 *in situ* vs *ex vivo* (A-A'') and E13.5 *in situ* vs. *ex vivo* anterior, middle and posterior regions. Statistical significance (P values) determined by ordinary 1-way ANOVA with Tukey's Multiple Comparisons Test. Sample size: see tables 3.3, 3.4 and 3.5. Error bars = mean with SD.

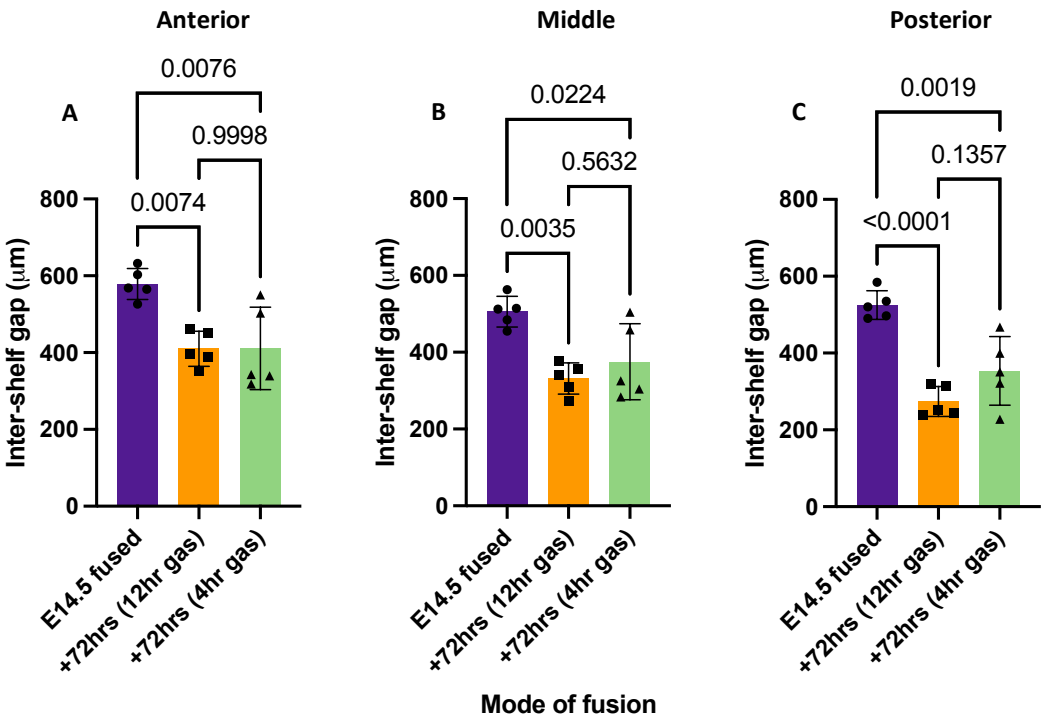

Figure 9.3 Inter-hinge gap comparison between E14.5 *in situ* fused and E13.5 fused *ex vivo*.

Graph comparing inter-hinge width difference between *in situ* fused and *ex vivo* culture fused PSs in middle and posterior regions. Statistical significance (P values) determined by ordinary 1-way ANOVA with Tukey's Multiple Comparisons Test. Sample size: see tables 3.3, 3.4 and 3.5. Error bars = mean with SD.

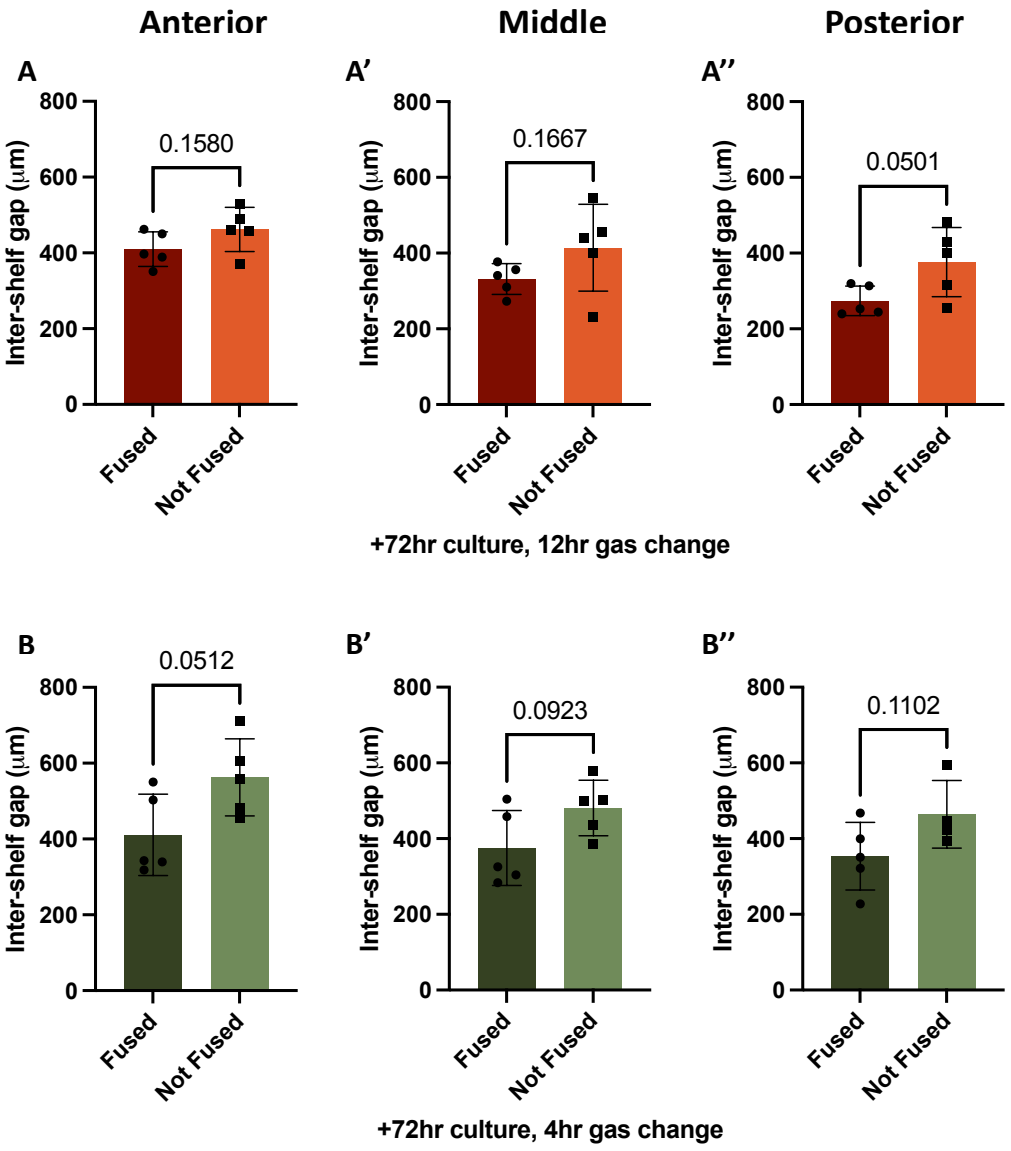

Figure 9.4 Inter-hinge gap comparison between E13.5 *ex vivo* culture fused and not fused explants at both gas changes

Graphs comparing inter-hinge width difference between fused and not fused E13.5 explants during *ex vivo* culture at during 12hr gas change (A-A'') and 4hr gas change (B-B'') in anterior, middle, and posterior regions. Statistical significance (P values) determined by two-tailed unpaired t-test (A-B') and Welch's t-test (B''). Sample size: see tables 3.3, 3.4 and 3.5. Error bars = mean with SD.

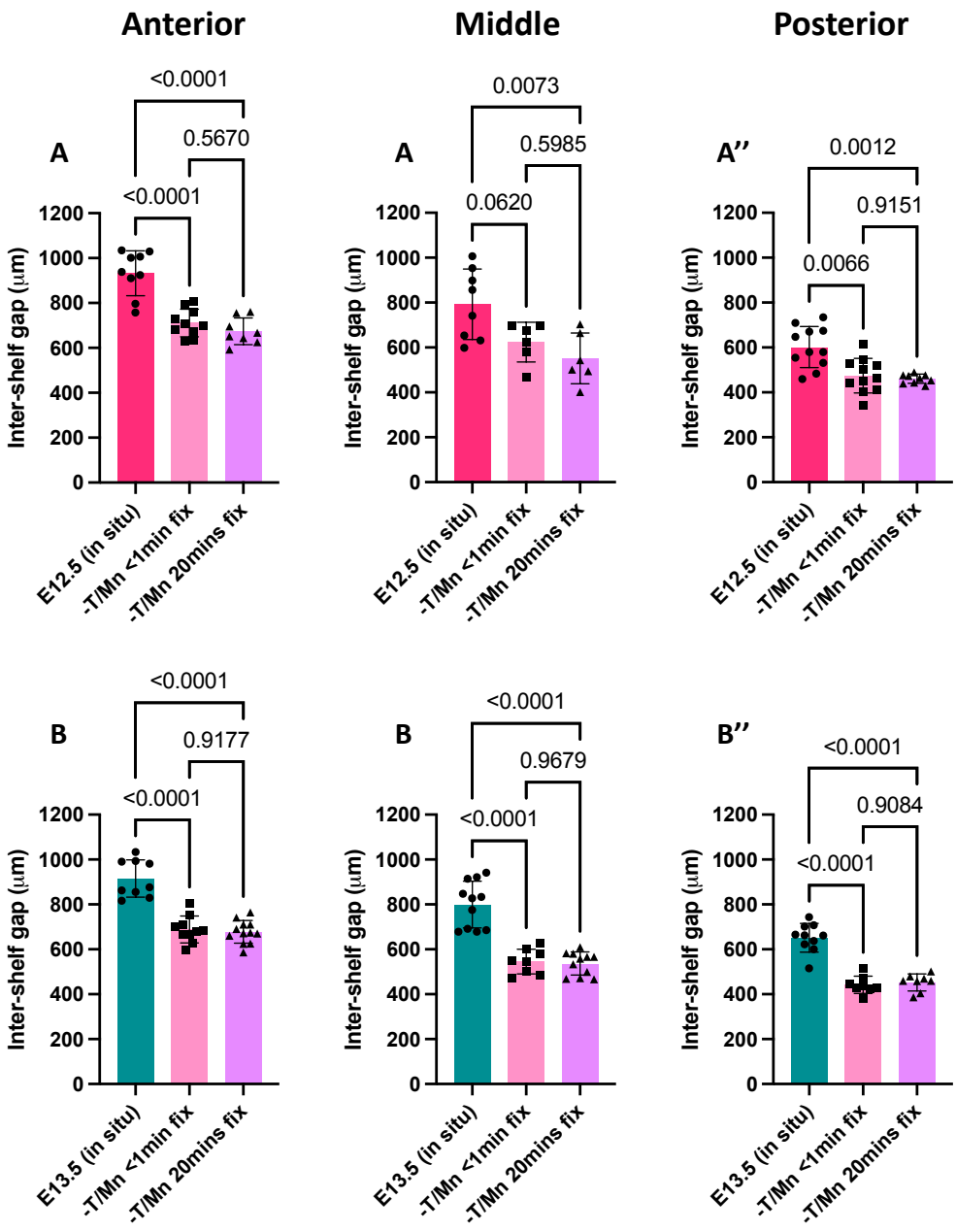

Figure 9.5 Inter-hinge gap comparison between E12.5 and E13.5 *in situ* and recoil study PSs

Graphs comparing inter-hinge width difference between E12.5 *in situ* vs recoil (A-A'') and E13.5 *in situ* vs. recoil (B-B'') in anterior, middle, and posterior regions. Statistical significance (P values) determined by ordinary 1-way ANOVA with Tukey's Multiple Comparisons Test (A, A', B-B'') and Brown-Forsythe & Welch's ANOVA with Dunnett's T3 Multiple Comparisons Test (A''). Sample size: see tables 3.3, 3.4 and 3.5. Error bars = mean with SD.

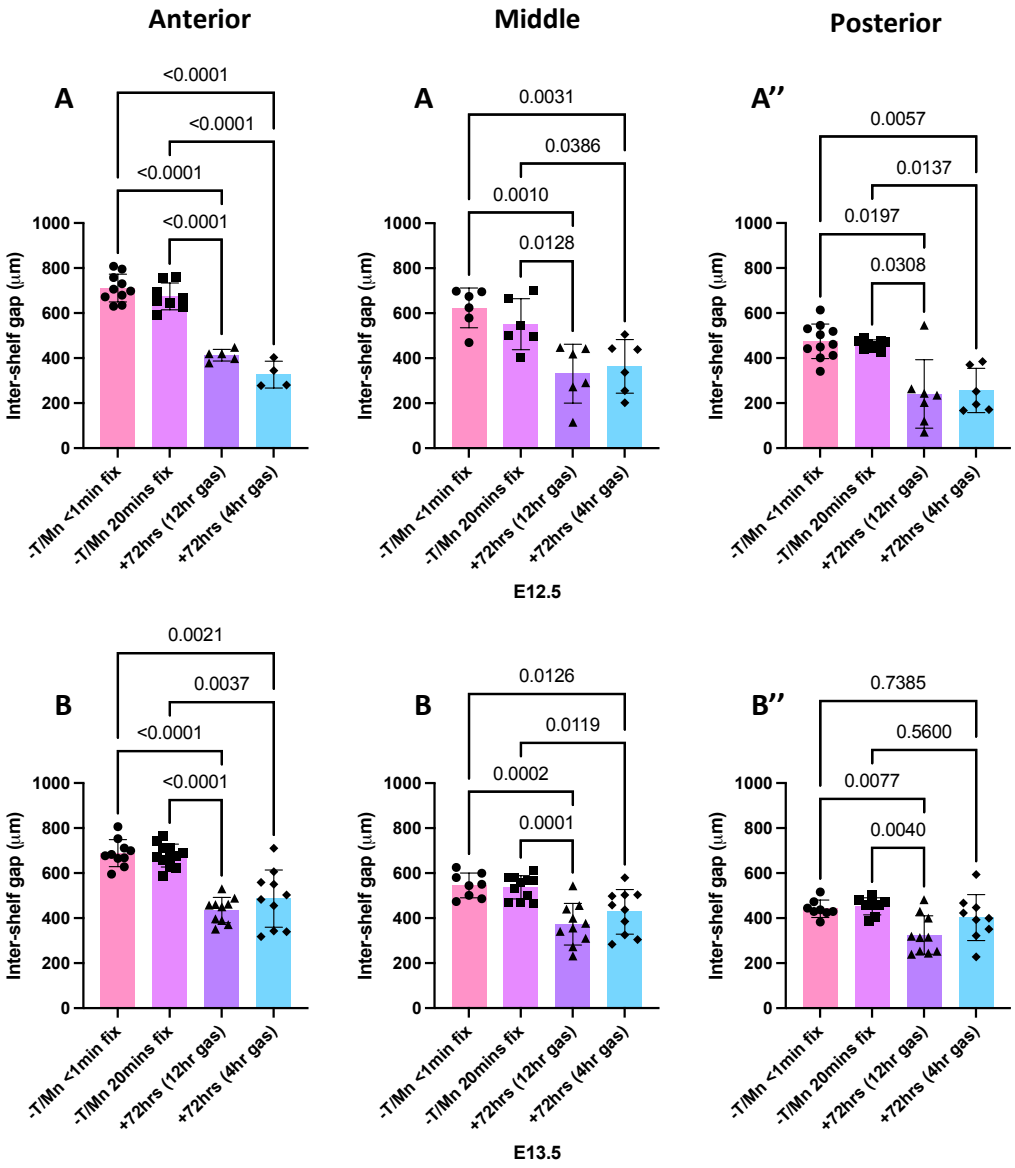

Figure 9.6 Inter-hinge gap comparison between E12.5 and E13.5 recoil study and *ex vivo* culture PSs.

Graphs comparing inter-hinge width difference between E12.5 recoil groups and *ex vivo* culture groups (A-A'') and E13.5 recoil groups and *ex vivo* culture groups (B-B'') in anterior, middle and posterior regions. Statistical significance (P values) determined by ordinary 1-way ANOVA with Tukey's Multiple Comparisons Test (A, A'&B') and Brown-Forsythe & Welch's ANOVA with Dunnett's T3 Multiple Comparisons Test (A'', B&B''). Sample size: see tables 3.3, 3.4 and 3.5. Error bars = mean with SD.

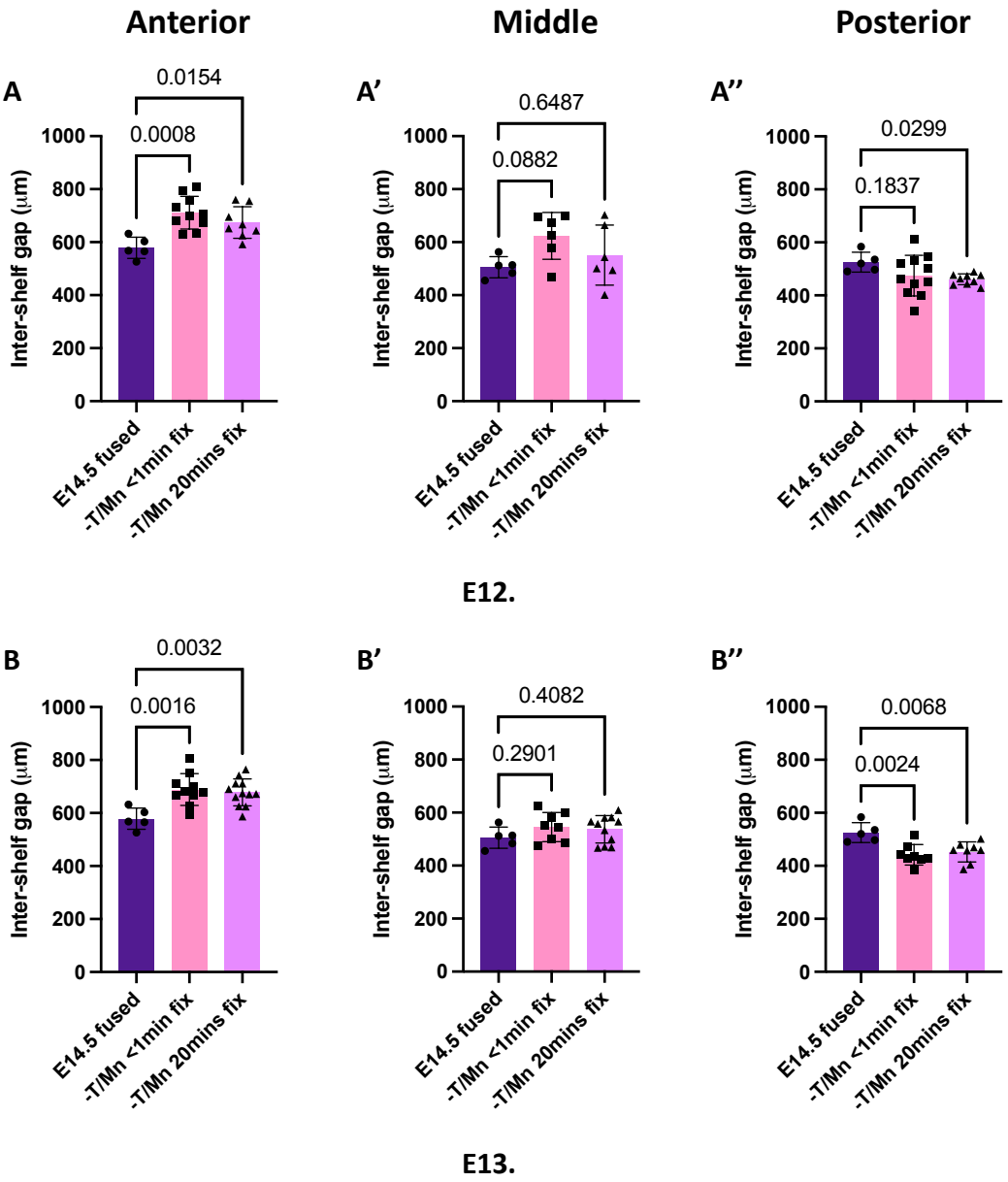

Figure 9.7 Inter-hinge gap comparison between E14.5 *in situ* fused and both recoil groups at E12.5 and E13.5

Graphs comparing inter-hinge gap between fused PSs *in situ* at E14.5 with both recoil groups at both E12.5 (A-A'') and E13.5 (B-B''). Statistical significance (P values) determined by ordinary 1-way ANOVA (A, A', B-B'') and Brown-Forsythe & Welch's ANOVA (A'') all with Dunnett's T3 Multiple Comparisons Test. Sample size: see tables 3.3, 3.4 and 3.5. Error bars = mean with SD.

Table 9.1 Mean, SD and sample number (n) of the inter-hinge gap in the anterior of each tested group across different embryonic day stages.

Anterior	*In vivo*			<1min fix			20mins fix			+72hrs culture (12hr gas change)			+72hrs culture (4hr gas change)		
	Mean	SD	N	Mean	SD	N	Mean	SD	N	Mean	SD	N	Mean	SD	N
E12.5	932.9	99.97	9	711.2	61.74	10	674.1	59.87	8	412.8	25.97	5	326.4	59.54	4
E13.5	915.4	83.19	9	688.6	59.81	10	677.7	50.69	12	435.9	56.47	10	486.8	127	10
E14.5	578.8	40.35	5												

Table 9.2 Mean, SD and sample number (n) of the inter-hinge gap in the middle of each tested group across different embryonic day stages.

Middle	*In vivo*			<1min fix			20mins fix			+72hrs culture (12hr gas change)			+72hrs culture (4hr gas change)		
	Mean	SD	N	Mean	SD	N	Mean	SD	N	Mean	SD	N	Mean	SD	N
E12.5	792.4	157	8	623.6	88.48	6	551.4	113.3	6	331.4	130.7	6	363.7	118.9	6
E13.5	799.4	103.7	11	545.3	54.94	8	536.8	51.71	11	373	92.23	10	428	99.2	10
E14.5	505.6	40.10	5												

Table 9.3 Mean, SD and sample number (n) of the inter-hinge gap in the posterior of each tested group across different embryonic day stages.

Posterior	*In vivo*			<1min fix			20mins fix			+72hrs culture (12hr gas change)			+72hrs culture (4hr gas change)		
	Mean	SD	N	Mean	SD	N	Mean	SD	N	Mean	SD	N	Mean	SD	N
E12.5	602	91.59	11	474.6	76.97	11	460.6	20.57	9	240.5	152	7	256.6	98.26	6
E13.5	651.4	63.88	10	442	38.82	8	452.5	38.22	8	325.3	85.42	10	402.7	101.9	9
E14.5	525.2	37.47	5												

9.3 Background to machine learning

In the Colab notebook, Stardist must first install and load key dependencies. The Colab session must then be initialised, which is essentially a checking step for GPU access (this is separate to the initialisation of training). About 12 hours of access time is granted to users at a time. The paired training dataset must be loaded from a Google Drive account, and so a Google Drive must be mounted.

The model training itself was then prepared for initialisation. 3 images were removed from the paired training datasets to serve as quality control or validation images post-training. Then, parameters were selected for use during training. The Colab notebook suggests using default parameters, though there is an option to vary different aspects of the network extensively. For example, editing the 'patch size' parameter will determine the area within each training image that will be used in training. The only parameter edited at this stage in the generation of my model was the number of epochs. An 'epoch' refers to one complete pass through the training dataset, with the Colab authors stating deep-learning models typically requiring up to 400 passes for a model to be fully trained (although preliminary results can be observed between 50-100 epochs). The number of epochs used can generally be considered as a trade-off between giving the model the maximum number of chances to make the right neural connections vs. overfitting to the data. In the case of overfitting, the model performs exceptionally well on the training data, but does not perform well on unseen data. This could be conceptualised as the model seeing and remembering all possible outcomes from a training dataset, but remaining incapable of applying what is has learnt to data (images) it hasn't been trained on. This can be, at least in part, addressed by using data augmentation and adding pre-trained weights.

Data augmentation amplifies differences in the dataset. Here, data augmentation stochastically creates variation by rotating and flipping images, or by intensifying certain parts of the image. This increases the range of data for the model to train on, thus reducing the chances of overfitting.

Next, weights from pre-trained models can be added. This is referred to as 'transfer learning' in machine learning more broadly, and essentially applies what has been learned by another model in previous training to improve the training of a new model. It is recommended by default that training weights are added from the default StarDist nuclei training model. The model is now ready for training.

Model training

Training a deep learning model is a computationally demanding task which refers to the generation of a model influenced by the parameters described previously. Broadly, the training of a deep learning model can be considered in five stages:

1. Forward propagation
2. Backpropagation
3. Iterative training
4. Hyperparameter training
5. Quality control testing

In the forward propagation step, the training data is run through the neural network, and the early model computes predictions and calculates the loss (error) compared to the target values via a loss function. The backpropagation step is essentially where the model attempts to correct its mistakes by adjusting its internal parameters to minimise loss. When calculating loss, the model uses the chain rule of calculus to determine how parameter adjustment effects the loss function. The chain rule can be considered as determining the product of two rates of change by knowing the rates of change between the variables indirectly, typically via a third variable, or "if a car travels twice as fast as a bicycle and the bicycle is four times as fast as a walking man, then the car travels $2 \cdot 4 = 8$ times as fast as the man" (Simons, 1996). The gradient (derivative) of each model parameter is then used as a reference to update the model parameters in reverse, thus directing model behaviour. Iterative training refers to the number of epochs run, i.e., the number of times the model is fed through the previous two steps. Hyperparameter training is the further adjustment of parameters (such as the previously described batch

size) though these were not adjusted here. Quality control is addressed separately in the context of my own model in *6.2.1.3*.

In total, I generated 21 individual models, varying the extent of augmentation, number of epochs and pre-training weight inclusion and their combinations. Overall, I found that a data augmentation of 4, the inclusion of pre-trained weight from the default StarDist model and 320 epochs generated a model which would automatically segment nuclei most accurately.

Inspection of the loss function

Prior to quality control testing it is possible to check the progress of training by assessing the loss function. This assesses how closely the model prediction fits the correct value following testing on unseen data (Nichols et al., 2019). A smaller loss function value represents a better-fitting model.

In the Colab notebook, an indication of the loss function is conveniently given by an automatically generated plot of training loss and validation loss against epoch number. Training loss is the loss function calculated against the training dataset, describing an error value which between prediction and target data for every epoch. Validation loss essentially does the same, but against unseen images from the validation dataset, which were removed from the paired training dataset pre-training as described. During training, both values should decrease to a minimal value before stabilising (represented by a flattening of the curve. At the point the curves flatten-out, the model has converged, and no further training is required. It is essential to analyse these curves as it gives insight into the quality of the model. For example, continually decreasing training and validation loss curves without levelling-off indicates that further training is required as a small loss function can be achieved. However, a sudden increase in previously descending validation loss with a training loss of 0 suggests overfitting is occurring i.e., the model is not generalising well to unseen data, and the training set needs to be increased.

My custom StarDist 2D model was trained for 320 epochs on 21 paired image patches with image dimensions and a patch size of 256 x 256 and batch size of 2. Functional

assessment was measured using a mean absolute error (MAE) loss function, using the StarDist 2D ZeroCostDL4Mic notebook (v 1.18) (von Chamier & Laine et al., 2021). The model was retrained from a pretrained model. Python packages used during training included tensorflow (v 2.11.0), csbdeep (v 0.7.3) and cuda (v 11.8.89Build cuda_11.8.r11.8/compiler.31833905_0). The training was accelerated using a Tesla T4 GPU.